

Durham E-Theses

The synthesis and photophysical studies of cyclometalated iridium(III) complexes

Bettington, Sylvia

How to cite:

Bettington, Sylvia (2003) *The synthesis and photophysical studies of cyclometalated iridium(III) complexes*, Durham theses, Durham University. Available at Durham E-Theses Online: <http://etheses.dur.ac.uk/1295/>

Use policy

The full-text may be used and/or reproduced, and given to third parties in any format or medium, without prior permission or charge, for personal research or study, educational, or not-for-profit purposes provided that:

- a full bibliographic reference is made to the original source
- a [link](#) is made to the metadata record in Durham E-Theses
- the full-text is not changed in any way

The full-text must not be sold in any format or medium without the formal permission of the copyright holders.

Please consult the [full Durham E-Theses policy](#) for further details.

A copyright of this thesis rests
with the author. No quotation
from it should be published
without his prior written consent
and information derived from it
should be acknowledged.

THE SYNTHESIS AND PHOTOPHYSICAL STUDIES OF CYCLOMETALATED IRIDIUM(III) COMPLEXES

Sylvia Bettington

Department of Chemistry,
University of Durham,
Durham, U.K.

Submitted in partial fulfilment of the requirements for the degree of
Doctor of Philosophy, University of Durham.



December 2003

28 APR 2004

Declaration

The work described in this thesis was carried out in the Department of Chemistry at the University of Durham between October 2000 and September 2003. This thesis is the work of the author except where acknowledged by reference and has not been submitted for any other degree.

Statement of Copyright

The copyright of this thesis rests with the author. No quotation from it should be published without her prior written consent and information derived from it should be acknowledged.

Abstract

In 1985, *fac*-Ir(ppy)₃ was characterised as the first triply *ortho*-metalated iridium(III) species. This bright yellow solid exhibits green phosphorescent emission. Since then, numerous related iridium(III) complexes of the formula Ir(L)₃ and Ir(L)₂acac have been synthesised utilising ligands such as 2-phenylpyridine (ppy), 4-(2-pyridyl)benzaldehyde (fppy), benzo[h]-quinoline (bzq) and 2-(2-thienyl)pyridine (thpy), to name but a few.

These complexes give rise to tuneable emission wavelengths *via* ligand modification and also exhibit electroluminescence allowing them to be used as phosphorescent dopants in Organic Light Emitting Devices (OLEDs), the next generation of flat panel displays.

In this work, *ortho*-metalating ligands, especially substituted 2-phenylpyridines, have been produced by a variety of synthetic pathways. The subsequent cyclometalating reactions of these ligands with iridium(III) and rhodium(III) have afforded a series of complexes whose photophysical properties can be related in part to the substituents upon the ligands. In general, these complexes exhibit phosphorescent emission that is derived from an excited metal to ligand charge transfer state (MLCT), which possesses mostly triplet character. Emission from this triplet excited state to the ground state is formally forbidden. However, strong spin-orbit coupling provides mixing of the ³MLCT state with higher energy singlet states thus providing this transition with intensity. Long lifetimes and oxygen-quenched emission are therefore typical of these complexes.

Tuning the emission wavelength of these complexes is possible by altering the relative energy of the emissive ³MLCT state and is achieved by altering the substituents that reside upon the cyclometalating ligands. The reversible oxidation of these complexes under anaerobic conditions has also been demonstrated. For these iridium(III) complexes the position of the oxidative wave follows a pattern in which more positive values are found for complexes of ligands bearing electron-withdrawing substituents and less positive values result from ligands with electron-donating substituents.

Studies of polymer films doped with these iridium(III) complexes have shown efficient energy transfer between the host and guest species. This is inferred by the lack of host emission even at doping concentrations as low as 0.5 % wt./wt. This is vital if these compounds are to be used as electroluminescent dopants in OLEDs.

Acknowledgements

First and foremost I would like to thank Dr Andrew Beeby for all his support and encouragement over the last three years. It has been his knowledge and enthusiasm for science that has helped me to stay immersed in my work and thankfully also kept me sane. I must also add that I'm glad to have been on the right side of his office window.

I also wish to thank EPSRC and CDT for their financial support and Dr Jon Pillow for his helpful advice and discussions.

In addition to this, there have been numerous members of the Beeby group who have played their part in providing a pleasant and relaxed environment in which to work. They are; Dr Allison Jones, Dr Lisa Bushby, Dr Simon FitzGerald, Karen Findlay, Simon Rutter and Kate Nicholson. Extra credit must go to Simon FitzGerald for the smooth running of the lab and his particularly helpful and supportive discussions throughout my time in CG 7.

I must also give many thanks to Amber Thompson who has become a particularly close and trusted friend over the past three years. She has also solved many crystal structures by working wonders with 'crystals' which were 'grown' in the magic cupboard in CG 7. This has been over and above her call of duty.

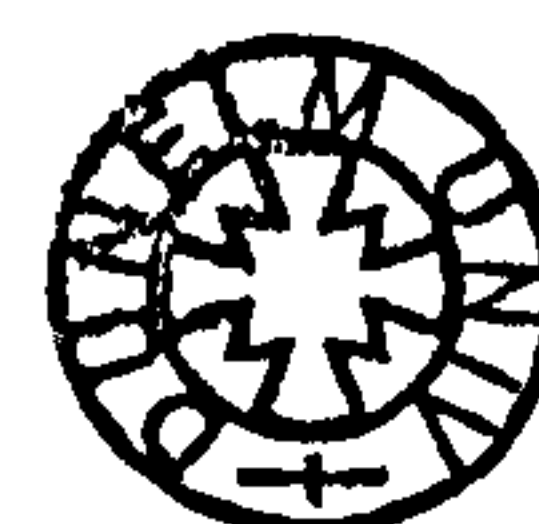
I would also like to thank Dr Alan Kenwright, Dr Mike Jones and Lara Turner for their advice on NMR and Mass Spectrometry samples and for their helpful discussions. For help and advice on the subject of cyclic voltammetry, thanks must also go Dr Paul Low and Michael Patterson. Paul has also been crucial in keeping a sly check on the Beeby group when Andy has been away (and you thought we didn't know who'd been spilling the beans).

Finally and most importantly, had it not been for the love and support of my parents, my brother Michael and my fiancé Joe, I surely would not have made it this far. Throughout my life and especially my years at Durham they have always believed in me. I am sure that the successes I have enjoyed have stemmed from this unwaveringly belief.

I can safely say that my experiences of Durham University and its chemistry department have been both enjoyable and memorable and it is to all those mentioned above that I have to thank for my seven fantastic years in Durham.

Table of Contents

Declaration and statement of copyright.....	i
Abstract.....	ii
Acknowledgements.....	iii
Contents.....	1
List of figures.....	7
List of tables.....	13
Abbreviations.....	16
 Chapter 1 The Synthesis and Photochemistry of Cyclometalated Iridium(III) Complexes	
1.1 Introduction.....	22
1.2 Iridium and Rhodium.....	23
1.3 Cyclometalated Organometallic Complexes of Iridium(III) and Rhodium(III).....	24
1.4 <i>Ortho</i> -metalation.....	24
1.5 Syntheses of 2-Phenylpyridines.....	26
1.5.1 Suzuki Cross-Coupling Reactions.....	26
1.5.2 Kröhnke Syntheses.....	28
1.5.3 The Arylation of Pyridine <i>via</i> the Gomberg Reaction.....	29
1.5.4 The use of Lithium Reagents to Afford 2-Phenylpyridines.....	29
1.6 Dichloro-bridged <i>Ortho</i> -metalated Complexes, $[\text{Ir}(\text{L})_2\text{Cl}]_2$	30
1.6.1 Synthesis and Structure.....	30
1.6.2 Electronic Structure.....	31
1.6.3 UV-Visible Absorption Spectra.....	32
1.6.4 Luminescence Properties.....	33
1.6.5 Summary.....	35
1.7 Monomeric <i>Ortho</i> -metalated Complexes of Iridium(III) and Rhodium(III).....	35
1.7.1 Introduction.....	35
1.7.2 Tris- <i>ortho</i> -metalated Complexes of Ir(III) and Rh(III).....	36
1.7.2.1 Synthesis.....	36



1.7.3	Bis- <i>ortho</i> -metalated Complexes of Ir(III) and Rh(III).....	38
1.7.3.1	Synthesis.....	38
1.7.4	Electronic Structure.....	39
1.7.5	UV-Visible Absorption Spectra.....	40
1.7.6	Luminescence Properties.....	41
1.7.6.1	Steady-State Spectra.....	41
1.7.6.2	Solvatochromatic Emission.....	42
1.7.6.3	Tuneable Emission.....	42
1.7.6.4	Luminescence Lifetimes and Quantum Yields.....	43
1.7.6.5	Singlet Oxygen Sensitisation and Quenching.....	44
1.7.7	Bis- <i>ortho</i> -metalated Complexes, Ir(L) ₂ X(Y).....	45
1.7.7.1	Luminescence Properties.....	45
1.7.7.2	Singlet Oxygen Sensitisation and Quenching.....	47
1.8	Conclusion.....	48
1.9	References.....	48
Chapter 2	Organic Light Emitting Devices	
2.1	Introduction.....	54
2.2	Photoluminescence and Electroluminescence in Molecular Solids.....	54
2.2.1	Photoluminescence.....	54
2.2.2	Electroluminescence.....	56
2.3	Efficient Electroluminescent Devices.....	57
2.3.1	Device Structure.....	57
2.3.2	The Electrodes.....	60
2.3.3	The Emitting Material.....	61
2.3.4	Spin Statistics.....	63
2.4	Device Lifetime and Degradation.....	63
2.4.1	Recoverable Degradation.....	63
2.4.2	Unrecoverable Degradation.....	65
2.5	Cyclometalated Iridium(III) Complexes in OLEDs.....	65
2.5.1	<i>Fac</i> -Ir(ppy) ₃ in OLEDs.....	66
2.5.2	Fluorine Substituted Iridium(III) Complexes for OLEDs.....	70
2.5.3	Tuneable Emission from OLEDs.....	72

2.5.4	Alkyl Substituted Iridium(III) Complexes for OLEDs.....	74
2.5.5	Oligomeric and Dendritic Iridium(III) Complexes for OLEDs with Reduced Self-quenching.....	75
2.6	Conclusion.....	79
2.7	References.....	79
Chapter 3	Synthesis: Cyclometalating Ligands and their Corresponding Ir(III) and Rh(III) Complexes	
	Table of Compounds used.....	84
3.1	Introduction.....	86
3.2	Ligands.....	86
3.2.1	2-Phenylpyridines and 2-Phenylpyrimidines.....	86
3.2.2	Phosphines.....	95
3.3	Bis-cyclometalated Dichloro-bridged Ir(III) and Rh(III) Complexes....	96
3.4	Monomeric $M(L)_3$ and $M(L)_2acac$ Complexes of Ir(III) and Rh(III).....	103
3.5	$Ir(L)_2X(Y)$ Complexes, where $X = Cl/CN$ and $Y =$ Monodentate ligand.....	116
3.6	Palladium(II) Species.....	123
3.7	References.....	124
Chapter 4	Experimental Techniques	
4.1	Introduction.....	126
4.2	UV-Visible Absorption Spectroscopy.....	126
4.3	Steady-State Luminescence Spectroscopy.....	126
4.3.1	Spectra.....	126
4.3.2	Luminescence Quantum Yields.....	127
4.4	Time Resolved Emission Spectroscopy (TRES).....	129
4.4.1	Luminescence Lifetime Measurements.....	129
4.4.2	Time Resolved Emission Spectra.....	130
4.5	Low Temperature Measurements.....	131
4.5.1	Sample Preparation.....	131
4.6	Cyclic Voltammetry.....	131

4.7	Spin-coating of Thin Polymer Films.....	132
4.8	References.....	132
Chapter 5	The Photophysical Studies of Cyclometalated Ir(L)₃ and Ir(L)₂acac Complexes	
5.1	Introduction.....	134
5.2	Synthesis.....	135
5.3	Structure.....	136
5.4	Electronic Structure.....	137
5.5	UV-Visible Absorption Spectra.....	138
5.6	Luminescence Properties.....	144
5.6.1	Steady-State Spectra.....	144
5.6.2	Solvatochromatic Emission of 4-(2-pyridyl)benzaldehyde (fppy) containing Complexes.....	147
5.6.3	Luminescence Lifetimes.....	149
5.7	Luminescence Quantum Yields.....	152
5.8	Cyclic Voltammetric Studies of Iridium(III) Complexes.....	154
5.9	Polymer Films containing Iridium(III) Complexes.....	160
5.10	OLEDs containing <i>Fac</i> -Ir(ppy) ₂ fppy.....	162
5.10.1	Thin Film Studies.....	162
5.10.2	OLED Studies.....	163
5.11	Conclusion.....	165
5.12	References.....	166
Chapter 6	The Photophysical Studies of Ir(L)₂X(Y) Complexes	
6.1	Introduction.....	170
6.2	Synthesis.....	171
6.2.1	NMR Spectra.....	172
6.3	Structure.....	173
6.4	UV-Visible Absorption Spectroscopy.....	176
6.5	Luminescence Properties.....	178
6.5.1	Steady-State Spectra.....	178
6.6	Time Resolved Emission Spectroscopy (TRES).....	182

6.6.1	Luminescence Lifetimes.....	182
6.7	Luminescence Quantum Yields.....	186
6.8	The Photodegradation of Ir(ppy) ₂ CN(CO).....	187
6.9	The Interaction of <i>Rac</i> -Ir(ppy) ₂ Cl(TAT) with DNA.....	189
6.10	Conclusion.....	193
6.11	References.....	195
Chapter 7	The Preliminary Catalytic Study of a Pyridyl-bridged Palladium(II) Complex	
7.1	Introduction.....	198
7.2	Isolation of <i>trans</i> -(P,N)-[PdBr(μ-C ₅ H ₄ N-C ² ,N)(PPh ₃)] ₂	198
7.2.1	Crystal Structure Determination of <i>trans</i> -(P,N)-[PdBr(μ-C ₅ H ₄ N-C ² ,N)(PPh ₃)] ₂	199
7.3	Catalysis - Part 1.....	201
7.3.1	Reaction A1.....	201
7.3.2	Reaction B1.....	202
7.3.3	Reaction C1.....	202
7.4	Alternative Preparation of <i>trans</i> -(P,N)-[PdBr(μ-C ₅ H ₄ N-C ² ,N)(PPh ₃)] ₂	204
7.5	Catalysis - Part 2.....	205
7.5.1	Reaction A2.....	205
7.5.2	Reaction B2.....	204
7.6	Conclusion.....	206
7.7	References.....	207
Appendix A	Crystallographic Information	
A1	X-ray crystal structure of 2-phenylpyrimidine.....	A1
A2	X-ray crystal structure of 2-(4-fluoren-9-ylidenemethyl-phenyl)-pyridine.....	A3
A3	X-ray crystal structure of indeno[1,2-b]pyridin-5-one.....	A5
A4	X-ray crystal structure of 4-methyl-2-phenyl-pyridine.....	A7
A5	X-ray crystal structure of	

	tetrakis(4-(2-pyridyl)benzaldehyde- C^2,N')(μ -chloro)diiridium.....	A9
A6	X-ray crystal structure of	
	tetrakis(2-(2,4-difluorophenyl)-pyridine- C^2,N')(μ -chloro)diiridium.....	A11
A7	X-ray crystal structure of	
	tetrakis(2,4-diphenylpyridine- C^2,N')(μ -chloro)diiridium.....	A13
A8	X-ray crystal structure of	
	tris-2-(2,4-difluoro-phenylpyridine- C^2,N')iridium.....	A15
A9	X-ray crystal structure of	
	bis-2-(2,4-difluoro-phenylpyridine- C^2,N')acetylacetonate iridium.....	A17
A10	X-ray crystal structure of	
	tris- <i>fac</i> -(2-Biphenyl-3-yl-4-phenyl-pyridine- C^2,N')iridium.....	A19
A11	X-ray crystal structure of	
	bis-(2-phenylpyridine- C^2,N')carbonyl iridium chloride.....	A21
A12	X-ray crystal structure of	
	bis-(2-phenylpyridine- C^2,N')triphenylphosphine iridium chloride.....	A23
A13	X-ray crystal structure of	
	bis-(2-(2,4-difluoro-phenyl)-pyridine- C^2,N')triphenylphosphine iridium chloride.....	A25
A14	X-ray crystal structure of <i>trans</i> -(P,N)-[PdBr(μ -C ₅ H ₄ N- C^2,N')(PPh ₃)] ₂ ..	A27
A15	X-ray crystal structure of <i>trans</i> -(P,N)-[PdBr(μ -C ₅ H ₄ N- C^2,N')(PPh ₃)] ₂ (Isolated from Suzuki reaction, as detailed in chapter 7).....	A29

Appendix B Courses, Work Experience Completed, Publications, Posters Presented and Conferences and Seminars Attended

B1	Publications.....	B1
B2	Posters Presented.....	B1
B3	Conferences Attended.....	B1
B4	Seminars Attended.....	B2
B5	Courses Completed.....	B4
B6	Work Experience.....	B5

List of Figures

Chapter 1

1.1	Synthetic scheme for <i>Fac</i> -Ir(ppy) ₃ (A) and [Ir(ppy) ₂ Cl] ₂ (B).....	24
1.2	<i>Ortho</i> -metalation in chlorotris(triphenylphosphine)iridium(I).....	25
1.3	(A) 2-phenylpyridine (ppy), (B) benzo[h]-quinone (bzq) and (C) 2-(2-thienylpyridine) (thpy).....	25
1.4	Suzuki Cross-Coupling reaction of a substituted aryl boronic acid and 2-bromopyridine to form a substituted 2-phenylpyridine.....	26
1.5	The outline of a catalytic cycle for a Suzuki cross-coupling reaction.....	27
1.6	A general mechanism for the Kröhnke synthesis of substituted pyridines.....	28
1.7	The diazotisation of aniline.....	29
1.8	The alkylation of pyridine using phenyllithium	29
1.9	A structural illustration of tetrakis(2-phenylpyridine-C ² ,N')(μ -dichloro)diiridium, [Ir(ppy) ₂ Cl] ₂	31
1.10	A structural illustration of <i>fac</i> -tris(2-phenylpyridine-C ² ,N')iridium(III), <i>fac</i> -Ir(ppy) ₃	36
1.11	A schematic of the electronic energy levels in an Ir(III)/Rh(III) complex, where * indicates an excited state, LC = ligand centered state and k _x = rate of process x.....	39
1.12	The normalised absorbance spectrum of <i>fac</i> -Ir(ppy) ₃ in aerated dichloromethane at 298 K.....	40
1.13	Luminescence spectra of <i>fac</i> -Ir(ppy) ₃ in degassed (black line) and aerated (grey line) dichloromethane at 298 K.....	41
1.14	A schematic representation of π -back-bonding in Ir(ppy) ₂ Cl(CO), from the Ir(III) center <i>via</i> d π -orbitals to the π^* orbital of CO, arrows indicate direction of electron donation.....	46
1.15	A structural illustration of the complex Ir(pbt) ₂ Cl(pyr), where pbt = 2-phenylbenzothiazole and pyr = pyridine.....	47

Chapter 2

2.1	A Jabłoński diagram representing the excitation and subsequent emission from a molecular solid, non-radiative processes are depicted by a zig-zag arrow and radiative processes by a straight arrow.....	55
2.2	The ground state, S_0 , and singlet excited state, S_1 , of a closed shell molecule....	56
2.3	Injection and migration of charge in an organic film.....	57
2.4	A schematic diagram showing the cross-section of a double heterostructure OLED	58
2.5	A band structure for a typical double heterostructure device.....	59
2.6	A band structure for a typical single heterostructure device.....	60
2.7	The phenomenon of spontaneous recovery and electric-field induced recovery in a double layer OLED.....	64
2.8	Proposed energy level structure for an electrophosphorescent device containing <i>fac</i> -Ir(ppy) ₃	66
2.9	The external quantum efficiency of OLEDs using Ir(ppy) ₃ :CBP emissive layers.....	67
2.10	1931 CIE Chromaticity Chart.....	74
2.11	Structures of first generation (G1) and second generation (G2) iridium(III) dendrimers.....	75
2.12	Oligofluorene iridium(III) complexes utilised in single layer devices.....	77

Chapter 3

Section 3.2	Structural illustrations of ligands.....	86
Section 3.3	Structural illustrations of bis-cyclometalated iridium(III) and rhodium(III) complexes.....	96
Section 3.4	Structural illustrations of monomeric $M(L)_3$ and $M(L)_2acac$ Complexes of Ir(III) and Rh(III).....	104
Section 3.5	Structural illustrations of $Ir(L)_2X(Y)$ complexes.....	116
Section 3.6	Structural illustration of <i>Trans</i> -(P,N)-[PdBr(μ -C ₅ H ₄ N-C ² ,N)(PPh ₃)] ₂	123

Chapter 4

- 4.1 A schematic of the Jobin Horiba Spex Fluorolog 3 spectrofluorimeter.....127
- 4.2 A typical single exponential fit obtained for a luminescence lifetime.....130

Chapter 5

- 5.1 A structural illustration of *fac*-tris(2-phenylpyridine- C^2,N')iridium(III),
fac-Ir(ppy)₃.....136
- 5.2 X-ray crystal structure of Ir(F₂ppy)₂acac.....137
- 5.3 A schematic of the electronic energy levels in an Ir(III)/Rh(III) complex,
where * indicates an excited state and k_x = rate of process x.....138
- 5.4 Normalised UV-Visible absorption spectra of Ir(F₂ppy)₂acac,
fac-Ir(ppy)₃ and *fac*-Ir(fppy)₃ in aerated dichloromethane at 298 K.....139
- 5.5 A molecular representation of the sodium-2-phenylpyridine
(Na-ppy) moiety used for CAChe energy level calculations.....140
- 5.6 The molecular orbital diagrams of the HOMO and LUMO
for Na-ppy, Na-fppy and Na-F₂ppy, as calculated by CAChe.....141
- 5.7 A schematic showing the relative HOMO-LUMO energy gaps (ΔE)
for Na-F₂ppy, Na-ppy and Na-fppy.....142
- 5.8 The normalised degassed and aerated (offset spectrum) emission spectrum
of *fac*-Ir(Cyclohex)₃ in dichloromethane at 298 K, $\lambda_{ex} = 355$ nm.....145
- 5.9 Normalised PL spectra of the phenyl ring substituted complexes
fac-Ir(ppy)₃, Ir(ppy)₂acac, *fac*-Ir(ppy)₂fppy, *fac*-Ir(fppy)₃,
Ir(F₂ppy)₃ and Ir(F₂ppy)₂acac in aerated toluene at 298 K, $\lambda_{ex} = 355$ nm.....146
- 5.10 Normalised PL spectra of the pyridine ring substituted complexes
fac-Ir(ppy)₃, *fac*-Ir(ppm)₃, *fac*-Ir(4-Meppy)₃, *fac*-Ir(Cyclohex)₃
and *fac*-Ir(dppy)₃ in aerated toluene at 298 K, $\lambda_{ex} = 355$ nm.....146
- 5.11 Normalised PL spectra of *fac*-Ir(ppy)₃ in aerated dichloromethane (1)
and *fac*-Ir(ppy)₂fppy in aerated toluene (2), dichloromethane (3),
acetonitrile (4) and ethanol (5), $\lambda_{ex} = 355$ nm.....147

5.12	The reversible oxidation waves of Ferrocene (FeCp_2) and $\text{Ir}(\text{dppy})_2\text{acac}$ in dichloromethane/0.1 M TBA[BF_4] at 298 K.....	157
5.13	Hammett Parameter (σ -value) versus half-wave oxidation potential for iridium(III) complexes 30-49 in degassed dichloromethane/0.1 M TBA[BF_4] at 298 K.....	159
5.14	The normalised luminescence spectra of iridium(III) complexes doped into PVK films at 5% wt/wt at 298 K, $\lambda_{\text{ex}} = 340 \text{ nm}$	161
5.15	PL spectra of (a) a 5% wt/wt <i>fac</i> - $\text{Ir}(\text{ppy})_2\text{fppy}$ doped PVK film, offset for clarity and (b) an aerated solution of <i>fac</i> - $\text{Ir}(\text{ppy})_2\text{fppy}$ in toluene at 298 K, $\lambda_{\text{ex}} = 350 \text{ nm}$	163
5.16	(a) EL spectra of <i>fac</i> - $\text{Ir}(\text{ppy})_2\text{fppy}$ doped into PVK with 6 wt%, offset for clarity and (b) PL spectra of <i>fac</i> - $\text{Ir}(\text{ppy})_2\text{fppy}$ in aerated toluene at 298 K, $\lambda_{\text{ex}} = 350 \text{ nm}$	164
5.17	Current versus Voltage for ITO/PEDOT/(PVK: <i>fac</i> - $\text{Ir}(\text{ppy})_2\text{fppy}$ 6%wt/wt)/Al. Inset: EL Brightness versus Current.....	164

Chapter 6

6.1	A schematic of the electronic energy levels in $\text{Ir}(\text{L})_2\text{X}(\text{Y})$ complexes, where * indicates an excited state and $k_x = \text{rate of process } x$	170
6.2	The ^1H -NMR (200 MHz) spectrum of $\text{Ir}(\text{F}_2\text{ppy})_2\text{Cl}(\text{CO})$ in CDCl_3 at 298 K.....	173
6.3	X-ray crystal structures of $\text{Ir}(\text{ppy})_2\text{Cl}(\text{CO})$, $\text{Ir}(\text{ppy})_2\text{Cl}(\text{PPh}_3)$, $\text{Ir}(\text{F}_2\text{ppy})_2\text{Cl}(\text{PPh}_3)$ and $[\text{Ir}(\text{F}_2\text{ppy})_2\text{Cl}]_2$	174
6.4	Normalised UV-Visible absorbance spectra of $\text{Ir}(\text{ppy})_2\text{Cl}(\text{CO})$, $\text{Ir}(\text{ppy})_2\text{Cl}(\text{PPh}_3)$, $\text{Ir}(\text{ppy})_2\text{Cl}(\text{Ph}_2\text{PPhCO}_2\text{H})$, $\text{Ir}(\text{ppy})_2\text{Cl}(\text{DMAP})$, $\text{Ir}(\text{F}_2\text{ppy})_2\text{Cl}(\text{CO})$ and $\text{Ir}(\text{F}_2\text{ppy})_2\text{Cl}(\text{PPh}_3)$ in aerated dichloromethane at 298 K.....	176
6.5	Normalised luminescence spectra of $\text{Ir}(\text{ppy})_2\text{Cl}(\text{CO})$, $\text{Ir}(\text{ppy})_2\text{Cl}(\text{PPh}_3)$, $\text{Ir}(\text{ppy})_2\text{Cl}(\text{DMAP})$, $\text{Ir}(\text{F}_2\text{ppy})_2\text{Cl}(\text{CO})$, $\text{Ir}(\text{F}_2\text{ppy})_2\text{Cl}(\text{PPh}_3)$, in aerated dichloromethane at 298 K, $\lambda_{\text{ex}} = 355 \text{ nm}$	179

6.6	Excitation spectra (left), $\lambda_{\text{em}} = 446$ nm and luminescence spectra, $\lambda_{\text{ex}} = 355$ nm, of $\text{Ir}(\text{F}_2\text{ppy})_2\text{Cl}(\text{CO})$ 59 in degassed (black line) and aerated (dashed lines) dichloromethane at 298 K.....	181
6.7	Excitation spectra (left), $\lambda_{\text{em}} = 462$ nm and luminescence spectra, $\lambda_{\text{ex}} = 355$ nm, of $\text{Ir}(\text{F}_2\text{ppy})_2\text{Cl}(\text{PPh}_3)$ 60 in degassed (black line) and aerated (dashed lines) dichloromethane at 298 K.....	181
6.8	Time-resolved low temperature luminescence spectra of $\text{Ir}(\text{ppy})_2\text{Cl}(\text{CO})$ (left) and $\text{Ir}(\text{F}_2\text{ppy})_2\text{Cl}(\text{CO})$ (right) in EPA at 77 K, $\lambda_{\text{ex}} = 355$ nm.....	185
6.9	Time resolved emission spectra of $\text{Ir}(\text{F}_2\text{ppy})_2\text{Cl}(\text{CO})$ in EPA at 77 K, $t = 0\text{-}5$ μs and $t = 40\text{-}80$ μs	185
6.10	Luminescence spectra of $\text{Ir}(\text{ppy})_2\text{CN}(\text{CO})$ in degassed benzene at 298 K, before (black line) and after (dashed line) irradiation at $\lambda_{\text{ex}} = 365$ nm.....	188
6.11	Normalised absorption spectra of $\text{Ir}(\text{ppy})_2\text{CN}(\text{CO})$ in degassed benzene at 298 K, before (black line) and after (dashed line) irradiation at $\lambda_{\text{ex}} = 365$ nm.....	189
6.12	A schematic representation of <i>rac</i> - $[\text{Ir}(\text{ppy})_2(\text{TAT})]\text{Cl}$	191
6.13	UV-Visible absorption spectra of <i>rac</i> - $\text{Ir}(\text{ppy})_2\text{Cl}(\text{TAT})$ in aerated 0.1 mmol HEPES/0.1 mmol NaCl buffer, pH = 7.4, in the absence (black line) and presence (dashed line) of calf thymus DNA at 298 K.....	192
6.14	Emission spectra of <i>rac</i> - $\text{Ir}(\text{ppy})_2\text{Cl}(\text{TAT})$ in aerated 0.1 mmol HEPES/0.1 mmol NaCl buffer, pH = 7.4, in the absence (dashed line) and presence (black line) of calf thymus DNA at 298 K, $\lambda_{\text{ex}} = 355$ nm.....	193

Chapter 7

7.1	Crystal structure of the palladium dimer with thermal ellipsoids at 50%.....	200
7.2	Suggested catalytic cycle of the dimeric Pd(II) complex.....	204

Appendix A

A1	X-ray crystal structure of 2-phenylpyrimidine.....	A2
A2	X-ray crystal structure of 2-(4-fluoren-9-ylidenemethyl-phenyl)-pyridine.....	A4
A3	X-ray crystal structure of indeno[1,2-b]pyridin-5-one.....	A6
A4	X-ray crystal structure of 4-Methyl-2-phenyl-pyridine.....	A8
A5	X-ray crystal structure of tetrakis(4-(2-pyridyl)benzaldehyde-C ² ,N')(μ-chloro)diiridium.....	A10
A6	X-ray crystal structure of tetrakis(2-(2,4-difluorophenyl)-pyridine-C ² ,N')(μ-chloro)diiridium.....	A12
A7	X-ray crystal structure of tetrakis(2,4-diphenylpyridine-C ² ,N')(μ-chloro)diiridium.....	A14
A8	X-ray crystal structure of tris-2-(2,4-difluoro-phenylpyridine-C ² ,N')iridium...	A16
A9	X-ray crystal structure of bis-2-(2,4-difluoro-phenylpyridine-C ² ,N')acetylacetonate iridium.....	A18
A10	X-ray crystal structure of tris- <i>fac</i> -(2-Biphenyl-3-yl-4-phenyl-pyridine-C ² ,N')iridium.....	A20
A11	X-ray crystal structure of bis-(2-phenylpyridine-C ² ,N')carbonyl iridium chloride.....	A22
A12	X-ray crystal structure of bis-(2-phenylpyridine-C ² ,N')triphenylphosphine iridium chloride.....	A24
A13	X-ray crystal structure of bis-(2-(2,4-difluoro-phenyl)-pyridine-C ² ,N')triphenylphosphine iridium chloride.....	A26
A14	X-ray crystal structure of <i>trans</i> -(P,N)-[PdBr(μ-C ₅ H ₄ N-C ² ,N)(PPh ₃)] ₂	A28
A15	X-ray crystal structure of <i>trans</i> -(P,N)-[PdBr(μ-C ₅ H ₄ N-C ² ,N)(PPh ₃)] ₂ (Isolated from Suzuki reaction, as detailed in chapter 7).....	A30

List of Tables

Chapter 1

1.1	Absorption Data for Ir(III) and Rh(III) Dichloro-Bridged Species of ppy and bzq in dichloromethane and chloroform at 298 K.....	32
1.2	Luminescence lifetimes of the $[M(L)_2Cl]_2$ species, where M = Rh, Ir and L = ppy, bzq.....	34
1.3	Emission and Cyclic Voltammetric Data for <i>fac</i> -tris- <i>ortho</i> -metalated Ir(III) Complexes.....	43
1.4	Luminescence and lifetime data for some tris- <i>ortho</i> -metalated Ir(III) complexes at 298 K.....	44
1.5	Quantum Yields for Singlet Oxygen generation (Φ_Δ), rate constants for the oxygen quenching of phosphorescence, $k_q(sv)$ and rate constants for singlet oxygen quenching by the iridium complex sensitiser, $k_q(^1O_2)$, $\lambda_{ex} = 355\text{ nm}$	45
1.6	Photophysical characteristics of bis- <i>ortho</i> -metalated Ir(III) complexes.....	45

Chapter 2

2.1	Performance characteristics of Ir(ppy) ₂ acac, Ir(bt) ₂ acac and Ir(btp) ₂ acac based OLEDs.....	73
2.2	Luminescence properties of oligofluorene iridium(III) complexes.....	78

Chapter 3

3.1	Compounds used for synthetic and photophysical studies.....	84
-----	---	----

Chapter 4

No tables are presented in this chapter

Chapter 5

5.1	Summary of synthetic data for complexes 30-49	135
5.2	HOMO and LUMO energies (eV) calculated by CAChe for Na-ppy, Na-fppy and Na-F ₂ ppy moieties	142
5.3	Absorption spectra features and extinction coefficients (ϵ) of selected iridium(III) complexes in aerated dichloromethane at 298 K	143
5.4	Maximum emission wavelengths (λ_{max}) for iridium(III) complexes 30-49 in aerated dichloromethane and toluene at 298 K, $\lambda_{\text{ex}} = 355 \text{ nm}$	144
5.5	Maximum emission wavelength (λ_{max}) of <i>fac</i> -Ir(ppy) ₃ , <i>fac</i> -Ir(ppy) ₂ fppy and <i>fac</i> -Ir(fppy) ₃ in aerated solvents at 298 K, $\lambda_{\text{ex}} = 355 \text{ nm}$	148
5.6	Luminescence lifetimes of iridium(III) complexes in both aerated and degassed dichloromethane (CH ₂ Cl ₂) and toluene (C ₆ H ₅ CH ₃) at 298 K, $\lambda_{\text{ex}} = 355 \text{ nm}$, emission wavelength (nm) in brackets	151
5.7	Luminescence quantum yields, Φ , and rate coefficients of oxygen quenching, k_q , of iridium(III) complexes in dichloromethane at 298 K, $\lambda_{\text{ex}} = 450 \text{ nm}$ (a) and 355 nm (b)	153
5.8	The half-wave potentials ($E_{1/2}$) for iridium(III) complexes in acetonitrile/0.1 M TBA[BF ₄] at 298 K	155
5.9	The half-wave oxidation potentials ($E_{1/2}$) for iridium(III) complexes 30-49 in dichloromethane/0.1 M TBA[BF ₄] at 298 K	156
5.10	The half-wave oxidation potentials ($E_{1/2}$) and Hammett Parameters (σ -value) for iridium(III) complexes in dichloromethane/0.1 M TBA[BF ₄] at 298 K	158
5.11	Chromaticity (CIE) co-ordinates for PVK films doped with iridium(III) complexes	162

Chapter 6

6.1	Summary of synthetic data for $\text{Ir}(\text{L})_2\text{X}(\text{Y})$ complexes 50-60.....	172
6.2	Comparison of selected bond distances (\AA) for $[\text{Ir}(\text{F}_2\text{ppy})_2\text{Cl}]_2$ and $\text{Ir}(\text{F}_2\text{ppy})_2\text{Cl}(\text{PPh}_3)$	175
6.3	Carbonyl and cyano infrared absorption bands of complexes 50, 51, 53 and 59 in nujol mulls on KBr discs.....	175
6.4	Absorption spectra features and extinction coefficients (ϵ) of $\text{Ir}(\text{L})_2\text{Cl}(\text{Y})$ complexes in aerated dichloromethane at 298 K.....	177
6.5	Emission maxima, λ_{max} , of some $\text{Ir}(\text{L})_2\text{X}(\text{Y})$ complexes in aerated dichloromethane at 298 K, $\lambda_{\text{ex}} = 355 \text{ nm}$	180
6.6	Luminescence lifetimes (τ) of $\text{Ir}(\text{L})_2\text{X}(\text{Y})$ complexes in degassed and aerated dichloromethane at 298 K, $\lambda_{\text{ex}} = 355 \text{ nm}$ (aerated lifetimes in brackets).....	183
6.7	Luminescence lifetimes (τ) of $\text{Ir}(\text{L})_2\text{X}(\text{Y})$ complexes in aerated EPA at 77 K, $\lambda_{\text{ex}} = 355 \text{ nm}$, λ_{max} (nm) in brackets.....	184
6.8	Luminescence quantum yields, Φ , and rate coefficients of oxygen quenching, k_q , of $\text{Ir}(\text{L})_2\text{X}(\text{Y})$ complexes in dichloromethane at 298 K, $\lambda_{\text{ex}} = 355 \text{ nm}$	186

Chapter 7

7.1	Crystallographic data for <i>trans</i> -(P,N)- $[\text{PdBr}(\mu\text{-C}_5\text{H}_4\text{N-C}^2\text{,N})(\text{PPh}_3)]_2$	199
-----	---	-----

Abbreviations

A

A = acceptor

acac/acacH = 2, 4-pentanedione/acetyl acetate

Alq₃ = tris-(8-hydroxyquinoline) aluminium

Ar-X = aryl halide

Å = angstrom (10^{-10} m)

B

BCP = 2,9-dimethyl-4,7-diphenyl-1,10-phenanthroline/bathocuproine

btp = 2-benzo[b]thiophen-2-yl-pyridine

bzq = benzo[h]-quinoline

bipy/bpy = 2,2'-bipyridine

C

CBP = 4,4'-N,N'-dicarbazole-biphenyl host

CCD = charge coupled device

CF = crystal field

CFSE = crystal field stabilisation energy

CH₂Cl₂ = dichloromethane

C₆H₅CH₃ = toluene

CIE = Commission Internationale de L'Eclairage co-ordinates

CNPPP = poly(2-(6-cyano-6-methyl)-heptyloxy-1,4-phenylene)

CO = carbon monoxide

D

D = donor

Decppy = 2-(4'-decylphenyl)pyridine

DecOppy = 2-(4'-(3'',7''-dimethyloctyloxy)phenyl)pyridine

DFT = density functional theory

DMAP = dimethylaminopyridine

DMF = dimethylformamide

DMSO = dimethylsulphoxide

DNA = deoxyribonucleic acid

dppz = dipyrido[3,2-a:2',3'-c]phenazine

dpq = dipyrido[3,2-a:2'3'-c]-quinoxaline

E

ΔE = energy gap

EL = electroluminescence

EM = emissive material (layer)

ET/ETL = electron transport (layer)

$E_{1/2}$ = half-wave potential

ϵ = extinction coefficient ($\text{dm}^3 \text{mol}^{-1} \text{cm}^{-1}$)

F

fac = facial

FeCp_2 = ferrocene

FeCp_2^* = *bis*(pentamethylcyclopentadienyl)iron(II)/iron(III)

FPD = flat panel display

fppy = 4-(2'-pyridyl)benzaldehyde

G

G1 = first generation dendrimer

G2 = second generation dendrimer

H

h = Planck's Constant ($6.626 \times 10^{-34} \text{ Js}$)

HOMO = highest occupied molecular orbital

HT/HTL = hole transport (layer)

I

IC = internal conversion

I_p = peak current (μA)

$\text{Ir}(\text{L})_3$ = triply *ortho*-metalated iridium(III) species

$\text{Ir(L)}_2\text{acac}$ = bis *ortho*-metalated iridium(III) acetyl acetonate species

$[\text{Ir(L)}_2\text{Cl}]_2$ = μ -dicloro-bridged iridium(III) species

$\text{Ir(L)}_2\text{X(Y)}$ = bis *ortho*-metalated iridium(III) species

ISC = inter-system crossing

IR = Infrared

ITO = indium tin oxide (anode)

J

J = spectral overlap integral between the absorption spectrum of the donor and the emission spectrum of the acceptor ($\text{cm}^6 \text{mol}^{-1}$)

K

k = rate constant

k_q = bimolecular quenching constant ($\text{dm}^3 \text{mol}^{-1} \text{s}^{-1}$)

L

L = cyclometalating ligand

LC = ligand centered state

LCD = liquid crystal display

LED = light emitting device

LUMO = lowest unoccupied molecular orbital

λ = emission wavelength

M

mer = meridonal

MLCT = metal to ligand charge transfer state

mppy = 3-methyl-2-phenylpyridine

MS = mass spectrometry

N

NBu_4BF_4 = tertiary butyl ammonium tetrafluoroborate

α -NPD = 4,4'-bis[N-(1-naphthyl)-N-phenylamino] biphenyl

nb = 2-naphthalen-1-yl-benzothiazole

NMR = nuclear magnetic resonance

NR = non-radiative

η_e = fraction of emitted photons that are coupled out of the device

η_r = fraction of injected charge carriers that form excitons on the donor

O

OLED = organic light emitting diode

$^1\text{O}_2$ = singlet oxygen

OXD-7 = 1,3-bis[4-tert-butylphenyl]-1,3,4-oxadiazolyl]phenylene

P

pbt = 2-phenylbenzothiazole

PBu₃ = tributylphosphine

Pd(dppb)₂Cl₂ = 1,4-bis(diphenylphosphino)butanepalladium(II) dichloride

Pd(OAc)₂ = palladium(II) acetate

Pd(PPh₃)₄ = tetrakis(triphenylphosphine)palladium(0)

PEDOT = polyethylenedioxythiophene-polystyrenesulfonic acid

phen = 1,10-phenanthroline

PL = photoluminescence

PLQY = photoluminescence quantum yield

PMMA = poly(methylmethacrylate)

PPh₃ = triphenylphosphine

ppy = 2-phenylpyridine

pq = 2-phenylquinoline

PtOEP = 2,3,7,8,12,13,17,18-octaethyl-21H,23H-porphine platinum(II)

ptpy = 2-(p-tolyl)pyridine

pyr = pyridine

PVK = poly(N-vinylcarbazole)

Q

Φ = quantum yield

R

R = radiative

r = the distance between the donor and acceptor (cm)

r_0 = critical quenching radius (cm)

rac = racemate/racemic mixture

S

S = solvent/ligating solvent

S_0 = singlet ground state

S_1 = singlet excited state

σ -value = Hammett Parameter

T

t = time

T_1 = triplet excited state

TAT = 1,4,8,9-tetraaza-triphenylene

TBA = tetrabutyl ammonium

THF = tetrahydrofuran

thpy = 2-(2-thienyl)pyridine

TRES = times resolved emission spectroscopy

τ = lifetime

U

UV = ultra-violet

V

ν = scan rate (Vs^{-1})

W

wt/wt = weight/weight

X

X = ancillary ligand

χ_s = fraction of singlet excitons

χ_t = the fraction of triplet excitons

Y

Y = ancillary ligand

Z

Chapter 1

The Synthesis and Photochemistry of Cyclometalated Iridium(III) Complexes

1.1 Introduction

This chapter describes a review of the synthetic methods used to synthesise cyclometalating ligands and the subsequent synthesis, characterisation and photophysical properties of cyclometalated iridium(III) complexes, in particular those containing substituted 2-phenylpyridine ligands. In places, analogous work on rhodium(III) complexes will be discussed for completeness.

The following chapter discusses organic light emitting devices (OLEDs), their components and properties as well as the application of cyclometalated iridium(III) complexes within these optical devices as electrophosphorescent dopants. Organic light emitting devices (OLEDs) are based on thin amorphous organic films that can be deposited on a variety of substrates, such as rigid glass or flexible polymer supports. There are various methods of depositing the doped polymer layer onto the OLED substrate; among others these include masked dye diffusion, microcontact printing, and hybrid inkjet printing. The wider viewing angles and increased brightness at low voltages of OLEDs compared to that of liquid crystal displays (LCDs) means that OLEDs may in fact one day replace LCDs in many display applications. In the case of OLEDs it is the use of the unique flexible polymer support that makes them an attractive option for applications such as portable/roll-up flat panel displays (FPDs) or as backlights.

Electrophosphorescent complexes that are capable of generating pure red, green and blue light are in high demand for their use as dopants in full colour organic light emitting displays. Iridium(III) complexes containing cyclometalating ligands, such as 2-phenylpyridine, have already been utilised in these kinds of devices with a great deal of success. Given the interest in the use of such compounds, it has been the aim of this thesis to produce new cyclometalated iridium(III) complexes and study their photophysical properties with the proposal that they may one day be used as phosphorescent dopants in OLEDs.

1.2 Iridium and Rhodium

Iridium and rhodium are exceedingly rare metals. They comprise only 0.001 ppm and 0.0001 ppm of the Earth's crust respectively. Iridium is usually obtained from its ores; osmiridium (Ir ~ 50 %) and iridosmium (Ir ~ 70 %), which are found mainly in Alaska and South Africa. Iridium has two stable isotopes: ^{191}Ir 37.3 % and ^{193}Ir 62.7 %. Rhodium has one isotope, ^{103}Rh , and is normally sourced from nickel-copper-sulfide ores in South Africa and Canada which contain ~ 0.1 % rhodium.

The electronic configurations of iridium and rhodium are $[\text{Xe}] 4f^{14} 5d^7 6s^2$ and $[\text{Kr}] 4d^8 5s^1$ respectively and the range of oxidation states that they may possess is small compared to elements in the preceding groups of the periodic table. This is due to the increasing stability of the (n-1)d electrons, where n = number of electrons in the highest energy d orbital, whose attraction to the large atomic nuclei of these elements is sufficient to prevent the highest oxidation states from being attained. Hence no oxidation states above +6 are found for iridium and rhodium, indeed examples of +5 and +6 oxidation states of iridium and rhodium are rare.

The effect of the crystal field stabilisation energy (CFSE)¹ for heavy elements such as these is more marked as their crystal field (CF)¹ splittings are much greater. A result of this is that the +3 state is the most important oxidation state for both iridium and rhodium, where $[\text{M}(\text{H}_2\text{O})_6]^{3+}$ and M = Ir(III)/Rh(III), is the only simple aquo complex formed by either element. However with π -acceptor ligands the +1 oxidation state is well known for both elements, examples of which are $[\text{Ir}(\text{CO})\text{Cl}(\text{PPh}_3)_2]$ and $[\text{Rh}(\text{PPh}_3)_3]^+$.¹

The most stable of the halide complexes of these two elements are the trihalides. The water-soluble hydrates of the tri-chloride, tri-bromide and tri-iodide are formed by dissolving hydrous Ir_2O_3 in the appropriate acid and, like its rhodium analogue, $\text{IrCl}_3 \cdot 3\text{H}_2\text{O}$ is an extremely useful starting material for a wide range of iridium chemistry.

1.3 Cyclometalated Organometallic Complexes of Iridium(III) and Rhodium(III)

The *ortho*-metalating reactions of iridium and rhodium chlorides, e.g. IrCl_3 , with ligands such as 2-phenylpyridine (ppy) form cyclometalated organometallic complexes such as *fac*- $\text{Ir}(\text{ppy})_3$ ² (A) and $[\text{Ir}(\text{ppy})_2\text{Cl}]_2$ ³ (B), figure 1.1.

In general, *fac*- $\text{Ir}(\text{ppy})_3$ and its related complexes are brightly coloured solids that are highly phosphorescent. These species have generated a great deal of interest over the past 30 years due to their varying photophysical properties. More recently, these phosphorescent organometallic moieties have been utilised as optical oxygen sensors^{4,5,6} and more widely as emissive dopants in solid^{7,8} and solution-state⁹ electroluminescent devices more commonly known as organic light emitting devices (OLEDs).

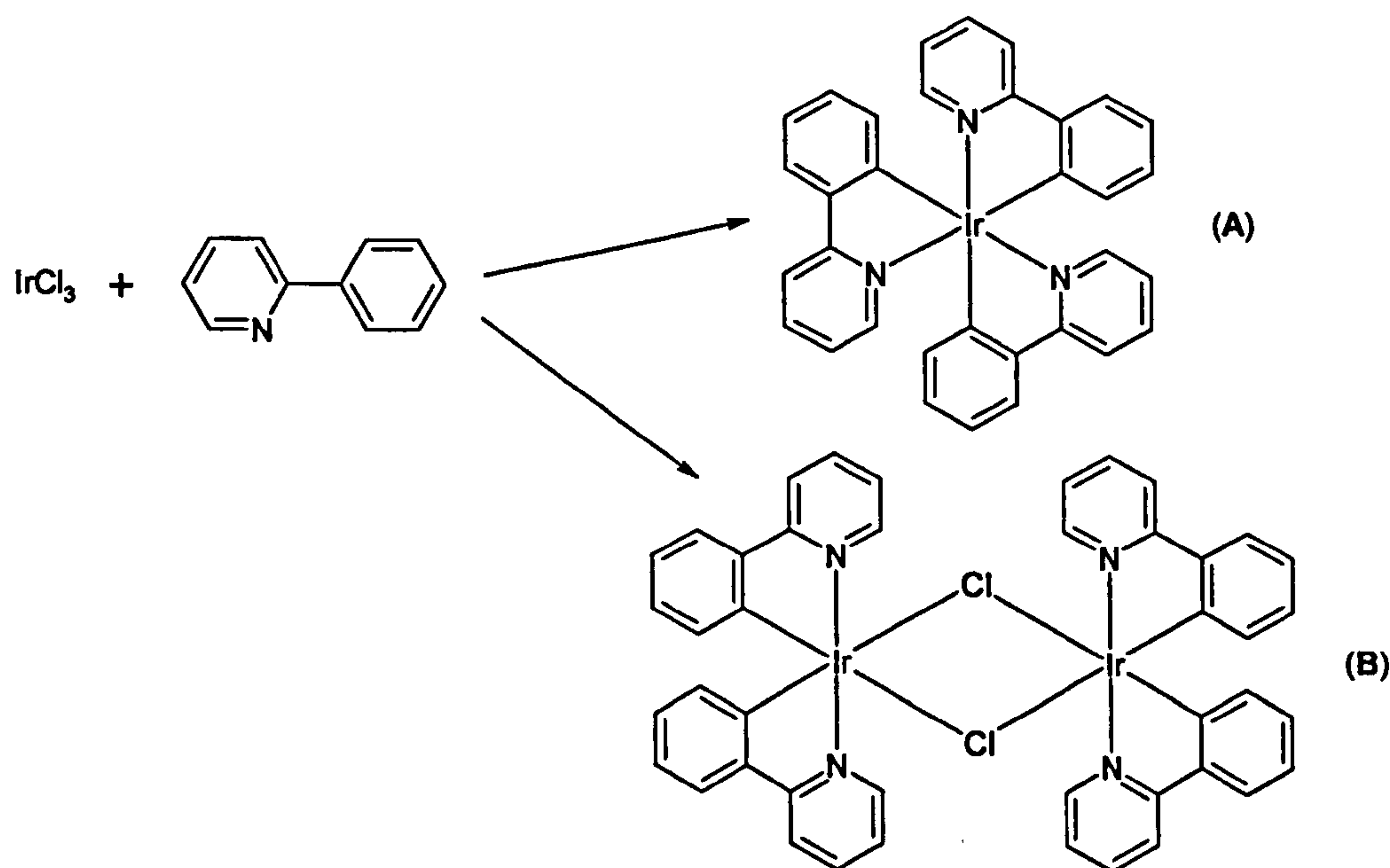


Figure 1.1 Synthetic scheme for *Fac*- $\text{Ir}(\text{ppy})_3$ (A) and $[\text{Ir}(\text{ppy})_2\text{Cl}]_2$ (B).

1.4 Ortho-metalation

Ortho-metalation reactions involve the cleavage of *ortho*-C-H bonds of aryl groups by a metal. This results in the formation of metal-carbon (M-C) bonds. The reaction is

frequently encountered with aryl groups bound to co-ordinated donor atoms such as nitrogen or phosphorus and with electron-rich metals in low oxidation states, which are able to undergo oxidative additions. An example of this is illustrated, figure 1.2, by the iridium phosphine complex, chlorotris(triphenylphosphine)iridium(I) as reported by Bennett *et al.*¹⁰ in 1967.

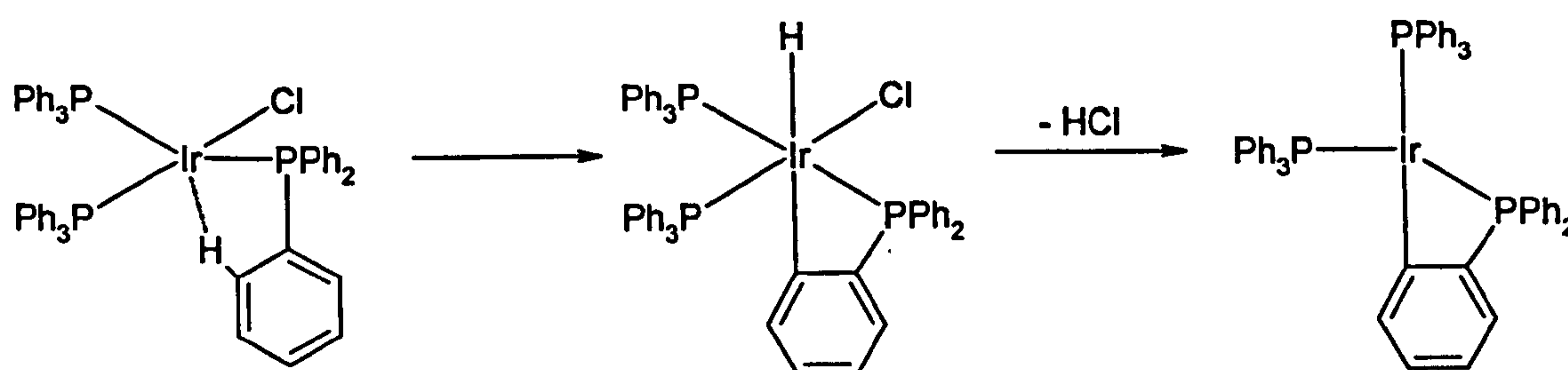


Figure 1.2 *Ortho*-metalation in chlorotris(triphenylphosphine)iridium(I).

Examples of *ortho*-metalating ligands include; 2-phenylpyridine (ppy), benzo[h]-quinoline (bzq) and 2-(2-thienyl)pyridine (thpy), as shown below in figure 1.3.

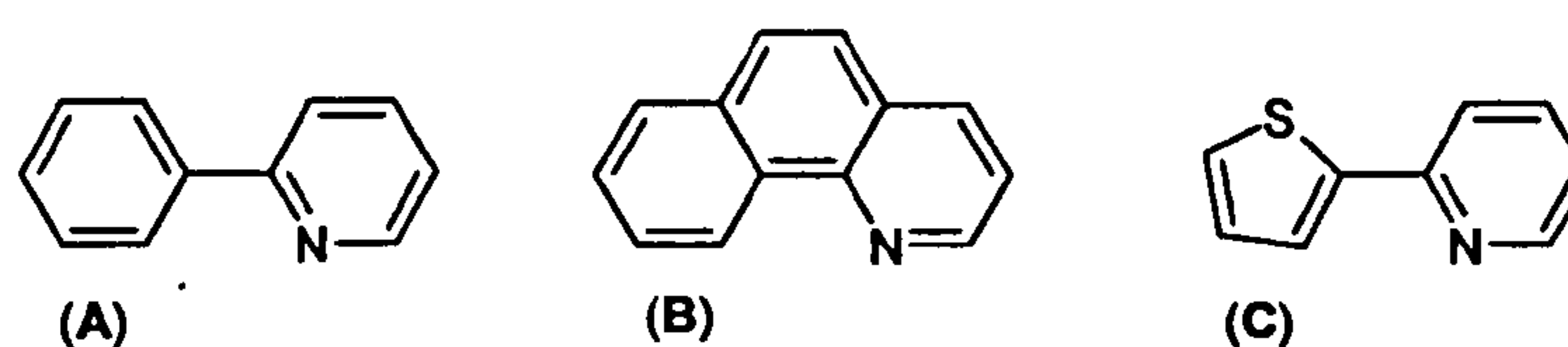


Figure 1.3 (A) 2-phenylpyridine (ppy), (B) benzo[h]-quinone (bzq) and (C) 2-(2-thienylpyridine) (thpy).

The work presented in this report will be focusing mainly on one particular class of cyclometalating ligand, 2-phenylpyridine and its substituted counterparts as well as other closely related ligands. 2-Phenylpyridines can be produced by a number of well-established synthetic pathways, these will be described in the following sections.

1.5 Syntheses of 2-Phenylpyridines

1.5.1 Suzuki Cross-Coupling Reactions

One of the most versatile methods of producing biaryl systems is the palladium catalysed Suzuki cross-coupling reaction.¹¹ In this reaction, an arylboronic acid, e.g. benzenboronic acid, may be coupled to an aryl halide, e.g. 2-bromopyridine, *via* the use of a palladium(0) catalyst under mild conditions, where R and R' can be a variety of different substituents, figure 1.4.

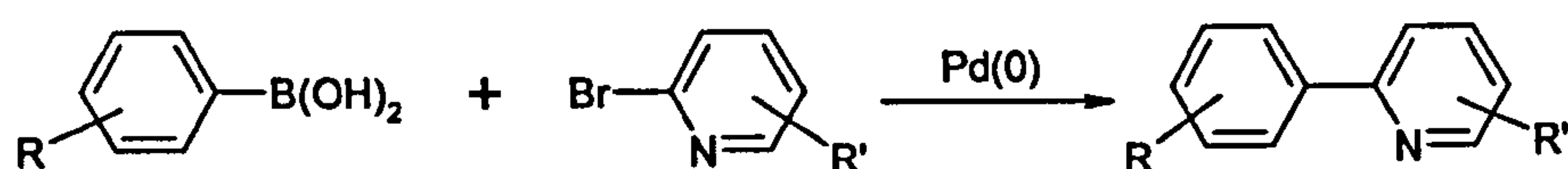


Figure 1.4 Suzuki cross-coupling reaction of a substituted aryl boronic acid and 2-bromopyridine to form a substituted 2-phenylpyridine.

In general the catalyst is either a palladium(0) or palladium(II) species containing phosphine ligands. Examples of these types of catalyst/catalyst precursors are, 1,4-bis(diphenylphosphino)butanepalladium(II) dichloride¹² ($\text{Pd(dppb)}_2\text{Cl}_2$) and tetrakis(triphenylphosphine)palladium(0)¹³ ($\text{Pd(PPh}_3)_4$) which are normally added to the reaction mixture in 1-5 mole % quantities under an inert atmosphere.

Some catalysts may also be generated *in situ*, by the addition of a precursor, such as palladium(II)acetate and the corresponding phosphine ligand, e.g. triphenylphosphine (PPh_3). It must also be noted that the percentage yields of these reactions vary greatly with the substituent groups, aryl halide, solvent, base and catalyst. Typical solvents used for this type of reaction include dimethylformamide (DMF) and toluene/water mixtures.

The outline of the catalytic cycle for a Suzuki reaction is shown in figure 1.5. The first step of this cycle is an oxidative addition reaction involving the palladium(0) species $\text{L}_n\text{Pd(0)}$ and the aryl halide Ar-X forming an intermediate palladium(II) species, $\text{L}_n\text{PdAr(X)}$. The subsequent transmetalation reaction involving the aryl boronic acid

$\text{Ar}'\text{-B(OH)}_2$ generates the bis-aryl species $\text{L}_n\text{PdAr(Ar')}$ which can then undergo reductive elimination to form the coupled product $\text{Ar-Ar}'$ and the palladium(0) species, $\text{L}_n\text{Pd(0)}$.

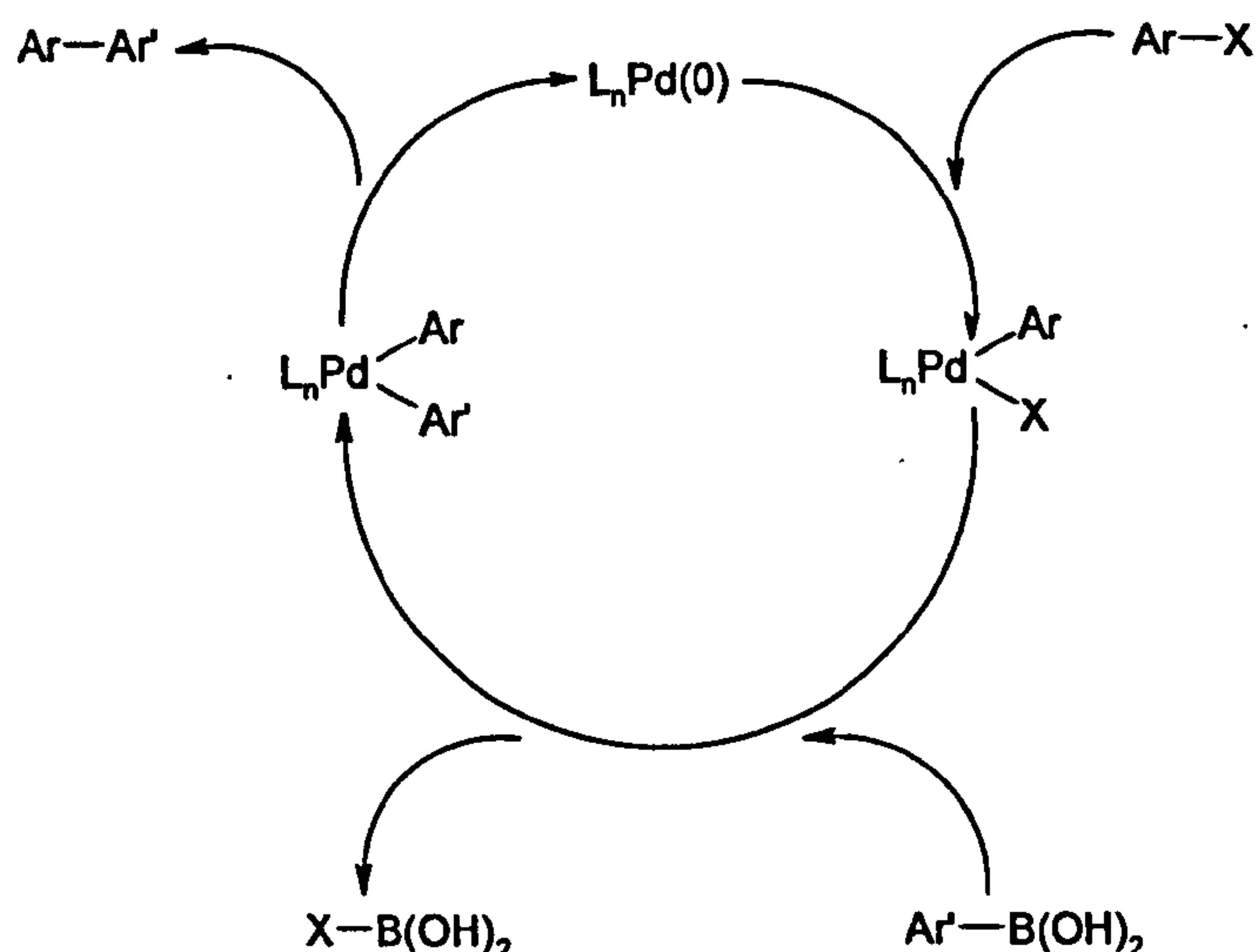


Figure 1.5 The outline of a catalytic cycle for a Suzuki cross-coupling reaction.

Palladium catalysts containing two or more phosphine ligands have been widely used for Suzuki cross-coupling reactions, as discussed by Miyaura¹⁴ in 1998. Work by Littke *et al.*¹⁵ suggests that palladium species containing a single phosphine ligand can act as effective catalysts for Suzuki coupling reactions. Examples of monophosphine adducts as catalysts are discussed in more depth in chapter 7.

Work by Reetz *et al.*¹⁶ regarding Suzuki cross-coupling reactions utilising phosphine free palladium catalysts has reported the presence of palladium nanoparticles in such solutions. Their study of a palladium(II)acetate catalysed reaction involving phenylboronic acid and *p*-bromoacetophenone in dimethylformamide (DMF) at 130 °C revealed the presence of colloidal Pd-species of 1.3 nm in diameter. These species were detected *in situ* by transmission electron microscopy (TEM) after product formation had been observed. They proposed that Pd(OAc)_2 had undergone thermolytic decomposition at 130 °C to yield a Pd(0) species in the form of a colloid. Their observations of the thermolysis of Pd(OAc)_2 at 100 °C (3h) in the likewise polar solvent propylene carbonate (PC), which quantitatively yielded PC-stabilised Pd colloidal particles, supported this assumption. Although the appearance of these Pd-colloids occurred simultaneously with the initiation of the reaction it cannot be viewed as proof

that the Pd-particles actually take part in the catalytic cycle, although earlier work has shown that preformed Pd colloids can catalyse Suzuki reactions.¹⁷

1.5.2 Kröhnke Syntheses

In 1976 Fritz Kröhnke reviewed the specific synthesis of substituted pyridines and polypyridines from methyl ketones *via* the following series of steps, as illustrated in figure 1.6.¹⁸ The methyl ketone (A) may be halogenated with either bromine or iodine to give the halomethyl ketone (B), which can then be reacted with pyridine to yield an acylpyridinium salt (C). These salts are produced in high yield and are stable enough to be stored under ambient conditions for later use. The salt is subsequently deprotonated and the zwitterion is treated with a 2,3-unsaturated aldehyde/ketone (D) to form a 1,5-diketone (E) intermediate *via* a Michael addition¹⁹ at 20-120 °C. This diketone (E) is rarely isolated and undergoes ring closure on treatment with ammonium acetate in acetic acid to give the substituted pyridine (F) by the loss of two equivalents of water.

Using this method the synthesis of bis-, ter- and up to septipyridines can be achieved, although the product yield varies with starting materials and solvent.

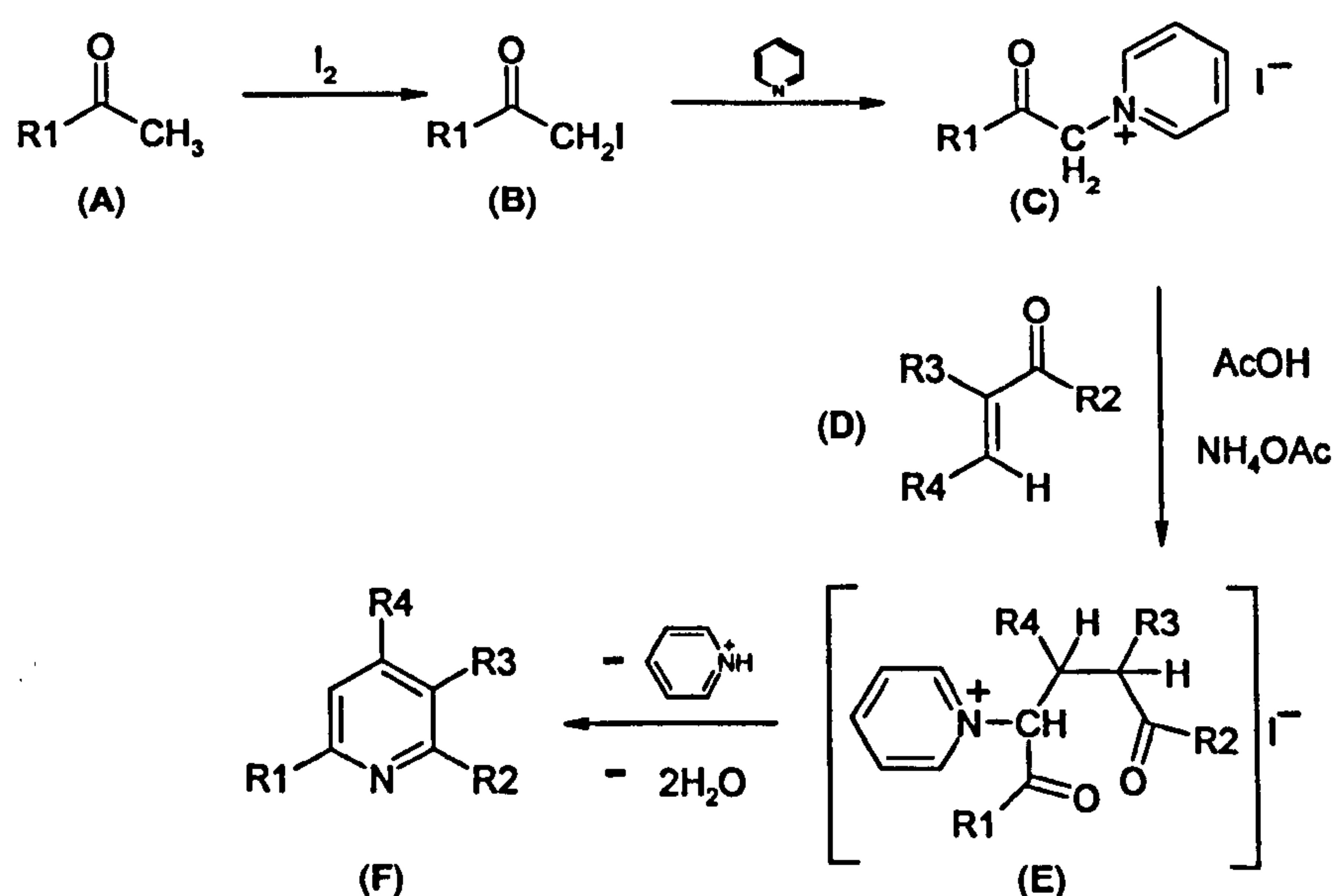


Figure 1.6 A general mechanism for the Kröhnke synthesis of substituted pyridines.

1.5.3 The Arylation of Pyridine *via* the Gomberg Reaction

Primary benzenamines (anilines) are attacked by cold nitrous acid in a reaction called diazotisation to yield relatively stable arenediazonium salts,²⁰ figure 1.7.

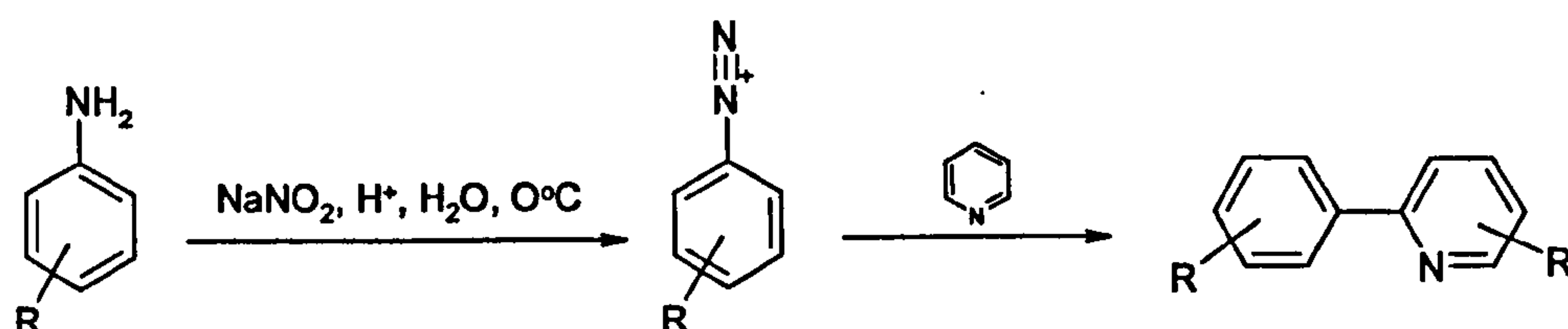


Figure 1.7 The diazotisation of aniline.

The acidic solution of the diazonium salt is subsequently made alkaline allowing the formation of a covalent compound which can then cleave to form free radicals which can then go on to react with another aryl group, i.e. pyridine, to form 2-phenylpyridine. This is known as the Gomberg reaction.²¹ The yields for these reactions are seldom high due to the lack of regioselectivity of the reaction and the many side-reactions undergone by diazonium salts. The 2-, 3- and 4- substituted isomers can be separated *via* distillation or column chromatography.

1.5.4 The use of Lithium Reagents to Afford 2-Phenylpyridines

Alkyl and aryl lithium add to the 2-position of pyridine to form a 2-alkyl(aryl)-1,2-dihydropyridine which upon work-up in oxidative conditions generates the 2-alkyl(aryl)pyridine. This treatment of pyridine with phenyllithium may be used to produce 2-phenylpyridines,²² as depicted in figure 1.8.

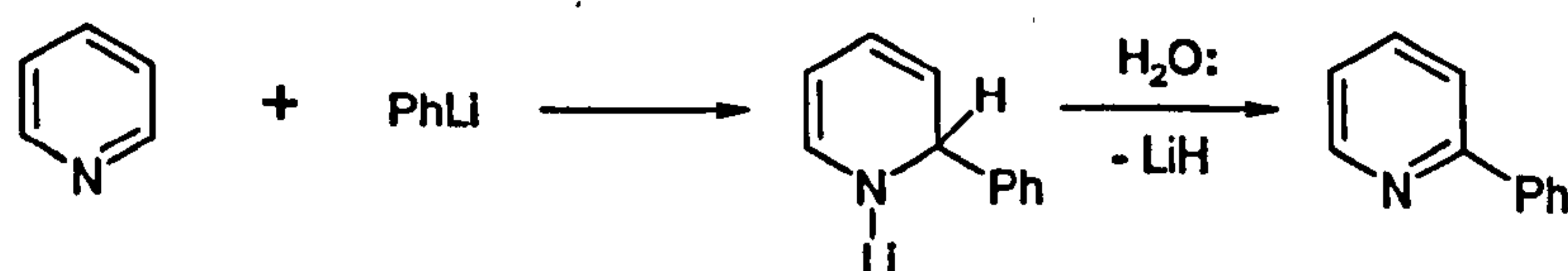


Figure 1.8 The alkylation of pyridine using phenyllithium.

The alkylation of 4-methylpyridine (4-picoline) using phenyllithium was reported by Osuch *et al.*²³ in 1956. The acidity of the methyl protons in 4-picoline allows the formation of 4-picolylithium which can subsequently react with benzene to form 2-phenyl-4-methylpyridine in 39 % yield. The drawback to these reactions is that multiple alkylations can occur, however with phenylpyridines the isomers can be separated relatively easily *via* column chromatography or fractional distillation.

1.6 Dichloro-bridged *Ortho*-metalated Complexes, $[M(L)_2Cl]_2$

1.6.1 Synthesis and Structure

Dichloro-bridged iridium and rhodium complexes of the type $[M(L)_2Cl]_2$, where $M = Ir(III)/Rh(III)$ and $L =$ a cyclometalating ligand, figure 1.1, can be readily synthesised in high yield. The corresponding metal salt, e.g. $IrCl_3 \cdot nH_2O$, is refluxed with an excess of the ligand, e.g. 2-phenylpyridine, in the presence of water in a high boiling point solvent, such as 2-ethoxyethanol. Refluxing of this solution for just an hour begins to yield the complex, tetrakis(2-phenylpyridine- C^2, N')(μ -dichloro)diiridium ($[Ir(ppy)_2Cl]_2$), as a yellow coloured precipitate, which is easily removed *via* filtration after the full reaction time has elapsed.

In 1984, Sprouse *et al.*³ described the synthesis, characterisation and photophysical properties of the first of these iridium and rhodium complexes containing 2-phenylpyridine (ppy) and benzo[h]-quinoline (bzq) ligands. Their 1H and ^{13}C NMR results confirmed the previous formulations²⁴ of the complexes as dichloro-bridged *ortho*-metalated species. Each iridium center has an octahedral environment with mutually *trans* Ir-N bonds and mutually *cis* Ir-C bonds, which are also *cis* to the bridging chlorines, figure 1.9.

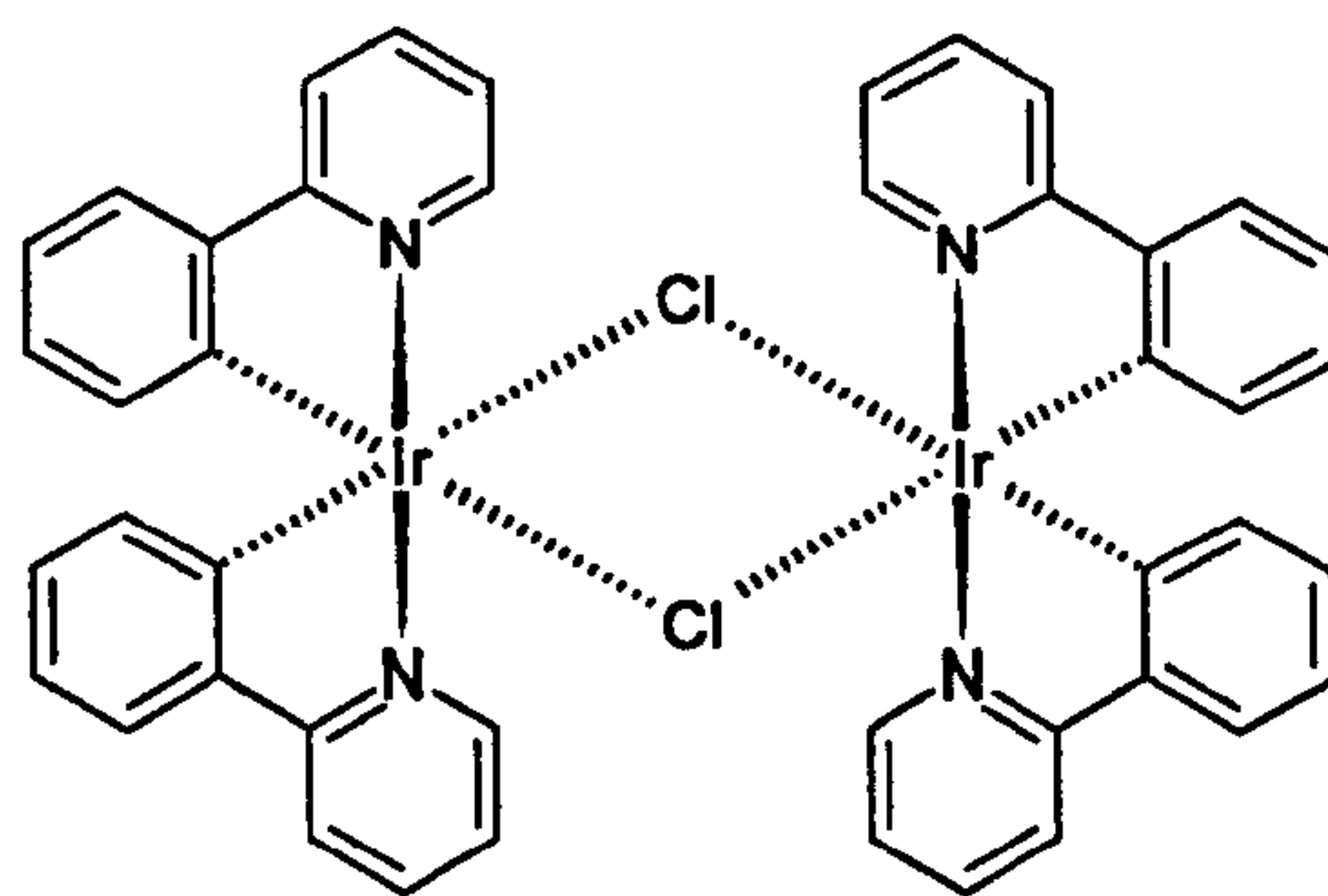


Figure 1.9 A structural illustration of tetrakis(2-phenylpyridine- C^2,N')(μ -dichloro)diiridium, $[Ir(ppy)_2Cl]_2$.

These cyclometalating reactions were carried out under relatively mild conditions in contrast to those for similar complexes containing 2,2'-bipyridine (bpy) ligands, which required more forcing conditions such as refluxing in glycerol. Sprouse *et al.*³ suggested that the phenyl ring in ppy is more readily metalated than a pyridine ring in bpy under the same conditions. If metalation were considered to occur *via* electrophilic attack²⁵ of the metal on the aromatic phenyl ring, then the relative deactivation of bpy would occur due to the presence of the electron-withdrawing nitrogen atom in each of the pyridine rings.

The tendency of ppy and bzq to form bridged species, in relation to the monomeric species favoured by bpy and 1,10-phenanthroline (phen) was viewed as a result of the enhanced electron density at the metal center, imposed by a larger σ -donation through the M-C bonds in the ppy and bzq complexes than that obtained *via* M-N bonds in complexes of bpy and phen. The reactions of $RhCl_3$ were also found to give higher yields than those carried out with $IrCl_3$, suggesting that Ir(III) has a greater tendency than Rh(III) to form mononuclear products.³

1.6.2 Electronic Structure

Consideration of these bridged species as M(III) bonded to anionic ligands leads to a formal count of 16 electrons per metal centre. The electronic configurations of iridium(III) and rhodium(III) in this environment are $[Xe] 4f^{14} 5d^6$ and $[Kr] 4d^6$ respectively and are both low-spin d^6 complexes. As suggested by Sprouse *et al.*³ the

comparison of these $[M(L)_2Cl]_2$ complexes with mononuclear species containing bpy and phen ligands indicates that they contain metal centres with electron density which is intermediate between that of mononuclear $M(I)$ and $M(III)$ complexes. For example, $M(L)_2Cl_2^+$, where $M = Ir(III)/Rh(III)$, e.g. $Rh(bpy)Cl_2^+$ ²⁶ (18 electron count), and $M(L)_2^+$, where $M = Ir(I)/Rh(I)$, e.g. $Rh(bpy)_2^+$ ²⁷ (16-electron count). This is consistent with a reactivity intermediate between the strong tendency of $Rh(bpy)_2^+$ to undergo oxidative addition reactions and the relatively inert character of $Rh(bpy)_3^{3+}$ towards reduction. The participation of the $[M(L)_2Cl]_2$ species in bridge cleaving reactions, particularly with good π -acceptor ligands, such as CO, to yield mononuclear species with a formal 18-electron count, reflects this intermediacy in their reactivity.²⁸

1.6.3 UV-Visible Absorption Spectra

The absorption spectra of the four dichloro-bridged species, $[Ir(ppy)_2Cl]_2$, $[Ir(bzq)_2Cl]_2$, $[Rh(ppy)_2Cl]_2$ and $[Rh(bzq)_2Cl]_2$ were studied by Sprouse *et al.*³ in 1984. A complete compilation of the spectral features and extinction coefficients is detailed in table 1.1.

Table 1.1 Absorption Data for Ir(III) and Rh(III) Dichloro-Bridged Species of ppy and bzq in dichloromethane and chloroform at 298 K.

Complex	Absorption Features, nm		$\epsilon / 10^3 \text{ mol dm}^{-3} \text{ cm}^{-1}$
	$CHCl_3$	CH_2Cl_2	
$[Ir(ppy)_2Cl]_2$	487 (sh)	484 (sh)	1.1
	436	434	4.2
	405	400	6.3
	355 (sh)	355 (sh)	11.0
	355	355	13.0
	260	260	68.0
$[Ir(bzq)_2Cl]_2$	480 (sh)	480 (sh)	3.1
	448	442	5.5
	365	363 (sh)	18.0
	349	347	20.0
	325	322	21.0
	260	260	77.0

[Rh(ppy) ₂ Cl] ₂	464	462	0.048
	397	393	7.7
	385 (sh)	380 (sh)	6.8
	335 (sh)	333 (sh)	15.0
	307	310 (sh)	29.0
	a	240	73.0
[Rh(bzq) ₂ Cl] ₂	b	440 (sh)	1.1
	415	410	8.2
	400	380 (sh)	6.5
	333	330 (sh)	23.0
	280 (sh)	277	48.0
	255 (sh)	255	76.0

Extinction coefficients determined in CH₂Cl₂. (a) = No absorption features observed due to solvent cut-off. (b) = Low energy shoulder (sh) not observed.

In addition to this, their absorption measurements of these complexes in dimethylformamide solutions were found to deviate markedly from Beer’s Law. The absorption features of the spectra continued to change for several days after the solutions had been prepared. The weaker solutions exhibited the greatest changes where the ‘low energy absorption features were found to be replaced by higher energy absorption bands with ageing.’ The NMR results indicated that the dichloro-bridged species had been cleaved to form monomeric species of the type M(L)₂Cl(S) in ligating solvents such as dimethylformamide (s = ligating solvent).

1.6.4 Luminescence Properties

Each of the [M(L)₂Cl]₂ complexes studies by Sprouse *et al.*,³ M = Ir(III)/Rh(III), L = ppy and bzq, was found to be luminescent in ethanol/methanol/dichloromethane glasses (4:1:1 by volume) at 77 K. Nitrogen flushed dichloromethane solutions of the Ir(III) complexes at ambient temperature showed that their emissions were sensitive to oxygen quenching. However, emission from the Rh(III) complexes under the same conditions was not observed.

The lifetimes of these four complexes were measured, table 1.2, showing that the Rh(III) species were considerably longer lived than those of Ir(III) and for each metal complex the bzq moiety was longer lived than that of the ppy.

Table 1.2 Luminescence lifetimes of the $[M(L)_2Cl]_2$ species,
where M = Ir(III)/Rh(III) and L = ppy, bzq.

Complex	Luminescence Lifetime	
	77 K ^a	298 K ^b
$[Ir(ppy)_2Cl]_2$	4.8 μs	0.14 μs
$[Ir(bzq)_2Cl]_2$	30.0 μs	1.4 μs
$[Rh(ppy)_2Cl]_2$	93.0 μs	c
$[Rh(bzq)_2Cl]_2$	2.7 ms	c

(a) = Measured in ethanol/methanol/dichloromethane glass (4:1:1 by volume). (b) = Measured in nitrogen-flushed dichloromethane. (c) = No luminescence observed in nitrogen-flushed dichloromethane.

The differences in luminescence lifetimes and energies in the luminescence spectra of these bridged species indicate dissimilar emissive states for the complexes of these two metals. Sprouse *et al.*³ assigned the emissive state as intraligand for the rhodium species and metal to ligand charge transfer (MLCT) for the iridium species.

The comparison of the ppy and bzq dimers with similar species, $Rh(bpy)_2Cl_2^+$ and $Rh(phen)_2Cl_2^+$,²⁶ indicated that ppy and bzq (*ortho*-metalated ligands) have considerably higher ligand field (LF) excited states than bpy and phen in the spectrochemical series. As well as increasing the energy of the ligand-field excited states in their complexes relative to similar bpy and phen species, these ligands induce lower energy charge-transfer transitions.

The relatively low energy MLCT emissions observed for the Ir(III) complexes indicated that they are good π -accepting ligands with sufficiently delocalised π^* orbitals to accommodate electron transfer from the Ir(III) metal center in the excited state. Furthermore, their Ir-C bonds allow suitably strong σ -donation, enriching the electron density at the metal and rendering the Ir(III) center more oxidisable than in the bpy and phen complexes. However, this synergistic combination of bonding effects is not adequate to induce MLCT emission from the rhodium complexes.

Studies of several *ortho*-metalated iridium(III) dichloro-bridged complexes containing methyl-substituted phenylpyridine ligands were reported in 1988 by Garces *et al.*²⁹ The methylated ligands were 2-(*p*-tolyl)pyridine (ptpy) and 3-methyl-2-phenylpyridine (mppy). The ultraviolet-visible absorption properties of the dimers were similar to those of the non-substituted ppy complexes. They exhibited low-energy MLCT bands ranging from 484 nm to 400 nm. The emission spectra were also similar to dichloro-bridged species containing non-substituted ppy ligands. At room temperature the methylated species showed broad emission bands at 515 nm and structured emission bands at 494 nm and 528 nm in glasses at 77 K. The cyclic voltammetric studies showed that these methyl-substituted complexes were easier to oxidise and harder to reduce relative to the non-substituted ppy complexes. This was exhibited by cathodic shifts (~ 100 mV) in the half-wave potentials compared to the potentials of the ppy complex. This suggested that the electron density around the iridium metal, which influences the reducing power of these complexes, may be controlled by inductive effects from the methyl group on the phenylpyridine ligands.

1.6.5 Summary

Although many novel dichloro-bridged species of this nature have been reported since, their preparation has primarily been for use as precursors for the preparation of monomeric *ortho*-metalated iridium(III) and rhodium(III) complexes and they have received no detailed attention.

1.7 Monomeric *Ortho*-metalated Complexes of Iridium(III) and Rhodium(III)

1.7.1 Introduction

In 1985 King *et al.*³⁰ characterised the first triply *ortho*-metalated iridium(III) species, *fac*-Ir(ppy)₃, figure 1.10. This monomeric species contains an iridium(III) centre in an octahedral environment.

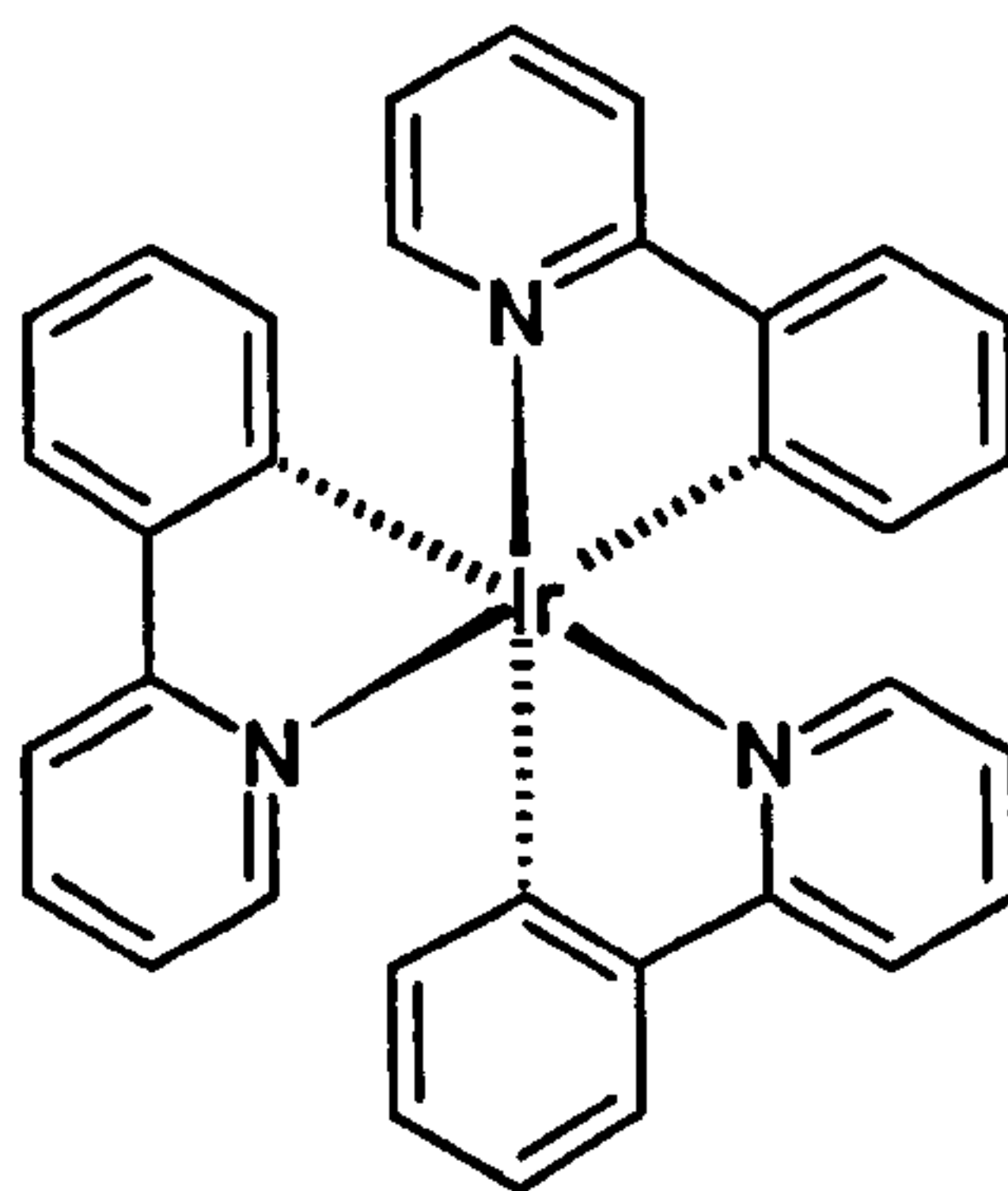


Figure 1.10 A structural illustration of *fac*-tris(2-phenylpyridine- C^2,N')iridium(III), *fac*-Ir(ppy)₃.

This complex was isolated as a side product in the preparation of the dichloro-bridged species $[Ir(ppy)_2Cl]_2$ from ethanol and acetone washings. The washings were evaporated to give a yellow solid in a 10 % yield. Elemental analysis confirmed the formulation of the monomeric complex, *fac*-Ir(ppy)₃. Following this, other synthetic strategies have been developed which allow the preparation of this complex in good yield. These synthetic pathways are discussed in more detail in the following section.

1.7.2 Tris-*ortho*-metalated Complexes of Ir(III) and Rh(III)

1.7.2.1 Synthesis

Triply *ortho*-metalated complexes may be produced *via* a variety of synthetic pathways. The product yield obtained depends heavily upon the ligands and the synthetic method of choice. The following section describes the range of possible pathways used to create these complexes.

Method A

This method, reported by Dedeian *et al.*³¹ in 1991, involves the use of the iridium(III) precursor tris(acetylacetonato)iridium(III), Ir(acac)₃. In a particularly pH sensitive reaction,³² involving iridium(III) chloride and 2,4-pentanedione (acacH), Ir(acac)₃ can be prepared and isolated in moderate yield (45 %). This compound is then refluxed with an

excess of the cyclometalating ligand in degassed glycerol at 220 °C for 10 hours. The addition of 1M hydrochloric acid to the reaction mixture after cooling results in the precipitation of the cyclometalated product. Dedeian *et al.*³¹ reported yields of ~ 40 % - 70 % utilising substituted 2-(X-phenyl)pyridine ligands, where X = 4-Me, 4-Pr, 4-^tBu, 4-F, 4-CF₃, 4-MeO and 5-MeO.

The success of this method is due to the elimination of chloride from the starting material and the *trans*-directing effect of the Ir-C bonds, which leads to preferential labilisation of the Ir-O bonds, located *trans* to the Ir-C bonds.³³

Method B

In 1994 Colombo *et al.*² reported on the use of silver(I) salts as chloride scavengers in the synthesis of triply *ortho*-metalated iridium(III) monomers from the dichloro-bridged precursors. Due to the nature of silver(I) salts the reaction must be carried out in an inert atmosphere and preferably in the absence of light. Yields of up to 50 % are possible but this depends upon the ligand and silver salt used. This basic synthetic method was later termed as a 'solvent free' synthesis by Grushin *et al.*³⁴ who produced a range of iridium(III) complexes containing a variety of fluorinated 2-phenylpyridine ligands in yields ranging from 8 % - 82 %.

These triply *ortho*-metalated complexes formed *via* methods A and B possess a facial (*fac*) geometry. The carbon donor atoms on the *ortho*-metalating ligands are able to reduce their negative charge more effectively if they are situated *trans* to a nitrogen atom, this is considered the major driving force behind the preference for the formation of the *fac* over *meridional* (*mer*) isomer formation.³⁵

Method C

More recently, Tamayo *et al.*³⁶ described the following synthetic method in which only the facial isomer is produced if temperatures of 200 °C and above are used. The reaction utilises the dichloro-bridged iridium(III) precursor, an excess of cyclometalating ligand and 5-10 molar equivalents of K₂CO₃ in glycerol under and an inert atmosphere.

The solution is then refluxed at 200 °C for 20-24 hours. Work-up and subsequent purification of the reaction mixture affords the pure *fac*-isomer in 65 % - 80 % yield.

1.7.3 Bis-*ortho*-metalated Monomers of Ir(III) and Rh(III)

1.7.3.1 Synthesis

Method A

The synthesis of bis-*ortho*-metalated complexes of the formula $\text{Ir}(\text{L})_2\text{X}$, where X = bidentate monoionic ligand, such as 2,4-pentanedione (acac), picolinic acid (pic) and N-methylsalicylamine (sal), were reported in 2001 by Lamansky *et al.*³⁷ This method utilises the dichloro-bridged complexes, $[\text{Ir}(\text{L})_2\text{Cl}]_2$, and an excess of XH, i.e. acacH, in the presence of a base, sodium carbonate. The materials are refluxed in 2-ethoxyethanol in an inert atmosphere for 12-15 hours, after which the precipitated complex can be collected *via* filtration in 75 % - 90 % yields. Unlike methods A and B (section 1.7.2.1), in which the excess 2-phenylpyridine acts as its own base as well as the metalating ligand, this method requires added base to aid the removal of the acacH proton.

Although this method does not produce triply *ortho*-metalated complexes, it does however produce monomeric iridium(III) complexes in high yields *via* a simple synthetic procedure. The bidentate acetylacetonate ligand also negates the use of a chloride scavenger.

Method B

Mononuclear iridium complexes of the formula $\text{Ir}(\text{L})_2\text{X}(\text{Y})$ were synthesised by King *et al.*²⁸ in 1984, where L = an *ortho*-metalating ligand, X = Cl and Y = pyridine (pyr), triphenylphosphine (PPh_3) and carbon monoxide (CO). The corresponding chloro-bridged complex is reacted with 2 equivalents of the monodentate ligand, Y, at room temperature. Subsequent concentration of the reaction mixture, followed by the addition of hexane allows the precipitation of the product in high yield.

1.7.4 Electronic Structure

For these low-spin d^6 transition-metal complexes, described in sections 1.6 and 1.7, the lowest lying excited state is MLCT-based,² $d\pi^6\pi^{*0} \rightarrow d\pi^5\pi^{*1}$, see figure 1.11 below. The promotion of an electron from a metal $d\pi$ orbital to a ligand π^* orbital by the absorption of a photon, with energy $= h\nu$, results in the formation of a singlet excited state, $^1\text{MLCT}^*$. The singlet excited state may then undergo intersystem crossing (ISC), a non-radiative process, to form a triplet excited state, $^3\text{MLCT}^*$. The excited triplet state can subsequently experience either non-radiative decay (NR) or radiative decay (R) and relax back to its ground electronic state, $M(d\pi^6\pi^0)$. In the latter case, involving a change in spin multiplicity, the energy given out is called phosphorescence as it derives from a state with triplet character.³⁸

This process is formally forbidden, however spin-orbit coupling, due to the heavy atom effect, between $^3\text{MLCT}^*$ and higher energy, spin-allowed $^1\text{MLCT}^*$ transitions increases the probability of this radiative decay process.²

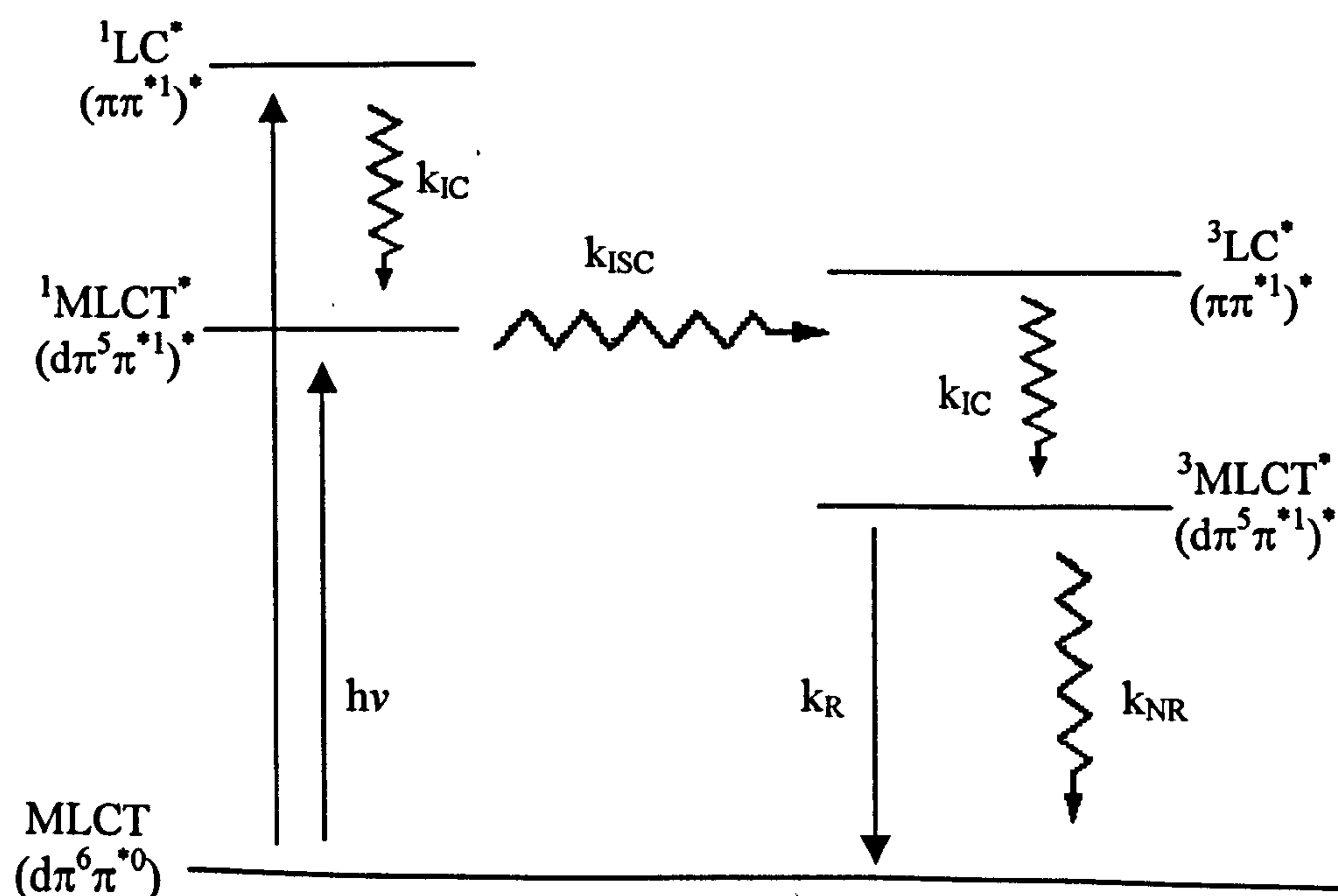


Figure 1.11 A schematic of the electronic energy levels in an Ir(III)/Rh(III) complex, where * indicates an excited state, LC = ligand centered state and k_x = rate of process x.

1.7.5 UV-Visible Absorption Spectra

The absorption spectra of *fac*-Ir(ppy)₃ in aerated dichloromethane is shown below in figure 1.12. As described by Colombo *et al.*,² the intense absorption band at $\sim 35,000$ cm⁻¹ (285 nm) has been assigned as a ligand centered (LC) spin-allowed $^1\pi-\pi^*$ transition. The broad absorption band at lower energy ($\sim 28,000$ cm⁻¹, 358 nm) is typical of spin-allowed $^1\text{MLCT}$ transitions and at even lower energies, the weaker bands which reach into the visible region are assigned as formally forbidden $^3\text{MLCT}$ transitions. These features acquire their intensity by spin-orbit coupling with higher energy $^1\text{MLCT}$ spin-allowed transitions.²

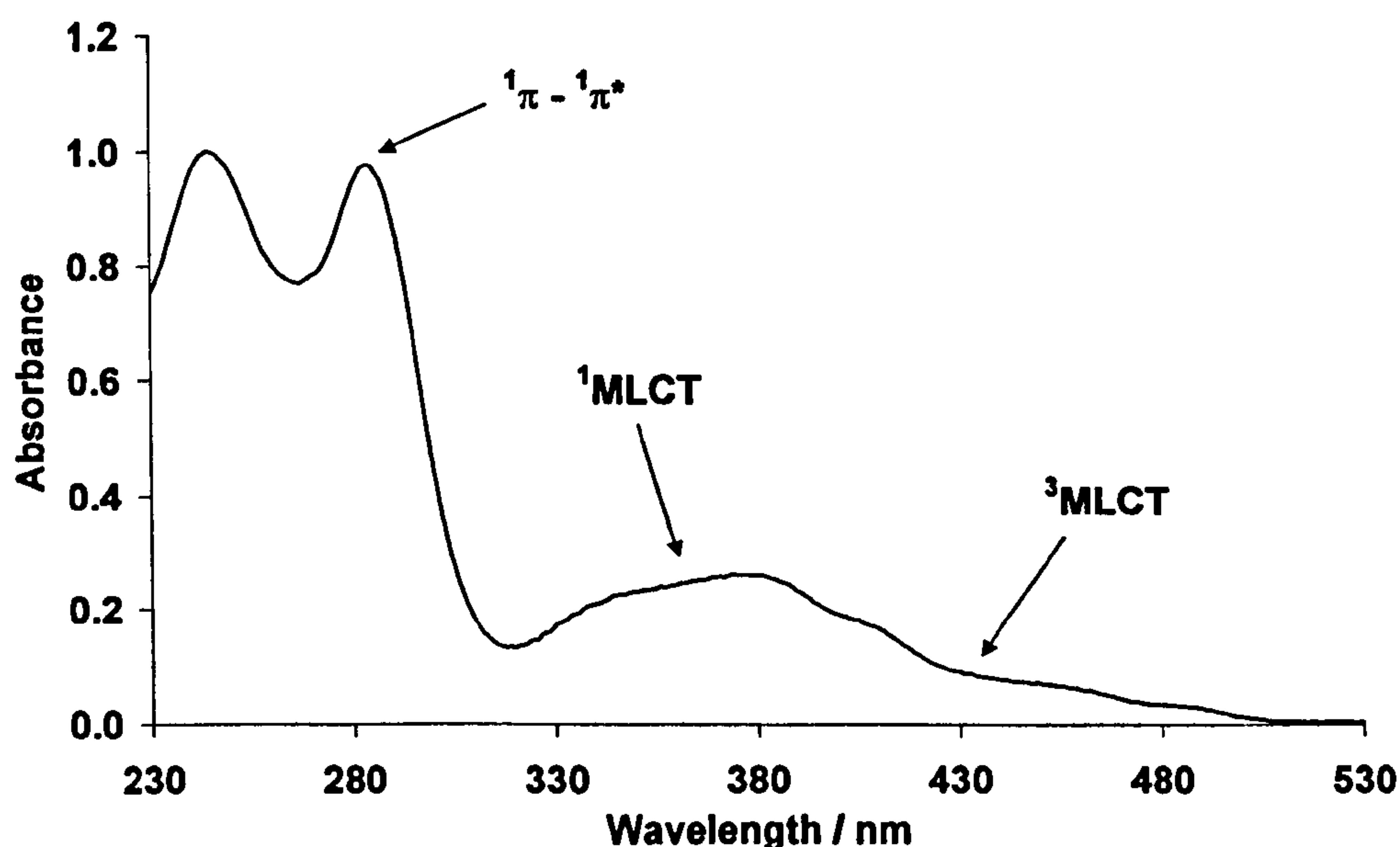


Figure 1.12 The normalised absorbance spectrum of *fac*-Ir(ppy)₃ in aerated dichloromethane at 298 K.

In some cases, i.e. Ir(tpy)₂acac, where tpy = 2-(*p*-tolyl)pyridine, the $^1\text{MLCT}$ and $^3\text{MLCT}$ bands are more clearly resolved.³⁷

The absorption features of related iridium and rhodium complexes were assigned in the same way. However, the $^3\text{MLCT}$ bands for rhodium complexes are weaker than those of iridium due to the smaller spin-orbit coupling constant of rhodium.

1.7.6 Luminescence Properties

1.7.6.1 Steady-State Spectra

The luminescence spectra of *fac*-Ir(ppy)₃ is shown in figure 1.13. This bright green emission, centered at ~ 515 nm, is produced by UV excitation, i.e. 355 nm, and arises from an excited ³MLCT state.²

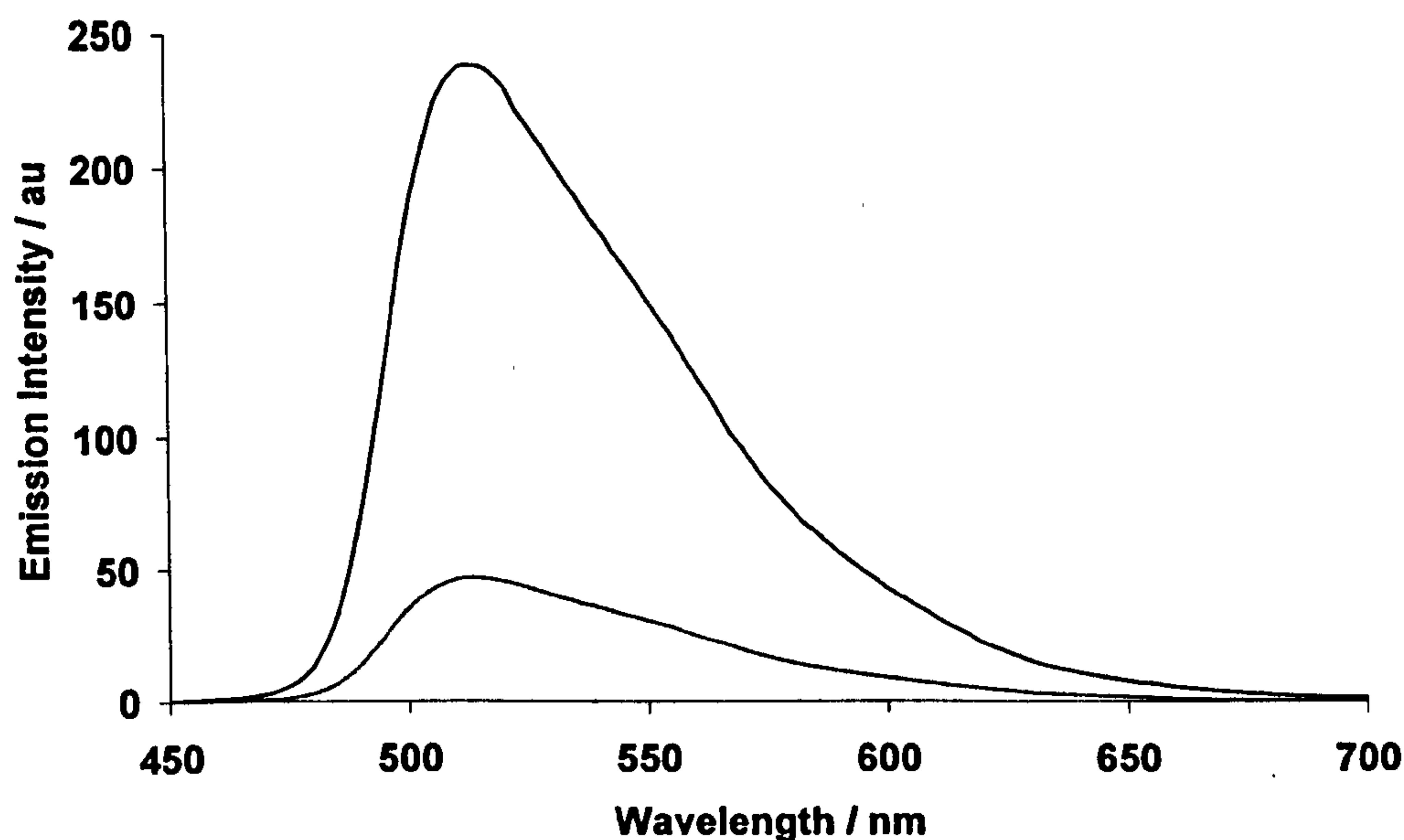


Figure 1.13 Luminescence spectra of *fac*-Ir(ppy)₃ in degassed (black line) and aerated (grey line) dichloromethane at 298 K.

Previous investigations of Ru(bipy)₃²⁺, using various absorption,^{39,40} electroabsorption⁴¹ and Raman techniques⁴² indicated that the lowest MLCT state was localised on a single ligand. Time-resolved studies of the formation of the triplet MLCT excited state with transient absorption pump-probe spectroscopy, showed the initial delocalisation of the excited state over all three ligands, followed by the charge localising onto a single ligand.⁴³ In cyclometalated iridium complexes the excitation processes can be both ligand-centred and MLCT in nature. Following excitation the emissive ³MLCT state is formed, and by analogy with the Ru(bipy)₃²⁺ complexes, it can therefore be assumed that this also localises upon a single ligand. In *fac*-Ir(ppy)₃ this can be any one of the three identical 2-phenylpyridine ligands. However, in the case of mixed ligand

complexes such as $\text{Ir(ppy)}_2\text{fppy}$,⁴⁴ where $\text{fppy} = 4\text{-(2'-pyridyl)benzaldehyde}$, the excitation is localised on the ligand which gives rise to the lowest energy complex. The presence of the carbonyl moiety on the fppy ligand lowers its energy in comparison with the ppy ligands. Hence it is upon the fppy ligand that the final excitation resides. Subsequent emission from the complex is therefore characterised by the substituted fppy ligand.

1.7.6.2 Solvatochromatic Emission

Many tris- and bis-*fac-ortho*-metalated complexes also exhibit solvatochromatic emission and the degree to which their emission wavelength is shifted by the solvent depends upon the ligand substituents. The emission maxima of *fac*- Ir(ppy)_3 in CH_2Cl_2 , $\text{C}_6\text{H}_5\text{CH}_3$, MeCN and EtOH shows no discernable shift. However the emission maxima of complexes containing more polar ligands, such as fppy,⁴⁵ are shifted by as much as 40 nm in these solvents. The solvatochromic emission in the fppy containing complexes is attributed to the greater delocalisation of charge in the excited $^3\text{MLCT}$ state. The formyl group acts as an electron acceptor and hence stabilises the negative charge that can be considered to reside on the ligand. The degree of stabilisation, and hence the extent of the red shift, depends upon the polarity of the environment.

1.7.6.3 Tuneable Emission

It has also been shown that the emission wavelength of iridium(III) complexes containing 2-phenylpyridine ligands can be tuned to give more red-shifted⁴⁴ or blue-shifted⁴⁵ emission by changing the substituents. Previous work by Dedeian *et al.*³¹ illustrated this with a series of Ir(L)_3 complexes, $\text{L} = 2\text{-(X-phenyl)pyridine}$, where $\text{X} = 4\text{-Me, 4-Pr, 4-}^t\text{Bu, 4-F, 4-CF}_3, 4\text{-MeO and 5-MeO}$. They also reported the half-wave potential for these complexes showing that the position of the oxidation wave, $\text{Ir(III)} \rightarrow \text{Ir(IV)}$, follows a pattern in which more positive values are found for complexes bearing electron-withdrawing substituents and less positive values for complexes bearing electron-donating substituents, table 1.3.

Table 1.3 Emission and Cyclic Voltammetric Data
for *fac*-tris-*ortho*-metalated Ir(III) Complexes.³¹

Complex	τ / μs ^a	λ_{em} / nm ^b	$E_{1/2}$ / V (+1/0) ^c
Ir(ppy) ₃	1.90	494	+ 0.77
Ir(4-Me-ppy) ₃	1.94	493	+ 0.70
Ir(4-Pr-ppy) ₃	1.93	496	+ 0.67
Ir(4- ^t Bu-ppy) ₃	1.97	497	+ 0.66
Ir(4-F-ppy) ₃	2.04	468	+ 0.97
Ir(4-CF ₃ -ppy) ₃	2.16	494	+ 1.08
Ir(4-MeO-ppy) ₃	2.24	481	+ 0.75
Ir(5-MeO-ppy) ₃	2.86	539	+ 0.55

(a) Degassed acetonitrile, (b) shortest wavelength feature in emission spectrum in ethanol/methanol glass (1:1 by volume) at 77 K and (c) half-wave potential in acetonitrile for [Ir(R-ppy)₃]⁺/Ir(R-ppy)₃ taken from cyclic voltammogram, V vs. SCE (internal reference $E_{1/2}(\text{Fc}^{+/0}) = 0.41$ V vs. SCE).

1.7.6.4 Luminescence Lifetimes and Quantum Yields

As expected, luminescence from these complexes is oxygen sensitive due to the long radiative lifetimes associated with these formally spin-forbidden transitions. The excited state lifetime, τ , for these complexes is controlled by the recombination rate of the charge-separated electron and hole (oxidised metal centre). It can therefore be described in terms of the non-radiative (vibrational relaxation) rate, k_{NR} , and the radiative decay rate, k_{R} , as shown in equation 1.2.

$$\frac{1}{\tau} = k_{\text{NR}} + k_{\text{R}} \quad 1.2$$

Table 1.4 illustrates the luminescence and lifetime data for a selection of tris-*ortho*-metalated iridium(III) complexes.

Table 1.4 Luminescence and lifetime data for selected tris-*ortho*-metalated Ir(III) complexes at 298 K.

Complex	Luminescence		$\Phi \pm 20 \%$
	Lifetime $\pm 10 \%$ / μs	λ_{max} / nm	
Ir(ppy) ₃ ^a	2.0	515	0.40
Ir(ppy) ₂ acac ^b	1.6	516	0.34
Ir(tpy) ₂ acac ^b	3.1	512	0.31

(a) Degassed toluene²⁹ and (b) degassed 2-methyltetrahydrofuran (2-MeTHF).³⁷

1.7.6.5 Singlet Oxygen Sensitisation and Quenching

The luminescence lifetimes and quantum yields of these cyclometalated species are severely reduced by the presence of oxygen. This photophysical feature prompted Gao *et al.*⁴⁶ to investigate these complexes as potential singlet oxygen sensitisers. They studied a series of bis-cyclometalated complexes of the formula, Ir(L)₂X, where L = 2-phenylquinoline (pq), 2-phenylbenzothiazole (pbt) and 2-naphthalen-1-yl-benzothiazole (nb), X = acac. The quantum yields of singlet oxygen formation (Φ_{Δ}) were obtained by measuring the intensity of the ¹O₂ phosphorescence at 1268 nm after excitation at 355 nm in aerated benzene solutions at concentrations where triplet-triplet annihilation was negligible. Their results clearly showed that these iridium(III) species were extremely efficient singlet oxygen sensitisers, with some complexes reported to have quantum yields of singlet oxygen production at or near unity. Table 1.5 reports the Φ_{Δ} values for some of these complexes as well as the rate constants for the oxygen quenching of phosphorescence, $k_q(\text{sv})$, determined by Stern-Volmer analysis and the rate constants for singlet oxygen quenching by the iridium complex sensitiser, $k_q(^1\text{O}_2)$.⁴⁶

Table 1.5 Quantum Yields for Singlet Oxygen generation (Φ_{Δ}), rate constants for the oxygen quenching of phosphorescence, $k_q(\text{sv})$ and rate constants for singlet oxygen quenching by the iridium complex sensitiser, $k_q(^1\text{O}_2)$, $\lambda_{\text{ex}} = 355 \text{ nm}$.

Sensitiser	Φ_{Δ}	$k_q(\text{sv}) \text{ (} 10^9 \text{ dm}^3 \text{ s}^{-1} \text{)}$	$k_q(^1\text{O}_2) \text{ (} 10^6 \text{ dm}^3 \text{ s}^{-1} \text{)}$
Ir(pq) ₂ acac	0.62 ± 0.05	7.2 ± 0.3	1.0 ± 0.2
Ir(pbt) ₂ acac	0.86 ± 0.07	5.9 ± 0.6	0.5 ± 0.2
Ir(nb) ₂ acac	0.54 ± 0.02	-	2.1 ± 0.5

It is therefore likely that related iridium(III) complexes are also singlet oxygen sensitisers and weak quenchers.

1.7.7 Bis-*ortho*-metalated Complexes, $\text{M(L)}_2\text{X(Y)}$

1.7.7.1 Luminescence Properties

The luminescence properties of the bis-*ortho*-metallated complexes, $\text{Ir(ppy)}_2\text{Cl(Y)}$, where $\text{Y} = \text{pyridine (pyr)}$, triphenylphosphine (PPh_3) and carbon monoxide (CO) were isolated and characterised by King *et al.*²⁸ in 1984. The photophysical data for these complexes and *fac*- Ir(ppy)_3 at 298 K and 77 K is summarised in table 1.6.

Table 1.6 Photophysical characteristics of bis-*ortho*-metalated Ir(III) complexes.

Complex	Lifetime	λ_{max}	Lifetime	λ_{max}
	77 K / μs ^a	77 K / nm ^{a,b}	298 K / μs ^c	298 K / nm ^c
Ir(ppy) ₃	5.0	495	0.60	530
Ir(ppy) ₂ Cl(pyr)	4.3	483	0.14	500
Ir(ppy) ₂ Cl(PPh ₃)	5.5	470	0.047	485
Ir(ppy) ₂ Cl(CO)	28	455	0.11	462

(a) Ethanol/methanol glass (4:1 by volume), (b) shortest wavelength peak in vibrational progression and (c) degassed dichloromethane.

King *et al.*²⁸ discussed the change in the character of the emissive states of these complexes according to the π -accepting ability of ligand Y. Due to strong σ -donation

from the C-bonded ppy ligands, the metal centers in these kinds of complexes possess enriched electron density. This proves to lower the energy of the metal to π -acceptor transitions. The MLCT character of the emissive state is therefore greatest in complexes where there are the maximum number of Ir-C bonds and the presence of a good delocalised π -acceptor ligand with relatively high energy ligand centered (LC) excited states, i.e. $\text{Ir(ppy)}_2\text{Cl(pyr)}$. On the other hand, the degree of LC character of the emissive state is greatest when there are fewer Ir-C bonds and the presence of a more localised π -accepting ligand with low energy LC excited states, i.e. $\text{Ir(ppy)}_2\text{Cl(CO)}$, figure 1.14.

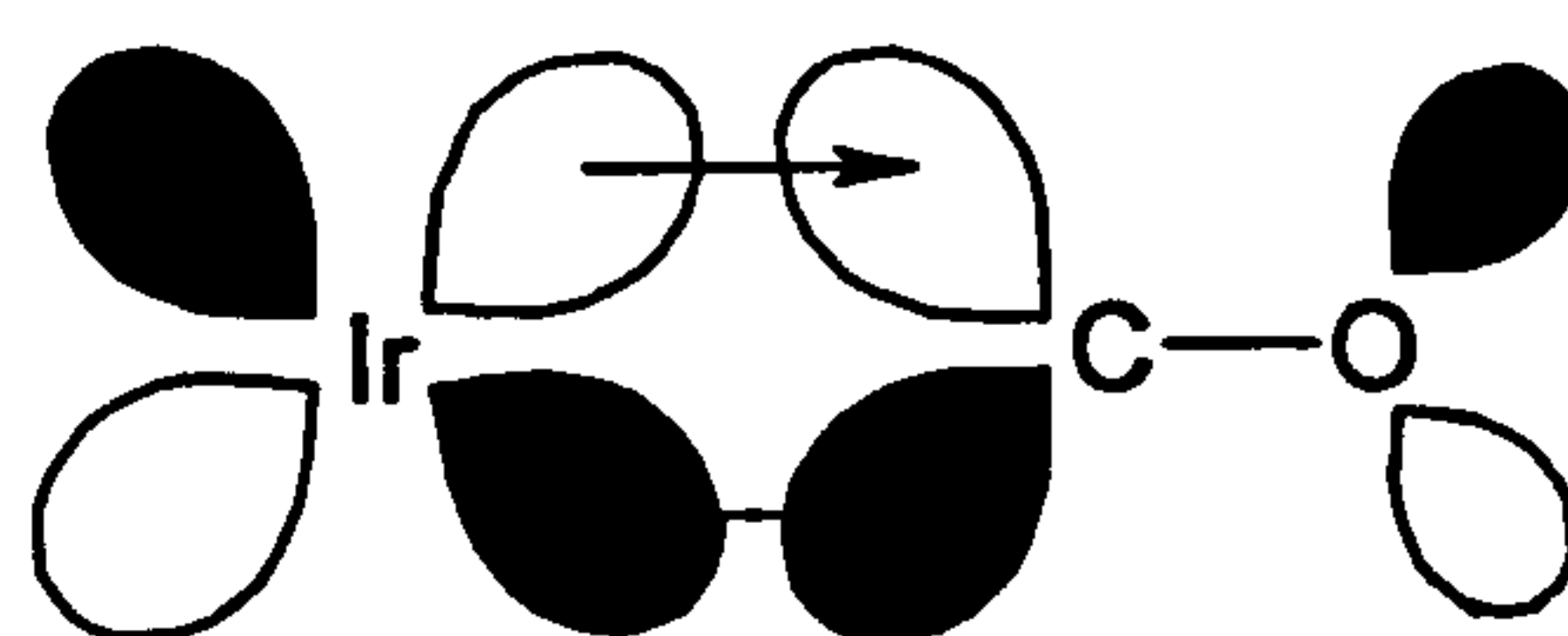


Figure 1.14 A schematic representation of π -back-bonding in $\text{Ir(ppy)}_2\text{Cl(CO)}$, from the Ir(III) center *via* $d\pi$ -orbitals to the π^* orbital of CO, arrows indicate direction of electron donation.

The progression of the emissive state from MLCT to LC character is illustrated nicely by the complexes in table 6. The blue-shifting of the highest energy wavelength feature in the 77 K emission spectra decreases from 483 nm to 455 nm going from pyridine (pyr) to CO, whilst the emission lifetimes increase from 4.3 μs to 28 μs . These trends correlate with an increase in the π -accepting ability of the variable ligand Y, in the series pyr, PPh_3 , CO from left to right.

The luminescent excited state of $\text{Ir(ppy)}_2\text{Cl(pyr)}$ is assigned as MLCT to the ppy ligand. However, when pyridine is replaced with PPh_3 the MLCT state is moved up in energy as electron density from the iridium centre is removed *via* π -back-bonding. Electrons are donated into the anti-bonding π^* orbital of PPh_3 , thus rendering charge transfer to the ppy ligand more difficult. King *et al.*²⁸ stated that the introduction of the CO ligand allowing strongly localised π -back-bonding into the co-ordination sphere appears to move the energy of the MLCT above that of the LC configuration. This therefore yields a complex whose emission spectrum and luminescence lifetime indicate

significantly more LC character than is present in the excited emissive states of $\text{Ir(ppy)}_2\text{Cl(pyr)}$ and $\text{Ir(ppy)}_2\text{Cl(PPh}_3\text{)}$.

Related iridium(III) complexes containing 2-(2-thienyl)pyridine (thpy) with tributylphosphine (PPh_3) and pyridine (pyr) have also been characterised by Nonoyama,⁴⁷ who also reported the formation of the solvent adduct $\text{Ir(thpy)}_2\text{Cl(DMSO)}$.

1.7.7.2 Singlet Oxygen Sensitisation and Quenching

The previously mentioned series of bis-cyclometalated complexes studied by Gao *et al.*⁴⁶ included the pyridyl complex, $\text{Ir(pbt)}_2\text{Cl(pyr)}$, figure 1.15.

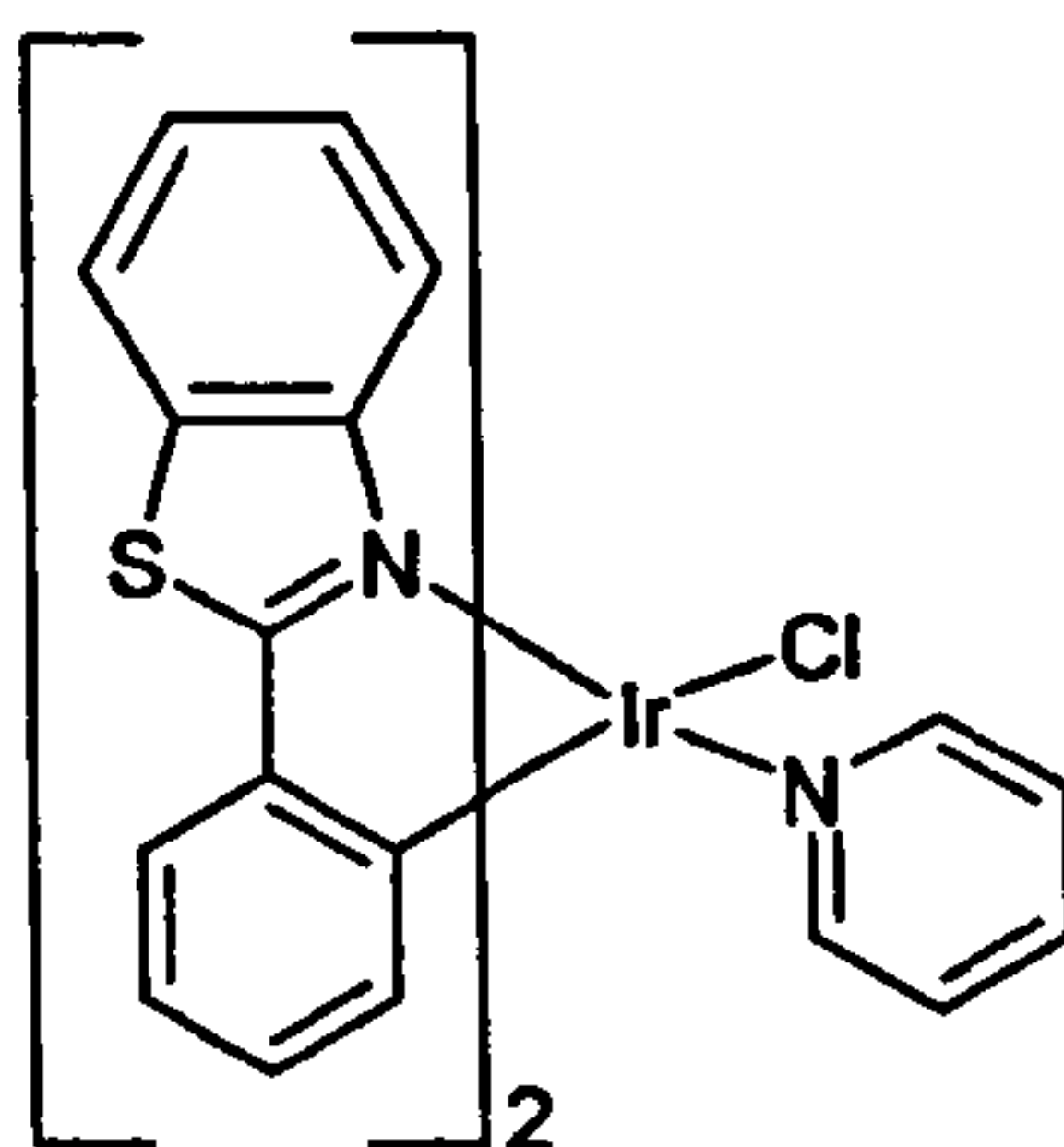


Figure 1.15 A structural illustration of the complex $\text{Ir(pbt)}_2\text{Cl(pyr)}$, where pbt = 2-phenylbenzothiazole and pyr = pyridine.

This complex was found to have a high quantum yield for singlet oxygen formation, $\Phi_{\Delta} = 0.95 \pm 0.09$ in benzene, at 355 nm excitation. In concurrence with the bis-cyclometalated complexes of the formula, $\text{Ir(L)}_2\text{X}$, where L = 2-phenylquinoline (pq), 2-phenylbenzothiazole (pbt) and 2-naphthalen-1-yl-benzothiazole (nb) and X = acac, whose rates of singlet oxygen quenching were low, $\text{Ir(pbt)}_2\text{Cl(pyr)}$ was reported to have no measurable rate of singlet oxygen quenching.

1.8 Conclusion

Monomeric iridium(III) complexes may be synthesised by a number of synthetic pathways. They are highly luminescent species and have solvent dependent lifetimes in the range of 20 ns (aerated) to 5 μ s (degassed). The excited emissive states of these complexes have been assigned as MLCT states that possess mainly triplet character, which accounts for the long-lived oxygen sensitive luminescence that is observed from these complexes. The emission intensity of these species is increased upon degassing and the spectral profile remains unchanged. Many of these iridium complexes also exhibit solvatochromatic emission. The emission characteristics including emission wavelength may be tuned by altering the electronic properties of the cyclometalating and ancillary ligands. Other properties include the reversible oxidation of these compounds in deoxygenated solutions as observed by cyclic voltammetry and their ability to sensitise singlet oxygen.

1.9 References

- 1 N. N. Greenwood and A. Earnshaw, *Chemistry of the Elements*, Pergamon Press, 1990, **19**, 1084-1101.
- 2 M. G. Colombo, T. C. Brunold, T. Riedener, H. U. Güdel, M. Förtsch and H. Bürgi, Facial Tris Cyclometalated Rh^{3+} and Ir^{3+} Complexes: Their Synthesis, Structure and Optical Spectroscopic Properties, *Inorg. Chem.*, 1994, **33**, 545-550.
- 3 S. Sprouse, K. A. King, P. J. Spellane and R. J. Watts, Photophysical Effects of Metal-Carbon σ bonds in Ortho-Metalated Complexes of Ir(III) and Rh(III), *J. Am. Chem. Soc.*, 1984, **106**, 6647-6653.
- 4 E. V. Donckt, B. Camerman, F. Hendrick, R. Herne and R. Vandeloise, Polystyrene Immobilised Ir(III) Complex as a New Material for Optical Oxygen Sensing, *Bull. Soc. Chim. Belg.*, 1994, **103**, 207-211.

- 5 G. Di Marco, M. Lanza, M. Pieruccini and S. Campagna, A Luminescent Iridium(III) Cyclometalated Complex Immobilised in a Polymeric Matrix as a Solid-State Oxygen Sensor, *Adv. Mater.*, 1996, **8**, 576-580.
- 6 Y. Amao, Y. Ishikawa and I. Okura, Green Luminescent Iridium(III) Complex Immobilised in Fluoropolymer film as Optical Oxygen-sensing Material, *Anal. Chim. Acta.*, 2001, **445**, 177-182.
- 7 M. A. Baldo, S. Lamansky, P. E. Burrows, M. E. Thompson and S. R. Forrest, Very High-efficiency Green Organic Light-emitting Devices based on Electrophosphorescence, *Appl. Phys. Lett.*, 1999, **75**, 4-6.
- 8 T. Tsutsui, M. Yang, M. Yahiro, K. Nakamura, T. Watanabe, T. Tsuji, Y. Fukuda, T. Wakimoto and S. Miyaguchi, High Quantum Efficiency in Organic Light-emitting Devices with Iridium-Complex as a Triplet Emissive Center, *Jpn. J. Appl. Phys.*, 1999, **38**, L1502-L1504.
- 9 K. Nishimura, Y. Hamada, T. Tsujioka, K. Shibata and T. Fuyuki, Solution Electrochemiluminescent Cell using Tris(phenylpyridine) Iridium, *Jpn. J. Appl. Phys.*, 2001, **40**, L945-L947.
- 10 M. A. Bennett and D. L. Milner, Chlorotris(triphenylphosphine)iridium(I): An Example of Hydrogen Transfer to a Metal from a Co-ordinated Ligand, *Chem. Commun. (London)*, 1967, **12**, 581-582.
- 11 N. Miyaura and A. Suzuki, Palladium-Catalysed Cross-Coupling Reactions of Organoboron Compounds, *Chem. Rev.*, 1995, **95**, 2457-2483.
- 12 N. M. Ali, A. McKillop, M. B. Mitchell, R. A. Rebelo and P. J. Wallbank, Palladium-Catalysed Cross-Coupling Reactions of Arylboronic Acids with π -Deficient Heteroaryl Chlorides, *Tetrahedron*, 1992, **48**(37), 8117-8126.
- 13 D. R. Coulson, Tetrakis(triphenylphosphine)palladium(0), *Inorg. Synth.*, 1990, **23**, 121-124.
- 14 N. Miyaura, *Advances in Metal-Organic Chemistry*, JAI Press Inc. 1998, **6**, 187-243.

- 15 A. F. Littke, C. Dai and G. C. Fu, Versatile Catalysts for the Suzuki Cross-Coupling of Arylboronic Acids with Aryl and Vinyl Halides and Triflates under Mild Conditions, *J. Am. Chem. Soc.*, 2000, **122**, 4020-4028.
- 16 M. T. Reetz and E. Westermann, Phosphane-Free Palladium-Catalysed Coupling Reactions: The Decisive Role of Pd Nanoparticles, *Angew. Chem. Int. Ed.*, 2000, **39**(1), 165-168.
- 17 M. T. Reetz, R. Breinbauer and K. Wanninger, Suzuki and Heck Reactions Catalyzed by Preformed Palladium Clusters and Palladium/Nickel Bimetallic Clusters, *Tet. Lett.*, 1996, **37**, 4499-4502.
- 18 F. Kröhnke, The Specific Synthesis of Pyridines and Oligopyridines, *Synthesis*, 1976, **1**, 1-24.
- 19 J. March, *Advanced Organic Chemistry, Reactions, Mechanisms and Structure*, Wiley Interscience, Fourth Edition, 1992, 795.
- 20 K. P. C. Vollhardt and N. E. Shore, *Organic Chemistry*, W. H. Freeman and Company, Second Edition, 1994.
- 21 R. Bolton and G. H. Williams, Homolytic Arylation of Aromatic and Polyfluoroaromatic Compounds, *Chem. Soc. Rev.*, 1986, **15**, 261-289.
- 22 B. S. Furniss, A. J. Hannaford, P. W. G. Smith and A. R. Tatchell, *Vogel's Textbook of Practical Organic Chemistry*, Longman Scientific and Technical, Fifth Edition, 1989, **8**, 1170-1171.
- 23 C. Osuch and R. Levine, The Use of Organolithium Compounds to Effect the Alkylation of 2- and 4-Picoline, *J. Am. Chem. Soc.*, 1956, **78**, 1723-1725.
- 24 M. Nonoyama, Benzo[h]quinolin-10-yl-N Iridium(III) Complexes, *Bull. Chem. Soc, Jpn.* 1974, **47**, 767-768.
- 25 G. W. Parshall, Intramolecular Aromatic Substitution in Transition Metal Complexes, *Acc. Chem. Res.*, 1970, **3**, 139-144.

- 26 D. H. W. Carstens and G. A. Crosby, Luminescence from Complexes of Rhodium(III), *J. Mol. Spectrosc.*, 1970, **34**, 113-135.
- 27 S. G. Yan, B. S. Brunschwig, C. Creutz, E. Fujita and N. Sutin, Reversible Formation of Bis(2,2'-bipyridine)rhodium(III) Dihydride from Bis(2,2'-bipyridine)rhodium(I) and Dihydrogen. Direct Transfer of Dihydrogen from Rhodium(III) Dihydride to Rhodium(I), *J. Am. Chem. Soc.*, 1998, **120**, 10553-10554.
- 28 K. A. King, M. F. Finlayson, P. J. Spellane and R. J. Watts, Luminescence Spectroscopy and Oxidative Quenching of Orthometalated Complexes of Iridium(III), *Sci. Papers I. P. C.R.*, 1984, **78**, 97-106.
- 29 F. O. Garces, K. A. King and R. J. Watts, Synthesis, Structure, Electrochemistry and Photophysics of Methyl-Substituted Phenylpyridine *Ortho*-Metalated Iridium(III) Complexes, *Inorg. Chem.*, 1988, **27**, 3464-3471.
- 30 K. A. King, P. J. Spellane and R. J. Watts, Excited-State Properties of a Triply *Ortho*-Metalated Iridium(III) Complex, *J. Am. Chem. Soc.*, 1985, **107**, 1431-1432.
- 31 K. Dedeian, P. I. Djurovich, F. O. Garces, G. Carlson and R. J. Watts, A New Synthetic Route to the Preparation of a Series of Strong Photoreducing Agents: *fac*-Tris-*Ortho*-Metalated Complexes of Iridium(III) with Substituted 2-Phenylpyridines, *Inorg. Chem.*, 1991, **30**, 1685-1687.
- 32 J. E. Collins, M. P. Castellani, A. L. Rheingold, E. J. Miller, W. E. Geiger, A. L. Rieger and P. H. Rieger, Synthesis, Characterisation and Molecular Structure of Bis(tetraphenylcyclopentadienyl)rhodium(II), *Organomet.*, 1995, **14**, 1232-1238.
- 33 A. Immirzi, Crystal Structures of Rhodacyclopentane Derivatives, *J. Organomet. Chem.*, 1974, **81**, 217-225.
- 34 V. V. Grushin, N. Herron, D. D. LeCloux, W. J. Marshall, V. A. Petrov and Y. Wang, New Efficient Electroluminescent Materials based on Organometallic Complexes, *Chem. Commun.*, 2001, **16**, 1494-1495.

- 35 E. C. Constable and C. E. Housecroft, The Electronic Structure of some Ruthenium(II) Complexes Related to $[\text{Ru}(\text{bipy})_3]^{2+}$: An Investigation of the Stepwise Replacement of N,N-donors by C,N-donors, *Polyhedron*, 1990, 9, 1939-1947.
- 36 A. B. Tamayo, B. D. Alleyne, P. I. Djurovich, S. Lamansky, I. Tysba, N. N. Ho, R. Bau and M. E. Thompson, Synthesis and Characterisation of Facial and Meridional Tris Cyclometalated Iridium(III) Complexes, *J. Am. Chem. Soc.*, 2003, 125, 7377-7387.
- 37 S. Lamansky, P. Djurovich, D. Murphy, F. Abdel-Razzaq, R. Kwong, I. Tsyba, M. Bortz, B. Mui, R. Bau and M. E. Thompson, Synthesis and Characterisation of Phosphorescent Cyclometalated Iridium Complexes, *Inorg. Chem.*, 2001, 40, 1704-1711.
- 38 J. C. Scaiano, *Handbook of Photochemistry*, CRC Press, 1989, 2, 448
- 39 H. Riesen, L. Wallace and E. Krausz, Localised $^3\text{MLCT}$ Excitations of $[\text{Ru}(\text{bpy})_{3-x}(\text{bpy}-6,6'\text{-d}_2)_x]^{2+}$ ($x = 0-3$) in $[\text{Zn}(\text{bpy})_3](\text{ClO}_4)_2$ ($\text{bpy} = 2,2'$ -bipyridine), *Inorg. Chem.*, 1996, 35, 6908-6909.
- 40 J. S. Gold, S. J. Milder, J. W. Lewis and D. S. Kliger, Transient Circular Dichroism of the Luminescent State of $\text{Ru}(\text{bpy})^{2+}$, *J. Am. Chem. Soc.*, 1985, 107, 8285-8286.
- 41 D. H. Oh, M. Sano and S. G. Boxer, Electroabsorption (Stark Effect) Spectroscopy of Mono- and Biruthenium, Charge-Transfer Complexes: Measurements of Changes in Dipole Moments and other Electrooptic Properties, *J. Am. Chem. Soc.*, 1991, 113, 6880-6890.
- 42 P. J. Carroll and L. E. Brus, Picosecond Raman Scattering Study of Electron Localisation in the Charge-Transfer Excited State of Tris(bipyridine)ruthenium(II), *J. Am. Chem. Soc.*, 1987, 109, 7613-7616.
- 43 A. T. Yeh, C. V. Shank and J. K. McCusker, Ultrafast Electron Localisation Dynamics Following Photo-induced Charge Transfer, *Science*, 2000, 289, 935-938.

- 44 A. Beeby, S. Bettington, I. D. W. Samuel and Z. Wang, Tuning the Emission of Cyclometalated Iridium Complexes by Simple Ligand modification, *J. Mater. Chem.*, 2003, **13**, 80-83.
- 45 P. I. Djurovich, S. A. Lamansky, M. A. Nugent, D. L. Murphy, R. C. Kwong and M. E. Thompson, Ir(III) Cyclometalated Complexes as Efficient Phosphorescent Emitters in Polymer Blend and Organic LEDs, *Polym. Prep.*, 2000, **41**, 770-771.
- 46 R. Gao, D. G. Ho, B. Hernandez, M. Selke, D. Murphy, P. I. Djurovich and M. E. Thompson, Bis-cyclometalated Ir(III) Complexes as Efficient Singlet Oxygen Sensitisers, *J. Am. Chem. Soc.*, 2000, **124**, 14828-14829.
- 47 M. Nonoyama, Synthesis of a Few Derivatives of Cycloiridiated 2-(2-Thienyl)pyridine, *Bull. Chem. Soc. Jpn.*, 1979, **52**, 3749-3750.

Chapter 2

Organic Light Emitting Devices

This chapter will present an introduction to organic light emitting devices (OLEDs) and following this, a review of the performance of cyclometalated iridium(III) complexes as phosphorescent dopants within these types of devices will be discussed.

2.1 Introduction

Organic light emitting devices (OLEDs) are based on thin amorphous organic films that can be deposited on a variety of substrates, such as rigid glass or flexible polymer supports. There are various methods of depositing the doped polymer layer onto the OLED substrate; among others these include masked dye diffusion,¹ microcontact printing² and hybrid inkjet printing.³ Potentially this makes the manufacture of OLEDs relatively cheap and simple.

In addition to this, inorganic light emitting devices (LEDs) such as those based on In, Ga, Al and As semiconductors require crystalline substrates that allow the epitaxial growth of the active materials onto the surface. The organic films used in OLEDs are usually of the order of 500-1000 Å thick, which allows them only a low optical density even at their peak wavelength of absorption. This coupled with a large Stokes shift between their absorption and emission band maxima makes them effectively transparent to their own emission. The wider viewing angles and increased brightness at low voltages of OLEDs compared to that of liquid crystal displays (LCDs) means that OLEDs may in fact one day replace LCDs in many display applications.

In the case of OLEDs it is these qualities along with the use of the unique flexible polymer support that makes them an attractive option for applications such as portable/roll-up flat panel displays (FPDs) or as backlights.

2.2 Photoluminescence and Electroluminescence in Molecular Solids

2.2.1 Photoluminescence

A schematic representation of the process of photoluminescence (PL) in an organic molecular solid is shown in figure 2.1.⁴ In this process a high-energy photon ($h\nu$) is absorbed, promoting the molecule from its ground state, S_0 , to a singlet excited state, S_1 . A molecule occupying an S_1 state is known as a Frenkel exciton. The molecule can also be excited to a higher energy excited state, e.g. S_2 , but this is normally followed by rapid relaxation to the S_1 state by a non-radiative process called internal conversion (IC).

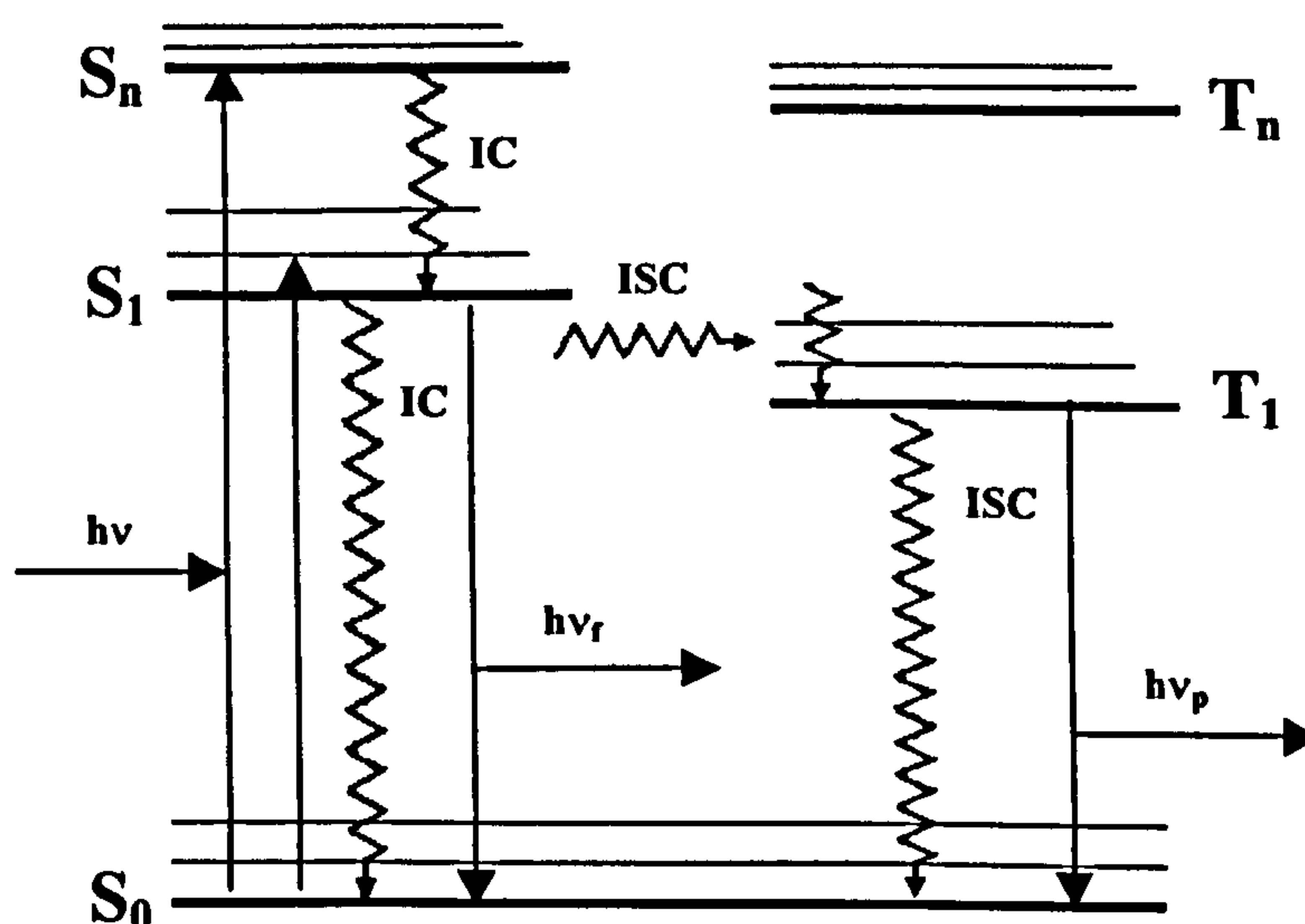


Figure 2.1 A Jabłonski diagram representing the excitation and subsequent emission from a molecular solid, non-radiative processes are depicted by a zig-zag arrow and radiative processes by a straight arrow.

In its excited state, the molecule undergoes a structural rearrangement, which causes the equilibrium geometries of the ground and excited states to be inequivalent. The geometries of S_0 and S_1 possess different interatomic separations (r -values) and this structural change results in the dominant transition being from the ground vibrational level of the ground state, S_0 , to a higher vibrational level of the excited state, S_1 . This is known as the Franck-Condon principle.⁵

The excited state molecule rapidly relaxes to its ground state *via* either a radiative (R) or a non-radiative (NR) energy process. In this instance, it will be assumed that this excited state molecule relaxes *via* a radiative decay process. Radiative relaxation from the lowest vibrational level of S_1 leads to a vibrationally excited state of S_0 , which rapidly relaxes to the ground state, the energy given out in this process is termed fluorescence.⁵

Another possibility is that the excited S_1 state may undergo inter-system crossing (ISC) to the triplet state T_1 . Subsequently, this vibrationally excited state may also undergo internal conversion to the lowest vibrationally excited state of T_1 and then may also undergo either radiative or non-radiative decay to the ground state, S_0 . The former process allows the emission of energy and is called phosphorescence.⁵

Overall, this figure illustrates that the excitation energy is greater than the energy of emission and that the difference between these two energies will be greatest for molecules, which have a large structural change between their ground and excited states.

2.2.2 Electroluminescence

Electroluminescence (EL) is a process where by a molecule may be electronically excited by the application of an electric field, thus allowing it to attain the states depicted in figure 2.1. In general, the shape of the EL spectrum is identical to that seen in photoluminescence. For closed shell molecules, the ground state, S_0 , has two spin-paired electrons in its highest occupied molecular orbital (HOMO) and a vacant lowest unoccupied molecular orbital (LUMO). In the S_1 state both the HOMO and the LUMO are singly occupied, as shown in figure 2.2.⁴

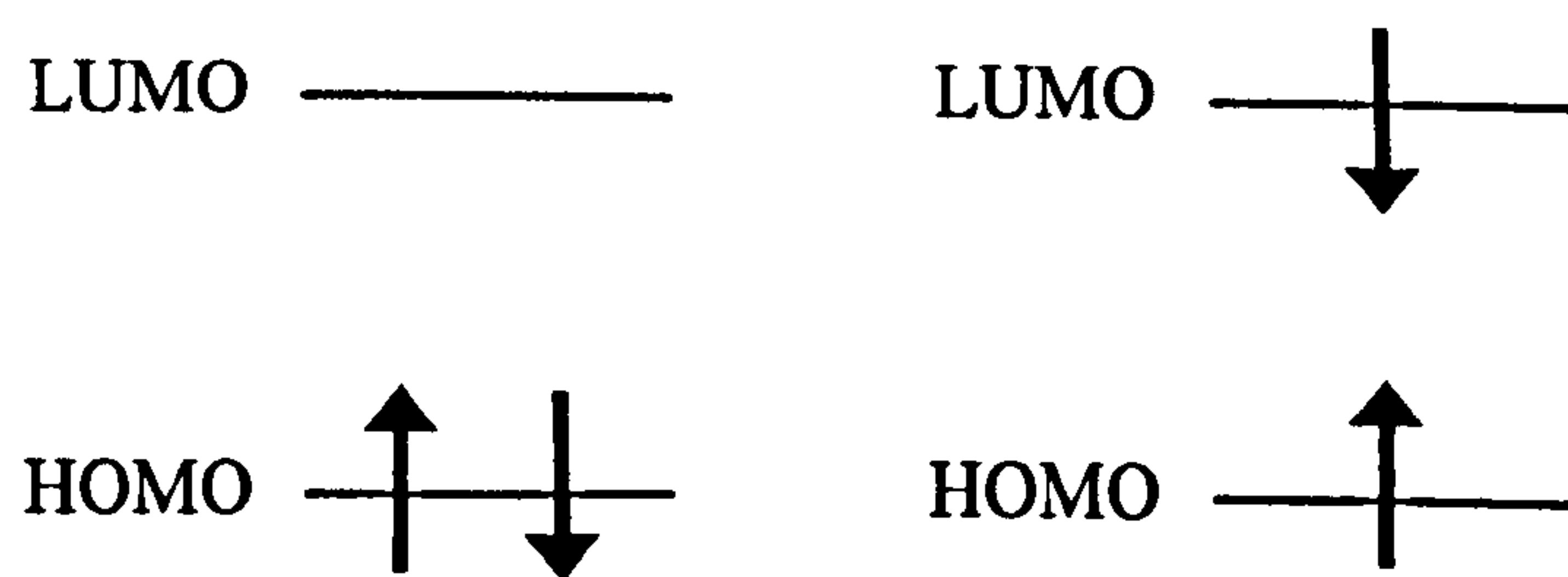


Figure 2.2 The ground state, S_0 , and singlet excited state, S_1 , of a closed shell molecule.

Consider a simple OLED, consisting of a thin organic film situated between an indium-tin oxide (ITO) anode and a metal cathode. When a potential is applied to the device, material is oxidised at the anode and reduced at the cathode. This corresponds to the injection of positive holes and electrons, respectively, into the thin-film, figure 2.3. The organic film consists of weakly interacting molecules, where the oxidised and reduced versions correspond to the molecular sites where the holes and electrons are

located respectively. In the presence of an applied field the holes and electrons are able to drift through the film *via* a hopping mechanism.

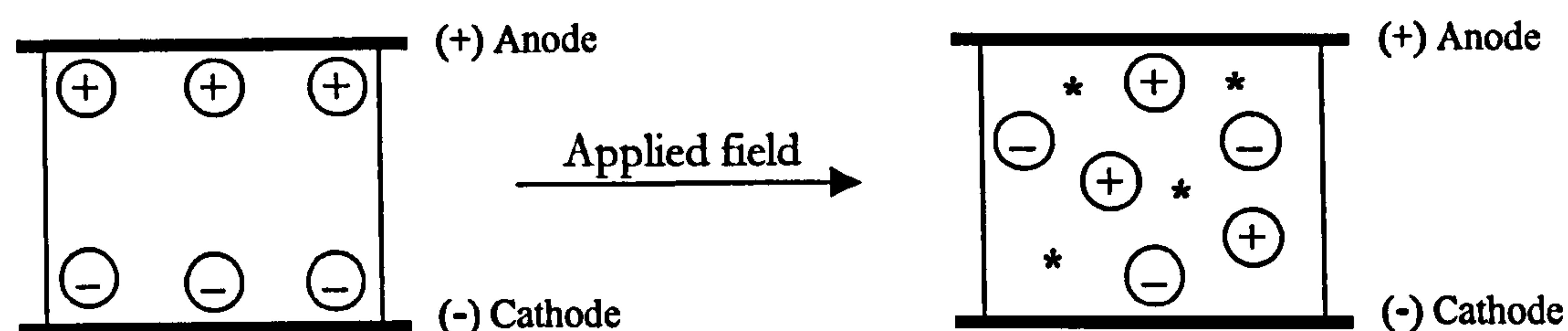


Figure 2.3 Injection and migration of charge in an organic film.

The holes and electrons are removed either at the opposite electrode or when they encounter an oppositely charged species within the film. In the latter case, electron transfer occurs from the electron carrier to the oxidised molecule (hole carrier) forming an exciton, an excited state molecule, which may decay radiatively to produce luminescence, this species is depicted by * in figure 2.3.

The products of this final hopping step are a molecule in its ground electronic state, S_0 , and an adjacent molecule in the S_1 (Frenkel) state. The excited S_1 state can then relax to its ground state by the same mechanisms as previously described for photoluminescence. The close relationship between EL and PL stems from the fact that the emission originates from the same excited state in both these processes, the Frenkel exciton. It is this relationship between PL and EL in molecular materials, which has been utilised in designing new chromophores for implementation in OLEDs. The PL spectrum of a compound is therefore used as a preliminary assessment of the EL spectrum of the material.

2.3 Efficient Electroluminescent Devices

2.3.1. Device Structure

A number of different criteria need to be satisfied to produce a high probability for electron and hole radiative recombination and hence emission within the film. Energy barriers for injection of holes and electrons need to be roughly equal to ensure a balance between the injected electron and hole densities.

This is achieved *via* the use of multiple organic layers, where each layer is optimised for its particular role as a charge carrier, charge injector or light emitter. An example of this is seen in figure 2.4.⁴ This shows a ‘double heterostructure’ OLED, which utilises an ITO coated glass substrate, upon which a hole transporting layer (HTL), an emissive material (EM) and an electron transporting layer (ETL) are sequentially deposited in a vacuum. This multi-layer system is capped with a low work function metal as the cathode, such as magnesium, aluminium or calcium.

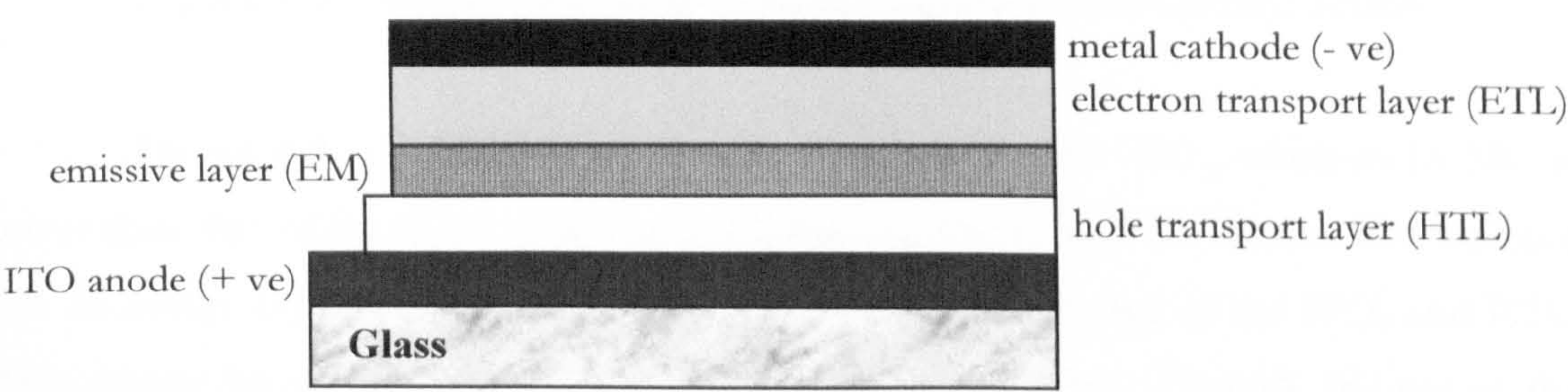


Figure 2.4 A schematic diagram showing the cross-section of a double heterostructure OLED.

The HTL and ETL have high mobilities for holes and electrons respectively, but very low mobilities for the oppositely charged carriers. If an electric field is applied to the device, holes will move through the HTL/EM interface and electrons will move through the ETL/EM interface. These carriers then combine to form an exciton in the EM layer and subsequent radiative relaxation leads to efficient light emission. The materials chosen for each of these individual layers are selected based on the relative energies of their S_0 and S_1 states as well as their transport properties. A band structure for a typical double heterostructure device is shown in figure 2.5.⁴

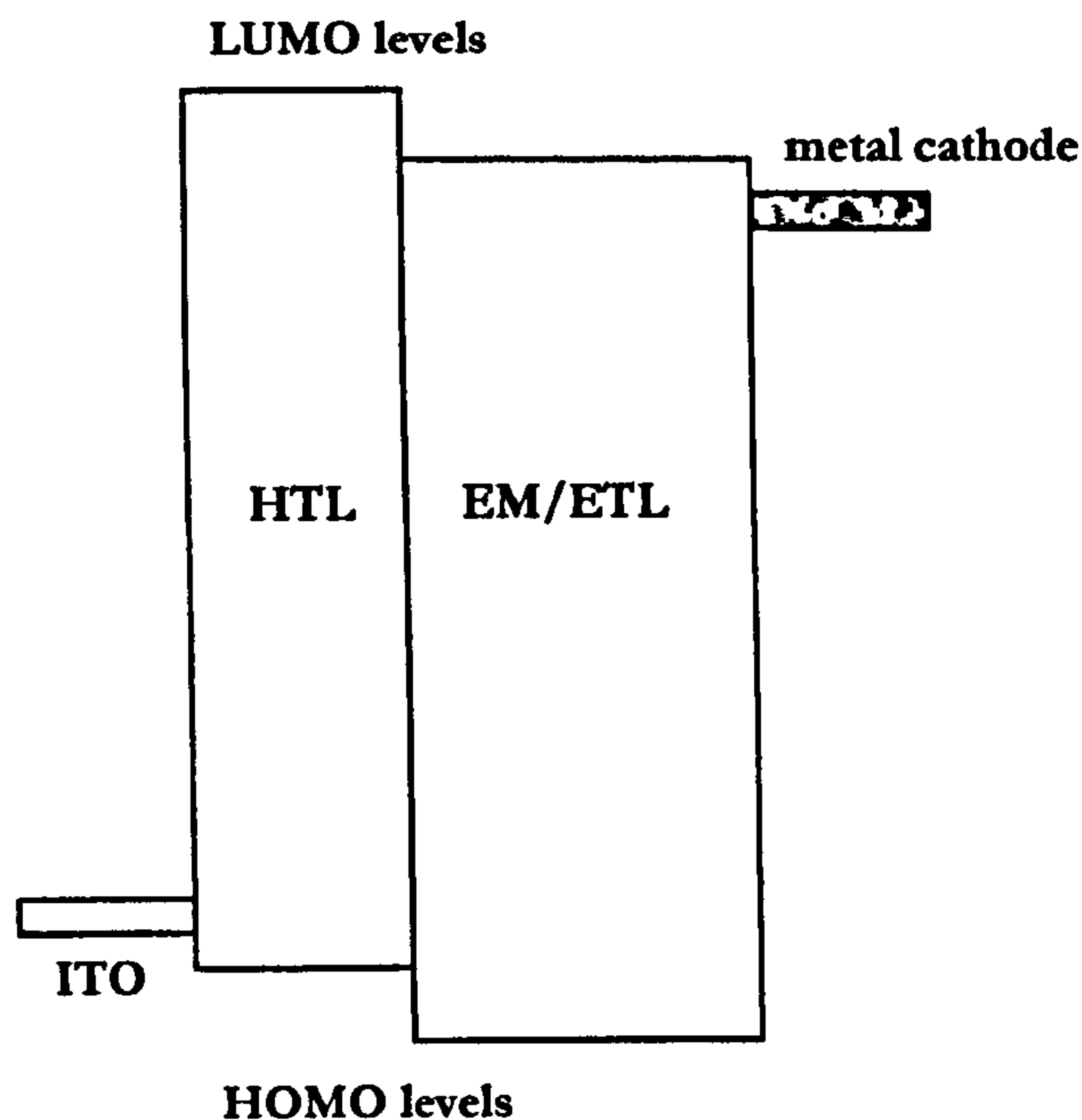


Figure 2.5 A band structure for a typical double heterostructure device.

The HOMO of the EM layer is higher than that of the HTL, whilst its LUMO is lower than that of the ETL. It is also important to ensure that the chosen EM material has an energy gap/band gap (HOMO-LUMO) smaller than that of the HTL and ETL. This causes the confinement of the excitons in the EM layer. Overall, the use of the suitable materials for the HTL and ETL makes it possible to trap/confine both carriers and excitons within this region, hence preventing non-radiative losses, at the electrode surfaces.

The thickness of each layer is also important. The first efficient EL device was a single heterostructure, shown schematically in figure 2.6, which comprised a tertiary amine as the HTL and an aluminium complex serving both as the ETL and EM in a single layer.⁶

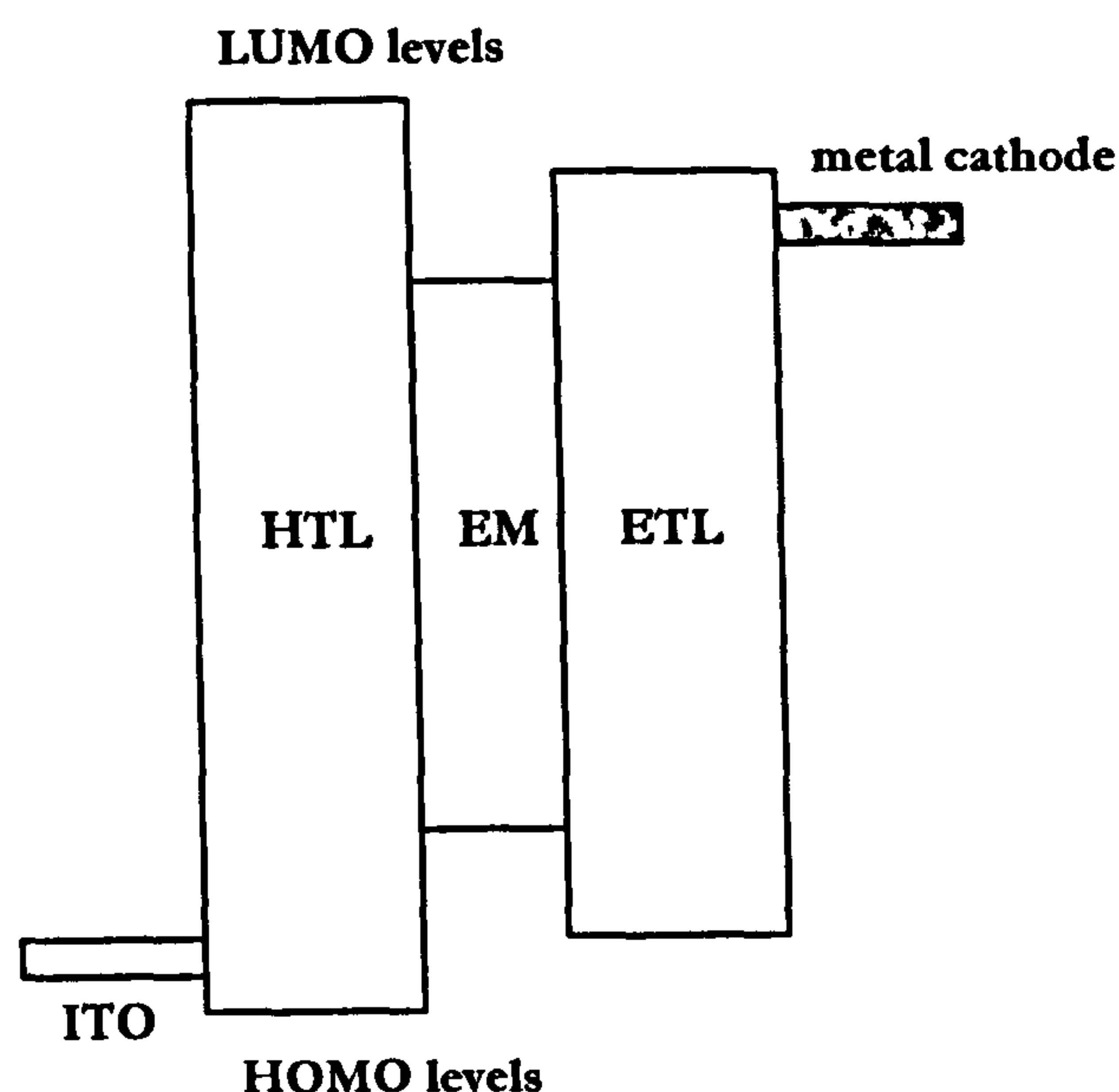


Figure 2.6 A band structure for a typical single heterostructure device.

In this particular device, the preferred conductivity of holes in the HTL and electrons in the ETL leads to a build up of carriers at the HTL/ETL interface. Hence excitons are formed at the interface, but are not spatially confined. As a result of this, it is important that the thickness of the ETL/EM layer is chosen so that the majority of the excitons decay radiatively prior to reaching the adjacent electrode.

In certain devices the HTL and ETL materials do not need to be segregated into individual layers to achieve high efficiency. A polymeric HTL and either a molecular or polymeric light emitter and an electron transport (ET) material can be prepared in a homogenous blend. The resulting OLED consists of a single organic film sandwiched between an ITO anode and a metal cathode, with the recombination occurring in the polymer thin film. Polymers and monomeric metal species have been used successfully in these devices to give colours that span the visible spectrum.⁷

2.3.2 The Electrodes

The choice of suitable materials/metals for the electrodes is based on the energies of the filled and vacant states of the organic material relative to the work functions of these contacts. ITO is well matched to inject holes into the HTL HOMO and low work

function metals such as magnesium, aluminum and calcium can inject electrons into the ETL LUMO.

Under forward bias (ITO positive) the injection of holes into the HTL and electrons into the ETL occurs at low potentials ($\sim 5\text{V}$), while reversing the bias requires a much higher potential to inject current density, i.e. it behaves as a diode.

2.3.3 The Emitting Material

The emissive layer (EM) need not consist solely of one emissive species for exciton confinement to occur. Self-quenching within a homogeneous emissive film can be avoided by doping a host layer with a much lower concentration of the emissive guest/dopant molecule.⁸ For the dopant to function as an efficient electron hole or trap, it must possess an energy gap that is smaller than that of the host in order to allow it to act as an 'exciton trap'.

If this is true, then rapid Förster⁹ energy transfer (exciton transfer) from the host matrix to the dopant, or charge carrier trapping by the dopant itself, more commonly known as Dexter excitation transfer,⁹ will allow excitons to be effectively trapped on the dopant molecules. This leads to improved EL efficiency and emission that is characteristic of the dopant species.

Dexter energy transfer (electron exchange excitation transfer) occurs as a result of an electron exchange mechanism.⁹ It requires the overlap of the wavefunctions of the donor and the acceptor. It is the dominant mechanism in triplet-triplet energy transfer, where the rate of energy transfer is given by, k_{ET} , in equation 2.1.

$$k_{\text{ET}} \propto \frac{h}{2\pi} P^2 J \exp \frac{-2r}{L} \quad 2.1$$

Where, h = Planck's Constant (6.626×10^{-34} Js), J = spectral overlap integral between the absorption spectrum of the donor (D) and the emission spectrum of the acceptor (A) ($\text{cm}^6 \text{mol}^{-1}$), r = the distance between the donor and acceptor (cm) and P and L = constants.

For a fluorescent dopant, induced dipole (Förster) energy transfer from the host to the guest's singlet state is a spin-allowed process. The rate of Förster energy transfer, $k_{D \rightarrow A}$, can also be written as shown in equation 2.2.⁹

$$k_{D \rightarrow A} = k \left(\frac{r_0}{r} \right)^6 \quad 2.2$$

Where, k = decay rate of excited state host molecules (s), r = distance between the donor and acceptor (cm), r_0 = critical quenching radius (cm), the distance at which $k_{D \rightarrow A}$ is equal to the inverse of the radiative lifetime.

Generally, a larger r_0 value is obtained when the emission spectrum of the host and the absorption spectrum of the guest overlap strongly.

For a phosphorescent dopant, Förster energy transfer to the triplet state is forbidden by spin conservation. However, energy transfer can occur by the sequential combination of Förster transfer to the singlet state with electron exchange (Dexter energy transfer). Dexter transfer is the physical coherent transfer of an exciton from a donor to an acceptor site at a rate proportional to the orbital overlap of the donor and acceptor molecules. Subsequently, this is a short-range process that attenuates exponentially with distance, as described in equation 2.2.

Dexter energy transfer processes allow for the transfer of triplet excitons because only the total spin of the donor-acceptor complex is conserved. Hence it is possible for both singlets and triplets to induce phosphorescence, thus increasing the theoretical efficiency of the OLED device.⁴

The external EL quantum efficiency, Φ_{EL} , of an OLED, which is the number of photons emitted per electron injected, can be described by equation 2.3.¹⁰

$$\Phi_{EL} = (\chi_s \Phi_f \eta_s + \chi_t \Phi_{ph} \eta_t) \eta_i \eta_e \quad 2.3$$

χ_s and χ_t are the fractions of singlet and triplet excitons, where $\chi_t = (1 - \chi_s)$, Φ_f and Φ_{ph} are the PL efficiencies of fluorescence and phosphorescence of the acceptor, η_s and η_t

are the transfer efficiencies of the singlet and triplet excitons from the donor to the acceptor molecules, η_i is the fraction of injected charge carriers that form excitons on the donor and η_e is the fraction of emitted photons that are coupled out of the device.

2.3.4 Spin Statistics

According to the simplest quantum mechanical assumption, the ratio of the production of singlet and triplet excited states is 1:3.¹¹ Under electrical excitation recombination of the hole/electron pairs can lead to excitons in both symmetry states. Thus harvesting luminescence from all excitons has the potential to yield significantly higher efficiencies than is possible in devices containing purely fluorescent emitters. This can of course be done using a phosphorescent dopant whereby both singlet and triplet excited states participate.

A range of luminescent and laser dyes have been developed with emission wavelengths which span the visible spectrum. The high luminescent quantum efficiencies of these materials in dilute solution make them excellent candidates as dopant emitters in OLEDs and many have already been incorporated into such devices. Examples of these emissive materials span polymeric materials such as carbazole derivatives,¹² dendrimers¹³ and small molecules such as *fac*-Ir(ppy)₃.¹⁴

2.4 Device Lifetime and Degradation

The degradation mechanisms of OLEDs can be divided into two categories, recoverable and unrecoverable degradation (real degradation).

2.4.1 Recoverable Degradation

Many OLED devices contain ionic impurities, which influence the lifetime of the device considerably. Degradation associated with these impurities is usually observed within the first few minutes after a bias has been applied. It is believed that ionic species may cause this degradation *via* the formation of an internal electric field in the opposite direction to

the applied external field.¹⁵ This may be the crucial feature as to why OLEDs prepared by solution processing are generally found to have poorer durability than those prepared by dry vacuum processing techniques.⁴

Zou *et al.*¹⁵ studied the recovery rates of a double layer OLED where the poly(N-vinylcarbazole) (PVCz) layer doped with coumarin-6 was fabricated from solution *via* spin-coating and the tris-(8-hydroxyquinoline)-aluminium (Alq₃) and Mg:Al layers were prepared by vacuum deposition. After applying a constant forward bias during the time interval between t_1 and t_2 a decrease in current density and luminance was clearly visible. At t_2 the forward bias was released for 10 minutes and at t_3 the bias was set to its initial value, as between t_1 and t_2 . The current density and luminance now displayed higher values at t_3 than at t_2 . This increase indicated that a spontaneous recovery had occurred between t_2 and t_3 . Subsequently, at t_3 they applied a forward bias and current density and luminance was observed at levels similar to those seen between t_1 and t_2 . At t_4 the forward bias was released and instead a negative bias was applied for 10 minutes and at t_5 the bias was re-set to its initial positive value. As a result of the applied negative bias higher current density and luminance levels were observed at t_5 than those at t_1 , this is depicted in figure 2.7 below.¹⁵

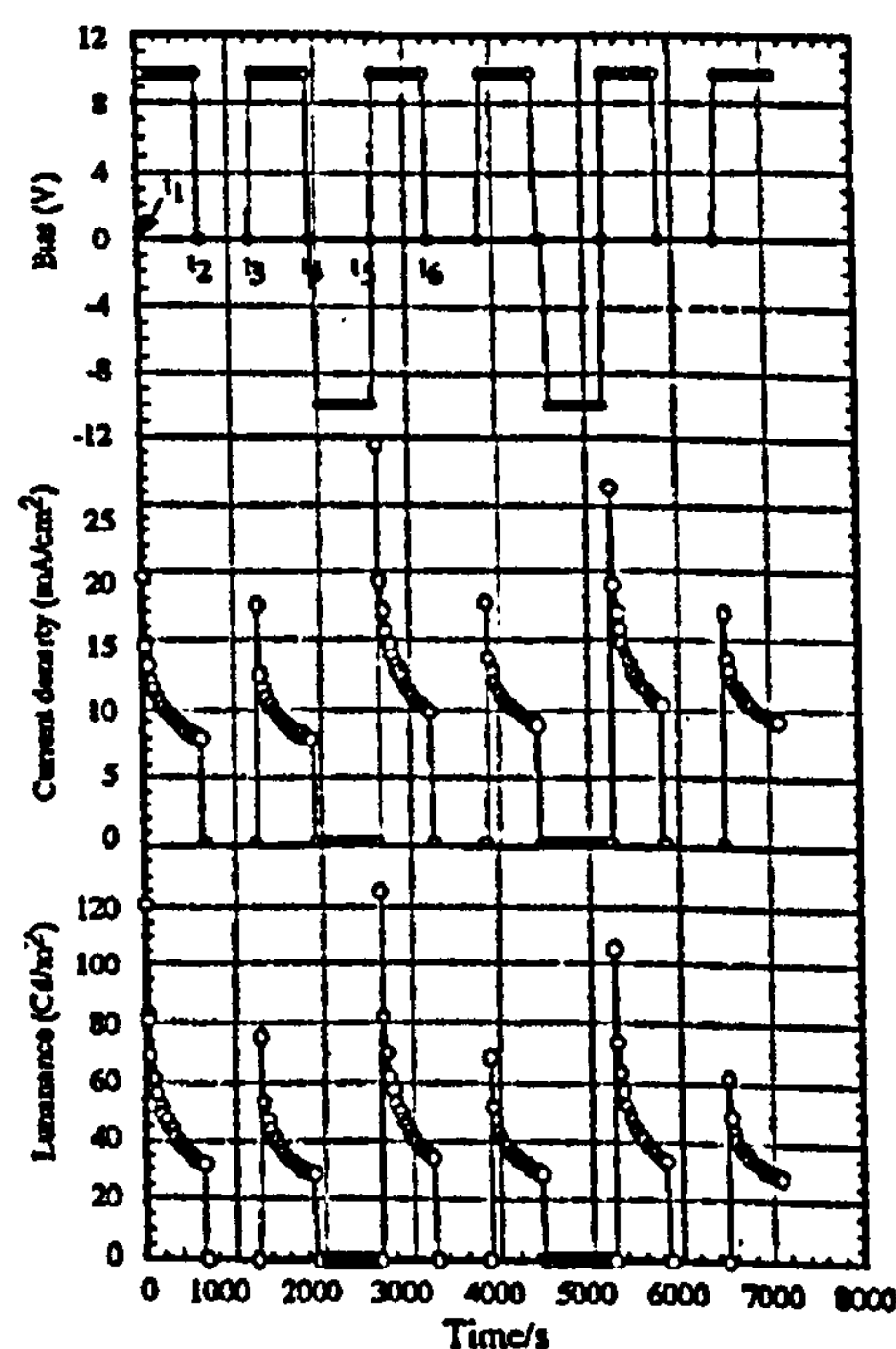


Figure 2.7 The phenomenon of spontaneous recovery and electric-field induced recovery in a double layer OLED.

This effect is referred to as an electric field induced recovery or electric-field induced enhancement. Zou *et al.*¹⁵ also demonstrated that this phenomenon is reproducible. In addition to this, their findings also illustrated that the recovery rate and speed depend upon the magnitude of the negative bias as well as the time interval over which the bias is applied.

2.4.2 Unrecoverable Degradation

This is the term used to describe the degradation that appears when layers in the device undergo a chemical and/or physical change. These alterations can stem from inhomogeneity and the presence of moisture and/or oxygen within the device and can manifest themselves as 'dark spots' and areas of crystallisation.⁴

2.5 Cyclometalated Iridium(III) Complexes in OLEDs

In 1998 Hoshino *et al.*¹⁶ reported one of the first examples of an OLED using an electrophosphorescent dopant in a polymer host. They observed the electroluminescence of benzophenone doped into poly(methylmethacrylate) (PMMA) at 100 K. Though only low-efficiency luminescence was achieved no emission from the host material was detected.

In 1999 Baldo *et al.*¹⁷ described the highly efficient phosphorescent emission from OLEDs containing the organometallic platinum porphine complex 2,3,7,8,12,13,17,18-octaethyl-21H,23H-porphine platinum(II) (PtOEP). The addition of Pt to the porphine ring reduced the phosphorescence lifetime by increasing the spin-orbit coupling of the system and effectively enhanced the inter-system crossing from the first singlet excited state to the triplet excited state. The host material, tris-(8-hydroxyquinoline) aluminium (Alq₃), also an electron transport material, was selected for its peak emission wavelength at 530 nm where PtOEP exhibits strong absorption.

2.5.1 *Fac*-Ir(ppy)₃ in OLEDs

In 1999, Baldo and co-workers¹⁴ also described the performance of an organic light-emitting device employing the green electrophosphorescent material *fac*-tris(2-phenylpyridine) iridium, *fac*-Ir(ppy)₃. The iridium complex was doped into a 4,4'-N,N'-dicarbazole-biphenyl host (CBP). The proposed energy level structure of the device is shown in figure 2.8.¹⁴

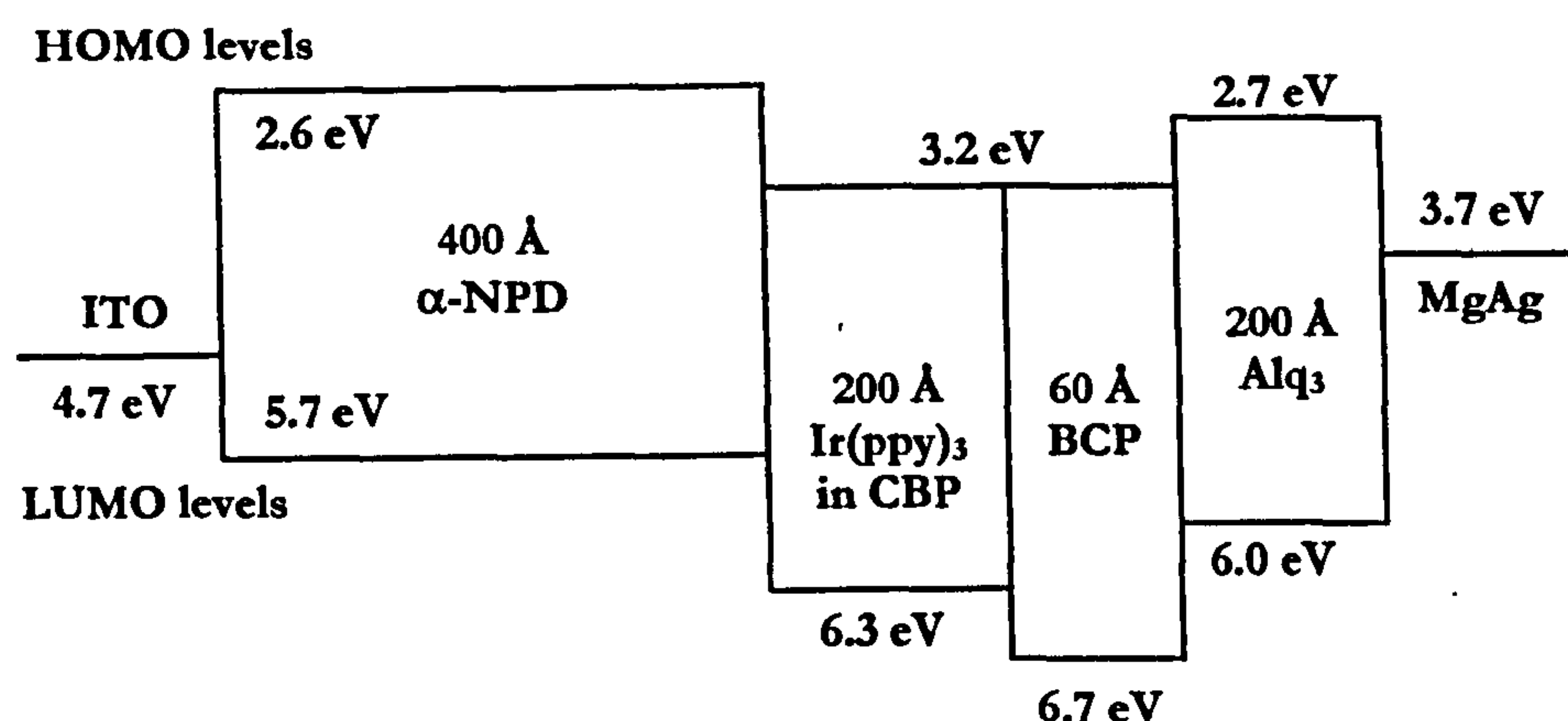


Figure 2.8 Proposed energy level structure for an electrophosphorescent device containing *fac*-Ir(ppy)₃.

The organic layers were deposited by high-vacuum (10^{-6} Torr) thermal evaporation onto a cleaned glass substrate that was precoated with a transparent layer of the conductive material indium-tin-oxide. A 400 Å thick layer of 4,4'-bis[N-(1-naphthyl)-N-phenylamino] biphenyl (α -NPD) was used to transport holes into the luminescent layer of Ir(ppy)₃ doped into CBP and a 200 Å thick layer of Alq₃ was used as the electron transport material. A shadow mask with 1mm-diameter openings was used to define the cathode consisting of a 1000 Å thick layer of 25:1 Mg:Ag.

O'Brien *et al.*¹⁸ reported the use of a thin (60 Å) barrier layer of 2,9-dimethyl-4,7-diphenyl-1,10-phenanthroline (bathocuproine/BCP) inserted between the CBP and the Alq₃ as necessary to confine excitons within the luminescent region and hence maintain high efficiencies. Here it was also argued that this layer prevented triplets from diffusing outside of the doped region. They also suggested that CBP may readily transport holes and that BCP may be required to force exciton formation within

the luminescent layer. Baldo *et al.*¹⁴ stated that transient studies of triplet exciton diffusion within CPB were needed to resolve this question. In either case the use of BCP, in figure 2.8¹⁴ above, clearly serves to trap excitons within the luminescent region. Figure 2.9¹⁴ shows the external quantum efficiencies of several Ir(ppy)₃-based OLEDs. All devices have the same structure as shown in figure 2.8, except for the 100 % device where the Ir(ppy)₃ layer is 300 Å thick and there is no BCP blocking layer and the 6 % device there is no BCP blocking layer.

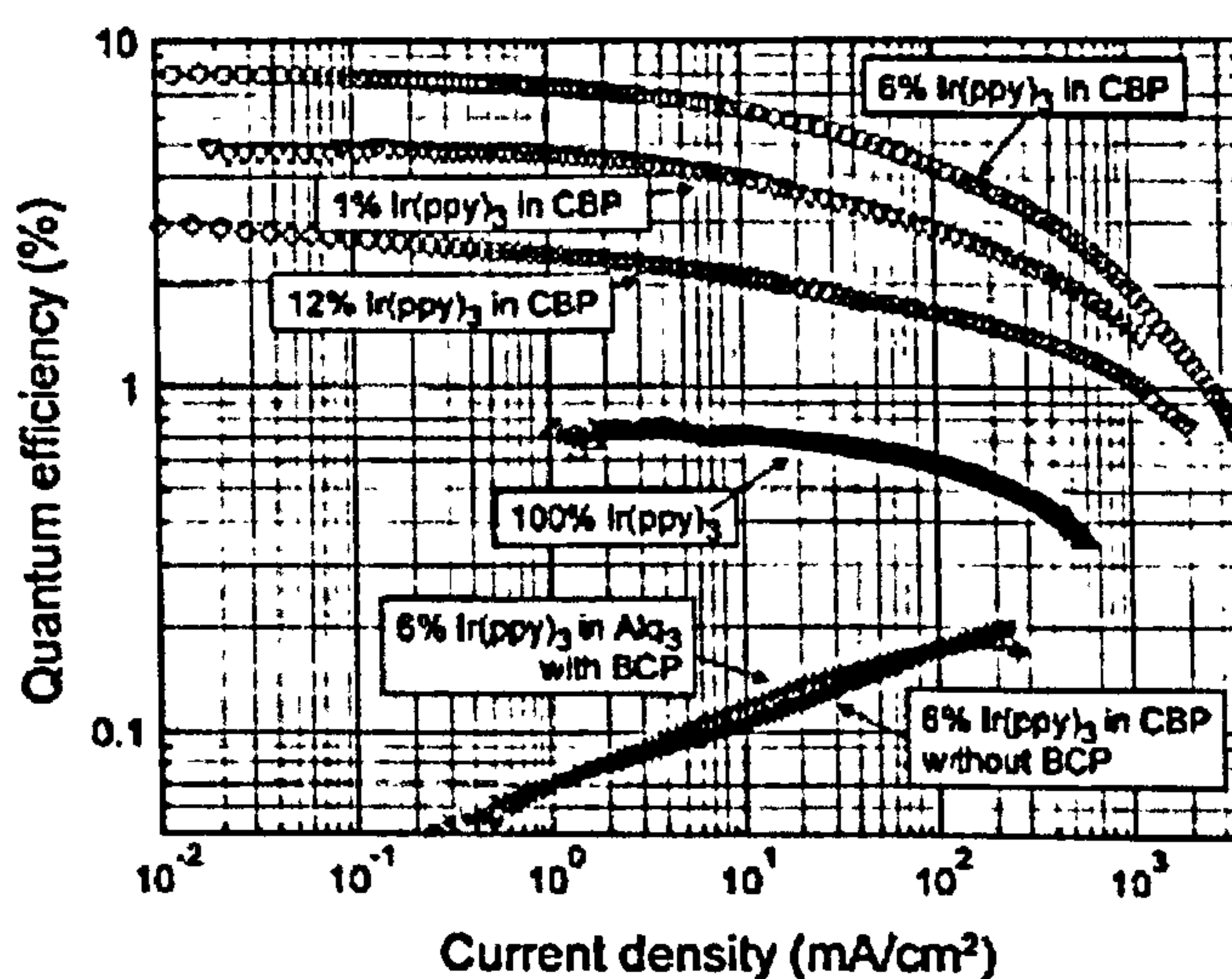


Figure 2.9 The external quantum efficiency of OLEDs using Ir(ppy)₃:CBP emissive layers.

There is a decrease in quantum efficiency with increasing current. This result is similar to that achieved in the Alq₃:PtOEP system,¹⁷ in which the doped device possessed a maximum efficiency of ~ 8% for mass ratios of Ir(ppy)₃:CBP of approximately 6%-8%. This fact also suggests that the energy transfer pathway for Ir(ppy)₃:CBP is likely to be similar to that in the Alq₃:PtOEP system,¹⁷ i.e. *via* short-range Dexter transfer of triplets from the host.

At low Ir(ppy)₃ concentrations, the lumophores often lie beyond the Dexter transfer radius of an excited Alq₃ molecule, while at high concentrations, aggregate quenching is increased. It should be noted that dipole-dipole (Förster) transfer is forbidden for triplet transfer and in the PtOEP:Alq₃ system direct charge trapping was not found to be significant. Baldo *et al.*¹⁴ also constructed a heterostructure device where the luminescent region was made from a homogeneous film of Ir(ppy)₃. The efficiency

the luminescent layer. Baldo *et al.*¹⁴ stated that transient studies of triplet exciton diffusion within CPB were needed to resolve this question. In either case the use of BCP, in figure 2.8¹⁴ above, clearly serves to trap excitons within the luminescent region. Figure 2.9¹⁴ shows the external quantum efficiencies of several Ir(ppy)₃-based OLEDs. All devices have the same structure as shown in figure 2.8, except for the 100 % device where the Ir(ppy)₃ layer is 300 Å thick and there is no BCP blocking layer and the 6 % device there is no BCP blocking layer.

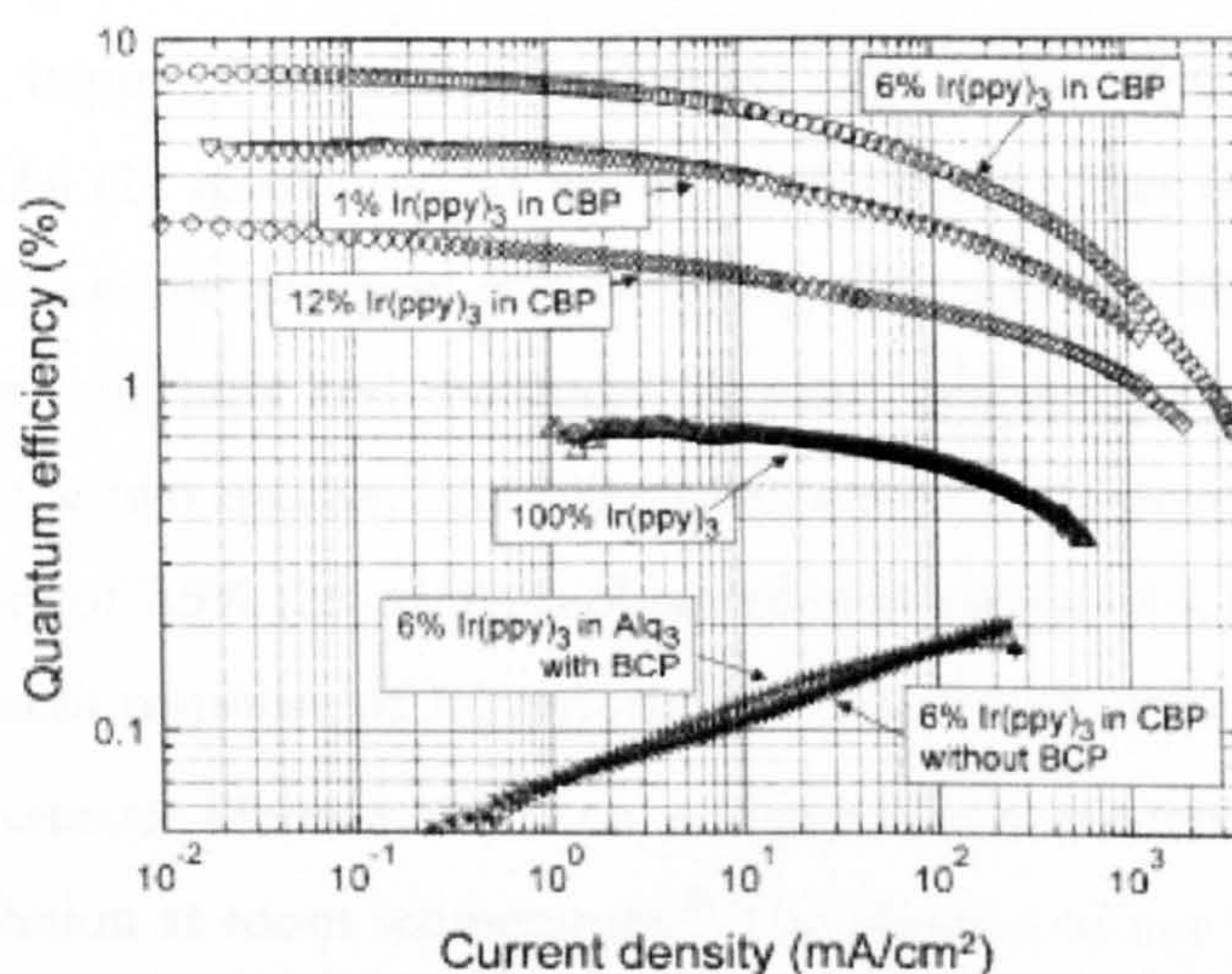


Figure 2.9 The external quantum efficiency of OLEDs using Ir(ppy)₃:CBP emissive layers.

There is a decrease in quantum efficiency with increasing current. This result is similar to that achieved in the Alq₃:PtOEP system,¹⁷ in which the doped device possessed a maximum efficiency of ~ 8% for mass ratios of Ir(ppy)₃:CBP of approximately 6%-8%. This fact also suggests that the energy transfer pathway for Ir(ppy)₃:CBP is likely to be similar to that in the Alq₃:PtOEP system,¹⁷ i.e. *via* short-range Dexter transfer of triplets from the host.

At low Ir(ppy)₃ concentrations, the lumophores often lie beyond the Dexter transfer radius of an excited Alq₃ molecule, while at high concentrations, aggregate quenching is increased. It should be noted that dipole-dipole (Förster) transfer is forbidden for triplet transfer and in the PtOEP:Alq₃ system direct charge trapping was not found to be significant. Baldo *et al.*¹⁴ also constructed a heterostructure device where the luminescent region was made from a homogeneous film of Ir(ppy)₃. The efficiency

of this device was found to be $\sim 0.8\%$, figure 2.8.¹⁴ This low efficiency was also reflected in the transient decay of the neat Ir(ppy)_3 film which had a lifetime of only ~ 100 ns and was found to deviate considerably from mono-exponential behaviour.

The 6% Ir(ppy)_3 :CBP devices with and without the BCP barrier layer can also be seen in figure 2.8.¹⁴ Very low quantum efficiencies are observed for these two device configurations, although they are found to increase with current. This behaviour suggests a saturation of non-radiative sites as excitons migrated into the Alq_3 , either in the luminescent region or adjacent to the cathode.

The 6% Ir(ppy)_3 :CBP device exhibited peak external quantum and power efficiencies of 8.0% (28 cd/A) and 31 lm/W, respectively. This remarkable result was ascribed to bipolar carrier transport in CBP along with a favourable triplet energy level alignment between the host and the guest (dopant), which promotes efficient energy transfer between the two species.¹⁹ At 100 cd/m², a power efficiency of 19 lm/W with a quantum efficiency of 7.5% (26 cd/A) is obtained at a voltage of 4.3 V.

The transient response of Ir(ppy)_3 in CBP was found to be a mono-exponential with a phosphorescence lifetime ~ 500 ns, compared to a lifetime of 2 μs in degassed dilute toluene solution at room temperature.²⁰ The absence of any Ir(ppy)_3 fluorescence in the transient response, as seen in solution, suggests that Ir(ppy)_3 possesses strong intersystem crossing from the singlet to the triplet state. Therefore all emission originates from the long-lived triplet state. This slow triplet relaxation can form a 'bottleneck' in electrophosphorescence, however the short triplet lifetime of Ir(ppy)_3 is a major advantage in this kind of system. This results in only a gradual decrease in efficiency with increasing current, leading to a maximum luminance of $\sim 100,000$ cd/m².

The electroluminescent spectrum of 6% Ir(ppy)_3 :CBP shows the peak wavelength to be 510 nm. The Commission Internationale de L'Eclairage (CIE) co-ordinates²¹ were found to be $x = 0.27$, $y = 0.63$ and are independent of current. At very high current densities (~ 100 mA/cm²) it was found that blue emission from CBP was negligible. This indicated that there was complete energy transfer.

As triplet emission is red-shifted from singlet emission, it may be difficult to find guest/host systems where the phosphorescent guest emits in the blue or green. Blue fluorescent emission has been demonstrated using polyfluorene, CBP and perylene,²² however the additional exchange energy loss must be overcome at some stage in the

energy transfer to the triplet state of the phosphorescent guest. This may be a problem in the blue, where wide-gap (~ 3.5 eV) host materials are necessary.

It is clear from work carried out by Baldo *et al.*¹⁴ that the efficiency improvements offered by phosphorescence outweigh the slight increase in voltage that results from the use of large-energy-gap materials. The alternative is to use the phosphorescent material as an undoped film resulting in a loss in efficiency. They concluded that the potential use of purely organic phosphors should not be ruled out and that the application of transition-metal compounds containing organic ligands in these types of devices had produced most promising results so far. The transition-metal itself mixes the singlet and triplet states which enhances inter-system crossing and reduces the lifetime of the triplet excited state. Their work demonstrated that reasonable photoluminescent efficiencies and lifetimes of the order of 1 μ s are sufficient for high-performance devices.

These results were confirmed by Tsutsui *et al.*²³ later that year. Their results also demonstrated that the durability of materials used for organic light-emitting devices with phosphorescent emitters is comparable to those used in conventional organic materials for singlet emitters.

Further work by Adachi *et al.*²⁴ described the use of different ET layers as hosts for the Ir(ppy)₃ species within both single and double heterostructure devices. A maximum external quantum efficiency (η_{ext}) of $15.4 \pm 0.2\%$ and a luminous power efficiency of 40 ± 2 lm/W were achieved using a naphthyl-triazole derivative as the ET layer host. Based on the performance characteristics of single and double heterostructures containing layers of different thicknesses they concluded that exciton formation in Ir(ppy)₃ occurred within close proximity to the hole transport layer/ETL:Ir(ppy)₃ interface.

Since then various host materials have been investigated for use in OLEDs containing Ir(III) complexes such as Ir(ppy)₃. Yang *et al.*²⁵ studied the use of poly(N-vinylcarbazole) (PVK) as the host material for Ir(ppy)₃. Their work included the fabrication of double and triple layer devices which used either Alq₃ or 1,3-bis[4-tert-butylphenyl]-1,3,4-oxadiazolyl]phenylene (OXD-7) as the electron transport layer. In addition to this they tested the efficiency of 2,9-dimethyl-4,7-diphenyl-1,10-phenanthroline (BCP) as a hole blocking layer. The double layer device which was composed of PVK doped with 6.8 wt% Ir(ppy)₃ and

OXD-7 gave an external quantum efficiency of 7.5% and power luminous efficiency of 5.8 lm/W at the luminance of 106 cd/m² (current density of 0.40 mA/cm² and drive voltage of 14.5 V).

Further work conducted by Lee *et al.*²⁶ using PVK as a host for Ir(ppy)₃, concluded that the emission spectrum of the device exhibited no emission from the PVK. This indicates that energy transfer from PVK to Ir(ppy)₃ is efficient. This also demonstrated that efficient electrophosphorescent light-emitting devices could be realised with polymers.

2.5.2 Fluorine Substituted Iridium(III) Complexes for OLEDs

In 2000 Djurovich *et al.*²⁷ synthesised and characterised the complex, *fac*-tris[2-(4',5'-difluorophenyl)pyridine-C',N] iridium(III) (FIrppy). PVK-based LEDs were chosen for its implementation based on its good solubility in organic solvents.

The single-layer polymer blend ITO/PVK:PBD:FIrppy/Mg:Ag/Ag PBD = 2-(4-biphenyl)-5-(4-tert-butylphenyl)-1,3,4-oxadiazole) devices showed efficient green electrophosphorescence originating from exciton radiative recombination on FIrppy molecules. The introduction of the electron-withdrawing fluorine atoms results in an increase in the triplet excitation energy and hence a blue-shift in the emission compared to that of Ir(ppy)₃. The quantum efficiency of the LEDs exhibited strong dye concentration dependence with a maximum of ca. 1.7% at 2.5% - 3.5 wt% of FIrppy. After reaching the peak quantum efficiency as a function of current passed the efficiency was found to drop more sharply than in conventional fluorescence-based LEDs, which indicated that a triplet-triplet annihilation process was occurring in the FIrppy devices.

The following year, Wang *et al.*²⁸ also described the use of the fluorinated iridium complex, *fac*-tris[5-fluoro-2-(5-trifluoromethyl-2-pyridinyl)phenyl-C,N]iridium (IrFppyCF₃), as an efficient EL material in an OLED device. The emissive layer within the device was made solely of a thin undiluted film of the IrFppyCF₃ complex in the absence of a charge transporting host material. The device produced intense electroluminescence at 525 nm with an efficiency of 20 cd/A and a maximum radiance of 4800 cd/m². This result indicates that IrFppyCF₃ has comparable charge transporting properties compared to Ir(ppy)₃ where lower efficiencies were obtained from similar

devices containing homogenous films of the complex.¹⁴ Wang *et al.*²⁸ described the improved efficiency as arising from the replacement of C-H bonds with C-F bonds. The C-H bond is an effective promoter of excited state radiationless decay, whereas a C-F bond, possessing a lower vibrational frequency, can reduce the rate of deactivation. The presence of fluorine atoms can sometimes enhance the electron mobility of the compound²⁹ and also aid sublimation to provide better film deposition. In addition to this, the difference in the molecular packing of IrFppyCF₃ compared to Ir(ppy)₃ may also serve to reduce the self-quenching behaviour in the films.

Work carried out by Adachi *et al.*³⁰ described the use of the fluorinated iridium(III) complexes bis-(4,6-difluorophenyl)-pyridinato-N,C^{2'})-picolate iridium(III) (Ir(F₂ppy)₂pic) and -acetylacetonate iridium(III) (Ir(F₂ppy)₂acac) in CBP-based OLEDs. At 100 K, the transient phosphorescence decay of a 6 % Ir(F₂ppy)₂pic:CBP film was recorded. In addition to the prompt phosphorescence observed from Ir(F₂ppy)₂pic, Adachi *et al.*³⁰ also recorded an extremely long decay component lasting for ~ 10 ms. Since the PL spectrum of this slow component coincides with that of Ir(F₂ppy)₂pic, this supports the idea that exothermic energy transfer from Ir(F₂ppy)₂pic to CBP occurs. The triplet state then migrates through the CBP host molecules and finally is endothermically transferred back to the Ir(F₂ppy)₂pic, resulting in the delayed blue phosphorescence.

Further research into OLEDs containing a series of fluorine substituted iridium(III) complexes has been carried out by Grushin *et al.*³¹ The position of the substituent group has been explored in terms of fine-tuning the emission wavelength of the device. These complexes also provide high device efficiencies and exhibit excellent processing properties, in particular the trifluoromethyl-substituted species.

There is therefore little doubt that these types of complexes will continue to generate much research into their use in OLEDs over the coming years. Indeed, work by Du Pont de Nemours and Company and Viacheslav *et al.*³² on fluorinated iridium complexes and their use in optical displays with blue shifted emission and improved efficiencies has already been patented.

2.5.3 Tuneable Emission from OLEDs

The further use of *ortho*-metalated ligands in Ir(III) complexes has allowed the formation of complexes and hence OLEDs with a range of different coloured emission wavelengths. Adachi *et al.*³³ demonstrated a high-efficiency red electrophosphorescent device containing the Ir(III) complex, bis(2-(2'-benzo[4,5-a]thienyl)pyridinato-N,C^{3'}) iridium(acetylacetonate), Ir(btp)₂acac, doped into a CBP host. This complex utilises the small π - π^* transition energy of the btp ligand which leads to a low energy triplet excited state, giving strong red phosphorescence. The short phosphorescence lifetime ($\sim 4 \mu\text{s}$) of Ir(btp)₂acac leads to a significant improvement in the external efficiency at high currents.³³ Later work by Chen *et al.*,³⁴ supported this argument. Polymer light emitting devices (PLEDs) utilising Ir(btp)₂acac doped into PVK were reported to possess reduced self-quenching (*via* excimer formation or triplet-triplet annihilation) and hence improved efficiencies compared to those doped with platinum(II)-2,8,12,17-tetraethyl-3,7,13,18-tetramethylporphyrin (PtOX). It is believed that the shorter lifetime of the iridium complex's triplet state is responsible for this effect.³⁴

Red phosphorescent emission has also been observed from tris-cyclometalated iridium(III) complexes doped into PVK-based OLEDs.³⁵ Beeby *et al.*³⁵ described the use of bis-(2-phenyl-pyridyl)-2-(4'-formylphenyl)pyridine iridium(III), Ir(ppy)₂fppy, in simple single layer OLEDs made with ITO and aluminium contacts. The peak quantum efficiency was found to be 0.02 % at 34 V. This low efficiency and high operating voltage were due to the large barrier to electron injection from aluminium into PVK, however a high efficiency would not be expected for such a simple device structure. The photoluminescence quantum yield (PLQY) can be a useful guide to the maximum conceivable efficiency for materials in OLEDs. Beeby *et al.*³⁵ also reported these values for Ir(ppy)₃ and Ir(ppy)₂fppy doped into PVK films, at 6 % weight, as $35 \pm 3 \%$ and $60 \pm 3 \%$ respectively. For Ir(ppy)₃ this value is similar to that obtained in degassed toluene,¹⁴ so the PLQY observed for Ir(ppy)₂fppy is particularly encouraging, suggesting that it may perform even better than Ir(ppy)₃ in optimised devices.

Recent work by Lamansky *et al.*³⁶ describes the implementation of three Ir(L)₂acac complexes, where L = 2-phenylpyridine (ppy), 2-phenylbenzothiozole (bt)

and 2-benzo[b]thiophen-2-yl-pyridine (btp), were doped into the emissive region of multilayer vapour-deposited OLEDs. The emission from these devices gave green, yellow and red electroluminescence respectively. Their performance characteristics are summarised in table 2.1.³⁶ For reference a CIE diagram is shown in figure 2.10 below.

Table 2.1 Performance characteristics of Ir(ppy)₂acac, Ir(bt)₂acac and Ir(btp)₂acac based OLEDs.ⁱ

Property	Dopant Phosphor		
	Ir(ppy) ₂ acac	Ir(bt) ₂ acac	Ir(btp) ₂ acac
EL colour	green	yellow	red
Peak wavelength / nm	525	565	617
CIE-X	0.31	0.51	0.68
CIE-Y	0.64	0.49	0.68
Luminance at 10 mA/cm ² (cd/m ²)	3.300	2500	470
Drive voltage / V at 10 mA/cm ² (cd/m ²)	9.3	9.5	11.6
External quantum efficiency / %			
at 1 mA/cm ²	10.0	9.7	6.6
at 10 mA/cm ²	7.6	8.3	6.0
at 100 mA/cm ²	5.4	5.5	4.6
Power efficiency / lm/W at 1 mA/cm ²	18	11	2.2

(i) Device structure: ITO/ α -NPD (500 Å)/doped CBP (300 Å)/BCP (100 Å)/Alq₃ (400 Å)/Mg-Ag with dopant at 7 % by weight loading in CBP layer.

These Ir(L)₂acac doped devices show some of the highest efficiencies reported for OLEDs. The high efficiencies result from efficient trapping and radiative relaxation of the singlet and triplet excitons formed in the electroluminescent process.

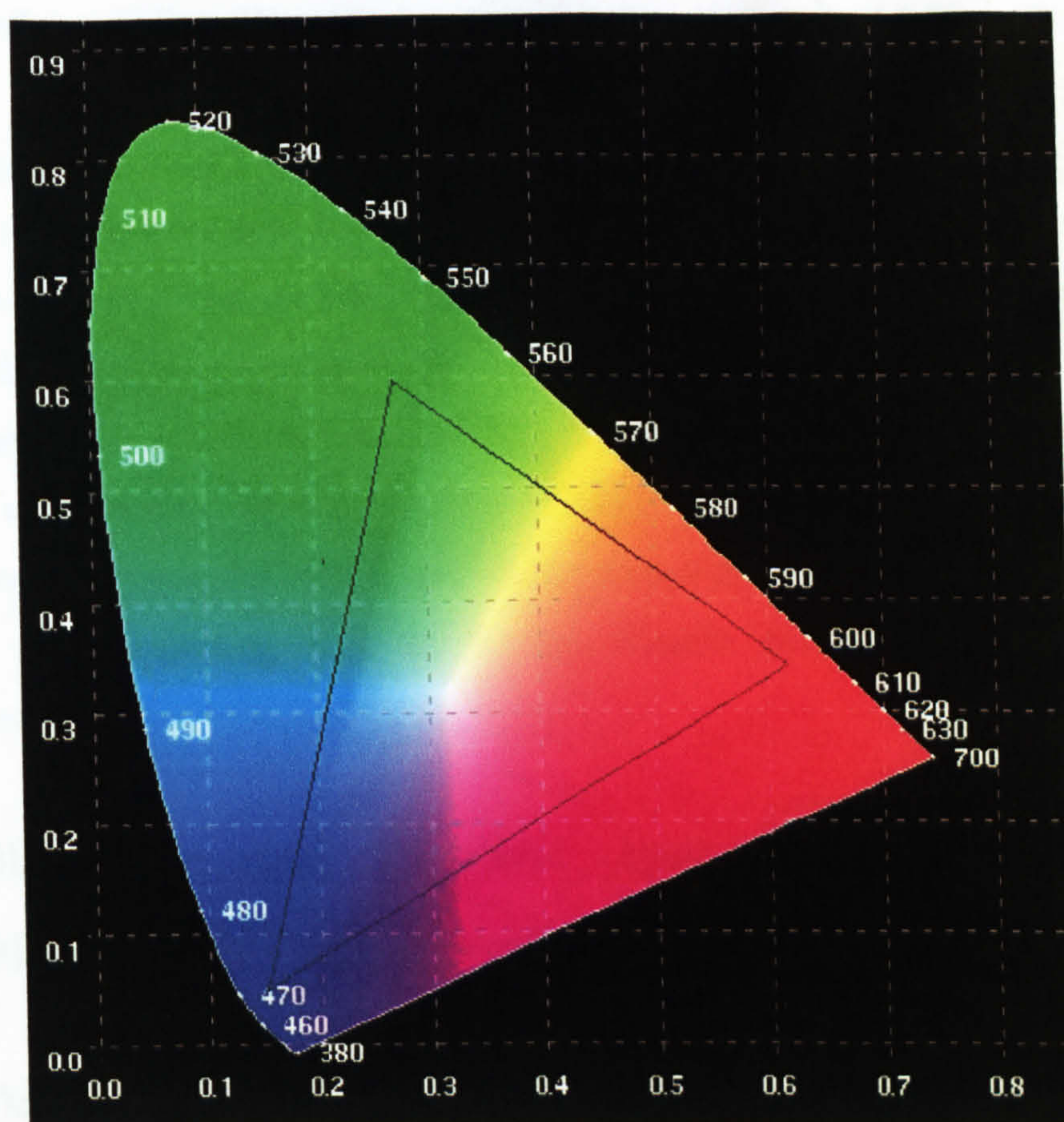


Figure 2.10 A 1931 CIE Chromaticity Chart.

2.5.4 Alkyl Substituted Iridium(III) Complexes for OLEDs

The intention of work by Zhu *et al.*³⁷, to substitute the phenylpyridine ligands of Ir(ppy)_3 with alkyl chains, was to improve the interaction of the metal complex guest with the conjugated polymer host. This improved interface was expected to inhibit phase segregation and improve the efficiency of the energy transfer. The tertiary butyl substituted complex, *fac*-tris-(2-(4-tert-butylphenyl)pyridine)iridium(III) (Ir(t-Buppy)_3), was doped into poly(2-(6-cyano-6-methyl)-heptyloxy-1,4-phenylene) (CNPPP) device and was shown to display a higher quantum efficiency than that of Ir(ppy)_3 for a given dopant concentration. More importantly, they suggested that the addition of the butyl group into the ppy ligand significantly suppress the decay of the device efficiency at high current density.

Work on iridium(III) complexes containing the *p*-substituted 2-phenylpyridine ligands, 2-(4'-(3'',7''-dimethyloctyloxy)phenyl)pyridine (DecOppy) and 2-(4'-decylphenyl)pyridine (Decppy) was also carried out by Zhu *et al.*³⁸ in 2003. However, these iridium doped CNPPP devices were found to display lower quantum efficiencies than that reported for Ir(ppy)₃. An overlap of the emission spectrum of the host and the absorption spectrum of the guest is an important condition in obtaining high efficiency. However, even though the three iridium complexes studied by Zhu *et al.*^{37,38} are all reported to have the same overlap between the emission spectrum of CNPPP and their own absorption spectra, the device performances obtained were very different, thus suggesting that the energy transfer process in these devices is complicated.

2.5.5 Oligomeric and Dendritic Iridium(III) Complexes for OLEDs with Reduced Self-quenching

In 2002, Markham *et al.*³⁹ reported the characteristics of efficient single layer OLEDs formed by spin-coating new solution processible phosphorescent iridium cored dendrimers. The first (G1) and second (G2) generation dendrimers, see figure 2.11, contain a *fac*-tris(2-phenylpyridine) iridium core, phenylene based dendrons and 2-ethylhexyloxy (R) surface groups.

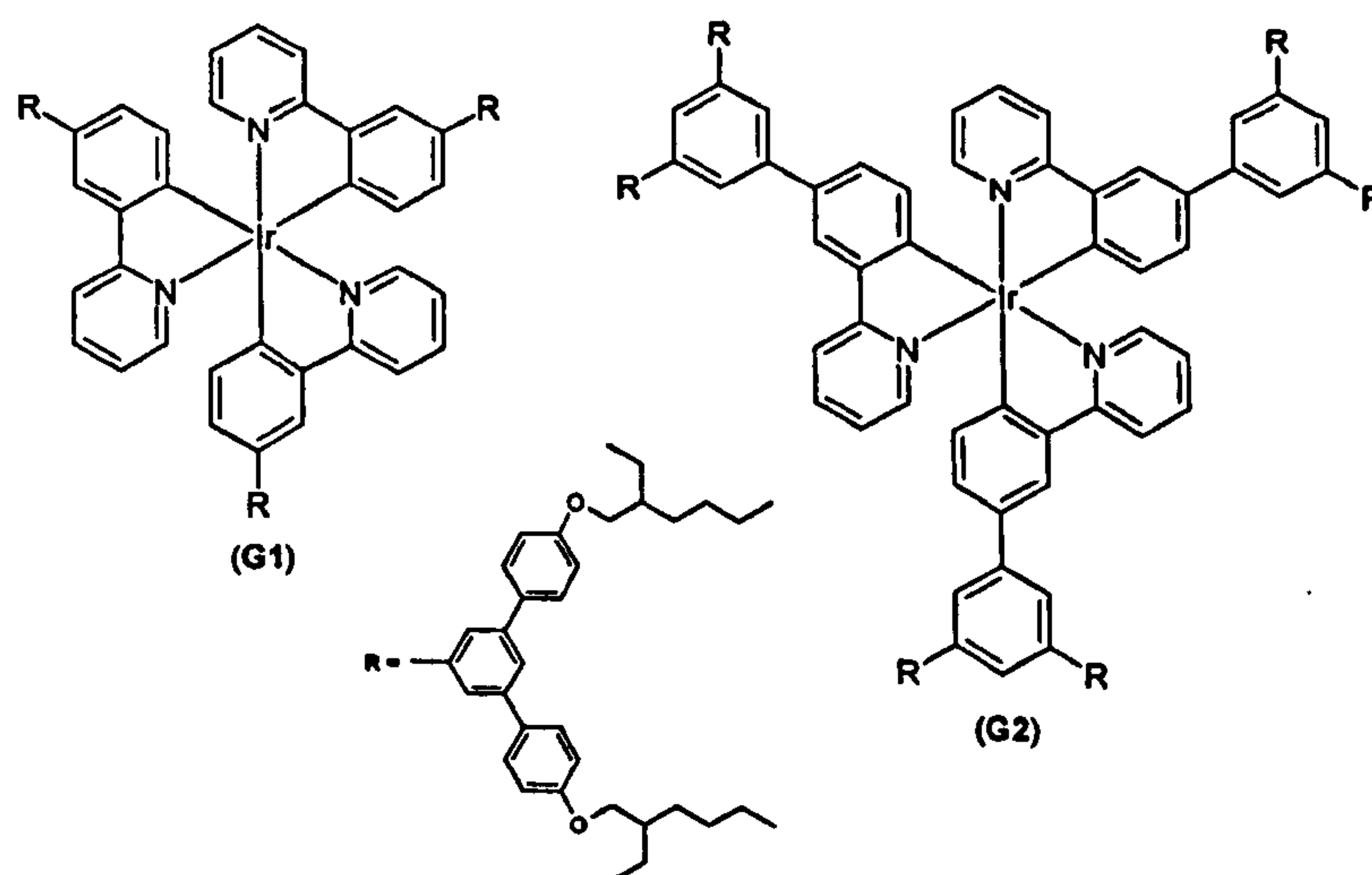


Figure 2.11 Structures of first generation (G1) and second generation (G2) iridium(III) dendrimers.

OLEDs based on neat films of **G1** and **G2** dendrimers were compared with a 20 wt% blend of **G1** in a CBP host. The absorption spectra of the **G1** and **G2** possess a band at 272 nm, assigned to the biphenyl dendrons, and a band between 325 nm and 475 nm, assigned to the *fac*-tris(2-phenylpyridine) iridium(III) core. The former increases in intensity with generation due to the increasing number of biphenyl units relative to the dendrimer core. Green electrophosphorescence, $\lambda_{\text{max}} = 518$ nm, was observed from all three devices with PLQYs recorded for the following thin films, $\Phi_{\text{G1}} = 0.22$, $\Phi_{\text{G2}} = 0.31$ and $\Phi_{\text{G1 blend}} = 0.78$. The higher PLQYs for the second generation and blend materials can be attributed to the greater separation of the iridium(III) based cores, thus reducing self-quenching effects.

OLEDs based on the neat films of the dendrimers exhibited lower external quantum efficiencies than those of equivalent blend devices. Markham *et al.*³⁹ also reported the striking dependence of the efficiency upon the generation, with the efficiency increasing by an order of magnitude from 0.2 % to 2.1 % in going from **G1** to **G2**. As the thin film PLQY only increases by a factor of 1.4 in going from **G1** to **G2** this illustrates the effect of the dendrons on the charge transport within the device. This feature of increasing device efficiency with dendrimer generation was previously observed by Lupton *et al.*¹³ with fluorescent dendrimers, where it was attributed to the reduction in charge mobility with generation. This effect slows the charge carriers and increases the probability of exciton formation within the bulk of the device.

The light output-voltage characteristics of the three devices studied by Markham *et al.*³⁹ were found to be similar, however the current at a given brightness was found to be lower in the **G2** based device compared to that of **G1** and lower still in that of the blend. This accounts for the higher efficiency of **G2** than **G1** and the even higher efficiency of the blend device. The enhanced film-forming properties of the dendrimers were found to prevent recrystallisation of the CBP host. The bipolar charge transport in the film and efficient injection of charge at the anode and cathode combined to enhance the efficiency of the devices. In comparison, a similar device fabricated from 6 wt% Ir(ppy)₃ in CBP¹⁴ with poorer stability and device characteristics has been reported and was found to be more insulating than that containing the dendrimer blend. Overall, this work has illustrated that electrophosphorescent dendrimers are a promising way of making efficient and easily fabricated spin-coated OLEDs.

Samuel *et al.*⁴⁰ and Lupton *et al.*⁴¹ have patented metal containing dendrimers for use in optical devices in conjunction with Isis Innovation. These highly branched organometallic dendrimers contain a metal cation core, i.e. Ir(III), and possess enhanced solution processability. The increased isolation of the metal core from adjacent chromophores also leads to reduced triplet-triplet annihilation.

In the same year, Ostrowski *et al.*⁴² described the use of amorphous dendritic iridium complexes in the fabrication of single layer OLEDs. The oligofluorene type moieties utilised in this work are displayed in figure 2.12, where R = n-hexyl chain.

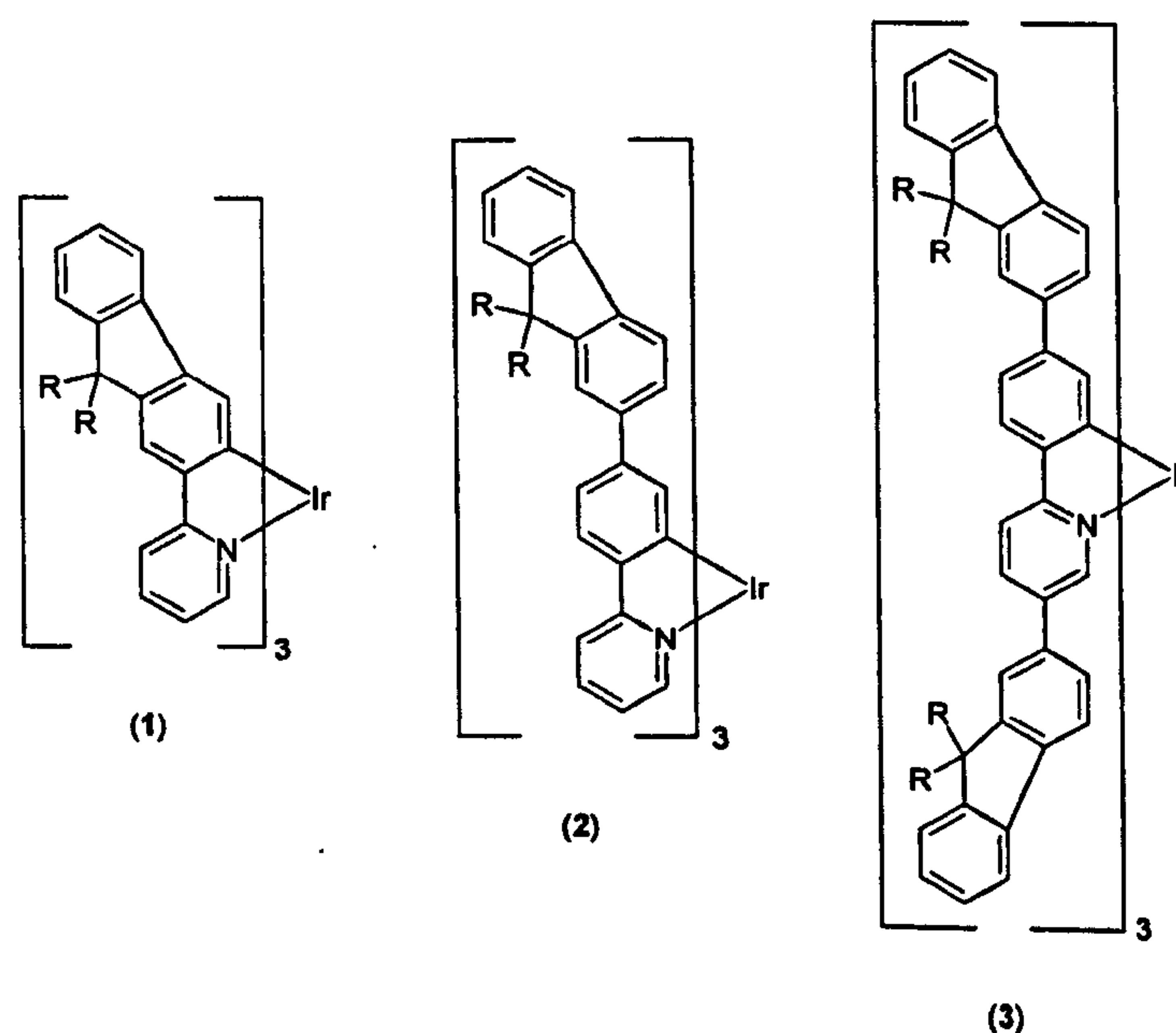


Figure 2.12 Oligofluorene iridium(III) complexes utilised in single layer devices.

Compounds 1 to 3 were designed to provide a progression of steric protection around the metal centre and allow the study of the effect of ligand substitution pattern on the bulk morphology and solid-state phosphorescence.⁴³ A summary of their luminescence properties is presented in table 2.2.

Table 2.2 Luminescence properties of oligofluorene iridium(III) complexes.

Complex	Φ (solution) ^a	Φ ^b (solid)/%	Absorbance ^a	Emission Maximum / nm ^a
1	0.59	1.3 ± 1	330, 412, 449, 470	545
2	0.61	1.7 ± 0.5	345, 401, 449, 470	550
3	0.63	11.2 ± 1	375, 441, 513	595

Φ (solution) = solution state quantum yield, Φ (solid) = solid state quantum yield (b) films were spun from toluene, (a) in degassed toluene solution.

It can be seen from table 2.2 that the extent of conjugation can be used to tune colour whereas the ligand environment controls the solid-state quenching. Differential scanning calorimetry (DSC) showed complexes 1-3 to be amorphous solids after solvent removal. All DSC data was collected at a scanning rate of $10\text{ }^{\circ}\text{Cmin}^{-1}$ and shows that the ligand framework influences the glass transition temperature and the stability of the amorphous state. Complexes 1 and 2 show glass transition temperatures of only $98\text{ }^{\circ}\text{C}$ and $110\text{ }^{\circ}\text{C}$ respectively, whereas complex 3 exhibits a glass transition temperature at $83\text{ }^{\circ}\text{C}$ followed by crystallisation at $130\text{ }^{\circ}\text{C}$. This indicates that the smaller ligands of complexes 1 and 2 give rise to higher glass transition temperatures and are more resistant to crystallisation.

Device performance was tested with a general LED architecture of ITO/PEDOT/Ir complex ($1000\text{ }\text{\AA}$)/Ca ($900\text{ }\text{\AA}$)/Ag ($1000\text{ }\text{\AA}$), where PEDOT = polyethylenedioxythiophene-polystyrenesulfonic acid and films of the iridium complexes were spin-coated from solution. Only modest efficiencies of 0.1 cd/A , 0.04 cd/A and 0.07 cd/A were observed for complexes 1-3 respectively and quantum efficiencies for all devices were 0.1% . Further optimisation of these OLEDs would be expected upon blending conjugated polymers with the iridium complexes and by improved device fabrication.

2.6 Conclusion

OLEDs have been manufactured and tested utilising a variety of iridium(III) complexes as the emissive species and numerous device structures. The emission wavelength, quantum efficiency, lifetime and other characteristics of these devices can be tuned by altering the substituents on the metal complex. In addition to this, device characteristics may also be improved by the use of emissive species with reduced self-quenching, doping the emissive species into a polymer layer and the addition of other charge carrying/blocking layers.

2.7 References

- 1 F. Pschenitzka and J. C. Sturm, Three-Colour Organic Light Emitting Diodes Patterned by Masked Dye Diffusion, *Appl. Phys. Lett.*, 1999, **74**, 1913-1915.
- 2 J. A. Rogers, Z. Bao and V. R. Raju, Nonphotolithographic Fabrication of Organic Transistors with Micron Feature Sizes, *Appl. Phys. Lett.*, 1998, **72**, 2716-2718.
- 3 S. Chang, J. Bharathan, Y. Yang, R. Helgeson, F. Wudl, M. B. Ramey and J. R. Reynolds, Dual-Colour Polymer Light Emitting Pixels Processed by Hybrid Inkjet Printing, *Appl. Phys. Lett.*, 1998, **73**, 2561-2563.
- 4 M. Roundhill and J. P. Fackler, Jr., *Optoelectronic Properties of Inorganic Compounds*, Plenum Press, New York, 1999, 2, S. Sibley, M. E. Thompson, P. E. Burrows and S. R. Forrest, *Electroluminescence in Molecular Materials*, 29-54.
- 5 Turro, N. J., *Modern Molecular Photochemistry*, Benjamin/Cummings Publishing, Menlo Park, Ca. 1978, 3.
- 6 C. W. Tang and S. A. Van Syke, Organic Electroluminescent Diodes, *Appl. Phys. Lett.*, 1987, **51**, 913-915.

- 7 J. Tian, C. C. Wu, M. E. Thompson, J. C. Sturm, R. A. Register, M. J. Marsella and T. M. Swager, Electroluminescent Properties of Self-Assembled Polymer Thin Films, *Adv. Mater.*, 1995, **7**, 395-398.
- 8 C. Hosokawa, H. Higashi, H. Nakamura and K. Kusumoto, Highly Efficient Blue Electroluminescence from a Distyrylarylene Emitting Layer with a New Dopant, *Appl. Phys. Lett.*, 1995, **67**, 3853-3855.
- 9 J. C. Scaiano, *Handbook of Organic Photochemistry*, CRC Press, 1989, 2.
- 10 M. A. Baldo, D. F. O'Brien, M. E. Thompson and S. R. Forrest, Electronic Singlet-Triplet Ratio in a Semiconducting Organic Thin Film, *Phys. Rev. B*, 1999, **60**, 14422-14428.
- 11 P. W. Atkins and R. S. Friedman, *Molecular Quantum Mechanics*, Oxford University Press, 1997, Third Edition, 113-119.
- 12 K. R. J. Thomas, J. T. Lin, Y. Tao and C. Ko, Light-Emitting Carbazole Derivatives: Potential Electroluminescent Materials, *J. Am. Chem. Soc.*, 2001, **123**, 9404-9411.
- 13 J. M. Lupton, I. D. W. Samuel, R. Beavington, P. L. Burn and H. Bässler, Control of Charge Transport and Intermolecular Interaction in Organic Light Emitting Dendrimer Generation, *Adv. Mater.*, 2001, **13**, 258-261.
- 14 M. A. Baldo, S. Lamansky, P. E. Burrows, M. E. Thompson and S. R. Forrest, Very High Efficiency Green Organic Light Emitting Devices based on Electrophosphorescence, *Appl. Phys. Lett.*, 1999, **75**, 4-6.
- 15 D. Zou, M. Yahiro and T. Tsutsui, Study on the Degradation Mechanism of Organic Light Emitting Diodes (OLEDs), *Synth. Met.*, 1997, **91**, 191-193.
- 16 S. Hoshino and H. Suzuki, Electroluminescence from Triplet Excited States of Benzophenone, *Appl. Phys. Lett.*, 1996, **69**, 224-226.

- 17 M. A. Baldo, D. F. O'Brien, Y. You, A. Shoustikov, S. Sibley, M. E. Thompson and S. R. Forrest, Highly Efficient Phosphorescent Emission from Organic Electroluminescent Devices, *Nature*, 1998, **395**, 151-154.
- 18 D. F. O'Brien, M. A. Baldo, M. E. Thompson and S. R. Forrest, Improved Energy Transfer in Electrophosphorescent Devices, *Appl. Phys. Lett.*, 1999, **74**, 442-444.
- 19 H. Kanai, S. Ichinosawa, and Y. Sato, Effect of Aromatic Diamines as a Cathode Interface Layer, *Synth. Met.*, 1997, **91**, 195-196.
- 20 K. A. King, P. J. Spellane and R. J. Watts, Excited-State Properties of a Triply Ortho-Metalated Iridium(III) Complex, *J. Am. Chem. Soc.*, 1985, **107**, 1431-1432.
- 21 R. W. Burnham, R. M. Hanes and C. James Bartleson, *Color: A Guide to Basic Facts and Concepts*, John Wiley and Sons, 1967, **6**, 123-150.
- 22 V. G. Kozlov, G. Parthasarathy, P. E. Burrows, and S. R. Forrest, Optically Pumped Blue Semiconductor Lasers, *Appl. Phys. Lett.*, 1998, **72**, 144-146.
- 23 T. Tsutsui, M. Yang, M. Yahiro, K. Nakamura, T. Watanabe, T. Tsuji, Y. Fukuda, T. Wakimoto and S. Miyaguchi, High Quantum Efficiency in Organic Light Emitting Devices with Iridium Complex as a Triplet Emissive Center, *Jpn. J. Appl. Phys.*, 1999, **38**, L1502-L1504.
- 24 C. Adachi, M. A. Baldo, S. R. Forrest and M. E. Thompson, High Efficiency Organic Electrophosphorescent Devices with Tris(2-phenylpyridine)iridium doped into Electron-transporting Materials, *Appl. Phys. Lett.*, 2000, **77**, 904-906.
- 25 M. Yang and T. Tsutsui, Use of Poly(9-vinylcarbazole) as Host Material for Iridium Complexes in High Efficiency Organic Light Emitting Devices, *Jpn. J. Appl. Phys.*, 2000, **39**, L828-L829.
- 26 C. Lee, K. Lee and J. Kim, Polymer Phosphorescent Light Emitting Devices doped with Tris(2-phenylpyridine)iridium as a Triplet Emitter, *Appl. Phys. Lett.*, 2000, **77**, 2280-2282.

- 27 P. I. Djurovich, S. A. Lamansky, M. R. Nugent, D. Murphy, R. C. Kwong and M. E. Thompson, Ir(III) Cyclometalated Complexes as Efficient Phosphorescent Emitters in Polymer Blend and Organic LEDs, *Polym. Prep.*, 2000, **41**, 770-771.
- 28 Y. Wang, N. Herron, V. V. Grushin, D. LeCloux and V. Petrov, Highly Efficient Electroluminescent Materials based on Fluorinated Organometallic Iridium Compounds, *Appl. Phys. Lett.*, 2001, **79**, 449-451.
- 29 Z. Bao, A. J. Lovinger and J. Brown, New Air Stable n-Channel Organic Thin Film Transistors, *J. Am. Chem. Soc.*, 1998, **120**, 207-208.
- 30 C. Adachi, R. C. Kwong, P. I. Djurovich, V. Adamovich, M. A. Baldo, M. E. Thompson and S. R. Forrest, Endothermic Energy Transfer: A Mechanism for generating Very Efficient High Energy Phosphorescent Emission in Organic Materials, *Appl. Phys. Lett.*, 2001, **79**, 2082-2084.
- 31 V. V. Grushin, N. Herron, D. LeCloux, W. J. Marshall, V. A. Petrov and Y. Wang, New Efficient Electroluminescent Materials based on Organometallic Complexes, *Chem. Commun.*, 2001, **16**, 1494-1495.
- 32 P. Viacheslav, W. Ying, G. Vladimir and Du Pont de Nemours and Company, Electroluminescent Iridium Compounds with Fluorinated Phenylpyridines, Phenylpyrimidines and Phenylquinolines and Devices made with such Compounds, WO 02/02714 A2, 10th January 2002.
- 33 C. Adachi, M. A. Baldo, S. R. Forrest, S. Lamansky, M. E. Thompson and R. C. Kwong, High Efficiency Red Electrophosphorescent Devices, *Appl. Phys. Lett.*, 2001, **78**, 1622-1624.
- 34 F. Chen, Y. Yang, M. E. Thompson and J. Kido, High Performance Polymer Light Emitting Diodes doped with a Red Phosphorescent Iridium Complex, *Appl. Phys. Lett.*, 2002, **80**, 2308-2310.
- 35 A. Beeby, S. Bettington, I. D. W. Samuel and Z. Wang, Tuning the Emission of Cyclometalated Iridium Complexes by Simple Ligand Modification, *J. Mater. Chem.*, 2003, **13**, 80-83.

- 36 S. Lamansky, P. Djurovich, D. Murphy, F. Abdel-Razzaq, H. Lee, C. Adachi, P. E. Burrows, S. R. Forrest and M. E. Thompson, Highly Phosphorescent Bis-cyclometalated Iridium Complexes: Synthesis, Photophysical Characterisation and use in Organic Light Emitting Diodes, *J. Am. Chem. Soc.*, 2001, **123**, 4304-4312.
- 37 W. Zhu, Y. Mo, M. Yuan and Y. Cao, Highly Efficient Electrophosphorescent Devices based on Conjugated Polymers with Iridium Complexes, *Appl. Phys. Lett.*, 2002, **80**, 2045-2047.
- 38 W. Zhu, C. Lui, L. Su, W. Yang, M. Yuan and Y. Cao, Synthesis of New Iridium Complexes and their Electrophosphorescent Properties in Polymer Light Emitting Diodes, *J. Mater. Chem.*, 2003, **13**, 50-55.
- 39 J. P. J. Markham, S. Lo, S. W. Magennis, P. L. Burn and I. D. W. Samuel, High Efficiency Green Phosphorescence from Spin-Coated Single Layer Dendrimer Light Emitting Diodes, *Appl. Phys. Lett.*, 2002, **80**, 2645-2647.
- 40 I. D. W. Samuel, S. Lo, P. L. Burn and Isis Innovation, Aryl-Aryl Dendrimers, WO 02/067343 A1, 29th August 2002.
- 41 J. M. Lupton, I. D. W. Samuel, S. Lo, V. Christou, P. L. Burn, J. N. G. Pillow and Isis Innovation, Metal Containing Dendrimers, WO 02/066552 A1, 29th August 2002.
- 42 J. C. Ostrowski, M. R. Robinson, A. J. Heeger and G. C. Bazan, Amorphous Iridium Complexes for Electrophosphorescent Light Emitting Devices, *Chem. Commun.*, 2002, 784-785.
- 43 H. Z. Xie, M. W. Liu, O. Y. Wang, X. H. Zhang, C. S. Lee, L. S. Hung, S. T. Lee, P. F. Teng, H. L. Kwong, H. Zheng and C. M. Che, Reduction of Self-quenching effect in Organic Electrophosphorescence Emitting Devices *via* the use of Sterically Hindered Spacers in Phosphorescence Molecules, *Adv. Mater.*, 2001, **13**, 1245-1248.

Chapter 3

Synthesis: Cyclometalating Ligands and their Corresponding Ir(III) and Rh(III) Complexes

Table 3.1 Compounds used for synthesis and photophysical studies.

Chemical name	Abbreviation	Supplier	Grade/Purity
acetic acid	AcOH	Fluka	99.8 %
acetonitrile	MeCN	Aldrich	99.9 %
ammonium acetate	NH ₄ OAc	Aldrich	99.99 %
β-carboline	-	Aldrich	99.99 %
benzaldehyde	-	Aldrich	99.5 %
benzeneboronic acid	-	Aldrich	97 %
2,2'-bipyridine	bipy/bpy	Lancaster	99 %
2-bromopyridine	-	Aldrich	99 %
2-bromo-4-methylpyridine	-	Aldrich	97 %
9-bromofluorene	-	Aldrich	-
cresyl violet	-	Aldrich	99.99 %
carbon monoxide	CO	BOC	C.P.
chloroform	CHCl ₃	Fischer	99.9 %
2-chloropyrimidine	-	Aldrich	95 %
cinnamaldehyde	-	BDH	98 %
cyclohexane	-	Aldrich	99.9 %
1-cyclohexane-1-carboxaldehyde	-	Aldrich	98 %
1,4-dibromobenzene	-	Aldrich	98 %
dichloromethane	CH ₂ Cl ₂	Fischer	99.9 %
diethylene glycol	-	Aldrich	99 %
diethyl ether	Et ₂ O	Fischer	99.9 %
2,4-difluorophenyl boronic acid	-	Aldrich	97 %
dimethoxyethane	DME	Aldrich	99.9 %
dimethylaminopyridine	DMAP	Aldrich	99 %
dimethylformamide	DMF	Avocado	99 %
diphenylphosphine chloride	-	Aldrich	98 %
ethanol	EtOH	Fischer	99.9 %
2-ethoxyethanol	-	Aldrich	99 %
ethyl acetate	EtOAc	Fischer	99.95 %
fluorescein	-	Aldrich	99.99 %
glycerol	-	Aldrich	99 %
hydrazine monohydrate	NH ₂ NH ₂ ·H ₂ O	Aldrich	98 %
iridium chloride	IrCl ₃ ·3H ₂ O	Precious Metals Online	99 %

malononitrile	$\text{CH}_2(\text{CN})_2$	Aldrich	99 %
methacrolein	-	Aldrich	95 %
methanol	MeOH	Prolabo	99.8 %
2-methoxyethyl ether	-	Aldrich	99 %
3-methyl-2-phenylpyridine	-	Lancaster	97 %
n-butyllithium in hexanes	n-BuLi	Aldrich	-
nitromethane	MeNO ₂	Aldrich	99 %
n-hexane	-	BDH	96 %
palladium acetate	Pd(OAc) ₂	Chemika	47 % Pd
2,4-pentanedione/acetyl acetone	AcAc/acac	BDH	98 %
2-phenylpyridine	ppy	Aldrich	98 %
2-phenyl-4-styryl-pyridine	-	T. Marder	-
piperidine	-	Aldrich	97 %
polyphosphoric acid	-	Aldrich	-
potassium permanganate	KMnO ₄	Aldrich	99 %
pyridinium p-toluene sulfonate	-	Aldrich	98 %
4-(2-pyridyl)benzaldehyde	fppy	Aldrich	97 %
quinine sulphate			
1R-(-)-myrtenal	-	Aldrich	98 %
rhodium chloride	RhCl ₃ .3H ₂ O	Alfa Aesar	99.9 %
silver (I) cyanide	AgCN	Aldrich	99 %
silver(I) trifluoroacetate	AgCF ₃ CO ₂	Aldrich	98 %
silver(I) trifluoromethane sulphonate	AgCF ₃ SO ₃	Aldrich	99 %
1,4,8,9-tetraaza-triphenylene	TAT	D. Parker	-
tetrahydrofuran	THF	Aldrich	99.9 %
tetrakis(triphenylphosphine)palladium(0)	Pd(PPh ₃) ₄	P. Low	-
Toluene	C ₆ H ₅ CH ₃	Fischer	99.9 %
triphenylphosphine	PPh ₃	Aldrich	99 %

3.1 Introduction

Electrophosphorescent complexes that are capable of generating pure red, green and blue light are in high demand for their use as dopants in full colour organic light emitting displays. Iridium(III) complexes containing cyclometalating ligands, such as 2-phenylpyridine, have already been utilised in these kinds of devices with a great deal of success. Given the interest in the use of such compounds it is important that new complexes are synthesised and their photophysical properties studied fully. This current chapter focuses on the synthesis of substituted 2-phenylpyridines, 2-phenylpyrimidines and phosphines in order to produce a series of new cyclometalated iridium(III) and rhodium(III) complexes. The photophysical studies of these compounds are discussed in detail in chapters 5 and 6.

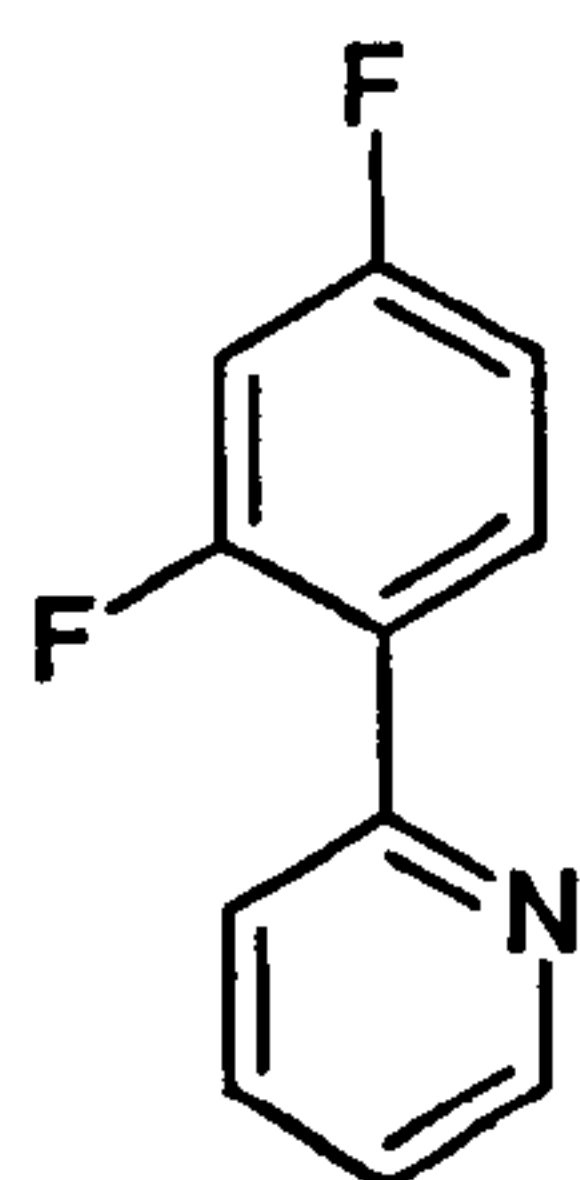
This chapter is split into three parts. The first section reports the methods used to synthesise the substituted 2-phenylpyridines/pyrimidines and phosphine ligands. The second part describes the synthesis of cyclometalated chloro-bridged bimetallic Ir(III)/Rh(III) species. The third part reports the synthesis of cyclometalated monometallic Ir(III)/Rh(III) complexes. Intermediate products are also included within the relevant part.

3.2 Ligands

3.2.1 2-Phenylpyridines and 2-Phenylpyrimidines

2-(2,4-Difluoro-phenyl)-pyridine (1)

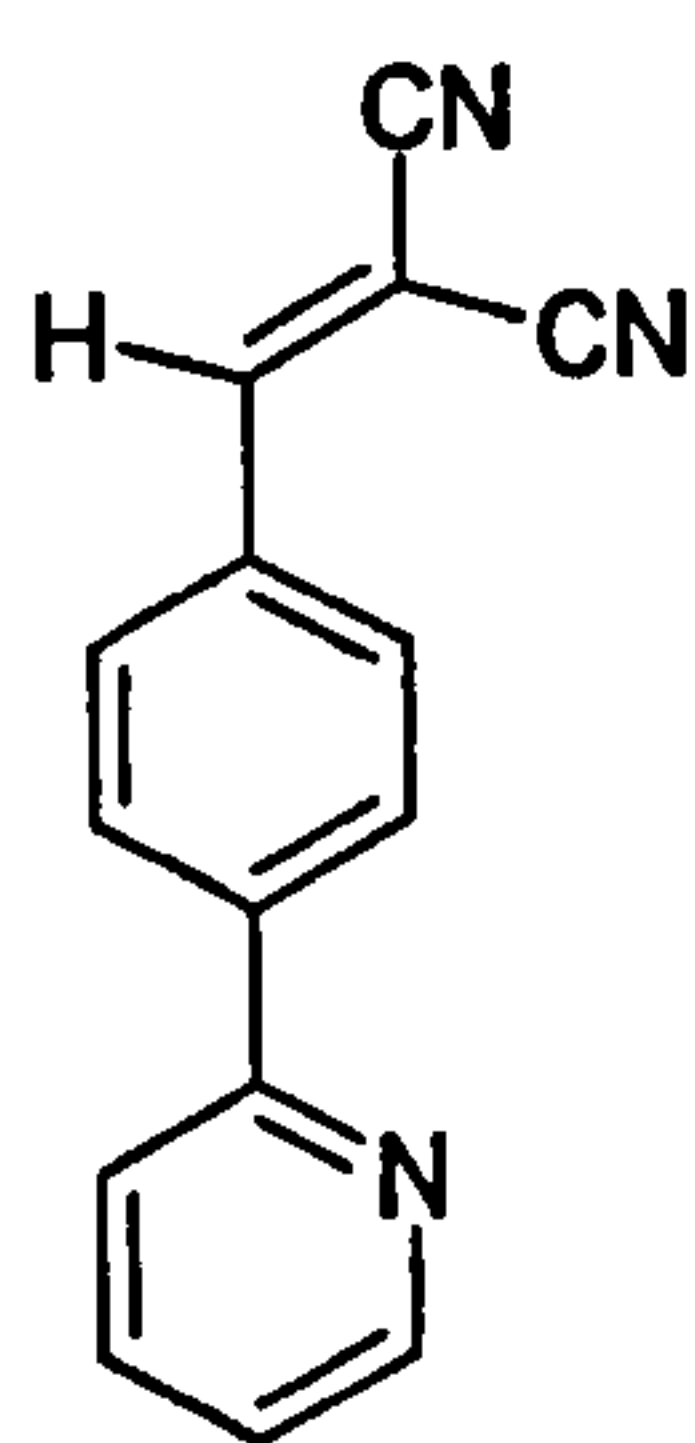
General synthesis adapted from work by O'Keefe *et al.*¹



2,4-Difluorophenyl boronic acid (5.0 g, 32 mmol), 2-bromopyridine (5.5 g, 34.8 mmol), aqueous sodium bicarbonate (2M, 50 mL) and tetrahydrofuran (100 mL) were placed in a reaction vessel and purged with nitrogen. Tetrakis(triphenylphosphine)palladium(0) (0.75 g, 0.60 mmol, 5 mol %) was added to the reaction mixture and the solution was

heated at 80 °C under a nitrogen atmosphere for 48 hours with continuous stirring. The resulting solution was cooled and the tetrahydrofuran was evaporated off and water (200 mL) was added. The mixture was extracted into ethyl acetate (4 x 50 mL) and the organic layers were dried over magnesium sulphate, filtered and evaporated to dryness to produce a dark oil. Column chromatography (silica gel, dichloromethane) afforded 1 as a pale yellow liquid (5.0 g, 82 %). ¹H-NMR 300 MHz (CDCl₃): δ 8.72 (1H, d, J = 3.3 Hz), 8.01 (1H, q, J = 6.9 Hz), 7.76 (2H, m), 7.27 (1H, m), 6.97 (2H, m). MS (ES⁺): m/z 191 (M)⁺, 172 (M-F)⁺.

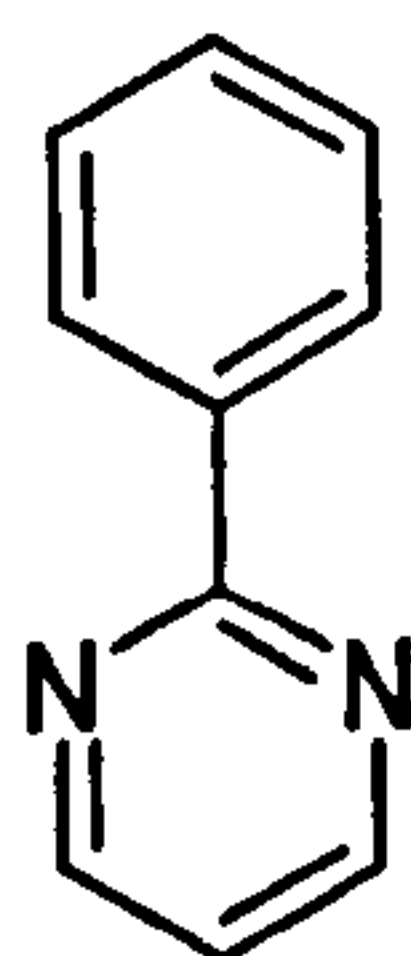
2-(4-Pyridin-2-yl-benzylidene)-malononitrile (2)



4-(2-Pyridyl)benzaldehyde (0.20 g, 1.0 mmol), malononitrile (0.096 g, 1.45 mmol), a drop of acetic acid and a drop of piperidine were refluxed in ethanol (15 mL) at 75 °C for 2 hours. The pale yellow-brown solution turned clear orange in colour. The solution was cooled to room temperature and evaporated to dryness. Column chromatography (silica gel, dichloromethane) afforded 2 as a pale solid (0.064 g, 26 %). ¹H-NMR 300 MHz (CDCl₃): δ 8.76 (1H, d, J = 5.1 Hz), 8.20 (2H, d, J = 8.4 Hz), 8.04 (2H, d, J = 8.4 Hz), 7.83 (3H, m), 7.35 (1H, q, J = 6.0 Hz). MS (EI⁺): m/z 231 (M)⁺, 205 (M-CN)⁺, 179 (M-C₂N₂)⁺.

2-Phenylpyrimidine (3)

General synthesis adapted from work by Ali *et al.*²

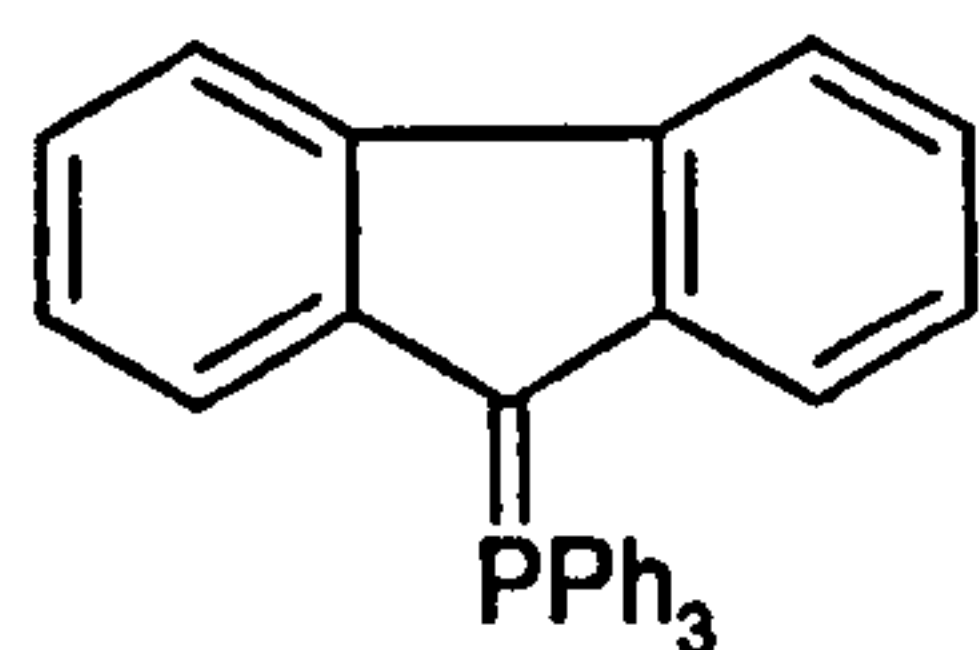


2-Chloropyrimidine (0.50 g, 4.37 mmol), benzenboronic acid (0.59 g, 4.8 mmol), potassium carbonate (0.79 g, 4.8 mmol), dimethoxyethane (20 mL) and water (10 mL) were purged with nitrogen. Palladium acetate (0.025 g, 0.11 mmol) and triphenylphosphine (0.12 g, 0.44 mmol) were added and the solution was heated at 100 °C for 18 hours with continuous stirring. The mixture was cooled to room temperature and the dimethoxyethane was

evaporated off. The aqueous residues were extracted into dichloromethane and the extract was dried over magnesium sulphate, filtered and evaporated to dryness. Column chromatography afforded **3** as a yellow liquid (0.48 g, 70 %). $^1\text{H-NMR}$ 300 MHz (CDCl_3): δ 8.84 (2H, d, $J = 4.8$ Hz), 8.58 (2H, m), 7.57 (2H, m), 7.18 (1H, t, $J = 7.2$ Hz), 6.96 (1H, m). MS (ES $^+$): m/z 156 (M) $^+$. The X-ray crystal structure and related data for **3** can be found in appendix A, part A1. Crystals were grown from dichloromethane.

Fluoren-9-ylidene-triphenylphosphane (**4**)

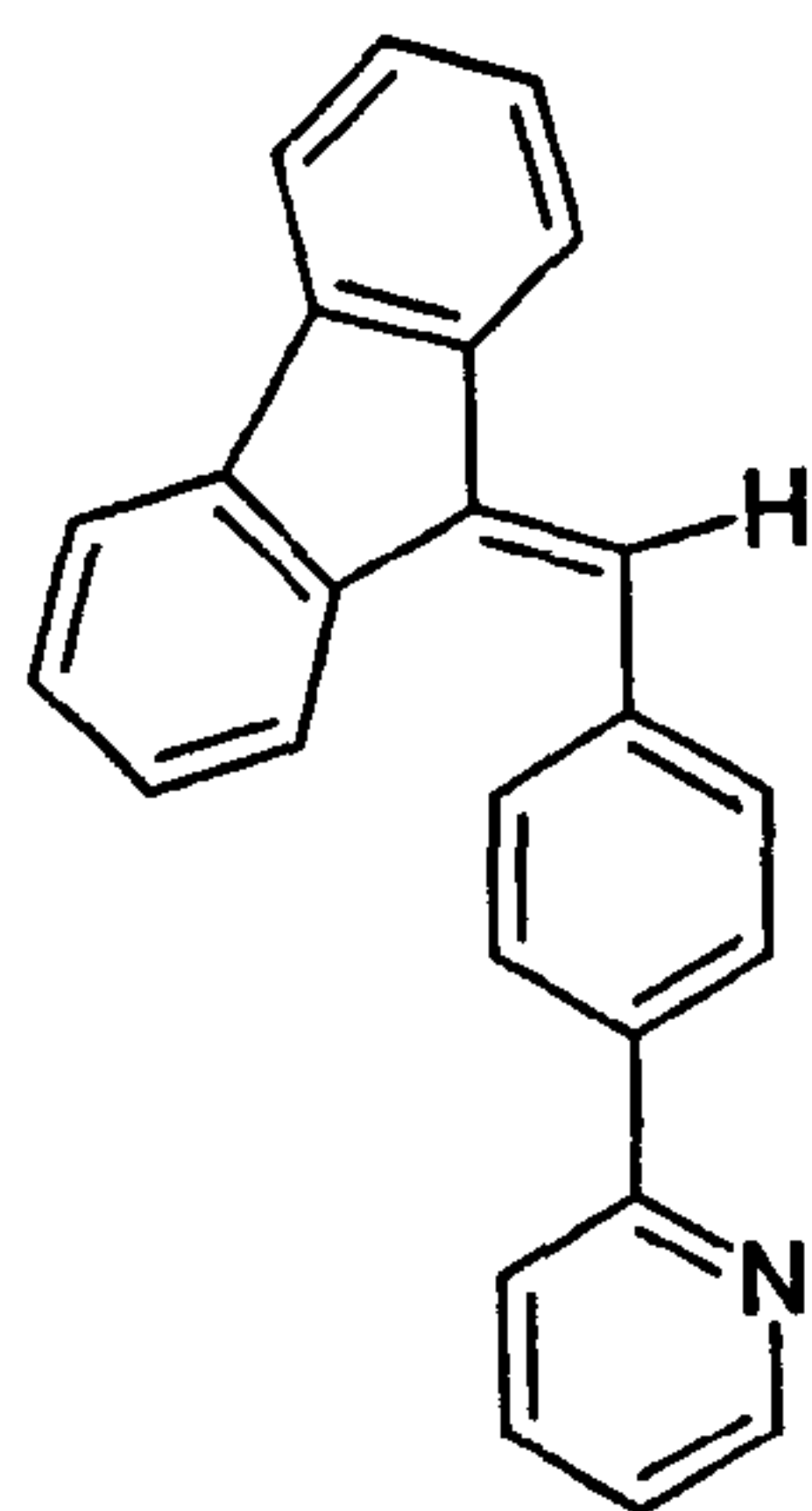
General synthesis adapted from work by Johnson *et al.*³ and Pinck *et al.*⁴



9-bromofluorene (3.01 g, 12.23 mmol) was dissolved in nitromethane (40 mL) with a little warming. To this clear solution triphenylphosphine (3.22 g, 12.23 mmol) was added slowly and an exothermic reaction ensued. After 2 hours under continuous stirring the clear pale green mixture became cloudy and white crystals of fluorenyl-9-triphenylphosphonium bromide precipitated out. The mixture was filtered and washed with nitromethane (50 mL) and subsequently recrystallised from boiling methanol to produce a white solid, fluorenyl-9-triphenylphosphonium bromide (5.09 g, 82 %). Fluorenyl-9-triphenylphosphonium bromide (1.50 g, 3.0 mmol) was dissolved in boiling methanol (75 mL) and 33% aqueous ammonia solution (5 mL) was added dropwise to the stirred solution. A bright yellow precipitate was immediately formed. The suspension was stirred for another 30 minutes. The cooled solution was filtered and washed with cold methanol and dried under *vacuo*, affording **4** a bright yellow solid (1.23 g, 95 %). $^1\text{H-NMR}$ 300 MHz (CDCl_3): δ 8.18 (2H, d, $J = 7.8$ Hz), 7.67 (15H, m), 7.01 (2H, t, $J = 7.2$ Hz), 6.90 (2H, t, $J = 6.9$ Hz), 6.35 (2H, d, $J = 7.8$ Hz).

2-(4-Fluoren-9-ylidenemethyl-phenyl)-pyridine (5)

General synthesis adapted from work by Johnson *et al.*³

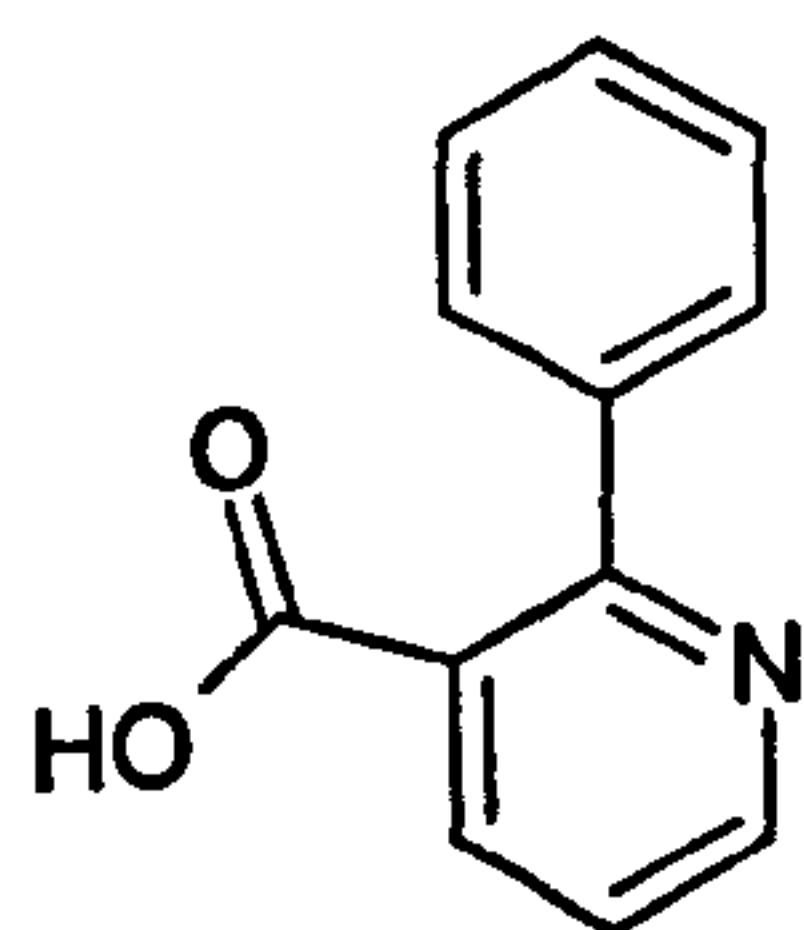


Fluoren-9-ylidene-triphenylphosphane **4** (0.50 g, 1.2 mmol) 4-(2-pyridyl)benzaldehyde (0.22 g, 1.2 mmol) were heated to 90 °C in chloroform (30 mL) for 10 hours. The solution was cooled to room temperature and evaporated to dryness. The crude residues were recrystallised from ethanol and water to afford **5** as a pale yellow solid (0.39 g, 98 %). ¹H-NMR 300 MHz (CDCl₃): δ 8.75 (1H, dt, J = 4.5 Hz), 8.11 (2H, m), 7.53 (9H, m), 7.35 (4H, m), 7.08 (1H, td, J = 6.6 Hz). MS (EI⁺): m/z 331 (M)⁺, 252 (M-C₅H₄N)⁺. The

X-ray crystal structure and related data for **5** can be found in appendix A, part A2. Crystals were grown from ethanol.

2-Phenyl-nicotinic acid (6)

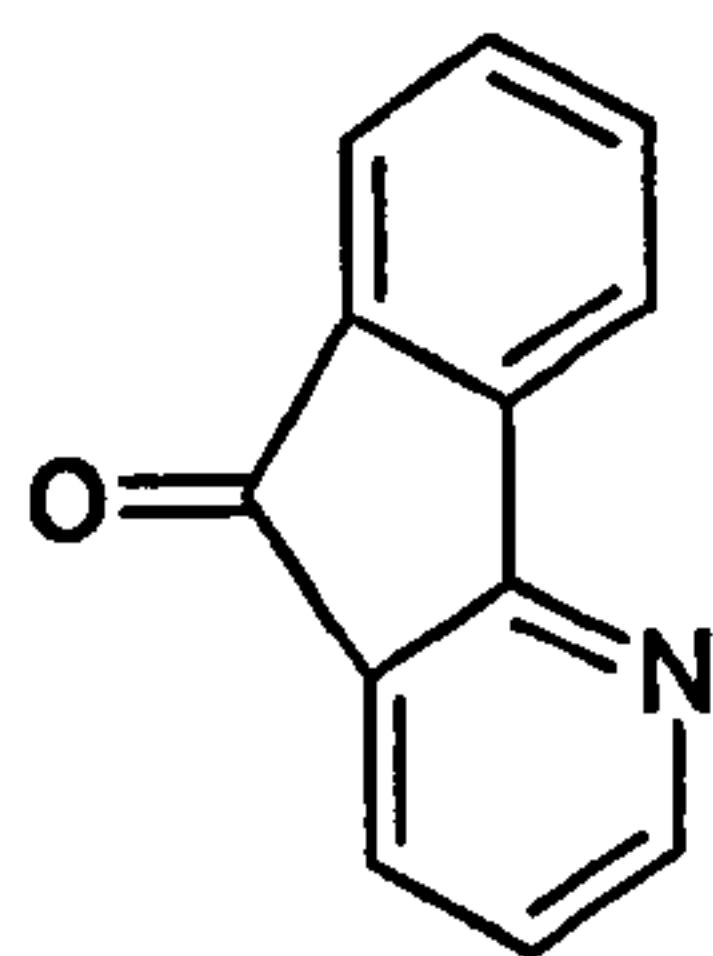
Synthesis taken from work by DuPriest *et al.*⁵



3-Methyl-2-phenylpyridine (10.0 g, 60 mmol), potassium permanganate (28.1 g, 0.18 mmol) and water (250 mL) were slowly heated to reflux over a period of 2 hours and refluxed for a further 3 hours with continuous stirring. When no permanganate remained the hot solution was filtered through celite and washed with hot water (100 mL). The aqueous filtrate was then continuously extracted into dichloromethane for 24 hours. The organic mixture was evaporated to dryness leaving a clear viscous syrup, which, upon trituration with diethyl ether, produced a white precipitate. The crude material was washed with more ether and dried under *vacuo* yielding **6** as a pure white light solid (5.97 g, 50 %). ¹H-NMR 300 MHz (CDCl₃/(CD₃)₂SO): δ 8.72 (1H, dd, J = 4.8 Hz), 8.11 (1H, dd, 7.89 Hz), 7.57 (2H, m), 7.38 (3H, m), 7.30 (1H, m), acid proton peak not seen, compound probably isolated as a salt.

Indeno[1,2-b]pyridin-5-one (7)

Synthesis taken from work by DuPriest *et al.*⁵

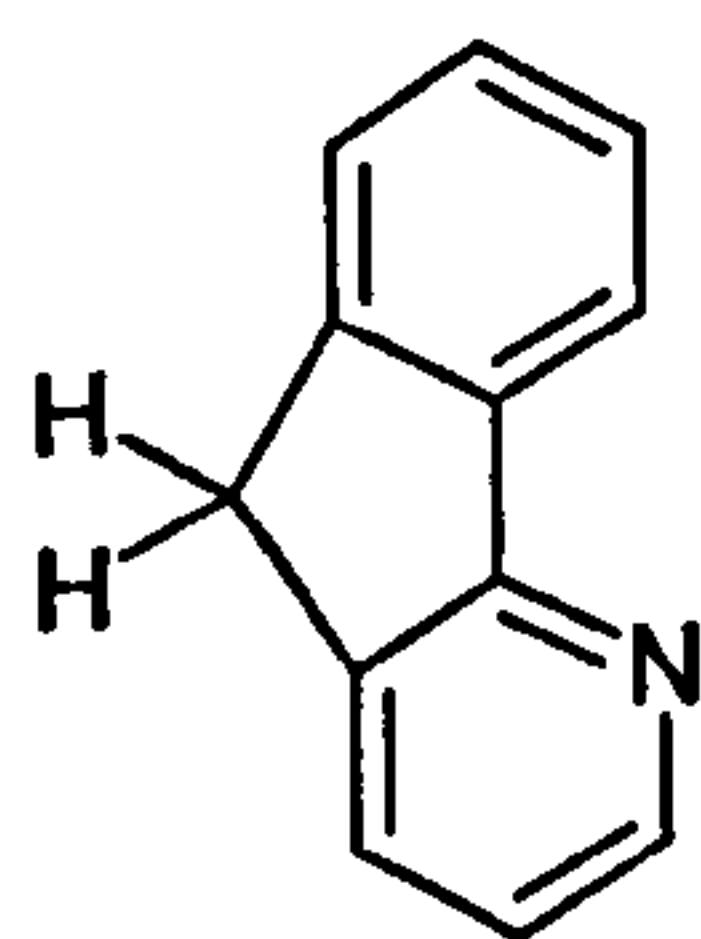


2-Phenyl-nicotinic acid **6** (0.78 g, 4.0 mmol) and polyphosphoric acid (12.0 g, excess) were heated at 170 °C for 3 hours. The initially clear syrup became a darker green-brown colour. The hot mixture was poured over cold aqueous sodium hydroxide (3M, 60 mL) precipitating a solid.

The slurry was extracted into ethyl acetate (60 mL), dried over magnesium sulphate and evaporated to dryness under *vacuo* producing **7** as a cream coloured solid (0.45 g, 63 %). ¹H-NMR 300 MHz (CDCl₃): δ 8.59 (1H, dd, *J* = 3.0 Hz), 7.86 (1H, d, *J* = 6.0 Hz), 7.81 (1H, d, *J* = 7.5 Hz), 7.69 (1H, d, *J* = 7.5 Hz), 7.57 (1H, t, *J* = 7.2 Hz), 7.40 (1H, t, *J* = 7.5 Hz), 7.18 (1H, m). The X-ray crystal structure and related data for **7** can be found in appendix A, part A3. Crystals were grown from ethyl acetate.

5H-Indeno[1,2-b]pyridine (8)

Synthesis taken from work by DuPriest *et al.*⁵

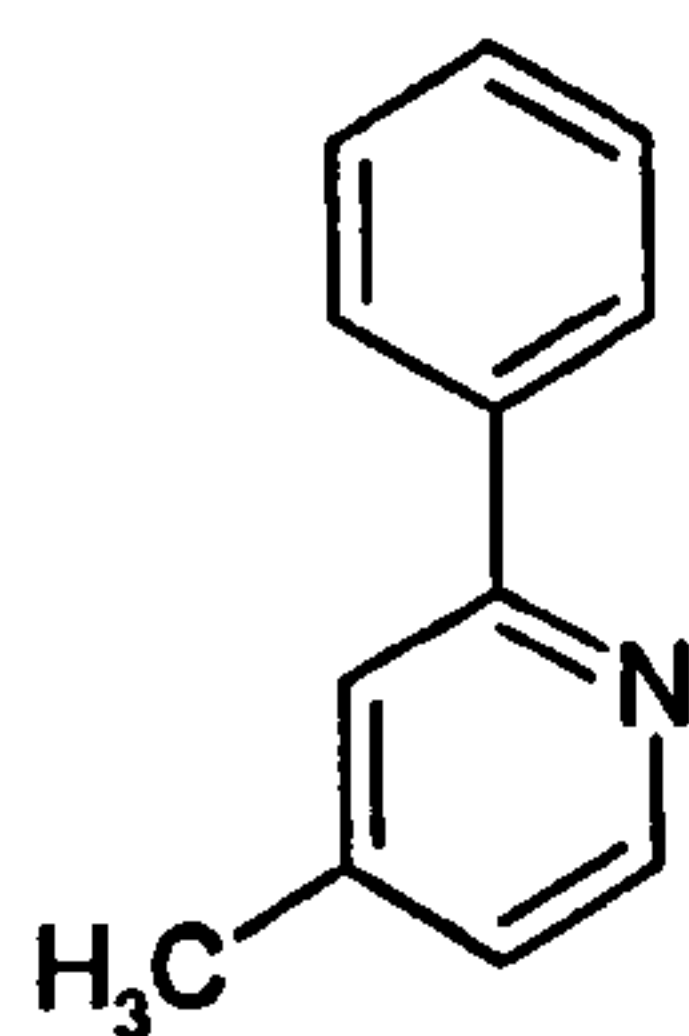


Indeno[1,2-b]pyridin-5-one **7** (0.30 g, 1.66 mmol), hydrazine hydrate (0.32 mL, 6.5 mmol) and diethylene glycol (20 mL) were heated at 180 °C for 3 hours. The mixture turned pale cream in colour. The cooled solution was poured into a mixture of water (30 mL) and brine (6 mL) and extracted into ethyl acetate (50 mL). The organic layer was washed

with water (20 mL) and dried over magnesium sulphate, filtered and dried under *vacuo* to **8** as a pale cream-yellow solid (0.20 g, 74 %). ¹H-NMR 300 MHz (CDCl₃): δ 8.60 (1H, d, *J* = 4.8 Hz), 8.12 (1H, d, *J* = 5.1 Hz), 7.81 (1H, d, *J* = 6.9 Hz), 7.58 (1H, d, *J* = 5.4 Hz), 7.47 (2H, m), 7.19 (1H, m), 3.87 (2H, s). MS (EI⁺): *m/z* 167 (M)⁺, 139 (M-C₂H₄)⁺, 113 (M-C₄H₆)⁺.

4-Methyl-2-phenyl-pyridine (9)

General synthesis adapted from work by O'Keefe *et al.*¹

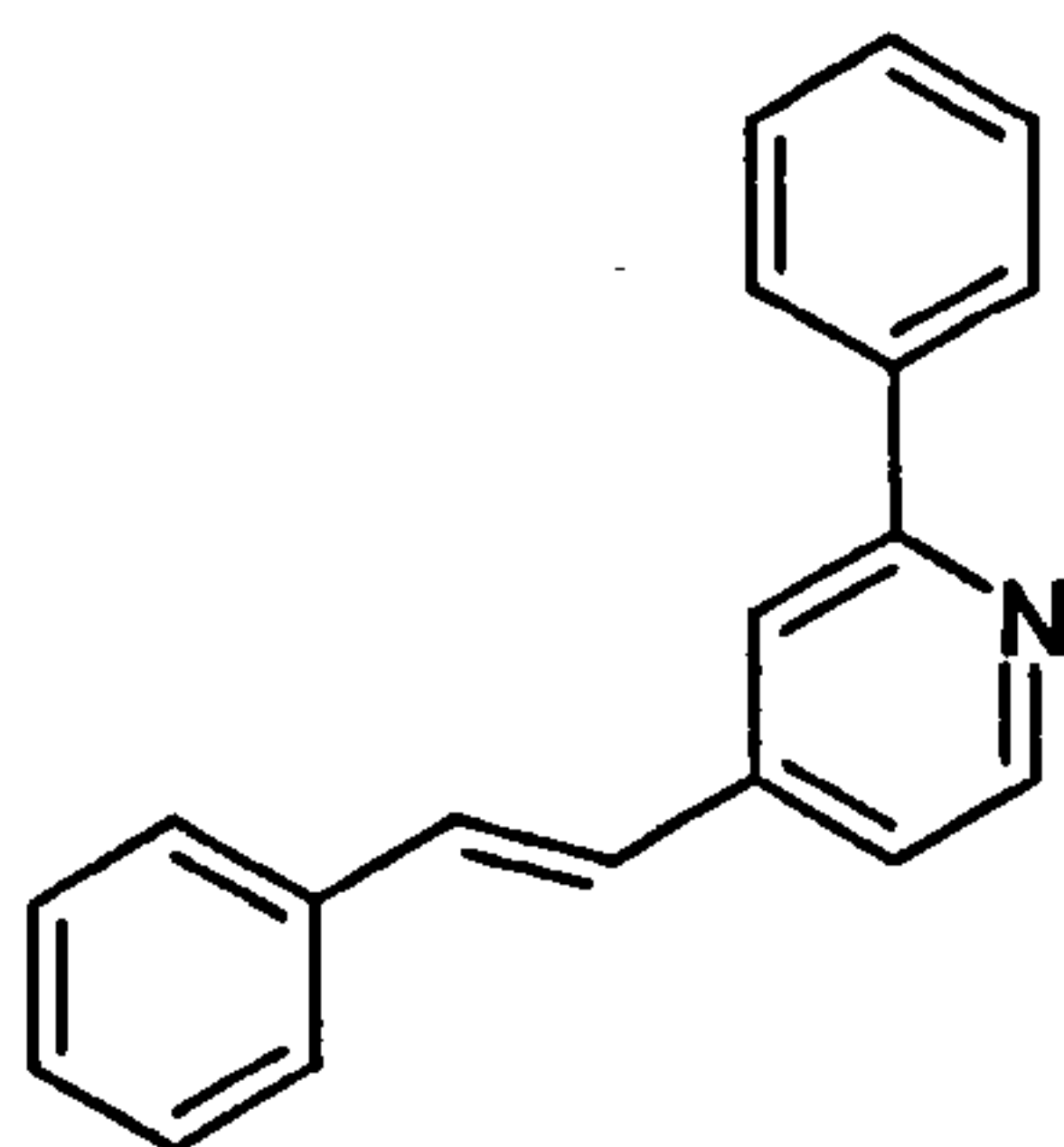


2-Bromo-4-methylpyridine (1.75 g, 10 mmol), benzene boronic acid (1.37 g, 11 mmol), aqueous sodium hydroxide (2M, 20 mL) and tetrahydrofuran (50 mL) were purged with nitrogen and tetrakis(triphenylphosphine)palladium(0) (0.25 g, 0.2 mmol) was added.

The solution was heated at 80 °C under a nitrogen atmosphere for 12 hours with continuous stirring. The mixture was cooled and the tetrahydrofuran was evaporated off. Water (50 mL) was added and the mixture was extracted into dichloromethane (50 mL). The organic layer was dried over magnesium sulphate, filtered and evaporated to dryness. Column chromatography (silica gel/dichloromethane) afforded **9** as a clear liquid (0.48 g, 28 %). ¹H-NMR 300 MHz (CDCl₃): δ 8.59 (1H, d, J = 7.8 Hz), 8.01 (2H, d, J = 7.8 Hz), 7.57 (1H, s), 7.47 (3H, m), 7.08 (1H, d, J = 5.1 Hz), 2.43 (3H, s). MS (ES⁺): m/z 169 (M)⁺, 154 (M-CH₃)⁺. The X-ray crystal structure and related data for **9** can be found in appendix A, part A4. Crystals were grown from dichloromethane.

2-Phenyl-4-styryl-pyridine (10)

General synthesis adapted from work by Maury *et al.*⁶



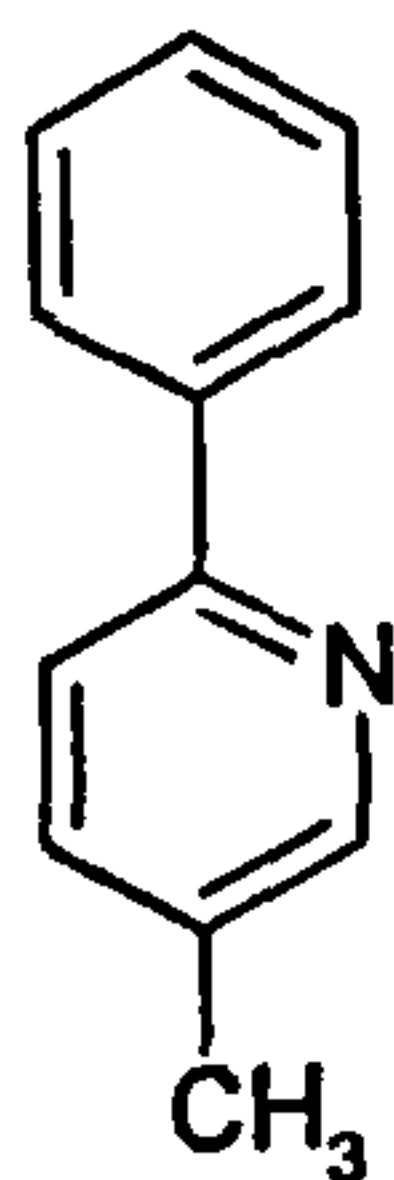
A solution of n-butyllithium in hexanes (1.6 M, 3.88 mL, 6.22 mmol) was added to dry degassed tetrahydrofuran (25 mL) at -78 °C. Following this, 4-Methyl-2-phenyl-pyridine **9** (1.0 g, 5.92 mmol) was dissolved and degassed in tetrahydrofuran (25 mL) and added dropwise to the n-butyllithium solution. The dark red-orange mixture was stirred for 1½ hours.

Benzaldehyde (0.63 g, 5.92 mmol) dissolved and degassed in tetrahydrofuran (25 mL) was then added dropwise to the flask and stirred for 2 hours at -78 °C and then overnight at room temperature. The solvent was removed from the dark yellow solution and the resulting material was dried under *vacuo* and then dissolved in dry toluene (25 mL). The solution was purged with nitrogen for 20 minutes and pyridinium

p-toluene sulfonate (0.20 g, 0.85 mmol) was added and the reaction mixture heated at 145 °C overnight. After cooling to room temperature, dichloromethane (2 x 50 mL) was added. The organic layers were combined, dried over magnesium sulphate, filtered and evaporated to dryness. Column chromatography (silica gel, dichloromethane) afforded the pure product **10** as a pale yellow solid (0.68 g, 45 %). ¹H-NMR 200 MHz (CDCl₃): δ 8.69 (1H, d, *J* = 5.0 Hz), 8.07 (2H, m), 7.81 (1H, s), 7.34 (11 H, m). MS (ES⁺): *m/z* 257 (M)⁺, 180 (M-C₆H₅)⁺, 155 (M-C₈H₇)⁺.

5-Methyl-2-phenyl-pyridine (**11**)

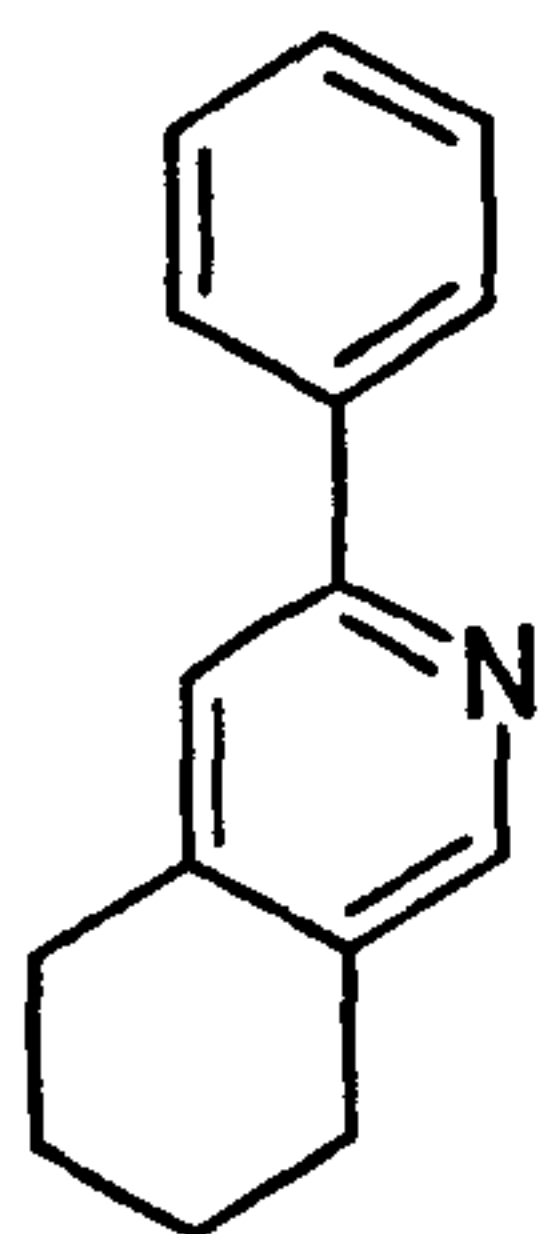
General synthesis adapted from work by Kröhnke *et al.*⁷



N-phenacylpyridinium iodide⁸ (9.8 g, 30.4 mmol), methacrolein (1.94 g, 27.6 mmol), ammonium acetate (4.26 g, 55.3 mmol) and dimethylformamide (50 mL) were heated at 80 °C for 15 hours under a nitrogen atmosphere. To the cooled solution, water (150 mL) was added and the mixture was extracted into ethyl acetate (150 mL). The organic extracts were dried over magnesium sulphate, filtered and evaporated to dryness. The crude material was distilled to afford **11** as a pale yellow solid (1.53 g, 33 %). ¹H-NMR 300 MHz (CDCl₃): δ 8.54 (1H, s), 7.98 (2H, d, *J* = 6.8 Hz), 7.62 (2H, m), 7.45 (3H, m), 2.38 (3H, s). MS (EI⁺): *m/z* 169 (M)⁺, 154 (M-CH₃)⁺.

3-Phenyl-5,6,7,8-tetrahydro-isoquinoline (**12**)

General synthesis adapted from work by Kröhnke *et al.*⁷

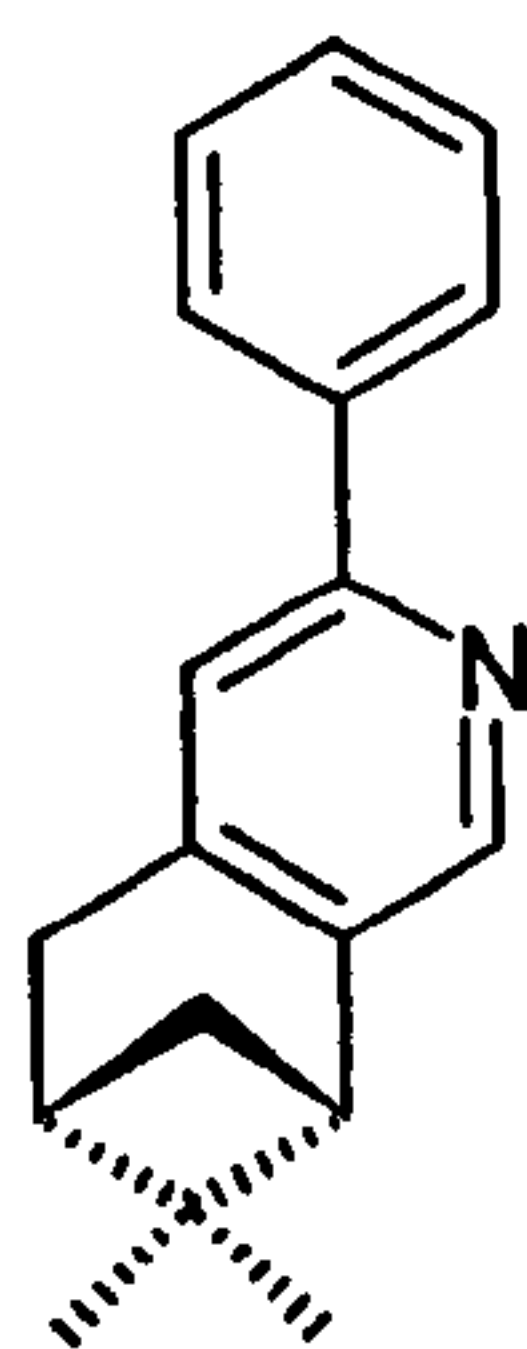


N-phenacylpyridinium bromide⁸ (3.79 g, 13.6 mmol), cyclohexane carboxaldehyde (1.0 g, 9.1 mmol), ammonium acetate (1.4 g, 18.2 mmol) and acetic acid (5 mL) were heated at 120 °C under a nitrogen atmosphere with continuous stirring for 12 hours. The mixture was allowed to cool to room temperature and aqueous potassium bicarbonate solution (150 mL) was added and the solution was extracted with ethyl acetate (4 x 50 mL). The organic layer was dried over magnesium sulphate, filtered and evaporated to dryness.

Distillation of the crude material afforded **12** as a yellow liquid (1.05 g, 58 %). $^1\text{H-NMR}$ 200 MHz (CDCl_3): δ 8.39 (1H, s), 7.96 (2H, dd, $J = 8.0$), 7.42 (4H, m), 2.79 (4H, m), 1.85 (4H, m). MS (ES $^+$): m/z 209 (M^+), 195 (M-CH_2^+), 180 ($\text{M-C}_2\text{H}_4^+$), 167 ($\text{M-C}_3\text{H}_5^+$), 153 ($\text{M-C}_4\text{H}_8^+$).

10,10-Dimethyl-5-phenyl-4-aza-tricyclo[7.1.1.0*2,7*]undeca-2(7),3,5-triene (**13**)

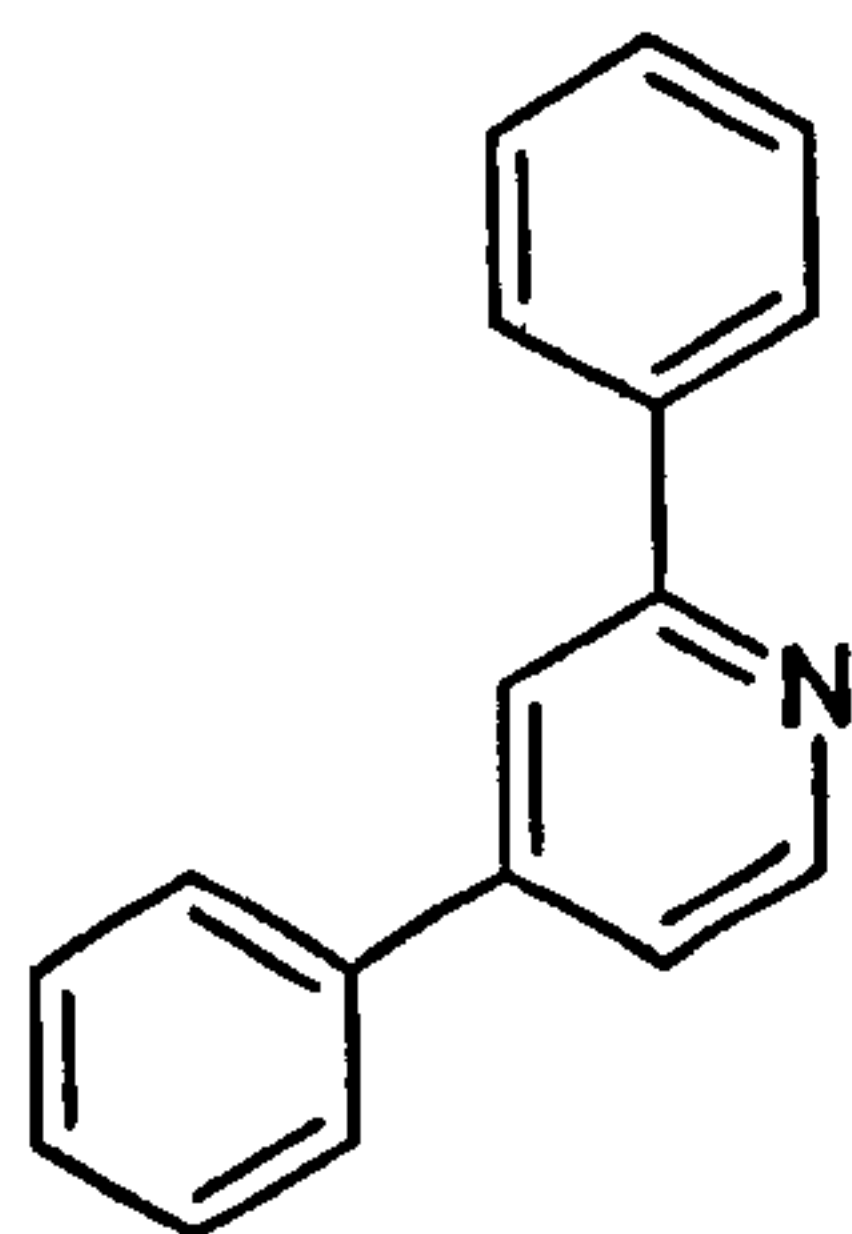
General synthesis adapted from work by Kröhnke *et al.*⁷



N-phenacylpyridinium iodide⁸ (9.84 g, 30.4 mmol), 1R-(-)-myrtenal (4.15 g, 27.6 mmol), ammonium acetate (5.13 g, 66.6 mmol) and dimethylformamide (50 mL) were heated at 75 °C under a nitrogen atmosphere with continuous stirring for 20 hours. The mixture was allowed to cool to room temperature and aqueous potassium bicarbonate solution (150 mL) was added and the solution was extracted with ethyl acetate (3 x 100 mL). The organic layer was dried over magnesium sulphate, filtered and evaporated to dryness. Column chromatography (silica gel, hexane/dichloromethane) afforded **13** as a pale yellow solid (2.7 g, 40 %). $^1\text{H-NMR}$ 400 MHz (CDCl_3) δ 8.25 (1H, s), 7.97 (1H, m), 7.95 (1H, m), 7.53 (1H, m), 7.46 (2H, t, $J = 7.6$ Hz), 7.38 (1H, m), 3.03 (2H, d, $J = 2.8$ Hz), 2.86 (1H, t, $J = 5.6$ Hz), 2.71 (1H, m), 2.32 (1H, m), 1.42 (3H, s), 1.25 (1H, d, $J = 9.6$ Hz), 0.67 (3H, s). $^{13}\text{C-NMR}$ 400 MHz (CDCl_3) δ 155.9, 146.1, 145.4, 141.4, 140.1, 128.9, 128.6, 126.9, 120.3, 44.5, 40.3, 39.6, 33.1, 32.1, 26.3, 21.7.

2,4-Diphenylpyridine (**14**)

General synthesis adapted from work by Kröhnke *et al.*⁷

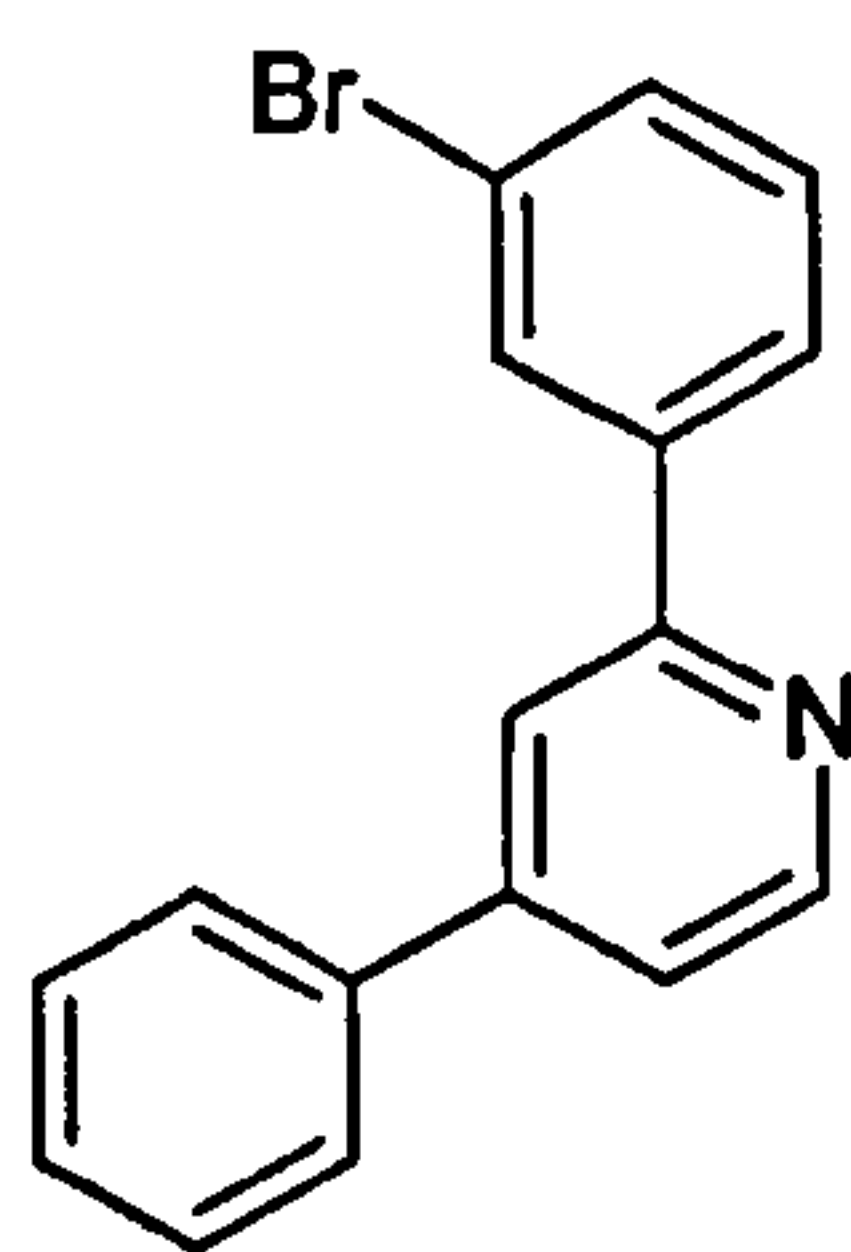


N-phenacylpyridinium iodide⁸ (9.8 g, 30.4 mmol), cinnamaldehyde (4.4 g, 33.2 mmol), ammonium acetate (5.14 g, 66.7 mmol) and DMF (50 mL) were heated at 75 °C under a nitrogen atmosphere with continuous stirring for 24 hours. The solution was allowed to cool to

room temperature and water (200 mL) was added and the solution was extracted with ethyl acetate (5 x 100 mL). The organic layer was extracted and dried over magnesium sulphate, filtered and evaporated to dryness. Column chromatography (silica gel, dichloromethane) afforded **14** as a pale yellow oil (1.22 g, 18 %). ¹H-NMR 300 MHz (CDCl₃): δ 8.56 (1H, d, J = 5.4 Hz), 7.84 (2H, dd, J = 5.8 Hz), 7.72 (1H, s), 7.49 (2H, dd, J = 6.0 Hz), 7.31 (7H, m). MS (EI⁺): m/z 231 (M)⁺, 154 (M-C₆H₅)⁺, 77 (M-C₁₂H₁₀)⁺.

2-(3-Bromo-phenyl)-4-phenyl-pyridine (**15**)

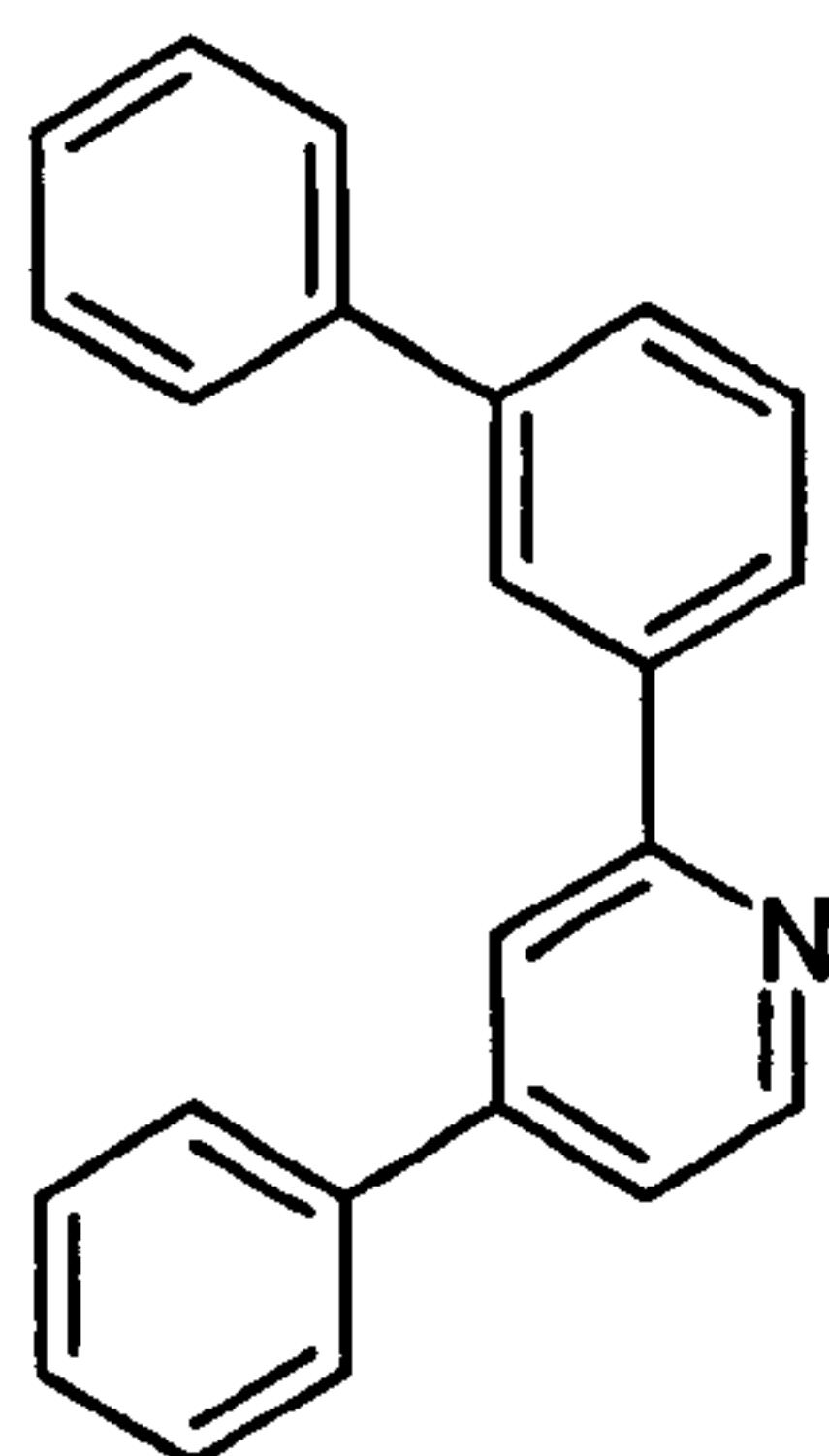
General synthesis adapted from work by Kröhnke *et al.*⁷



1-(3-Bromo-benzoyl)-pyridinium iodide⁸ (10.0 g, 25 mmol), cinnamaldehyde (4.9 g, 37.5 mmol), ammonium acetate (5.8 g, 75 mmol) and acetic acid (25 mL) were heated at 120 °C under a nitrogen atmosphere with continuous stirring for 36 hours. The mixture was cooled to room temperature and aqueous potassium bicarbonate solution (500 mL) was added and subsequently extracted with ethyl acetate (5 x 100 mL). The organic layer was dried over magnesium sulphate, filtered and evaporated to dryness. Column chromatography (silica gel, dichloromethane) afforded **15** as a brown liquid (2.1 g, 27 %). ¹H-NMR 300 MHz (CDCl₃): δ 8.75 (1H, dd, J = 5.7 Hz), 8.24 (1H, m), 7.99 (1H, dt, J = 10.5 Hz), 7.90 (1H, m), 7.70 (2H, m), 7.52 (5H, m), 7.37 (1H, t, J = 7.8 Hz). MS (EI⁺): m/z 309 (M)⁺, 230 (M-Br)⁺, 154 (M-Br-C₆H₅)⁺.

2-Biphenyl-3-yl-4-phenyl-pyridine (**16**)

General synthesis adapted from work by O'Keefe *et al.*¹



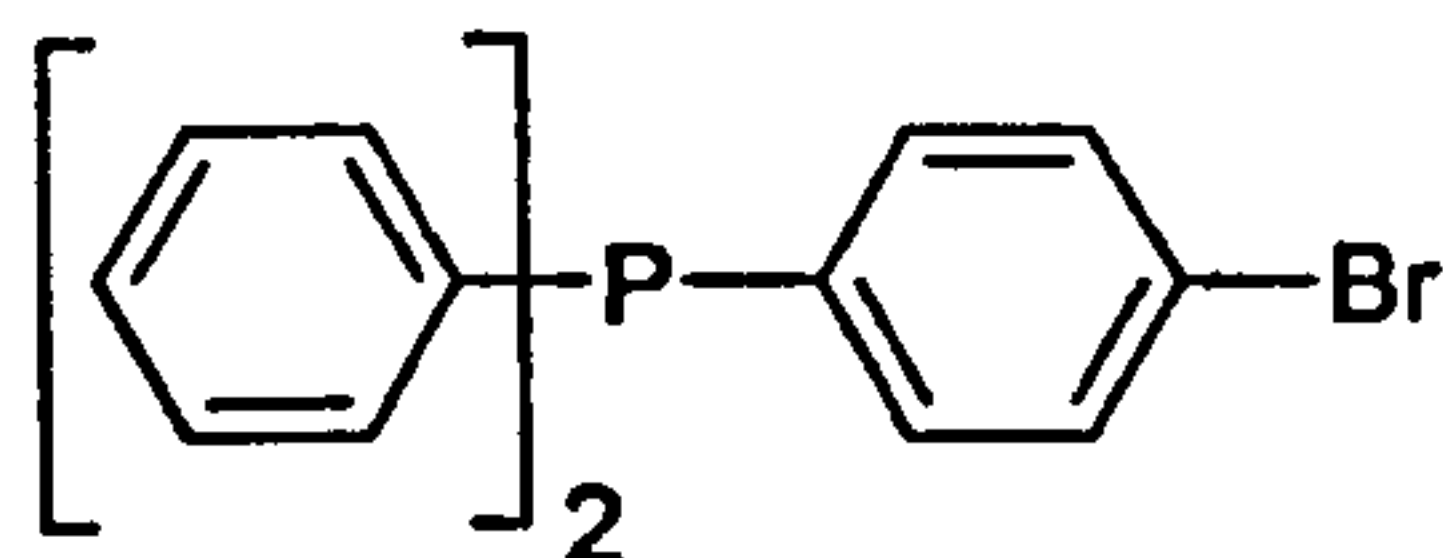
2-(3-Bromo-phenyl)-4-phenyl-pyridine **15** (0.65 g, 0.21 mmol), benzeneboronic acid (0.31 g, 2.5 mmol), potassium carbonate (0.35 g, 2.5 mmol), dimethoxyethane (40 mL) and water (10 mL) were purged with nitrogen. Palladium acetate (0.05 g, 0.053 mmol) and

triphenylphosphine (0.22 g, 0.084 mmol) were added and the solution was heated at 100 °C for 24 hours with continuous stirring. The mixture was cooled to room temperature and water (50 mL) and dichloromethane (100 mL) was added. The organic layer was extracted, dried over magnesium sulphate, filtered and evaporated to dryness. Column chromatography (silica gel: dichloromethane) afforded **16** as a pale yellow oil (0.58 g, 90 %). ¹H-NMR 200 MHz (CDCl₃): δ 8.80 (1H, d, J = 5.0 Hz), 8.33 (1H, s), 8.07 (1H, dt, J = 6.0 Hz), 8.02 (1H, s), 7.57 (13 H, m). MS (EI⁺): m/z 307 (M)⁺, 230 (M-C₆H₅)⁺, 154 (M-C₁₂H₉)⁺.

3.2.2 Phosphines

(4-Bromophenyl)-diphenyl-phosphane (**17**)

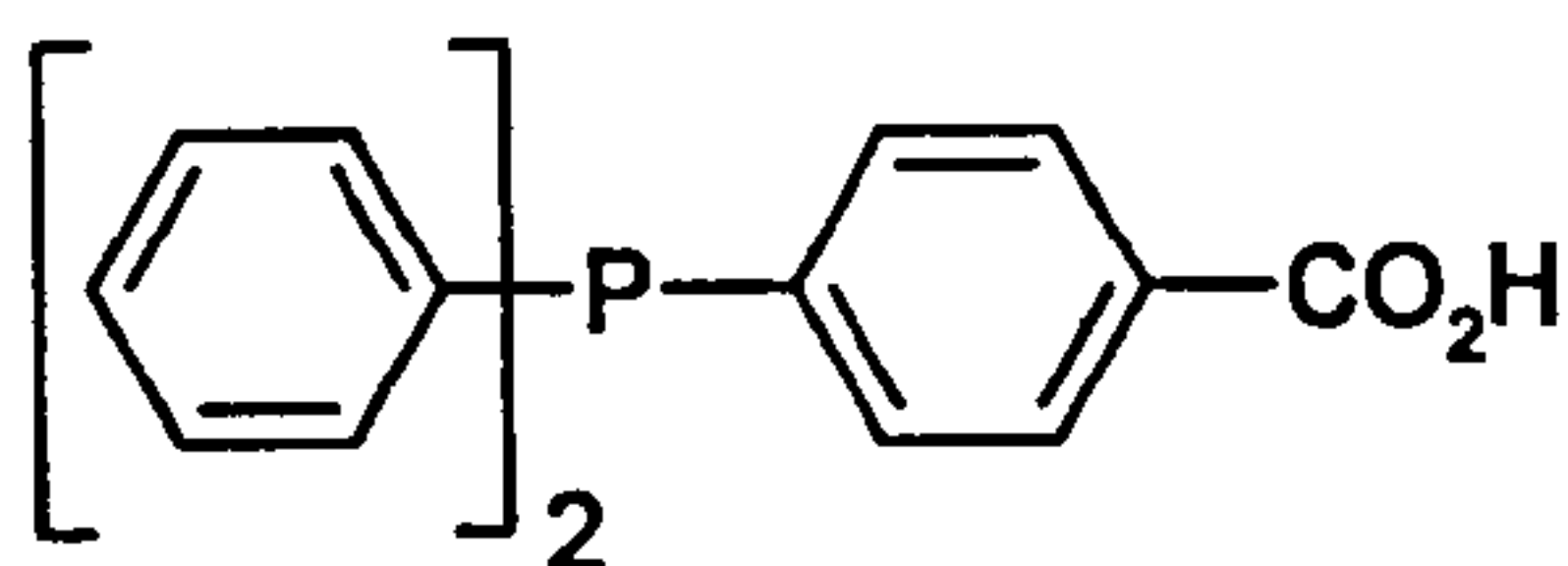
General synthesis adapted from work by Ravindar *et al.*⁹



1,4-dibromobenzene (5.0 g, 0.021 mmol) was dissolved in dry degassed tetrahydrofuran (20 mL) and cooled to -78 °C. The solution was treated with a solution of n-butyllithium in hexanes (1.6 M, 13.2 mL, 0.021 mmol). Diphenylphosphine chloride (3.77 mL, 0.021 mmol) was added dropwise to the reaction mixture and stirred for 1 hour. The solution was then allowed to warm to room temperature. The reaction was quenched with water (30 mL) and extracted with diethyl ether (2 x 20 mL). The organic layers were dried over magnesium sulphate, filtered and evaporated to dryness. Column chromatography (silica gel: dichloromethane/n-hexane (2:1)) afforded **17** as a clear liquid (3.5 g, 48 %). ¹H-NMR 200 MHz (CDCl₃): δ 7.51 (2H, dd, J = 1.2 Hz), 7.37 (10H, m), 7.19 (2H, dt, J = 7.0 Hz). ³¹P-NMR 200 MHz (CDCl₃): δ -5.25 (1P). MS (EI⁺): m/z 341 (M)⁺, 262 (M-Br)⁺, 183 (M-C₆H₅)⁺.

4-Diphenylphosphanyl-benzoic acid (18)

General synthesis adapted from work by Ravindar *et al.*⁹



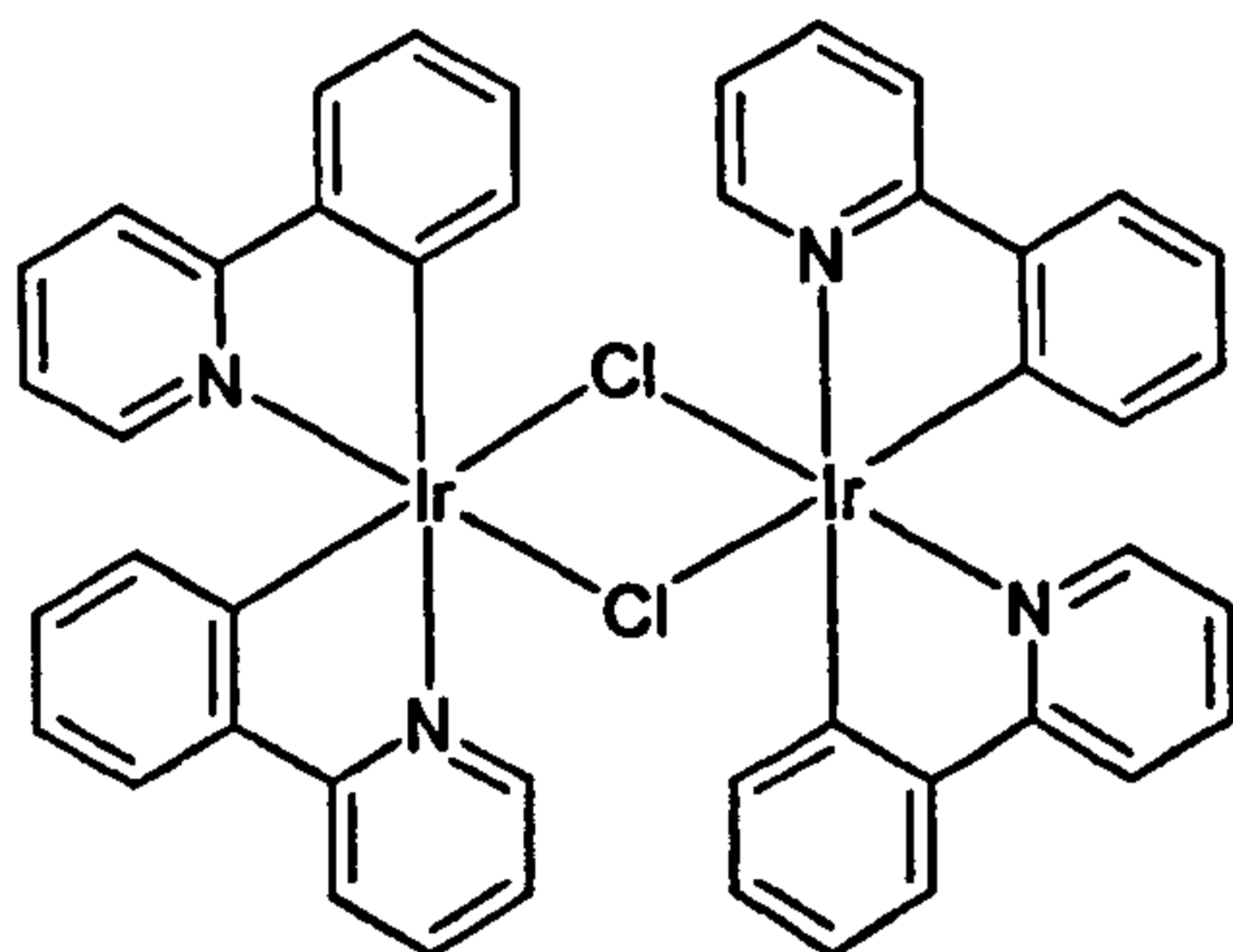
(4-Bromo-phenyl)-diphenyl-phosphane **17** (1.42 g, 4.2 mmol) was dissolved in dry degassed tetrahydrofuran (30 mL) and cooled to -78 °C. The solution was

treated with *n*-butyllithium (1.6 M, 4 mL, 6.4 mmol) in hexanes *via* dropwise addition. Solid CO₂ (excess) was then added to the reaction vessel which was allowed to warm to room temperature with continuous stirring over 1 hour. The mixture was quenched with water (20 mL) and basified using sodium hydroxide and extracted with diethyl ether (2 x 20 mL). The remaining aqueous layer was acidified and then extracted with diethyl ether (2 x 20 mL) and evaporated to dryness. Column chromatography (silica gel: acetone) afforded **18** as a white solid (0.33 g, 26 %). ¹H-NMR 200 MHz (CDCl₃): δ 10.75 (1H, s), 8.05 (2H, d, *J* = 7.4 Hz), 7.34 (12H, m). ³¹P-NMR 200 MHz (CDCl₃): δ - 3.64 (1P). MS (EI⁺): *m/z* 306 (M)⁺, 183 (M-C₇H₅O₂)⁺, 107 (M-C₁₃H₁₀O₂)⁺.

3.3 Bis-cyclometalated Dichloro-bridged Complexes of Ir(III) and Rh(III)

Tetrakis(2-phenylpyridine-C²,N')(μ -chloro)diiridium, [Ir(ppy)₂Cl]₂ (**19**)

General synthesis adapted from work by Sprouse *et al.*¹⁰



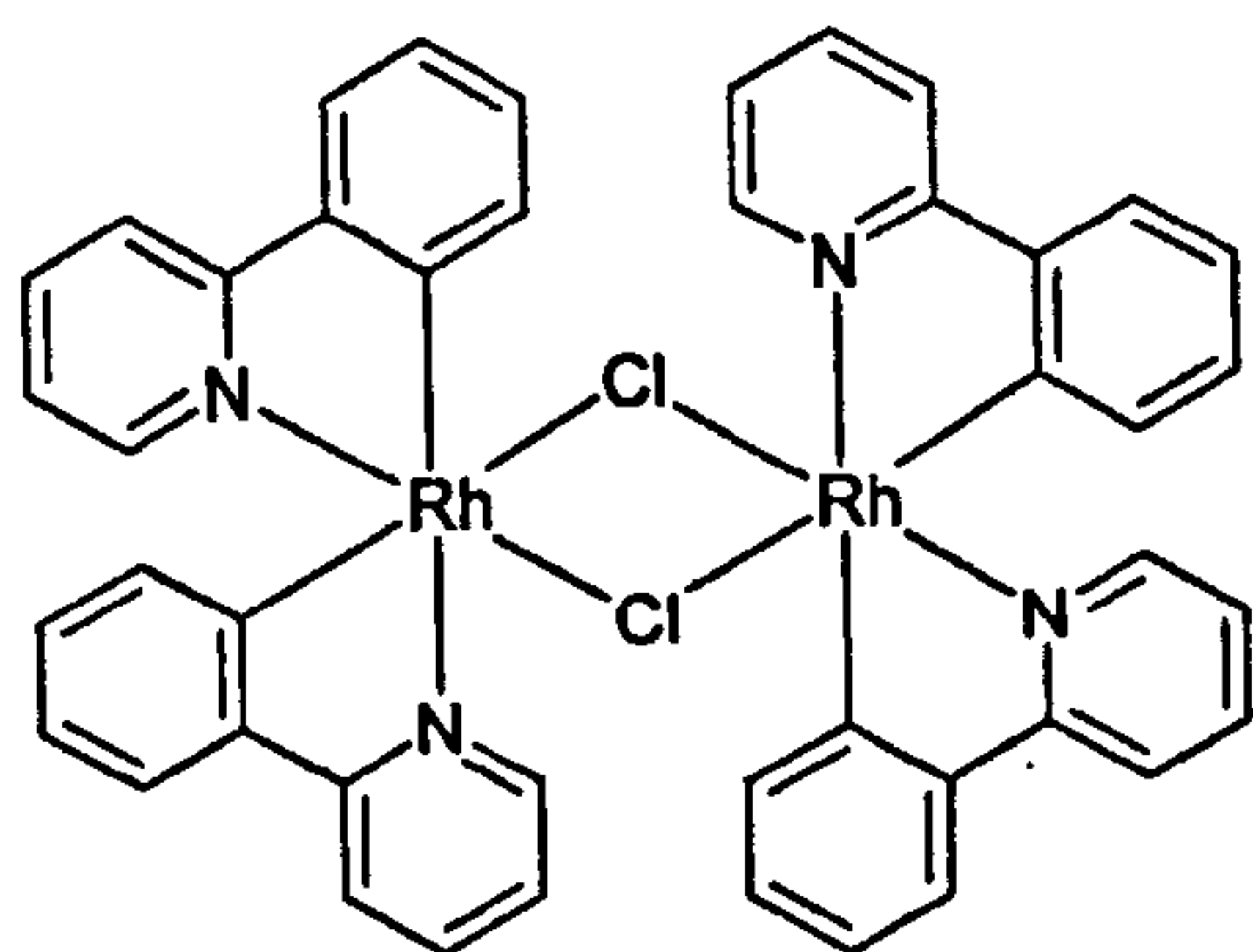
Iridium chloride (IrCl₃·3H₂O, 0.20 g, 5.67 mmol), 2-phenylpyridine (2.64 g, 17 mmol), 2-ethoxyethanol (30 mL) and water (15 mL) were placed in a reaction vessel and heated to 110 °C for 8 hours with under continuous stirring. The initial dark brown solution became lighter in colour and a

yellow precipitate formed. The solution was cooled to room temperature and was filtered. The resulting solid was washed with ethanol (2 x 10 mL) and acetone (2 x 10

ml) and the remaining solid dissolved in dichloromethane. Column chromatography (silica gel, dichloromethane) afforded **19** as a bright yellow solid (2.18 g, 72 %). $^1\text{H-NMR}$ 300 MHz (CD_2Cl_2): δ 9.23 (4H, dt $J = 2.4$ Hz), 7.92 (4H, d, $J = 7.5$ Hz), 7.77 (4H, td, $J = 8.1$ Hz), 7.55 (4H, dd, $J = 7.5$ Hz), 6.80 (8H, m), 6.58 (4H, td, $J = 7.5$ Hz), 5.85 (4H, dd, $J = 3.9$ Hz). MS (EI+): m/z 1072 (M^+), 1036 (M-H-Cl^+), 580 ($\text{M-Ir-C}_{22}\text{H}_{16}\text{N}_2\text{Cl}^+$), 501 ($\text{M-Ir-C}_{22}\text{H}_{16}\text{N}_2\text{Cl}_2^+$).

Tetrakis(2-phenylpyridine- C^2, N')(μ -chloro)dirhodium, $[\text{Rh}(\text{ppy})_2\text{Cl}]_2$ (**20**)

General synthesis adapted from work by Sprouse *et al.*¹⁰

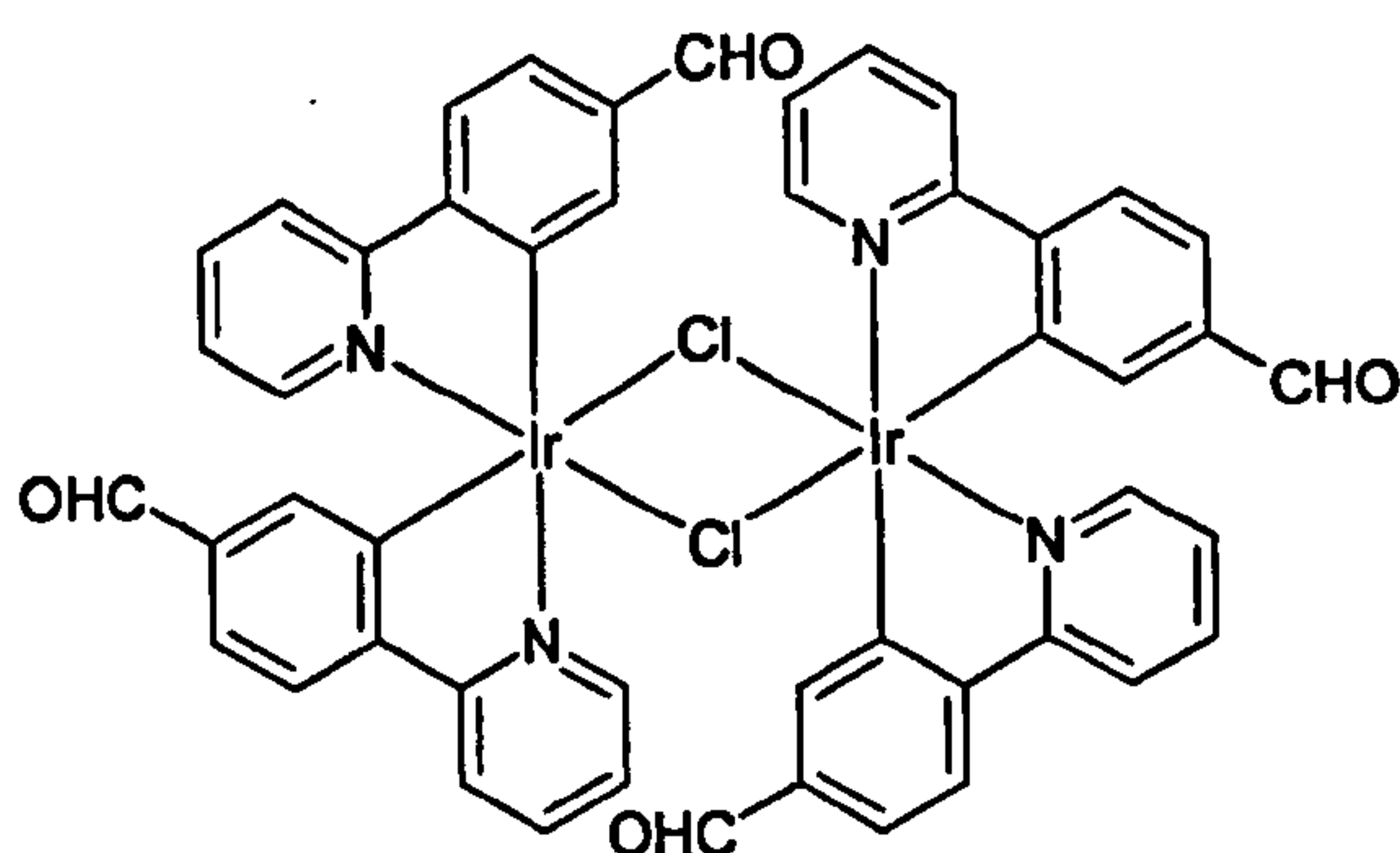


Rhodium chloride ($\text{RhCl}_3 \cdot 2\text{H}_2\text{O}$, 0.21 g, 1.0 mmol), 2-phenylpyridine (0.84 g, 5.0 mmol), 2-ethoxyethanol (15 ml) and water (10 ml) were placed in a reaction vessel and heated to 110 °C for 8 hours with under continuous stirring. The initial dark brown solution became lighter in colour and a

pale green-yellow precipitate formed. The solution was cooled to room temperature and was filtered. The resulting solid was washed with ethanol (2 x 10 ml) and acetone (2 x 10 ml). The product was dissolved in dichloromethane and column chromatography (silica gel, dichloromethane) afforded **20** as a pale green-yellow solid (0.42 g, 70 %). $^1\text{H-NMR}$ 300 MHz (CDCl_3): δ 9.22 (4H, d, $J = 5.7$ Hz), 7.85 (8H, m), 7.55 (4H, dd, $J = 7.8$ Hz), 6.80 (8H, m), 6.65 (4H, td, $J = 7.5$ Hz), 5.95 (4H, d, $J = 7.5$ Hz). MS (EI+): m/z 892 (M^+), 737 ($\text{M-C}_{11}\text{H}_8\text{N}^+$), 446 ($\text{M-RhC}_{22}\text{H}_{16}\text{N}_2\text{Cl}^+$), 411 ($\text{M-RhC}_{22}\text{H}_{16}\text{N}_2\text{Cl}_2^+$), 257 ($\text{M-RhC}_{33}\text{H}_{24}\text{N}_3\text{Cl}_2^+$), 103 ($\text{M-RhC}_{44}\text{H}_{32}\text{N}_4\text{Cl}_2^+$).

Tetrakis(4-(2-pyridyl)benzaldehyde- C^2,N')(μ -chloro)diiridium, $[\text{Ir}(\text{fppy})_2\text{Cl}]_2$ (21)

General synthesis adapted from work by Sprouse *et al.*¹⁰

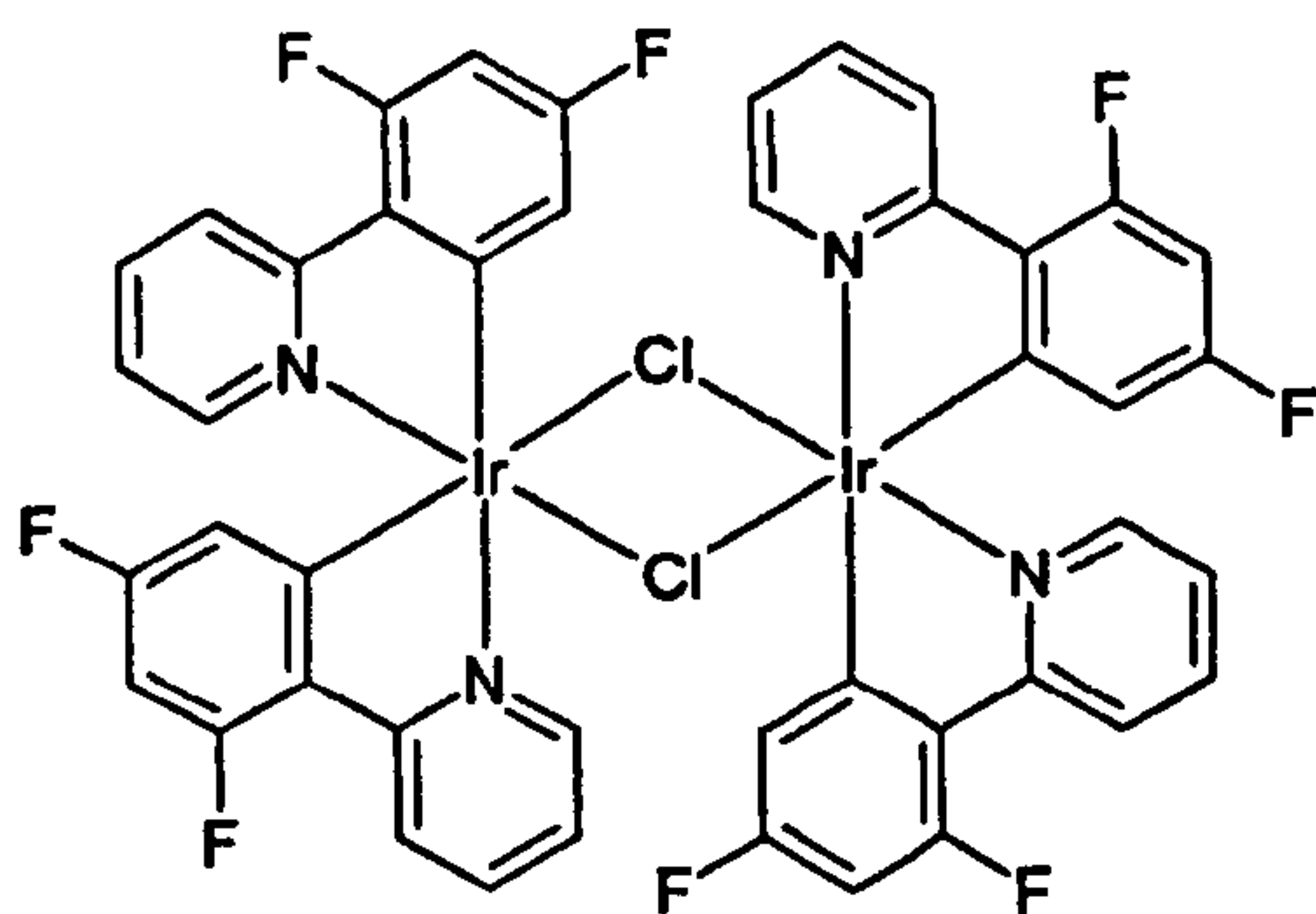


$\text{IrCl}_3 \cdot 3\text{H}_2\text{O}$ (0.35 g, 1.0 mmole), 4-(2-pyridyl)benzaldehyde (0.92 g, 5.0 mmole), 2-ethoxyethanol (15 ml) and water (7 ml) were placed in a reaction vessel and heated to 110 °C for 8 hours with under continuous stirring. The initial dark brown solution became lighter in

colour and an orange precipitate formed. The solution was cooled to room temperature and was filtered. The resulting solid was washed with ethanol (2 x 10 ml) and acetone (2 x 10 ml). The product was dissolved in dichloromethane and column chromatography (silica gel, dichloromethane) afforded **21** as a bright orange solid (0.44 g, 73 %). $^1\text{H-NMR}$ 300 MHz (CDCl_3): δ 9.53 (4H, s), 9.27 (4H, d, $J = 4.8$ Hz), 8.07 (4H, d, $J = 7.8$ Hz), 7.94 (4H, td, $J = 8.0$ Hz), 7.68 (4H, d, $J = 8.4$ Hz), 7.32 (4H, dd, $J = 1.5$ Hz), 6.91 (4H, td, $J = 6.0$ Hz), 6.29 (4H, d, $J = 1.5$ Hz). MS (EI⁺): m/z 1184 (M^+), 592 ($\text{M-IrC}_{24}\text{H}_{16}\text{N}_2\text{O}_2\text{-Cl}^+$), 557 ($\text{M-IrC}_{24}\text{H}_{16}\text{N}_2\text{O}_2\text{-Cl}_2^+$). The X-ray crystal structure and related data for **21** can be found in appendix A, part A5. Crystals were grown from dichloromethane.

Tetrakis(2-(2,4-difluorophenyl)-pyridine- C^2,N')(μ -chloro)diiridium, $[\text{Ir}(\text{F}_2\text{ppy})_2\text{Cl}]_2$ (22)

General synthesis adapted from work by Sprouse *et al.*¹⁰

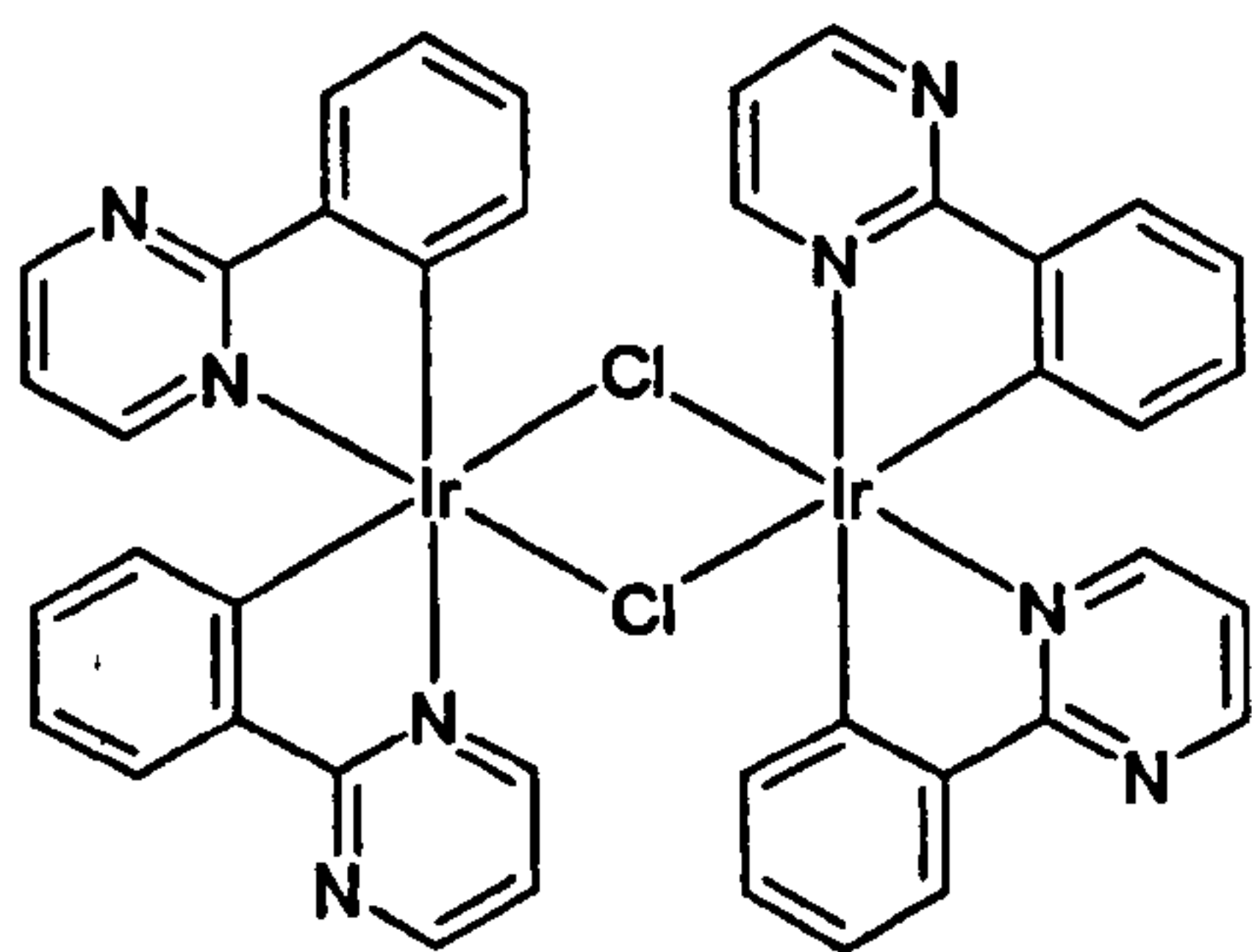


$\text{IrCl}_3 \cdot 3\text{H}_2\text{O}$ (0.31 g, 0.85 mmol), 2-(2,4-difluorophenyl)pyridine **1** (0.72 g, 3.81 mmol), 2-ethoxyethanol (20 ml) and water (10 mL) were placed in a reaction vessel and heated to 110 °C for 8 hours with under continuous stirring. The initial dark brown solution became lighter in colour and a yellow precipitate formed. The

solution was cooled to room temperature and filtered. The resulting solid was washed with ethanol (2 x 10 ml) and acetone (2 x 10 ml) and dissolved in dichloromethane. Column chromatography (silica gel, dichloromethane) afforded **22** as a bright yellow solid (0.42 g, 78 %). $^1\text{H-NMR}$ 300 MHz (CD_2Cl_2): δ 9.09 (4H, d, $J = 6.0$ Hz), 8.31 (4H, d, $J = 8.4$ Hz), 7.85 (4H, t, $J = 7.2$ Hz), 6.85 (4H, td, $J = 6.0$ Hz), 6.36 (4H, td, $J = 11.25$ Hz), 5.48 (4H, d, $J = 9.3$ Hz). MS (EI+): m/z 1216 (M^+), 608 ($\text{M-Ir-C}_{22}\text{H}_{12}\text{F}_4\text{N}_2\text{Cl}^+$), 573 ($\text{M-Ir-C}_{22}\text{H}_{12}\text{F}_4\text{N}_2\text{Cl}_2^+$). The X-ray crystal structure and related data for **22** can be found in appendix A, part A6. Crystals were grown from dichloromethane.

Tetrakis(2-phenylpyrimidine- C^2, N')(μ -chloro)diiridium, $[\text{Ir}(\text{ppm})_2\text{Cl}]_2$ (**23**)

General synthesis adapted from work by Sprouse *et al.*¹⁰

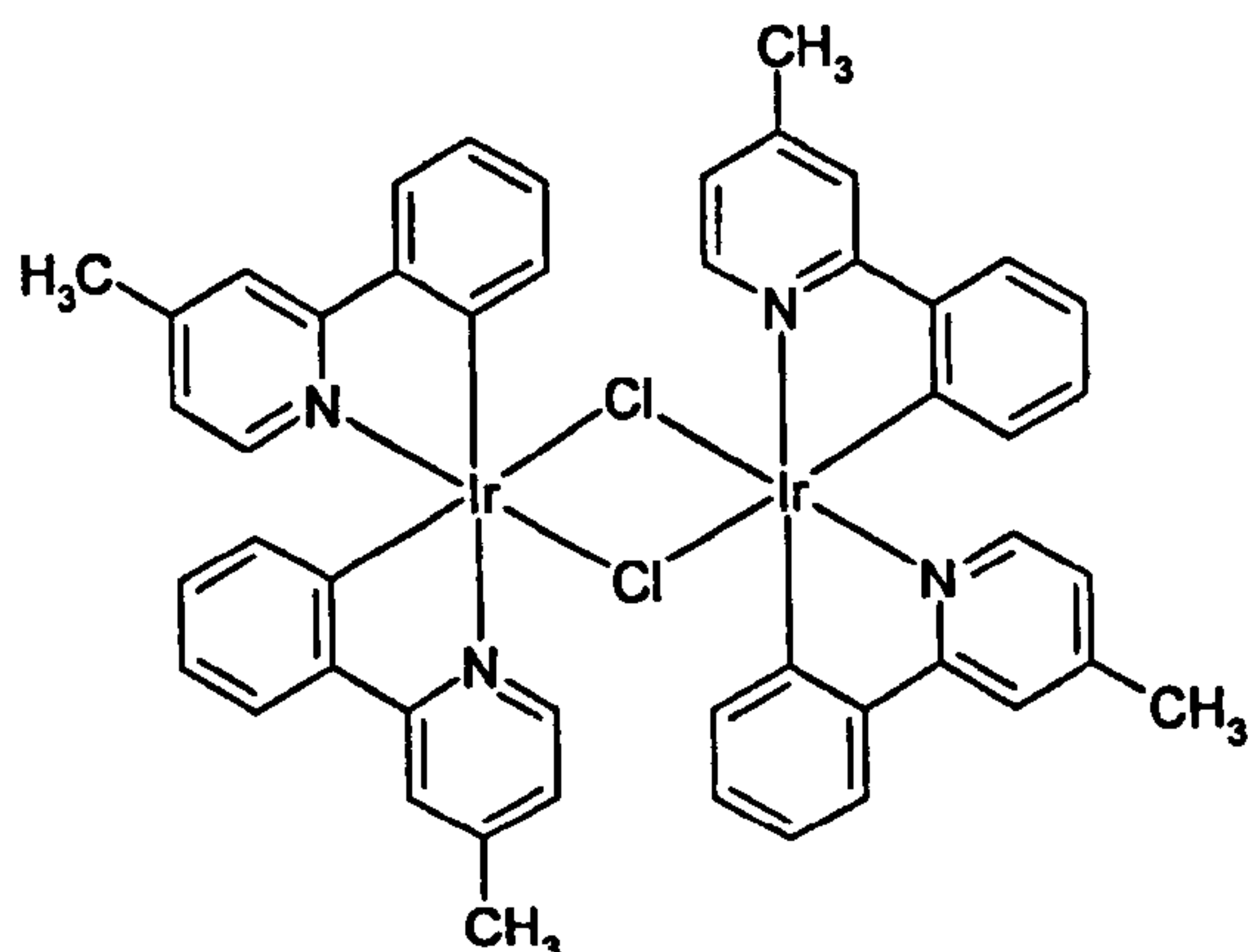


$\text{IrCl}_3 \cdot 3\text{H}_2\text{O}$ (0.076 g, 0.22 mmol), 2-phenylpyrimidine **3** (0.14 g, 0.87 mmol), 2-ethoxyethanol (20 mL) and water (10 mL) were placed in a reaction vessel and heated to 110 °C for 8 hours with under continuous stirring. The initial dark brown solution became lighter in colour and a

golden orange precipitate formed. The solution was cooled to room temperature and filtered. The resulting solid was washed with ethanol (2 x 10 mL) and acetone (2 x 10 mL) and dissolved in dichloromethane. Column chromatography (silica gel, dichloromethane) afforded **23** as an orange solid (0.06 g, 40 %). $^1\text{H-NMR}$ 300 MHz (CDCl_3): δ 9.42 (4H, dd, $J = 1.4$ Hz), 8.83 (4H, dd, $J = 2.25$ Hz), 7.93 (4H, dd, $J = 7.5$ Hz), 6.87 (8H, m), 6.72 (4H, td, $J = 7.8$ Hz), 5.97 (4H, d, $J = 7.2$ Hz). MS (EI+): m/z 1077 (M^+), 1039 (M-Cl^+), 920 ($\text{M-C}_{10}\text{H}_7\text{N}_2^+$), 538 ($\text{M-IrC}_{20}\text{H}_{14}\text{N}_4\text{Cl}^+$), 503 ($\text{M-IrC}_{20}\text{H}_{14}\text{N}_4\text{Cl}_2^+$), 423 ($\text{M-IrC}_{30}\text{H}_{28}\text{N}_8\text{Cl}_3^+$).

**Tetrakis(4-methyl-2-phenylpyridine- C^2,N')(μ -chloro)diiridium,
[Ir(4-Meppy) $_2$ Cl] $_2$ (24)**

General synthesis adapted from work by Sprouse *et al.*¹⁰

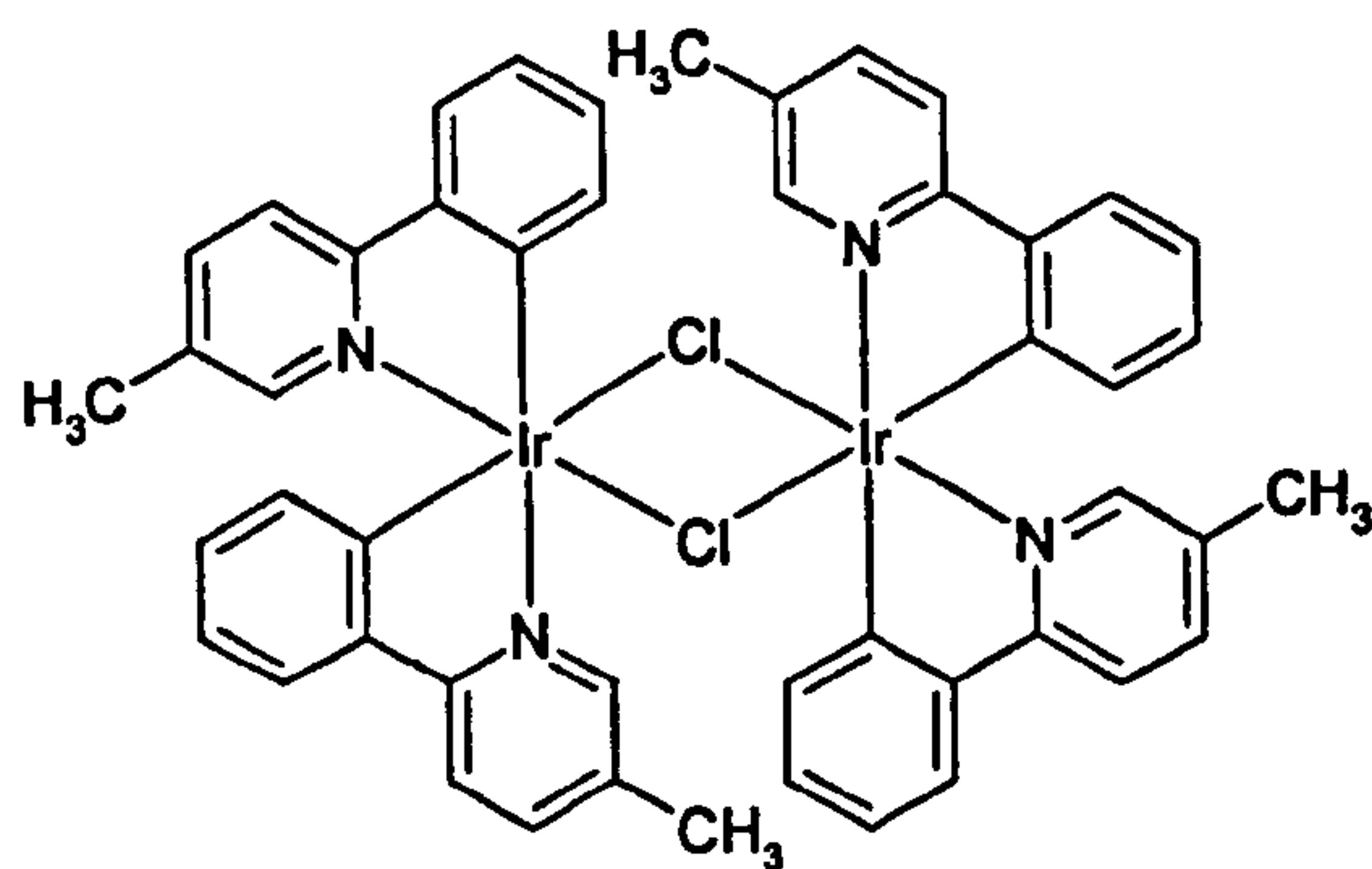


IrCl $_3$ ·3H $_2$ O (0.30 g, 0.85 mmol), 2-phenyl-4-methylpyridine **9** (0.64 g, 3.8 mmol), 2-ethoxyethanol (10 ml) and water (5 ml) were placed in a reaction vessel and heated to 110 °C for 8 hours with under continuous stirring. The initial dark brown solution became lighter in colour and a yellow precipitate formed. The solution

was cooled to room temperature and filtered. The resulting solid was washed with ethanol (2 x 10 ml) and acetone (2 x 10 ml) and dissolved in dichloromethane. Column chromatography (silica gel, dichloromethane) afforded **24** as a bright yellow solid (0.36 g, 75 %). $^1\text{H-NMR}$ 300 MHz (CDCl $_3$): δ 9.05 (4H, d, J = 5.7 Hz), 7.68 (4H, s), 7.47 (4H, d, J = 7.2 Hz), 6.73 (4H, t, J = 6.9 Hz), 6.55 (8H, m), 5.96 (4H, d, J = 8.7 Hz), 2.65 (12H, s). MS (EI $^+$): m/z 1128 (M) $^+$, 564 (M-IrC $_{24}$ H $_{20}$ N $_2$ Cl) $^+$, 529 (M-IrC $_{24}$ H $_{20}$ N $_2$ Cl $_2$) $^+$.

**Tetrakis(5-methyl-2-phenylpyridine- C^2,N')(μ -chloro)diiridium,
[Ir(5-Meppy) $_2$ Cl] $_2$ (25)**

General synthesis adapted from work by Sprouse *et al.*¹⁰



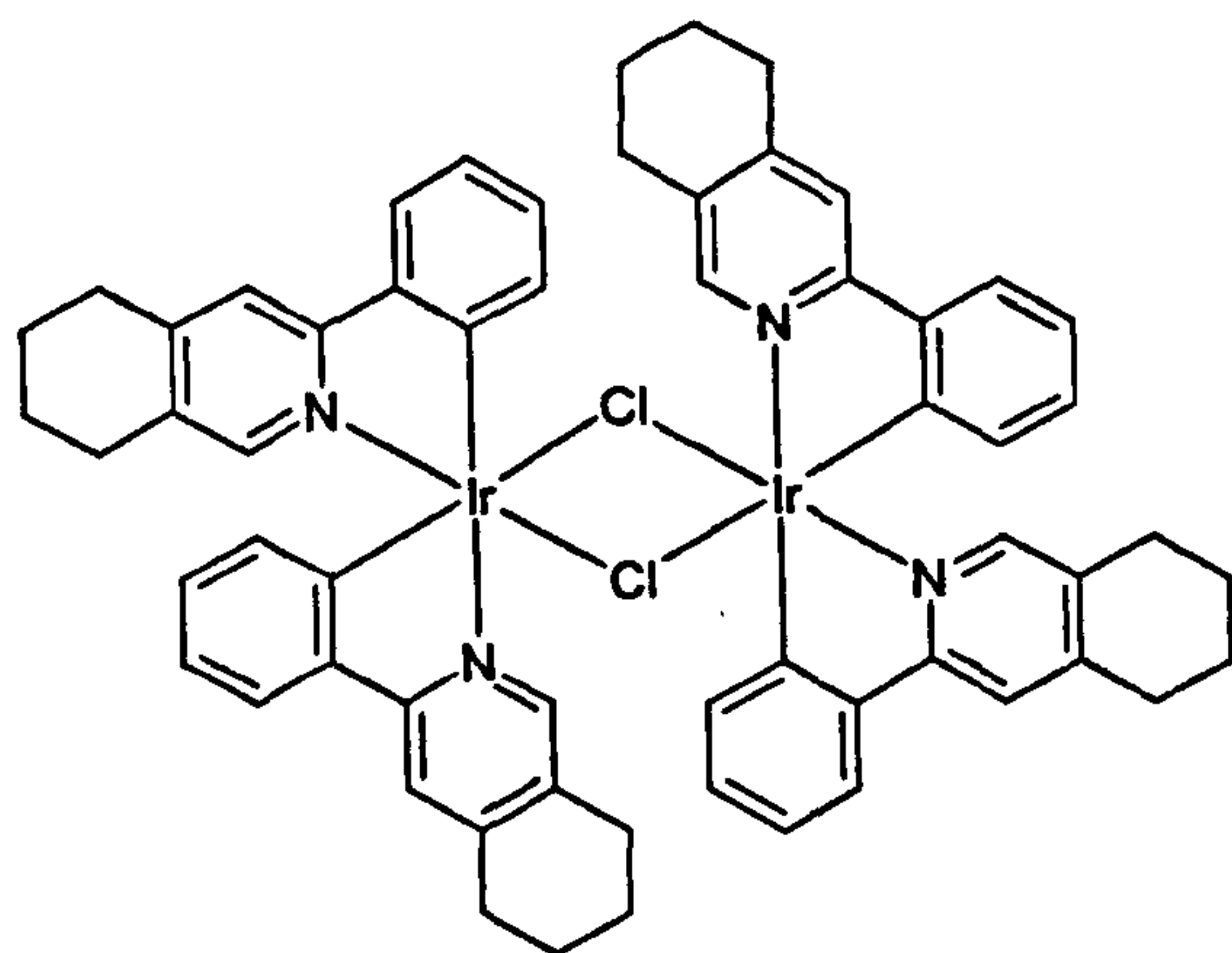
IrCl $_3$ ·3H $_2$ O (0.27 g, 0.77 mmol), 2-phenyl-5-methylpyridine **11** (0.50 g, 3.0 mmol), 2-ethoxyethanol (10 ml) and water (10 ml) were placed in a reaction vessel and heated to 110 °C for 8 hours with under continuous stirring. The initial dark brown solution became lighter in colour

and a yellow precipitate formed. The solution was cooled to room temperature and

filtered. The resulting solid was washed with ethanol (2 x 10 ml) and acetone (2 x 10 ml) and dissolved in dichloromethane. Column chromatography (silica gel, dichloromethane) afforded **25** as a bright yellow solid (0.36 g, 83 %). $^1\text{H-NMR}$ 300 MHz (CDCl_3): δ 9.12 (4H, s), 7.77 (4H, d, $J = 8.4$ Hz), 7.61 (4H, d, $J = 9.9$ Hz), 7.44 (4H, d, $J = 6.9$ Hz), 6.75 (4H, t, $J = 7.5$ Hz), 6.55 (4H, t, $J = 7.5$ Hz), 5.85 (4H, d, $J = 8.1$ Hz), 1.57 (12H, s). MS (EI $^+$): m/z 1128 (M^+), 564 ($\text{M-C}_{24}\text{H}_{20}\text{Cl}^+$).

Tetrakis(3-phenyl-5,6,7,8-tetrahydro-isoquinoline-C²,N')(μ -chloro)diiridium, [Ir(Cyclohex)₂Cl]₂ (26**)**

General synthesis adapted from work by Sprouse *et al.*¹⁰



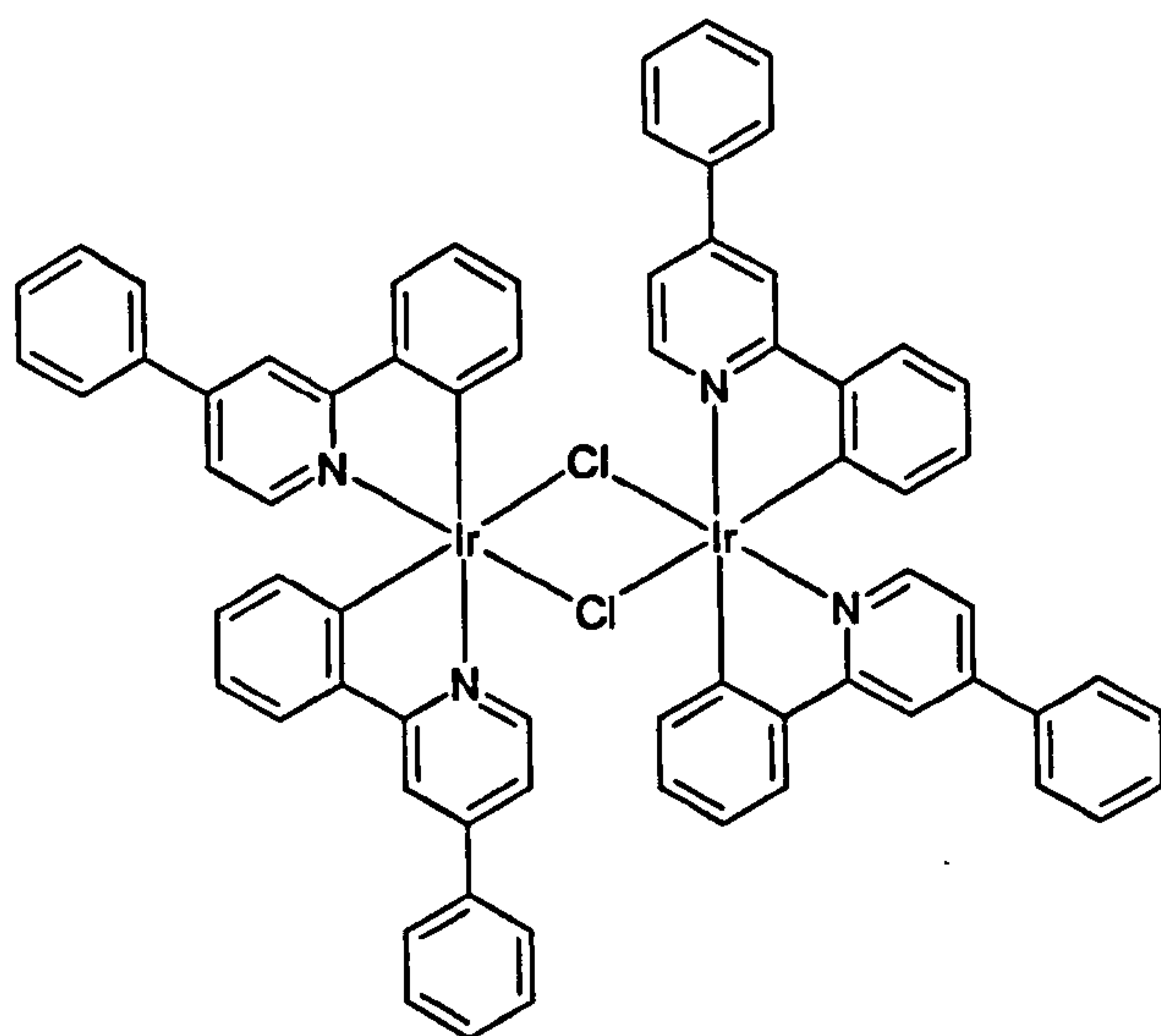
$\text{IrCl}_3 \cdot 3\text{H}_2\text{O}$ (0.21 g, 0.60 mmol), 3-phenyl-5,6,7,8-tetrahydro-isoquinoline **12** (0.50 g, 2.4 mmol), 2-ethoxyethanol (10 ml) and water (10 ml) were placed in a reaction vessel and heated to 110 °C for 8 hours with under continuous stirring. The initial dark brown solution became lighter in colour and a yellow-orange precipitate

formed. The solution was cooled to room temperature and filtered. The resulting solid was washed with ethanol (2 x 10 ml) and acetone (2 x 10 ml) and was dissolved in dichloromethane. Column chromatography (silica gel, dichloromethane) afforded **26** as a yellow solid (0.37 g, 92 %). $^1\text{H-NMR}$ 300 MHz (CDCl_3): δ 9.12 (4H, s), 7.51 (4H, s), 7.37 (4H, d, $J = 6.6$ Hz), 6.69 (4H, t, $J = 7.8$ Hz), 6.52 (4H, t, $J = 7.7$ Hz), 5.76 (4H, d, $J = 7.8$ Hz), 3.06 (8H, m), 2.64 (4H, m), 2.08 (4H, m), 1.90 (16H, m). MS (EI $^+$): m/z 1288 (M^+), 1253 (M-Cl^+), 1215 (M-Cl_2^+), 1079 ($\text{M-C}_{15}\text{H}_{14}\text{N}^+$), 1043 ($\text{M-C}_{15}\text{H}_{14}\text{NCl}^+$).



Tetrakis(2,4-diphenylpyridine-C²,N')(μ -chloro)diiridium, [Ir(dppy)₂Cl]₂ (27)

General synthesis adapted from work by Sprouse *et al.*¹⁰

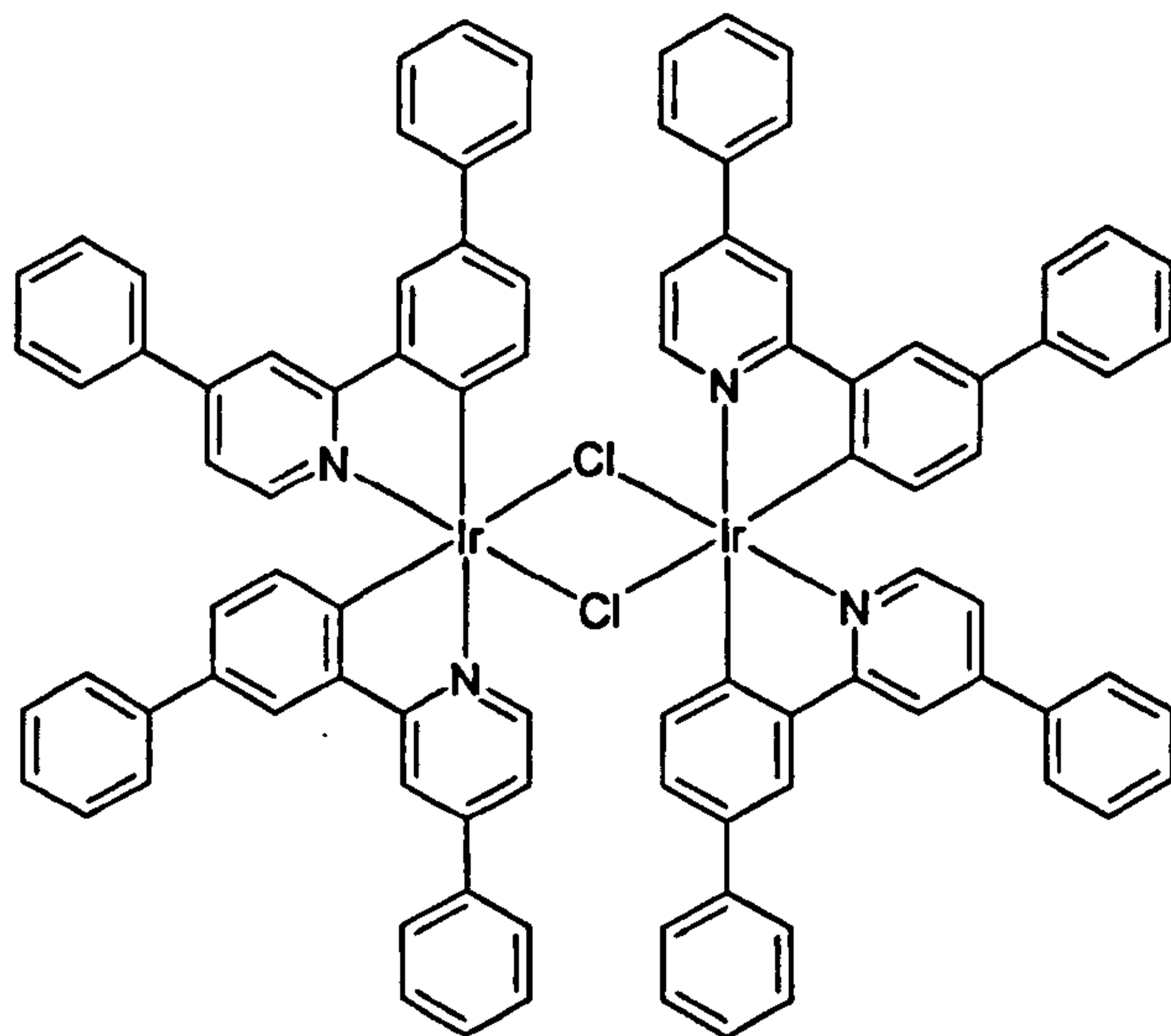


$\text{IrCl}_3 \cdot 3\text{H}_2\text{O}$ (0.18 g, 0.50 mmol), 2,4-diphenylpyridine **14** (0.47 g, 2.0 mmol), 2-ethoxyethanol (10 ml) and water (5 ml) were placed in a reaction vessel and heated to 110 °C for 8 hours with under continuous stirring. The initial dark brown solution became lighter in colour and an orange precipitate formed. The solution was cooled to room

temperature and filtered. The resulting solid was washed with ethanol (2 x 10 ml) and acetone (2 x 10 ml) and dissolved in dichloromethane. Column chromatography (silica gel, dichloromethane) afforded **27** as an orange solid (0.28 g, 83 %). ¹H-NMR 300 MHz (CDCl_3): δ 9.30 (4H, d, J = 6.3 Hz), 8.12 (4H, d, J = 2.1 Hz), 7.63 (12H, m), 7.51 (12H, m), 6.91 (4H, dd, J = 8.1 Hz), 6.80 (4H, d, J = 6.6 Hz), 6.63 (4H, t, J = 7.2 Hz), 6.14 (4H, d, J = 6.9 Hz). MS (EI⁺): m/z 1376 (M)⁺, 1340 (M -Cl)⁺, 1145 (M -C₁₇H₂₄N)⁺, 1109 (M -C₁₇H₂₄NCl)⁺. The X-ray crystal structure and related data for **27** can be found in appendix A, part A7. Crystals were grown from dichloromethane and toluene.

**Tetrakis(2-biphenyl-3-yl-4-phenyl-pyridine-C²,N')(μ -chloro)diiridium,
[Ir(bippy)₂Cl]₂ (28)**

General synthesis adapted from work by Sprouse *et al.*¹⁰



IrCl₃.3H₂O (0.11 g, 0.31 mmol), 2-biphenyl-3-yl-4-phenyl-pyridine 16 (0.39 g, 1.25 mmol), 2-ethoxyethanol (15 ml) and water (8 ml) were placed in a reaction vessel and heated to 110 °C for 8 hours with under continuous stirring. The initial dark brown solution became lighter in colour and a brown-orange precipitate formed. The solution

was cooled to room temperature and filtered. The resulting solid was washed with ethanol (2 x 10 ml) and acetone (2 x 10 ml) and dissolved in dichloromethane. Column chromatography (silica gel, dichloromethane) afforded 28 as a dark orange solid (0.20 g, 76 %). ¹H-NMR 200 MHz (CDCl₃): δ 9.37 (4H, d, J = 6.2 Hz), 8.23 (4H, s), 7.98 (4H, s), 7.84 (4H, d, J = 1.6), 7.56 (36H, m), 6.99 (4H, dd, J = 8.2 Hz), 6.91 (4H, dd, J = 9.6 Hz), 6.30 (4H, d, J = 8.0 Hz). MS (ES⁺): m/z 1686 (M)⁺, 1266 (M-C₁₁₀H₈₀Cl)⁺, 843 (M-C₄₆H₃₂N₂Cl)⁺, 805 (M-C₄₆H₃₂N₂Cl₂)⁺.

3.4 Monomeric M(L)₃ and M(L)₂acac Complexes of Ir(III) and Rh(III)

Tris-(acetylacetonato)iridium, Ir(acac)₃ (29)

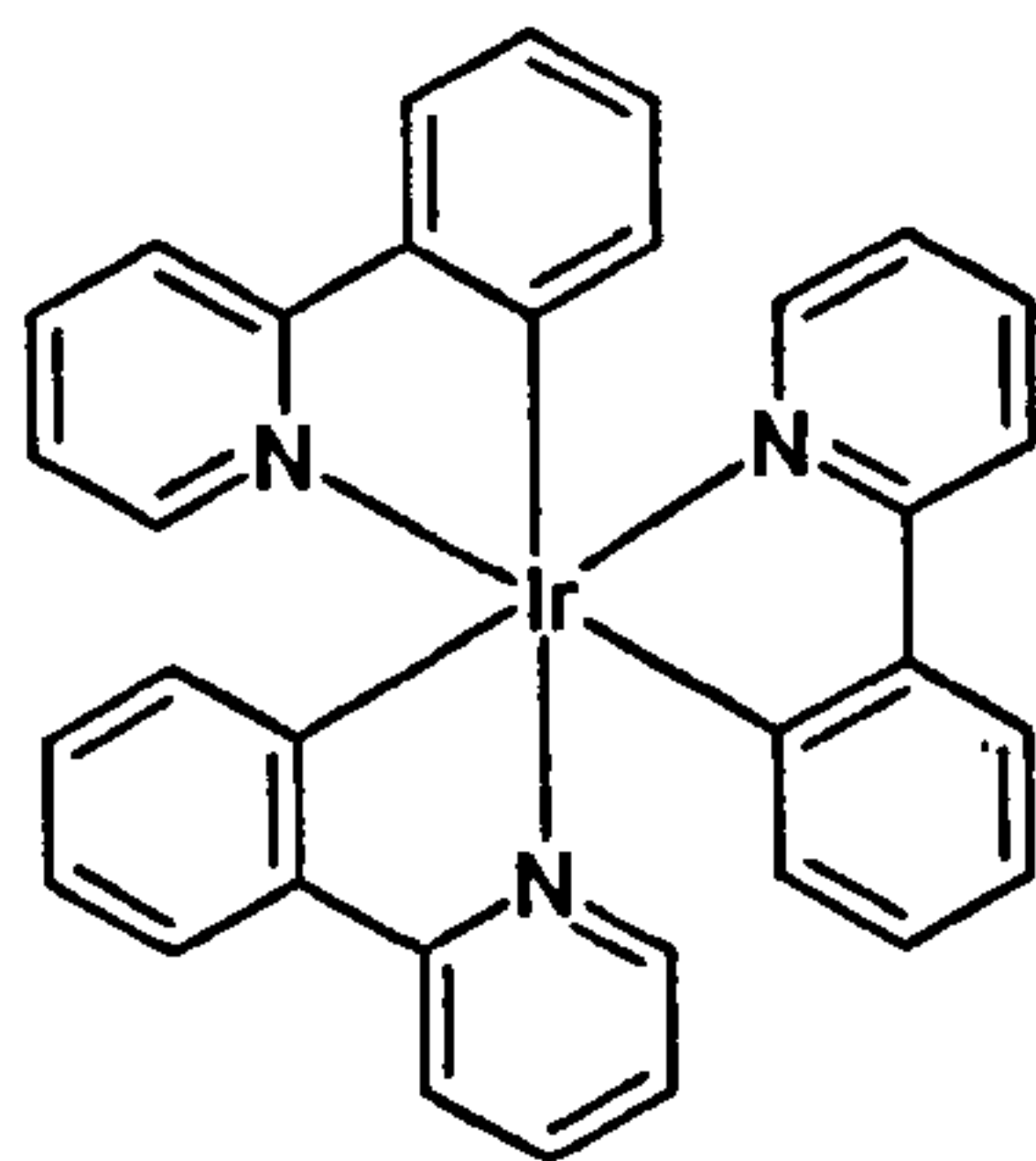
Synthesis taken from work by Collins *et al.*¹¹

IrCl₃.3H₂O (1.0 g, 2.86 mmol) and water (10ml) were placed in a reaction vessel and the pH was adjusted to pH 4-5 using sodium bicarbonate and 1M HCl. The solution was refluxed for 30 minutes and then allowed to cool to room temperature and

2,4-pentanedione (2.86 g, 28.6 mmol, 2.63 mL) was added, the resulting solution was then refluxed for a further 30 minutes. After cooling to room temperature, the acidity was adjusted again to pH 4-5 and the resulting solution was refluxed for 24 hours. The mixture was cooled to room temperature and evaporated to dryness to give an orange-yellow solid. The crude material was recrystallised from hot methanol to give **29** as a bright orange-yellow solid (0.89 g, 64%). MS (EI+): m/z 490 (M)⁺, 391 ($M-C_5H_7O_2$)⁺, 291 ($M-C_{10}H_{15}O_4$)⁺. Elemental analysis showed the presence of chloride. Analysis calculated for $C_{15}H_{21}IrO_6$ (MW 489.5): Cl: 0 %. Found Cl: 26.33. The presence of a large proportion of chlorine containing species clearly illustrates the inadequacy of this purification method.

***Fac*-tris-(2-phenylpyridine- C^2,N')iridium, *fac*-Ir(ppy)₃ (**30**)**

General synthesis adapted from work by Colombo *et al.*¹²

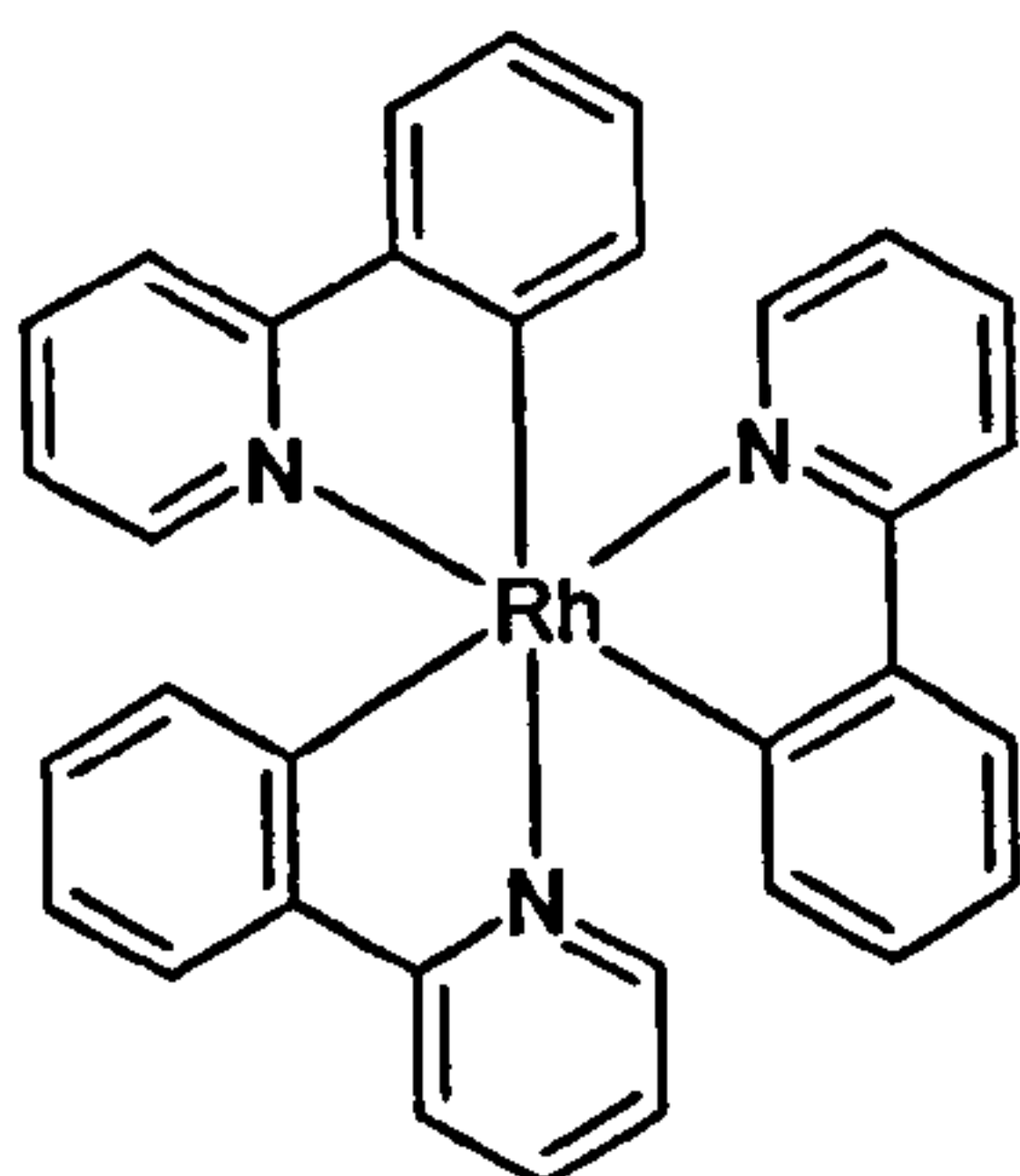


[Ir(ppy)₂Cl]₂ **19** (0.11 g, 0.10 mmol), 2-phenylpyridine (0.95 g, 6.1 mmol) and silver(I) trifluoromethanesulphonate (0.05 g, 0.19 mmol) were placed in a reaction vessel and purged with nitrogen. The mixture was heated to 110 °C for 8 hours with continuous stirring. The suspension was cooled to room temperature and filtered through a glass filter frit. The

precipitate was washed with ethanol (2 x 10 mL) to remove any remaining ligand. Column chromatography (silica gel, dichloromethane) afforded **30** as a bright yellow solid (0.09 g, 67 %). ¹H-NMR 300MHz (CD₂Cl₂): δ 8.0 (1H, d, J = 8.1 Hz), 7.64 (2H, m), 7.55 (1H, d, J = 5.4 Hz), 6.89 (2H, m), 6.75 (2H, m). MS (EI+): m/z 655 (M)⁺, 577 ($M-C_5H_4N$)⁺, 501 ($M-C_{11}H_8N$)⁺. Elemental analysis $Ir_1C_{33}H_{24}N_3$, $M(654.79)$; Expected C: 60.53 %, H: 3.69 %, N: 6.42 %, Obtained C: 59.81 %, H: 3.84 %, N: 6.26 % corresponding to $Ir_1C_{33}H_{24}N_3 \cdot H_2O$.

***Fac*-tris-(2-phenylpyridine- C^2,N')rhodium, *fac*-Rh(ppy)₃ (31)**

General synthesis adapted from work by Colombo *et al.*¹²

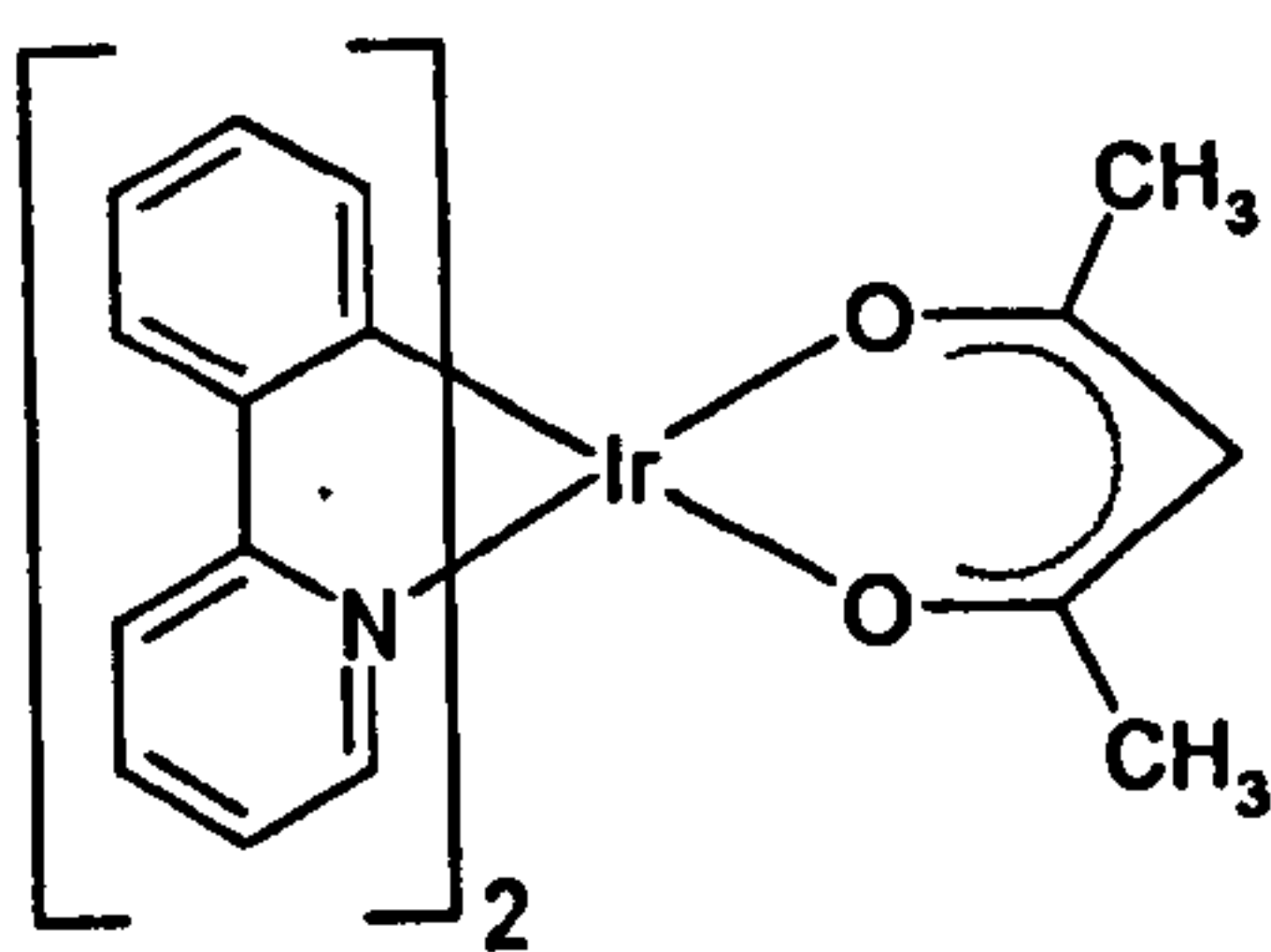


[Rh(ppy)₂Cl]₂ **20** (0.10 g, 0.11 mmol), 2-phenylpyridine (1.2 g, 7.73 mmol) and silver(I) trifluoromethanesulphonate (0.073 g, 0.28 mmol) were placed in a reaction vessel and purged with nitrogen. The mixture was heated to 110 °C for 8 hours with continuous stirring. The solution was cooled to room temperature and filtered through a glass filter frit. The

precipitate was washed with ethanol (2 x 10 ml) to remove any remaining ligand. Column chromatography (silica gel, dichloromethane) afforded **31** as a pale yellow solid (0.008 g, 6.2 %). ¹H-NMR 300 MHz (CD₂Cl₂): δ 7.92 (3H, d, J = 8.1 Hz), 7.70 (6H, m), 7.56 (3H, d, J = 4.5 Hz) 6.92 (6H, m), 6.80 (6H, m). MS (EI⁺): m/z 565 (M)⁺, 410 (M-C₁₁H₈N)⁺. HRMS (EI⁺): m/z 565.1033 (M)⁺, 410.0300 (M-C₁₁H₈N)⁺.

Bis-(2-phenylpyridine- C^2,N')acetylacetonate iridium, Ir(ppy)₂AcAc (32)

General synthesis adapted from work by Colombo *et al.*¹²

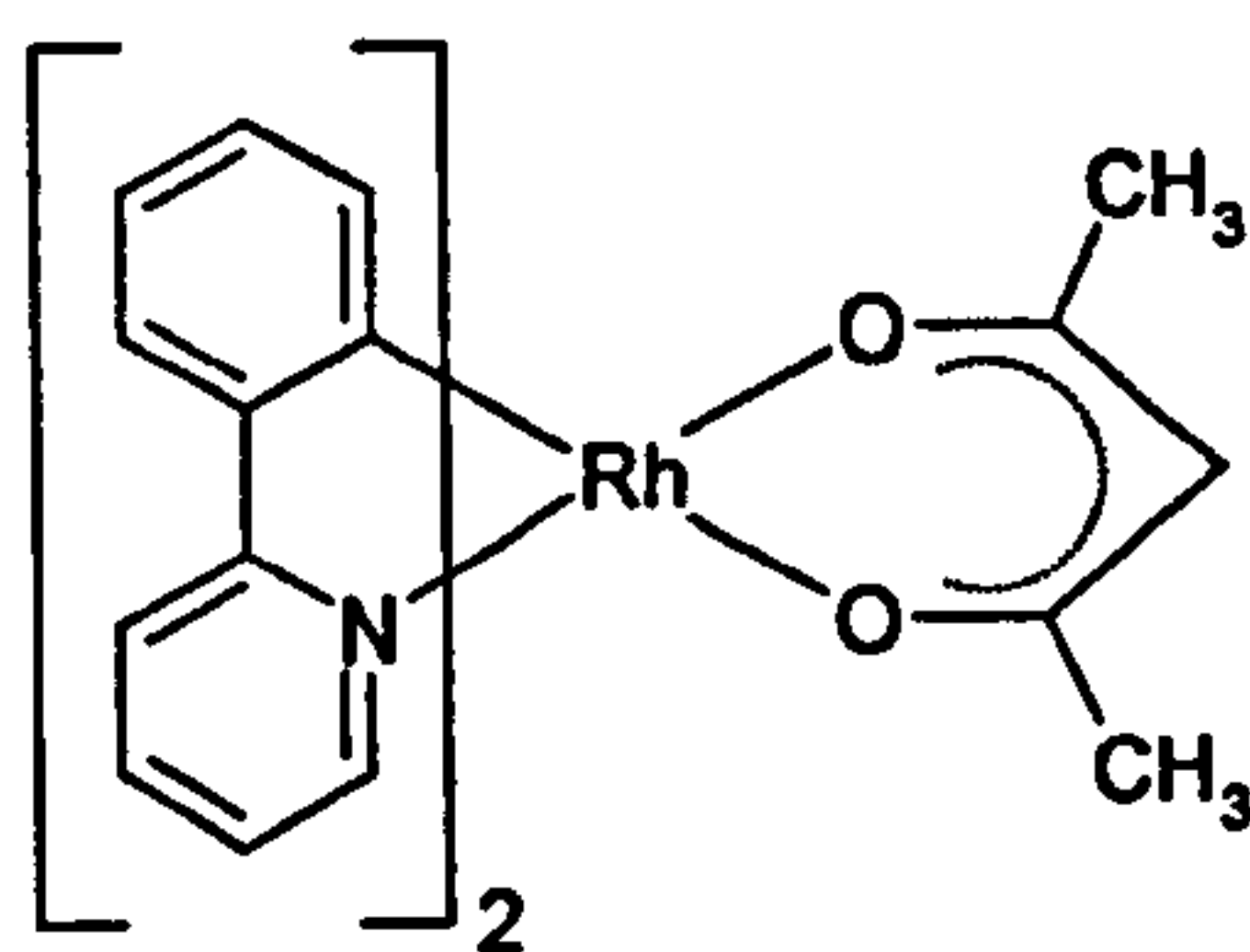


[Ir(ppy)₂Cl]₂ **19** (0.11 g, 0.10 mmol), 2,4-pentanedione (mass, 0.05 g, 0.5 mmol) silver(I) trifluoromethanesulphonate (0.13 g, 0.5 mmol) and 2-methoxyethyl ether (2 mL) were placed in a reaction vessel and purged with nitrogen. The mixture was heated

to 110 °C for 1 hour. The solution was cooled to room temperature and water (10 ml) and dichloromethane (2 x 10 ml) were added. The organic layer was extracted, dried over magnesium sulphate, filtered and evaporated to dryness. Column chromatography (silica gel, dichloromethane) afforded **32** as a yellow-orange solid (0.06 g, 52 %). ¹H-NMR 300 MHz (CDCl₃): δ 8.52 (2H, d, J = 6.0 Hz), 7.86 (2H, d, J = 8.1 Hz), 7.74 (2H, td, J = 8.0 Hz), 7.55 (2H, dd, J = 7.8 Hz), 7.15 (2H, td, J = 6.5 Hz), 6.82 (2H, td, J = 6.8 Hz), 6.69 (2H, td, J = 7.5 Hz), 6.27 (2H, dd, J = 6.6 Hz), 5.22 (1H, m), 1.79 (6H, s). MS (EI⁺): m/z 600 (M)⁺, 501 (M-C₅H₇O₂)⁺, 444 (M-C₁₁H₁₀N)⁺. HRMS (EI⁺): m/z 600.1394 (M)⁺, 501.0945 (M-C₅H₇O₂)⁺.

Bis-(2-phenylpyridine-C²,N')acetylacetonate rhodium, Rh(ppy)₂AcAc (33)

General synthesis adapted from work by Colombo *et al.*¹²

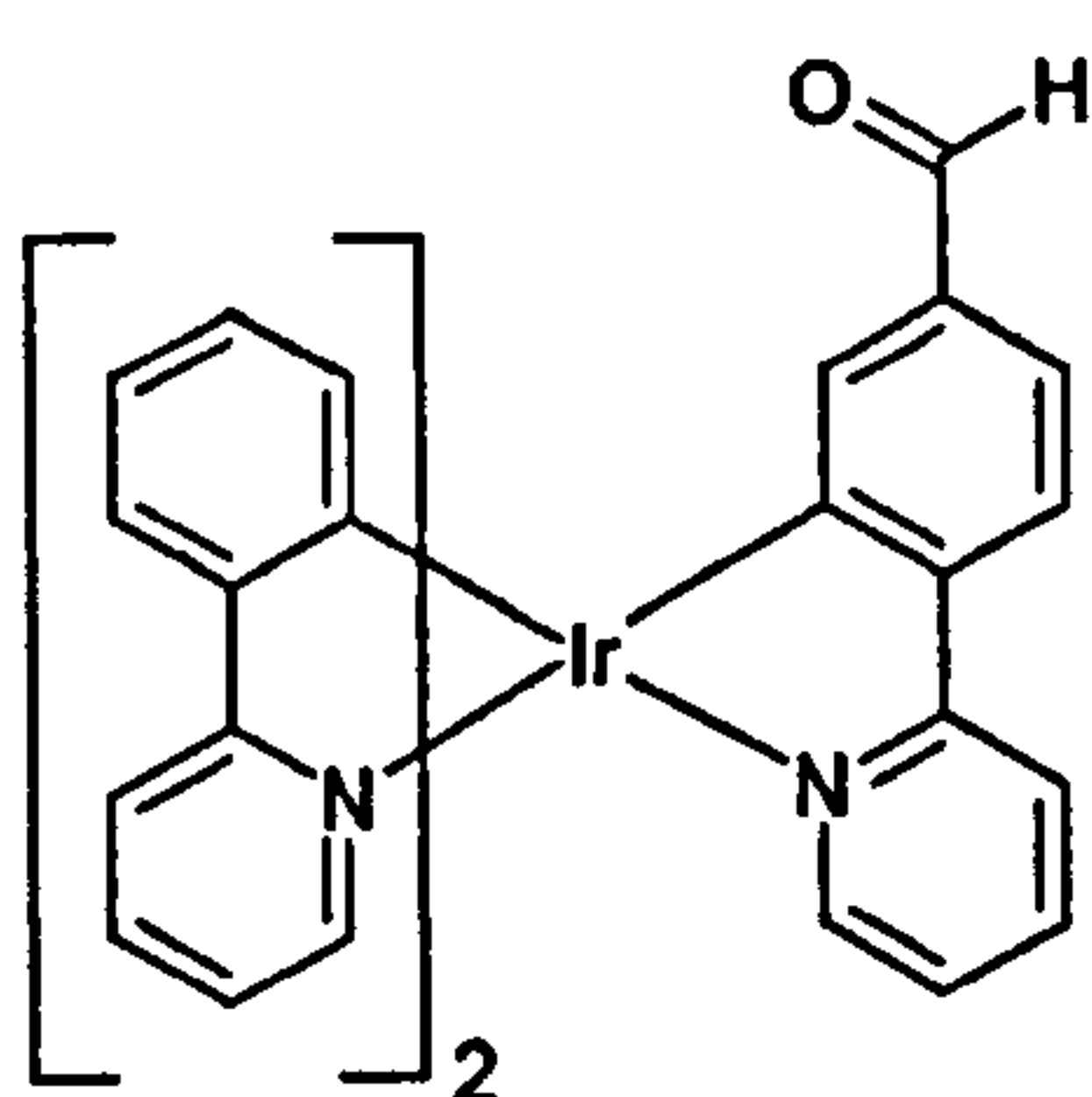


[Rh(ppy)₂Cl]₂ 20 (0.10 g, 0.11 mmol), 2,4-pentanedione (0.022 g, 0.22 mmol), silver(I) trifluoromethanesulphonate (0.06 g, 0.23 mmol) and 2-methoxyethyl ether (1 mL) were placed in a reaction vessel and purged with nitrogen. The mixture was heated

to 110 °C for 30 minutes. The solution was cooled to room temperature and water (10 ml) and dichloromethane (2 x 10 ml) were added. The organic layer was extracted, dried over magnesium sulphate, filtered and evaporated to dryness. Column chromatography (silica gel, dichloromethane) afforded 32 as a pale yellow solid (0.06 g, 49 %). ¹H-NMR 300 MHz (CDCl₃): δ 8.51 (2H, dd, J = 6.6 Hz), 7.86 (4H, m), 7.59 (2H, dd, J = 6.3 Hz), 7.21 (2H, td, J = 2.4 Hz), 6.89 (2H, td, J = 8.1 Hz), 6.77 (2H, td, J = 8.7 Hz), 6.29 (2H, d, J = 7.8 Hz), 5.23 (1H, s), 1.88 (6H, s). MS (EI⁺): m/z 510 (M)⁺, 411 (M-C₅H₇O₂)⁺.

Fac-Bis-(2-phenylpyridine-C²,N')-2-(4'-formylphenylpyridine-C²,N')iridium, Fac-Ir(ppy)₂fppy (34)

General synthesis adapted from work by Colombo *et al.*¹²



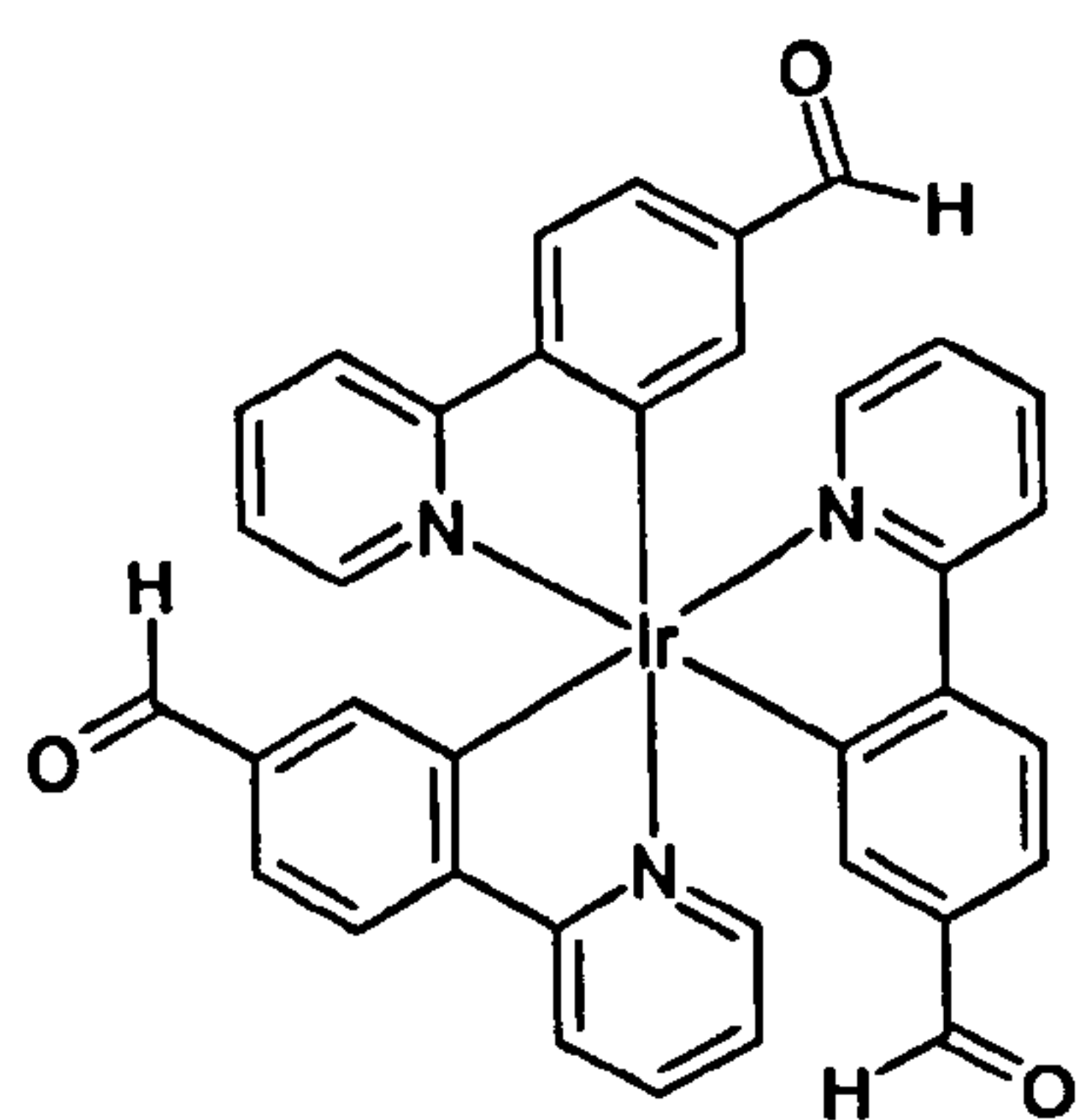
[Ir(ppy)₂Cl]₂ 19 (0.21 g, mmol), 4-(2-pyridyl)benzaldehyde (0.37 g, 2.0 mmol), silver(I) trifluoromethanesulphonate (0.11 g, 0.43 mmol) and 2-methoxyethyl ether (2 mL) were placed in a reaction vessel and purged with nitrogen. The mixture was heated to 110 °C for 8 hours. The solution was cooled to room temperature and water (10

ml) and dichloromethane (2 x 10 ml) were added. The organic layer was extracted, dried over magnesium sulphate, filtered and evaporated to dryness. Column chromatography (silica gel, dichloromethane) afforded 34 as a red solid (0.07 g, 27 %). ¹H-NMR 300 MHz (CD₂Cl₂): δ 9.64 (1H, s), 8.01 (1H, d, J = 8.4 Hz), 7.92 (2H, d, J = 8.1 Hz), 7.78 (2H, m), 7.67 (6H, m), 7.53 (2H, q, J = 7.5 Hz), 7.36 (1H, dd, J = 8.1 Hz), 7.22 (1H, d,

$J = 1.8$ Hz), 7.02 (1H, m), 6.83 (6H, m), 6.65 (1H, dd, $J = 7.5$ Hz). MS (EI+): m/z 683 (M)⁺, 655 (M -CO)⁺, 605 (M -C₅H₄N)⁺, 529 (M -C₁₁H₈N)⁺, 501 (M -C₁₂H₉NO)⁺. HRMS (EI+): m/z 683.1537 (M)⁺, 655.1701 (M -CO)⁺, 529.0578 (M -C₁₁H₈N)⁺, 501.0757 (M -C₁₂H₈NO)⁺.

***Fac*-tris-2-(4'-formylphenylpyridine-C²,N')iridium, *fac*-Ir(fppy)₃ (35)**

General synthesis adapted from work by Colombo *et al.*¹²

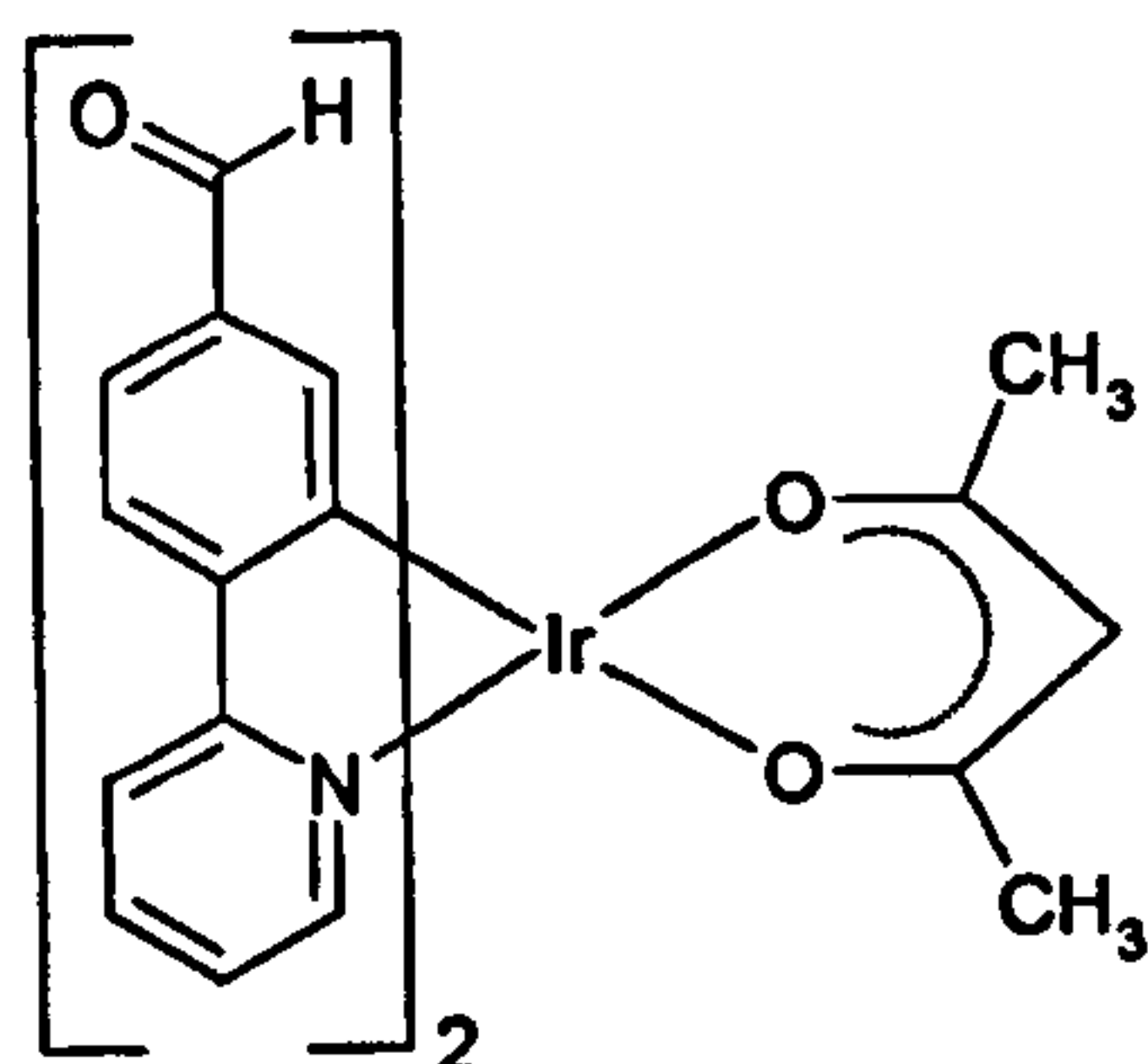


[Ir(fppy)₂Cl]₂ **21** (0.12 g, 0.1 mmole), 4-(2-pyridyl)benzaldehyde (0.047 g, 0.25 mmole), silver(I) trifluoromethanesulphonate (0.064 g, 0.25 mmole) and 2-methoxyethyl ether (2 mL) were placed in a reaction vessel and purged with nitrogen. The mixture was heated to 110 °C for 1 hour. The solution was cooled to room temperature and water (10

ml) and dichloromethane (2 x 10 ml) were added. The organic layer was extracted, dried over magnesium sulphate, filtered and evaporated to dryness. Column chromatography (silica gel, dichloromethane) afforded **35** as a dark red solid (0.032 g, 22 %). ¹H-NMR 300MHz (CD₂Cl₂): δ 9.64 (3H, s), 8.05 (3H, d, $J = 7.8$ Hz), 7.83 (3H, d, $J = 8.1$ Hz), 7.75 (3H, td, $J = 7.1$ Hz), 7.60 (3H, d, $J = 5.1$ Hz), 7.43 (3H, dd, $J = 6.6$ Hz), 7.16 (3H, d, $J = 1.5$ Hz), 7.04 (3H, td, $J = 6.0$ Hz). MS (EI+): m/z 739 (M)⁺, 711 (M -CO)⁺, 683 (M -C₂O₂)⁺, 557 (M -C₁₂H₈NO)⁺, 329 (M -C₁₃H₁₀NO₃)⁺. HRMS (EI+): m/z 739.1460 (M)⁺, 711.1528 (M -CO)⁺, 683.1358 (M -C₂O₂)⁺, 655.1629 (M -C₃O₃)⁺, 577.0854 (M -C₁₂H₈NO)⁺.

**Bis-2-(4'-formylphenylpyridine-C²,N')acetylacetonate iridium,
Ir(fppy)₂AcAc (36)**

General synthesis adapted from work by Colombo *et al.*¹²

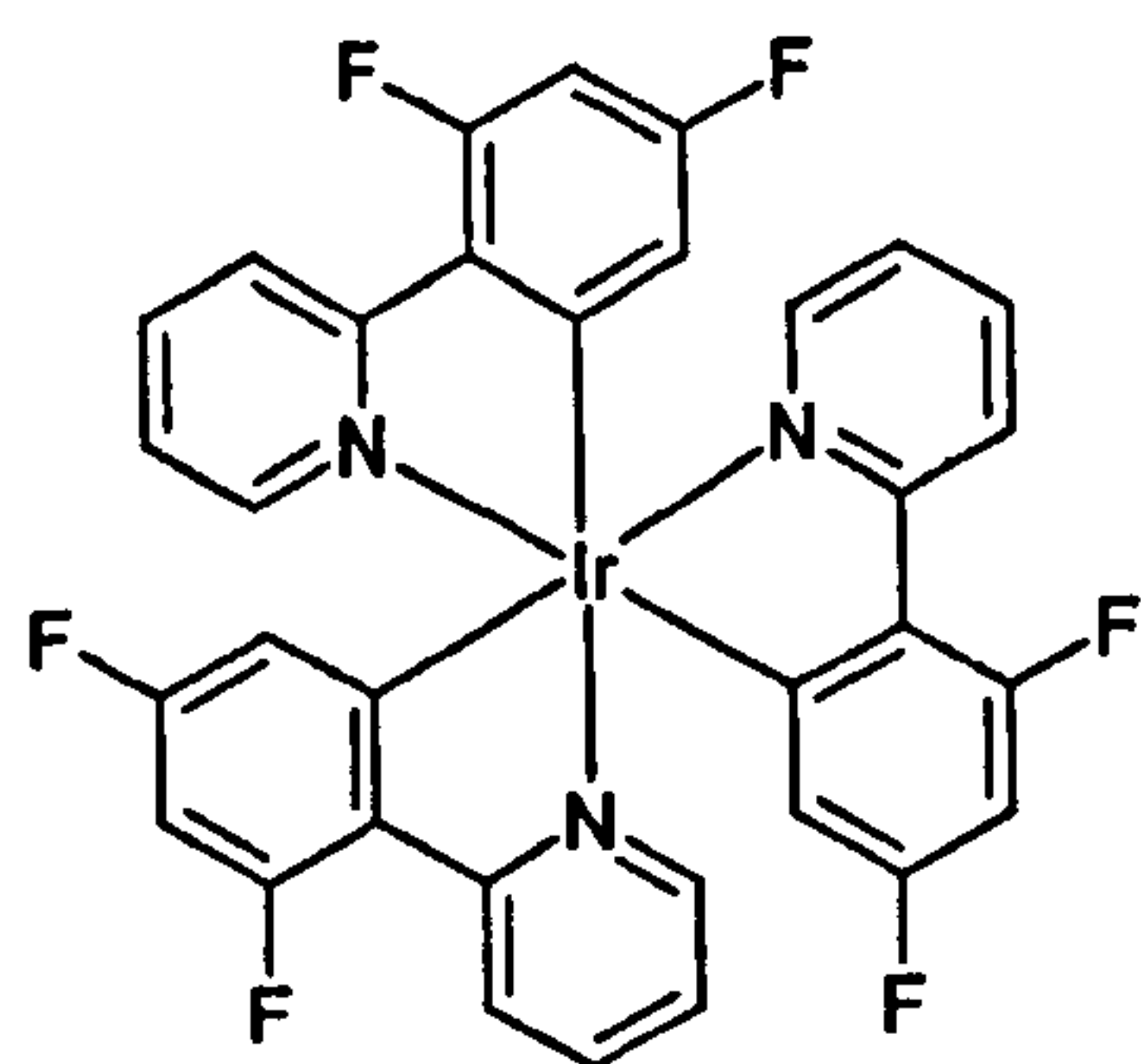


[Ir(fppy)₂Cl]₂ **21** (0.12 g, 0.1 mmol), 2,4-pentanedione (0.05 g, 0.25 mmoles), silver(I) trifluoromethanesulphonate (0.050 g, 0.25 mmoles) and 2-methoxyethyl ether (2 mL) were placed in a reaction vessel and purged with nitrogen. The mixture was heated to 110 °C for 1 hour. The solution was cooled to room

temperature and water (10 mL) and dichloromethane (2 x 10 mL) were added. The organic layer was extracted, dried over magnesium sulphate, filtered and evaporated to dryness. Column chromatography (silica gel, dichloromethane) afforded **36** as a red solid (0.009 g, 7 %). ¹H-NMR 300 MHz (CDCl₃): δ 9.64 (2H, s), 8.58 (2H, d, J = 5.1 Hz), 8.01 (2H, d, J = 7.8 Hz), 7.89 (2H, td, J = 7.4 Hz), 7.71 (2H, d, J = 8.1 Hz), 7.32 (4H, m), 6.71 (2H, d, J = 1.5 Hz), 5.27 (1H, s), 1.81 (1H, s). MS (EI⁺): m/z 656 (M)⁺, 557 (M-C₅H₇O₂)⁺.

Tris-2-(2,4-difluoro-phenylpyridine-C²,N')iridium, Ir(F₂ppy)₃ (37)

General synthesis adapted from work by Colombo *et al.*¹²



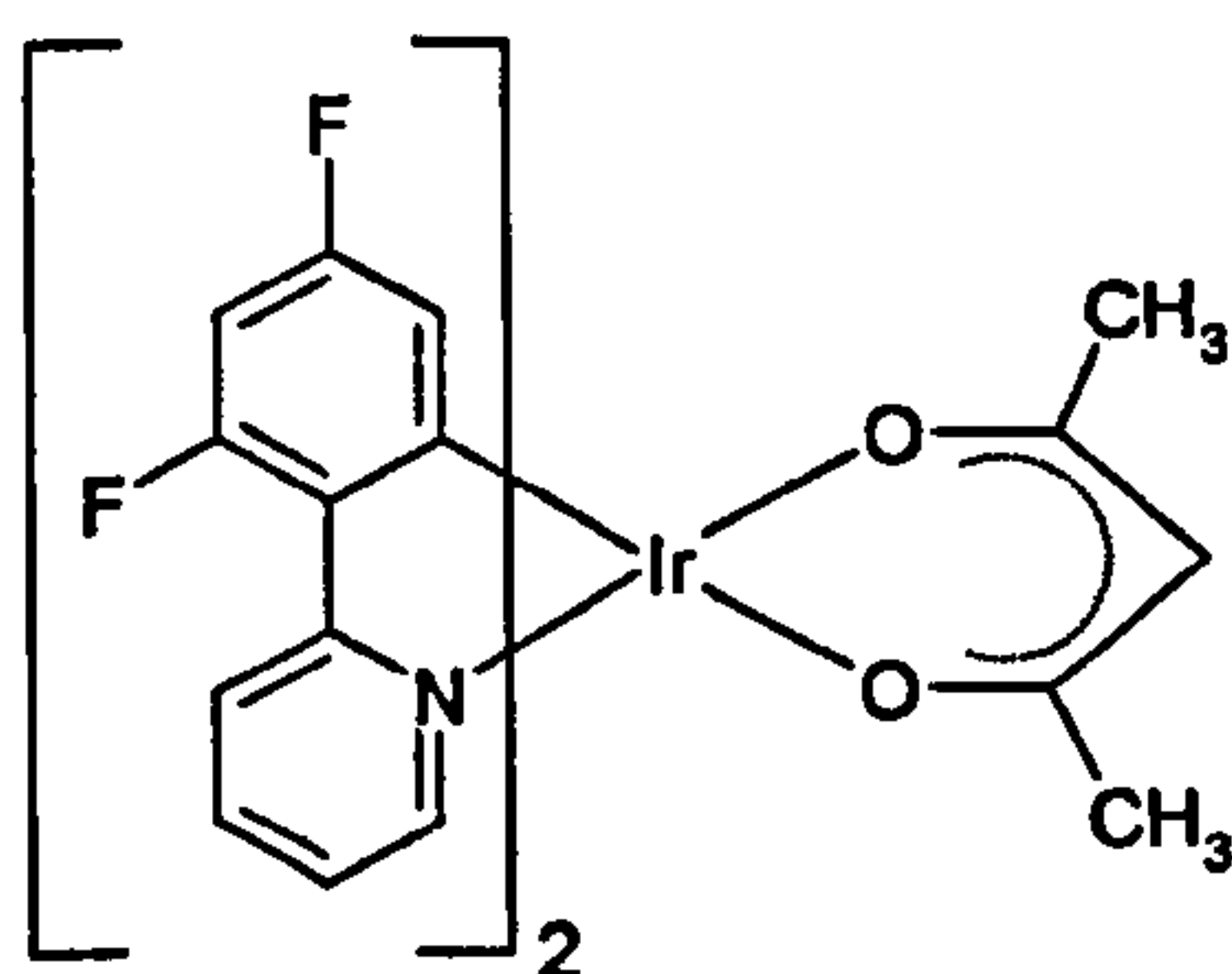
[Ir(F₂ppy)₂Cl]₂ **22** (0.20 g, 0.16 mmol), 2-(2,4-difluorophenylpyridine) (0.08 g, 0.41 mmol), silver(I) trifluoromethanesulphonate (0.10 g, 0.41 mmol) and 2-methoxyethyl ether (2 mL) were placed in a reaction vessel and purged with nitrogen. The mixture was heated to 110 °C for 2 hours. The solution was

cooled to room temperature and water (10 mL) and dichloromethane (2 x 10 mL) were added. The organic layer was extracted, dried over magnesium sulphate, filtered and evaporated to dryness. Column chromatography (silica gel, dichloromethane) afforded **37** as a bright yellow solid (0.063 g, 25 %). ¹H-NMR 300 MHz (CDCl₃): δ 8.30 (3H, m),

7.76 (6H, m), 7.03 (3H, m), 6.12 (6H, m). ^{19}F -NMR 200 MHz (CDCl_3): δ -108.11 (1F, q, $J = 10.6$ Hz), -109.03 (2F, m), -109.22 (1F, q, $J = 106$ Hz), -109.80 (1F, t, $J = 10.8$ Hz), -110.30 (1F, t, $J = 10.6$ Hz), -110.71 (1F, t, $J = 10.8$ Hz), -111.52 (1F, t, $J = 13.6$ Hz). MS (EI $^{+}$): m/z 763 (M^{+}), 722 ($\text{M}-\text{C}_3\text{H}_5$) $^{+}$, 571 ($\text{M}-\text{C}_{11}\text{H}_6\text{NF}_2$) $^{+}$, 381 ($\text{M}-\text{C}_{22}\text{H}_{12}\text{N}_2\text{F}_4$) $^{+}$. HRMS (EI $^{+}$): m/z 763.1033 (M^{+}), 571.0501 ($\text{M}-\text{C}_{11}\text{H}_6\text{NF}_2$) $^{+}$. The X-ray crystal structure and related data for **37** can be found in appendix A, part A8. Crystals were grown from dichloromethane.

Bis-2-(2,4-difluoro-phenylpyridine- C^2, N^1)acetylacetonate iridium,
 $\text{Ir}(\text{F}_2\text{ppy})_2\text{AcAc}$ (38**)**

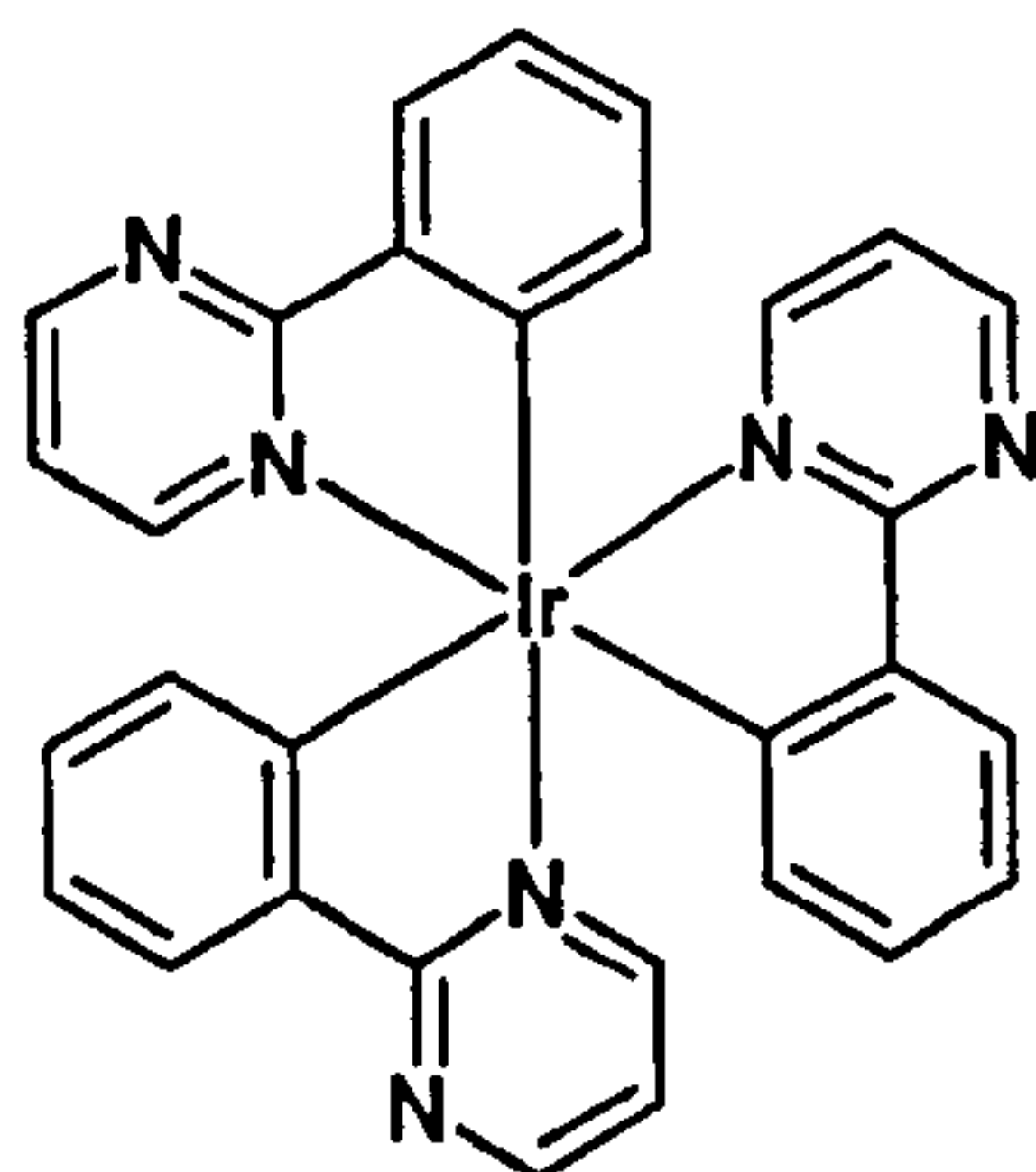
General synthesis adapted from work by Colombo *et al.*¹²



$[\text{Ir}(\text{F}_2\text{ppy})_2\text{Cl}]_2$ **22** (0.10 g, 0.08 mmol), 2,4-pentanedione (0.04 g, 9.7 mmol), silver(I) trifluoromethanesulphonate (0.04 g, 0.16 moles) and 2-methoxyethyl ether (2 mL) were placed in a reaction vessel and purged with nitrogen. The mixture was heated to 110 °C for 30 minutes. The solution was cooled to room temperature and water (10 ml) and dichloromethane (2 x 10 ml) were added. The organic layer was extracted, dried over magnesium sulphate, filtered and evaporated to dryness. Column chromatography (silica gel, dichloromethane) afforded **38** as a bright yellow solid (0.032 g, 30 %). ^1H -NMR 300 MHz (CDCl_3): δ 8.45 (2H, dd, $J = 3.0$ Hz), 8.26 (2H, d, $J = 8.4$ Hz), 7.81 (2H, d, $J = 8.4$ Hz), 7.20 (2H, td, $J = 6.0$ Hz), 6.34 (2H, t, $J = 10.8$ Hz), 5.66 (2H, dd, $J = 6.3$ Hz), 5.23 (1H, s), 1.82 (6H, s). ^{19}F -NMR 300 MHz (CDCl_3): δ -109.262 (2F, q, $J = 9.6$ Hz), -111.52 (2F, t, $J = 12.0$ Hz). MS (EI $^{+}$): m/z 672 (M^{+}), 573 ($\text{M}-\text{C}_5\text{H}_7$) $^{+}$. HRMS (EI $^{+}$): 672.1002 (M^{+}), 573.0515 ($\text{M}-\text{C}_5\text{H}_7$) $^{+}$. The X-ray crystal structure and related data for **38** can be found in appendix A, part A9. Crystals were grown from dichloromethane.

***Fac*-tris-(2-phenylpyrimidine- C^2,N')iridium, *fac*-Ir(ppm)₃ (39)**

General synthesis adapted from work by Grushin *et al.*¹³

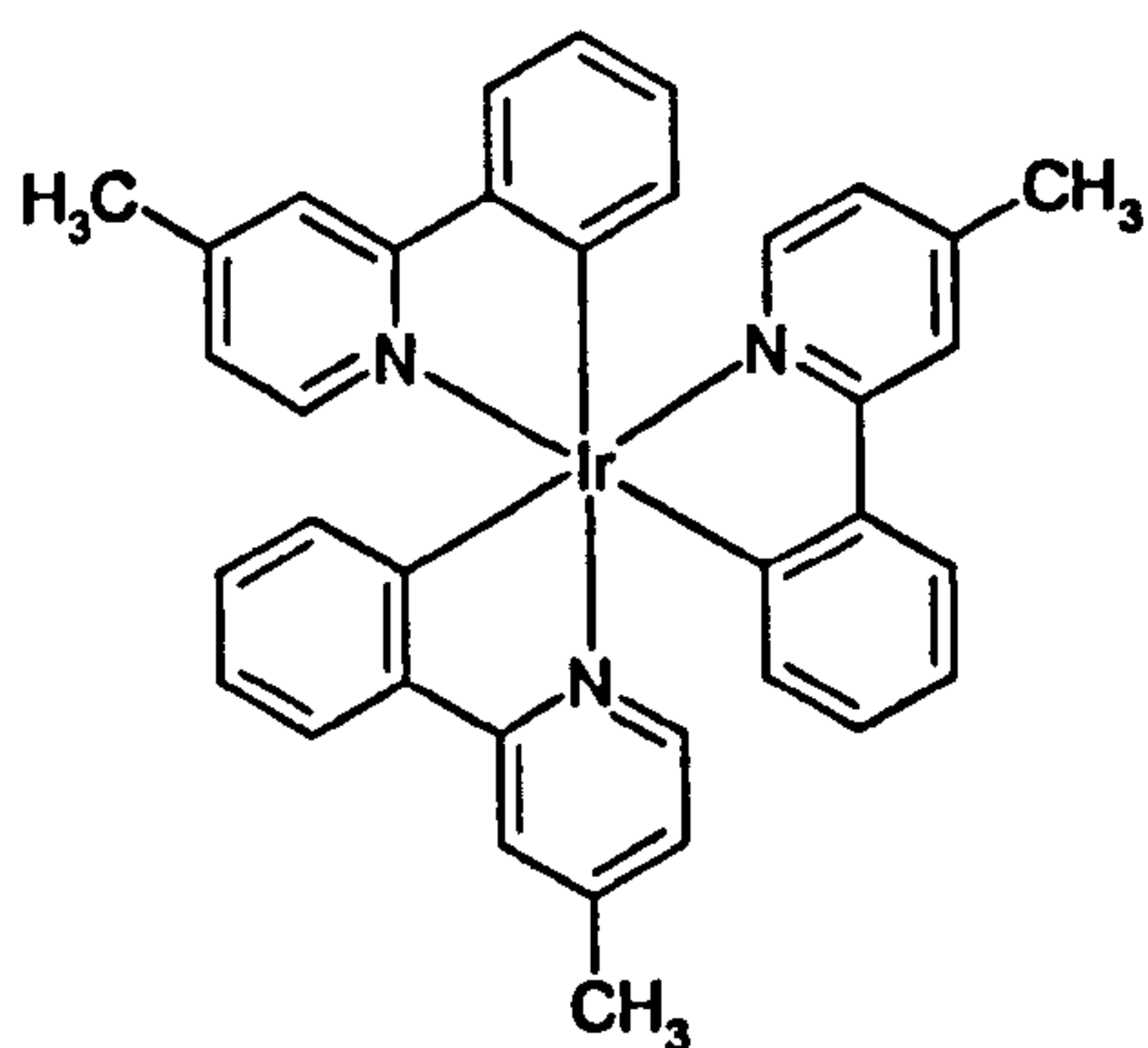


IrCl₃·3H₂O (0.075 g, 0.21 mmol), 2-phenylpyrimidine **23** (0.33 g, 2.1 mmol) and silver(I) trifluoroacetate (0.165 g, 0.75 mmol) were placed in a reaction vessel and purged with nitrogen. The mixture was heated to 190 °C for 10 hours. The solution was cooled to room temperature and water (10 ml) and dichloromethane (2 x 10 ml) were added. The

organic layer was extracted, dried over magnesium sulphate, filtered and evaporated to dryness. Column chromatography (silica gel, dichloromethane) afforded **39** as a bright yellow solid (0.042 g, 30 %). ¹H-NMR 200 MHz (CDCl₃): δ 8.70 (3H, m), 8.10 (3H, m), 7.78 (3H, dd, J = 5.5 Hz), 6.91 (12H, m). ¹³C-NMR 200 MHz (CDCl₃): δ 159.71, 157.29, 154.46, 147.33, 140.98, 137.02, 132.44, 128.24, 121.24, 118.17. MS (EI⁺): m/z 658 (M)⁺, 579 (M-C₄H₃N₂)⁺, 503 (M-C₁₀H₇N₂)⁺. HRMS (EI⁺): m/z 658.1442 (M)⁺, 579.1136 (M-C₄H₃N₂)⁺, 503.0842 (M-C₁₀H₇N₂)⁺.

Tris-(4-Methyl-2-phenyl-pyridine- C^2,N')iridium, Ir(4-Meppy)₃ (40)

General synthesis adapted from work by Grushin *et al.*¹³



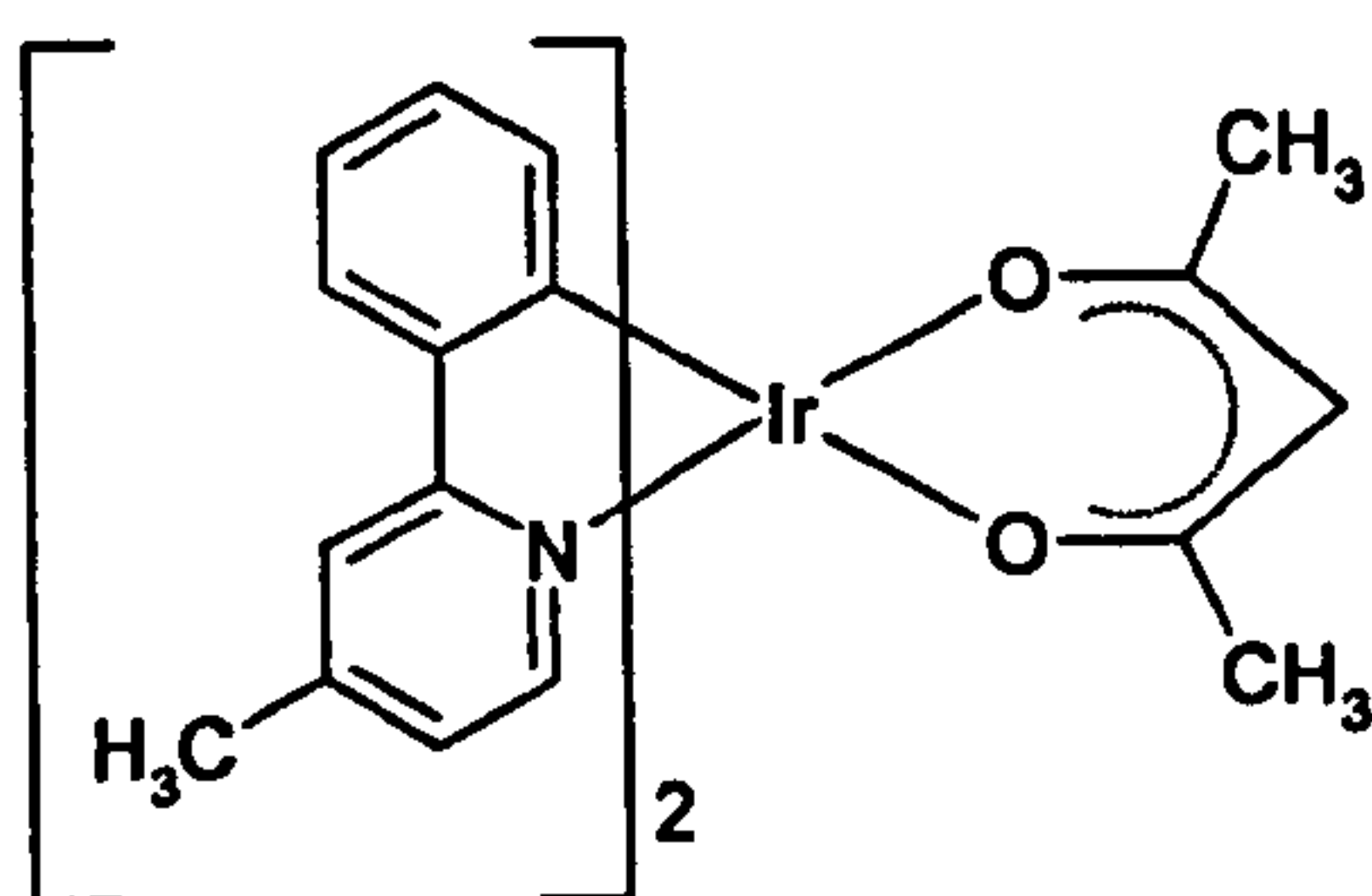
IrCl₃·3H₂O (0.060 g, 0.17 mmol), 4-methyl-2-phenylpyridine **9** (0.35 g, 1.7 mmol) and silver(I) trifluoroacetate (0.112 g, 0.51 mmol) were placed in a reaction vessel and purged with nitrogen. The mixture was heated to 190 °C for 24 hours. The solution was cooled to room temperature and water (10 ml) and dichloromethane (2 x 10 ml) were added.

The organic layer was extracted, dried over magnesium sulphate, filtered and evaporated to dryness. Column chromatography (silica gel, dichloromethane) afforded **40** as a bright yellow solid (0.014 g, 10 %). ¹H-NMR 300 MHz (CDCl₃): δ 8.06 (2H, d, J = 9.6 Hz), 7.73 (1H, s), 7.67 (1H, s), 7.64 (1H, d, J = 7.5 Hz), 7.47 (3H, m), 7.40 (1H, d, J =

5.7 Hz), 6.86 (4H, m), 6.67 (1H, d, $J = 5.7$ Hz), 2.51 (3H, s), 2.40 (3H, s). MS (ES⁺): m/z 720 (M+Na)⁺, 698 (M+H)⁺, 696 (M)⁺, 684 (M-CH₃)⁺.

**Bis-(4-methyl-2-phenyl-pyridine-C²,N')acetylacetonate iridium,
Ir(4-Meppy)₂AcAc (41)**

General synthesis adapted from work by Lamansky *et al.*¹⁴

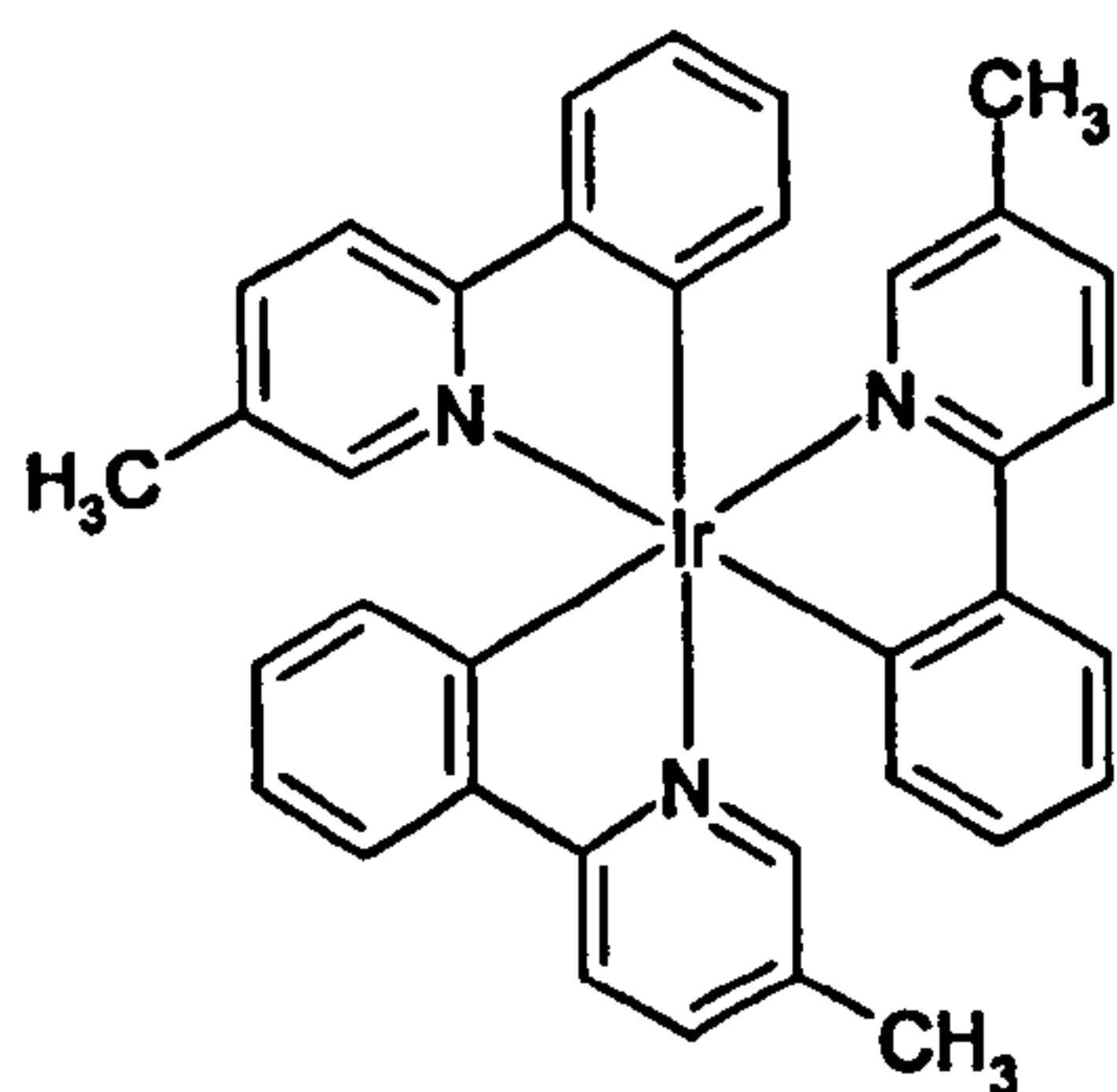


Ir(4-Meppy)₂Cl₂ 24 (0.091 g, 0.09 mmol), 2,4-pentanedione (0.020 g, 0.20 mmol), sodium carbonate (0.10 g, 0.94 mmol) and 2-ethoxyethanol (8 mL) were placed in a reaction vessel and purged with nitrogen gas. The mixture was heated to 120 °C for 16 hours, with continuous stirring. The

solution was cooled to room temperature and then filtered. The resulting precipitate was washed with cyclohexane (10 ml) and ether (10ml). Column chromatography (silica gel, dichloromethane) afforded 41 as a yellow-orange solid (0.048 g, 49 %). ¹H-NMR 300 MHz (CDCl₃): δ 8.34 (2H, d, $J = 5.7$ Hz), 7.66 (2H, s), 7.53 (2H, d, $J = 7.8$ Hz), 6.97 (2H, d, $J = 5.4$ Hz), 6.80 (2H, t, $J = 7.5$ Hz), 6.68 (2H, t, $J = 7.2$ Hz), 6.28 (2H, d, $J = 7.8$ Hz), 5.20 (1H, s), 2.59 (6H, s). MS (EI⁺): m/z 628 (M)⁺, 529 (M-C₅H₇O₂)⁺.

Fac-tris-(5-methyl-2-phenyl-pyridine-C²,N')iridium, fac-Ir(5-Meppy)₃ (42)

General synthesis adapted from work by Grushin *et al.*¹³

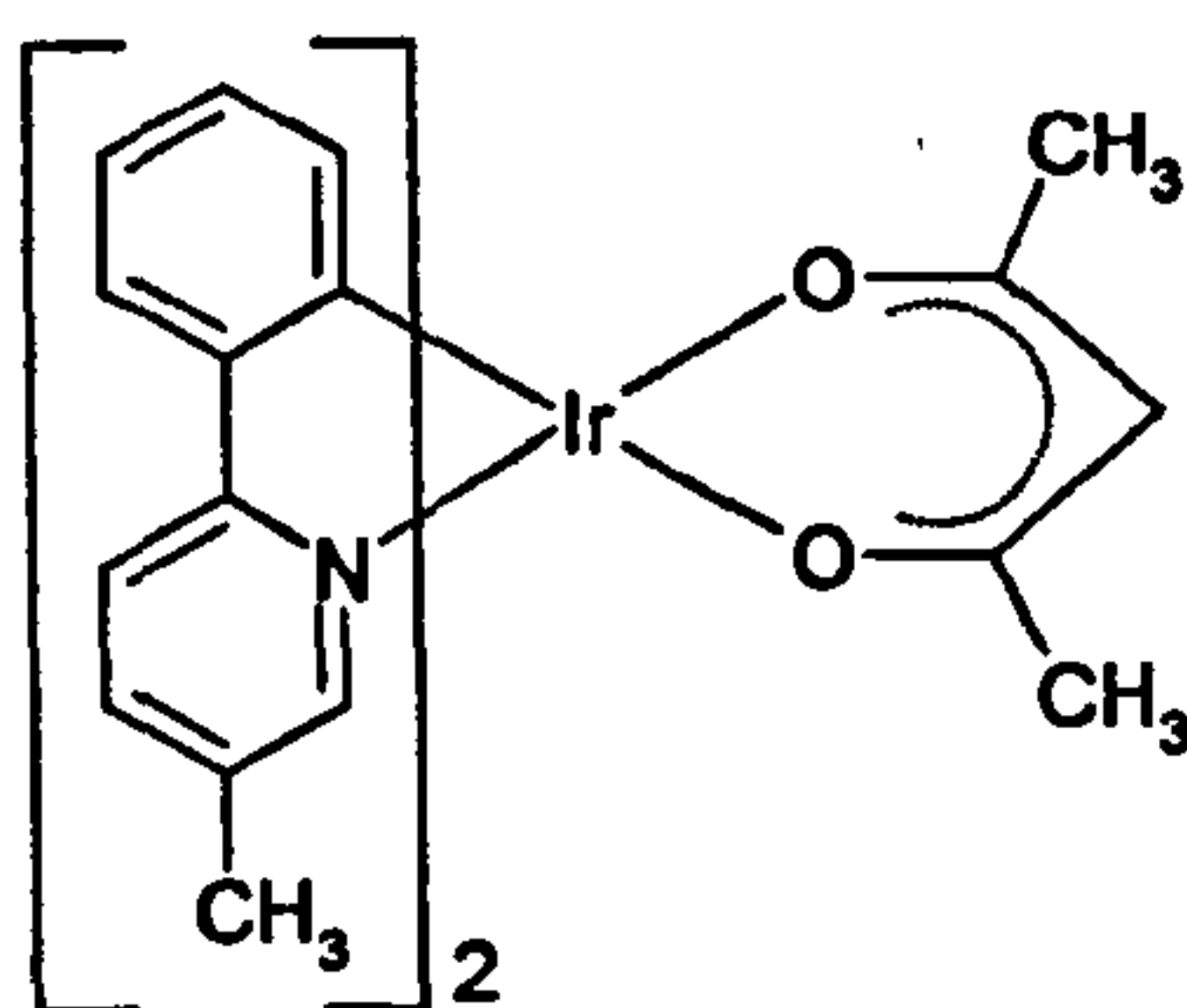


IrCl₃·3H₂O (0.088 g, 0.25 mmol), 5-methyl-2-phenylpyridine 10 (0.212 g, 1.25 mmol) and silver(I) trifluoroacetate (0.166 g, 0.75 mmol) were placed in a reaction vessel and purged with nitrogen. The mixture was heated to 200 °C for 10 hours. The solution was cooled to room temperature and water (10 ml) and dichloromethane (2 x 10 ml) were added. The organic layer was extracted, dried over magnesium sulphate, filtered and evaporated to dryness. Column chromatography (silica

gel, dichloromethane) afforded **42** as a bright yellow solid (0.027 g, 15 %). $^1\text{H-NMR}$ 200 MHz (CDCl_3): δ 7.78 (3H, d, $J = 8.2$ Hz), 7.62 (3H, d, $J = 7.0$ Hz), 7.41 (3H, dd, $J = 8.2$ Hz), 7.32 (3H, s), 6.83 (9H, m), 2.14 (9H, m). MS (EI+): m/z 697 (M) $^+$, 529 ($\text{M-C}_{12}\text{H}_{10}\text{N}$) $^+$.

**Bis-(5-methyl-2-phenyl-pyridine- C^2, N^1)acetylacetonate iridium,
 $\text{Ir}(\text{5-Meppy})_2\text{AcAc}$ (**43**)**

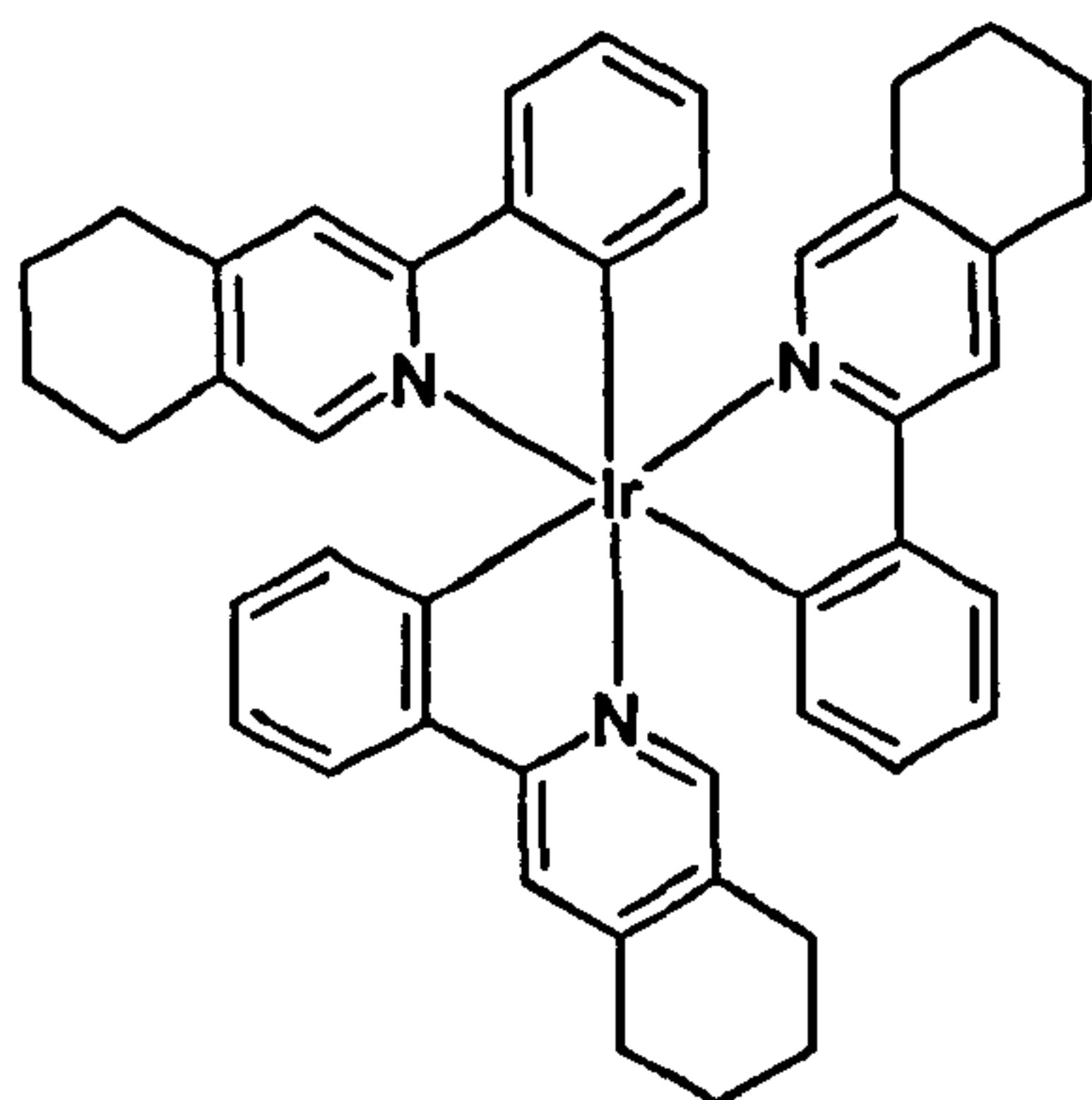
General synthesis adapted from work by Lamansky *et al.*¹⁴



$\text{Ir}(\text{5-Meppy})_2\text{Cl}]_2$ **25** (0.113 g, 0.10 mmol), 2,4-pentanedione (0.026 g, 0.26 mmol), sodium carbonate (0.10 g, 0.94 mmol) and 2-ethoxyethanol (8 mL) were placed in a reaction vessel and purged with nitrogen gas. The mixture was heated to 120 °C for 15 hours, with continuous stirring. The solution was cooled to room temperature and then filtered. The resulting precipitate was washed with cyclohexane (10 mL) and ether (10 mL). Column chromatography (silica gel, dichloromethane) afforded **43** as a yellow-orange solid (0.048 g, 38 %). $^1\text{H-NMR}$ 300 MHz (CDCl_3): δ 8.34 (2H, s), 7.74 (2H, d, $J = 8.4$ Hz), 7.53 (4H, m), 6.79 (2H, t, $J = 7.5$ Hz), 6.67 (2H, t, $J = 7.2$ Hz), 6.24 (2H, d, $J = 7.5$ Hz), 5.22 (1H, s), 2.41 (6H, s), 1.80 (6H, s). MS (EI+): m/z 628 (M) $^+$, 529 ($\text{M-C}_5\text{H}_7\text{O}_2$) $^+$.

***Fac*-tris-(3-phenyl-5,6,7,8-tetrahydro-isoquinoline- C^2, N^1)iridium,
 $\text{Fac-Ir}(\text{Cyclohex})_3$ (**44**)**

General synthesis adapted from work by Colombo *et al.*¹²

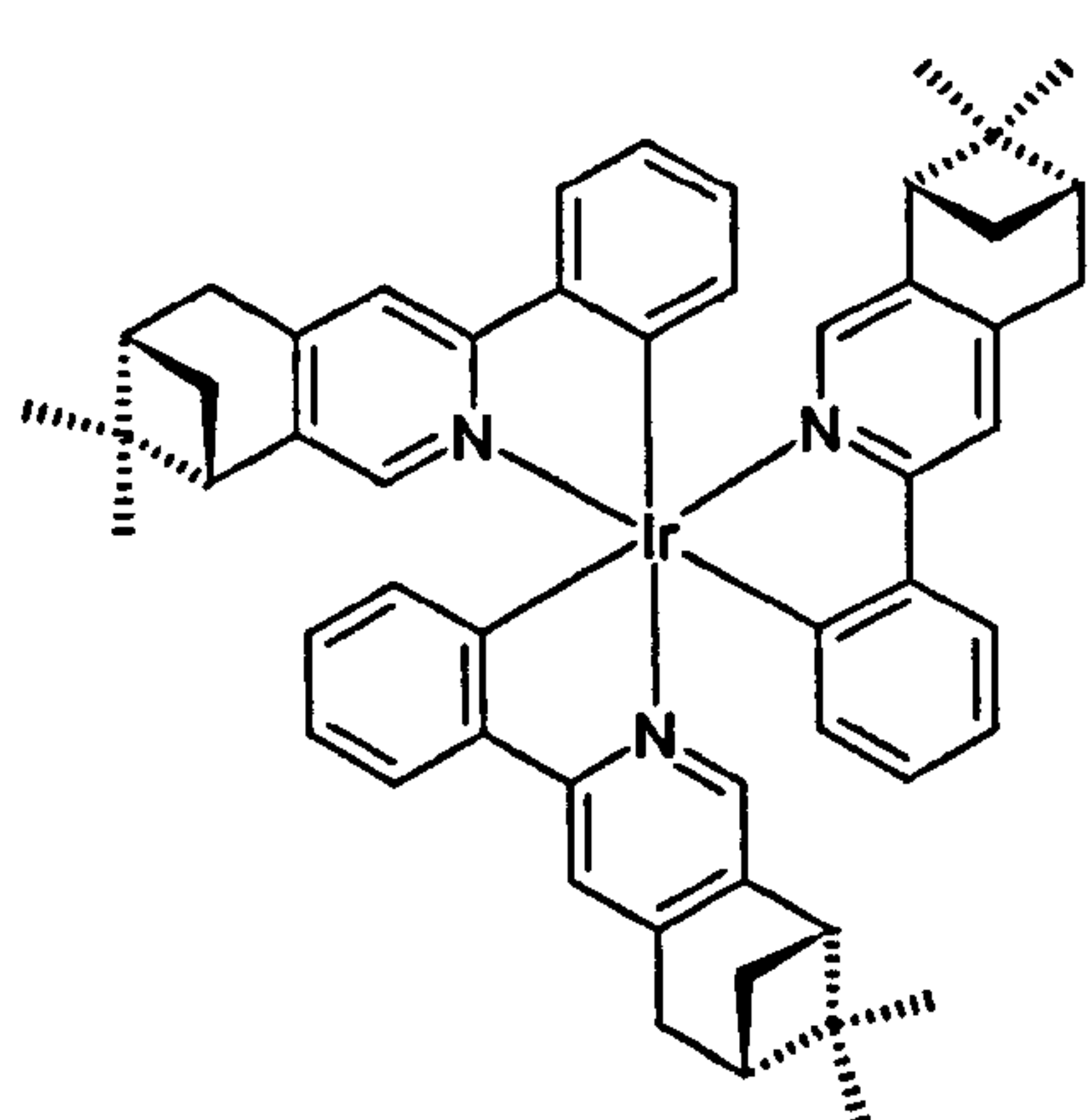


$[\text{Ir}(\text{Cyclohex})_2\text{Cl}]_2$ **26** (0.129 g, 0.20 mmol), 3-phenyl-5,6,7,8-tetrahydro-isoquinoline **12** (0.084 g, 0.40 mmol), silver(I) trifluoroacetate (0.077 g, 0.30 mmol) and 2-methoxyethyl ether (2 mL) were placed in a

reaction vessel and purged with nitrogen. The mixture was heated to 195 °C for 8 hours. The solution was cooled to room temperature and water (10 ml) and dichloromethane (2 x 10 ml) were added. The organic layer was extracted, dried over magnesium sulphate, filtered and evaporated to dryness. Column chromatography (silica gel, n-hexane: dichloromethane (1:4)) afforded **44** as a yellow-orange solid (0.017 g, 10 %). ¹H-NMR 300 MHz (CDCl₃): δ 7.60 (3H, t, J = 5.1 Hz), 7.53 (3H, s), 7.22 (3H, s), 6.82 (6H, m), 6.65 (3H, m), 2.84 (6H, m), 2.53 (6H, m), 1.76 (12H, m). MS (EI⁺): m/z 817 (M)⁺, 607 (M-C₁₅H₁₄N)⁺. HRMS (ES⁺): m/z 818.3040 (M+H)⁺.

***Fac*-Tris-(10,10-Dimethyl-5-phenyl-4-aza-tricyclo[7.1.1.0*2,7*]undeca-2(7),3,5-triene-C²,N')iridium, *fac*-Ir(Myrt)₃ (**45**)**

General synthesis adapted from work by Dedeian *et al.*¹⁵

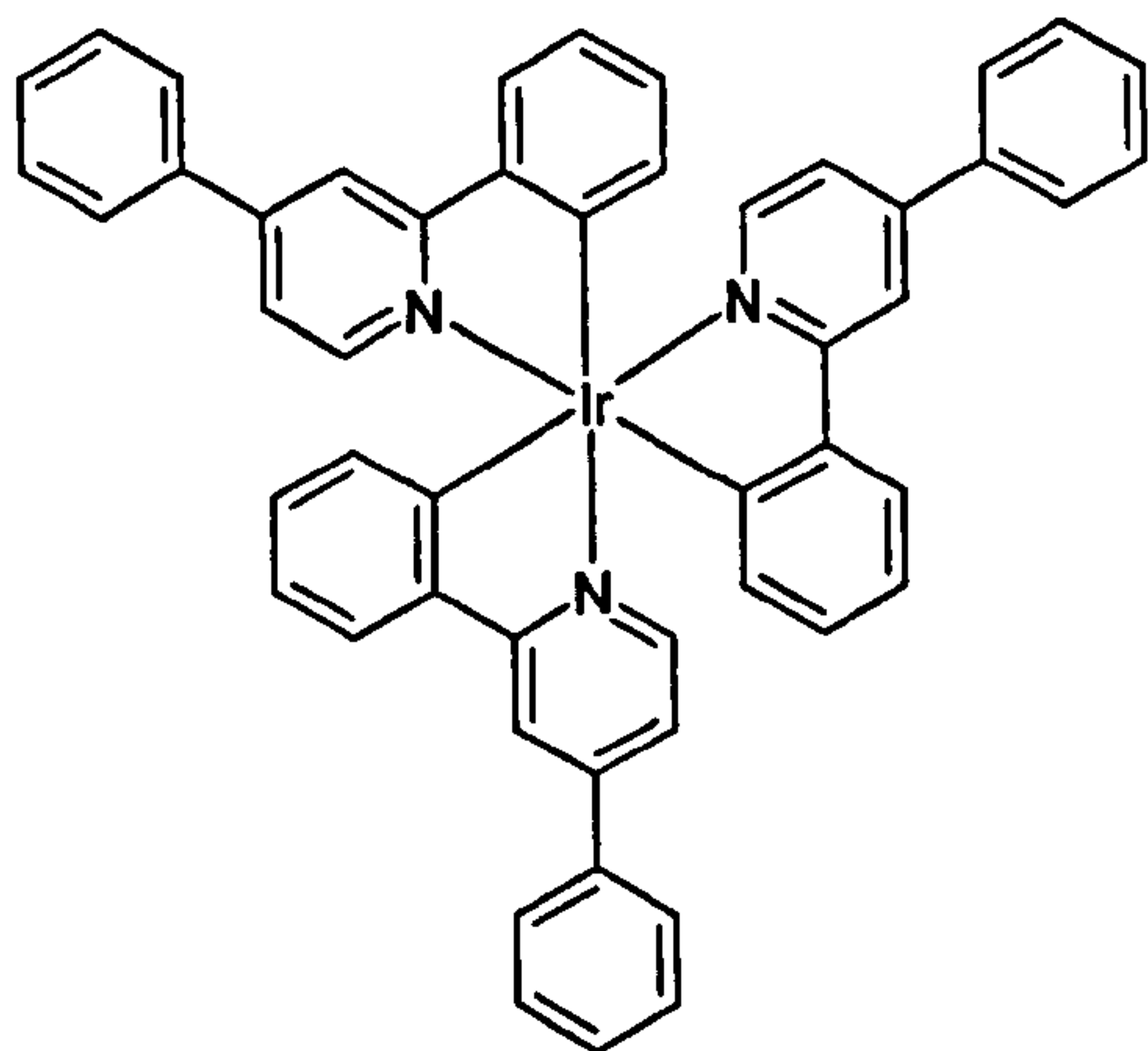


Ir(acac)₃ **29** (0.207 g, 0.42 mmol) and 10,10-dimethyl-5-phenyl-4-aza-tricyclo-[7.1.1.0*2,7]-undeca-2(7),3,5-triene **13** (0.41 g, 1.68 mmol) were dissolved in glycerol (15 mL) and purged under nitrogen. The mixture was heated to 220 °C for 10 hours. The solution was cooled to room temperature and HCl (1M, 30 mL) was added causing precipitation of the product. The crude

material was collected on a filter frit, washed with water (30 mL), dissolved in dichloromethane, dried over magnesium sulphate, filtered and evaporated to dryness. Column chromatography afforded **45** as a bright yellow solid (0.118 g, 30 %). ¹H-NMR 500 MHz (CDCl₃): δ 7.63 (6H, d, J = 8.0 Hz), 7.56 (6H, m), 7.14 (3H, m), 6.96 (3H, s), 6.88 (6H, m), 6.81 (6H, m), 6.69 (3H, s), 3.04 (12H, m), 2.66 (3H, m), 2.53 (3H, m), 2.41 (3H, t, J = 5.5 Hz), 2.27 (6H, m), 2.20 (3H, m), 1.56 (9H, s), 1.31 (12H, m), 1.22 (3H, d, J = 10.0 Hz), 1.14 (3H, d, 10.0 Hz), 0.64 (9H, s), 0.49 (9H, s). The ¹H-NMR NMR spectrum is particularly complex due to the presence of both diastereoisomers. MS (EI⁺): m/z 938 (M)⁺, 687 (M-C₁₈H₁₈N)⁺. HRMS (ES⁺): m/z 960.3930 (M+Na)⁺. Elemental analysis C₅₄H₅₄IrN₃ (M = 937.26); Expected C: 69.18 %, H: 5.81 %, N: 4.48 %, Obtained C: 66.51 %, H: 5.61 %, N: 4.17 % corresponding to C₅₄H₅₄IrN₃·½CH₂Cl₂.

***Fac*-tris-(2,4-diphenylpyridine- C^2,N')iridium, *fac*-Ir(dppy)₃ (46)**

General synthesis adapted from work by Grushin *et al.*¹³



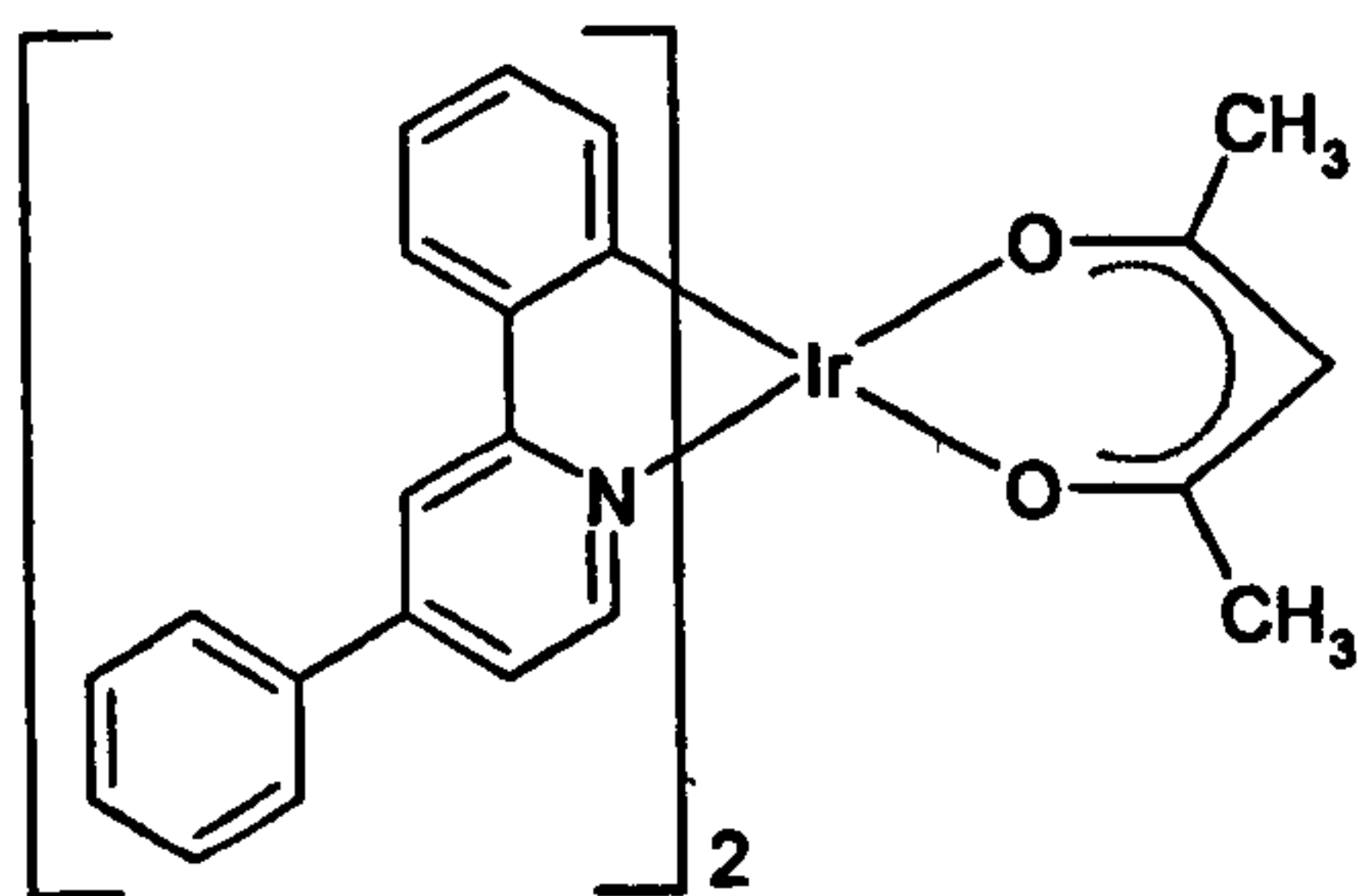
[Ir(dppy)₂Cl]₂ **27** (0.137 g, 0.20 mmol), 2,4-diphenylpyridine **14** (0.093 g, 0.40 mmol), and silver(I) trifluoroacetate (0.077 g, 0.30 mmol) were placed in a reaction vessel and purged with nitrogen. The mixture was heated to 195 °C for 15 hours. The solution was cooled to room temperature and water (10 ml) and dichloromethane (2 x 10 ml) were added. The organic layer was extracted, dried over

magnesium sulphate, filtered and evaporated to dryness. Column chromatography (silica gel, dichloromethane: acetic acid (1:398) afforded **46** as an orange solid (0.102 g, 58 %).

¹H-NMR 300 MHz (CDCl₃): δ 8.11 (3H, s), 7.79 (3H, d, J = 7.2 Hz), 7.69 (9H, m), 7.49 (9H, m), 7.14 (3H, dd, J = 5.7 Hz), 6.92 (9H, m). MS (EI⁺): m/z 883 (M)⁺, 806 (M-C₆H₅)⁺. HRMS (ES⁺): m/z 906.2421 (M+Na)⁺.

Bis-(2,4-diphenylpyridine- C^2,N')acetylacetonate iridium, Ir(dppy)₂AcAc (47)

General synthesis adapted from work by Lamansky *et al.*¹⁴



Ir(dppy)₂Cl]₂ **27** (0.138 g, 0.10 mmol), 2,4-pentanedione (0.026 g, 0.26 mmol), sodium carbonate (0.10 g, 0.94 mmol) and 2-ethoxyethanol (8 mL) were placed in a reaction vessel and purged with nitrogen gas.

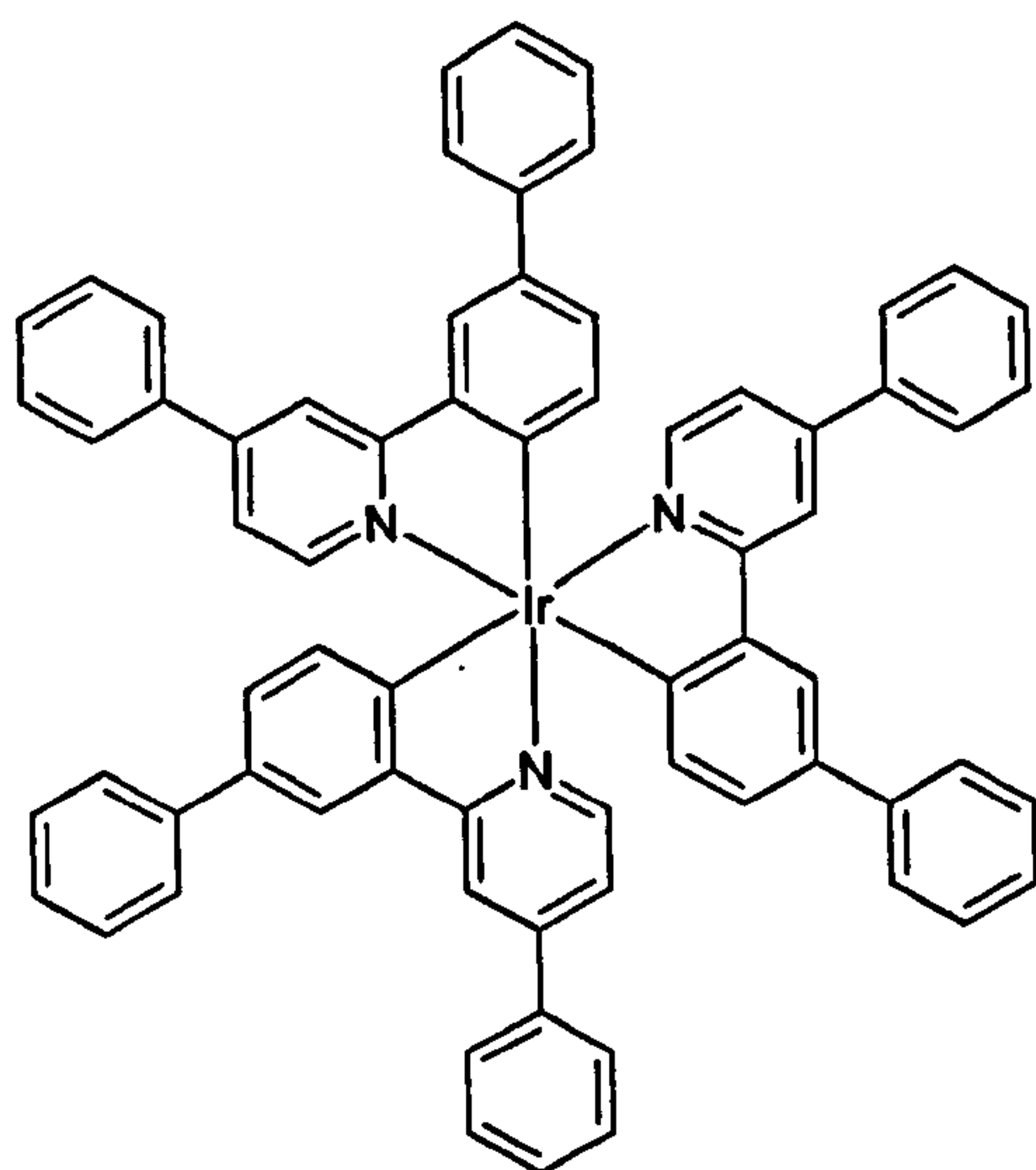
The mixture was heated to 120 °C for 15 hours,

with continuous stirring. The solution was cooled to room temperature and then filtered. The resulting precipitate was washed with diethyl ether (2 x 10ml). Column chromatography (silica gel, dichloromethane) afforded **47** as an orange solid (0.030 g, 20 %). ¹H-NMR 300 MHz (CDCl₃): δ 8.57 (2H, d, J = 6.3 Hz), 8.07 (2H, s), 7.81 (4H, d, J

= 6.9 Hz), 7.66 (2H, d, $J = 7.8$ Hz), 7.55 (8H, m), 7.38 (2H, dd, $J = 6.0$ Hz), 6.82 (2H, t, $J = 7.5$ Hz), 6.73 (2H, t, $J = 8.7$ Hz), 6.38 (2H, d, $J = 6.6$ Hz), 5.26 (1H, s), 1.83 (6H, s). MS (EI+): m/z 752 (M)⁺, 653 ($M-C_5H_7O_2$)⁺.

***Fac*-tris-(2-Biphenyl-3-yl-4-phenyl-pyridine- C^2,N')iridium, *fac*-Ir(bippy)₃ (48)**

General synthesis adapted from work by Colombo *et al.*¹²

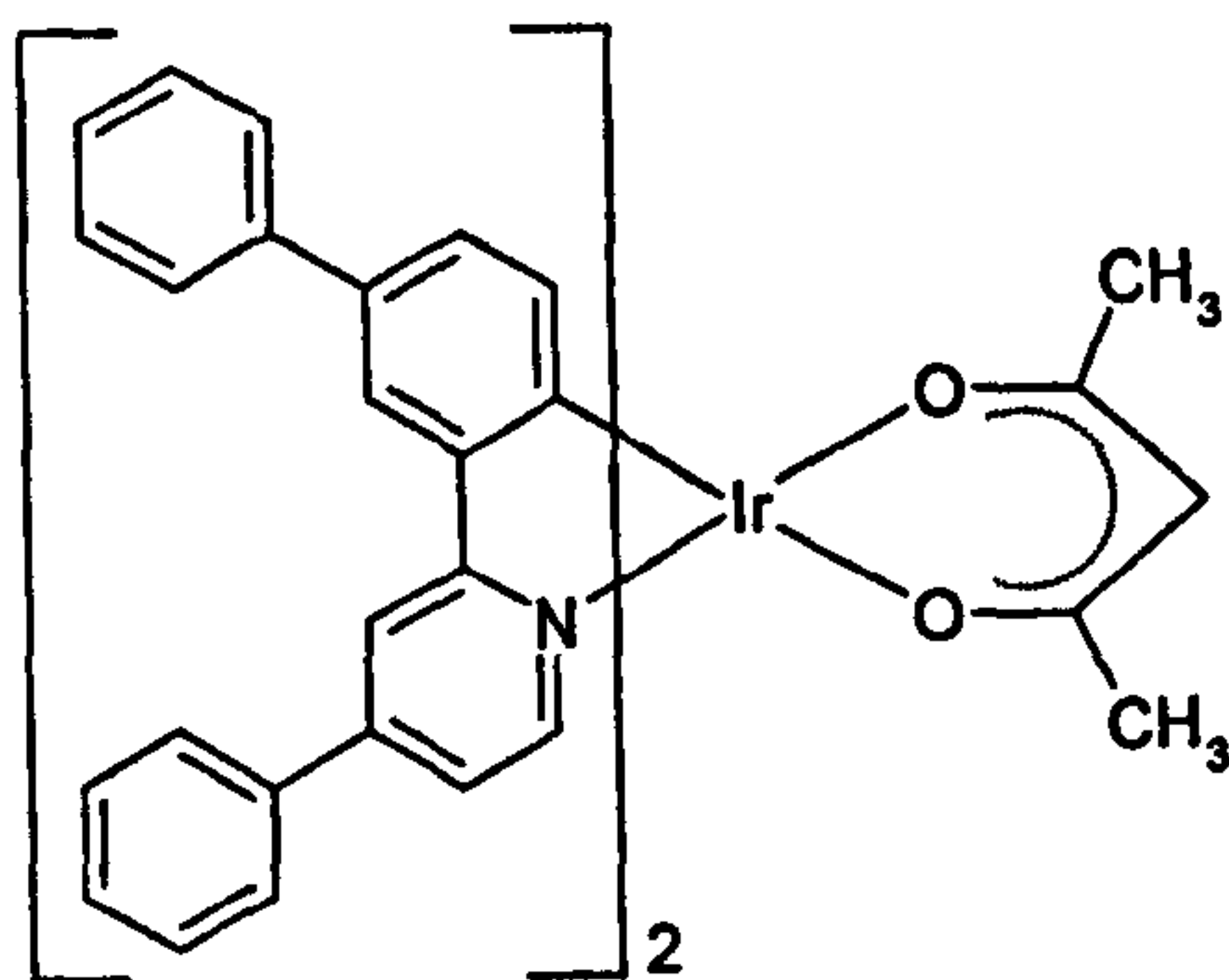


[Ir(bippy)₂Cl]₂ 28 (0.94 g, 0.06 mmol), 2-biphenyl-3-yl-4-phenyl-pyridine 16 (0.069 g, 0.22 mmol), silver(I) trifluoroacetate (0.037 g, 0.17 mmol) and 2-methoxyethyl ether (2 mL) were placed in a reaction vessel and purged with nitrogen. The mixture was heated to 195 °C for 15 hours. The solution was cooled to room temperature and water (10 mL) and dichloromethane (2 x 10 mL) were added. The organic layer was extracted, dried over magnesium sulphate, filtered and evaporated

to dryness. Column chromatography (silica gel, toluene) afforded 48 as an orange solid (0.023 g, 18 %). ¹H-NMR 200 MHz (CDCl₃): δ 8.45 (3H, s), 8.22 (3H, d, $J = 8.0$ Hz), 7.98 (3H, s), 7.73 (18H, m), 7.71 (21H, m). MALDI MS (EI+): m/z 1111.302 (M)⁺, 1033.259 ($M-C_6H_5$)⁺, 805.177 ($M-C_{23}H_{16}N$)⁺. The X-ray crystal structure and related data for 48 can be found in appendix A, part A10. Crystals were grown from dichloromethane and toluene.

**Bis-(2-Biphenyl-3-yl-4-phenyl-pyridine-C²,N')acetylacetonate iridium,
Ir(bippy)₂AcAc (49)**

General synthesis adapted from work by Lamansky *et al.*¹⁴



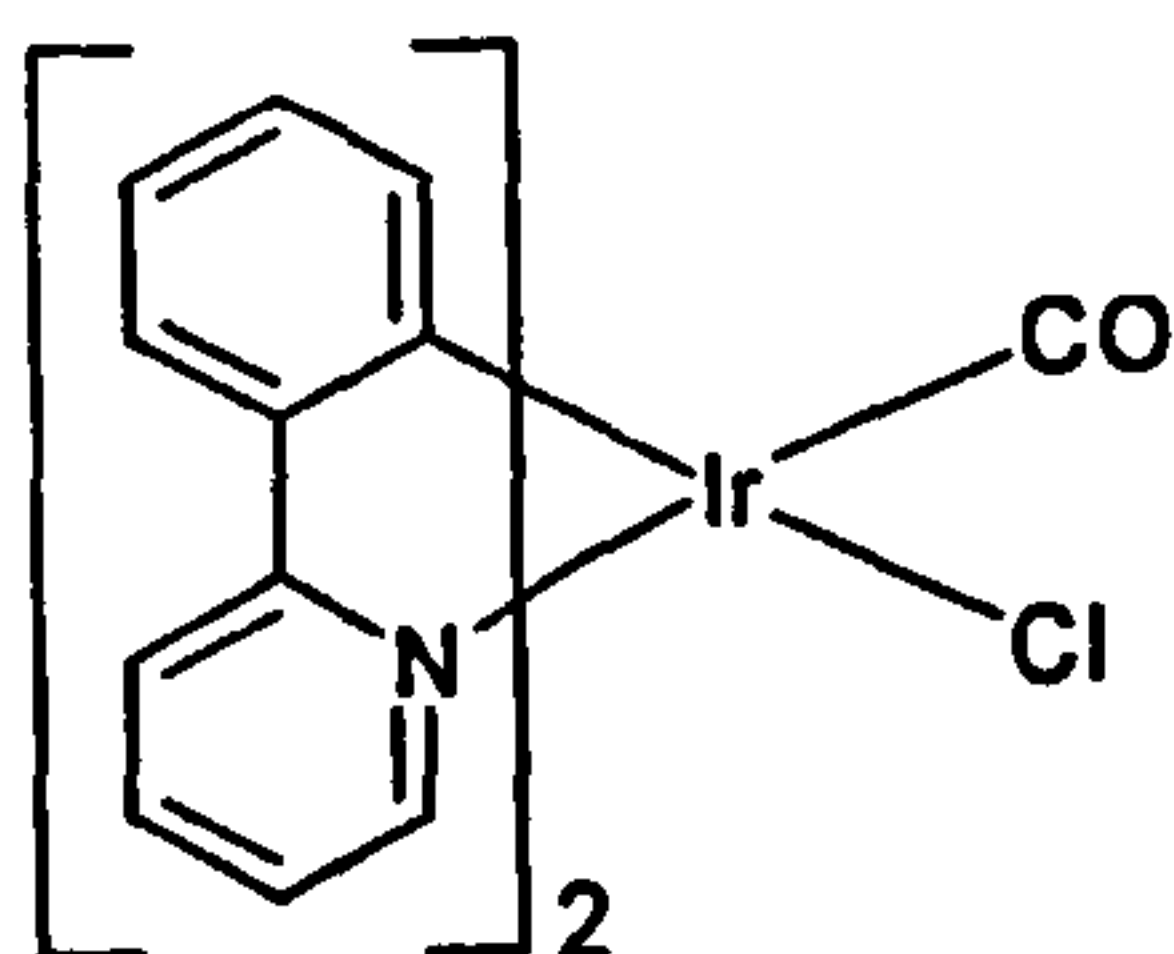
Ir(bippy)₂Cl₂ 28 (0.169 g, 0.10 mmol), 2,4-pentanedione (0.040 g, 0.40 mmol), sodium carbonate (0.10 g, 0.94 mmol) and 2-ethoxyethanol (8 mL) were placed in a reaction vessel and purged with nitrogen gas. The mixture was heated to 120 °C for 12 hours, with continuous stirring. The solution was

cooled to room temperature and water (10 mL) was added. The resulting mixture was filtered and the precipitate washed with water (2 x 10 mL). The crude solid was dissolved in dichloromethane, dried over magnesium sulphate, filtered and evaporated to dryness. Column chromatography (silica gel, dichloromethane) afforded 49 as a bright orange solid (0.072 g, 40 %). ¹H-NMR 200 MHz (CDCl₃): δ 8.54 (2H, d, J = 6.2 Hz), 8.09 (2H, s), 7.76 (6H, m), 7.37 (18H, m), 6.93 (2H, d, J = 6.2 Hz), 6.43 (2H, d, J = 8.0 Hz), 5.21 (1H, s), 1.79 (6H, s). MALDI MS (EI⁺): m/z 904.295 (M)⁺, 805.345 (M-C₅H₇O₂)⁺.

**3.5 Ir(L)₂X(Y) Complexes, where X = Cl/CN
and Y = Monodentate ligand**

Bis-(2-phenylpyridine-C²,N')carbonyl iridium chloride, Ir(ppy)₂Cl(CO) (50)

General synthesis adapted from work by King *et al.*¹⁶



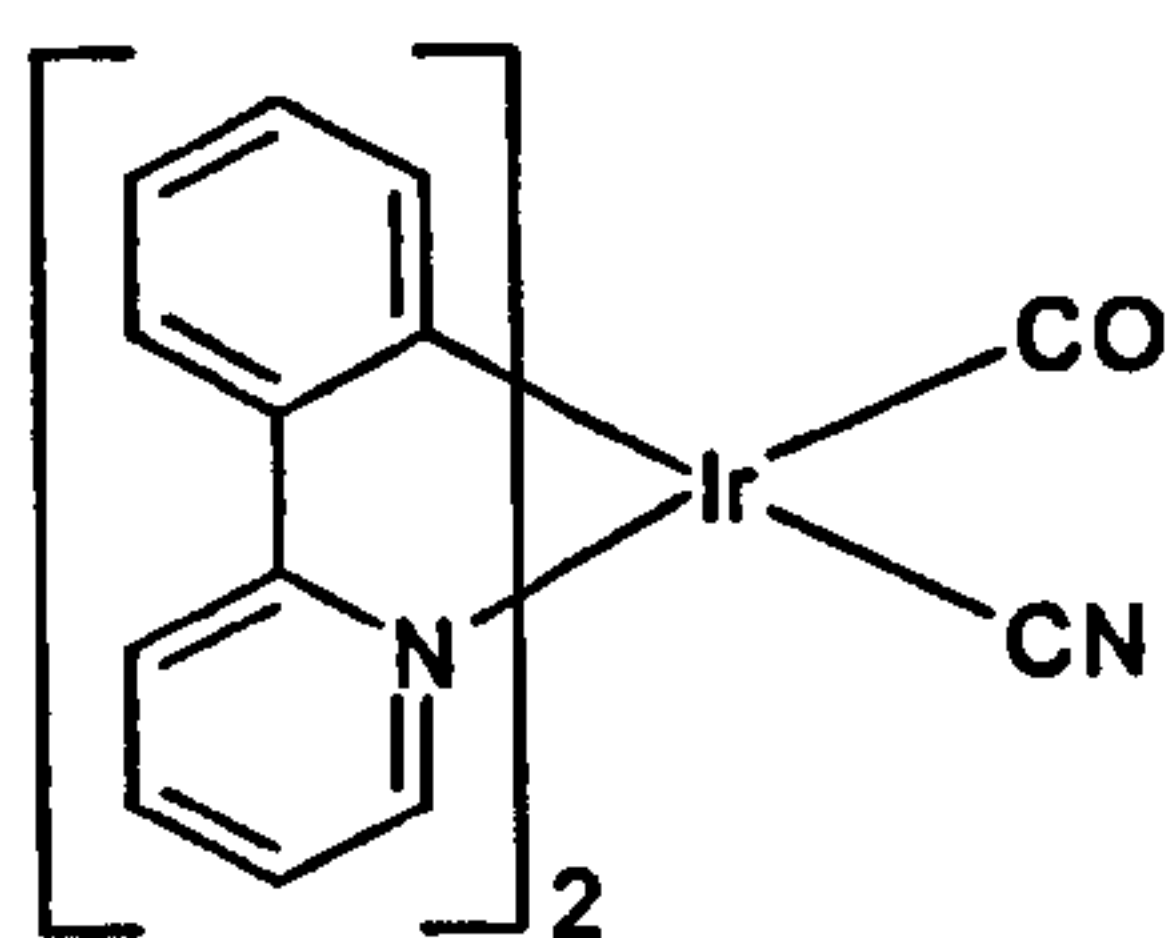
[Ir(ppy)₂Cl]₂ 19 (0.23 g, 0.21 mmol) was suspended in dichloromethane (15 mL) and the flask was purged with CO several times. The reaction mixture was stirred continuously at room temperature for 12 hours under a blanket of carbon monoxide. The now clear solution was evaporated to dryness

and column chromatography afforded 50 as a green-yellow solid (0.239 g, 98 %).

$^1\text{H-NMR}$ 500 MHz (CDCl_3): δ 9.87 (1H, d, $J = 6.0$ Hz), 9.10 (1H, d, $J = 6.0$ Hz), 7.94 (4H, m), 7.63 (2H, t, $J = 9.0$ Hz), 7.36 (1H, q, $J = 5.0$ Hz), 7.26 (1H, d, $J = 9.5$ Hz), 6.97 (2H, m), 6.86 (2H, m), 6.40 (1H, d, $J = 7.5$ Hz), 5.96 (1H, d, $J = 7.5$ Hz). MS (EI+): m/z 564 (M^+), 536 (M-CO^+), 501 (M-COCl^+), 347 ($\text{COClC}_{11}\text{H}_8\text{N}^+$). IR (Nujol: KBr): $\nu(\text{C=O})$ 2032 cm^{-1} . The X-ray crystal structure and related data for 50 can be found in appendix A, part A11. Crystals were grown from dichloromethane and cyclohexane.

Bis-(2-phenylpyridine- C^2, N^1)carbonyl iridium cyanide, $\text{Ir}(\text{ppy})_2\text{CN}(\text{CO})$ (51)

General synthesis adapted from work by King *et al.*¹⁶

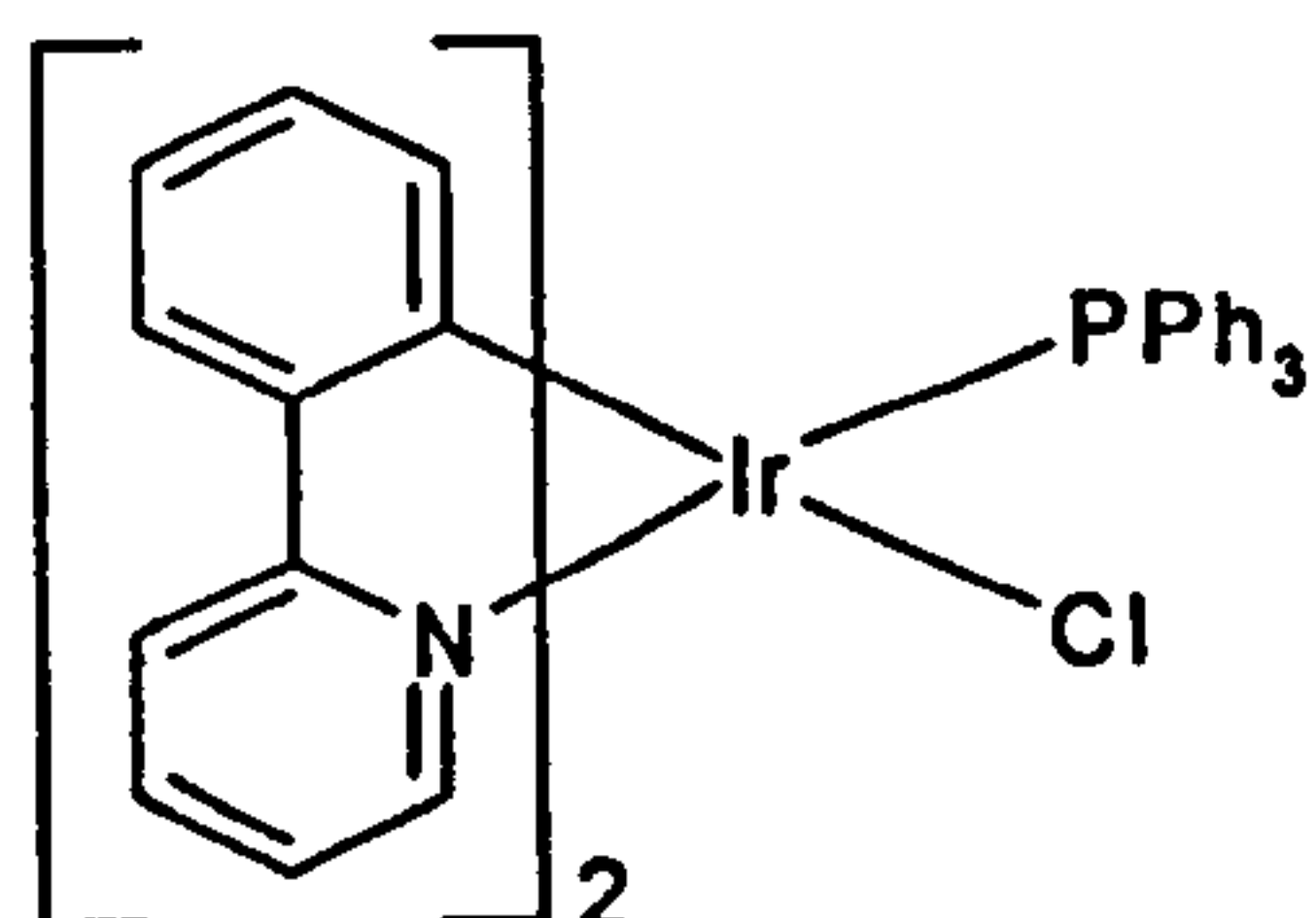


$\text{Ir}(\text{ppy})_2\text{Cl}(\text{CO})$ 50 (0.055 g, 0.10 mmol) was dissolved in acetonitrile (5 mL) with gentle warming and silver(I) cyanide (0.013 g, 0.10 mmol) was added. The reaction mixture was stirred continuously at room temperature for 1 hour and then water (10 mL) was added. The slurry was filtered through

celite and washed with more water (2 x 20 mL) and subsequently dissolved in dichloromethane. The filtrate was dried over magnesium sulphate, filtered and evaporated to dryness. Column chromatography afforded 51 as a yellow solid (0.022 g, 40 %). $^1\text{H-NMR}$ 200 MHz (CDCl_3): δ 9.72 (1H, d, $J = 5.8$ Hz), 9.01 (1H, d, $J = 5.8$ Hz), 7.95 (4H, m), 7.64 (2H, td, $J = 7.6$ Hz), 7.32 (2H, m), 7.42 (2H, m), 6.92 (4H, m), 6.32 (1H, d, $J = 8.2$ Hz), 6.01 (1H, d, $J = 7.2$ Hz). MS (EI+): m/z (M^+) not seen, 526 (M-CO^+), 501 (M-COCN^+). IR (Nujol: KBr): $\nu(\text{C=O})$ 2042 cm^{-1} , $\nu(\text{C}\equiv\text{N})$ 2126 cm^{-1} .

Bis-(2-phenylpyridine- C^2, N^1)triphenylphosphine iridium chloride, $\text{Ir}(\text{ppy})_2\text{Cl}(\text{PPh}_3)$ (52)

General synthesis adapted from work by King *et al.*¹⁶

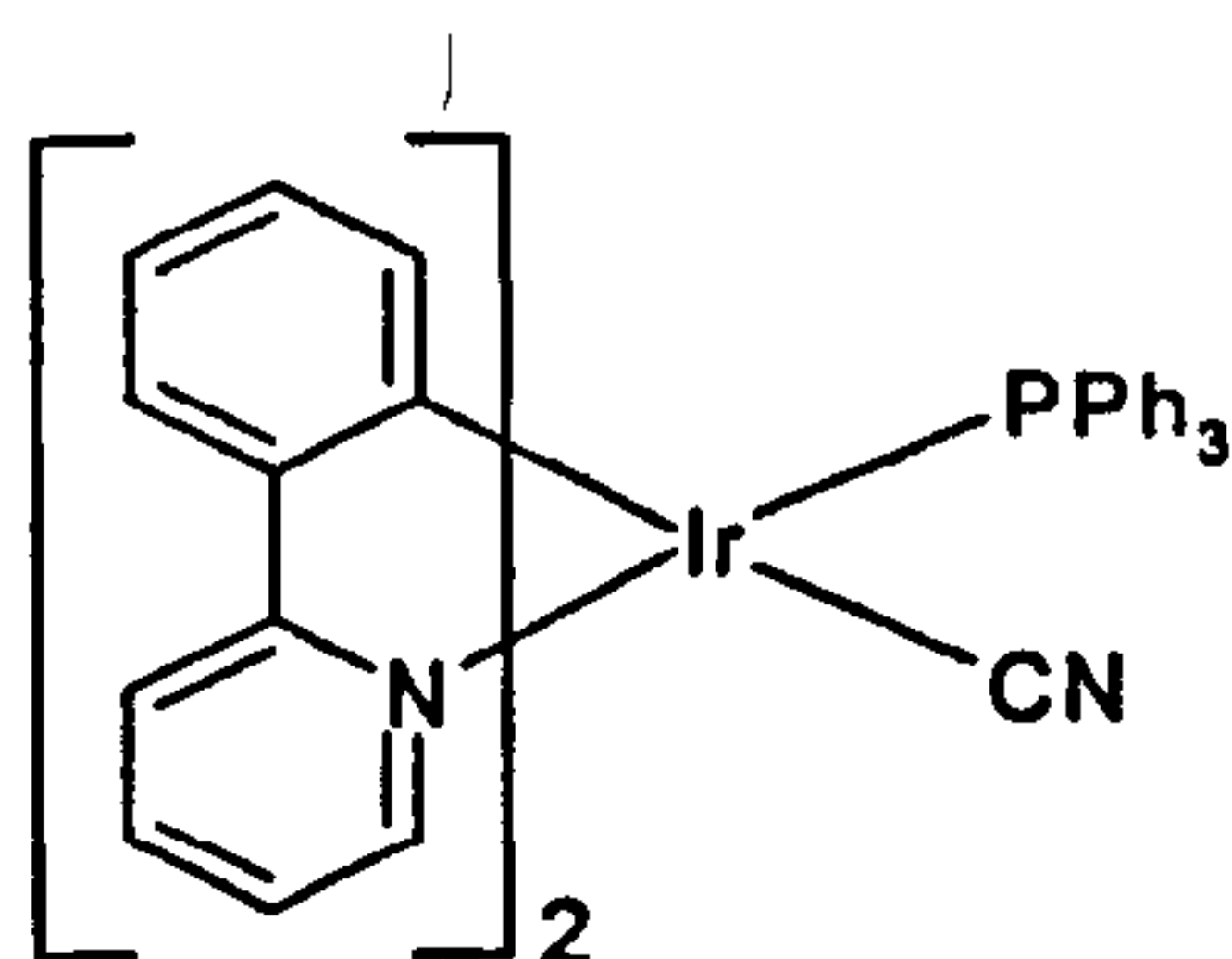


$[\text{Ir}(\text{ppy})_2\text{Cl}]_2$ 19 (0.11 g, 0.10 mmol) and triphenylphosphine (0.052 g, 0.20 mmol) were suspended in dichloromethane (15 mL) and warmed gently. The

reaction mixture was stirred continuously at room temperature for 2 hours. The now clear solution was evaporated to dryness and the residual solid was washed repeatedly with cyclohexane and then dried under vacuum to afford **52** as a green-yellow solid (0.140 g, 88 %). $^1\text{H-NMR}$ 400 MHz (CD_2Cl_2): δ 9.15 (1H, d, $J = 6.0$ Hz), 8.87 (1H, d, $J = 6.4$ Hz), 7.93 (1H, d, $J = 9.6$ Hz), 7.76 (1H, t, $J = 8.0$ Hz), 7.60 (2H, m), 7.48 (2H, m), 7.25 (12 H, m), 7.11 (3H, m), 6.88 (1H, t, $J = 8.0$ Hz), 6.82 (2H, m), 6.74 (2H, m), 6.55 (1H, t, $J = 8.0$ Hz), 5.95 (1H, d, $J = 8.0$ Hz), 5.78 (1H, q, $J = 5.2$ Hz). $^{13}\text{C-NMR}$ 500 MHz (CD_2Cl_2): δ 169.3 (d, $J = 25.0$ Hz), 167.0, 162.2, 161.4, 155.5 (d, $J = 30.5$ Hz), 151.4, 148.4 (d, $J = 17.0$ Hz), 143.8, 143.4, 137.3, 136.4, 134.6 (d, $J = 38.0$ Hz), 131.5, 131.4, 131.1, 130.0, 129.9, 129.5, 127.9 (d, $J = 36.5$ Hz), 124.1 (d, $J = 19.0$ Hz), 123.9, 122.5, 122.4, 121.0, 119.9, 118.1. $^{31}\text{P-NMR}$ 400 MHz (CDCl_3): δ -0.39 (1P). MS (EI+): m/z 798 (M) $^+$, 536 ($\text{M-PC}_{18}\text{H}_{15}$) $^+$, 501 ($\text{M-PC}_{18}\text{H}_{15}\text{Cl}$) $^+$, 347 ($\text{M-PC}_{29}\text{H}_{23}\text{ClN}$) $^+$. The X-ray crystal structure and related data for **52** can be found in appendix A, part A12. Crystals were grown from dichloromethane and cyclohexane.

**Bis-(2-phenylpyridine- C^2, N^1)triphenylphosphine iridium cyanide,
 $\text{Ir}(\text{ppy})_2\text{CN}(\text{PPh}_3)$ (**53**)**

General synthesis adapted from work by King *et al.*¹⁶

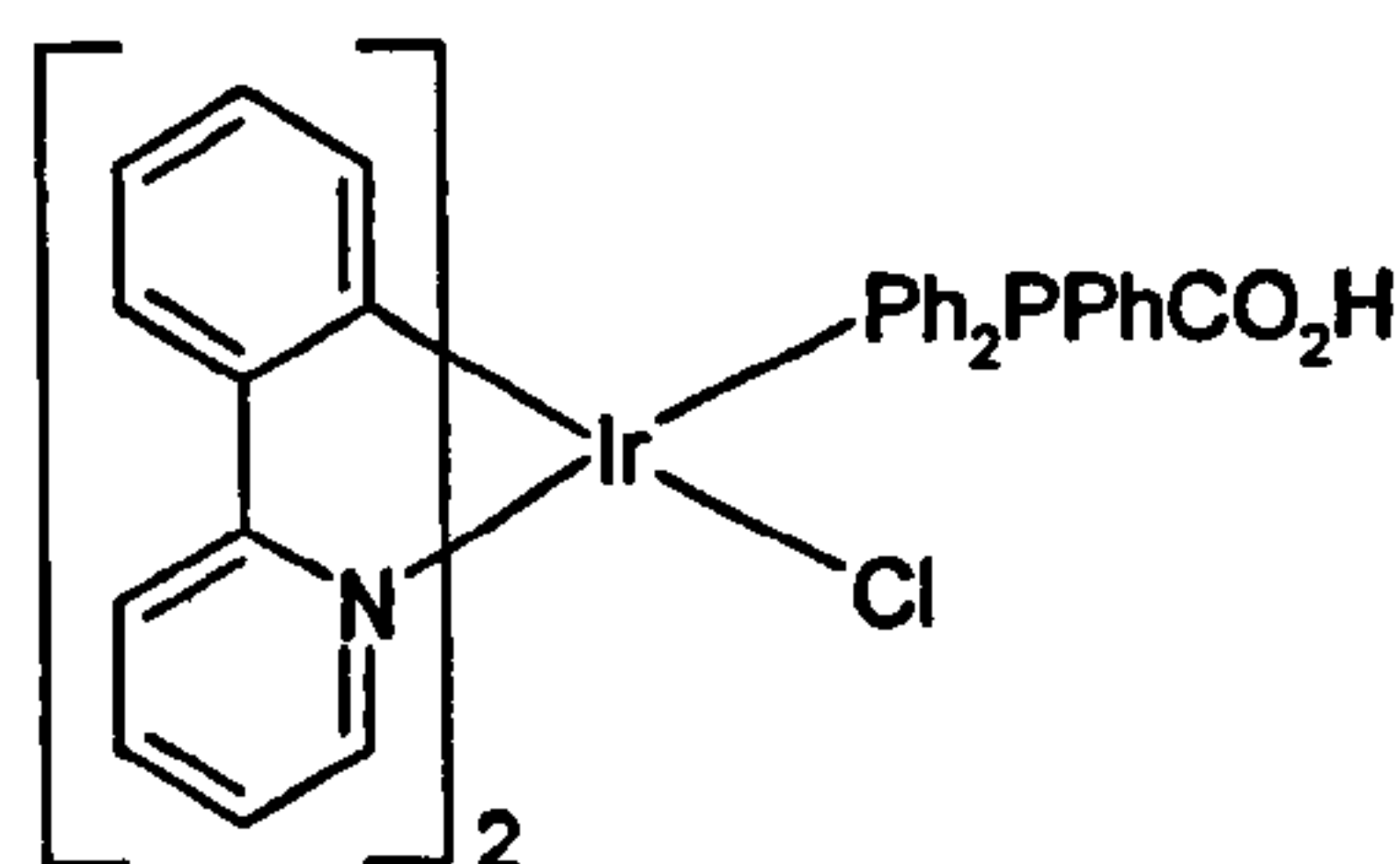


$\text{Ir}(\text{ppy})_2\text{Cl}(\text{PPh}_3)$ **52** (0.160 g, 0.20 mmol) and silver(I) cyanide (0.026 g, 0.20 mmol) were dissolved in acetonitrile (5 mL) and warmed gently. The reaction mixture was stirred continuously for 2 hours with gentle warming. The solution was evaporated to dryness and the residual solid

was washed repeatedly with cyclohexane and subsequently dried under vacuum to afford **53** as a yellow solid (0.129 g, 82 %). $^1\text{H-NMR}$ 200 MHz (CDCl_3): δ 9.00 (1H, d, $J = 5.8$ Hz), 8.64 (1H, d, $J = 5.4$ Hz), 7.60 (11H, m), 7.22 (8H, m), 6.81 (8H, m), 5.99 (1H, q, $J = 4.8$ Hz), 5.91 (1H, d, $J = 7.4$ Hz). $^{31}\text{P-NMR}$ 300 MHz (CDCl_3): -1.05 (1P). MS (EI+): m/z 788 (M) $^+$, 527 (M-PPh_3) $^+$. IR (Nujol: KBr): $\nu(\text{C}\equiv\text{N})$ 2102 cm^{-1} .

Bis-(2-phenylpyridine-C²,N')4-diphenylphosphane-benzoic acid iridium chloride, Ir(ppy)₂Cl(Ph₂PPhCO₂H) (54)

General synthesis adapted from work by King *et al.*¹⁶

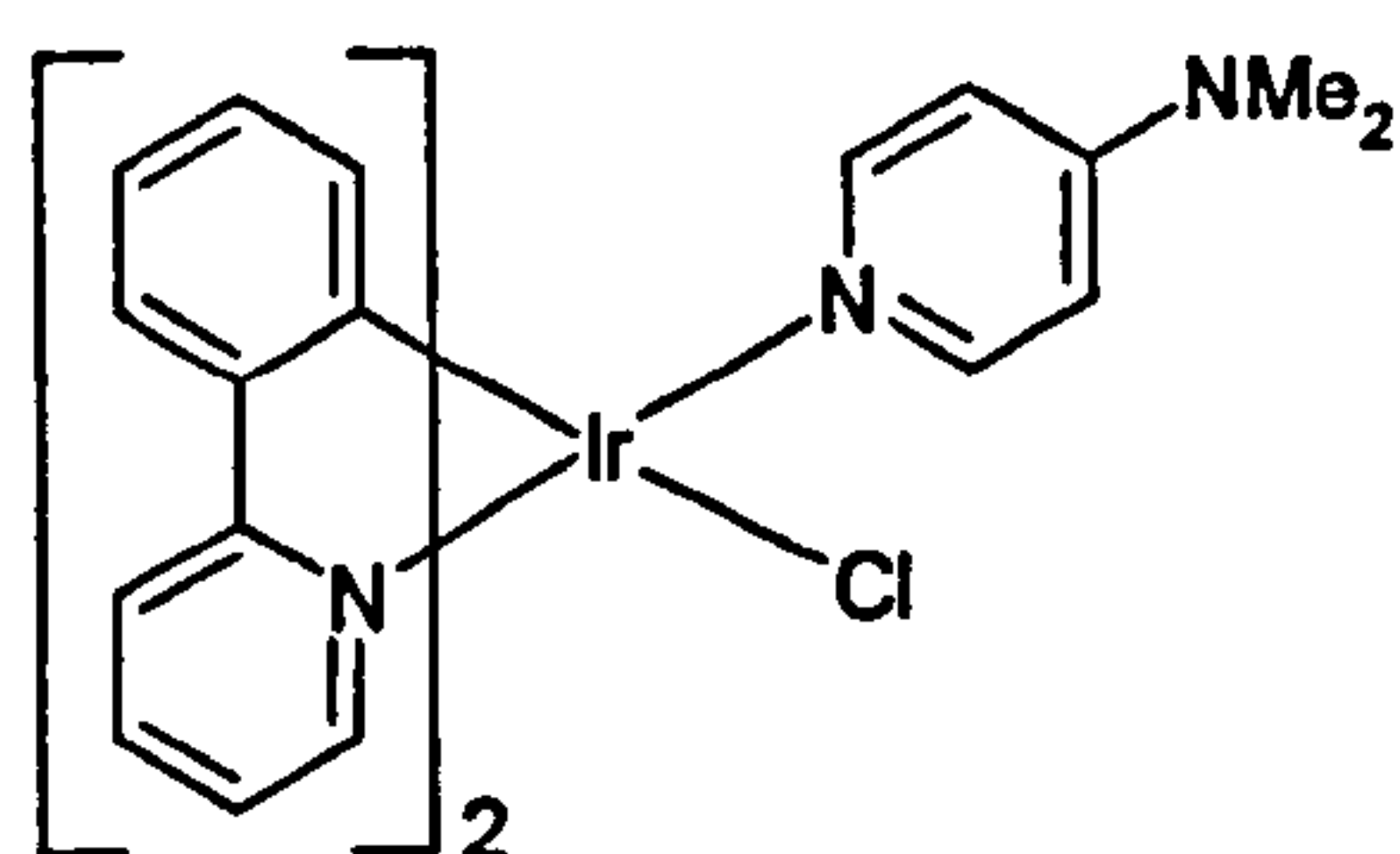


[Ir(ppy)₂Cl]₂ **19** (0.11 g, 0.10 mmol) and 4-diphenylphosphanyl-benzoic acid **18** (0.062 g, 0.20 mmol) were suspended in dichloromethane (5 mL) and warmed gently. The reaction mixture was stirred continuously at room temperature for 1 hour.

The now clear solution was evaporated to dryness and the residual solid was washed repeatedly with cyclohexane and subsequently dried under vacuum to afford **54** as a green-yellow solid (0.163 g, 97 %). ¹H-NMR 300 MHz (CDCl₃): δ 9.32 (1H, d, J = 5.7 Hz), 8.83 (1H, d, J = 5.7 Hz), 7.92 (1H, d, J = 7.8 Hz), 7.60 (3H, m), 7.56 (2H, t, J = 7.5 Hz), 7.49 (2H, t, J = 7.8 Hz), 7.40 (2H, t, J = 8.1 Hz), 7.28 (5H, m), 7.19 (5H, m), 6.85 (5H, m), 6.56 (1H, t, J = 7.8 Hz), 5.90 (1H, d, J = 8.1 Hz), 5.84 (1H, m). ³¹P-NMR 300 MHz (CDCl₃): -0.48 (1P). MS (EI⁺): m/z 842 (M)⁺, 806 (M-Cl)⁺.

Bis-(2-phenylpyridine-C²,N')dimethylaminopyridine iridium chloride, Ir(ppy)₂Cl(DMAP) (55)

General synthesis adapted from work by King *et al.*¹⁶



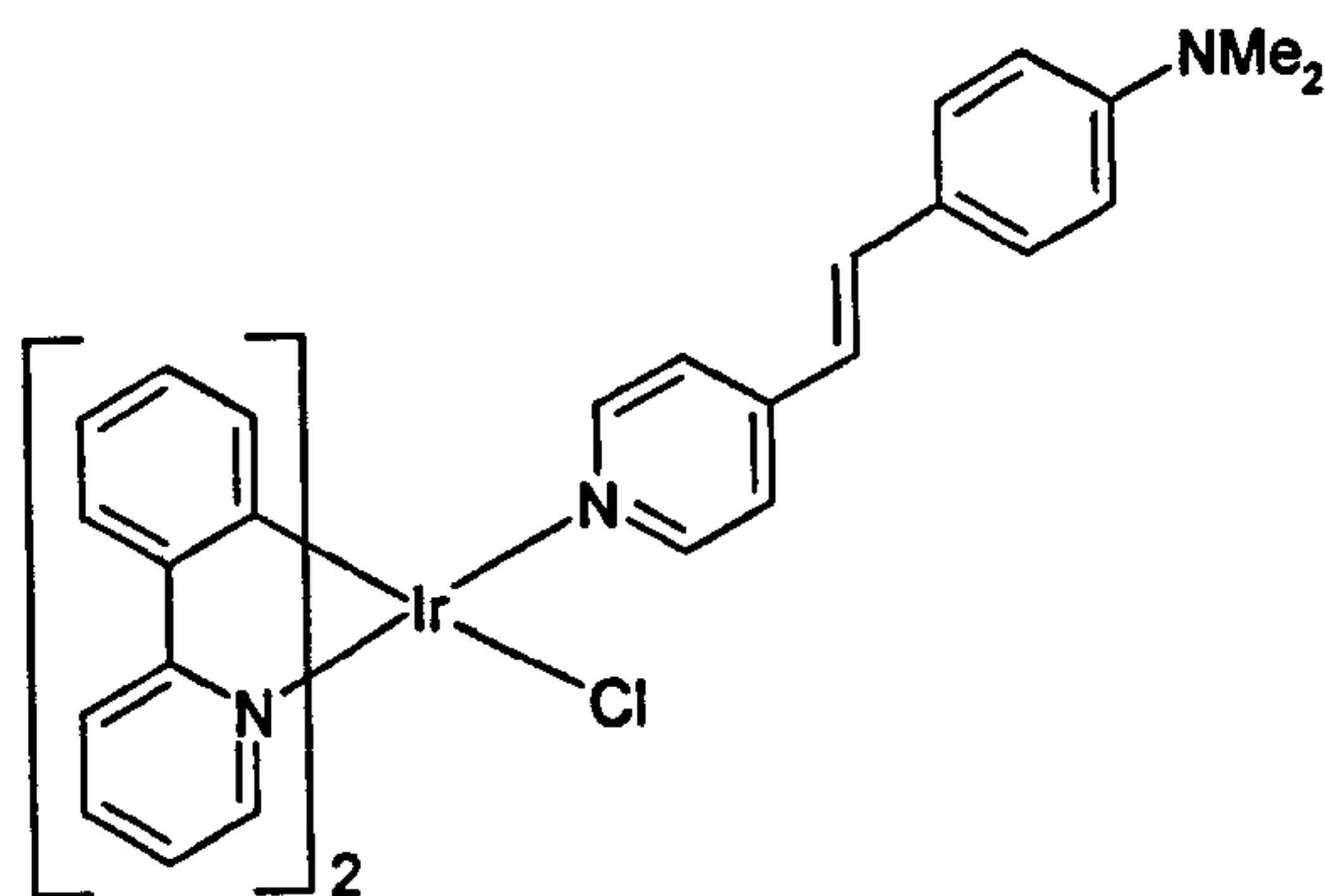
[Ir(ppy)₂Cl]₂ **19** (0.11 g, 0.10 mmol) and dimethylaminopyridine (DMAP) (0.025 g, 0.20 mmol) were suspended in dichloromethane (5 mL) and warmed gently. The reaction mixture was stirred continuously at room temperature for 1 hour. The

now clear solution was evaporated to dryness and the residual solid was washed repeatedly with cyclohexane and subsequently dried under vacuum to afford **55** as an orange solid (0.058 g, 44 %). ¹H-NMR 200 MHz (CDCl₃): δ 9.94 (1H, d, J = 5.8 Hz), 8.19 (1H, d, J = 6.0 Hz), 7.88 (1H, d, J = 9.0 Hz), 7.66 (3H, m), 7.52 (2H, q, J = 8.0 Hz), 7.15 (1H, t, J = 5.6 Hz), 6.84 (1H, t, J = 7.4 Hz), 6.75 (5H, m), 6.32 (4H, m), 6.21 (1H,

d, $J = 1.6$ Hz), 2.94 (6H, s). MS (EI⁺): m/z 658 (M)⁺, 536 (M-C₆H₇N)⁺, 501 (M-C₆H₇NCl)⁺.

**Bis-(2-phenylpyridine-C²,N')2-Phenyl-4-styryl-pyridine iridium chloride,
Ir(ppy)₂Cl(pyCH=CHPhNMe₂) (56)**

General synthesis adapted from work by King *et al.*¹⁶

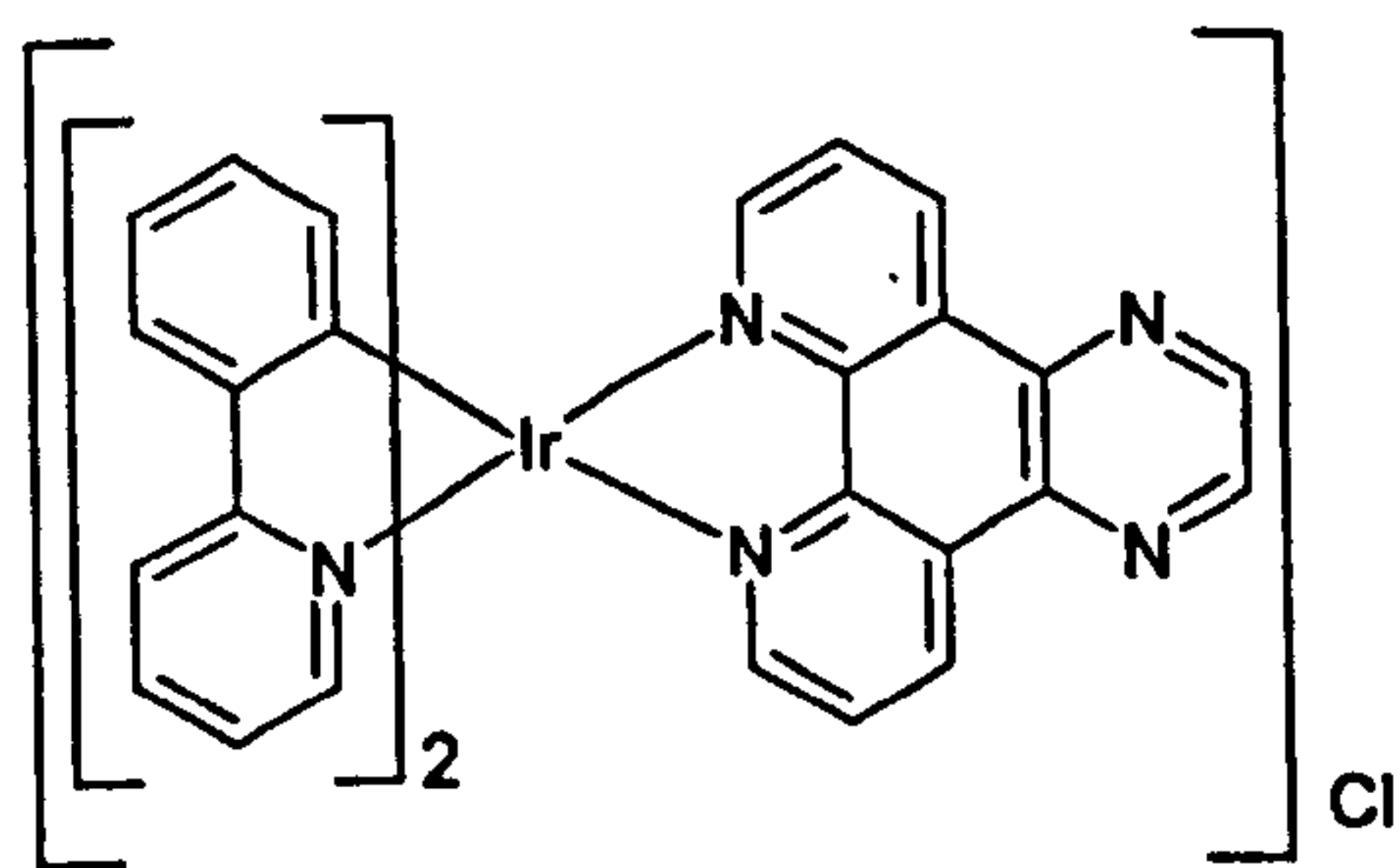


[Ir(ppy)₂Cl]₂ **19** (0.11 g, 0.10 mmol) and 2-phenyl-4-styryl-pyridine (pyCH=CHPhNMe₂) **10** (0.045 g, 0.20 mmol) were suspended in dichloromethane (5 mL) and warmed gently. The reaction mixture was stirred continuously at room temperature for 1

hour. The now clear solution was evaporated to dryness and the residual solid was washed repeatedly with cyclohexane and subsequently dried under vacuum to afford **56** as an orange solid (0.140 g, 92 %). ¹H-NMR 200 MHz (CDCl₃): δ 9.94 (1H, d, $J = 7.8$ Hz), 8.15 (1H, d, $J = 8.7$ Hz), 7.90 (1H, d, 10.5 Hz), 7.67 (3H, m), 7.54 (2H, m), 7.39 (2H, d, 12.9 Hz), 7.17 (4H, m), 7.02 (1H, t, $J = 9.3$ Hz), 6.77 (9H, m), 6.35 (1H, d $J = 10.5$ Hz), 6.22 (1H, d, $J = 10.5$ Hz), 3.01 (6H, s). MS (EI⁺): m/z 760 (M)⁺.

**Rac-Bis-(2-phenylpyridine-C²,N')1,4,8,9-tetraaza-triphenylene iridium chloride,
Ir(ppy)₂Cl(TAT) (57)**

General synthesis adapted from work by King *et al.*¹⁶



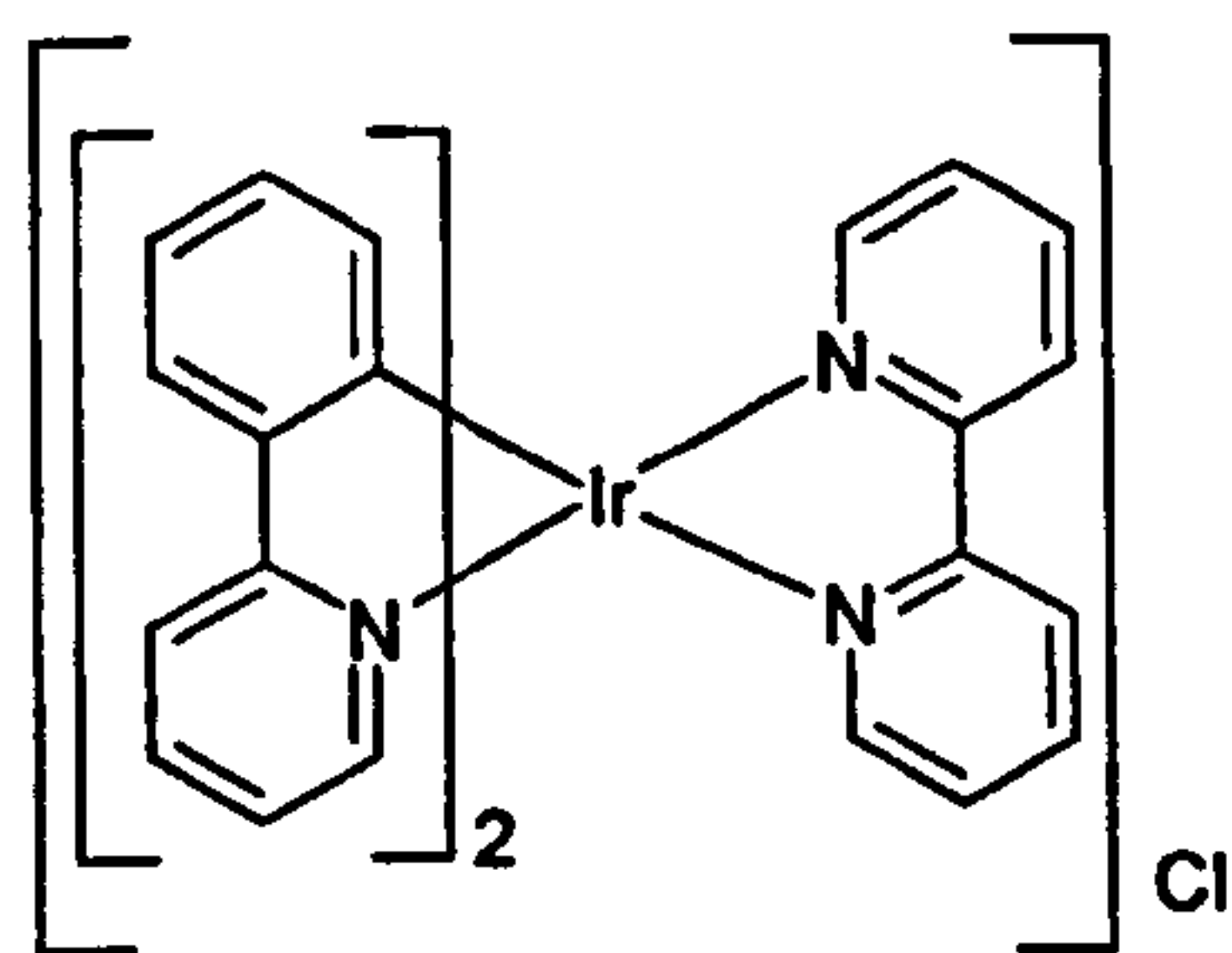
[Ir(ppy)₂Cl]₂ **19** (0.053 g, 0.05 mmol) and 1,4,8,9-tetraaza-triphenylene (TAT) (0.023 g, 0.10 mmol) were suspended in dichloromethane (5 mL) and warmed gently. The reaction mixture was stirred continuously at room temperature overnight. The now clear orange solution was

evaporated to dryness and the residual solid was washed repeatedly with toluene and then diethyl ether and subsequently dried under vacuum to afford **57** as a bright orange solid (0.070 g, 91 %). $^1\text{H-NMR}$ 300 MHz (CDCl_3): δ 7.72 (1H, d, $J = 7.8$ Hz), 9.19 (1H, s), 8.39 (1H, d $J = 4.5$ Hz), 8.06 (1H, m), 7.95 (1H, m), 7.75 (2H, m), 7.45 (1H, d, $J = 5.1$ Hz), 7.08 (1H, t, $J = 7.2$ Hz), 6.96 (2H, m), 6.39 (1H, d, $J = 7.5$ Hz). MS (ES⁺): m/z 733 (M-Cl)⁺.

***Rac*-Bis-(2-phenylpyridine- C^2, N')2,2'-bipyridine iridium chloride,**

$\text{Ir}(\text{ppy})_2\text{Cl}(\text{bipy})$ (58**)**

General synthesis adapted from work by King *et al.*¹⁶

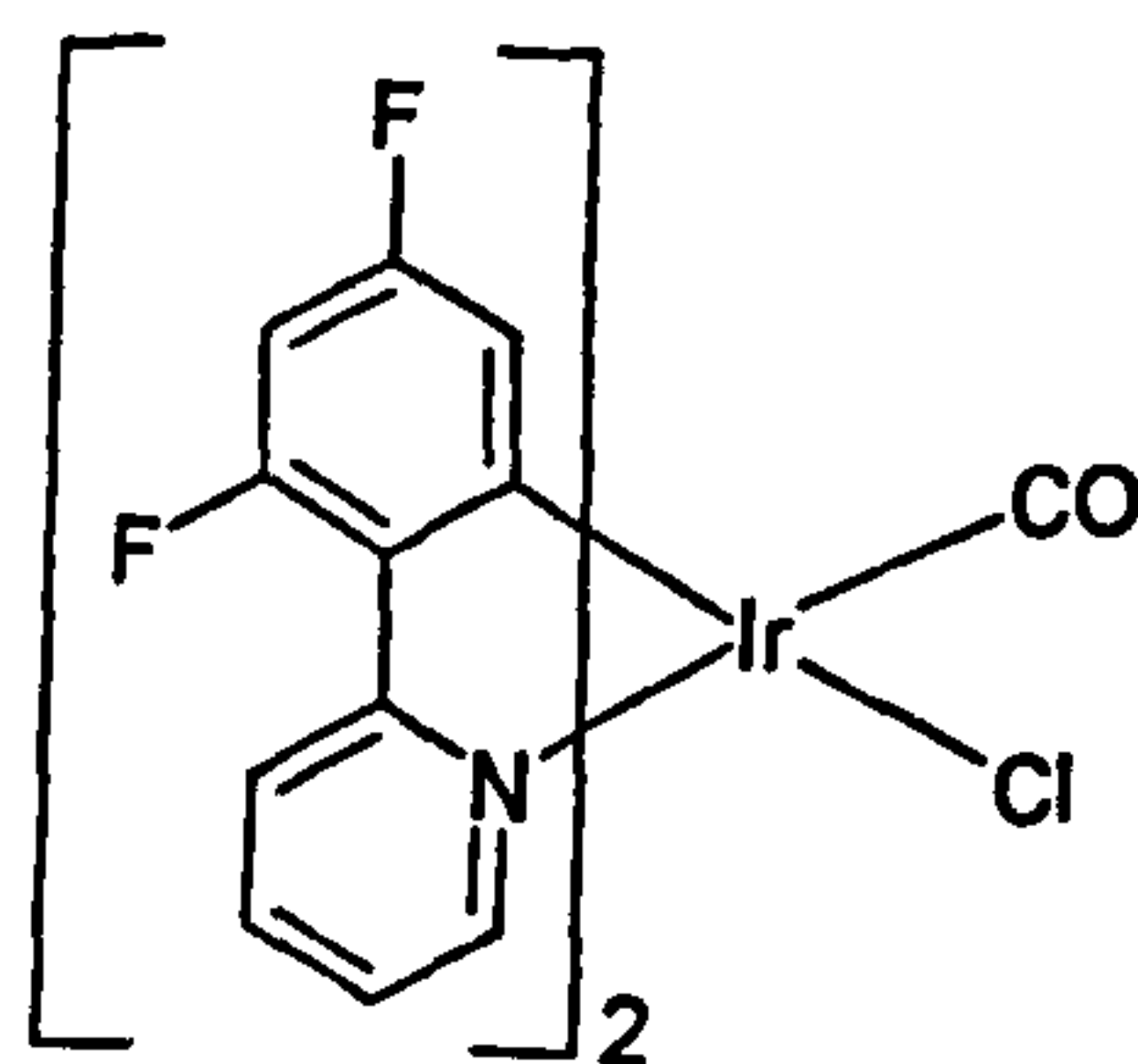


$[\text{Ir}(\text{ppy})_2\text{Cl}]_2$ **19** (0.10 g, 0.093 mmol) and 2,2'-bipyridine (bipy) (0.029 g, 0.187 mmol) were suspended in dichloromethane (5 mL) and warmed gently. The reaction mixture was stirred continuously at room temperature overnight. The now clear yellow solution was evaporated to dryness and the residual solid was

washed repeatedly with toluene and then diethyl ether and subsequently dried under vacuum to afford **58** as a bright yellow solid (0.110 g, 85 %). $^1\text{H-NMR}$ 300 MHz (CDCl_3): δ 9.71 (1H, d, $J = 8.1$ Hz), 9.24 (1H, d, $J = 5.4$ Hz), 8.26 (1H, t, $J = 8.1$ Hz), 7.88 (3H, m), 7.70 (4H, m), 7.47 (2H, m), 7.37 (1H, t, $J = 6.9$ Hz), 7.23 (2H, m), 6.94 (4H, m), 6.76 (2H, m), 6.58 (1H, t, $J = 14.7$ Hz), 6.30 (1H, d, $J = 7.8$ Hz), 5.93 (1H, d, $J = 7.8$ Hz). MS (ES⁺): m/z 657 (M-Cl)⁺.

**Bis-(2-(2,4-difluoro-phenyl)-pyridine- C^2,N')carbonyl iridium chloride,
 $Ir(F_2ppy)_2Cl(CO)$ (59)**

General synthesis adapted from work by King *et al.*¹⁶

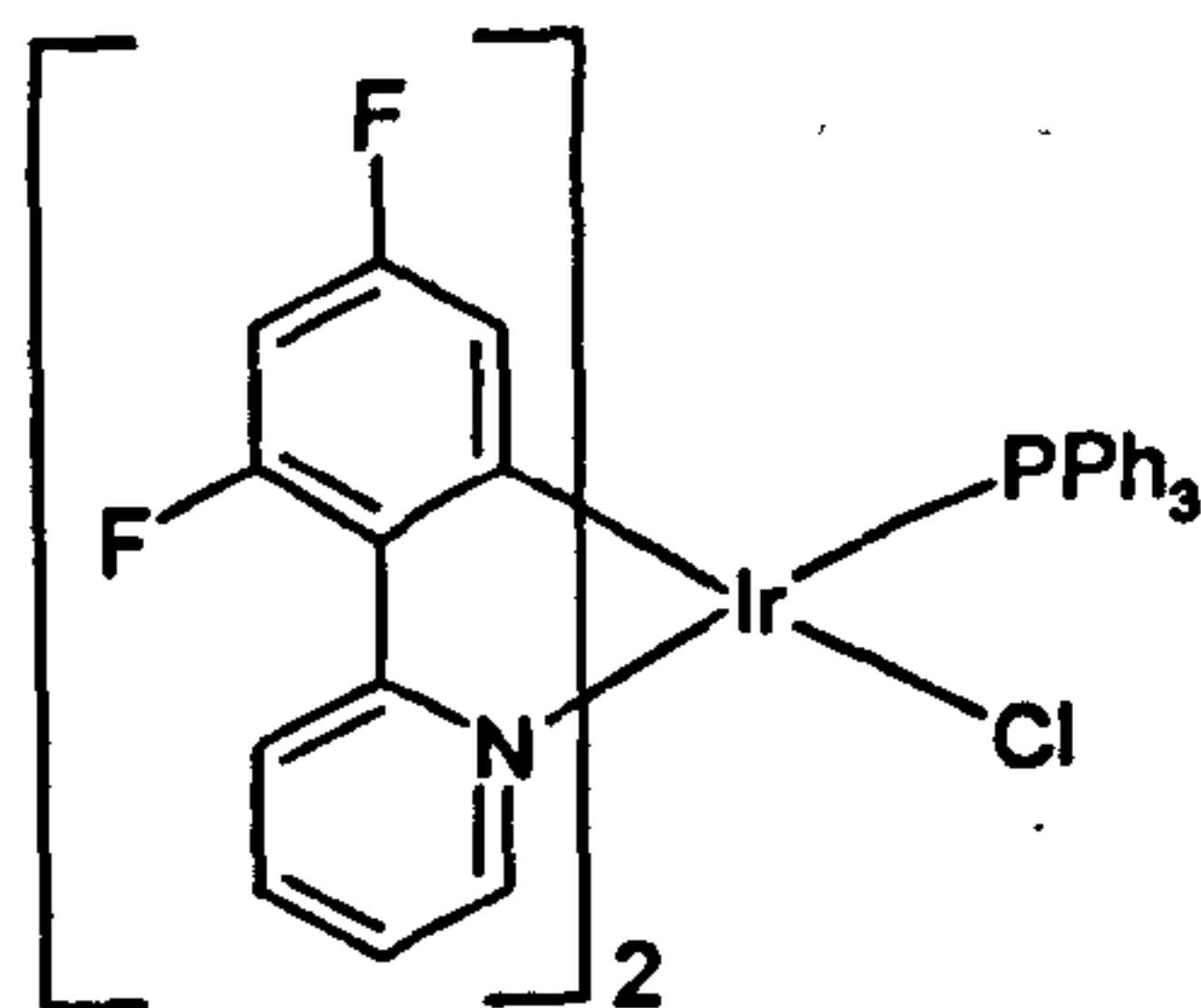


$[Ir(F_2ppy)_2Cl]_2$ 22 (0.20 g, 0.164 mmol) was suspended in dichloromethane (15 mL) and the flask was purged with CO several times. The reaction mixture was stirred continuously at room temperature for 12 hours under a blanket of carbon monoxide. The now clear solution was evaporated to dryness and column chromatography afforded 59 as a pale

yellow solid (0.160 g, 77 %). 1H -NMR 200 MHz ($CDCl_3$): δ 9.86 (1H, d, $J = 4.8$ Hz), 9.06 (1H, d, $J = 5.2$ Hz), 8.34 (2H, m), 8.00 (2H, q, $J = 7.8$ Hz), 7.41 (1H, t, $J = 7.0$ Hz), 7.31 (1H, m), 6.48 (2H, m), 5.84 (1H, dd, $J = 8.0$ Hz), 5.38 (1H, d, $J = 8.0$ Hz). ^{13}C -NMR 500 MHz ($CDCl_3$): δ 172.3, 167.0 (d, $J = 24.5$ Hz), 164.8 (q, $J = 45.5$ Hz), 164.3 (m), 162.7 (m), 162.3, 160.6 (d, $J = 24.0$ Hz), 160.3 (d, $J = 51.5$ Hz), 154.0, 152.1, 143.6 (d, $J = 30.5$ Hz), 140.0, 139.4, 128.0 (m), 127.8 (m), 124.8 (d, $J = 84.0$ Hz), 124.6, 123.9 (d, $J = 80.0$ Hz), 114.1 (dd, $J = 87.5$ Hz), 112.3 (dd, $J = 61.0$ Hz), 101.0 (t, $J = 105.0$ Hz), 100.2 (t, $J = 105.0$ Hz). ^{19}F -NMR 200 MHz ($CDCl_3$): δ -106.10 (2F, m), -108.99 (2F, m). MS (EI⁺): m/z 635 (M)⁺, 608 ($M-CO$)⁺, 573 ($M-COCl$)⁺, 382 ($M-C_{23}H_{12}F_4OCl$)⁺. IR (Nujol: KBr): $\nu(C=O)$ 2056 cm^{-1} , 2038 cm^{-1} . The two carbonyl stretches indicate the presence of more than one isomer.

**Bis-(2-(2,4-difluoro-phenyl)-pyridine- C^2,N')triphenylphosphine iridium chloride,
 $Ir(F_2ppy)_2Cl(PPh_3)$ (60)**

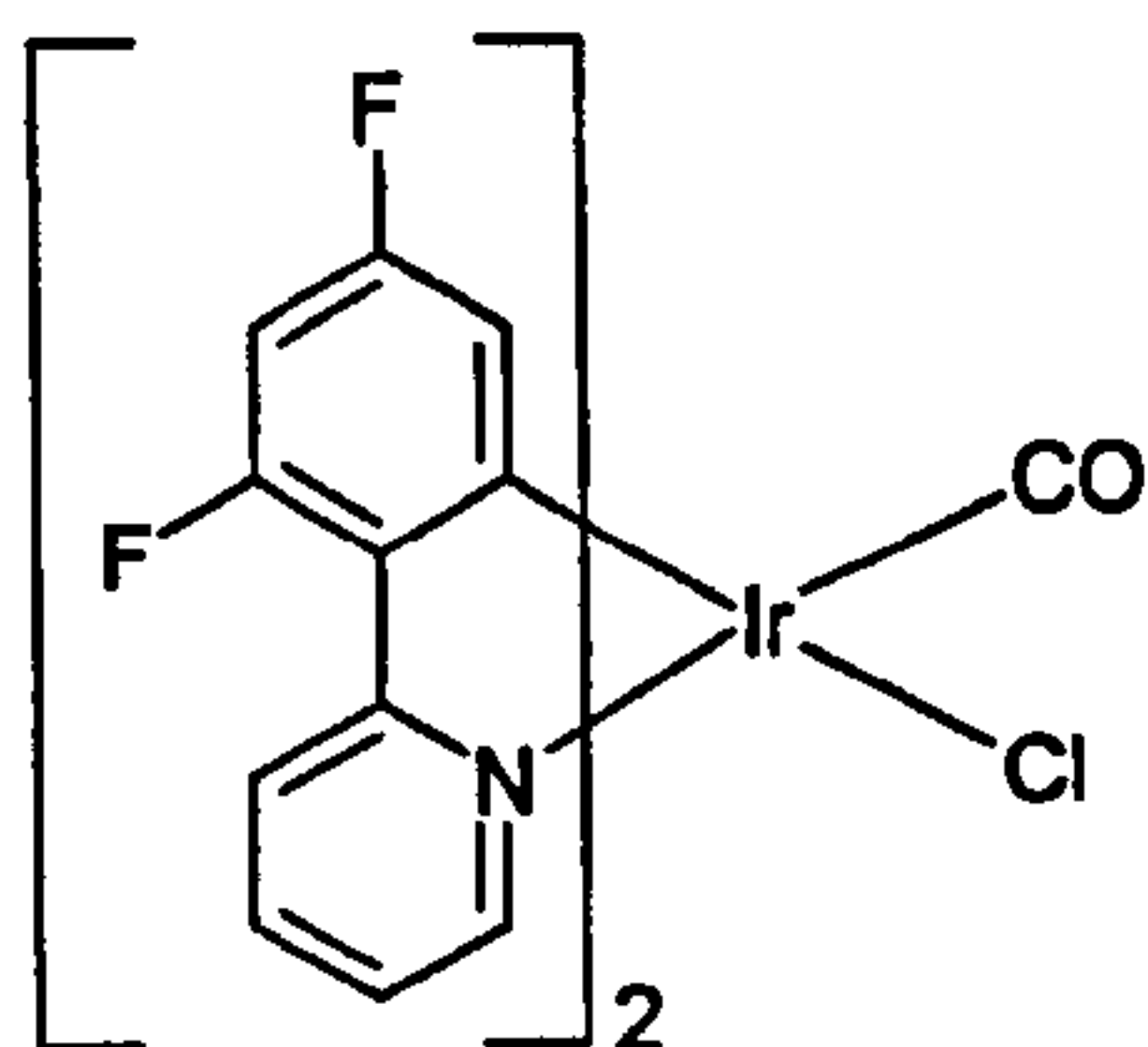
General synthesis adapted from work by King *et al.*¹⁶



$[Ir(F_2ppy)_2Cl]_2$ 22 (0.122 g, 0.10 mmol) and triphenylphosphine (PPh_3) (0.053 g, 0.20 mmol) were suspended in dichloromethane (5 mL) and warmed gently. The reaction mixture was stirred continuously at room temperature overnight. The now clear yellow solution was

**Bis-(2-(2,4-difluoro-phenyl)-pyridine- C^2,N')carbonyl iridium chloride,
 $\text{Ir}(\text{F}_2\text{ppy})_2\text{Cl}(\text{CO})$ (59)**

General synthesis adapted from work by King *et al.*¹⁶

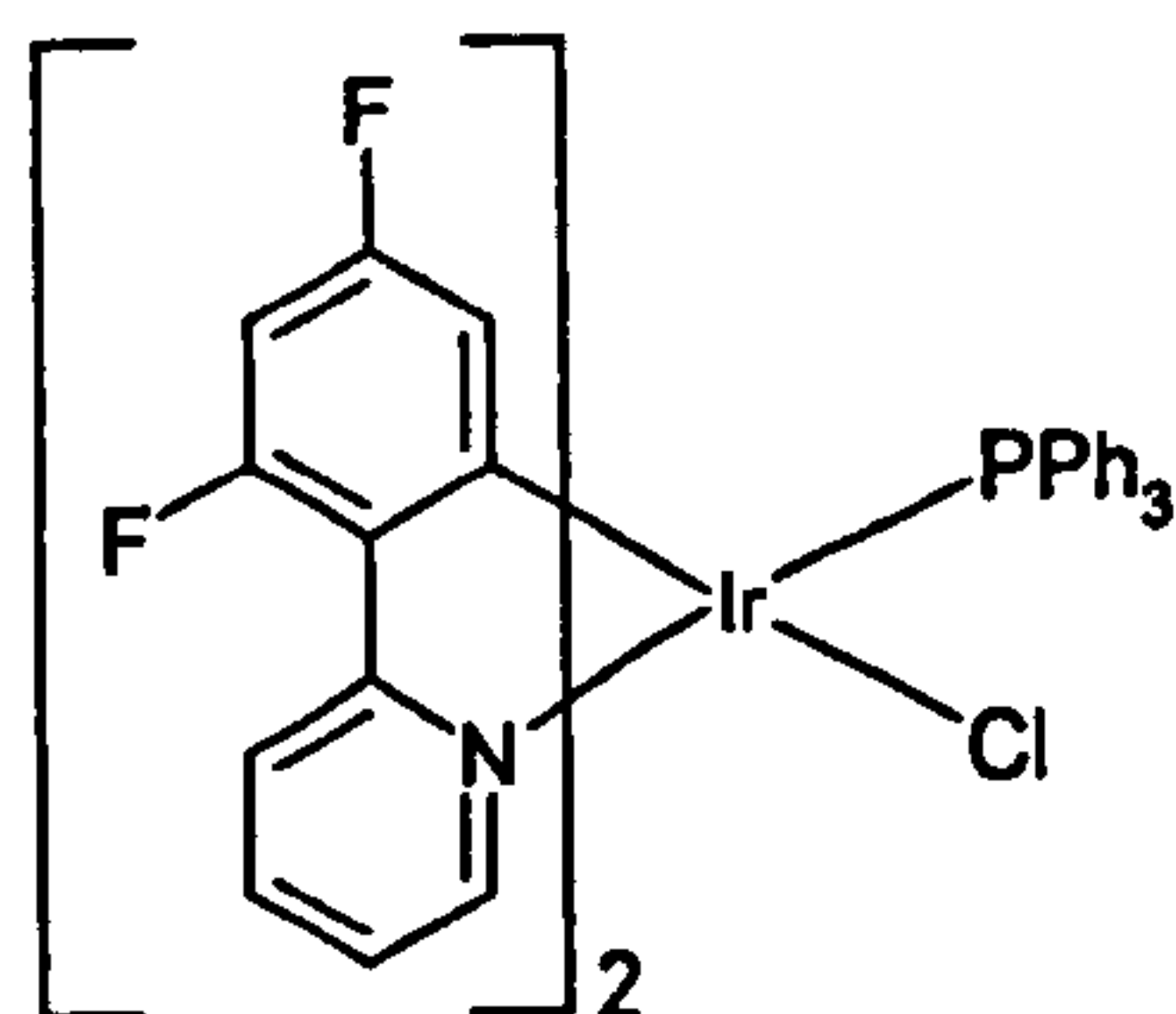


$[\text{Ir}(\text{F}_2\text{ppy})_2\text{Cl}]_2$ 22 (0.20 g, 0.164 mmol) was suspended in dichloromethane (15 mL) and the flask was purged with CO several times. The reaction mixture was stirred continuously at room temperature for 12 hours under a blanket of carbon monoxide. The now clear solution was evaporated to dryness and column chromatography afforded 59 as a pale

yellow solid (0.160 g, 77 %). ^1H -NMR 200 MHz (CDCl_3): δ 9.86 (1H, d, $J = 4.8$ Hz), 9.06 (1H, d, $J = 5.2$ Hz), 8.34 (2H, m), 8.00 (2H, q, $J = 7.8$ Hz), 7.41 (1H, t, $J = 7.0$ Hz), 7.31 (1H, m), 6.48 (2H, m), 5.84 (1H, dd, $J = 8.0$ Hz), 5.38 (1H, d, $J = 8.0$ Hz). ^{13}C -NMR 500 MHz (CDCl_3): δ 172.3, 167.0 (d, $J = 24.5$ Hz), 164.8 (q, $J = 45.5$ Hz), 164.3 (m), 162.7 (m), 162.3, 160.6 (d, $J = 24.0$ Hz), 160.3 (d, $J = 51.5$ Hz), 154.0, 152.1, 143.6 (d, $J = 30.5$ Hz), 140.0, 139.4, 128.0 (m), 127.8 (m), 124.8 (d, $J = 84.0$ Hz), 124.6, 123.9 (d, $J = 80.0$ Hz), 114.1 (dd, $J = 87.5$ Hz), 112.3 (dd, $J = 61.0$ Hz), 101.0 (t, $J = 105.0$ Hz), 100.2 (t, $J = 105.0$ Hz). ^{19}F -NMR 200 MHz (CDCl_3): δ -106.10 (2F, m), -108.99 (2F, m). MS (EI $^+$): m/z 635 (M^+), 608 ($\text{M}-\text{CO}^+$), 573 ($\text{M}-\text{COCl}^+$), 382 ($\text{M}-\text{C}_{23}\text{H}_{12}\text{F}_4\text{OCl}^+$). IR (Nujol: KBr): $\nu(\text{C}=\text{O})$ 2056 cm^{-1} , 2038 cm^{-1} . The two carbonyl stretches indicate the presence of more than one isomer.

**Bis-(2-(2,4-difluoro-phenyl)-pyridine- C^2,N')triphenylphosphine iridium chloride,
 $\text{Ir}(\text{F}_2\text{ppy})_2\text{Cl}(\text{PPh}_3)$ (60)**

General synthesis adapted from work by King *et al.*¹⁶



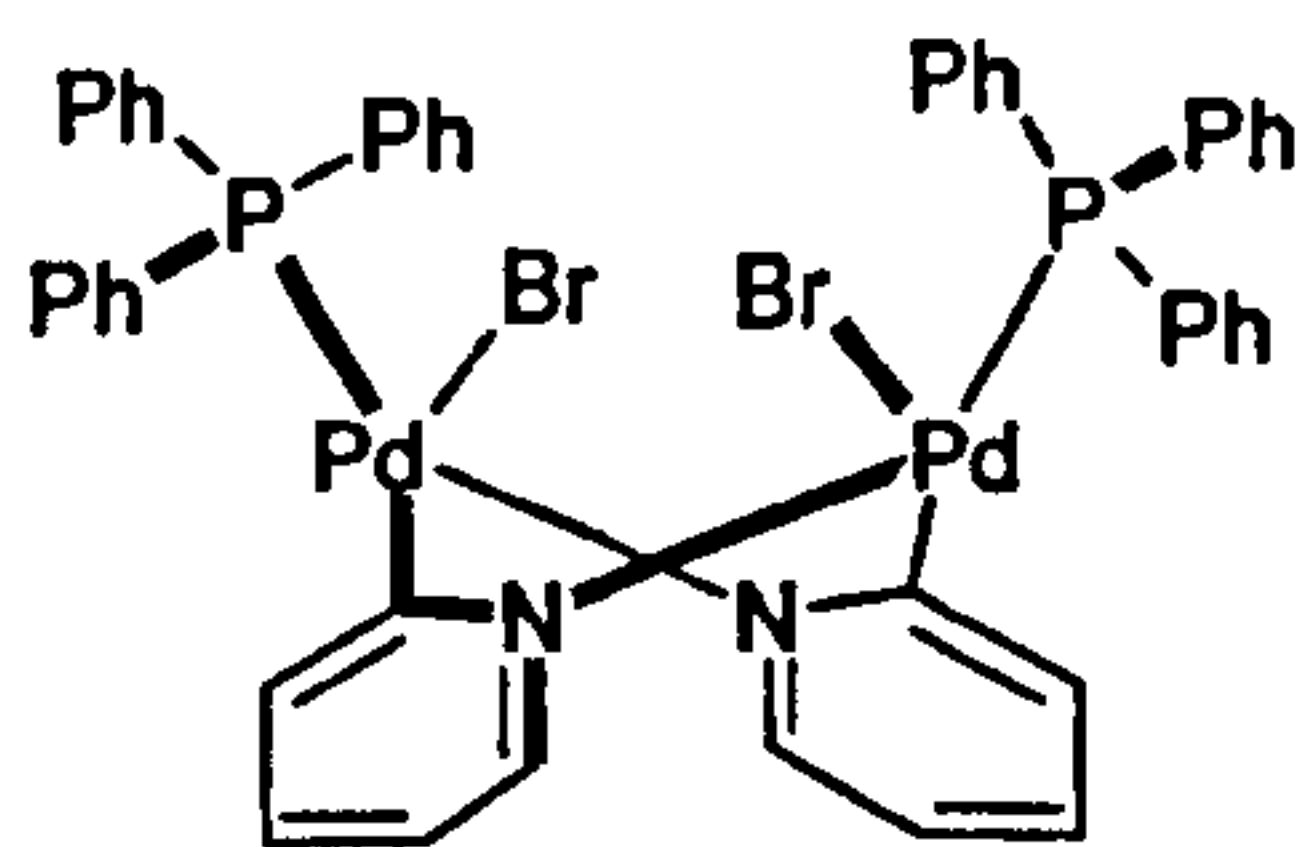
$[\text{Ir}(\text{F}_2\text{ppy})_2\text{Cl}]_2$ 22 (0.122 g, 0.10 mmol) and triphenylphosphine (PPh_3) (0.053 g, 0.20 mmol) were suspended in dichloromethane (5 mL) and warmed gently. The reaction mixture was stirred continuously at room temperature overnight. The now clear yellow solution was

evaporated to dryness and the residual solid was washed repeatedly cyclohexane and subsequently dried under vacuum to afford **60** as a pale yellow solid (0.156 g, 89 %). ^1H -NMR 300 MHz (CDCl_3): δ 8.28 (1H, d, $J = 6.0$ Hz), 8.90 (1H, d, $J = 6.0$ Hz), 8.37 (1H, d, 7.5 Hz), 8.03 (1H, d, 8.7 Hz), 7.80 (1H, t, $J = 7.5$ Hz), 7.57 (1H, t, $J = 7.8$ Hz), 7.21 (10H, m), 7.19 (5H, m), 6.80 (2H, m), 6.40 (2H, m), 5.37 (1H, d, $J = 9.0$ Hz), 5.62 (1H, m). ^{19}F -NMR 300 MHz (CDCl_3): δ -107.42 (1F, m), -108.49 (1F, m), -110.17 (1F, q, $J = 12.0$ Hz), -110.81 (1F, t, $J = 12.0$ Hz). ^{31}P -NMR 300 MHz (CDCl_3): δ -2.98 (1P). MS (EI+): m/z 870 (M^+), 608 ($\text{M}-\text{C}_{18}\text{H}_{15}\text{P}^+$), 573 ($\text{M}-\text{C}_{18}\text{H}_{15}\text{PCl}^+$). The X-crystal structure and related data for **60** can be found in appendix A, part A13. Crystals were grown from dichloromethane and cyclohexane.

3.6 Palladium(II) Species

Trans-(P,N)-[PdBr(μ - $\text{C}_5\text{H}_4\text{N}-\text{C}^2,\text{N}$)(PPh_3)]₂ (**61**)

General synthesis adapted from work by Chin *et al.*¹⁷



Tetrakis(triphenylphosphine) palladium(0) ($\text{Pd}(\text{PPh}_3)_4$) (0.60 g, 0.48 mmol) was dissolved in degassed toluene (40 mL) forming a bright yellow solution. 2-bromopyridine (0.137 g, 0.87 mmol) was added dropwise and the reaction mixture

was refluxed at 90 °C for 4 hours during which time the solution became cloudy. The mixture was cooled to room temperature and filtered. The resulting solid was washed repeatedly with diethyl ether and recrystallised from chloroform to afford **61** as a yellow-green solid (0.205 g, 81 %). ^1H -NMR 300 MHz (CDCl_3): δ 8.58 (2H, m), 7.86 (12H, m), 7.36 (6H, m), 7.28 (12H, m), 6.61 (2H, m), 6.49 (4H, m). ^{31}P -NMR 300 MHz (CDCl_3): δ 31.79. MS (ES+) (CH_3CN): m/z 973 ($\text{M}-\text{Br}^+$), 817 ($\text{M}-\text{Br}_2\text{C}_6\text{H}_5^+$), 488 ($\text{M}-\text{Br}_2+\text{C}_4\text{H}_6\text{N}_2$)²⁺. The X-crystal structure and related data for **61** can be found in appendix A, part A14. Crystals were grown from chloroform.

3.7 References

- 1 D. F. O'Keefe, M. C. Dannock and S. M. Marcuccio, Palladium Catalysed Coupling of Halobenzenes with Arylboronic Acids: Role of the Triphenylphosphine Ligand, *Tet. Lett.*, 1992, **33**, 6679-6680.
- 2 N. M. Ali, A. McKillop, M. B. Mitchell, R. A. Rebelo and P. J. Wallbank, Palladium Catalysed Cross Coupling Reactions of Arylboronic Acids with π -deficient Heteroaryl Chlorides, *Tetrahedron*, 1992, **48**, 8117-8126.
- 3 A. W. Johnson, Triphenylphosphoniumfluorenylide, *J. Org. Chem.*, 1959, **24**, 282-284.
- 4 L. A. Pinck and G. A. Hilbert, Triphenylphosphine Fluorenylidenide, *J. Am. Chem. Soc.*, 1947, **69**, 723.
- 5 M. T. DuPriest, C. L. Schmidt, D. Kuzmich and S. B. Williams, A Facile Synthesis of 7-Halo-5H-Indeno[1,2-b]pyridones and -pyridin-5-ones, *J. Org. Chem.* 1986, **51**, 2021-2023.
- 6 O. Maury, J. Guégan, T. Renouard, A. Hilton, P. Dupau, N. Sandon, L. Toupet and H. Le Bozec, Design and Synthesis of 4,4'- π -conjugated[2,2']bipyridines: A Versatile Class of Tuneable Chromophores and Fluorophores, *New. J. Chem.*, 2001, **25**, 1553-1566.
- 7 F. Kröhnke, The Specific Synthesis of Pyridines and Oligopyridines, *Synthesis (Reviews)*, 1976, 1-24.
- 8 All pyridinium iodide salts were obtained by the reaction of the corresponding acetophenone and pyridine in the presence of iodine. N-phenacylpyridinium bromide was obtained from the reaction of 2-bromoacetophenone and pyridine.
- 9 V. Ravindar, H. Hemling, H. Schumann and J. Blum, A New Synthesis of Hydrophilic Carboxylated Arylphosphines, *Synth. Commun.*, 1992, **22**, 841-851.

- 10 S. Sprouse, K. A. King, P. J. Spellane and R. J. Watts, Photophysical Effects of Metal-Carbon σ Bonds in *Ortho*-metalated Complexes of Ir(III) and Rh(III), *J. Am. Chem. Soc.*, 1984, **106**, 6647-6653.
- 11 J. E. Collins, M. P. Rheingold, E. J. Miller, W. E. Geiger, A. L. Rieger and P. H. Rieger, Synthesis, Characterisation and Molecular Structure of Bis(tetraphenylcyclopentadienyl)rhodium(II), *Organomet.*, 1995, **14**, 1232-1238.
- 12 M. C. Colombo, T. C. Brunold, T. Riedener, H. U. Güdel, M. Förtsch and H. Bürgi, Facial Tris Cyclometalated Rh^{3+} and Ir^{3+} Complexes, Their Synthesis, Structure and Optical and Spectroscopic Properties, *Inorg. Chem.*, 1994, **33**, 545-550.
- 13 V. V. Grushin, N. Herron, D. D. LeCloux, W. J. Marshall, V. A. Petrov and Y. Wang, New Efficient Electroluminescent Materials based on Organometallic Complexes, *Chem. Commun.*, 2001, **16**, 1494-1495.
- 14 S. Lamansky, P. I. Djurovich, D. Murphy, F. Abdel-Razzaq, R. C. Kwong, I. Tsyba, M. Bortz, B. Mui, R. Bau and M. E. Thompson, Synthesis and Characterisation of Phosphorescent Cyclometalated Iridium Complexes, *Inorg. Chem.*, 2001, **40**, 1704-1711.
- 15 K. Dedeian, P. I. Djurovich, F. O. Garces, G. Carlson and R. J. Watts, A New Synthetic Route to the Preparation of a Series of Strong Photoreducing Agents: *fac*-Tris-*Ortho*-Metalated Complexes of Iridium(III) with Substituted 2-Phenylpyridines, *Inorg. Chem.*, 1991, **30**, 1685-1687.
- 16 K. A. King, M. F. Finlayson, P. J. Spellane and R. J. Watts, Luminescent Spectroscopy and Oxidative Quenching of Orthometalated Complexes of Iridium(III), *Sci. Papers I. P. C. R.*, 1984, **78**, 97-106.
- 17 C. C. H. Chin, J. S. L. Yeo, Z. H. Loh, J. J. Vittal, W. Henderson and T. S. A. Hor, Synthesis and Electrospray Mass Spectrometry of Palladium(II) Diphosphine Complexes from Oxidative Addition to 2-bromopyridine to Pd^0 , *J. Am. Chem. Soc., Dalton Trans.*, 1998, 3777-3784.

Chapter 4

Experimental Techniques

4.1 Introduction

This chapter describes in detail the experimental techniques and instrumentation used to carry out the photophysical measurements, which are described in chapters 5 and 6.

4.2 UV-Visible Absorption Spectroscopy

Background corrected UV-Visible absorption spectra were recorded using an ATI Unicam UV/Vis UV2 spectrometer. Spectra were recorded over an appropriate wavelength range using quartz cuvettes with a pathlength of 1 cm.

Assuming the Beer-Lambert law, the absorption of light can be related to the concentration of the absorbing species present in the solution as follows.

$$\text{Log}_{10}\left(\frac{I_0}{I_t}\right) = A_\lambda = \epsilon_\lambda c l \quad 4.1$$

where, A_λ is the absorbance at a particular wavelength, c is the concentration of the absorbing species in mol dm^{-3} and l is the pathlength of the cuvette in cm. Therefore the units of ϵ_λ , the molar extinction coefficient, are $\text{dm}^3 \text{mol}^{-1} \text{cm}^{-1}$.

4.3 Steady-State Luminescence Spectroscopy

4.3.1 Spectra

Emission and excitation spectra were recorded on a Perkin Elmer LS-50B luminescence spectrometer and a Jobin Horiba Spex Fluorolog 3 spectrofluorimeter using quartz cuvettes with a pathlength of 1 cm. A right angle illumination method was used and appropriate optical filters were selected to remove 2nd order peaks and Raman scatter.¹ Each spectrum obtained was corrected for the spectral response of the machine. A

schematic of the Jobin Horiba Spex Fluorolog 3 spectrofluorimeter is shown in figure 4.1.

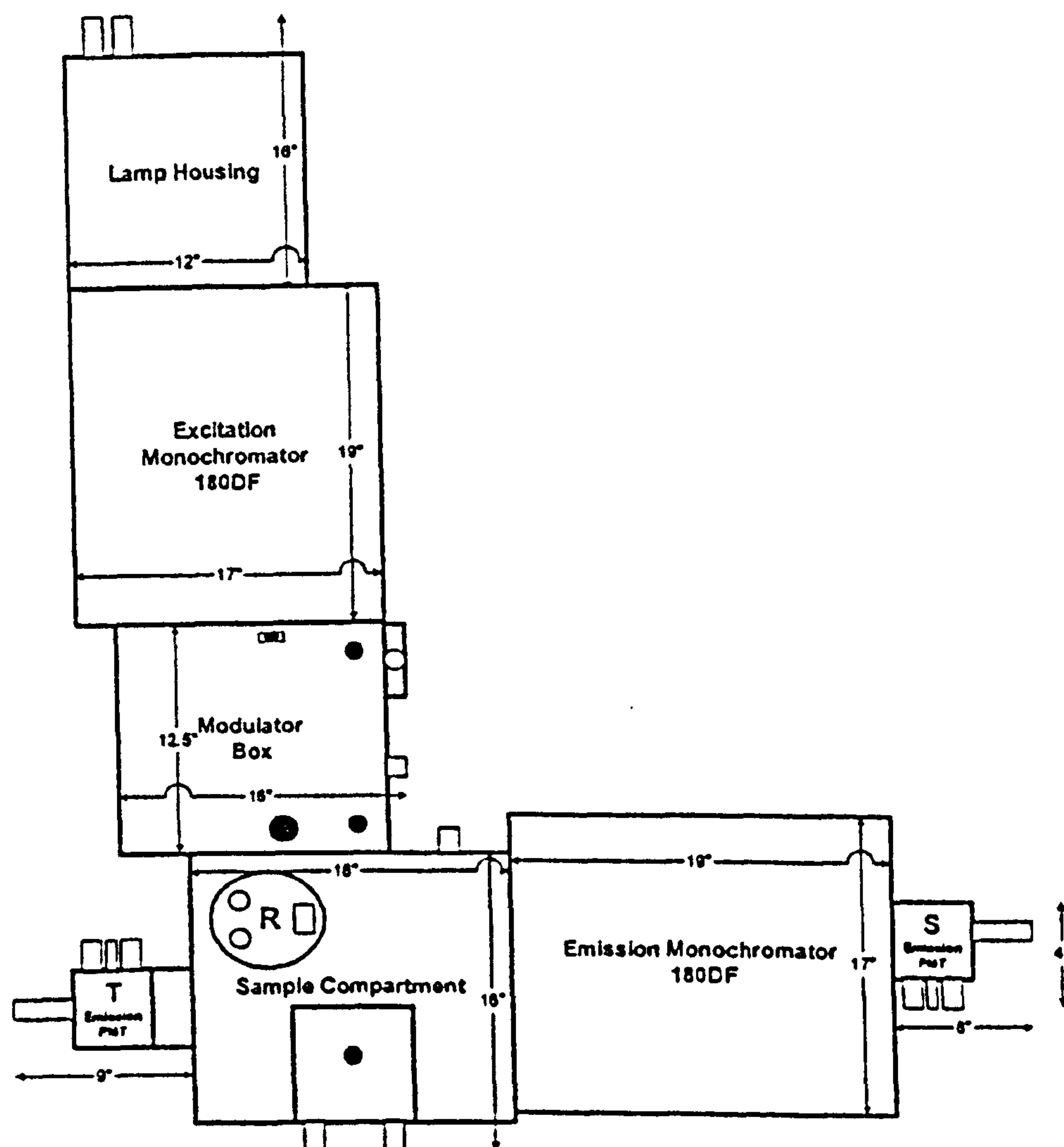


Figure 4.1 A schematic of the Jobin Horiba Spex Fluorolog 3 spectrofluorimeter.

4.3.2 Luminescence Quantum Yields

The luminescence quantum yield, Φ , is defined as the ratio of the number of photons emitted to the number of photons absorbed per unit time. In terms of competing decay processes, and assuming steady-state conditions (such that the rate of formation of

singlet state equals the rate of decay), the luminescence quantum yield, Φ , can be represented by equation 4.2.

$$\Phi = \frac{k_r}{k_r + k_{nr}} \quad 4.2$$

where, k_r and k_{nr} represent the rate constants for radiative and non-radiative processes, respectively.

Luminescence quantum yields in this work were recorded using the method of Demas *et al.*² and by means of the following pairs of standards, fluorescein ($\Phi = 0.95 \pm .03$)³ in 0.1 M aqueous sodium hydroxide and cresyl violet ($\Phi = 0.54$)⁴ in methanol and quinine bisulphate ($\Phi = 0.546$)⁵ and β -carboline ($\Phi = 0.60$)⁶ in 1N H₂SO₄. Relative to the standard compound, the quantum yield of the unknown sample is presented in equation 4.3.

$$\Phi_X = \Phi_{ST} \left(\frac{A_{ST}}{A_X} \right) \left(\frac{I_X}{I_{ST}} \right) \left(\frac{\eta_X^2}{\eta_{ST}^2} \right) \quad 4.3$$

The subscripts X and ST denote the unknown and standard solutions respectively, Φ is the quantum yield, A is the absorbance at the excitation wavelength, I is the integrated area of luminescence emission (all spectra were corrected for the spectral response of the machine before integration) and η is the refractive index of the solvent.

For aerated quantum yields, measurements were taken using 5 different concentrations of each lumophore to ensure the absence of concentration effects and all solutions were prepared with absorbances of less than 0.1, at the excitation wavelength, in a 10 mm pathlength cell to minimise inner-filter effects.¹ Degassed quantum yields were estimated by the comparison of the integrated emission intensity of a degassed and aerated solution of the sample. Rate constants of oxygen quenching, k_q , were then estimated using the aerated and degassed quantum yields with the Stern-Volmer equation, equation 4.4.¹ The associated error with both measured and calculated quantum yields is $\pm 10 \%$.

$$\frac{\Phi^0}{\Phi} = 1 + \tau^0 k_q [Q] \quad 4.4$$

where, Φ^0 and Φ represent the luminescence quantum yields in the absence and presence of quencher respectively, τ^0 = the lifetime in the absence of quencher (s), k_q = bimolecular quenching constant ($\text{dm}^3 \text{mol}^{-1} \text{s}^{-1}$), $[Q]$ = the concentration of quencher (mol dm^{-3}).

4.4 Time Resolved Emission Spectroscopy (TRES)

4.4.1 Luminescence Lifetime Measurements

Lifetimes were measured using a home-built ns-laser pumped fluorimeter. The samples were excited by a 10 Hz train of 3rd harmonic (355 nm) radiation from a Q-switched Nd:YAG laser (Spectra Physics GCR-150-10). The energy of the laser was typically 1-2 mJ per pulse with a FWHM of approximately 6 ns. Stray light at 1064 nm (fundamental) and 532 nm (2nd harmonic) was removed by the use of optical filters. Luminescence was collected at 90° to the excitation beam and focused onto the entrance slits of a monochromator (Jobin Yvon Horiba, Triax 320) using a bandpass in the range of 0.1-2.0 nm. The intensity of light at a given wavelength was monitored by a photomultiplier (PMT) tube (Hamamatsu R928). The transient decays were digitised and averaged by a digital storage oscilloscope (Tetronix TDS-340) over at least 64 laser pulses. The data was transferred to a PC for analysis by Microsoft Excel.

The emission lifetime of a single excited state species follows a single exponential decay curve. To obtain the lifetime from the data, the decay is fitted to a single exponential function, equation 4.5,

$$I(t) = A_1 \exp(-t/\tau_1) \quad 4.5$$

where, $I(t)$ is the intensity of light at time t , t is time and τ_1 is the luminescence lifetime of the species. For a process that contains two emitting species, a second term is added to the function, equation 4.6, and so on for an increasing number of emissive species.

$$I(t) = A_1 \exp(-t/\tau_1) + A_2 \exp(-t/\tau_2) \quad 4.6$$

The quality of the fit was judged by the randomness of the residuals and by the extent of minimisation of the sum of the squared residuals. The associated error with measured lifetimes is $\pm 10\%$. A typical pump profile, decay and fit are shown in figure 4.2.

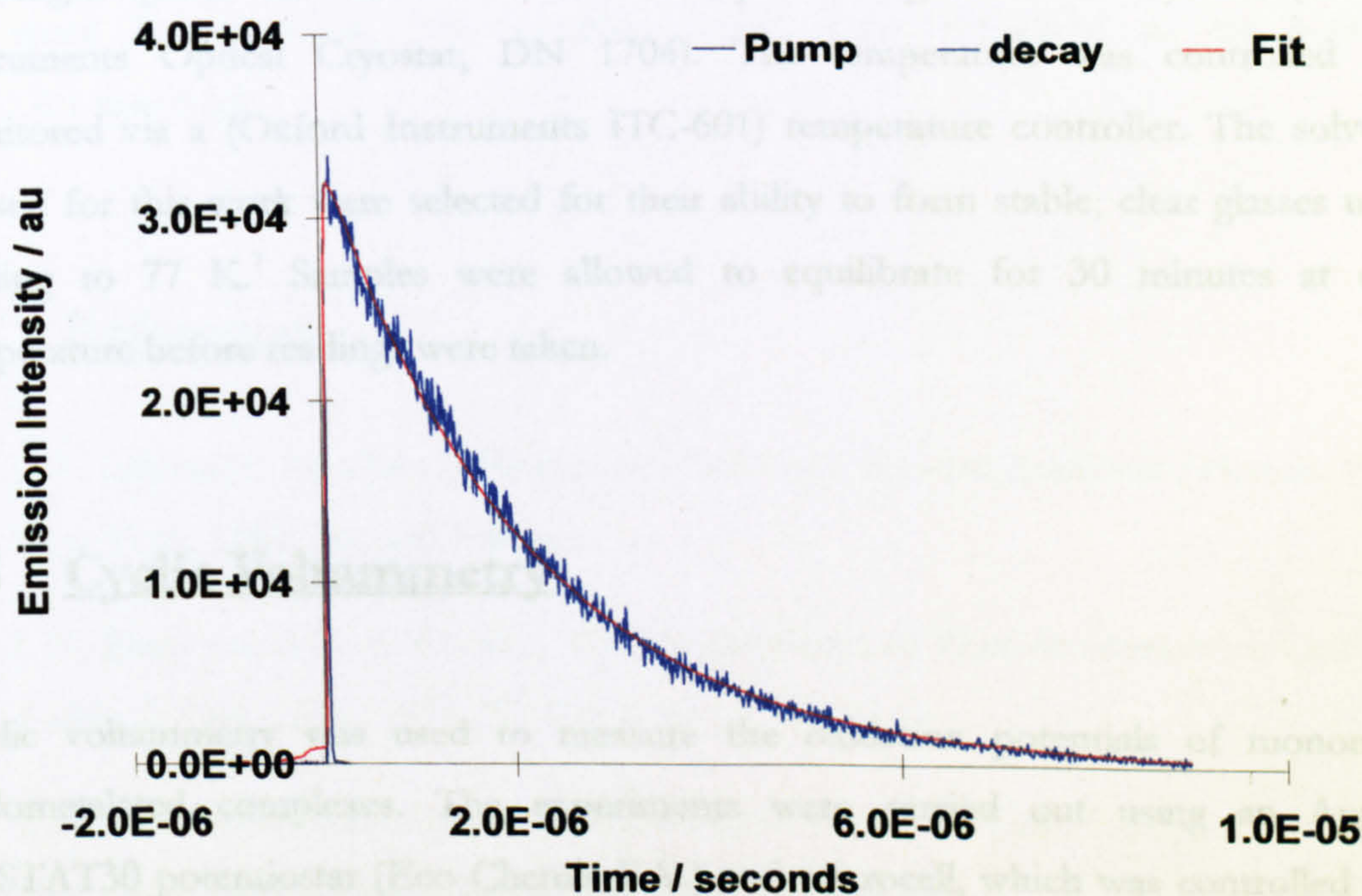


Figure 4.2 A typical single exponential fit obtained for a luminescence lifetime.

4.4.2 Time Resolved Emission Spectra

The instrumental set up for this experiment is the same as that used for the luminescence lifetime measurements in section 4.4.1 where a transient decay is averaged over a set number of laser shots. In this experiment a background is automatically subtracted from each decay. Sequences of decays are recorded at regular emission wavelengths so that a 3-dimensional data matrix can be generated. It is then possible to

obtain either kinetic behaviour at each wavelength or a time-resolved luminescence spectrum (TRES).

4.5 Low Temperature Measurements

4.5.1 Sample Preparation

All low temperature spectra and lifetimes were obtained from samples held in 10 mm pathlength quartz cuvettes and held in a liquid nitrogen cooled cryostat (Oxford Instruments Optical Cryostat, DN 1704). The temperature was controlled and monitored via a (Oxford Instruments ITC-601) temperature controller. The solvents chosen for this work were selected for their ability to form stable, clear glasses upon cooling to 77 K.⁷ Samples were allowed to equilibrate for 30 minutes at each temperature before readings were taken.

4.6 Cyclic Voltammetry

Cyclic voltammetry was used to measure the oxidation potentials of monomeric cyclometalated complexes. The experiments were carried out using an Autolab PGSTAT30 potentiostat (Eco Chemie B.V.) and microcell, which was controlled via a PC using the computer package GPES Manager. Solutions of the complex in dichloromethane containing 0.1 M NBu_4BF_4 as the electrolyte were purged with nitrogen and scanned at 100, 200, 400, 600 and 800 mV/s using platinum wires as the scanning, working and reference electrodes. Oxidation potentials were referenced using internal standards of either ferrocene or *bis*(pentamethylcyclopentadienyl)iron(II). The ferrocene-ferrocenium (FeCp_2) redox couple = 0.46 V versus the saturated calomel electrode (SCE) and the *bis*(pentamethylcyclopentadienyl)iron(II)/iron(III) (FeCp^*_2) redox couple is – 0.02 V versus SCE.⁸

4.7 Spin-coating of Thin Polymer Films

The preparation and spin coating of thin polymer thin films doped with cyclometalated complexes was carried out in the following manner. The polymer (host) and the complex (guest) were both dissolved in known volumes of dichloromethane. Relevant aliquots of each solution were then combined to give the doping concentrations of 0.5, 1.0, 2.5 and 5 % weight/weight (wt/wt) of complex/host. The resulting solutions were then shaken vigorously to ensure homogeneity. Following this, an aliquot of the solution was dropped onto a spinning glass slide, where the solvent evaporated over a period of seconds, leaving a thin film on the substrate. Various spin speeds were used to obtain the most homogeneous film possible. Films were estimated to be between 0.01 - 0.1 mm thick.

4.8 References

- 1 J. R. Lakowicz, *Principles of Fluorescence Spectroscopy*, Kluwer Academic/Plenum Press, New York, 1999, Second Edition.
- 2 J. N. Demas and G. A. Crosby, The Measurement of Photoluminescence Quantum Yields, *J. Phys. Chem.*, 1971, **75**, 991-1024.
- 3 J. H. Brannon and D. Magde, Absolute Quantum Yield Determination by Thermal Blooming. Fluorescein, *J. Phys Chem.*, 1978, **82**, 705-709.
- 4 D. Madge, J. H. Brannon, T. L. Cremers and J. Olmsted, Absolute Luminescence Yield of Cresyl Violet. A Standard for the Red, *J. Phys Chem.*, 1979, **83**, 696-699.
- 5 W. H. Melhuish, Absolute Spectrofluorometry, *J. Research*, NBS-A: Physics and Chemistry, 1972, **76A**, 547-560.
- 6 K. P. Ghiggino, P. F. Skilton and P.J. Thistlethwaite, β -Carboline as a Fluorescence Standard, *J. Photochem.*, 1985, **31**, 113-121.

- 7 J. C. Scaiano, *Handbook of Organic Photochemistry*, CRC Press, Volume 2, Chapter 16, 355-258.
- 8 N. G. Connelly and W. E. Geiger, Chemical Redox Agents for Organometallic Chemistry. *Chem. Rev.*, 1996, **96**, 877-910.

Chapter 5

The Synthesis and Photophysical Studies of Cyclometalated Ir(L)₃ and Ir(L)₂acac Complexes

5.1 Introduction

In 1985 King *et al.*¹ characterised the first triply *ortho*-metalated iridium(III) species, *fac*-Ir(ppy)₃, a bright yellow solid with green phosphorescent emission. Since then, numerous related iridium(III) and rhodium(III) complexes of the formula Ir(L)₃ and Ir(L)₂acac have been synthesised utilising ligands such as 2-phenylpyridine (ppy),² 4-(2-pyridyl)benzaldehyde (fppy),³ benzo[h]-quinoline (bzq)⁴ and 2-(2-thienyl)pyridine (thpy),² to name but a few.

UV excitation of these species causes them to undergo metal to ligand charge transfer (MLCT), thus forming a MLCT excited state, which possesses mostly triplet character. Phosphorescent emission from the lowest energy triplet excited state, ³MLCT, gives rise to emission that is characteristic of the lowest energy ligand. Hence these complexes give rise to emission wavelengths tuneable *via* ligand modification.

The luminescence spectra of these complexes increase in intensity upon degassing but the spectral profile remains unchanged. This is indicative of oxygen quenching of the long-lived excited triplet species. Radiative lifetimes of these complexes range between 1-2 μs in degassed solvents to 20-200 ns in aerated solutions.

In addition to this, cyclometalated iridium(III) complexes are also known to be electroluminescent. The use of these species as electrophosphorescent dopants in OLEDs,⁵ allows the utilisation of both singlet and triplet excitons within these devices, thus increasing their efficiency compared to that of purely fluorescent systems. These small molecules have therefore been widely studied for their use in OLEDs, the next generation of flat panel displays. Numerous companies worldwide are currently seeking phosphorescent dopants of this kind, which provide pure red, green and blue light to enable a full colour display.

This chapter presents the synthesis and subsequent photophysical studies of a selection of both previously reported and new iridium(III) and rhodium(III) complexes. The synthesis of new complexes, which contain a variety of substituted ligands, provides the opportunity for further study of their luminescence properties with respect to ligand modification. In particular, the tuneability of emission wavelength and the ability to reduce self-quenching with respect to ligand substituents will be studied.

5.2 Synthesis

The monomeric complexes of the formula $\text{Ir}(\text{L})_3$ and $\text{Ir}(\text{L})_2\text{acac}$ shown in table 5.1, were synthesised by a variety of synthetic pathways. These are described fully in chapter 3. In general, the $\text{Ir}(\text{L})_3$ complexes were either synthesised from $\text{Ir}(\text{acac})_3$ or their dichloro-bridged precursor, $[\text{Ir}(\text{L})_2\text{Cl}]_2$, whereas the $\text{Ir}(\text{L})_2\text{acac}$ complexes were synthesised solely from their dichloro-bridged precursors. A summary of the monomeric complexes synthesised is listed in table 5.1. Complexes marked with an asterisk (*) are new compounds.

Table 5.1 Summary of synthetic data for complexes 30-49.

Complex	Synthesis Number (Chapter 3)	% Yield
<i>fac</i> - $\text{Ir}(\text{ppy})_3$	30	67
$\text{Ir}(\text{ppy})_2\text{acac}$	32	52
<i>fac</i> - $\text{Ir}(\text{ppy})_2\text{fppy}$	34*	27
<i>fac</i> - $\text{Ir}(\text{fppy})_3$	35*	22
$\text{Ir}(\text{fppy})_2\text{acac}$	36*	7
$\text{Ir}(\text{F}_2\text{ppy})_3$	37 ^a	25
$\text{Ir}(\text{F}_2\text{ppy})_2\text{acac}$	38	30
<i>fac</i> - $\text{Ir}(\text{ppm})_3$	39*	30
$\text{Ir}(4\text{-Meppy})_3$	40*	10
$\text{Ir}(4\text{-Meppy})_2\text{acac}$	41*	49
<i>fac</i> - $\text{Ir}(5\text{-Meppy})_3$	42*	15
$\text{Ir}(5\text{-Meppy})_2\text{acac}$	43*	38
<i>fac</i> - $\text{Ir}(\text{Cyclohex})_3$	44*	10
<i>fac</i> - $\text{Ir}(\text{Myrt})_3$	45	30
<i>fac</i> - $\text{Ir}(\text{dppy})_3$	46*	58
$\text{Ir}(\text{dppy})_2\text{acac}$	47*	20
<i>fac</i> - $\text{Ir}(\text{bippy})_3$	48*	18
$\text{Ir}(\text{bippy})_2\text{acac}$	49*	40

(a) Complexes $\text{Ir}(\text{F}_2\text{ppy})_3$ 37 and $\text{Ir}(4\text{-Meppy})_3$ 40, were isolated as mixtures of the facial and meridonal isomers.

The percentage yields of the complexes listed in table 5.1 vary a great deal. This is generally because a variety of synthetic pathways have been used and so a direct comparison of their ease of synthesis cannot be made. Low percentage yields may have also arisen due to the use of reaction temperatures below 200 °C, which have only recently been shown to favour the formation of the meridional isomer over that of the facial.⁶

5.3 Structure

The monomeric Ir(L)_3 species contain a metal(III) centre in an octahedral environment with a facial geometry, figure 5.1 illustrates this with *fac*- Ir(ppy)_3 .

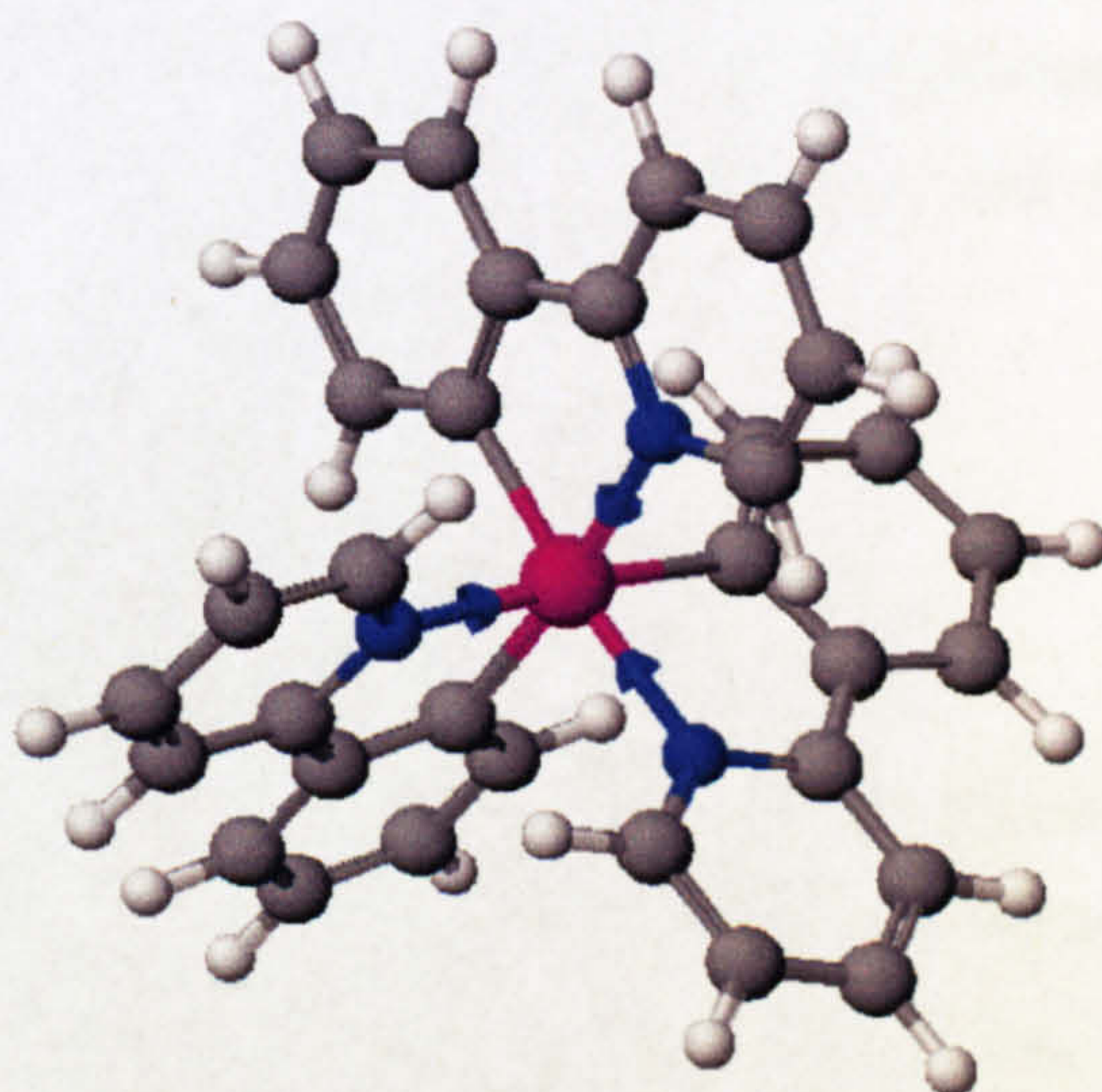


Figure 5.1 A structural illustration of *fac*-tris(2-phenylpyridine- C^2, N')iridium(III), *fac*- Ir(ppy)_3 **30**, atom key: pink = iridium, blue = nitrogen, grey = carbon and white = hydrogen.

However, for $\text{Ir(L)}_2\text{acac}$ complexes, though the metal centre remains in an octahedral geometry the two cyclometalated ligands are positioned such that the *cis*-C,C and *trans*-N,N disposition of the dichloro-bridged precursor is retained. This is illustrated by the X-ray crystal structure obtained from crystals of $\text{Ir(F}_2\text{ppy)}_2\text{acac}$ **38** (bis-2-(2,4-difluoro-phenylpyridine- C^2, N')acetylacetonate iridium), figure 5.2. Crystal

structures of $\text{Ir}(\text{L})_2\text{acac}$ complexes possessing this type of geometry have been widely reported in the literature, for example $\text{Ir}(\text{tpy})_2\text{acac}$, where $\text{tpy} = 2\text{-(}p\text{-tolyl)pyridine}$.⁴

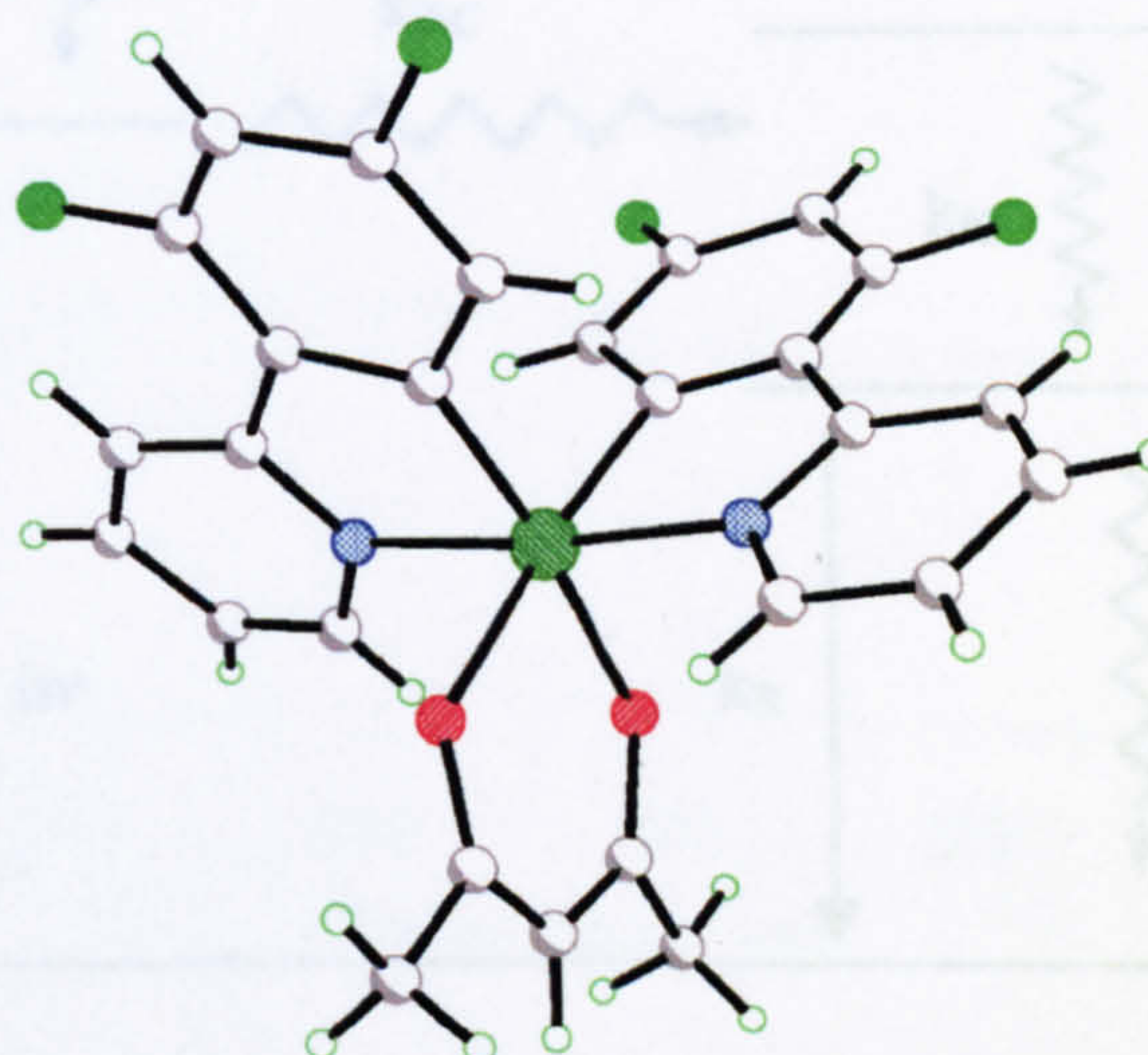


Figure 5.2 X-ray crystal structure of Bis-2-(2,4-difluoro-phenylpyridine- C^2, N')acetylacetonate iridium, $\text{Ir}(\text{F}_2\text{ppy})_2\text{acac}$ **38** at 120 K, all atoms refined as isotropic with 50 % occupancy.

5.4 Electronic Structure

For these low-spin d^6 transition-metal complexes, described in sections 1.4 and 1.5, the lowest lying excited state is MLCT-based, $d\pi^6\pi^{*0} \rightarrow d\pi^5\pi^{*1}$, see figure 5.3 below, where LC = ligand centred state. The promotion of an electron from a metal $d\pi$ orbital to a ligand π^* orbital by the absorption of a photon, with energy = $h\nu$, results in the formation of a singlet excited state, $^1\text{MLCT}^*$. The singlet excited state may then undergo intersystem crossing (ISC), a non-radiative process, to form a triplet excited state, $^3\text{MLCT}^*$. The excited triplet state can subsequently experience either non-radiative decay (NR) or radiative decay (R) (phosphorescence) and relax back to its ground electronic state, $\text{M}(d\pi^6\pi^{*0})$.

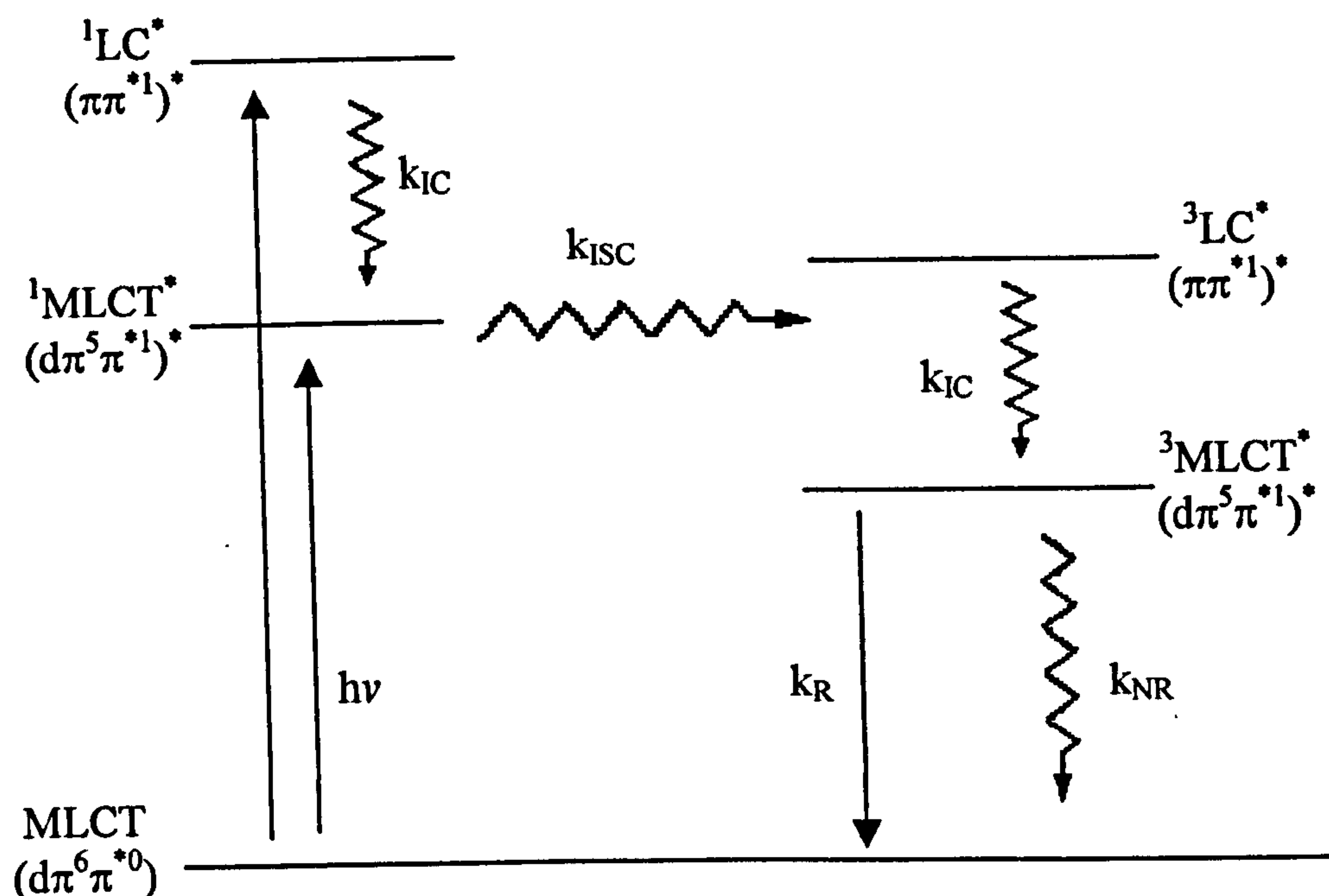


Figure 5.3 A schematic of the electronic energy levels in an Ir(III)/Rh(III) complex, where * indicates an excited state and k_x = rate of process x.

5.5 UV-Visible Absorption Spectra

The absorption spectra of complexes 30-49 were found to exhibit the features associated with cyclometalated iridium(III) and rhodium(III) complexes.² This is illustrated by Ir(F₂ppy)₂acac 38, *fac*-Ir(ppy)₃ 30 and *fac*-Ir(fppy)₃ 35 in aerated dichloromethane, figure 5.4. Intense absorption bands at 240-350 nm can be assigned as a ligand centred (LC) spin-allowed $^1\pi-\pi^*$ transition. The broad absorption bands at lower energies 360-480 nm are typical of spin-allowed $^1\text{MLCT}$ transitions and at even lower energies, the weaker bands which reach into the visible region are assigned as formally forbidden $^3\text{MLCT}$ transitions. These features acquire their intensity by mixing with higher energy $^1\text{MLCT}$ spin-allowed transitions on the cyclometalating ligands. This mixing is facilitated by the strong spin-orbit coupling of the iridium(III) center.

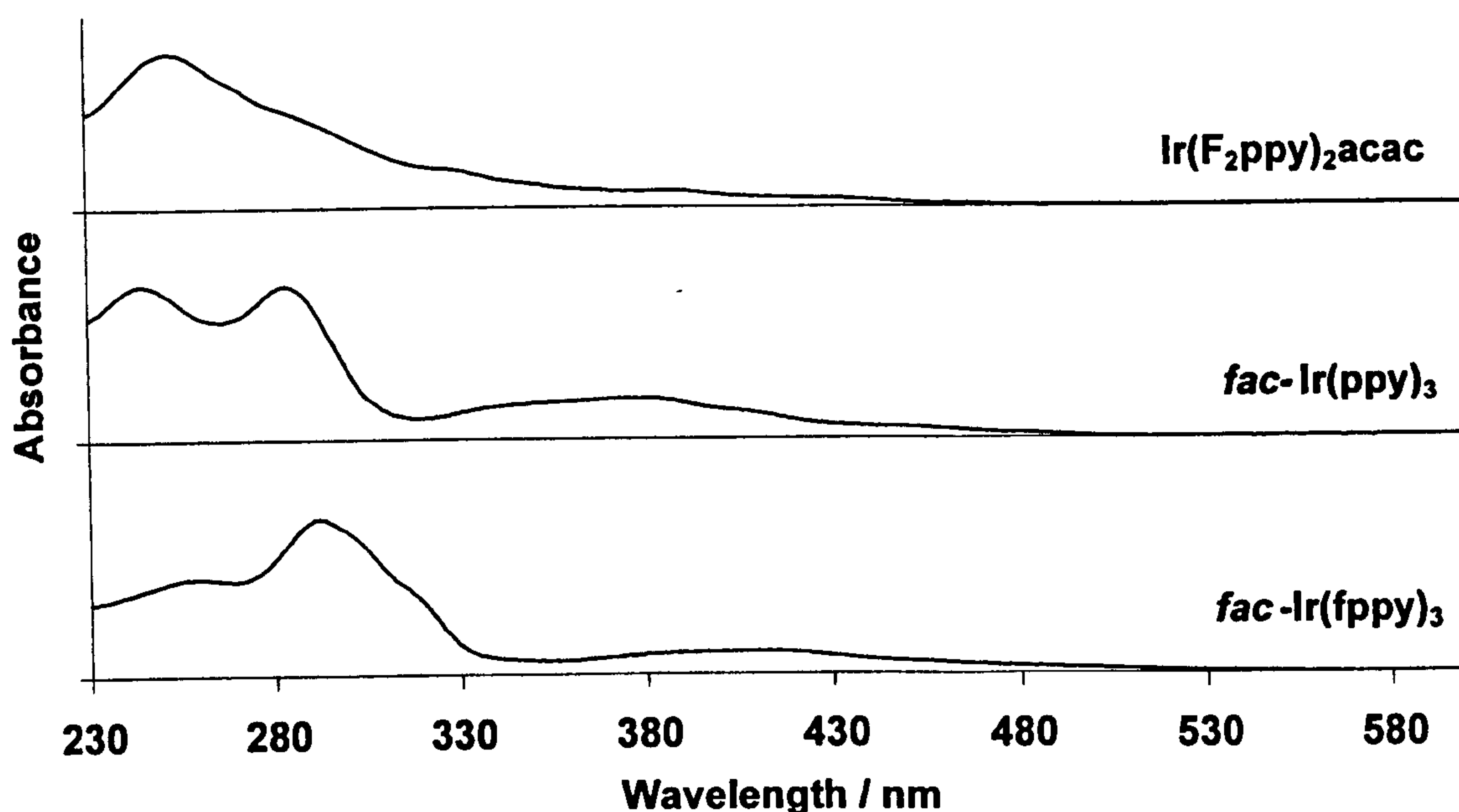


Figure 5.4 Normalised UV-Visible absorption spectra of $\text{Ir}(\text{F}_2\text{ppy})_2\text{acac}$ **38**, $\text{fac-Ir}(\text{ppy})_3$ **30** and $\text{fac-Ir}(\text{fppy})_3$ **35** in aerated dichloromethane at 298 K, spectra **30** and **38** are offset for clarity.

Although each of these spectra possess the absorption bands expected for a cyclometalated iridium(III) complex, what is particularly important is the shifting position of the $^3\text{MLCT}$ band which reaches into the visible region of the spectrum. In $\text{Ir}(\text{F}_2\text{ppy})_2\text{acac}$ **38** we observe a hypsochromic shift (blue shift) of the $^3\text{MLCT}$ band compared to that of $\text{fac-Ir}(\text{ppy})_3$ **30**. The reverse of this is true for the $^3\text{MLCT}$ band of $\text{fac-Ir}(\text{fppy})_3$ **35**, which undergoes a bathochromic shift (red shift) compared to that of the parent compound.

If we consider each of these complexes as an Ir(III) centre surrounded by three monoanionic ligands then the effect of different substituents upon the $^3\text{MLCT}$ state can be described in terms of their ability to stabilise the negative charge which is considered to reside upon the ligands. Both the fluorine atoms and the formyl group are electron-withdrawing substituents, but actually produce different effects upon the $^3\text{MLCT}$ absorption bands. The fluorine atoms are inductively withdrawing whereas the formyl groups cause a mesomeric effect.

The energy gap (ΔE) between the HOMO and LUMO of these complexes, and hence the energy of the excited state, depends upon the energies of the cyclometalating ligands within each molecule. To model how the substituents upon a 2-phenylpyridine

ligand affect the HOMO and LUMO energy levels within cyclometalated iridium(III) complexes, several density functional theory (DFT)⁷ calculations were carried out in CAChe 5.0. The HOMO and LUMO were generated by a MOPAC/PM3 wavefunction for the chemical sample at a geometry determined by MOPAC using PM3 parameters. Due to the limitations of the calculation the iridium-ligand interaction was modelled using a sodium cation attached to a monoanionic ligand moiety (Na-ppy) as depicted in figure 5.5.

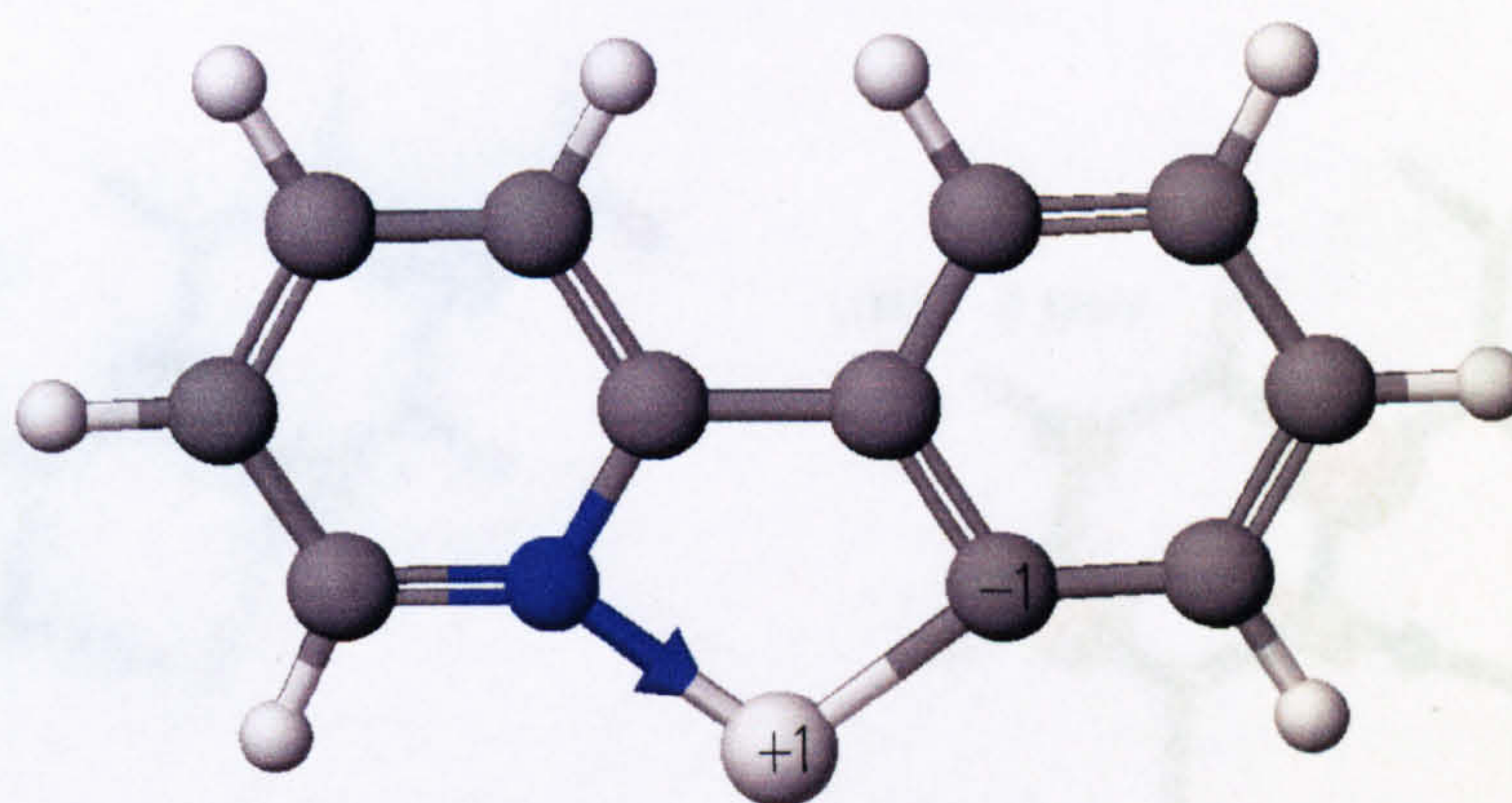


Figure 5.5 A molecular representation of the sodium-2-phenylpyridine (Na-ppy) moiety used for CAChe energy level calculations.

The energy of the HOMO and LUMO for 2-phenylpyridine (ppy), 4-(2-pyridyl)benzaldehyde (fppy) and 2-(2,4-difluoro-phenyl)-pyridine (F₂ppy) ligands were calculated by this method, the molecular orbital diagrams for each of the HOMO and LUMOs are shown in figure 5.6.

It must be noted that the calculated values of the HOMO energy levels relate only to the ligand and do not consider the metal orbitals in these approximations. This is in contrast to cyclometalated iridium(III) complexes with MLCT states, where the HOMO resides upon the metal centre. However, the MLCT excited state of these kinds of complexes also involves the LUMO of the ligand. Hence, the distribution of electron density within the LUMOs of these structures is important in determining the energy of the excited state.

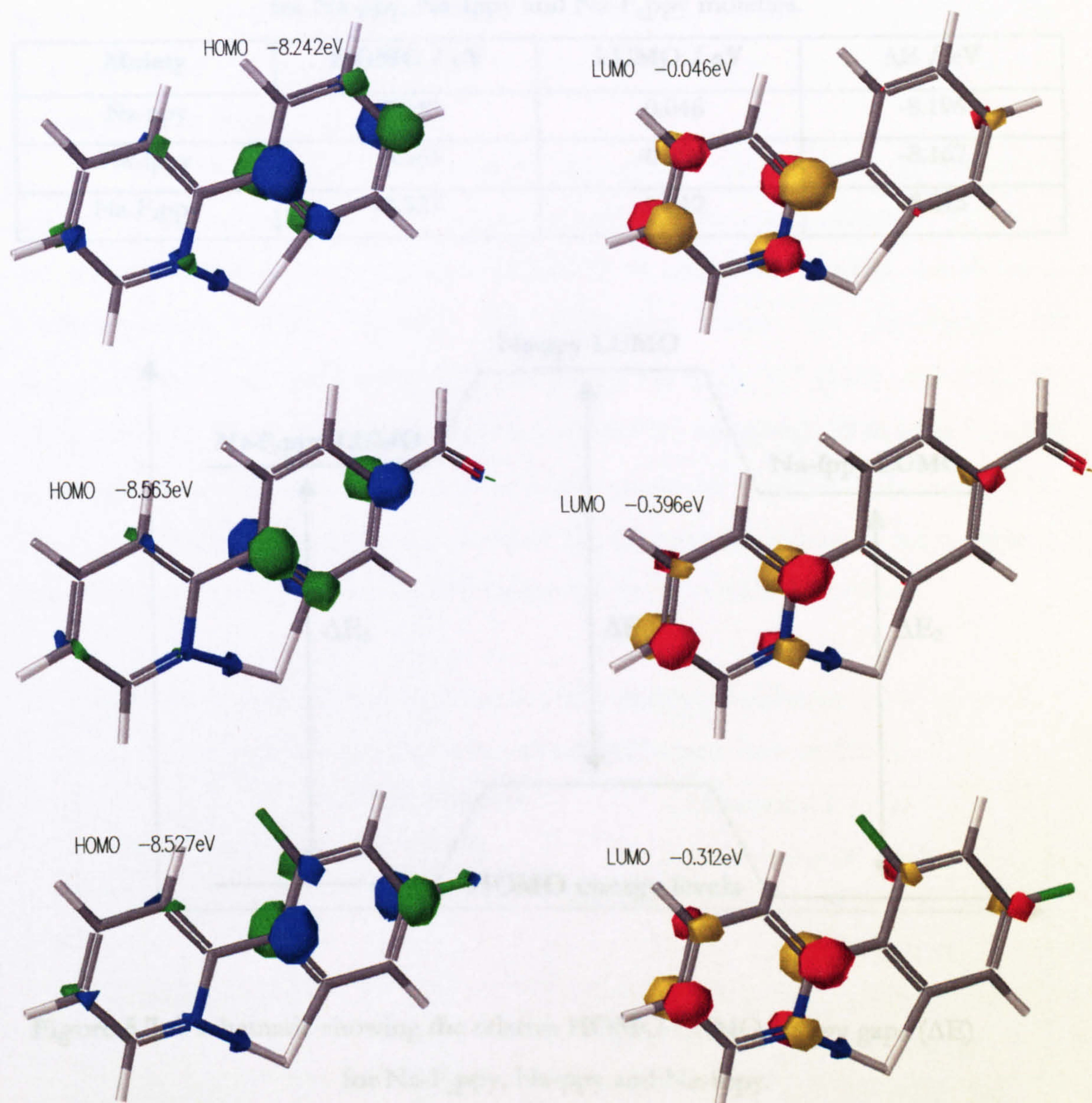


Figure 5.6 The molecular orbital diagrams of the HOMO and LUMO for Na-ppy, Na-fppy and Na-F₂ppy, as calculated by CAChe.

The energies for each of the HOMO and LUMOs are reported in table 5.2 and a schematic energy level diagram comparing the relative energy gaps between these states is shown in figure 5.7.

Table 5.2 HOMO and LUMO energies (eV) calculated by CAChe
for Na-ppy, Na-fppy and Na-F₂ppy moieties.

Moiety	HOMO / eV	LUMO / eV	ΔE / eV
Na-ppy	-8.242	-0.046	-8.196
Na-fppy	-8.563	-0.396	-8.167
Na-F ₂ ppy	-8.527	-0.312	-8.215

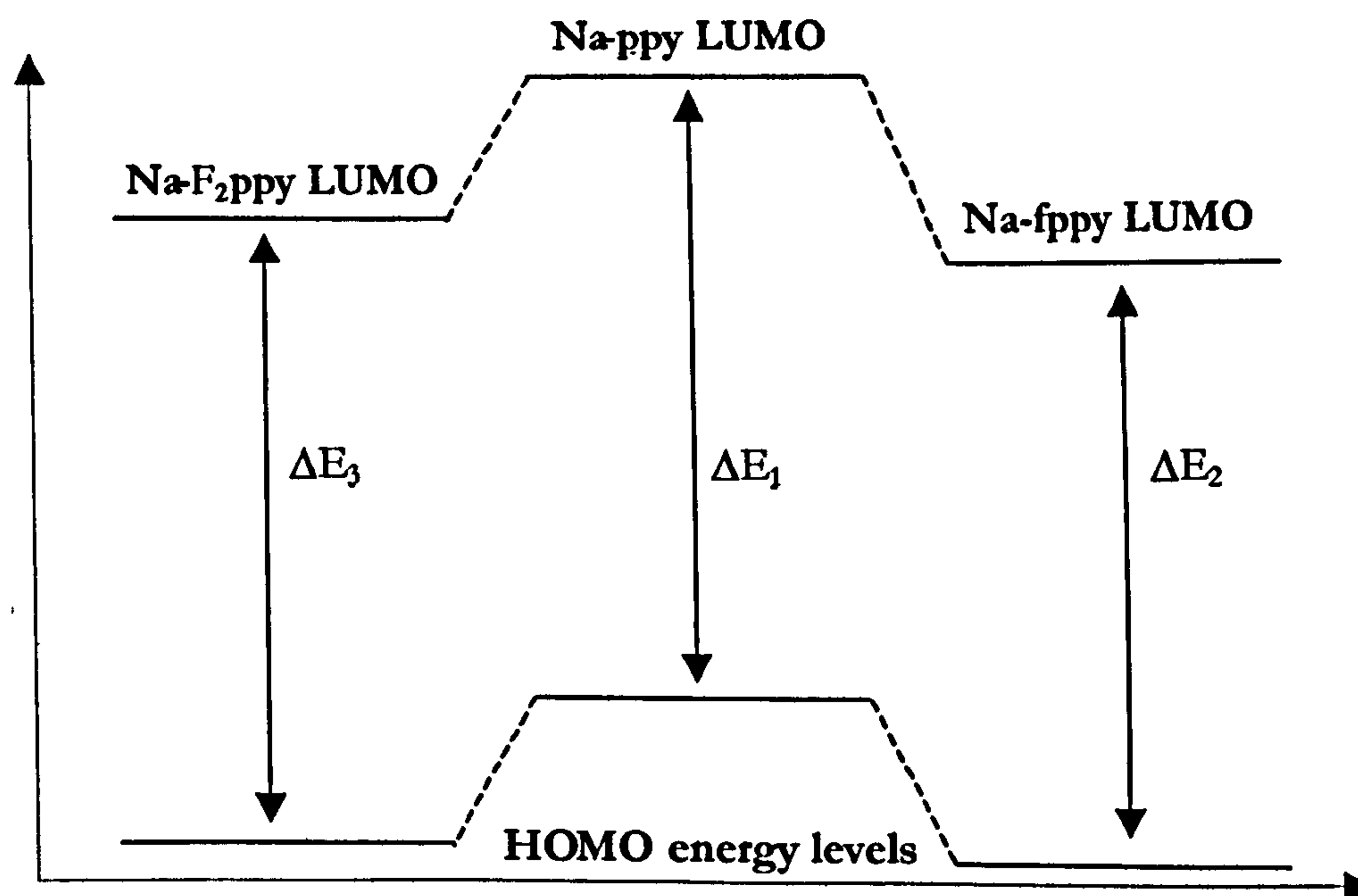


Figure 5.7 A schematic showing the relative HOMO-LUMO energy gaps (ΔE)
for Na-F₂ppy, Na-ppy and Na-fppy.

Applying these results to the cyclometalated species 30–49, indicates that the addition of either a formyl group or fluorine atoms to the parent complex *fac*-Ir(ppy)₃, 30 giving *fac*-Ir(fppy)₃, 35 or Ir(F₂ppy)₃, 37 respectively, causes the energy of the LUMO to be lowered. In addition to this, there must also be a decrease in energy of the HOMO for both of the substituted complexes. For the fluorine substituted complex, this produces an energy gap (ΔE) greater than that of the parent complex *fac*-Ir(ppy)₃, 30, which causes a hypsochromic shift in the energy of the ³MLCT band. However, the addition of the formyl group to give *fac*-Ir(fppy)₃, 35 serves to produce an HOMO-LUMO energy gap which is smaller than that of the parent complex and leads to a bathochromic shift in

the energy of the $^3\text{MLCT}$ band. In summary, $\Delta E_3 > \Delta E_1 > \Delta E_2$, i.e. in qualitative agreement with that of the iridium(III) complexes, 38, 39 and 35 respectively. The position of $^3\text{MLCT}$ absorption bands in other complexes in this series can also be rationalised in a similar way.

Table 5.3 comprises a summary of the spectral features from the absorption spectra of selected iridium(III) complexes, including extinction coefficients. Tamayo *et al.*⁶ recently reported the extinction coefficients of several iridium(III) complexes in dichloromethane. They reported the following values for *fac*-Ir(ppy)₃, 30; λ_{max} (ϵ , $10^3 \text{ dm}^3 \text{ mol}^{-1} \text{ cm}^{-1}$) 244 (45.5), 283 (44.8), 341 (9.2), 377 (12.0), 405 (8.1), 455 (2.8), 488 (1.6). The extinction coefficients obtained for *fac*-Ir(ppy)₃, 30 in table 5.3 are in good agreement with these values and are within reasonable experimental error ($\pm 5\%$).

The extinction coefficients obtained for the other complexes listed in table 5.3 are of the same order of magnitude as those reported for similar complexes.²

Table 5.3 Absorption spectra features and extinction coefficients (ϵ) of selected iridium(III) complexes in aerated dichloromethane at 298 K.

Complex	Synthesis Number (Chapter 3)	Absorption λ / nm (ϵ / $10^3 \text{ dm}^3 \text{ mol}^{-1} \text{ cm}^{-1}$)
<i>fac</i> -Ir(ppy) ₃	30	244 (44.0), 283 (42.9), 341 (9.3), 377 (11.4), 405(7.8), 455 (2.8), 488 (1.1)
<i>fac</i> -Ir(ppy) ₂ fppy	34	246 (51.8), 286 (57.7), 318 (22.3), 360 (11.9), 410 (9.9), 454 (4.1), 490 (1.8)
<i>fac</i> -Ir(fppy) ₃	35	258 (49.3), 293 (75.7), 318 (41.0), 390 (10.7), 415 (11.3), 457 (5.3), 490 (3.1)
Ir(F ₂ ppy) ₂ acac	38	254 (43.4), 287 (26.3), 330 (10.9), 374 (4.5), 390 (4.6), 440 (1.9)
<i>fac</i> -Ir(Cyclohex) ₃	44	247 (40.8), 288 (36.0), 340 (10.0), 370 (10.1), 404 (6.0), 440 (2.3)
<i>fac</i> -Ir(dppy) ₃	46	261 (83.8), 288 (60.0), 372 (19.6), 390 (19.6), 420 (13.8), 465 (5.5), 500 (3.0)
<i>fac</i> -Ir(bippy) ₃	48	273 (60.8), 296 (59.0), 325 (24.7), 373 (11.5), 395 (12.1), 425 (9.5), 473 (3.2)

5.6 Luminescence Properties

5.6.1 Steady-State Spectra

The steady-state emission spectra of dilute solutions of complexes 30-49 in aerated dichloromethane and toluene were recorded using an excitation wavelength of 355 nm. The maximum emission wavelengths (λ_{max}) for these complexes in both solvents are summarised in table 5.4.

Table 5.4 Maximum emission wavelengths (λ_{max}) for iridium(III) complexes 30-49 in aerated dichloromethane and toluene at 298 K, $\lambda_{\text{ex}} = 355$ nm.

Complex	Synthesis Number (Chapter 3)	Dichloromethane $\lambda_{\text{max}} / \text{nm}$	Toluene $\lambda_{\text{max}} / \text{nm}$
<i>fac</i> -Ir(ppy) ₃	30	510	510
Ir(ppy) ₂ acac	32	520	520
<i>fac</i> -Ir(ppy) ₂ fppy	34	615	580
<i>fac</i> -Ir(fppy) ₃	35	580	560
Ir(fppy) ₂ acac	36	600	585
Ir(F ₂ ppy) ₃	37	495*	475*
Ir(F ₂ ppy) ₂ acac	38	485	480
<i>fac</i> -Ir(ppm) ₃	39	530	525
Ir(4-Meppy) ₃	40	510	510
Ir(4-Meppy) ₂ acac	41	515	515
<i>fac</i> -Ir(5-Meppy) ₃	42	510	510
Ir(5-Meppy) ₂ acac	43	515	515
<i>fac</i> -Ir(Cyclohex) ₃	44	495	495
<i>fac</i> -Ir(Myrt) ₃	45	505	505
<i>fac</i> -Ir(dppy) ₃	46	575	560
Ir(dppy) ₂ acac	47	560	550
<i>fac</i> -Ir(bippy) ₃	48	575	560
Ir(bippy) ₂ acac	49	565	555

* Ir(F₂ppy)₃ is a mixture of the facial and meridonal isomers.

Degassed solutions of the complexes in dichloromethane and toluene were also studied. The emission intensities were found to increase dramatically, upon degassing, however the spectral profiles remained unchanged. This is indicative of oxygen quenching of the relatively long-lived triplet MLCT state and is illustrated, in figure 5.8, by the degassed and aerated emission spectra of *fac*-Ir(Cyclohex)₃, 44 in dichloromethane. In this case the maximum emission intensity, $\lambda_{\text{max}} = 495$ nm, increased by a factor of 33.5 upon degassing.

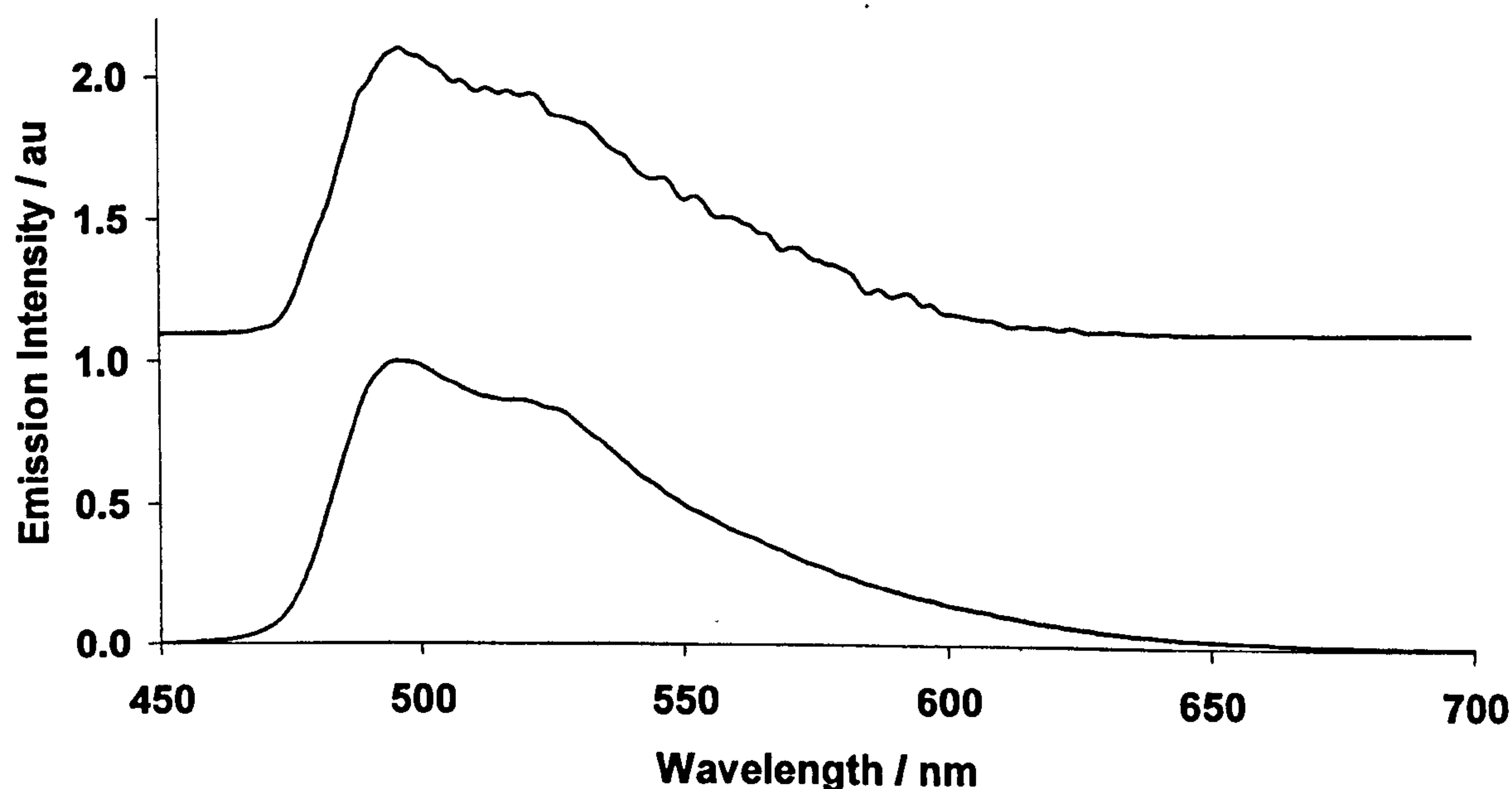


Figure 5.8 The normalised degassed and aerated (offset spectrum) emission spectrum of *fac*-Ir(Cyclohex)₃, 44 in dichloromethane at 298 K, $\lambda_{\text{ex}} = 355$ nm.

In general, emission maxima were found to differ at most by up to 5 nm between solvents. However, for complexes containing the formyl-substituted ligands (fppy), this was not the case. This will be discussed in more detail in the following section 5.6.2.

The photoluminescence (PL) spectra of the phenyl and pyridine ring substituted complexes in aerated toluene are shown in figures 5.9 and 5.10 below respectively, these plots illustrate that the emission wavelength/colour of these complexes can be tuned by utilising different substituents upon the cyclometalating ligands.

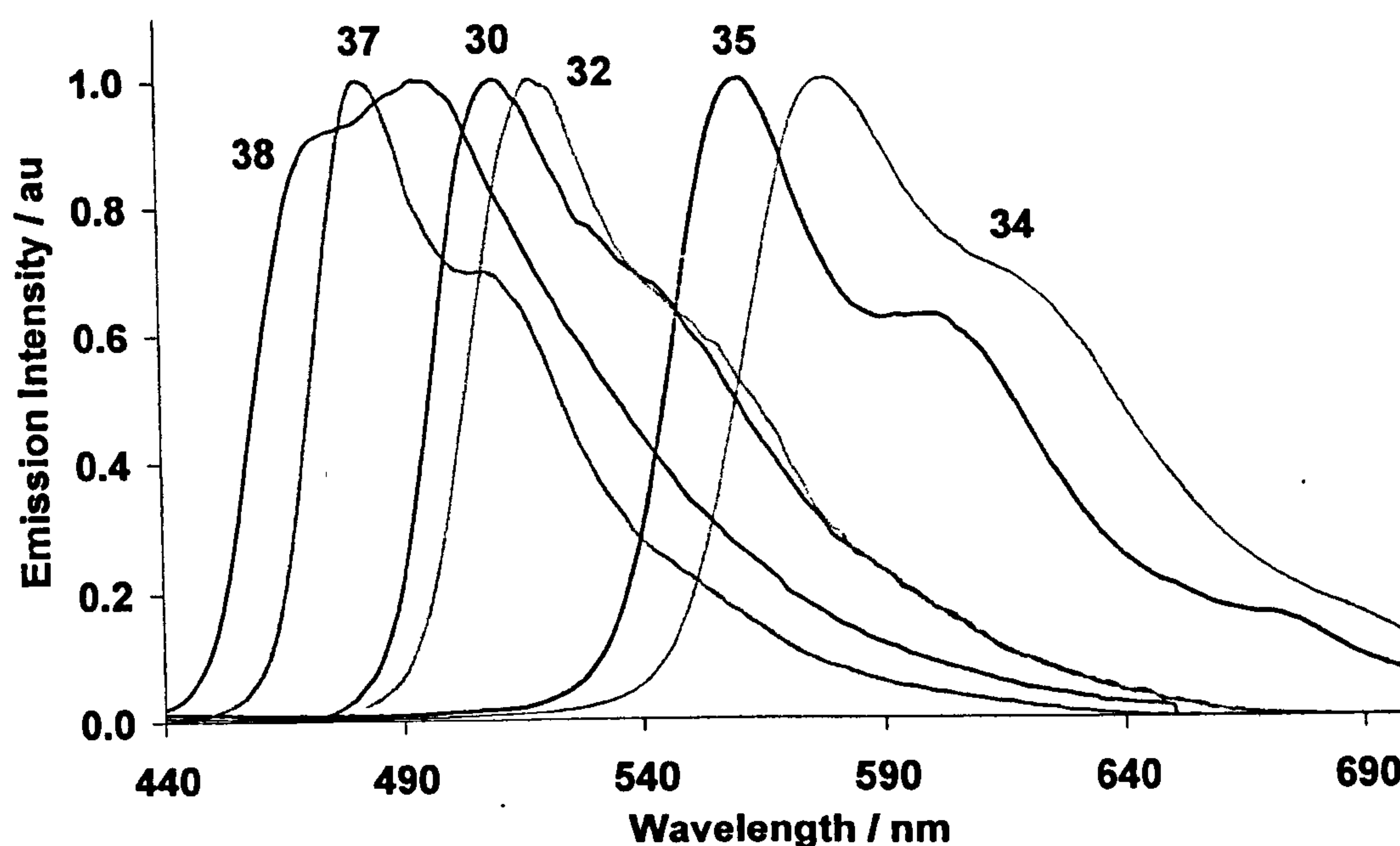


Figure 5.9 Normalised PL spectra of the phenyl ring substituted complexes *fac*-Ir(ppy)₃ 30, Ir(ppy)₂acac 32, *fac*-Ir(ppy)₂fppy 34, *fac*-Ir(fppy)₃ 35, Ir(F₂ppy)₃ 37 and Ir(F₂ppy)₂acac 38 in aerated toluene at 298 K, $\lambda_{\text{ex}} = 355$ nm.

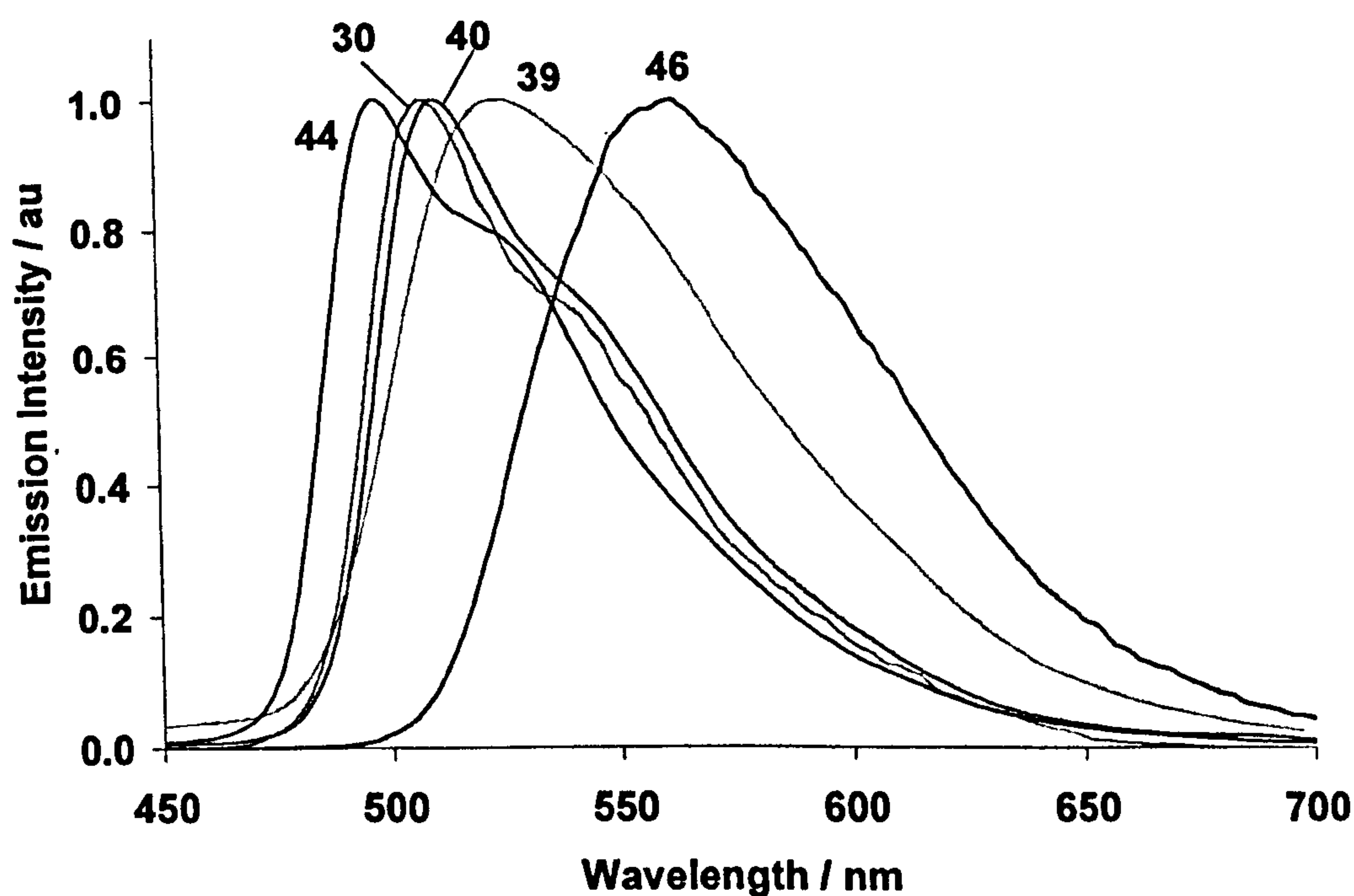


Figure 5.10 Normalised PL spectra of the pyridine ring substituted complexes *fac*-Ir(ppy)₃ 30, *fac*-Ir(ppm)₃ 39, Ir(4-Meppy)₃ 40, *fac*-Ir(Cyclohex)₃ 44 and *fac*-Ir(dppy)₃ 46 in aerated toluene at 298 K, $\lambda_{\text{ex}} = 355$ nm.

The change in emission maxima of these complexes with respect to their ligand substituents can be rationalised in terms of the relative stabilisation of the HOMO and LUMO energy levels, as described in detail in section 5.5. The presence of vibrational structure in some of these emission spectra indicates that the excited state may also possess some $^3\pi-\pi^*$ character.

5.6.2 Solvatochromatic Emission of 4-(2-pyridyl)benzaldehyde (fppy) containing Complexes

Iridium(III) complexes containing formyl-substituted (complexes 34-36) ligands were found to exhibit solvatochromatic emission. An example of this is illustrated by the formyl substituted complex, *fac*-Ir(ppy)₂fppy 34 as shown in figure 5.11 below and summarised in table 5.5. Solvatochromatic emission is also observed for other formyl substituted complexes such as *fac*-Ir(fppy)₃ 35, see table 5.5.

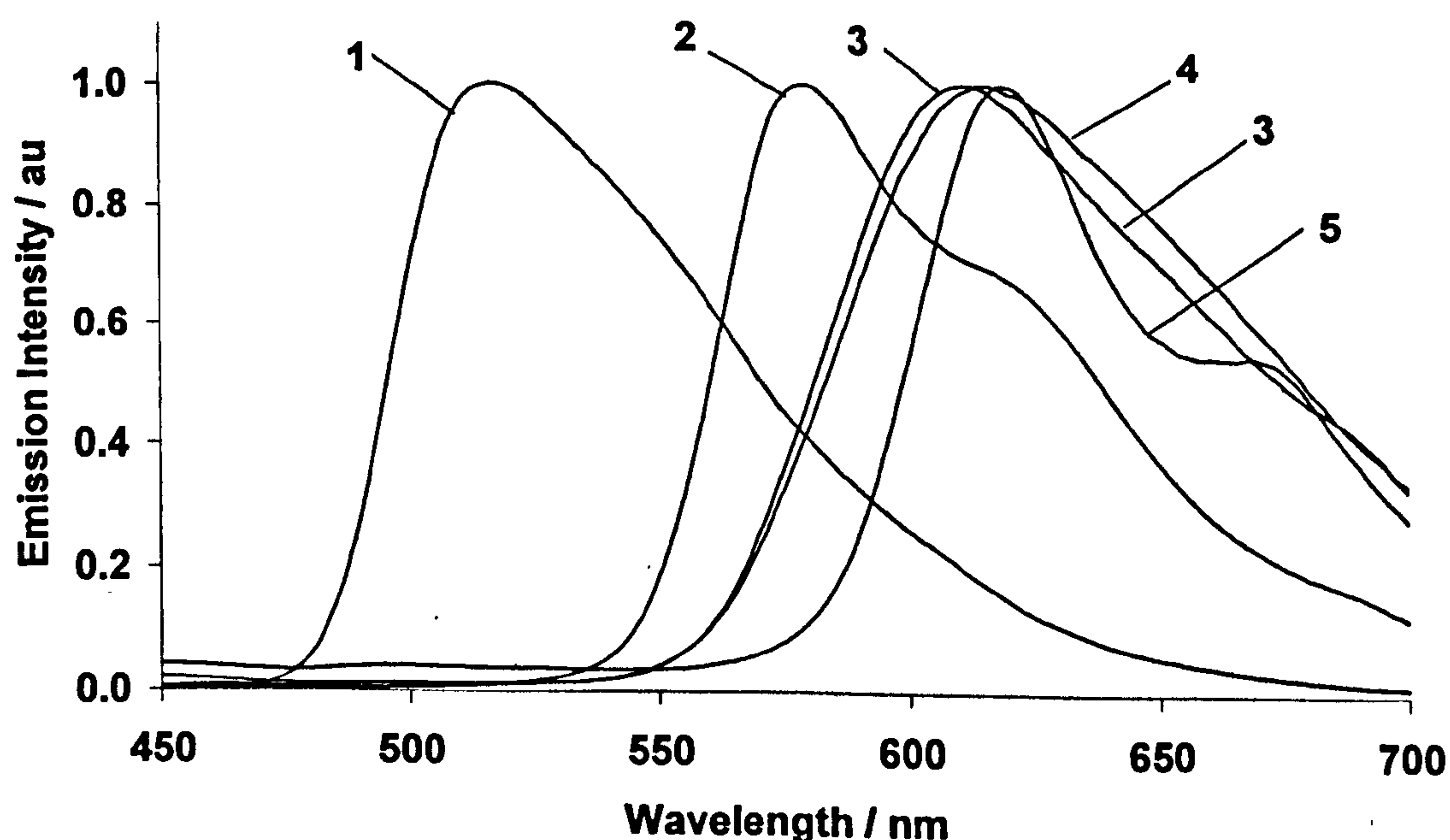


Figure 5.11 Normalised PL spectra of *fac*-Ir(ppy)₃ 30 in aerated dichloromethane (1) and *fac*-Ir(ppy)₂fppy 34 in aerated toluene (2), dichloromethane (3), acetonitrile (4) and ethanol (5), $\lambda_{\text{ex}} = 355$ nm.

As expected, the emission spectra of these complexes were found to increase in intensity upon degassing, but the spectral profiles remained unchanged.

Table 5.5 Maximum emission wavelength (λ_{max}) of *fac*-Ir(ppy)₃ **30**, *fac*-Ir(ppy)₂fppy **34** and *fac*-Ir(fppy)₃ **35** in aerated solvents at 298 K, $\lambda_{\text{ex}} = 355$ nm.

Complex	Synthesis Number (Chapter 3)	Solvent	$\lambda_{\text{max}} / \text{nm}$
<i>fac</i> -Ir(ppy) ₃	30	dichloromethane	517
<i>fac</i> -Ir(ppy) ₂ fppy	34	toluene	580
<i>fac</i> -Ir(ppy) ₂ fppy	34	dichloromethane	612
<i>fac</i> -Ir(ppy) ₂ fppy	34	acetonitrile	616
<i>fac</i> -Ir(ppy) ₂ fppy	34	ethanol	619
<i>fac</i> -Ir(fppy) ₃	35	toluene	565
<i>fac</i> -Ir(fppy) ₃	35	dichloromethane	586
<i>fac</i> -Ir(fppy) ₃	35	acetonitrile	596
<i>fac</i> -Ir(fppy) ₃	35	ethanol	605

The solvatochromatic emission exhibited by *fac*-Ir(ppy)₂fppy **34** and *fac*-Ir(fppy)₃ **35** can be described in terms of greater electron delocalisation in the excited ³MLCT state. The formyl group acts as an electron acceptor and hence stabilises the negative charge that can be considered to reside on the ligand. The degree of stabilisation, and hence the extent of the bathochromic shift, depends upon the polarity of the environment.

Previous investigations of Ru(bipy)₃²⁺ using various absorption,^{8,9} electroabsorption¹⁰ and Raman techniques¹¹ indicated that the lowest MLCT state was localised on a single ligand. Time-resolved studies of the formation of the triplet MLCT excited state with transient absorption pump-probe spectroscopy showed the initial delocalisation of the excited state over all three ligands, followed by the charge localising onto a single ligand.¹² In cyclometalated iridium complexes excitation processes can be both ligand-centred (LC) and MLCT in nature. Following excitation the emissive ³MLCT state is formed, and by analogy with the Ru(bipy)₃²⁺ complexes, it is proposed that this is localised on a single ligand. In the *fac*-Ir(ppy)₃ **30** complex this can be any one of the three identical 2-phenylpyridine ligands. However, in the case of *fac*-Ir(ppy)₂fppy

34, the presence of the carbonyl moiety on the 4-(2-pyridyl)benzaldehyde (fppy) ligand lowers both its HOMO and LUMO energies in comparison with the 2-phenylpyridine ligand. Hence it is upon this ligand that the final excitation resides. Subsequent emission from the complex is characterised by the substituted ligand.

The emission profile of complex 34 in toluene, figure 5.11, spectrum 2, indicates that there is some mixing of the destabilised $^3\text{MLCT}^*$ state with $^3\pi\text{-}\pi^*$ states in this solvent, thus causing the vibrational structure that is seen. The more stabilising solvents, dichloromethane (3) and acetonitrile (4), produce broad featureless emission profiles that are characteristic of MLCT transitions. However, in ethanol (5), we see a more structured emission profile. This is unlikely to be due to MLCT and LC state mixing, but is perhaps caused by acetal formation yielding two separate emission profiles. On the other hand, excitation spectra recorded at these emission wavelengths were identical in profile.

Luminescence measurements of *fac*-Ir(fppy)₃ 35 show similar solvatochromism to the singly substituted complex *fac*-Ir(ppy)₂fppy 34, although in all solvents the emission from *fac*-Ir(fppy)₃ 35 is blue shifted by approximately 15-25 nm compared with that of *fac*-Ir(ppy)₂fppy 34, as shown in table 5.5.

5.6.3 Luminescence Lifetimes

Typical literature values for the luminescence lifetimes of cyclometalated iridium(III) complexes at room temperature are of the order of 1-2 μs in degassed solvents^{1,4,6} and 100 ns in aerated media¹ and are characteristic of the emitting $^3\text{MLCT}$ state.

Luminescence lifetimes of dilute solutions of cyclometalated iridium(III) complexes were recorded using the technique described in chapter 4, section 4.4. Unless otherwise stated, each decay was fitted to a single exponential decay; these are reported in table 5.6.

In general, the lifetimes obtained for complexes 30-49 are 1-2 μs for degassed solutions and 20-200 ns in aerated solvents and are of the expected order of magnitude for iridium(III) species of this nature. There does not seem to be any obvious pattern between the lifetime and steric hindrance of the substituents. More bulkily substituted

complexes may have been expected to give longer lifetimes due to reduced self-quenching effects.

For complex **37**, Ir(F₂ppy)₃, already characterised by ¹H-NMR as a mixture of the facial and meridonal isomers, bi-exponential lifetimes were obtained in both solvents. The longer degassed lifetimes of 1.7 μs and 1.5 μs in dichloromethane and toluene respectively, are of the same order as that obtained for a pure sample of *fac*-Ir(F₂ppy)₃ in 2-methyltetrahydrofuran (2-MeTHF), τ = 1.6 μs, by Tamayo *et al.*⁶ The shorter lifetimes of 46 ns and 17 ns in dichloromethane and toluene respectively, can therefore be assigned to the meridonal isomer of this difluoro-substituted complex. Tamayo *et al.*⁶ reported the lifetime of this pure meridonal complex in 2-MeTHF as 0.21 μs at 298 K.

The individual lifetimes obtained for these bi-exponential decays may only be used as an estimate for that of the pure isomers under the same conditions, as possible quenching between isomers cannot be excluded.

Table 5.6 Luminescence lifetimes of iridium(III) complexes in both aerated and degassed dichloromethane (CH₂Cl₂) and toluene (C₆H₅CH₃) at 298 K, λ_{ex} = 355 nm, emission wavelength (nm) in brackets.

Complex	Synthesis Number	Degassed solvent		Aerated solvent	
		τ ± 10 % / μs (λ/nm)		τ ± 10 ns / ns (λ/nm)	
		CH ₂ Cl ₂	C ₆ H ₅ CH ₃	CH ₂ Cl ₂	C ₆ H ₅ CH ₃
<i>fac</i> -Ir(ppy) ₃	30	1.6 (510)	1.4 (510)	60 (510)	20 (510)
Ir(ppy) ₂ acac	31	1.9 (520)	1.6 (520)	80 (520)	30 (520)
<i>fac</i> -Ir(ppy) ₂ fppy	34	0.4 (615)	1.3 (580)	140 (615)	70 (580)
<i>fac</i> -Ir(fppy) ₃	35	1.2 (580)	1.9 (560)	170 (580)	70 (560)
Ir(fppy) ₂ acac	36	0.9 (600)	1.8 (585)	240 (600)	140 (585)
Ir(F ₂ ppy) ₃	37	τ ₁ = 1.7 μs, A ₁ = 0.63, τ ₂ = 46 ns, A ₂ = 0.37 (495)	τ ₁ = 1.5 μs, A ₁ = 0.58, τ ₂ = 17 ns, A ₂ = 0.42 (475)	τ ₁ = 90 ns, A ₁ = 0.33, τ ₂ = 40 ns, A ₂ = 0.67 (495)	τ ₁ = 40 ns, A ₁ = 0.47, τ ₂ = 10 ns, A ₂ = 0.53 (475)
Ir(F ₂ ppy) ₂ acac	38	1.1 (485)	1.1 (480)	100 (485)	100 (480)
<i>fac</i> -Ir(ppm) ₃	39	1.2 (530)	1.6 (525)	80 (530)	40 (525)
Ir(4-Meppy) ₃	40	1.5 (510)	1.3 (510)	50 (510)	20 (510)
Ir(4-Meppy) ₂ acac	41	1.6 (515)	1.5 (515)	60 (515)	30 (515)
<i>fac</i> -Ir(5-Meppy) ₃	42	1.8 (510)	1.6 (510)	50 (510)	20 (510)
Ir(5-Meppy) ₂ acac	43	1.7 (515)	1.6 (515)	70(515)	30 (515)
<i>fac</i> -Ir(Cyclohex) ₃	44	1.7 (495)	1.4 (495)	50 (495)	20 (495)
<i>fac</i> -Ir(Myrt) ₃	45	1.5 (505)	1.3 (505)	60 (505)	20 (505)
<i>fac</i> -Ir(dppy) ₃	46	2.0 (575)	1.9 (560)	100 (575)	50 (560)
Ir(dppy) ₂ acac	47	1.2 (560)	1.0 (550)	100 (560)	40 (550)
<i>fac</i> -Ir(bippy) ₃	48	1.6 (575)	1.6 (560)	100 (575)	50 (560)
Ir(bippy) ₂ acac	49	1.1 (565)	0.9 (555)	100 (565)	40 (555)

5.7 Luminescence Quantum Yields

Luminescence quantum yields in aerated dichloromethane were carried out at 298 K using the optically dilute method described by Demas *et al.*,¹³ these are reported in table 5.7. Estimated values for the degassed quantum yields were determined by the comparison of the integrated degassed and aerated emission intensity from a single solution at room temperature. Rate constants of oxygen quenching, k_q , were also determined using the Stern-Volmer equation, 5.1.

$$\Phi^0/\Phi = 1 + k_q\tau[\text{O}_2] \quad 5.1$$

where; Φ^0 = quantum yield in the absence of oxygen, Φ = in the presence of oxygen, k_q = bimolecular quenching constant ($\text{dm}^3 \text{mol}^{-1} \text{s}^{-1}$), τ^0 = radiative lifetime in the absence of oxygen (s) and $[\text{O}_2]$ is the concentration of oxygen in dichloromethane = $10.7 \times 10^{-3} \text{mol dm}^{-3}$.¹⁴

The value of the bimolecular quenching constant, k_q , can reflect the efficiency of quenching or the accessibility of the lumophores to the quencher. Diffusion controlled quenching typically results in values of k_q near to $10^{10} \text{dm}^3 \text{mol}^{-1} \text{s}^{-1}$. Smaller values indicate steric shielding and larger values of k_q indicate some sort of binding interaction with the quencher itself.¹⁵

In general the measured luminescence quantum yields, table 5.7, were found to be greatest for complexes with more bulky substituents. In particular *fac*-Ir(Myrt)₃ 45, *fac*-Ir(dppy)₃ 46, Ir(dppy)₂acac 47, *fac*-Ir(bippy)₃ 48 and Ir(bippy)₂acac 49, which were found to be in the region of 70-100%. This result may be due to a reduction in self-quenching of the complexes luminescent core by the larger substituent groups, however, this is not reflected by the lifetime data for these complexes.

The degassed quantum yields of *fac*-Ir(ppy)₃ 30, Ir(ppy)₂acac 31 and *fac*-Ir(Myrt)₃ 45 in dichloromethane are high compared to those previously reported in other solvents; $\Phi = 0.40$ for *fac*-Ir(ppy)₃ in degassed toluene¹ and 2-MeTHF,⁴ $\Phi = 0.34$ for

$\text{Ir(ppy)}_2\text{acac}$ in degassed 2-MeTHF⁴ and $\Phi = 0.71$ for fac-Ir(Myrt)_3 in degassed methanol¹⁶ using UV excitation.

Table 5.7 Luminescence quantum yields, Φ , and rate coefficients of oxygen quenching, k_q , of iridium(III) complexes in dichloromethane at 298 K, $\lambda_{\text{ex}} = 450$ nm (a) and 355 nm (b).

Complex	Synthesis Number	$\Phi \pm 10\%$ (Aerated)	Estimated $\Phi \pm 10\%$ (Degassed)	$k_q / \text{dm}^3 \text{mol}^{-1} \text{s}^{-1}$
fac-Ir(ppy)_3	30 ^a	0.060	0.87	8.2×10^8
$\text{Ir(ppy)}_2\text{acac}$	31 ^a	0.057	0.71	5.8×10^8
$\text{fac-Ir(ppy)}_2\text{fppy}$	34 ^a	0.037	0.046	5.7×10^7
fac-Ir(fppy)_3	35 ^a	0.047	0.18	2.2×10^8
$\text{Ir(fppy)}_2\text{acac}$	36 ^a	0.036	0.053	4.8×10^7
$\text{Ir(F}_2\text{ppy)}_2\text{acac}$	38 ^b	0.035	0.46	1.1×10^9
fac-Ir(ppm)_3	39 ^a	0.039	0.23	3.8×10^8
fac-Ir(4-Meppy)_3	40 ^a	0.031	0.41	7.5×10^8
$\text{Ir(4-Meppy)}_2\text{acac}$	41 ^a	0.034	0.43	6.8×10^8
fac-Ir(5-Meppy)_3	42 ^a	0.011	0.062	2.9×10^8
$\text{Ir(5-Meppy)}_2\text{acac}$	43 ^a	0.019	0.16	4.2×10^8
$\text{fac-Ir(Cyclohex)}_3$	44 ^b	0.015	0.52	1.9×10^9
fac-Ir(Myrt)_3	45 ^a	0.075	1.00	8.1×10^8
fac-Ir(dppy)_3	46 ^a	0.061	0.68	4.7×10^8
$\text{Ir(dppy)}_2\text{acac}$	47 ^a	0.112	0.96	5.9×10^8
fac-Ir(bippy)_3	48 ^a	0.097	0.90	4.7×10^8
$\text{Ir(bippy)}_2\text{acac}$	49 ^a	0.113	1.00	7.2×10^8

Standards used: (a) fluorescein and cresyl violet, (b) quinine bisulphate and β -carboline.

A recent paper by Nazeeruddin *et al.*¹⁷ reported the luminescence quantum yields for $[\text{Ir(ppy)}_2(\text{CN})_2]\text{TBA}$, $[\text{Ir(ppy)}_2(\text{NCS})_2]\text{TBA}$ and $[\text{Ir(ppy)}_2(\text{NCO})_2]\text{TBA}$, where TBA = tetrabutyl ammonium, in degassed dichloromethane at 298 K to be 0.94 ± 0.05 , 0.97 ± 0.05 and 0.99 ± 0.05 respectively. However, luminescence quantum yields for

these complexes in degassed acetonitrile were reported as 0.79 ± 0.1 , 0.99 ± 0.05 and 0.69 ± 0.1 respectively, under the same conditions.

Complexes which have a luminescence quantum yield less than that of *fac*-Ir(ppy)₃, **30** may possess substituents which promote self-quenching compared to that of the parent complex.

The estimated values of the bimolecular quenching constants, k_q , were all found to be less than $10^{10} \text{ dm}^3 \text{ mol}^{-1} \text{ s}^{-1}$ and therefore indicate that the quenching processes involved with these complexes are limited by some degree of steric shielding of the luminescent core. Literature values of k_q for bis-cyclometalated iridium(III) complexes¹⁸ range from $(0.5-6.3) \times 10^6 \text{ dm}^3 \text{ mol}^{-1} \text{ s}^{-1}$ and for the triply *ortho*-metalated complex, Ru(bipy)₃²⁺, k_q ranges from $(1-3) \times 10^9 \text{ dm}^3 \text{ mol}^{-1} \text{ s}^{-1}$.¹⁹ The values obtained in table 5.7 are therefore of the expected order of magnitude for these kinds of species.

5.8 Cyclic Voltammetric Studies of Iridium(III) Complexes

Dedeian *et al.*²⁰ stated that for the series of phenyl-substituted iridium(III) complexes they had studied in acetonitrile, the position of the oxidative wave followed a pattern. More positive oxidation potentials were found for complexes of ligands bearing electron-withdrawing substituents and less positive oxidation potentials result from ligands with electron-donating substituents. In these systems iridium(III) is oxidised to iridium(IV).

The half-wave oxidation potentials ($E_{1/2}$) of a selection of iridium(III) complexes were measured in degassed acetonitrile, table 5.8. The values obtained were found to be consistent with those reported by Dedeian *et al.*,²⁰ $E_{1/2} = + 0.77 \text{ V}$ for *fac*-Ir(ppy)₃, and also followed the trend for the half-wave potential versus ligand substituent as described above.

Table 5.8 The half-wave potentials ($E_{1/2}$) for iridium(III) complexes in acetonitrile/0.1 M TBA[BF₄] at 298 K.

Complex	Synthesis Number (Chapter 3)	$E_{1/2}/V$
<i>fac</i> -Ir(ppy) ₃	30	+ 0.74
Ir(ppy) ₂ acac	31	+ 0.82
<i>fac</i> -Ir(ppy) ₂ fppy	34	+ 0.81
Ir(fppy) ₂ acac	35	+ 0.98
<i>fac</i> -Ir(fppy) ₃	36	+ 0.97
Ir(F ₂ ppy) ₂ acac	37	+ 1.14
Ir(F ₂ ppy) ₃	38	+ 1.09

The half-wave oxidation potentials for the full series of iridium complexes 30-49 were then measured in degassed dichloromethane at 298 K, due to the ease of obtaining a cleaner background scan in dichloromethane than acetonitrile. Each complex was found to be as electrochemically reversible as ferrocene (FeCp₂) or bis(pentamethylcyclopentadienyl)iron(II) (FeCp*₂) under the same conditions.

A full list of the half-wave potential obtained for complexes 30-49 can be seen in table 5.9.

Table 5.9 The half-wave oxidation potentials ($E_{1/2}$) for iridium(III) complexes 30-49 in dichloromethane/0.1 M TBA[BF₄] at 298 K.

Complex	Synthesis Number (Chapter 3)	$E_{1/2}$ / V
<i>fac</i> -Ir(ppy) ₃	30	0.76
Ir(ppy) ₂ acac	32	0.87
<i>fac</i> -Ir(ppy) ₂ fppy	34	0.82
<i>fac</i> -Ir(fppy) ₃	35	1.02
Ir(fppy) ₂ acac	36	1.07
Ir(F ₂ ppy) ₃	37	1.13
Ir(F ₂ ppy) ₂ acac	38	1.36
<i>fac</i> -Ir(ppm) ₃	39	0.89
Ir(4-Meppy) ₃	40	0.70
Ir(4-Meppy) ₂ acac	41	0.82
<i>fac</i> -Ir(5-Meppy) ₃	42	0.69
Ir(5-Meppy) ₂ acac	43	0.83
<i>fac</i> -Ir(Cyclohex) ₃	44	0.64
<i>fac</i> -Ir(Myrt) ₃	45	0.65
<i>fac</i> -Ir(dppy) ₃	46	0.72
Ir(dppy) ₂ acac	47	0.87
<i>fac</i> -Ir(bippy) ₃	48	0.73
Ir(bippy) ₂ acac	49	0.83

As an example, figure 5.12 shows the electrochemically reversible oxidation waves of Ir(dppy)₂acac 47 and ferrocene, FeCp₂.

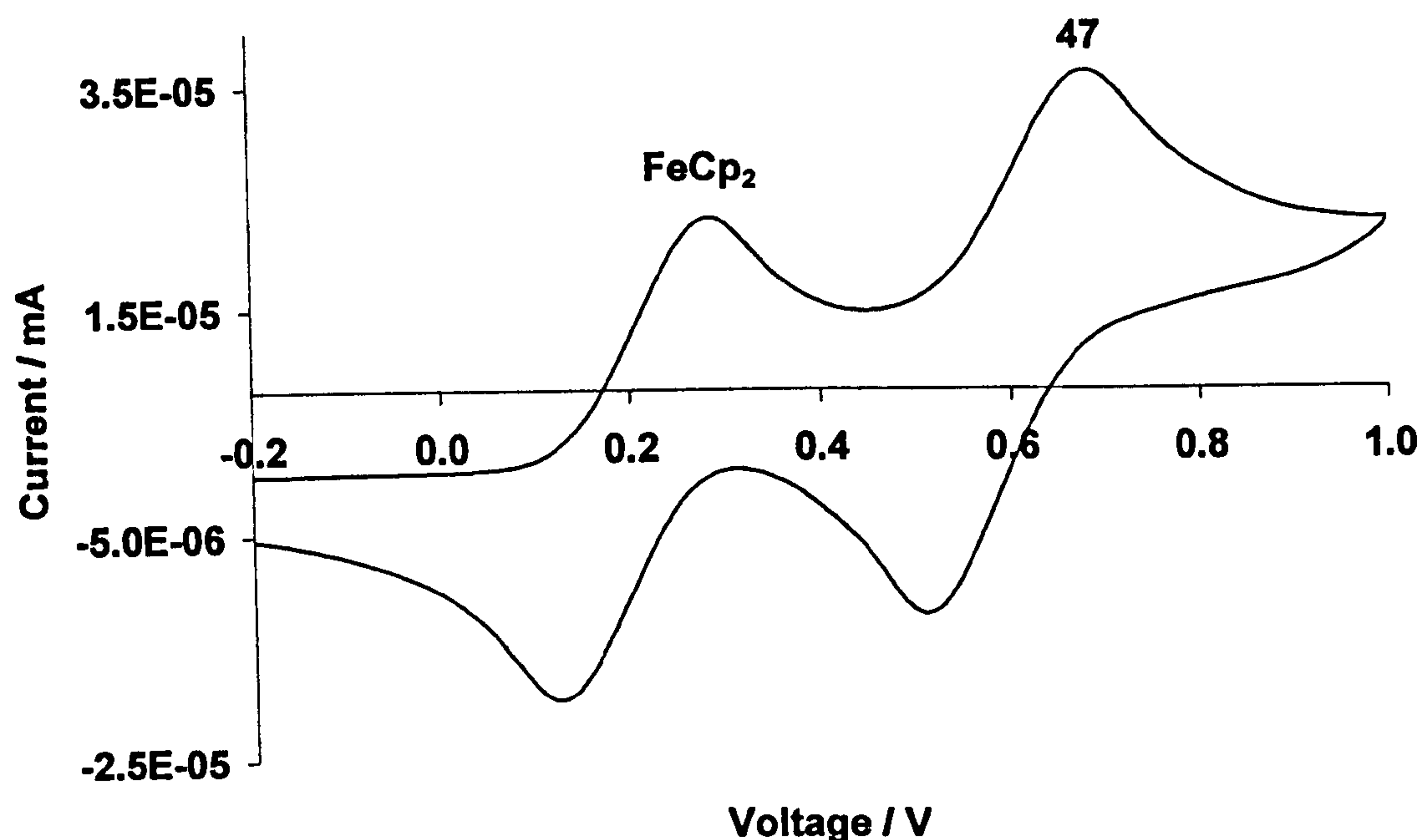


Figure 5.12 The reversible oxidation waves of Ferrocene (FeCp_2) and $\text{Ir(dppy)}_2\text{acac}$ **47** in dichloromethane/0.1 M $\text{TBA}[\text{BF}_4]$ at 298 K.

Each set of cyclic voltammograms was studied as a function of scan rate and can be described by equation 5.2, which expresses the peak current of an oxidised or reduced species in solution in relation to the scan rate for linear diffusion.²¹

$$I_p = (2.687 \times 10^5) n^{3/2} A D^{1/2} C v^{1/2} \quad 5.2$$

where; I_p = peak current (μA), n = number of electrons involved in the oxidation or reduction, A = area of the electrode (cm^2), D = diffusion coefficient of the electro-active species in solution (mmoles^{-1}) and v = scan rate (Vs^{-1}).

In order to examine the trend of oxidation potential versus ligand substituent in more detail, the Hammett Parameter,²² table 5.10, was plotted against the oxidation potential for each complex, figure 5.13.

Table 5.10 The half-wave oxidation potentials ($E_{1/2}$) and Hammett Parameters²² (σ -value) for iridium(III) complexes in dichloromethane/0.1 M TBA[BF₄] at 298 K.

Complex	Synthesis Number (Chapter 3)	$E_{1/2}$ / V	Hammett Parameter (σ -value)
<i>fac</i> -Ir(ppy) ₃	30	0.76	0
Ir(ppy) ₂ acac	32	0.87	0
<i>fac</i> -Ir(ppy) ₂ fppy	34	0.82	0.36
<i>fac</i> -Ir(fppy) ₃	35	1.02	0.36
Ir(fppy) ₂ acac	36	1.07	0.36
Ir(F ₂ ppy) ₃	37	1.13	0.68
Ir(F ₂ ppy) ₂ acac	38	1.36	0.68
<i>fac</i> -Ir(ppm) ₃	39	0.89	0
Ir(4-Meppy) ₃	40	0.70	-0.17
Ir(4-Meppy) ₂ acac	41	0.82	-0.17
<i>fac</i> -Ir(5-Meppy) ₃	42	0.69	-0.07
Ir(5-Meppy) ₂ acac	43	0.83	-0.07
<i>fac</i> -Ir(Cyclohex) ₃	44	0.64	-0.48
<i>fac</i> -Ir(Myrt) ₃	45	0.65	-0.48
<i>fac</i> -Ir(dppy) ₃	46	0.72	0.01
Ir(dppy) ₂ acac	47	0.87	0.01
<i>fac</i> -Ir(bippy) ₃	48	0.73	0.02
Ir(bippy) ₂ acac	49	0.83	0.02

Plotting the oxidation potential as a function of the Hammett parameter (σ -value) shows that there is good correlation, as illustrated by figure 5.13. Extrapolation of this data then allows the estimation of the half-wave potential that would be achieved by an iridium(III) complex containing specifically substituted 2-phenylpyridine ligands.

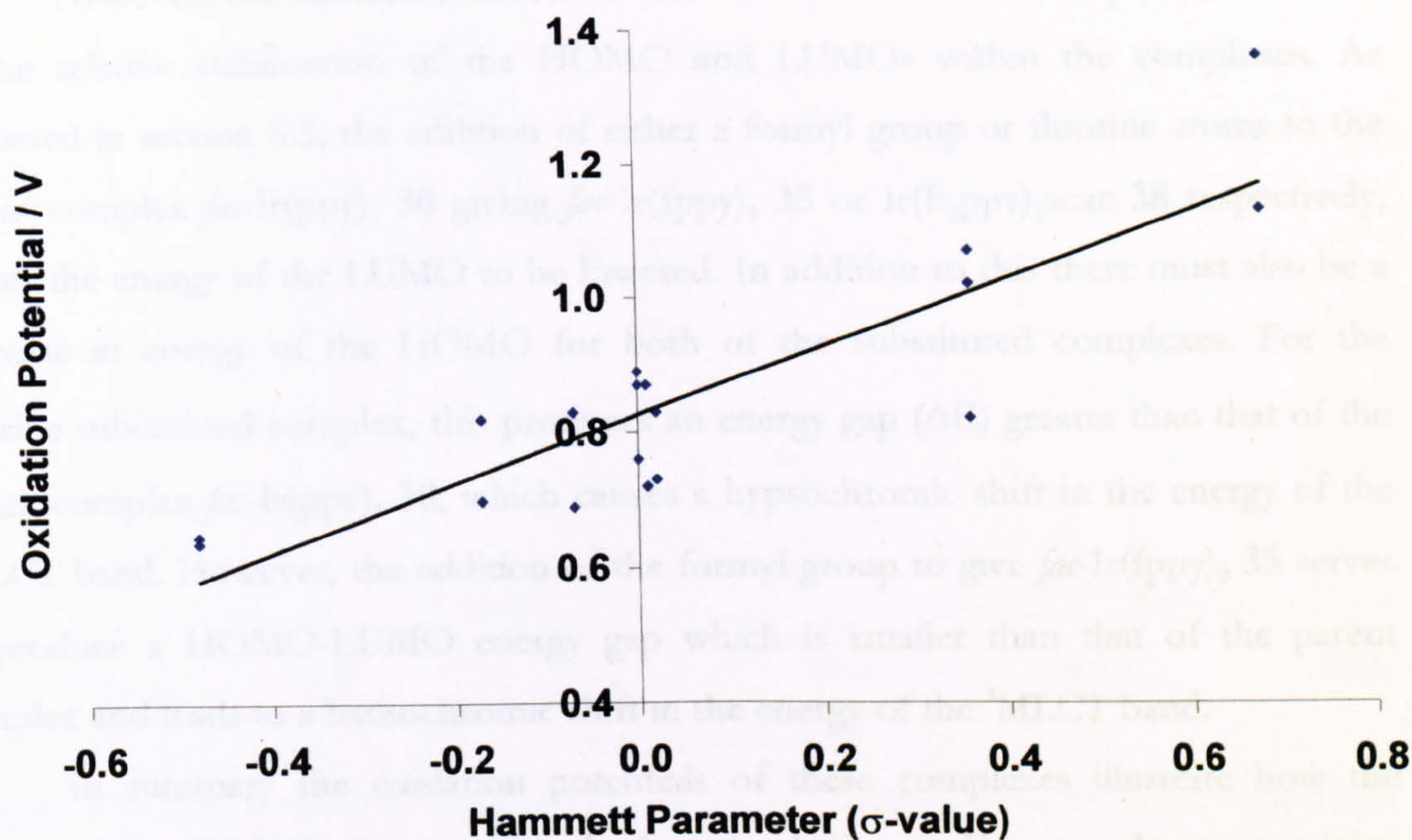


Figure 5.13 Hammett Parameter (σ -value) versus half-wave oxidation potential for iridium(III) complexes **30-49** in degassed dichloromethane/0.1 M TBA[BF₄] at 298 K.

The 4,6-difluoro substituents as found in Ir(F₂ppy)₃ **37** and Ir(F₂ppy)₂acac and the 4-formyl substituents as found in *fac*-Ir(ppy)₂fppy **34**, *fac*-Ir(fppy)₃ **35** and Ir(fppy)₂acac **36**, have Hammett parameters of 0.68 and 0.36 respectively. Therefore, they would both be expected to have an increased reduction potential and blue shifted emission compared to that of the parent complex, *fac*-Ir(ppy)₃ **30**, $\lambda_{\text{max}} = 510$ nm.

The 4,6-difluoro complexes correlate well with this trend, $\lambda_{\text{max}} \sim 490$ nm, however the 4-formyl complexes exhibit red-shifted emission, $\lambda_{\text{max}} \sim 580$ -615 nm in dichloromethane. The use of polar/inductive (σ_I) and resonance/mesomeric (σ_R) σ -values for these substituents, from the extended Hammett approach²³ does not improve the correlation between the emission wavelength and substituent.

The electronic effects of the fluorine and formyl groups are very different. The fluorine atoms exert a strong inductively electron-withdrawing effect and simplistically can be viewed as stabilising the negative charge on the phenyl ring of the complex. In the case of the formyl group, this negative charge is delocalised and hence stabilised by a mesomeric effect.

However, the electronic effects of these substituents can be expressed in terms of the relative stabilisation of the HOMO and LUMOs within the complexes. As discussed in section 5.5, the addition of either a formyl group or fluorine atoms to the parent complex *fac*-Ir(ppy)₃ **30** giving *fac*-Ir(fppy)₃ **35** or Ir(F₂ppy)₂acac **38** respectively, causes the energy of the LUMO to be lowered. In addition to this there must also be a decrease in energy of the HOMO for both of the substituted complexes. For the fluorine substituted complex, this produces an energy gap (ΔE) greater than that of the parent complex *fac*-Ir(ppy)₃ **30**, which causes a hypsochromic shift in the energy of the ³MLCT band. However, the addition of the formyl group to give *fac*-Ir(fppy)₃ **35** serves to produce a HOMO-LUMO energy gap which is smaller than that of the parent complex and leads to a bathochromic shift in the energy of the ³MLCT band.

In summary the oxidation potentials of these complexes illustrate how the energy of the HOMO changes with the ligand substituent. For complexes containing electron-withdrawing substituents we observe more positive oxidation potentials. This indicates a lowering in energy of the HOMO. The reverse of this is implied for complexes containing electron-donating substituents.

5.9 Polymer Films containing Iridium(III) Complexes

Polyvinylcarbazole (PVK) films doped with 5 % wt/wt *fac*-Ir(ppy)₃ **30**, Ir(ppy)₂acac **31**, *fac*-Ir(ppy)₂fppy **34**, Ir(fppy)₂acac **36** and Ir(F₂ppy)₂acac **38** were spun onto glass slides and the luminescence spectrum of each film, including a blank polyvinylcarbazole spectrum **A**, recorded. These are exhibited in figure 5.14.

The emission spectra of the doped films shows none of the characteristic PVK fluorescence indicating that efficient energy transfer is occurring between the host and guest species. In addition to this, the emission profile of each complex remains unaltered in the film with respect to that of the solution state spectra. This suggests that there is no perturbation of the iridium(III) complexes within the PVK films and that PVK could be a possible host for these iridium(III) complexes within an organic light emitting device.

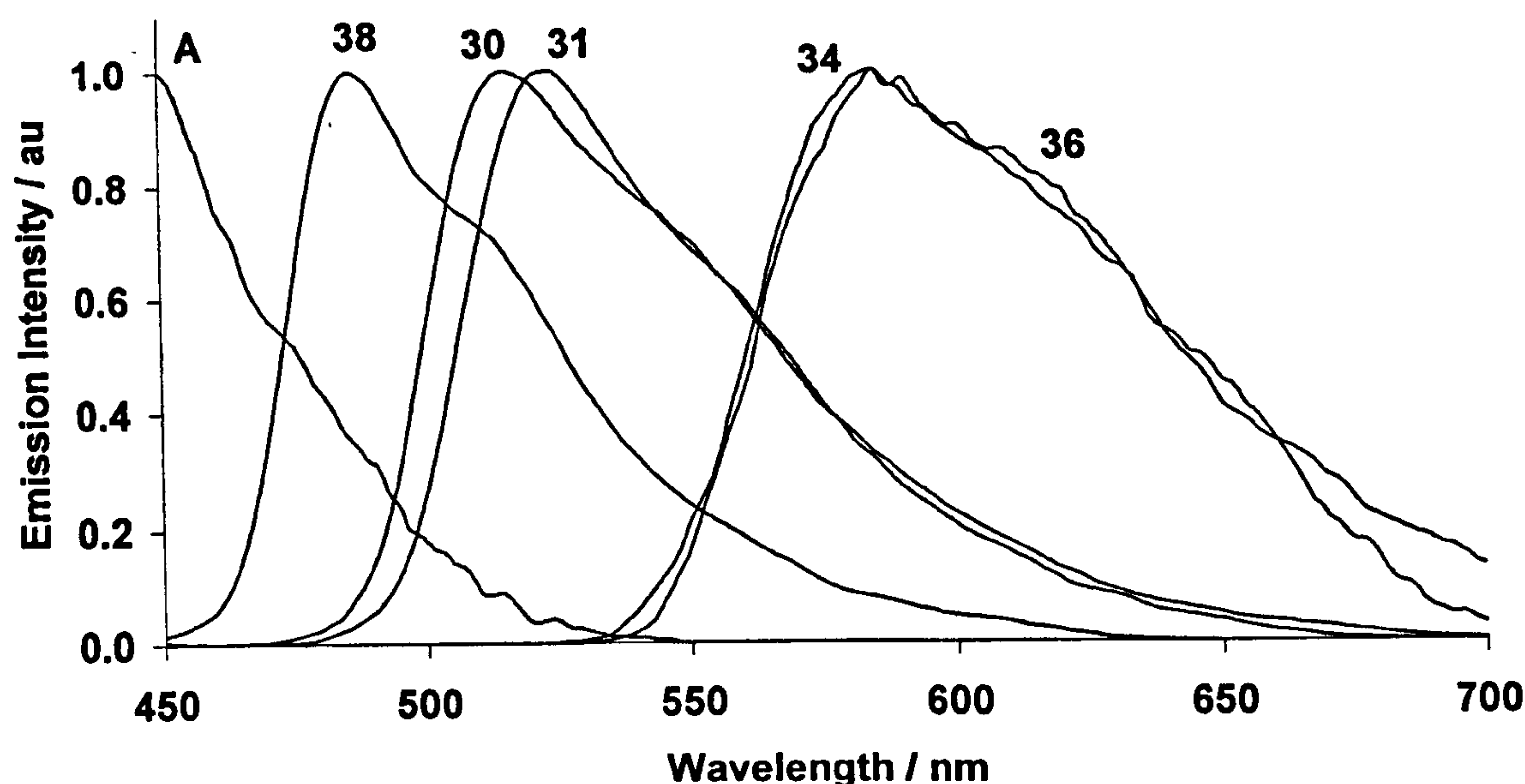


Figure 5.14 The normalised luminescence spectra of iridium(III) complexes doped into PVK films at 5% wt/wt at 298 K, $\lambda_{ex} = 340$ nm.

The Commission Internationale de L'Eclairage (CIE) chromaticity co-ordinates²⁴ calculated from the 5 % wt./wt. doped films' emission spectra are listed in table 5.11. CIE co-ordinates are calculated for each emission spectrum to determine the relative amounts, x , y and z , of each of the primary colours, X , Y and Z , present. The colour, C , of wavelength, λ , is expressed by equation 5.3.

$$C_{\lambda} = xX + yY + zZ \quad 5.3$$

Where; X , Y and Z are called the tristimulus values/co-ordinates.

Table 5.11 Chromaticity (CIE) co-ordinates for PVK films
doped with iridium(III) complexes.

Dopant phosphor	Synthesis Number	Colour	Peak wavelength/nm	CIE-x	CIE-y
<i>fac</i> -Ir(ppy) ₃	30	Green	512 nm	0.28	0.65
Ir(ppy) ₂ acac	31	Green	520 nm	0.29	0.66
<i>fac</i> -Ir(ppy) ₂ fppy	34	Orange-Red	580 nm	0.56	0.44
Ir(fppy) ₂ acac	36	Orange-Red	584 nm	0.55	0.44
Ir(F ₂ ppy) ₂ acac	38	Turquoise	480 nm	0.14	0.44

5.10 OLEDs containing *Fac*-Ir(ppy)₂fppy

5.10.1 Thin Film Studies

The photoluminescence spectra of spin-coated polyvinylcarbazole (PVK) and polymethylmethacralate (PMMA) films containing 0.5-5% wt./wt of *fac*-Ir(ppy)₂fppy 34 show similar emission spectra to those observed in toluene solutions following excitation at 350 nm, figure 5.15. The relative absorbance of each iridium(III) complex compared to that of PVK in each film is small, therefore the majority of the excitation light will be absorbed by PVK.

The emission spectra observed from the PVK films show none of the characteristic PVK fluorescence, indicating there to be efficient energy transfer from the host to guest, and suggesting that these formyl-substituted iridium complexes could be used as phosphorescent dopants in polymer films. There is a small difference in peak position between the toluene solution and PVK and PMMA films, which can be attributed to differences in the polarity of the medium surrounding the iridium complex. Following low-energy pulsed excitation, 0.1 mJ cm⁻², PMMA films containing low concentrations of the complex showed single exponential decays with a lifetime of $\tau = 1.35 \pm 0.1 \mu\text{s}$. As the pulse energies and/or concentrations were increased the observed decays became progressively non-single exponential, indicating the increasing significance of excited state–excited state quenching processes. PVK films doped with

fac-Ir(ppy)₂fppy showed more complex behaviour, indicating an energy transfer process which occurs by several pathways.

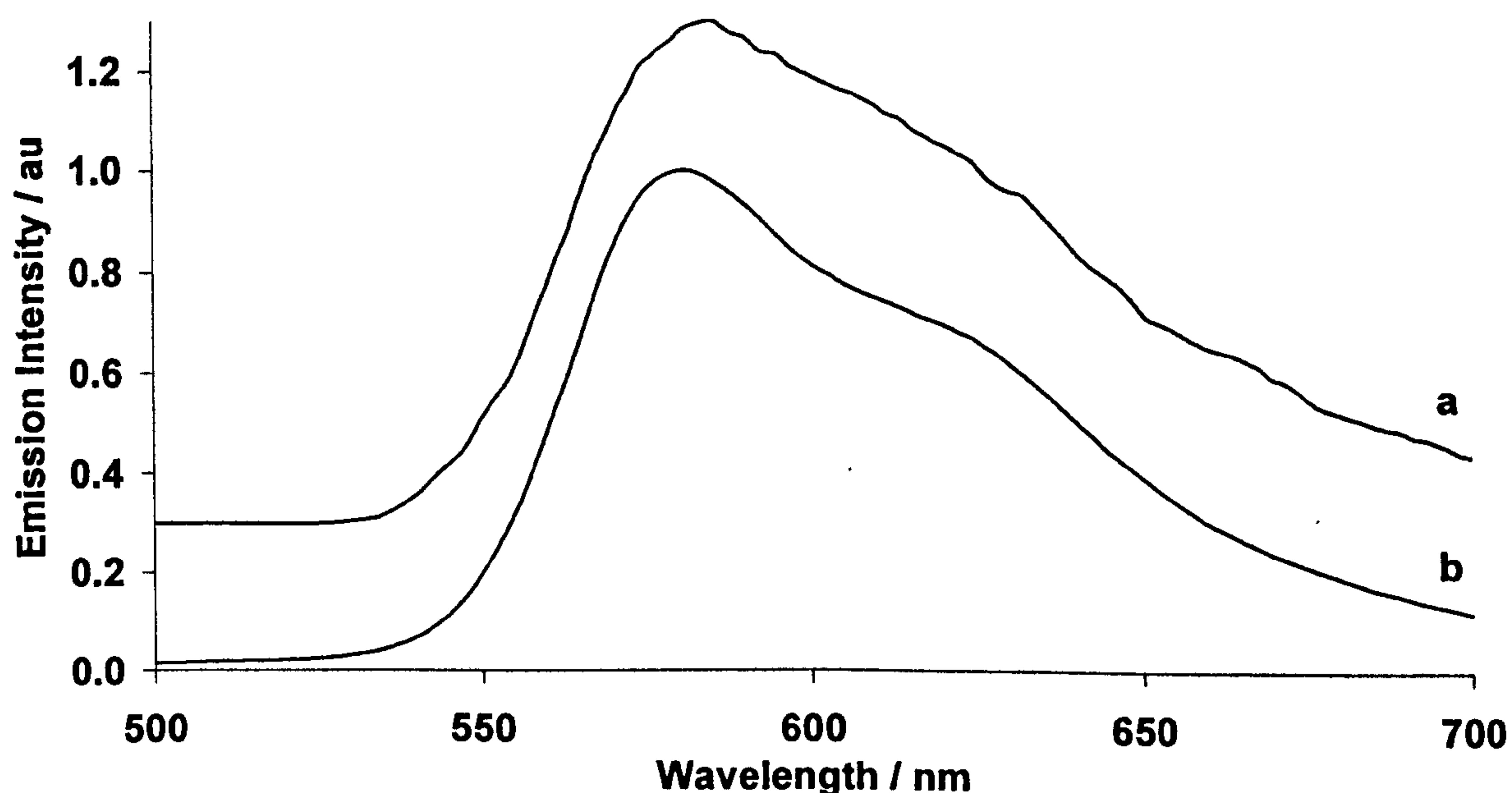


Figure 5.15 PL spectra of (a) a 5% wt/wt *fac*-Ir(ppy)₂fppy **34** doped PVK film, offset for clarity and (b) an aerated solution of *fac*-Ir(ppy)₂fppy **34** in toluene at 298 K, $\lambda_{\text{ex}} = 350$ nm.

5.10.2 OLED Studies

The work described in this section was completed by Ifor. D. W. Samuel's research group at the University of St. Andrew's, UK. Single layer OLEDs consisting of *fac*-Ir(ppy)₂fppy doped into PVK were fabricated on Indium Tin-Oxide (ITO) substrates, which were cleaned by sonication in acetone and isopropanol, air dried and coated with a PEDOT hole-injecting layer. *Fac*-Ir(ppy)₂fppy doped into PVK was spin-coated on top of the ITO layer, with a typical layer thickness of 100 nm and capped with aluminium cathodes. The electroluminescence (EL) observed from these devices was found to be identical to that obtained by photoluminescence (PL) in aerated toluene, figure 5.16.

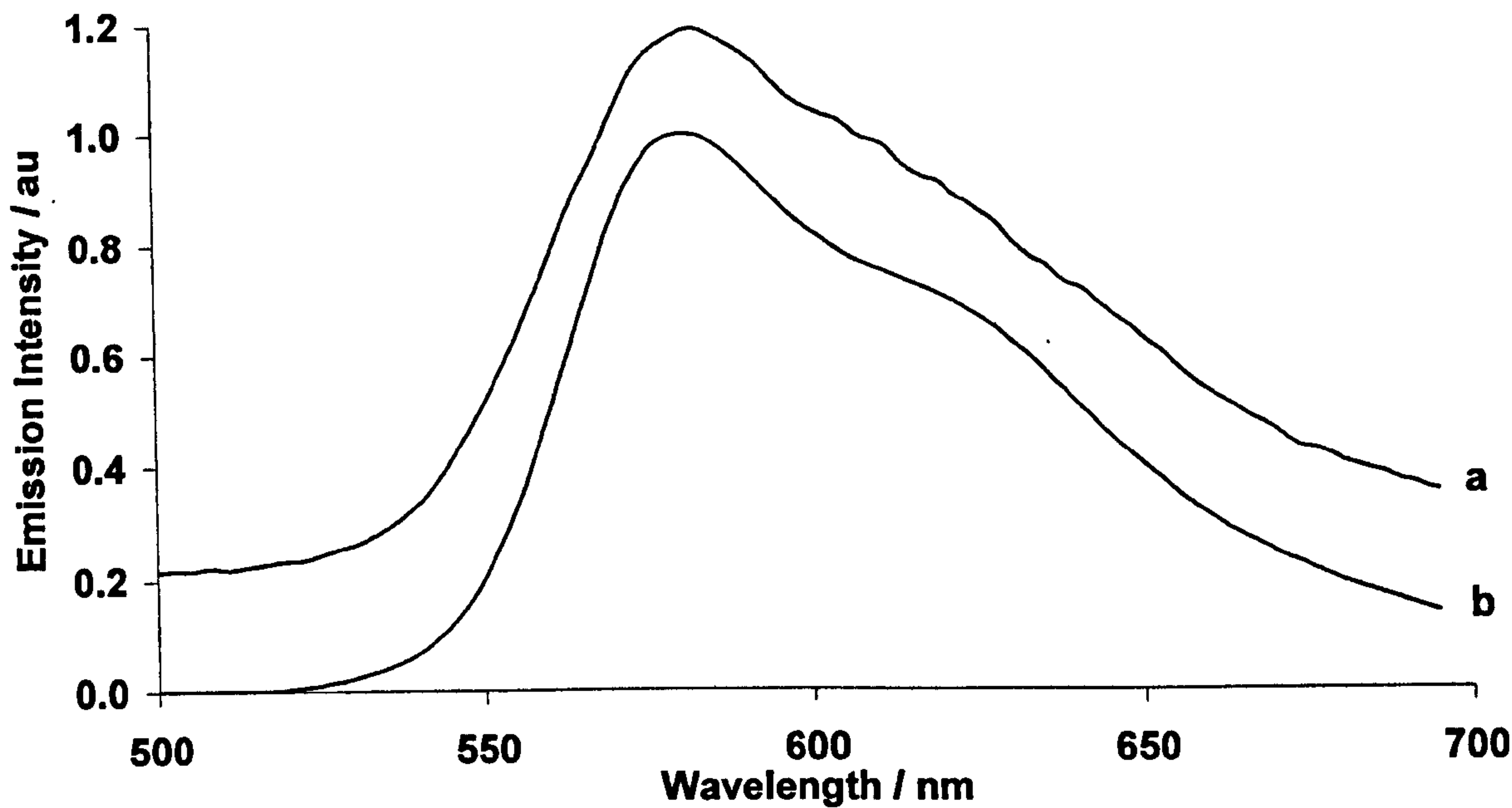


Figure 5.16 (a) EL spectra of *fac*-Ir(ppy)₂fppy doped into PVK with 6 wt%, offset for clarity and (b) PL spectra of *fac*-Ir(ppy)₂fppy in aerated toluene at 298 K, $\lambda_{\text{ex}} = 350$ nm.

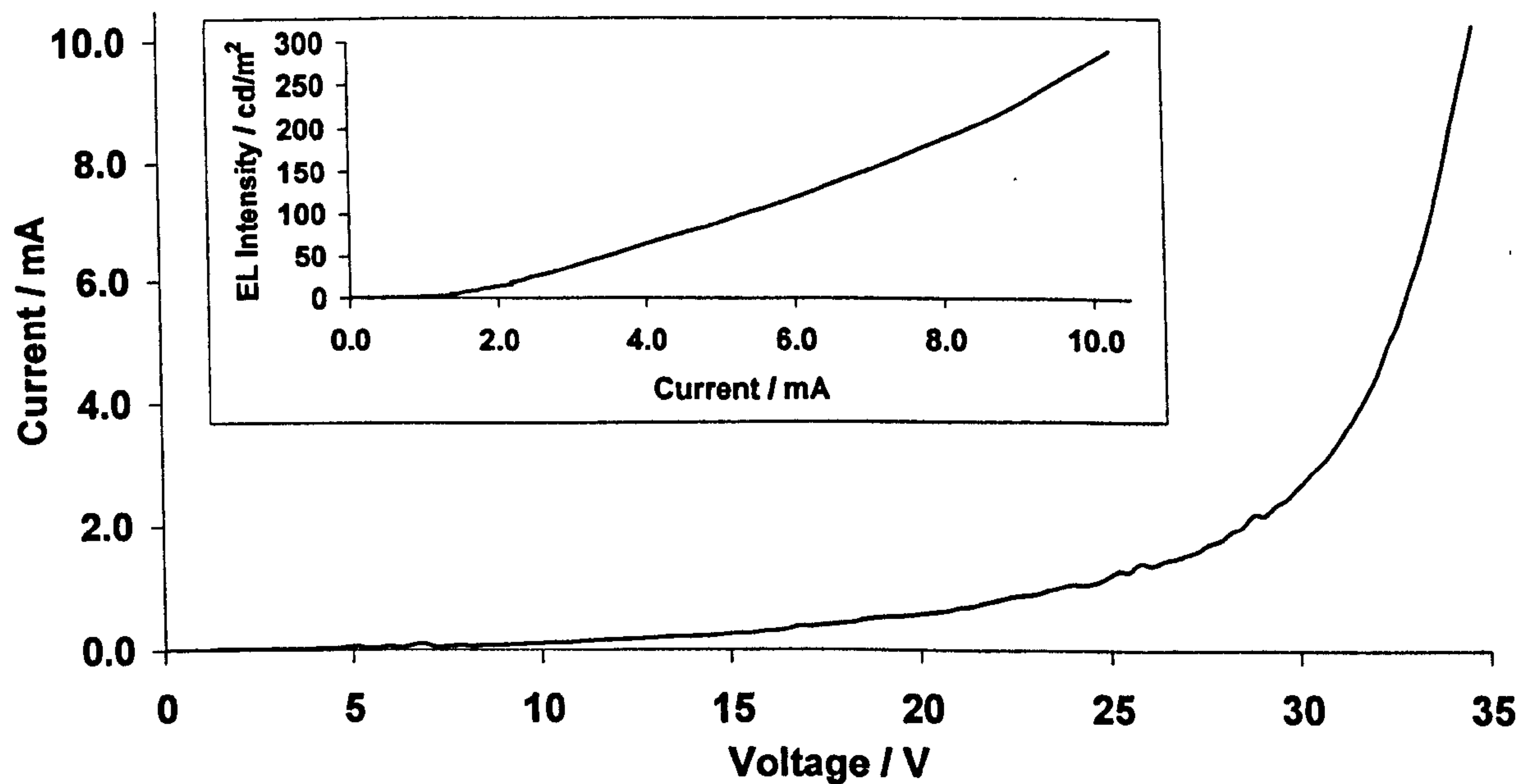


Figure 5.17 Current versus Voltage for ITO/PEDOT/(PVK: *fac*-Ir(ppy)₂fppy 6 % wt/wt)/Al.
Inset: EL Brightness versus Current.

The photoluminescence quantum yield (PLQY) can be a useful guide to the maximum conceivable efficiency for materials for OLEDs. These values were measured for *fac*-Ir(ppy)₃ and *fac*-Ir(ppy)₂fppy doped into PVK (6 %wt.) using an integrating sphere with CCD (charge coupled device) detection.^{25,26} For *fac*-Ir(ppy) a value of $35 \pm 3\%$ was obtained, which is similar to that in toluene solution. For *fac*-Ir(ppy)₂fppy $60 \pm 3\%$ was obtained, which is very encouraging and suggests that it may perform even better than *fac*-Ir(ppy)₃ in optimised devices. An attractive method for fabricating full colour displays would be to spin-cast a high-quality blue-emitting polymer film and then use screen printing,²⁷ microcontact printing²⁸ or hybrid inkjet printing²⁹ to deposit green *fac*-Ir(ppy)₃ and orange *fac*-Ir(ppy)₂fppy.

This novel phosphorescent iridium(III) complex, *fac*-Ir(ppy)₂fppy 34, which shows a strong orange emission in the region of 600 nm, illustrates that a small modification of one ligand is sufficient to cause a substantial change in the emission spectrum, and a large increase in the photoluminescence quantum yield. This approach provides a powerful way of tuning the properties of iridium complexes, which are a very important class of materials for OLEDs. The lifetime, effect of oxygen, and solvatochromism, section 5.6.2, show that a triplet MLCT is responsible for the light-emission. In addition to this *fac*-Ir(ppy)₂fppy 34 has also been demonstrated as a possible phosphorescent dopant for use in polymer OLEDs made via evaporation.

5.11 Conclusion

In summary, these iridium(III) complexes have been shown to exhibit a tuneable emission wavelength which is related to the substituents upon the cyclometalating ligands. The red shifted emission of *fac*-Ir(ppy)₂fppy 34 compared to that of the parent complex *fac*-Ir(ppy)₃ 30, illustrates that only a small modification of one ligand is needed to cause a substantial change in the emission spectrum.

The lowest energy excited state of these molecules has been assigned as a triplet metal to ligand charge transfer state, ³MLCT, state and gives rise to phosphorescent emission. In degassed solutions the emission intensity is greatly increased, but the spectral profile remains unchanged, this is indicative of oxygen quenching of the triplet character excited state. Luminescence lifetimes range from 1-2 μs in degassed solutions

and from 20-200 ns in aerated media. PL quantum yields of these complexes measured in dichloromethane were found to be in the range of 0.01-0.1 and 0.05-1.0 for aerated and degassed solutions respectively.

Thin films of PVK and PMMA doped with 0.5-6 % wt/wt of the iridium(III) complexes were spin-coated onto glass slides. Upon excitation these films exhibited only the dopant emission, suggesting efficient energy transfer between the guest and polymer host materials. Further work, utilising a simple PVK doped polymer OLED device containing the red emitting complex, *fac*-Ir(ppy)₂fppy **34**, illustrated that these complexes are promising phosphorescent dopants for use in OLEDs made via evaporation.

5.12 References

- 1 K. A. King, P. J. Spellane and R. J. Watts, Excited-State Properties of a Triply Ortho-Metalated Iridium(III) Complex, *J. Am. Chem. Soc.*, 1985, **107**, 1431-1432.
- 2 M. C. Colombo, T. C. Brunold, T. Riedener, H. U. Güdel, M. Förtsch and H. Bürgi, Facial Tris Cyclometalated Rh³⁺ and Ir³⁺ Complexes: Their Synthesis, Structure and Optical Spectroscopic Properties, *Inorg. Chem.*, 1994, **33**, 545-550.
- 3 A. Beeby, S. Bettington, I. D. W. Samuel and Z. Wang, Tuning the Emission of Cyclometalated Iridium Complexes by Simple Ligand modification, *J. Mater. Chem.*, 2003, **13**, 80-83.
- 4 S. Lamansky, P. Djurovich, D. Murphy, F. Abdel-Razzaq, R. Kwong, I. Tsyba, M. Bortz, B. Mui, R. Bau and M. E. Thompson, Synthesis and Characterisation of Phosphorescent Cyclometalated Iridium Complexes, *Inorg. Chem.*, 2001, **40**, 1704-1711.
- 5 M. A. Baldo, S. Lamansky, P. E. Burrows, M. E. Thompson and S. R. Forrest, Very High Efficiency Green Organic Light Emitting Devices based on Electrophosphorescence, *Appl. Phys. Lett.*, 1999, **75**, 4-6.
- 6 A. B. Tamayo, B. D. Alleyne, P. I. Djurovich, S. Lamansky, I. Tysba, N. N. Ho, R. Bau and M. E. Thompson, Synthesis and Characterisation of facial and Meridonal

- Tris-Cyclometalated Iridium(III) Complexes, *J. Am. Chem. Soc.*, 2003, **125**, 7377-7387.
- 7 P. W. Atkins, R. S. Friedman, *Molecular Quantum Mechanics*, Third Edition, Oxford University Press, 1997.
 - 8 H. Riesen, L. Wallace and E. Krausz, Localised $^3\text{MLCT}$ Excitations of $[\text{Ru}(\text{bpy})_{3-x}(\text{bpy}-6,6'\text{-d}_2)_x]^{2+}$ ($x = 0\text{-}3$) in $[\text{Zn}(\text{bpy})_3](\text{ClO}_4)_2$ ($\text{bpy} = 2,2'$ bipyridine), *Inorg. Chem.*, 1996, **35**, 6908-6909.
 - 9 J. S. Gold, S. J. Milder, J. W. Lewis and D. S. Kliger, Transient Circular Dichroism of the Luminescent State of $\text{Ru}(\text{bpy})^{2+}$, *J. Am. Chem. Soc.*, 1985, **107**, 8285-8286.
 - 10 D. H. Oh, M. Sano and S. G. Boxer, Electroabsorption (Stark Effect) Spectroscopy of Mono- and Biruthenium Charge-Transfer Complexes: Measurements of Changes in Dipole Moments and Other Electrooptic Properties, *J. Am. Chem. Soc.*, 1991, **113**, 6880-6890.
 - 11 P. J. Carroll and L. E. Brus, Picosecond Raman Scattering Study of Electron Localisation in the Charge Transfer State of Tris(bipyridine)ruthenium(II), *J. Am. Chem. Soc.*, 1987, **109**, 7613-7616.
 - 12 A. T. Yeh, C. V. Shank and J. K. McCusker, Ultrafast Electron Localisation Dynamics Following Photo-Induced Charge Transfer, *Science*, 2000, **289**, 935-938.
 - 13 J. N. Demas and G. A. Crosby, The Measurement of Photoluminescence Quantum Yields. A Review, *J. Phys Chem.*, 1971, **75**, 991-1023.
 - 14 S. L. Murov, I. Carmichael and G. L. Hug, *Handbook of Photochemistry*, 2nd edition, Marcel Dekker, Inc. 1993.
 - 15 J. R. Lakowicz, *Principles of Fluorescence Spectroscopy*, Second Edition, Kluwer Academic/Plenum Publishers, 1999.
 - 16 H. Z. Xie, M. W. Liu, O. Y. Wang, X. H. Zhang, C. S. Lee, L. S. Hung, S. T. Lee, P. F. Teng, H. L. Kwong, H. Zheng and C. M. Che, Reduction in Self-Quenching

- Effect in Organic Electrophosphorescent Emitting Devices via the Use of Sterically Hindered Spacers in Phosphorescence Molecules, *Adv. Mater.*, 2001, **13**, 1245-1248.
- 17 M. K. Nazeeruddin, R. Humphry-Baker, D. Berner, S. Rivier, L. Zuppiroli and M. Graetzel, Highly Phosphorescent Iridium Complexes and Their Application in Organic Light-Emitting Devices, *J. Am. Chem. Soc.*, 2003, **125**, 8790-8797.
- 18 R. Gao, D. G. Ho, B. Hernandez, M. Selke, D. Murphy, P. I. Djurovich and M. E. Thompson, Bis-Cyclometalated Complexes as Efficient Singlet Oxygen Sensitisers, *J. Am. Chem. Soc.*, 2000, **124**, 14828-14829.
- 19 M. I. Gutiérrez, C. G. Martinez, D. Garcia-Fresnadillo, A. M. Castro, G. Orellano, A. M. Braun and E. Oliveros, Singlet oxygen ($^1\Delta_g$) Production by Ruthenium(II) Complexes in Microheterogeneous Systems, *J. Phys. Chem. A*, 2003, **107**, 3397-3403.
- 20 K. Dedeian, P. I. Djurovich, F. O Garces, G. Carlson and R. J. Watts, A New Synthetic Route to the Preparation of a Series of Strong Photoreducing Agents: *Fac* Tris *Ortho*-Metalated Complexes of Iridium(III) with Substituted 2-Phenylpyridines, *Inorg. Chem.*, 1991, **30**, 1685-1687.
- 21 J. B. Headridge, *Electrochemical Techniques for Inorganic Chemists*, Chapter 5, Academic Press, 1969.
- 22 G. B. Barlin and D. D. Perrin, Prediction of the Strengths of Organic Acids, *Quart. Rev. (London)*, 1966, **20**, 75-101.
- 23 R. Jones, *Physical and Mechanistic Organic Chemistry*, Second edition, Cambridge University Press, 1984.
- 24 R. W. Burnham, R. M. Hanes and C. James Bartleson, *Color: A Guide to Basic Facts and Concepts*, John Wiley and Sons, 1967, **6**, 123-150.
- 25 N. C. Greenham, I. D. W. Samuel, G. R. Hayes, R. T. Phillips, Y. A. R. R. Kessener, S. C. Moratti and A. B. Holmes, Measurement of Absolute Photoluminescence Quantum Efficiencies in Conjugated Polymers, *Chem. Phys. Lett.*, 1995, **241**, 89-96.

- 26 J. C. de Mello, H. F. Wittmann and R. H. Friend, An Improved Experimental Determination of External Photoluminescence Quantum Efficiency, *Adv. Mater.*, 1997, **9**, 230-232.
- 27 F. Pschenitzka and J. C. Sturm, Three-Colour Organic Light Emitting Diodes Patterned by Masked Dye Diffusion, *Appl. Phys. Lett.*, 1999, **74**, 1913-1915.
- 28 J. A. Rogers, Z. Bao and V. R. Raju, Nonphotolithographic Fabrication of organic Transistors with Micron Feature Sizes, *Appl. Phys. Lett.*, 1998, **72**, 2716-2718.
- 29 S. Chang, J. Bharathan, Y. Yang, R. Helgeson, F. Wudl. M. B. Ramey, J. R. Reynolds, Dual Colour Polymer Light Emitting Pixels Processed by Hybrid Inkjet Printing, *Appl. Phys. Lett.*, 1998, **73**, 2561-2563.

Chapter 6

The Synthesis and Photophysical Studies of $\text{Ir}(\text{L})_2\text{X}(\text{Y})$ Complexes

6.1 Introduction

Mononuclear bis-cyclometalated iridium complexes of the formula $\text{Ir}(\text{L})_2\text{X}(\text{Y})$, where L = an *ortho*-metalating ligand, X = Cl and Y (ancillary ligand) = pyridine (pyr), triphenylphosphine (PPh_3) and carbon monoxide (CO) were characterised by King *et al.*¹ in 1984. In addition to this, related complexes such as $\text{Ir}(\text{pbt})_2\text{Cl}(\text{pyr})$,² where pbt = 2-phenylbenzothiazole, and $\text{Ir}(\text{2-thpy})_2\text{Cl}(\text{DMSO})$,³ where 2-thpy = 2-(2-thienyl)pyridine and DMSO = dimethylsulphoxide, have also been studied by Nonoyama and Gao *et al.* respectively. Since then, an array of complexes where L = 2-(4,6-difluorophenyl)pyridine (F_2ppy), X = Cl or CN and Y = a monodentate ligand such as tertiary butyl-isocyanide, pyridine, triphenylphosphine and 4-phenylpyridine have been reported by Lamansky *et al.*⁴

For these low-spin d^6 transition-metal complexes, described in sections 1.6 and 1.7, the lowest lying excited state is MLCT-based, $d\pi^6\pi^{*0} \rightarrow d\pi^5\pi^{*1}$. The promotion of an electron from a metal $d\pi$ orbital to a ligand π^* orbital by the absorption of a photon, with energy = $h\nu$, results in the formation of a singlet excited state, $^1\text{MLCT}^*$. The singlet excited state may then undergo intersystem crossing (ISC), a non-radiative process, to form a triplet excited state, $^3\text{MLCT}^*$, figure 6.1.

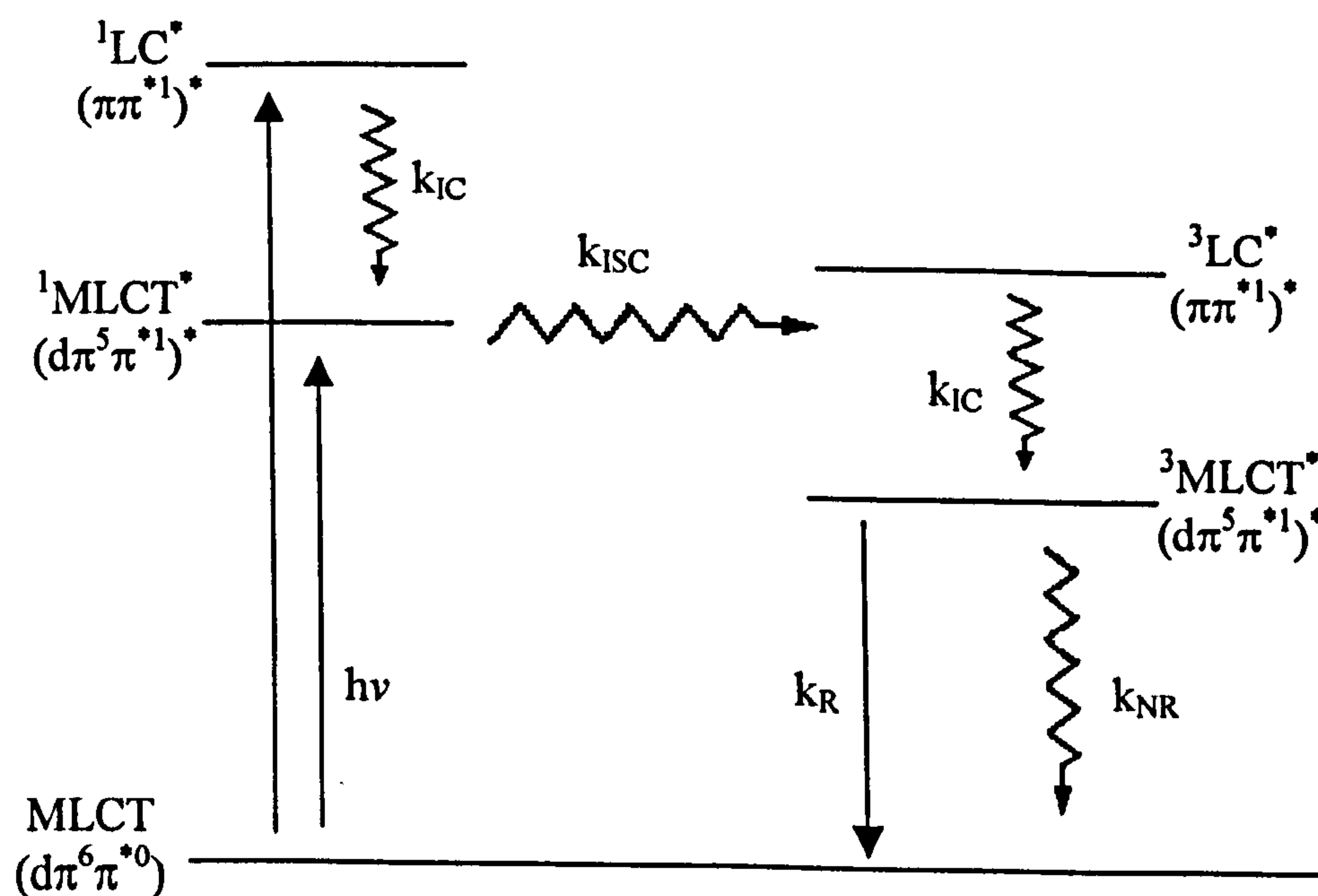


Figure 6.1 A schematic of the electronic energy levels in $\text{Ir}(\text{L})_2\text{X}(\text{Y})$ complexes, where * indicates an excited state and k_x = rate of process x.

The excited triplet state can subsequently experience either non-radiative decay (NR) or radiative decay (R) and relax back to its ground electronic state, MLCT ($d\pi^6\pi^0$). In the latter case, involving a change in spin multiplicity, this process is formally forbidden, however mixing between $^3\text{MLCT}^*$ and higher energy spin-allowed $^1\text{MLCT}^*$ transitions increases the probability of this radiative decay process. This mixing is facilitated by the strong spin-orbit coupling of the iridium(III) center.

The complexes reported by King *et al.*¹ possess shorter luminescent lifetimes, ~ 50-150 ns in degassed dichloromethane, than that of the triply *ortho*-metalated complexes, such as *fac*-Ir(ppy)₃, 30, 1.90 μs in degassed acetonitrile.⁵

King *et al.*¹ discussed the change in the character of the emissive states of these complexes according to the π -accepting ability of the ancillary ligand, Y. Due to strong σ -donation from the C-bonded ppy ligands, the metal centres in these kinds of complexes possess enriched electron density. This lowers the energy of the metal to π -acceptor transitions. The MLCT character of the emissive state was shown to be greatest in complexes where there are the maximum number of Ir-C bonds and the presence of a good delocalised π -acceptor ligand with relatively high energy ligand centered (LC) excited states, i.e. Ir(ppy)₂Cl(pyr). On the other hand, the degree of LC character of the emissive state is greatest when there are fewer Ir-C bonds and the presence of a more localised π -accepting ligand with low energy LC excited states, i.e. Ir(ppy)₂Cl(CO).⁶ In complexes where the emissive state possessed LC character, Ir(ppy)₂Cl(CO), a blue shift in emission wavelength was observed in addition to a much longer luminescence lifetime, 28 μs , at 77 K, compared to that of those with less LC character, 4-5 μs .^{1,6}

6.2 Synthesis

The corresponding dichloro-bridged complex, [Ir(L)₂Cl]₂, was reacted with 2 equivalents of the ancillary ligand, Y, at room temperature. Subsequent concentration of the reaction mixture, followed by the addition of hexane allowed the precipitation of the product, Ir(L)₂Cl(Y), in high yield. The detailed syntheses of these bis-cyclometalated complexes 50-60 can be found in chapter 3 and are summarised in table 6.1.

Table 6.1 Summary of synthetic data for Ir(L)₂X(Y) complexes 50-60.

Complex	Synthesis Number (Chapter 3)	% Yield
Ir(ppy) ₂ Cl(CO)	50*	98
Ir(ppy) ₂ CN(CO)	51*	40
Ir(ppy) ₂ Cl(PPh ₃)	52	88
Ir(ppy) ₂ CN(PPh ₃)	53*	82
Ir(ppy) ₂ Cl(Ph ₂ PPhCO ₂ H)	54*	97
Ir(ppy) ₂ Cl(DMAP)	55*	44
Ir(ppy) ₂ Cl(pyCH=CHPhNMe ₂)	56*	92
<i>rac</i> -Ir(ppy) ₂ Cl(TAT)	57*	91
<i>rac</i> -Ir(ppy) ₂ Cl(bipy)	58	85
Ir(F ₂ ppy) ₂ Cl(CO)	59*	77
Ir(F ₂ ppy) ₂ Cl(PPh ₃)	60	89

Complexes marked with an asterisk (*) are new; all others have been previously reported.

The high percentage yields of these complexes are due to the ease of Ir-Cl bond cleavage of the dichloro-bridged precursor by these ligands. The low yield of Ir(ppy)₂CN(CO) 51 is probably due the photodegradation of the product during purification, see section 6.5.4.

The presence of two carbonyl stretches in the IR spectrum of compound 59 indicates the existence of a second isomer of this species. The formation of other isomers of this complex are possible *via* ligand scrambling. This has already been observed in complex 37, Ir(F₂ppy)₃ containing the same ligand.

6.2.1 NMR Spectra

The proton NMR spectra of the bis-cyclometalated complexes, Ir(L)₂X(Y) are distinctive from that of the dichloro-bridged starting material, they possess two sets of peaks one for each chemically inequivalent cyclometalating ligand. This is in agreement with that observed by Nonoyama³ for Ir(2-thpy)₂Cl(DMSO) and is clearly illustrated by the ¹H-NMR spectrum of Ir(F₂ppy)₂Cl(CO) 59 in CDCl₃ in figure 6.2, ¹H-NMR 200 MHz (CDCl₃): δ 9.86 (1H₇, d, J = 4.8 Hz), 9.06 (1H₁, d J = 5.2 Hz), 8.34 (2H, H₄ and

H_{10} , m), 8.00 (2H, H_5 and H_{11} , q, $J = 7.8$ Hz), 7.41 (1H, H_9 , t, $J = 7.0$ Hz), 7.31 (1H, H_3 , m), 6.48 (2H, H_2 and H_8 , m), 5.84 (1H, H_{12} , d, $J = 8.0$ Hz), 5.38 (1H, H_6 , d, $J = 8.0$ Hz). The appearance of

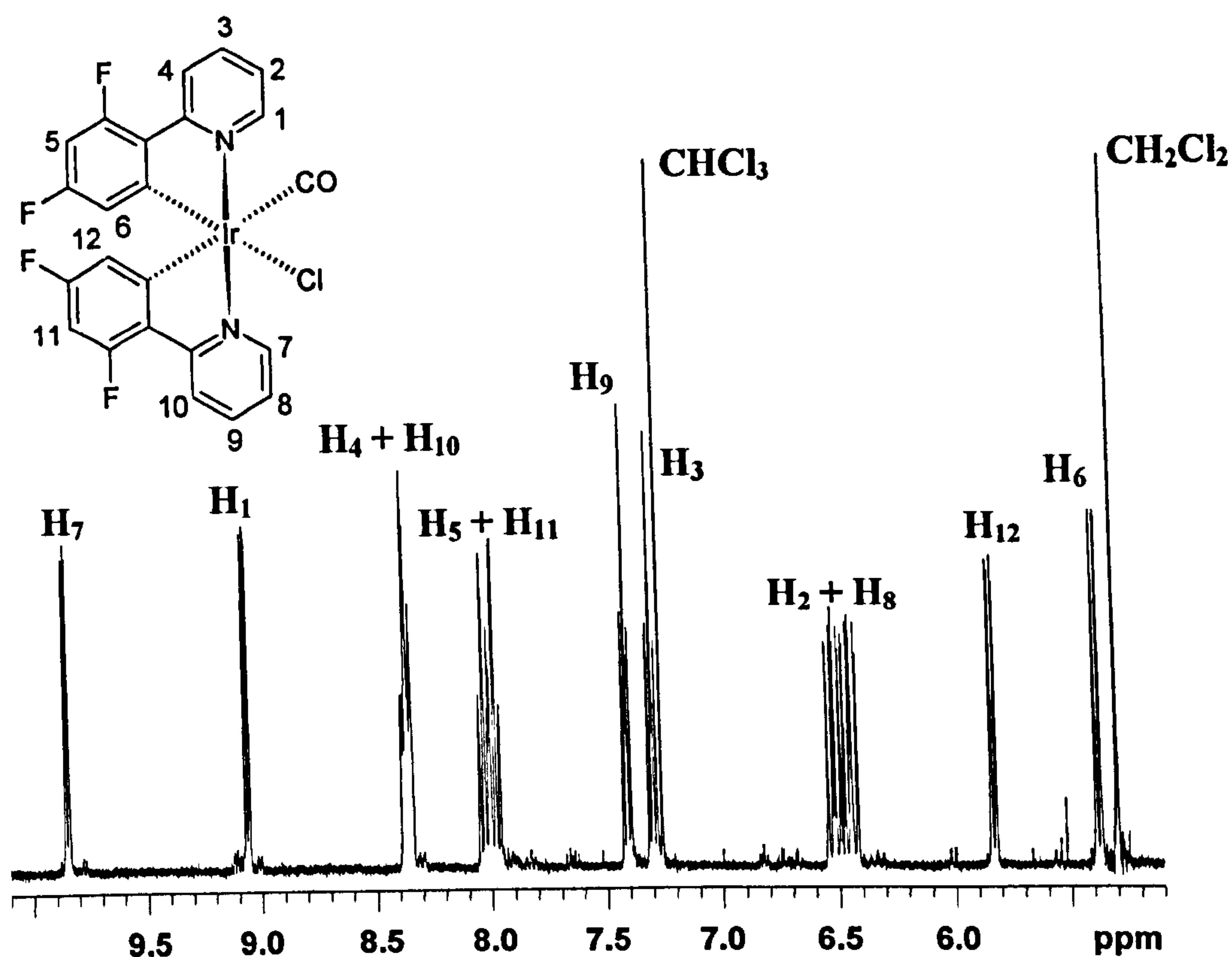


Figure 6.2 The ^1H -NMR (200 MHz) spectrum of $\text{Ir}(\text{F}_2\text{ppy})_2\text{Cl}(\text{CO})$ 59 in CDCl_3 at 298 K, inset shows the proton assignment for the complex.

6.3 Structure

The crystal structures of complexes $\text{Ir}(\text{ppy})_2\text{Cl}(\text{CO})$ 50, $\text{Ir}(\text{ppy})_2\text{Cl}(\text{PPh}_3)$ 52 and $\text{Ir}(\text{F}_2\text{ppy})_2\text{Cl}(\text{PPh}_3)$ 60, figure 6.3, show the central iridium atom residing in an octahedral geometry. The stereochemistry of these complexes is retained from the dichloro-bridged precursor where the cyclometalating ligands are positioned so that the nitrogen atoms are *trans* to one another and the carbon atoms are *cis*. This stereochemistry is in concurrence with that initially suggested by Nonoyama³ for the $\text{Ir}(\text{2-thpy})_2\text{Cl}(\text{DMSO})$ complex, and is also in accord with that of $\text{Ir}(\text{L})_2\text{acac}$ complexes.⁷

Figure 6.3 illustrates this retention of stereochemistry with the crystal structures of the dichloro-bridged precursor $[\text{Ir}(\text{F}_2\text{ppy})_2\text{Cl}]_2$ **22** and its related monomer $\text{Ir}(\text{F}_2\text{ppy})_2\text{Cl}(\text{PPh}_3)$ **60**; full crystallographic data for these structures can be found in appendix A.

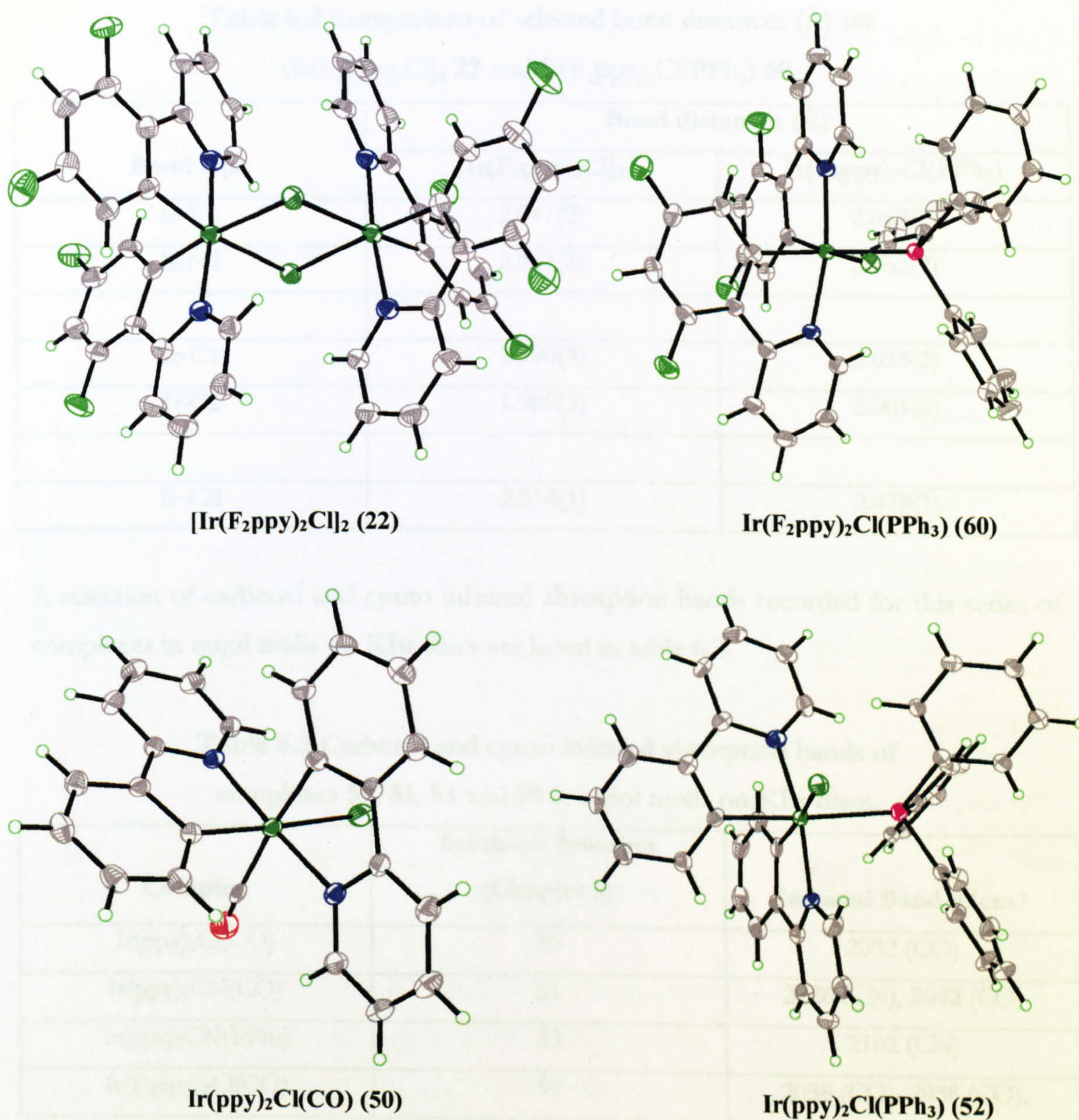


Figure 6.3 X-ray crystal structures of $\text{Ir}(\text{ppy})_2\text{Cl}(\text{CO})$ **50**, $\text{Ir}(\text{ppy})_2\text{Cl}(\text{PPh}_3)$ **52**, $\text{Ir}(\text{F}_2\text{ppy})_2\text{Cl}(\text{PPh}_3)$ **60** and $[\text{Ir}(\text{F}_2\text{ppy})_2\text{Cl}]_2$ **22** at 120 K, thermal ellipsoids depict 50 % occupancy.

A comparison of bond lengths, shown in table 6.2, also illustrates the similarity between $\text{Ir}(\text{F}_2\text{ppy})_2\text{Cl}(\text{PPh}_3)$ **60** and $[\text{Ir}(\text{F}_2\text{ppy})_2\text{Cl}]_2$ **22**. In comparison with literature values, the lengths of the Ir-N, Ir-C and Ir-Cl bonds are in accordance with those reported by DeRosa *et al.*⁸ for $\text{Ir}(\text{ppy})_2\text{Cl}(\text{vpy})$, where vpy = 4-vinylpyridine.

Table 6.2 Comparison of selected bond distances (Å) for $[\text{Ir}(\text{F}_2\text{ppy})_2\text{Cl}]_2$ **22** and $\text{Ir}(\text{F}_2\text{ppy})_2\text{Cl}(\text{PPh}_3)$ **60**.

Bond type	Bond distances (Å)	
	$[\text{Ir}(\text{F}_2\text{ppy})_2\text{Cl}]_2$	$\text{Ir}(\text{F}_2\text{ppy})_2\text{Cl}(\text{PPh}_3)$
Ir-N1	2.047(2)	2.062(2)
Ir-N2	2.044(2)	2.052(2)
Ir-C1	1.990(3)	2.035(2)
Ir-C2	1.989(3)	2.001(2)
Ir-Cl1	2.514(1)	2.478(1)

A selection of carbonyl and cyano infrared absorption bands recorded for this series of complexes in nujol mulls on KBr discs are listed in table 6.3.

Table 6.3 Carbonyl and cyano infrared absorption bands of complexes **50**, **51**, **53** and **59** in nujol mulls on KBr discs.

Complex	Synthesis Number (Chapter 3)	Infrared Band ν/cm^{-1}
$\text{Ir}(\text{ppy})_2\text{Cl}(\text{CO})$	50	2032 (CO)
$\text{Ir}(\text{ppy})_2\text{CN}(\text{CO})$	51	2126 (CN), 2042 (CO)
$\text{Ir}(\text{ppy})_2\text{CN}(\text{PPh}_3)$	53	2102 (CN)
$\text{Ir}(\text{F}_2\text{ppy})_2\text{Cl}(\text{CO})$	59	2058 (CO), 2038 (CO),

The position of the carbonyl infrared stretching bands for complexes in table 6.3 are in the same spectral region to those reported by Hiraki *et al.*⁹ for cyclometalated ruthenium(II) complexes, $\nu(\text{C}=\text{O}) = 1923\text{-}2050\text{ cm}^{-1}$, such as $\text{RuCl}(\text{ppy})(\text{CO})_2(\text{PPh}_3)$. The cyanide stretching vibrations are of a similar order of magnitude to that reported by Kunkely *et al.*¹⁰ for $[\text{Rh}(\text{ppy})_2(\text{CN})_2]\text{Bu}_4\text{N}$, where $\nu(\text{CN}) = 2129$ and 2104 cm^{-1} .

6.4 UV-Visible Absorption Spectroscopy

The UV-visible absorbance spectra of $\text{Ir(ppy)}_2\text{Cl(CO)}$ **50**, $\text{Ir(ppy)}_2\text{CN(CO)}$ **51**, $\text{Ir(ppy)}_2\text{Cl(PPh}_3\text{)}$ **52** and $\text{Ir(ppy)}_2\text{Cl(DMAP)}$ **55** are depicted in figure 6.4 below. The more intense absorption bands between 225 nm and 280 nm are assigned as a ligand centered (LC) spin-allowed $^1\pi\text{-}\pi^*$ transitions. The broader absorption bands at lower energy between 300 nm and 350 nm are typical of spin-allowed $^1\text{MLCT}$ transitions and at even lower energies, the weaker bands, which reach into the visible region, are assigned as formally forbidden $^3\text{MLCT}$ transitions. These features acquire their intensity by mixing with higher energy $^1\text{MLCT}$ spin-allowed transitions. This mixing is facilitated by the strong spin-orbit coupling of the iridium(III) center.

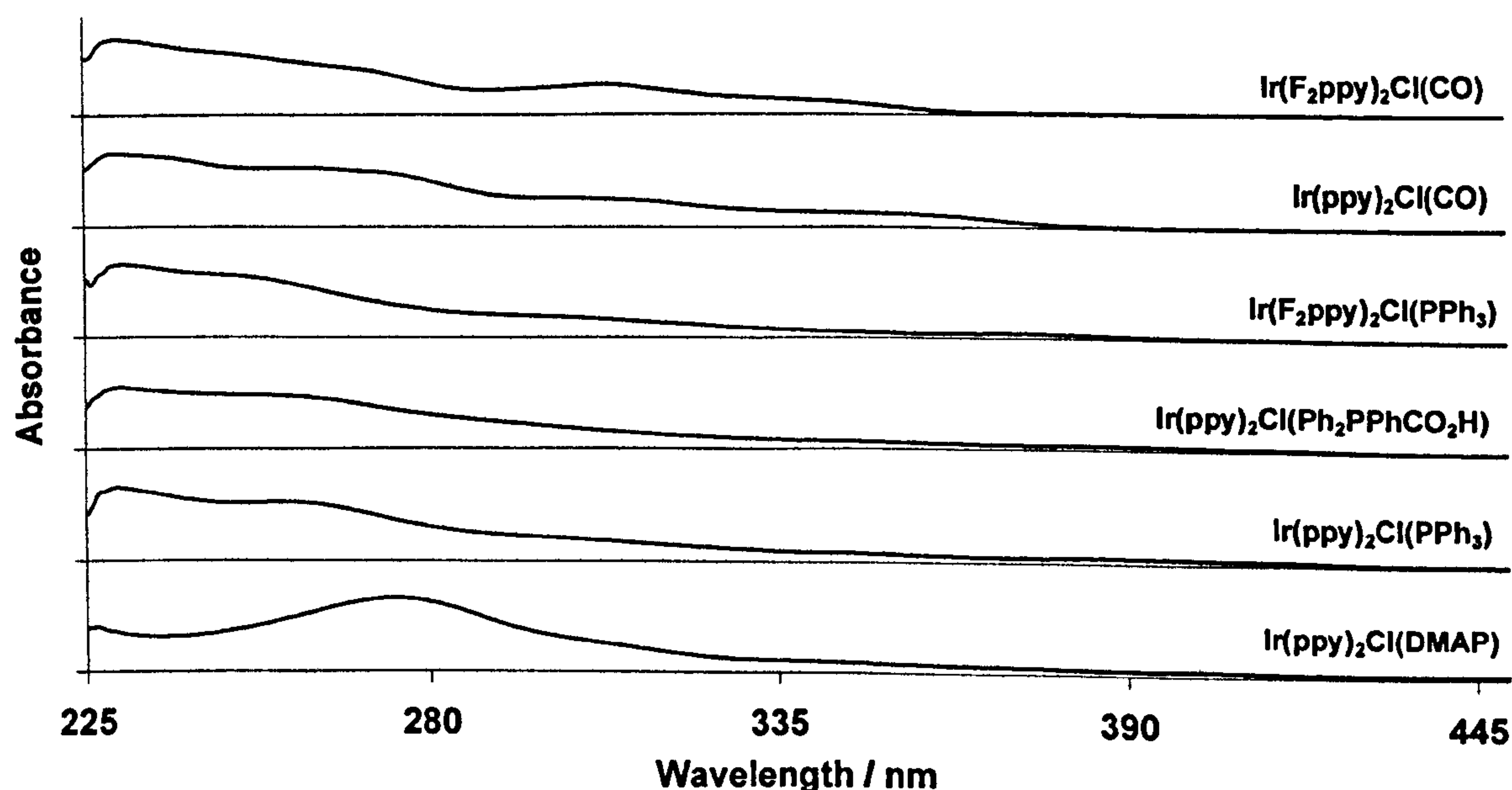


Figure 6.4 Normalised UV-Visible absorbance spectra of $\text{Ir(ppy)}_2\text{Cl(CO)}$ **50**, $\text{Ir(ppy)}_2\text{Cl(PPh}_3\text{)}$ **52**, $\text{Ir(ppy)}_2\text{Cl(Ph}_2\text{PPhCO}_2\text{H)}$ **54**, $\text{Ir(ppy)}_2\text{Cl(DMAP)}$ **55**, $\text{Ir(F}_2\text{ppy)}_2\text{Cl(CO)}$ **59** and $\text{Ir(F}_2\text{ppy)}_2\text{Cl(PPh}_3\text{)}$ **60** in aerated dichloromethane at 298 K.

Each of these spectra possesses the absorption bands expected for a cyclometalated iridium(III) complex. However, what is particularly important is the shifting positions of these bands with regards to the ligands L and Y within the complexes.

In Ir(F₂ppy)₂Cl(PPh₃) **60** we observe a hysochromic shift (blue shift) of the ³MLCT band compared to that of Ir(ppy)₂Cl(PPh₃) **52**. This has been rationalised in terms of the relative stabilisations of the HOMO and LUMOs by the fluorine substituents, similar to that observed for the Ir(L)₃ and Ir(L)₂acac complexes as described in chapter 5, section 5.5.

We also observe additional hypsochromic shifts in the absorption bands in the series; Ir(ppy)₂Cl(DMAP) **55** to Ir(ppy)₂Cl(PPh₃) **52** to Ir(ppy)₂Cl(CO) **50**, with complex **50** being the most blue shifted. This is caused by the change in ancillary ligand, Y, from DMAP to PPh₃ to CO. As the π-electron-accepting ability of the ancillary ligand, Y, increases from DMAP to PPh₃ to CO, additional electron density is removed from the iridium center. This renders the metal to ligand charge transfer process more energetic and hence increases the energy of MLCT state further. Table 6.4 comprises a summary of the spectral features from the absorption spectra of the iridium(III) complexes **50**, **52**, **54**, **55**, **59** and **60**, in aerated dichloromethane, including extinction coefficients.

Table 6.4 Absorption spectra features and extinction coefficients (ε) of Ir(L)₂Cl(Y) complexes in aerated dichloromethane at 298 K.

Complex	Synthesis Number (Chapter 3)	Absorption λ / nm (ε / 10 ³ dm ³ mol ⁻¹ cm ⁻¹)
Ir(ppy) ₂ Cl(CO)	50	231 (29.5), 262 (24.1), 274 (22.0), 300 (12.2), 316 (10.7), 350 (5.9), 364 (4.6)
Ir(ppy) ₂ Cl(PPh ₃)	52	232 (43.9), 260 (37.7), 295 (16.6), 332 (7.6), 354 (5.2), 390 (3.8)
Ir(ppy) ₂ Cl(Ph ₂ PPhCO ₂ H)	54	230 (49.5), 257 (39.9), 295 (20.8), 345 (6.5), 390 (3.8), 425 (1.5)
Ir(ppy) ₂ Cl(DMAP)	55	276 (4304), 307 (1806), 340 (7.3), 376 (3.8), 407 (2.9), 450 (10.1)
Ir(F ₂ ppy) ₂ Cl(CO)	59	230 (33.6), 255 (27.3), 272 (21.1), 310 (14.6), 338 (7.4), 360 (2.2)
Ir(F ₂ ppy) ₂ Cl(PPh ₃)	60	231 (48.5), 253 (38.0), 283 (17.1), 307 (13.3), 335 (6.4), 378 (3.5)

The values obtained for the extinction coefficients are similar to those obtained for triply *ortho*-metalated complexes,¹¹ and bis-cyclometalated species of similar structure.^{8,10}

6.5 Luminescence properties

6.5.1 Steady-State Spectra

As previously described by King *et al.*¹ the character of the emissive states of these $\text{Ir(L)}_2\text{X(Y)}$ type complexes changes according to the π -accepting ability of ligand Y. Due to strong σ -donation from the C-bonded ppy ligands, the metal centres in these kinds of complexes possess increased electron density. This proves to lower the energy of the metal to π -acceptor transitions. The MLCT character of the emissive state is therefore greatest in complexes where there are the maximum number of Ir-C bonds and the presence of a good delocalised π -acceptor ligand with relatively high energy ligand centred (LC) excited states, i.e. $\text{Ir(ppy)}_2\text{Cl(pyr)}$. On the other hand, the degree of LC character of the emissive state is greatest when there are fewer Ir-C bonds and the presence of a more localised π -accepting ligand with low energy LC excited states, i.e. $\text{Ir(ppy)}_2\text{Cl(CO)}$.

The room temperature luminescence spectra of a selection of $\text{Ir(L)}_2\text{X(Y)}$ complexes from species 50-60, in degassed dichloromethane is shown in figure 6.5.

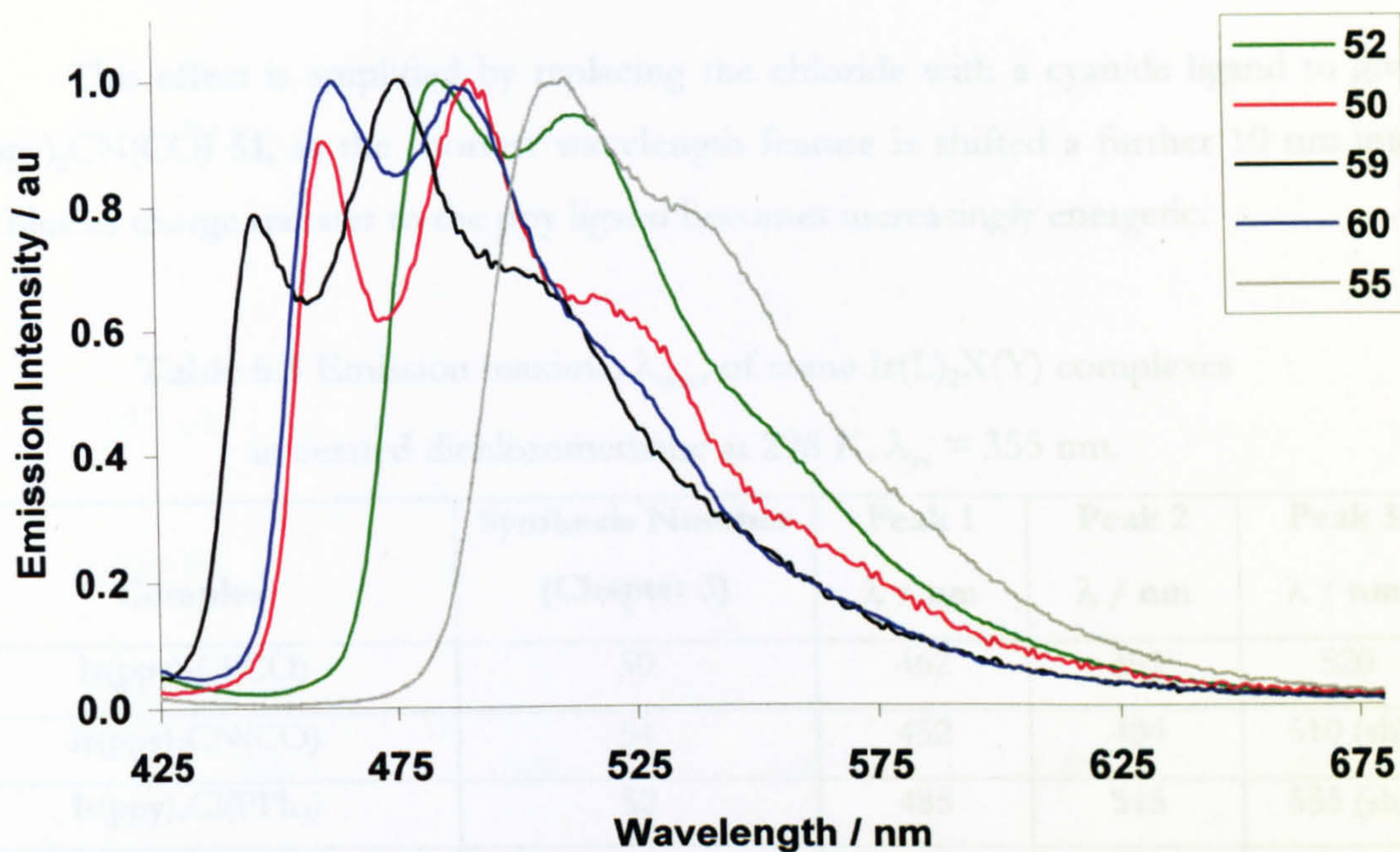


Figure 6.5 Normalised luminescence spectra of $\text{Ir(ppy)}_2\text{Cl(CO)}$ **50**, $\text{Ir(ppy)}_2\text{Cl(PPh}_3\text{)}$ **52**, $\text{Ir(ppy)}_2\text{Cl(DMAP)}$ **55**, $\text{Ir(F}_2\text{ppy)}_2\text{Cl(CO)}$ **59**, $\text{Ir(F}_2\text{ppy)}_2\text{Cl(PPh}_3\text{)}$ **60**, in aerated dichloromethane at 298 K, $\lambda_{\text{ex}} = 355$ nm.

The spectral details from figure 6.5 are fully summarised in table 6.5. The highest energy wavelength feature in the spectra is blue-shifted from 510 nm to 460 nm upon changing the ancillary ligand, Y, from DMAP to PPh_3 to CO. These trends correlate with an increase in the π -accepting ability of the variable ligand Y, in the series DMAP, PPh_3 , CO from left to right.

The luminescent excited state of $\text{Ir(ppy)}_2\text{Cl(DMAP)}$ **55** is assigned as MLCT to the ppy ligand, however the vibrational structure seen in this emission spectra also indicates the presence of some $^3\pi\text{-}\pi^*$ (LC) character in the excited state. When DMAP is replaced with PPh_3 the MLCT state is moved up in energy as electron density from the iridium center is removed by π -back-bonding. Electrons are donated into the anti-bonding π^* orbital of PPh_3 , thus rendering charge transfer to the ppy ligand more difficult. In agreement with King *et al.*¹ the introduction of the CO ligand, which allows strongly localised π -back-bonding into the anti-bonding π^* orbital of CO, moves the energy of the MLCT state above that of the LC excited state. The result is an emissive excited state with increased LC character whose emission spectrum possesses additional vibrational structure.

This effect is amplified by replacing the chloride with a cyanide ligand to give $\text{Ir(ppy)}_2\text{CN(CO)}$ **51**, as the shortest wavelength feature is shifted a further 10 nm into the blue as charge transfer to the ppy ligand becomes increasingly energetic.

Table 6.5 Emission maxima, λ_{max} , of some $\text{Ir(L)}_2\text{X(Y)}$ complexes in aerated dichloromethane at 298 K, $\lambda_{\text{ex}} = 355$ nm.

Complex	Synthesis Number (Chapter 3)	Peak 1 λ / nm	Peak 2 λ / nm	Peak 3 λ / nm
$\text{Ir(ppy)}_2\text{Cl(CO)}$	50	462	492	520
$\text{Ir(ppy)}_2\text{CN(CO)}$	51	452	484	510 (sh)
$\text{Ir(ppy)}_2\text{Cl(PPh}_3\text{)}$	52	485	515	555 (sh)
$\text{Ir(ppy)}_2\text{CN(PPh}_3\text{)}$	53	468	500	530 (sh)
$\text{Ir(ppy)}_2\text{Cl(Ph}_2\text{PPhCO}_2\text{H)}$	54	485	512 (sh)	-
$\text{Ir(ppy)}_2\text{Cl(DMAP)}$	55	510	540 (sh)	570 (sh)
$\text{Ir(F}_2\text{ppy)}_2\text{Cl(CO)}$	59	447	477	510
$\text{Ir(F}_2\text{ppy)}_2\text{Cl(PPh}_3\text{)}$	60	462	490	550 (sh)

sh = shoulder

As observed with the triply *ortho*-metalated complexes in chapter 5, the vibrational structure of the emission spectra of these complexes can also arise from inherent mixing of the excited MLCT state with LC transitions. The additional shift towards an excited state with increased LC character is provided by the addition of strong σ -donors and π -acceptors such as CO.

In addition to this, the emission wavelength may also be tuned by altering the cyclometalating ligand. A shift of ~ 15 nm to the blue is observed by replacing ppy in complex $\text{Ir(ppy)}_2\text{Cl(CO)}$ **50** with F_2ppy in complex $\text{Ir(F}_2\text{ppy)}_2\text{Cl(CO)}$ **59**. This effect is in concurrence with the wavelength shift seen with the triply cyclometalated complexes *fac*- Ir(ppy)_3 **30** and $\text{Ir(F}_2\text{ppy)}_2\text{acac}$ **38**. These complexes exhibit the most blue shifted emission reported for iridium(III) complexes so far.

The degassed and aerated luminescence spectra of $\text{Ir(F}_2\text{ppy)}_2\text{Cl(CO)}$ **59** and $\text{Ir(F}_2\text{ppy)}_2\text{Cl(PPh}_3\text{)}$ **60** in dichloromethane, are depicted in figures 6.6 and figure 6.7 respectively, as well as the corresponding excitation spectra for the shortest emission wavelength.

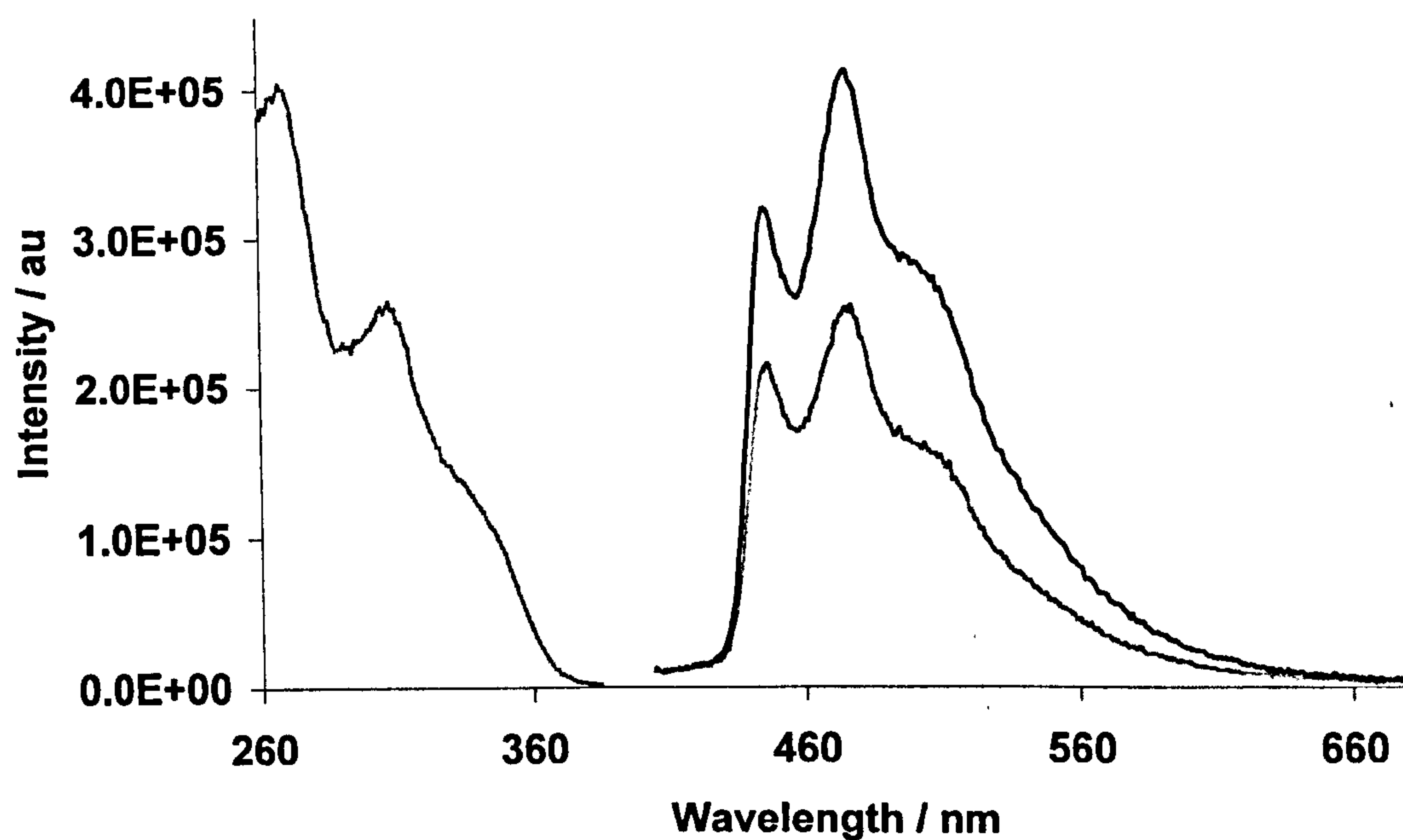


Figure 6.6 Excitation spectra (left), $\lambda_{\text{em}} = 446$ nm and luminescence spectra, $\lambda_{\text{ex}} = 355$ nm, of $\text{Ir}(\text{F}_2\text{ppy})_2\text{Cl}(\text{CO})$ **59** in degassed (black line) and aerated (dashed lines) dichloromethane at 298 K.

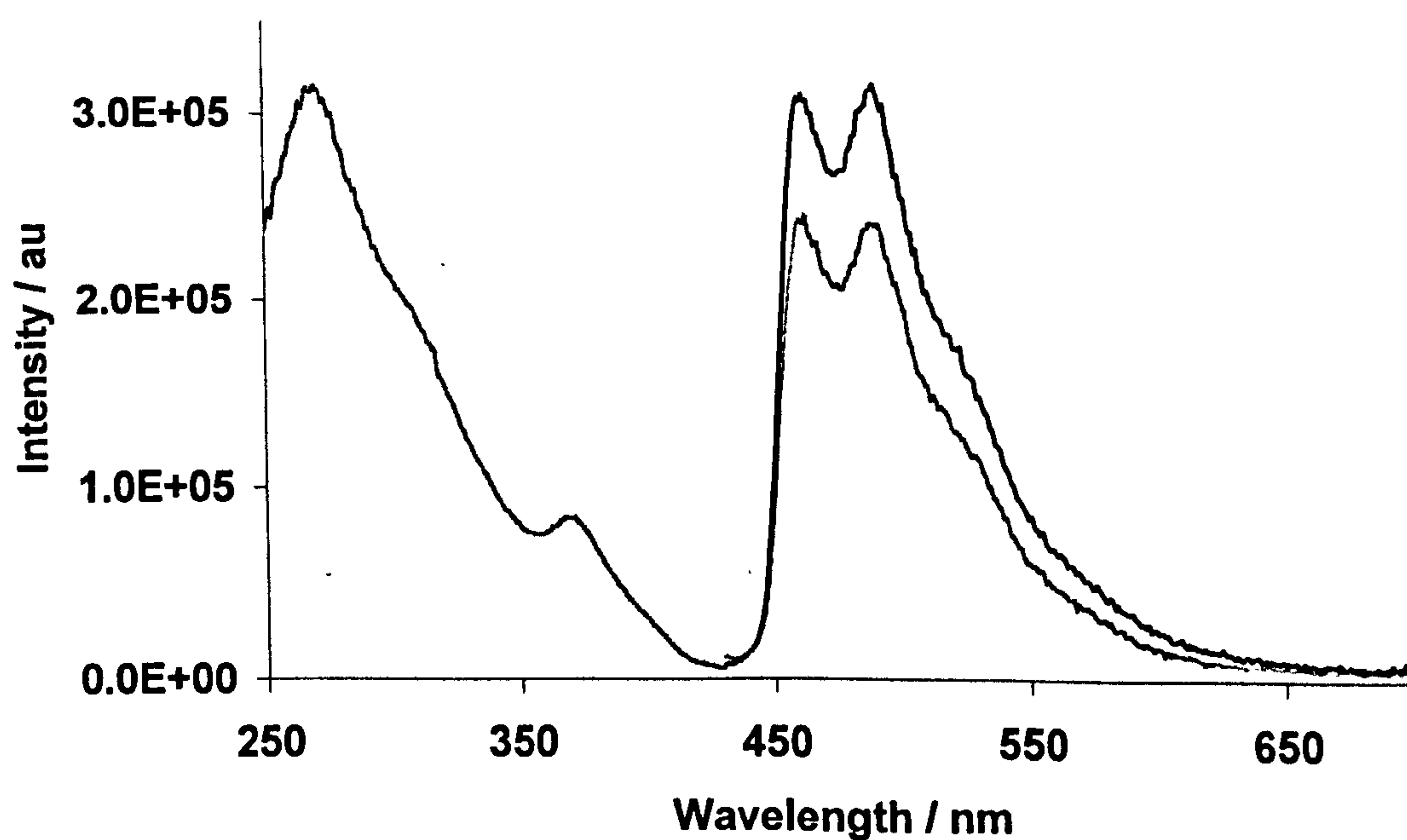


Figure 6.7 Excitation spectra (left), $\lambda_{\text{em}} = 462$ nm and luminescence spectra, $\lambda_{\text{ex}} = 355$ nm, of $\text{Ir}(\text{F}_2\text{ppy})_2\text{Cl}(\text{PPh}_3)$ **60** in degassed (black line) and aerated (dashed lines) dichloromethane at 298 K.

As illustrated in figures 6.6 and 6.7 above the profiles of the excitation spectra match that of the relevant absorption spectra, as shown in figure 6.4. In addition to this, the emission intensity increases upon degassing but the spectral profiles remain unchanged. This is indicative of phosphorescent compounds whose luminescence is quenched by oxygen.

However, the emission intensity of these iridium(III) complexes does not appear to be affected by oxygen quenching as much as the cyclometalated Ir(L)_3 and $\text{Ir(L)}_2\text{acac}$ complexes.^{7,11} The maximum emission intensity of *fac*- $\text{Ir}(\text{Cyclohex})_3$ 44 in dichloromethane, was found to increase by a factor of 33.5 upon degassing. In contrast to this, the maximum emission intensities of complexes $\text{Ir}(\text{F}_2\text{ppy})_2\text{Cl}(\text{CO})$ 59, $\lambda_{\text{max}} = 477 \text{ nm}$, and $\text{Ir}(\text{F}_2\text{ppy})_2\text{Cl}(\text{PPh}_3)$ 60 $\lambda_{\text{max}} = 462 \text{ nm}$, are found to increase by factors of 1.7 and 1.3 respectively. This indicates that for $\text{Ir(L)}_2\text{X(Y)}$ species where $\text{Y} = \text{CO}$, PPh_3 and $\text{Ph}_2\text{PPhCO}_2\text{H}$ the luminescent lifetimes at 298 K are much shorter than those of Ir(L)_3 and $\text{Ir(L)}_2\text{acac}$ complexes. Hence the excited states of these $\text{Ir(L)}_2\text{X(Y)}$ complexes are less affected by oxygen quenching.

6.6 Time Resolved Emission Spectroscopy (TRES)

6.6.1 Luminescence Lifetimes

The luminescence lifetimes of the $\text{Ir(L)}_2\text{X(Y)}$ complexes at 298 K are listed in table 6.6. In degassed dichloromethane, the longer microsecond lifetimes listed for $\text{Ir(ppy)}_2\text{Cl(DMAP)}$ 55 are in stark contrast to the nanosecond lifetimes listed for the other complexes. This illustrates the differences between complexes that possess varying degrees of $^3\text{MLCT}$ and ^3LC character in their lowest energy excited state. The lowest energy excited state for complex 55 can be assigned as $^3\text{MLCT}$ due to its long lifetime. However, the shorter luminescence lifetimes of complexes 50, 52, 54, 59 and 60 indicate that there are different emitting states involved. The presence of the ancillary ligands, CO , PPh_3 and $\text{Ph}_2\text{PPhCO}_2\text{H}$, increase the energy of the $^3\text{MLCT}$ due to π -back-bonding. The $^3\text{MLCT}$ and ^3LC states can now be considered as closer in energy than those of triply *ortho*-metalated complexes, such as *fac*- Ir(ppy)_3 30.

As illustrated in figures 6.6 and 6.7 above the profiles of the excitation spectra match that of the relevant absorption spectra, as shown in figure 6.4. In addition to this, the emission intensity increases upon degassing but the spectral profiles remain unchanged. This is indicative of phosphorescent compounds whose luminescence is quenched by oxygen.

However, the emission intensity of these iridium(III) complexes does not appear to be affected by oxygen quenching as much as the cyclometalated $\text{Ir}(\text{L})_3$ and $\text{Ir}(\text{L})_2\text{acac}$ complexes.^{7,11} The maximum emission intensity of *fac*- $\text{Ir}(\text{Cyclohex})_3$ 44 in dichloromethane, was found to increase by a factor of 33.5 upon degassing. In contrast to this, the maximum emission intensities of complexes $\text{Ir}(\text{F}_2\text{ppy})_2\text{Cl}(\text{CO})$ 59, $\lambda_{\text{max}} = 477$ nm, and $\text{Ir}(\text{F}_2\text{ppy})_2\text{Cl}(\text{PPh}_3)$ 60 $\lambda_{\text{max}} = 462$ nm, are found to increase by factors of 1.7 and 1.3 respectively. This indicates that for $\text{Ir}(\text{L})_2\text{X}(\text{Y})$ species where $\text{Y} = \text{CO}$, PPh_3 and $\text{Ph}_2\text{PPhCO}_2\text{H}$ the luminescent lifetimes at 298 K are much shorter than those of $\text{Ir}(\text{L})_3$ and $\text{Ir}(\text{L})_2\text{acac}$ complexes. Hence the excited states of these $\text{Ir}(\text{L})_2\text{X}(\text{Y})$ complexes are less affected by oxygen quenching.

6.6 Time Resolved Emission Spectroscopy (TRES)

6.6.1 Luminescence Lifetimes

The luminescence lifetimes of the $\text{Ir}(\text{L})_2\text{X}(\text{Y})$ complexes at 298 K are listed in table 6.6. In degassed dichloromethane, the longer microsecond lifetimes listed for $\text{Ir}(\text{ppy})_2\text{Cl}(\text{DMAP})$ 55 are in stark contrast to the nanosecond lifetimes listed for the other complexes. This illustrates the differences between complexes that possess varying degrees of $^3\text{MLCT}$ and ^3LC character in their lowest energy excited state. The lowest energy excited state for complex 55 can be assigned as $^3\text{MLCT}$ due to its long lifetime. However, the shorter luminescence lifetimes of complexes 50, 52, 54, 59 and 60 indicate that there are different emitting states involved. The presence of the ancillary ligands, CO , PPh_3 and $\text{Ph}_2\text{PPhCO}_2\text{H}$, increase the energy of the $^3\text{MLCT}$ due to π -back-bonding. The $^3\text{MLCT}$ and ^3LC states can now be considered as closer in energy than those of triply *ortho*-metalated complexes, such as *fac*- $\text{Ir}(\text{ppy})_3$ 30.

Table 6.6 Luminescence lifetimes (τ) of $\text{Ir}(\text{L})_2\text{X}(\text{Y})$ complexes in degassed and aerated dichloromethane at 298 K, $\lambda_{\text{ex}} = 355$ nm (aerated lifetimes in brackets).

Complex	Synthesis Number (Chapter 3)	Peak 1 τ / ns	Peak 2 τ / ns	Peak 3 τ / ns
$\text{Ir}(\text{ppy})_2\text{Cl}(\text{CO})$	50	140 (108)	130 (109)	150 (104)
$\text{Ir}(\text{ppy})_2\text{Cl}(\text{PPh}_3)$	52	50 (35)	50 (36)	60 (35)
$\text{Ir}(\text{ppy})_2\text{Cl}(\text{Ph}_2\text{PPhCO}_2\text{H})$	54	30 (19)	30 (23)	-
$\text{Ir}(\text{ppy})_2\text{Cl}(\text{DMAP})$	55	1700 (70)	1740 (68)	1790 (64)
$\text{Ir}(\text{F}_2\text{ppy})_2\text{Cl}(\text{CO})$	59	300 (266)	320 (290)	300 (261)
$\text{Ir}(\text{F}_2\text{ppy})_2\text{Cl}(\text{PPh}_3)$	60	70 (49)	70 (51)	80 (57)

The room temperature lifetimes for complexes 50 and 52 are the same, within experimental error, as those reported by King *et al.*,¹ $\tau = 110$ ns and $\tau = 47$ ns, respectively. The aerated lifetime of $\text{Ir}(\text{ppy})_2\text{Cl}(\text{DMAP})$ is very similar to that obtained by DeRosa *et al.*⁸ for $\text{Ir}(\text{ppy})_2\text{Cl}(\text{vpy})$ in toluene $\tau = 60$ ns, where vpy = 4-vinylpyridine. The lifetimes of the other complexes reported in this table fit well with these literature values.

The low temperature, 77 K, lifetimes of these complexes in EPA (ethanol: iso-pentane: diethyl ether) also illustrate this change in emissive state, table 6.7.

As inferred by Colombo *et al.*,¹² who studied the mixed ligand complex $[\text{Ir}(\text{ppy})_2(\text{bpy})]\text{PF}_6$, for complexes that possess $^3\text{MLCT}$ and ^3LC ($^3\pi\text{-}\pi^*$) states of similar energy, the lowest energy excited state depends upon the environment. In solutions and glasses at room temperature the $^3\text{MLCT}$ is stabilised with respect to the ^3LC state, whilst in crystalline hosts at low temperatures this order is reversed. The enhanced rigidity of the glass moves the $^3\text{MLCT}$ state up in energy when the temperature is lowered. At some point the energy of the $^3\text{MLCT}$ state will cross that of the ^3LC state, which will then become the emitting state.

Due to the broad inhomogeneous distribution of sites in the glass, Colombo *et al.*,¹² concluded that there must be excited state complexes on both sides of the crossing point. As a result of this they observed a superposition of both the $^3\text{MLCT}$ and ^3LC luminescence of $[\text{Ir}(\text{ppy})_2(\text{bpy})]\text{PF}_6$ at low temperatures. At 10 K the ^3LC state became the emitting state.

Table 6.7 Luminescence lifetimes (τ) of $\text{Ir}(\text{L})_2\text{X}(\text{Y})$ complexes
in aerated EPA at 77 K, $\lambda_{\text{ex}} = 355 \text{ nm}$, λ_{max} (nm) in brackets.

Complex	Number (Chapter 3)	$\tau \pm 10\%$ ($\lambda_{\text{max}} / \text{nm}$)
$\text{Ir}(\text{ppy})_2\text{Cl}(\text{CO})$	50	31 μs (458) $\tau_1 = 30 \mu\text{s}$, $A_1 = 0.61$, $\tau_2 = 3.3 \mu\text{s}$, $A_2 = 0.39$ (490) $\tau_1 = 31 \mu\text{s}$, $A_1 = 0.43$, $\tau_2 = 5.3 \mu\text{s}$, $A_2 = 0.57$ (520)
$\text{Ir}(\text{ppy})_2\text{Cl}(\text{PPh}_3)$	52	5.9 μs (473), 5.5 μs (505), 5.4 μs (535)
$\text{Ir}(\text{ppy})_2\text{Cl}(\text{Ph}_2\text{PPhCO}_2\text{H})$	54	5.9 μs (473), 5.5 μs (505), 5.2 μs (525)
$\text{Ir}(\text{ppy})_2\text{Cl}(\text{DMAP})$	55	3.9 μs (490), 4.3 μs (528), 4.6 μs (570)
$\text{Ir}(\text{F}_2\text{ppy})_2\text{Cl}(\text{CO})$	59	35 μs (440) $\tau_1 = 32 \mu\text{s}$, $A_1 = 0.93$, $\tau_2 = 3.3 \mu\text{s}$, $A_2 = 0.07$ (472) $\tau_1 = 38 \mu\text{s}$, $A_1 = 0.15$, $\tau_2 = 3.7 \mu\text{s}$, $A_2 = 0.85$ (505)
$\text{Ir}(\text{F}_2\text{ppy})_2\text{Cl}(\text{PPh}_3)$	60	5.5 μs (453), 5.4 μs (485), 5.6 μs (560)

The differences in the lifetimes of the complexes listed in table 6.5 serve to support this argument of fluctuating $^3\text{MLCT}$ and ^3LC levels. The low temperature lifetimes of complexes $\text{Ir}(\text{ppy})_2\text{Cl}(\text{CO})$ 50 and $\text{Ir}(\text{F}_2\text{ppy})_2\text{Cl}(\text{CO})$ 59, of their highest energy features, are found to be mono-exponential. These long microsecond lifetimes are in accord with that of $\text{Ir}(\text{ppy})_2\text{Cl}(\text{CO})$, $\tau = 28 \mu\text{s}$, reported by King *et al.*¹ and are typical of ^3LC ($^3\pi\text{-}\pi^*$) states.^{6,12} The bi-exponential lifetimes of complexes 50 and 59 at longer wavelengths serve to illustrate the superimposition of both the $^3\text{MLCT}$ and ^3LC luminescence of these species at low temperature, indicating that these two states possess similar energies at 77K. The time-resolved emission spectra of $\text{Ir}(\text{ppy})_2\text{Cl}(\text{CO})$ 50 and $\text{Ir}(\text{F}_2\text{ppy})_2\text{Cl}(\text{CO})$ 59 are shown in figure 6.8. Figure 6.9 illustrates the 77 K emission spectra for $\text{Ir}(\text{F}_2\text{ppy})_2\text{Cl}(\text{CO})$ 59 at different time intervals. The emission of $\text{Ir}(\text{F}_2\text{ppy})_2\text{Cl}(\text{CO})$ 59 at $t = 0\text{-}5 \mu\text{s}$ (solid line) exhibits greater intensities at longer wavelengths. At the longer time interval, $t = 40\text{-}80 \mu\text{s}$ (dashed line) emission intensities at the shorter wavelengths are greatest. This indicates that the bluer shifted emission wavelengths ($\tau \sim 35 \mu\text{s}$) derive from a ^3LC excited state and the longer emission wavelengths ($\tau \sim 3 \mu\text{s}$) derive from a mixed $^3\text{MLCT/LC}$ excited state.

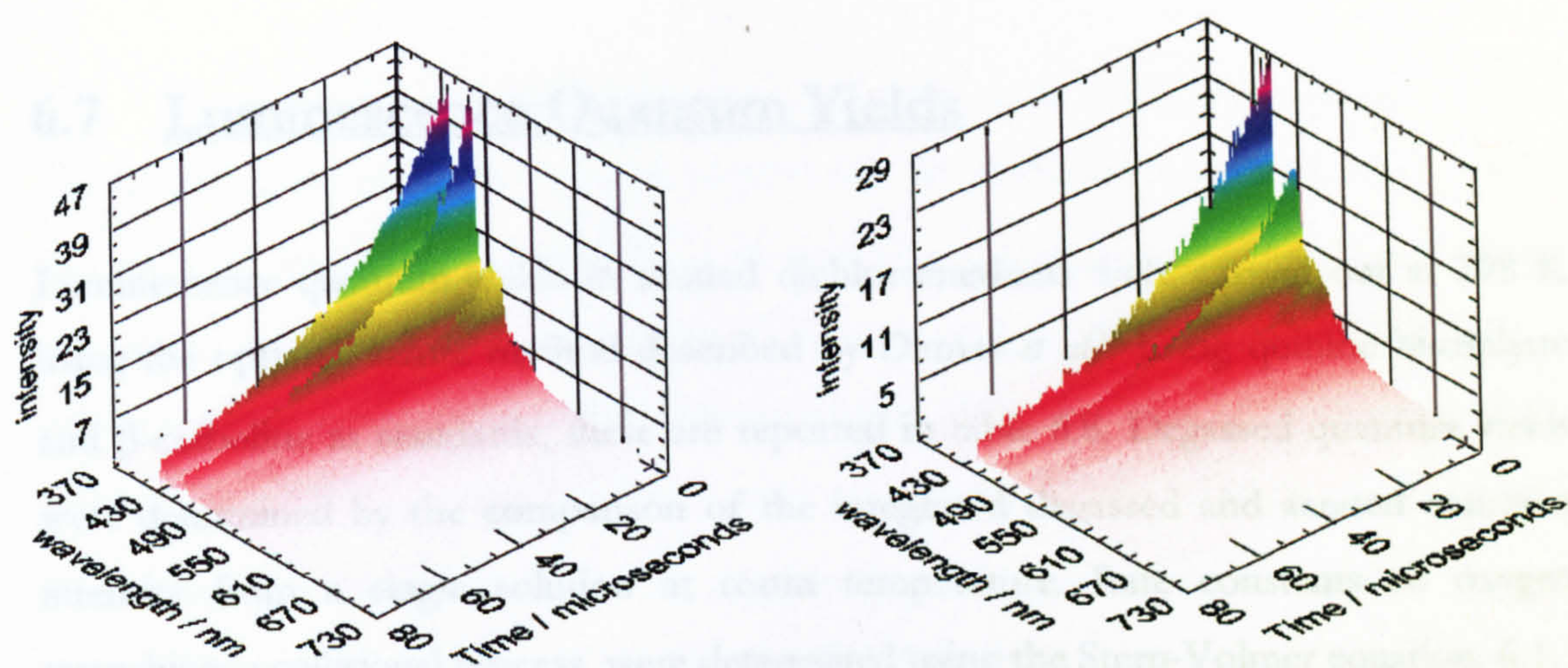


Figure 6.8 Time-resolved low temperature luminescence spectra of Ir(ppy)₂Cl(CO) **50** (left) and Ir(F₂ppy)₂Cl(CO) **59** (right) in EPA at 77 K, $\lambda_{\text{ex}} = 355$ nm.

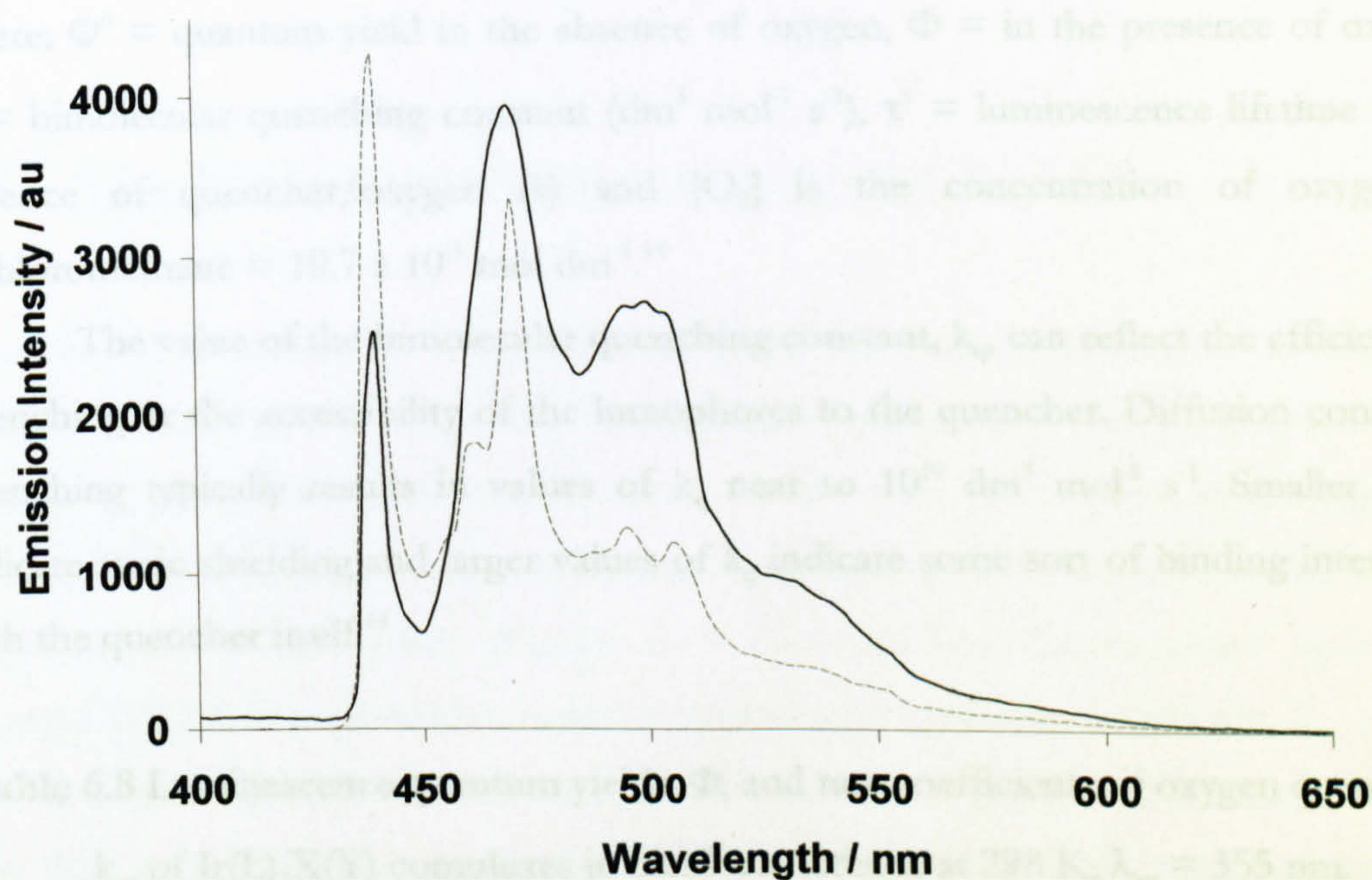


Figure 6.9 Time-resolved low temperature luminescence spectra of Ir(F₂ppy)₂Cl(CO) **59** in EPA at 77 K, $\lambda_{\text{ex}} = 355$ nm, $t = 0-5$ μs (solid line) and $t = 40-80$ μs (dashed line).

In contrast to this, complexes Ir(ppy)₂Cl(PPh₃) **52**, Ir(ppy)₂Cl(Ph₂PPhCO₂H) **54**, Ir(ppy)₂Cl(DMAP) **55** and Ir(F₂ppy)₂Cl(PPh₃) **60** exhibit mono-exponential lifetimes at all emission wavelengths. This suggests that although the ³MLCT state may have increased in energy with decreasing temperature, it has not exceeded that of the lowest energy ³LC excited state. Thus emission spectra possessing vibrational structure are seen, which most likely stem from a single ³MLCT/LC state.

6.7 Luminescence Quantum Yields

Luminescence quantum yields in aerated dichloromethane were carried out at 298 K using the optically dilute method described by Demas *et al.*,¹³ using quinine bisulphate and β -carboline as standards, these are reported in table 6.8. Degassed quantum yields were determined by the comparison of the integrated degassed and aerated emission intensity from a single solution at room temperature. Rate constants of oxygen quenching, a collisional process, were determined using the Stern-Volmer equation, 6.1.

$$\Phi^0/\Phi = 1 + k_q\tau^0[\text{O}_2] \quad 6.1$$

where; Φ^0 = quantum yield in the absence of oxygen, Φ = in the presence of oxygen, k_q = bimolecular quenching constant ($\text{dm}^3 \text{mol}^{-1} \text{s}^{-1}$), τ^0 = luminescence lifetime in the absence of quencher/oxygen (s) and $[\text{O}_2]$ is the concentration of oxygen in dichloromethane = $10.7 \times 10^{-3} \text{mol dm}^{-3}$.¹⁴

The value of the bimolecular quenching constant, k_q , can reflect the efficiency of quenching or the accessibility of the lumophores to the quencher. Diffusion controlled quenching typically results in values of k_q near to $10^{10} \text{dm}^3 \text{mol}^{-1} \text{s}^{-1}$. Smaller values indicate steric shielding and larger values of k_q indicate some sort of binding interaction with the quencher itself.¹⁵

Table 6.8 Luminescence quantum yields, Φ , and rate coefficients of oxygen quenching, k_q , of $\text{Ir}(\text{L})_2\text{X}(\text{Y})$ complexes in dichloromethane at 298 K, $\lambda_{\text{ex}} = 355 \text{ nm}$.

Complex	Synthesis Number (Chapter 3)	Φ (aerated)	Φ (degassed)	$k_q / \text{dm}^3 \text{mol}^{-1} \text{s}^{-1}$
$\text{Ir}(\text{ppy})_2\text{Cl}(\text{CO})$	50	0.0022	0.0027	1.6×10^8
$\text{Ir}(\text{ppy})_2\text{Cl}(\text{PPh}_3)$	52	0.0048	0.0074	9.4×10^8
$\text{Ir}(\text{ppy})_2\text{Cl}(\text{Ph}_2\text{PPhCO}_2\text{H})$	54	0.0031	0.0047	1.5×10^9
$\text{Ir}(\text{ppy})_2\text{Cl}(\text{DMAP})$	55	0.020	0.42	1.1×10^9
$\text{Ir}(\text{F}_2\text{ppy})_2\text{Cl}(\text{CO})$	59	0.0037	0.0038	3.3×10^8
$\text{Ir}(\text{F}_2\text{ppy})_2\text{Cl}(\text{PPh}_3)$	60	0.0063	0.0080	3.6×10^8

In general the aerated and degassed quantum yields of these complexes are low. The aerated quantum yields for these compounds are of the same order of magnitude as that reported for $[\text{Rh}(\text{ppy})_2(\text{CN})_2]\text{Bu}_4\text{N}$, $\Phi = 0.006$, in aerated acetonitrile.¹⁰ In contrast to this, the degassed luminescent quantum yield for $\text{Ir}(\text{ppy})_2\text{Cl}(\text{DMAP})$ **55**, $\Phi = 0.42$, is similar to those reported for cyclometalated iridium(III) complexes of the formula $\text{Ir}(\text{L})_3$ and $\text{Ir}(\text{L})_2\text{acac}$.^{7,11} The aerated quantum yield of complex **55**, $\Phi = 0.02$, is comparable to that reported by DeRosa *et al.*⁸ for $\text{Ir}(\text{ppy})_2\text{Cl}(\text{vpy})$ in aerated toluene, $\Phi = 0.06$.

The estimated values of the bimolecular quenching constants, k_q , were all found to be less than $10^{10} \text{ dm}^3 \text{ mol}^{-1} \text{ s}^{-1}$ and therefore indicate that the quenching processes involved with these complexes are limited by some degree of steric shielding of the luminescent core.

6.8 The Photodegradation of $\text{Ir}(\text{ppy})_2\text{CN}(\text{CO})$

The photodegradation of $\text{Ir}(\text{ppy})_2\text{CN}(\text{CO})$ **51** was initially observed in degassed dichloromethane whilst measuring luminescence lifetimes. However, cyclometalated iridium(III) complexes have already been shown to be photoactive in deoxygenated halogenated solvents,¹⁶ therefore benzene, a non-ligating and non-halogenated solvent, was chosen for this study. Figure 6.10 illustrates the luminescence spectra of $\text{Ir}(\text{ppy})_2\text{CN}(\text{CO})$ in degassed benzene before and after irradiation at 365 nm.

The comparison of the proton NMR spectra in degassed d_6 -benzene before and after 365 nm irradiation shows the loss of starting material to form a species that possesses chemically equivalent cyclometalating ligands. The formation of such a species is possible by the loss of either the carbonyl or cyanide ligand. The electrospray mass spectrometry data shows that the carbonyl is lost before the cyanide, suggesting that the iridium-carbonyl bond is the most susceptible to cleavage.

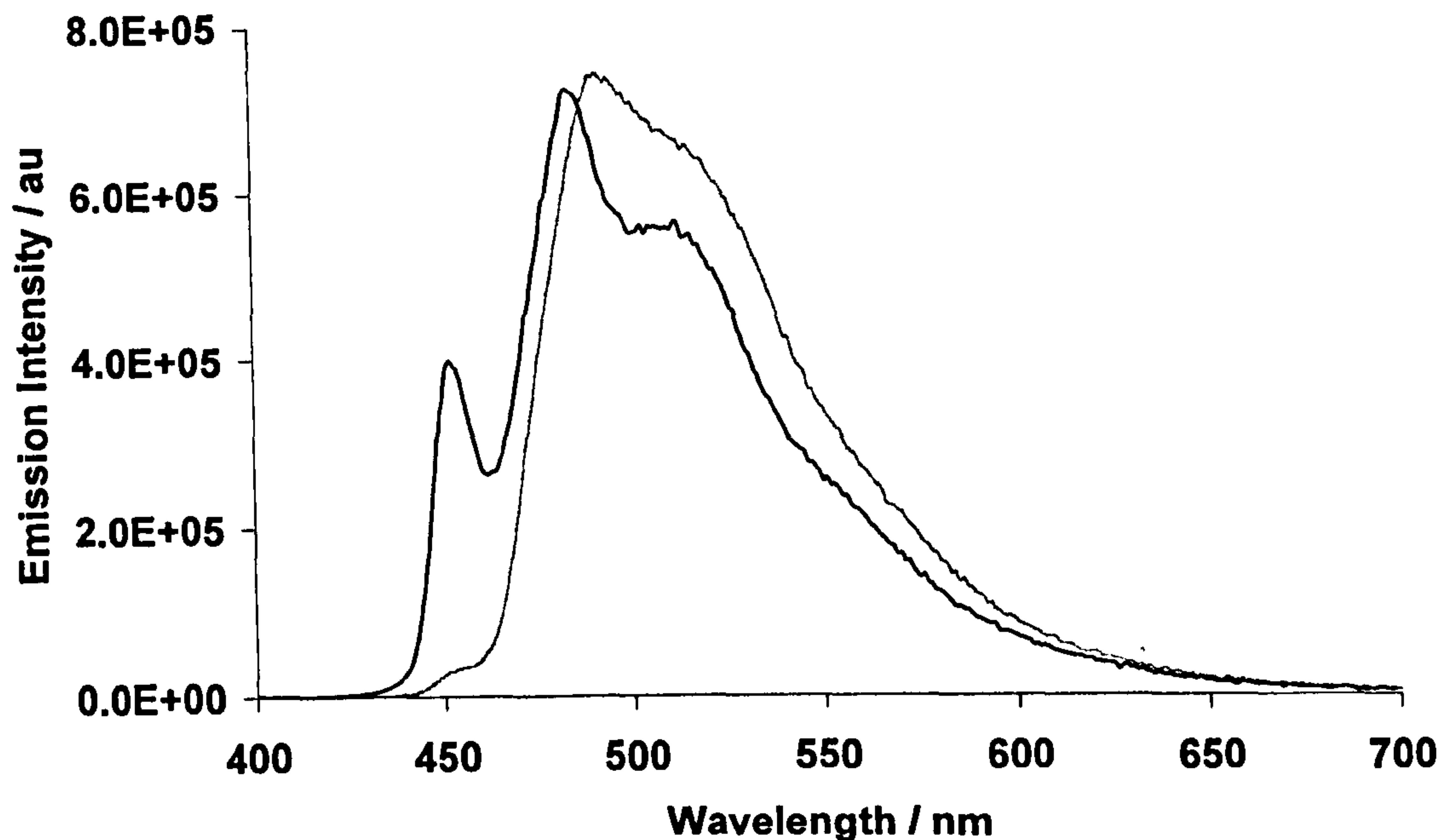


Figure 6.10 Luminescence spectra of Ir(ppy)₂CN(CO) **51** in degassed benzene at 298 K, before (black line) and after (dashed line) irradiation at $\lambda_{\text{ex}} = 365$ nm.

The luminescence of these Ir(L)₂X(Y) complexes has previously been described, section 6.5.1, as having both LC and MLCT character. The addition of an ancillary ligand, Y, such as CO that has strong localised π -back-bonding increases the energy of MLCT transitions so that they are similar to that of the LC transitions. This causes a hypsochromic shift of the emission spectra.

Upon irradiation, the bluest emission peak of Ir(ppy)₂CN(CO) **51**, figure 6.9, decreases dramatically in intensity, whereas the other two emission maxima seem only to be red-shifted by ~ 5 -10 nm. These longer emission wavelengths are typical of those expected from a bis- or tris-cyclometalated species,⁷ i.e. emission from a ³MLCT state. This also indicates the loss of either a carbonyl or cyanide ligand from the starting material species. This process is also indicated by the absorption spectra of Ir(ppy)₂CN(CO) in degassed benzene, figure 6.11. The longest wavelength absorption bands of the starting material are seen to decrease in intensity upon irradiation and the growth of a longer wavelength band is observed. This broad absorption band, which reaches into the visible region of the spectrum, is characteristic for a ³MLCT transition, and hence for a ³MLCT emitting species, such as *fac*-Ir(ppy)₃.⁷

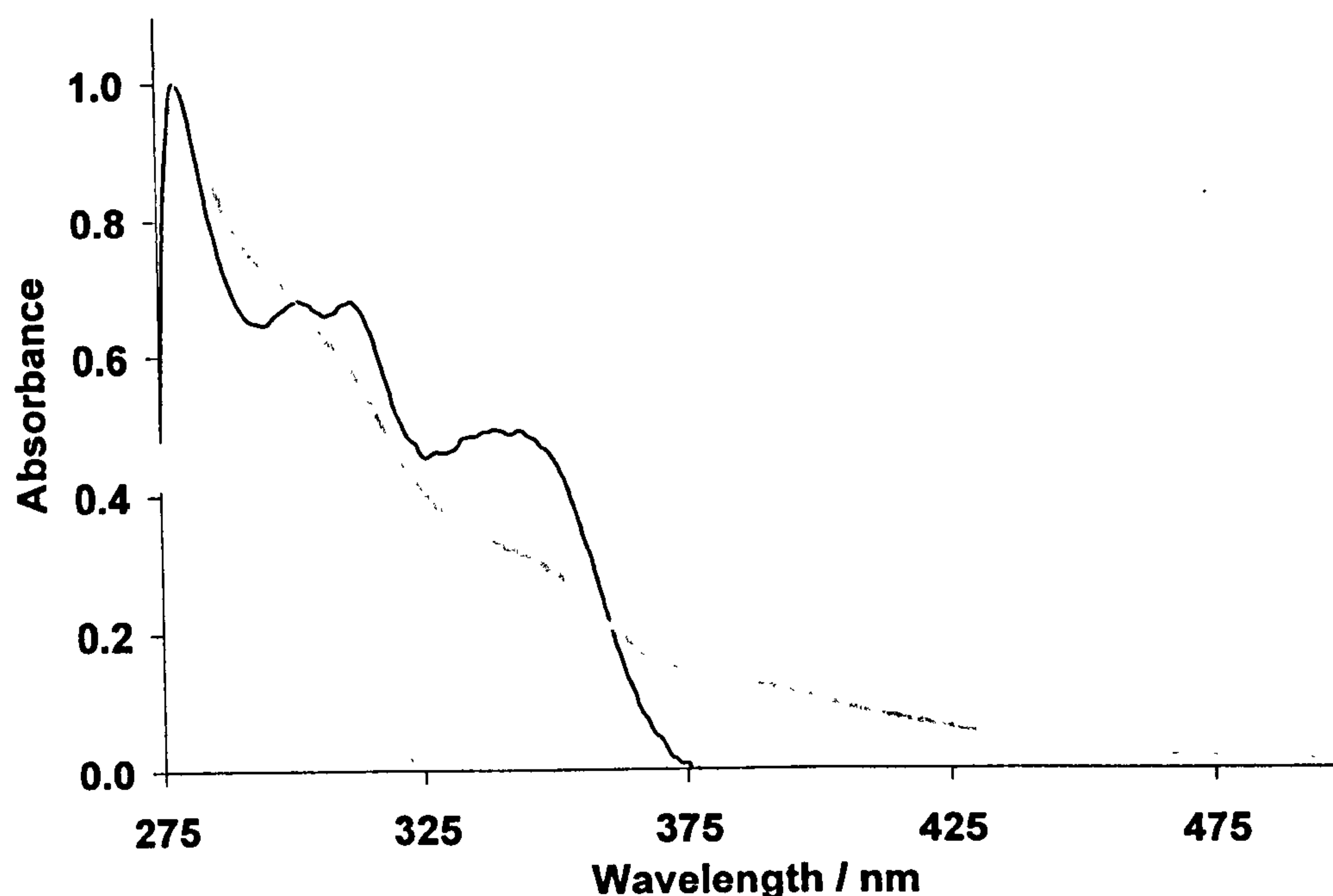


Figure 6.11 Normalised absorption spectra of Ir(ppy)₂CN(CO) **51** in degassed benzene at 298 K, before (black line) and after (dashed line) irradiation at $\lambda_{\text{ex}} = 365$ nm.

Work carried out by Heberhold *et al.*¹⁷ on carbonyl complexes of chromium, molybdenum and tungsten illustrates that the loss of a single carbonyl group occurs with ease in daylight and occurs at an even faster rate upon UV irradiation. This is therefore a likely scenario for these iridium carbonyl complexes. The loss of a cyanide ligand is less likely as this would leave a charged species and is therefore the more energetic process.

The electrospray mass spectrometry data for the irradiated species did not yield any insight to any other possible stable photoproducts of this reaction. It is possible that solvent molecules are able to fill the free co-ordination site.

6.9 The Interaction of *Rac*-Ir(ppy)₂Cl(TAT) with DNA

The use of metalointercalators as non-radioactive probes for DNA has been a growing topic of research over the last decade. During this time ruthenium(II) complexes, such as $[\text{Ru}(\text{phen})_2(\text{dpq})]_2^+$, where phen = 1,10-phenanthroline and

dpq = dipyrido[3,2-a:2'3'-c]-quinoxaline are the ancillary and intercalating ligands respectively, have been reported by Beck¹⁸ and Pellegrini.¹⁹

Beck *et al.*¹⁸ studied the ruthenium(II) metallointercalators, $[\text{Ru}(\text{phen})_3]^{2+}$ and $[\text{Ru}(\text{phen})_2(\text{dpq})]^{2+}$ which have similar charge, size and shape and were therefore expected to show a similar degree of electrostatic attraction towards the anionic phosphodiester backbone of DNA. Consequently, significant differences in DNA binding affinities of these ruthenium compounds were attributed to variations in their ability to act as minor groove binders or intercalators.

The ability of these types of compounds to act as intercalators varies as a consequence of the replacement of the 1,10-phenanthroline (phen) ligand in $[\text{Ru}(\text{phen})_3]^{2+}$ by larger ligands that can more readily insert into the DNA base stack.

Complexes containing larger ligands such as dipyrido[3,2-a:2',3'-c]phenazine (dppz) together with ancillary ligands such as phen and bpy have been studied by Friedman²⁰ and Jenkins²¹ as racemates and in their pure enantiomeric forms by Hiort *et al.*²² In these complexes charge transfer is directed from the metal centre to the phenazine ring and the major non-radiative pathway is likely to involve the protonation of the phenazine nitrogen atoms in the excited state. In aqueous solvents no luminescence is observed at ambient temperatures, however intense photoluminescence is observed in the presence of double-helical DNA.

In contrast to other ruthenium complexes, such as $\text{Ru}(\text{bpy})_3^{2+}$, the extended planar structure of dppz allows $\text{Ru}(\text{bpy})_2\text{dppz}^{2+}$ to bind to DNA by intercalation. The preferential charge transfer to the intercalating dppz ligand provides a sensitive probe for the helical DNA environment. Since then cyclometalated rhodium(III),²³ iridium(III)²⁴ and platinum(II)²⁵ complexes of a similar nature have also been studied for their use as luminescent probes for DNA.

The aim of this study was to synthesise an analogous iridium(III) complex which could undergo intercalation with DNA. The complex *rac*- $\text{Ir}(\text{ppy})_2\text{Cl}(\text{TAT})$ **57** was prepared by the following method. $[\text{Ir}(\text{ppy})_2\text{Cl}]_2$ **19** (0.053 g, 0.05 mmol) and 1,4,8,9-tetraaza-triphenylene (TAT) (0.023 g, 0.10 mmol) were suspended in dichloromethane (5 mL) and warmed gently. The reaction mixture was stirred continuously at room temperature overnight. The now clear orange solution was evaporated to dryness and the residual solid was washed repeatedly with toluene and then diethyl ether and subsequently dried under vacuum to yield **57** as a bright orange

solid (0.070 g, 91 %), figure 6.12. The higher percentage yield obtained for this iridium(III) complex compared to those for related rhodium(III) complexes²³ may be due to the more simplified synthetic pathway allowed by the ease of cleavage of the dichloro-bridged iridium(III) species and/or the greater tendency of iridium(III) over rhodium(III) to form mononuclear products.²⁶ This complex was characterised by ¹H-NMR and mass spectrometry, chapter 3.

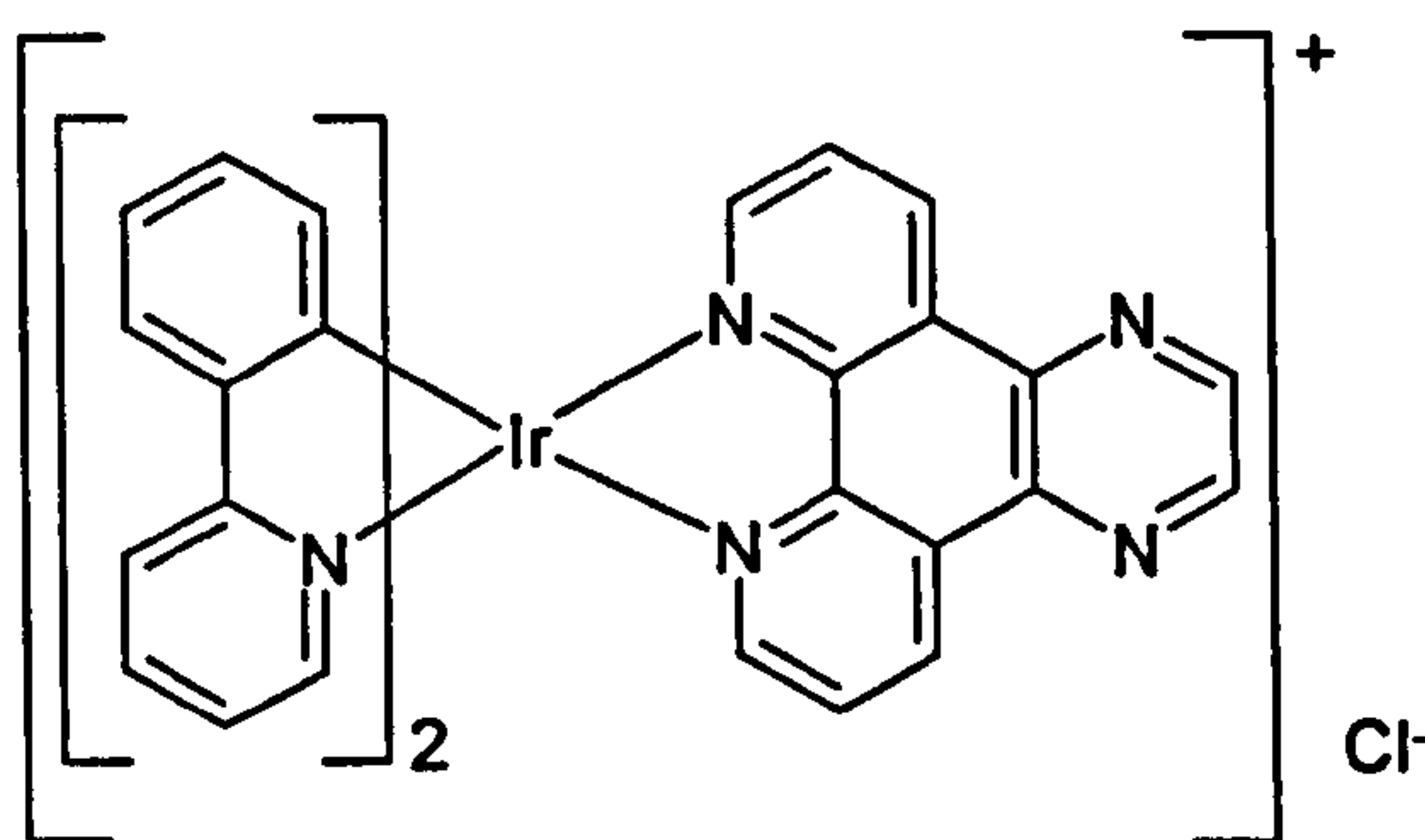


Figure 6.12 A schematic representation of *rac*-[Ir(ppy)₂(TAT)]Cl 57.

The UV-Visible absorbance and emission spectra of complex 57 dissolved in aerated 0.1 mmol HEPES/0.1 mmol NaCl solution (pH 7.4) were measured in the absence and presence of calf thymus DNA, these spectra are shown in figures 6.13 and 6.14.

The UV-visible absorption spectrum of *rac*-[Ir(ppy)₂(TAT)]Cl 57 in aerated 0.1 mmol HEPES/0.1 mmol NaCl solution is found to be similar to that of *rac*-[Ir(bpy)(phen)(phi)]³⁺²⁴ and those of *rac*-[Rh(ppy)₂chrysi]Cl and *rac*-[Rh(ppy)₂phi]Cl,²³ where chrysi = 5,6-diaminochrysene and phi = 9,10-diaminophenanthrene. The absorption bands can be assigned as ³LC (³π-π*) at ~ 210-300 nm, ¹MLCT at ~300-380 nm and ³MLCT at ~ 380-500 nm.

The addition of calf-thymus DNA causes hyperchromism of the ligand-centered absorption bands, ~ 210-300 nm, indicating a change in ligand environment. Little change in the overall shape of the spectrum is observed. This is consistent with the changes in absorption spectra seen for related ruthenium(II)²¹ complexes.

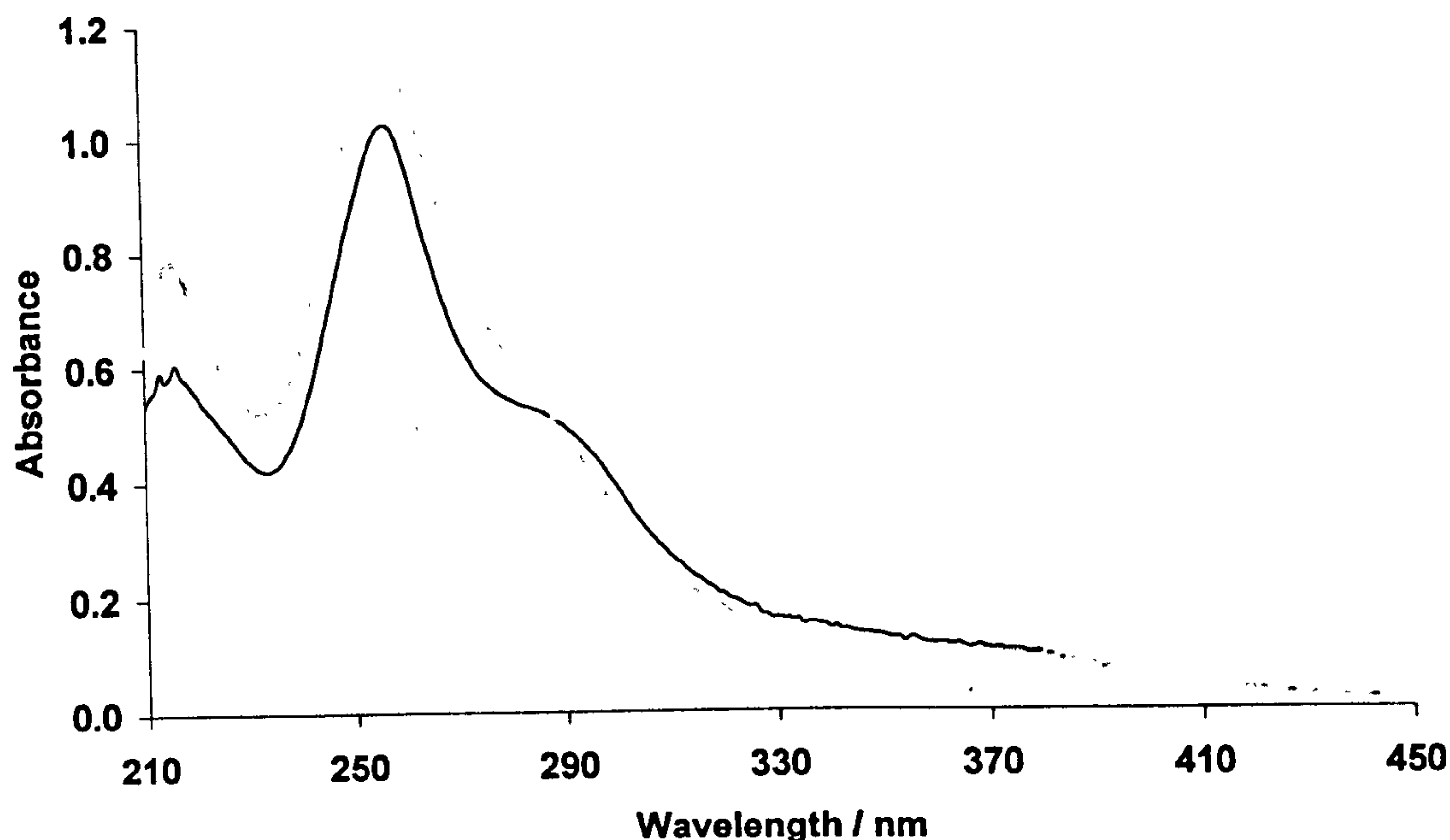


Figure 6.13 UV-Visible absorption spectra of *rac*-Ir(ppy)₂Cl(TAT) **57** in aerated 0.1 mmol HEPES/0.1 mmol NaCl buffer, pH = 7.4, in the absence (black line) and presence (dashed line) of calf thymus DNA at 298 K.

The weak photoluminescence, $\lambda_{\text{max}} \sim 610$ nm, observed for *rac*-Ir(ppy)₂Cl(TAT) **57** in buffer solution at ambient temperature can be attributed to the quenching of the luminescent excited state. Like related ruthenium(II) complexes, in aqueous solvents charge transfer in *rac*-Ir(ppy)₂Cl(TAT) **57** is likely to be directed from the metal center to the tetraaza-triphenylene (TAT) ligand and the major non-radiative pathway is likely to involve the protonation of the tetraaza-triphenylene nitrogen atoms in the excited state.

Upon addition of calf-thymus DNA, the photoluminescent intensity of *rac*-Ir(ppy)₂Cl(TAT) **57** at 610 nm increases by $I/I_0 \sim 16$. Although this is not as great an increase in intensity as that seen in platinum(II) metallointercalators, $I/I_0 = 271$, the fact remains, that this change in luminescent intensity indicates that *rac*-Ir(ppy)₂Cl(TAT) **57** interacts in some way with DNA, most likely by intercalation.

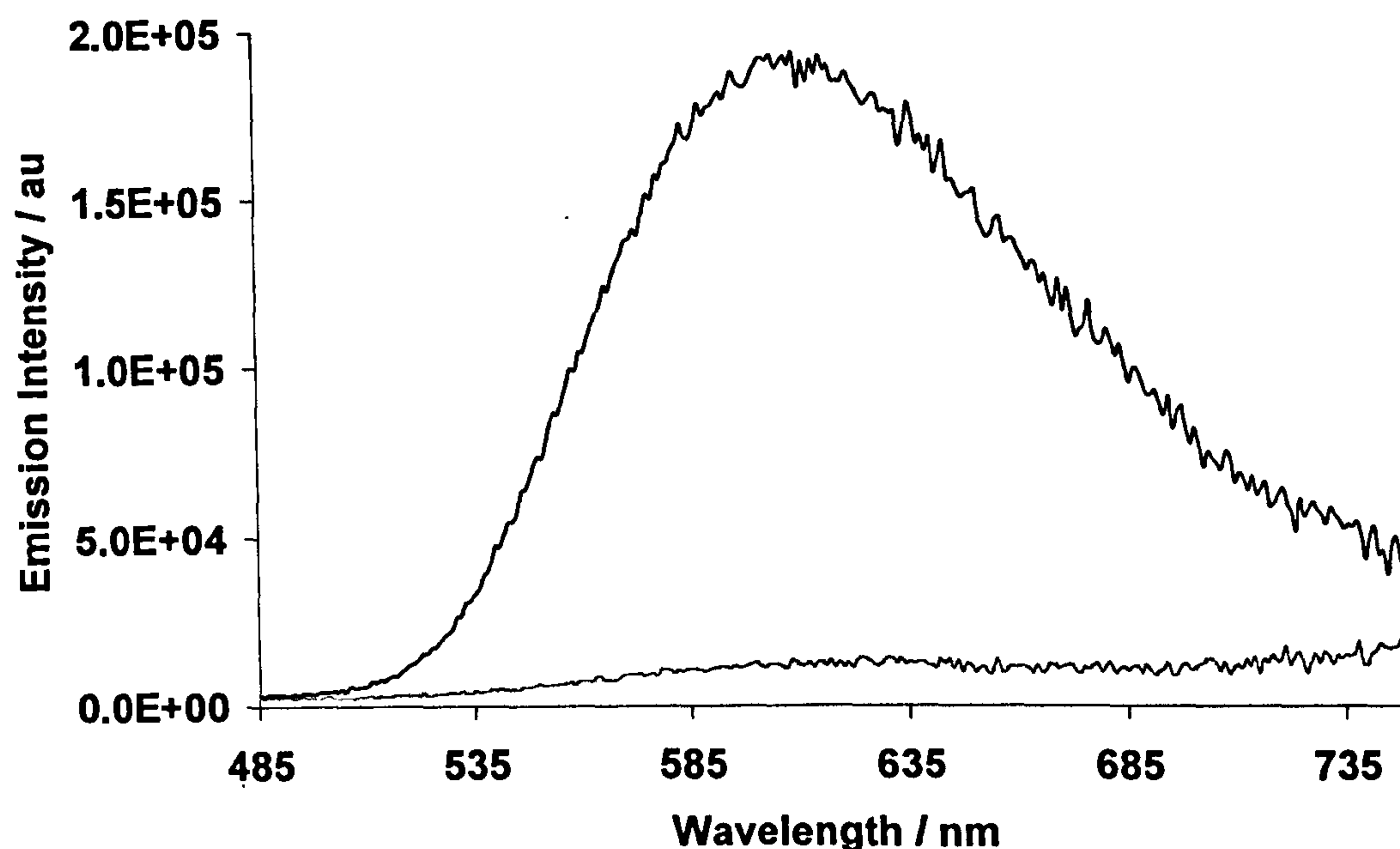


Figure 6.14 Emission spectra of *rac*-Ir(ppy)₂Cl(TAT) **57** in aerated 0.1 mmol HEPES/0.1 mmol NaCl buffer, pH = 7.4, in the absence (dashed line) and presence (black line) of calf thymus DNA at 298 K, $\lambda_{\text{ex}} = 355$ nm.

In summary, the results of this preliminary photophysical study suggest that *rac*-Ir(ppy)₂Cl(TAT) **57** may undergo intercalation with calf-thymus DNA in aqueous solution. The effect DNA interaction causes an increase in the ligand-centred absorption bands and a large increase in the photoluminescence at 610 nm.

In addition to this, the high synthetic yields of this cyclometalated iridium(III) complex means that closely related complexes of this nature should be as simple to synthesise. This is a distinct advantage over the related cyclometalated rhodium(III) complexes.²³

6.10 Conclusion

This chapter has described the synthesis and photophysical studies of several new cyclometalated iridium(III) complexes.

The series of $\text{Ir(L)}_2\text{X(Y)}$ compounds exhibit some of the bluest emitters reported so far for iridium(III) complexes, e.g. $\text{Ir(ppy)}_2\text{Cl(CO)}$ 50 and $\text{Ir(F}_2\text{ppy)}_2\text{Cl(CO)}$ 59. The position of the $^3\text{MLCT}$ state is tuned by all three ligands, L, X and Y.

In general, these complexes have short lifetimes at room temperature, $\tau \sim 50\text{-}300$ ns, and exhibit reduced luminescence quenching by oxygen in comparison to that of cyclometalated iridium(III) complexes of the formula Ir(L)_3 and $\text{Ir(L)}_2\text{acac}$. This has been attributed a lesser degree of triplet character present in the emissive MLCT state.

At low temperature the $^3\text{MLCT}$ state increases in energy due to the enhanced rigidity of the glassy media and reaches energies that are similar to those of the ^3LC states. In most of the complexes only $^3\text{MLCT}$ emission is observed and a mono-exponential lifetime is seen. However, in complexes with ancillary ligands, such as CO, which has particularly strong localised π -back-bonding, the superimposition of both ^3LC and $^3\text{MLCT}$ photoluminescence is observed. In agreement with this, bi-exponential lifetimes are seen; these have been illustrated clearly by the use of time-resolved emission spectroscopy (TRES). Quantum yields are low for the majority of the $\text{Ir(L)}_2\text{X(Y)}$ complexes studied, but are found to be of the same order as those reported for similar complexes.

In addition to this, the photo-degradation of $\text{Ir(ppy)}_2\text{CN(CO)}$ in degassed solutions of both dichloromethane and benzene has been observed. Proton NMR studies inferred a photoproduct containing chemically equivalent cyclometalating ligands. Mass spectrometry showed that the carbonyl ligand is the most labile ligand and therefore the loss of this species is likely to be the first step in the degradation process.

The synthesis of a new iridium(III) species, $\text{Ir(ppy)}_2\text{Cl(TAT)}$ 57 in high yield and its use as a DNA metallointercalator has also been reported. This complex exhibits weak luminescence in aqueous solution at room temperature. This has been ascribed to the deactivation of the metal to TAT ligand charge transfer process by the protonation of the nitrogen atoms upon the TAT ligand, causing a non-radiative decay mechanism to occur. However, upon addition of DNA, a dramatic increase in photoluminescence is observed. This is due to the interaction of the complex with the DNA, shielding the TAT ligand nitrogens, most likely *via* intercalation. This idea is supported by the change in absorption spectrum, which increases in intensity in the LC regions of the spectrum.

The successful use of this cyclometalated iridium(III) complex as a metallointercalator has highlighted a simple synthetic approach to making a new range of iridium(III) complexes for use as molecular 'light switches' for DNA.

6.11 References

- 1 K. A. King, M. F. Finlayson, P. J. Spellane and R. J. Watts, Luminescence Spectroscopy and Oxidative Quenching of Orthometalated Complexes of Iridium(III), *Sci. Papers I. P. C. R.*, 1984, **78**, 97-106.
- 2 R. Gao, D. G. Ho, B. Hernandez, M. Selke, D. Murphy, P. I. Djurovich and M. E. Thompson, Bis-cyclometalated Ir(III) Complexes as Efficient Singlet Oxygen Sensitisers, *J. Am. Chem. Soc.*, 2000, **124**, 14828-14829.
- 3 M. Nonoyama, Synthesis of a Few Derivatives of Cycloiridiated 2-(2-thienyl)pyridine, *Bull. Chem. Soc. Jpn.*, 1979, **52**, 3749-3750.
- 4 S. Lamansky, M. E. Thompson, V. Adamovich, P. I. Djurovich, C. Adachi, M. A. Baldo, S. R. Forrest and R. Kwong, *Organometallic Compounds and Emission-Shifting Organic Electrophosphorescence*, WO 02/15645 A1, 21st February 2002.
- 5 K. Dedeian, P. I. Djurovich, F. O. Garces, G. Carlson and R. J. Watts, A New Synthetic Route to the Preparation of a Series of Strong Photoreducing Agents: *fac* Tris *Ortho*-Metalated Complexes of Iridium(III) with Substituted 2-phenylpyridines, *Inorg. Chem.*, 1991, **30**, 1685-1687.
- 6 M. C. Colombo, T. C. Brunold, T. Riedener, H. U. Güdel, M. Förtsch and H. Bürgi, Facial Tris Cyclometalated Rh³⁺ and Ir³⁺ Complexes: Their Synthesis, Structure and Optical Spectroscopic Properties, *Inorg. Chem.*, 1994, **33**, 545-550.
- 7 S. Lamansky, P. Djurovich, D. Murphy, F. Abdel-Razzaq, R. Kwong, I. Tysba, M. Bortz, B. Mui, R. Bau and M. E. Thompson, Synthesis and Characterisation of Phosphorescent Cyclometalated Iridium Complexes, *Inorg. Chem.*, 2001, **40**, 1704-1711.

- 8 M. C. DeRosa, P. J. Mosher, G. P. A. Yap, K. S. Focsaneanu, R. L. Crutchley and C. E. B. Evans, Synthesis, Characterisation and Evaluation of $[\text{Ir}(\text{ppy})_2(\text{vpy})\text{Cl}]$ as a Polymer-Bound Oxygen Sensor, *Inorg. Chem.*, 2003, **42**, 4864-4872.
- 9 K. Hiraki, Y. Obayashi and Y. Oki, Preparations and Characterisation of Cycloruthenated Complexes Derived from 1-Phenylpyrazole, 2-Phenylpyridine and Benzo[h]-quinoline, *Bull. Chem. Soc. Jpn.*, 1979, **52**, 1372-1376.
- 10 H. Kunkely and A. Vogler, Photoluminescence of $[\text{Rh}(\text{phpy})_2(\text{CN})_2]^-$, *Chem. Phys. Lett.*, 2000, **319**, 486-488.
- 11 A. B. Tamayo, B. D. Alleyne, P. I. Djurovich, S. Lamansky, I. Tysba, N. N. Ho, R. Bau and M. E. Thompson, Synthesis and Characterisation of Facial and Meridional Tris-cyclometalated Iridium(III) Complexes, *J. Am. Chem. Soc.*, 2003, **125**, 7377-7387.
- 12 M. G. Colombo, A. Hauser and H. U. Güdel, Evidence for Strong Mixing between the LC and MLCT Excited States in Bis(2-phenylpyridinato- C^2, N^1)(2,2'-bipyridine)iridium(III), *Inorg. Chem.*, 1993, **32**, 3088-3092.
- 13 J. N. Demas and G. A. Crosby, The Measurement of Photoluminescence Quantum Yields. A Review, *J. Phys Chem.*, 1971, **75**, 991-1023.
- 14 S. L. Murov, I. Carmichael and G. L. Hug, *Handbook of Photochemistry*, 2nd edition, Marcel Dekker, Inc. 1993.
- 15 J. R. Lakowicz, *Principles of Fluorescence Spectroscopy*, 2nd Edition, Kluwer Academic/Plenum Publishers, 1999.
- 16 K. A. King, P. J. Spellane and R. J. Watts, Excited-State Properties of a Triply *Ortho*-metalated Iridium(III) Complex, *J. Am. Chem. Soc.*, 1985, **107**, 1431-1432.
- 17 M. Heberhold, C. Köhler, W. Milius and B. Wrackmeyer, Carbonylated Complexes ($\text{M}=\text{Cr}, \text{Mo}, \text{W}$) Derived from N-bis(diisopropylamino)phosphinyl-N'-tert-butyl Sulfur Diimide. Novel Five-membered PNSNM Metallacycles, *Inorg. Chim. Acta.*, 1995, **231**, 249-254.

- 18 J. L. Beck, R. Gupta, T. Urathamakul, N. L. Williamson, M. M. Sheil, J. R. Aldrich-Wright and S. F. Ralph, Probing DNA Selectivity of Ruthenium Metallointercalators using ESI Mass Spectroscopy, *Chem. Commun.*, 2003, 626-627.
- 19 P. P. Pellegrini and J. R. Aldrich-Wright, Evidence for Chiral Discrimination of Ruthenium(II) Polypyridyl Complexes by DNA, *J. Chem. Soc. Dalton. Trans.*, 2003, 176-183.
- 20 A. E. Friedman, J. Chambron, J. Sauvage, N. J. Turro and J. K. Barton, Molecular 'Light Switch' for DNA: $\text{Ru}(\text{bpy})_2(\text{dppz})^{2+}$, *J. Am. Chem. Soc.*, 1990, **112**, 4960-4962.
- 21 Y. Jenkins, A. E. Friedman, N. J. Turro and J. K. Barton, Characterisation of Dipyridophenazine Complexes of Ruthenium(II): The Light Switch Effect as a Function of Nucleic Acid Sequence and Conformation, *Biochem.*, 1992, **31**, 10809-10816.
- 22 C. Hiort, P. Lincoln and B. Nordén, DNA Binding of Δ - and Λ - $[\text{Ru}(\text{phen})_2(\text{dppz})]^{2+}$, *J. Am. Chem. Soc.*, 1993, **115**, 3448-3454.
- 23 J. L. Kisko and J. K. Barton, Recognition of DNA Base Pair Mismatches by a Cyclometalated Rh(III) Intercalator, *Inorg. Chem.*, 2000, **39**, 4942-4949.
- 24 C. Stinner, M. D. Wightman, S. O. Kelley, M. G. Hill and J. K. Barton, Synthesis and Spectroelectrochemistry of $\text{Ir}(\text{bpy})(\text{phen})(\text{phi})^{3+}$, a Tris(heteroleptic) Metallointercalator, *Inorg. Chem.*, 2001, **40**, 5245-5250.
- 25 H. Lui, T. Cheung and C. Che, Cyclometalated Platinum(II) Complexes as Luminescent Switches for Calf-thymus DNA, *Chem. Commun.*, 1996, 1039-1040.
- 26 S. Sprouse, K. A. King, P. J. Spellane and R. J. Watts, Photophysical Effects of Metal-Carbon σ -bonds in Ortho-Metalated Complexes of Ir(III) and Rh(III), *J. Am. Chem. Soc.*, 1984, **106**, 6647-6653.

Chapter 7

The Preliminary Catalytic Study of a Pyridyl-bridged Palladium(II) Complex

7.1 Introduction

Palladium-catalysed reactions have become an increasingly popular synthetic tool for carbon-carbon bond forming processes over the last few decades. In particular, the metal-catalysed coupling reactions of Suzuki¹ and Stille,² which utilise organometallic catalysts such as tetrakis(triphenylphosphine) palladium(0),³ $\text{Pd}(\text{PPh}_3)_4$, are used for the preparation of biaryls. There has been some discussion in the literature about the nature of the 'catalytically active' species, in particular, the number of phosphine ligands necessary to stabilise the palladium centre. Palladium catalysts containing two or more phosphine ligands have been widely used for Suzuki cross-coupling reactions, as discussed by Miyaura⁴ in 1998. However, work by Littke *et al.*⁵ suggests that palladium species containing a single phosphine ligand can act as effective catalysts for these kinds of reactions.

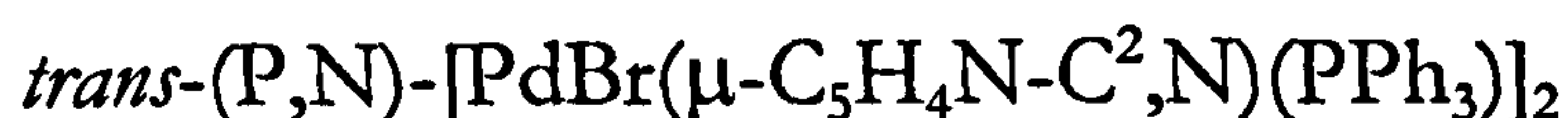
Oxidative addition of 2-, 3- and 4-bromopyridines to $\text{Pd}(\text{PPh}_3)_4$ has been shown to result in the formation of the bimetallic pyridine species *trans*- $[\text{PdBr}(\eta^1\text{-C}_5\text{H}_4\text{N-C}^n)(\text{PPh}_3)_2]$, where $n = 2, 3$ or 4 . No full crystallographic structural analyses were reported for these compounds.⁶ Chin *et al.* also reported the synthesis of a range of complexes derived from 2-bromopyridine and mono and diphosphine ligands.⁷ These complexes have been reported to undergo metathesis with anions such as ClO_4^- , BF_4^- and PF_6^- .⁸ In 1981, Isobe *et al.* reported the use of *trans*-(P,N)- $[\text{PdBr}(\mu\text{-C}_5\text{H}_4\text{N-C}^2, \text{N})(\text{PPh}_3)]_2$ as a catalyst for the coupling reaction of chloropyridine with methylmagnesium bromide.⁷ Chin *et al.* rationalised this observation as the reaction of the catalyst with an incoming nucleophile, Nuc, to generate $[\text{Pd}(\text{Nuc})(\eta^1\text{-C}_5\text{H}_4\text{N-C}^n)(\text{PPh}_3)_2]$, where $n = 3$ or 4 . Reductive elimination yields $\text{Nuc-C}_5\text{H}_4\text{N}$ as the hetero-coupled product and regenerates $\text{Pd}(\text{PPh}_3)_2$ as the active catalytic species.⁶

7.2 Isolation of *trans*-(P,N)- $[\text{PdBr}(\mu\text{-C}_5\text{H}_4\text{N-C}^2, \text{N})(\text{PPh}_3)]_2$

2,4-difluorophenylboronic acid (5.0 g, 32 mmol), 2-bromopyridine (5.5 g, 3.3 mL, 35 mmol, 1.1 eq.), Na_2CO_3 (1M (aq), 50 mL), THF (100 mL) and $\text{Pd}(\text{PPh}_3)_4$ (0.75 g, 0.6

mmol, 2 mole %) were heated overnight in a nitrogen atmosphere at 80 °C with continuous stirring. The reaction was cooled to room temperature and water (200 mL) was added. The resulting mixture was extracted with ethyl acetate (5 x 100 mL), dried over MgSO₄, filtered and evaporated to dryness. Column chromatography afforded the product, 2-(2,4-difluorophenyl)pyridine, as a pale yellow liquid in 82 % yield (5.0 g). The Pd(II) complex, *trans*-(P,N)-[PdBr-(μ-C₅H₄N-C²,N)(PPh₃)]₂, was isolated as pale yellow diamond shaped crystals, 1.1x10⁻³ % yield (0.02 g), from a fraction containing the impure product.

7.2.1 Crystal Structure determination of



Single crystal X-ray diffraction experiments were carried out at 120 K using graphite monochromated Mo K α radiation (λ = 0.71073 Å). Crystal data and structure refinement parameters are presented in table 7.1.

Table 7.1 Crystallographic data for *trans*-(P,N)-[PdBr(μ-C₅H₄N-C²,N)(PPh₃)]₂.

Empirical Formula	C51.50 H41.50 Br2 F N2.50
Crystal system	Triclinic
Space group	P $\bar{1}$
Crystal size /mm	0.40 x 0.08 x 0.04
Temperature /K	120(2)
<i>a</i> /Å	10.4525(4)
<i>b</i> /Å	13.0911(5)
<i>c</i> /Å	17.7535(6)
α /°	81.5170(10)°
β /°	78.849(2)°
γ /°	70.8180(10)°
Volume /Å ³	2241.84(14)
Z	2
Formula weight	1148.93
Density /mg m ⁻³	1.702
μ /mm ⁻¹	2.699
R _{int}	4.18%
Observed data [<i>I</i> >2σ(<i>I</i>)]	11754

R ₁ index [I>2σ(I)]	4.31%
R ₁ index (all data)	6.80%
wR ₂ index [I>2σ(I)]	8.98%
wR ₂ index (all data)	10.02%
Goodness of fit (S)	1.035
N° of variables	561

A characteristic specimen was analysed using X-ray single crystal diffraction and found to be a co-crystal of the palladium(II) species, *trans*-(P,N)-[PdBr(μ-C₅H₄N-C²,N)(PPh₃)]₂, and the reaction product 2-(2,4-difluorophenyl)pyridine, see figure 7.1.

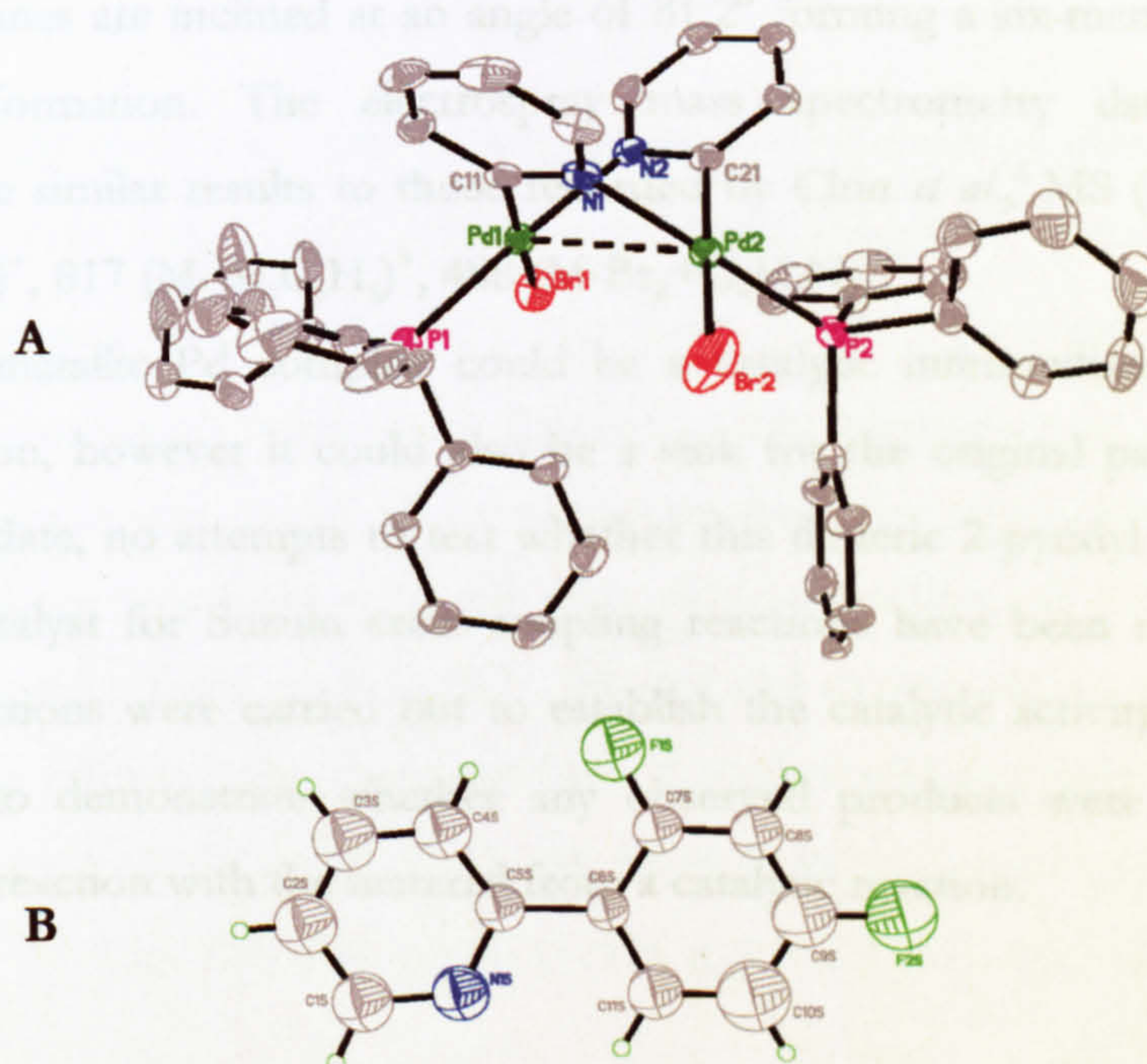


Figure 7.1 Crystal structure of the palladium dimer with thermal ellipsoids at 50% (**A**).

Two of the triphenylphosphine rings were found to be disordered, each with 50% occupancy. Crystal structure of the Suzuki coupling reaction product,

2-(2,4-difluorophenyl)pyridine (**B**) at 120 K.

Palladium(II) species of this nature were first reported in 1980 by Nakatsu *et al.*⁶ and its chloride analogue in 1985 by Anderson *et al.*⁹ Since then, other C,N-bonded derivatives have been isolated, such as the 2-chloroisoquinoline structure characterised

by Alcock *et al.*¹⁰ The structural characteristics of our complex are consistent with those previously reported.^{6,9,10}

Each palladium atom exhibits a square-planar geometry. The Pd-Pd interatomic distance is 3.2338(4) Å, and is consistent with the structure reported by Nakatsu *et al.*⁶ (3.194(2) Å) and the chlorine analogue⁹ (3.165(3) Å) already published. This suggests that the interaction may be weak; although a search of the Cambridge Structural Database¹¹ (Version 1.5, November 2002, 272066 entries) using ConQuest¹² shows that similar species occupy a range of 2.543-3.315 Å with a mean average of 2.795 Å. The central ring of the structure possesses two pyridine rings bridging the palladium atoms with the nitrogen trans to triphenylphosphine and carbon trans to bromine in both cases. These planes are inclined at an angle of 81.2° forming a six-membered ring in a boat-type conformation. The electrospray mass spectrometry data obtained in acetonitrile gave similar results to those recorded by Chin *et al.*,⁶ MS (ES+) (CH₃CN): *m/z* 973 (M-Br)⁺, 817 (M-Br₂C₆H₅)⁺, 488 (M-Br₂+C₄H₆N₂)²⁺.

This bimetallic Pd complex could be a catalytic intermediate in this Suzuki coupling reaction, however it could also be a sink for the original palladium catalyst, Pd(PPh₃)₄. To date, no attempts to test whether this dimeric 2-pyridyl Pd(II) adduct is an effective catalyst for Suzuki cross-coupling reactions have been reported. Several small-scale reactions were carried out to establish the catalytic activity of this isolated complex and to demonstrate whether any observed products were the result of a stoichiometric reaction with the material from a catalytic reaction.

7.3 Catalysis - Part 1

Crystals of the isolated palladium(II) complex were washed with diethyl ether and left to dry prior to use in the following catalytic test reactions.

7.3.1 Reaction A1

Phenylboronic acid (0.05 g, 0.41 mmol), 2-bromopyridine (0.07 g, 0.45 mmol), Na₂CO₃ (1M (aq), 1 ml), THF (1.5 mL) and Pd-dimer crystals (0.001 g, 0.95 μmol) were degassed

by three 'freeze-pump-thaw' cycles. The resulting mixture was heated at 80 °C overnight during which the clear solution became bright yellow in colour. The reaction mixture was allowed to cool to room temperature after which water (10 mL) was added. The mixture was then extracted with dichloromethane (3 x 10 mL) and the organic extracts were dried over MgSO_4 , filtered and evaporated to dryness. Column chromatography afforded the pure product, 2-phenylpyridine, as a pale yellow liquid, in 67 % yield (0.043 g). $^1\text{H-NMR}$ 300 MHz (CDCl_3) δ : 8.66 (1H, dt, $J = 4.2$ Hz), 7.91 (2H, m), 7.70 (2H, m), 7.42 (3H, m), 7.21 (1H, m). MS (ES⁺): 156.1 ($\text{M}+\text{H}$)⁺.

7.3.2 Reaction B1

Phenylboronic acid (0.05 mg, 0.41 mmol), 2-bromo-6-methoxypyridine (0.09 mg, 0.45 mmol), Na_2CO_3 (1M (aq), 1 mL), THF (1.5 mL) and Pd-dimer crystals (0.001 g, 0.95 μmol) were degassed by three 'freeze-pump-thaw' cycles. The resulting mixture was heated at 80 °C overnight during which the clear solution became pale yellow in colour. The reaction mixture was cooled to room temperature after which water (10 mL) was added. The mixture was then extracted with dichloromethane (3 x 10 mL) and the organic extracts were dried over MgSO_4 , filtered and evaporated to dryness. Column chromatography afforded the pure product, 2-methoxy-6-phenylpyridine, as a clear liquid, in 77 % yield (0.058 g). $^1\text{H-NMR}$ 300 MHz (CDCl_3) δ : 8.09 (2H, d, $J = 7.2$ Hz), 7.65 (1H, t, $J = 7.5$ Hz), 7.45 (4H, m), 6.73 (1H, d, $J = 8.1$ Hz), 4.08 (3H, s). MS (ES⁺): 186.1 ($\text{M}+\text{H}$)⁺.

7.3.3 Reaction C1

Phenylboronic acid (0.05 mg, 0.41 mmol), bromobenzene (0.07 g, 0.45 mmol), Na_2CO_3 (1M (aq), 1 mL), THF (1.5 mL) and Pd-dimer crystals (0.001 g, 0.95 μmol) were degassed by three 'freeze-pump-thaw' cycles. The resulting mixture was heated at 80 °C overnight during which the clear solution became pale yellow in colour. The reaction mixture was allowed to cool to room temperature after which water (10 mL) was added. The mixture was then extracted with dichloromethane (3 x 10 mL) and the organic extracts were dried over MgSO_4 , filtered and evaporated to dryness. Column

chromatography afforded the pure product, biphenyl, as a white solid, in 59 % yield (0.037 g). $^1\text{H-NMR}$ 300 MHz (CDCl_3) δ : 7.68 (4H, m), 7.52 (4H, m) 7.42 (2H, m). MS (EI+): 154 (M) $^+$.

The first reaction, **A1**, involved the coupling of 2-bromopyridine with phenylboronic acid. NMR and MS analysis of the isolated reaction product showed the formation of the hetero-coupled product, 2-phenylpyridine. The second test, reaction **B1**, utilised 2-methoxy-6-bromopyridine and phenylboronic acid and produced the hetero-coupled product, 2-methoxy-6-phenylpyridine in good yield. Finally in reaction **C1** the coupling of bromobenzene and phenylboronic acid afforded biphenyl in moderate yield. These reactions indicate that *trans*-(P,N)-[PdBr(μ -C₅H₄N-C²,N)(PPh₃)]₂, and most likely its related complexes, are active catalysts in the Suzuki cross-coupling reactions of 2-bromoarenes and aryl boronic acids.

As suggested by Alcock *et al.*¹⁰ the catalytic cycle is most likely to proceed by a monomeric Pd(II) species **X**. The displacement of the bromide from **X** by the aryl group from ArB(OH)₂ would lead to species **Y** which can undergo reductive elimination of the product. Subsequent oxidative addition of another molecule of the aryl-halide would regenerate the monomeric species, **X** which is likely to be in equilibrium with the dimer, **Z**. This catalytic cycle is shown in figure 7.2.

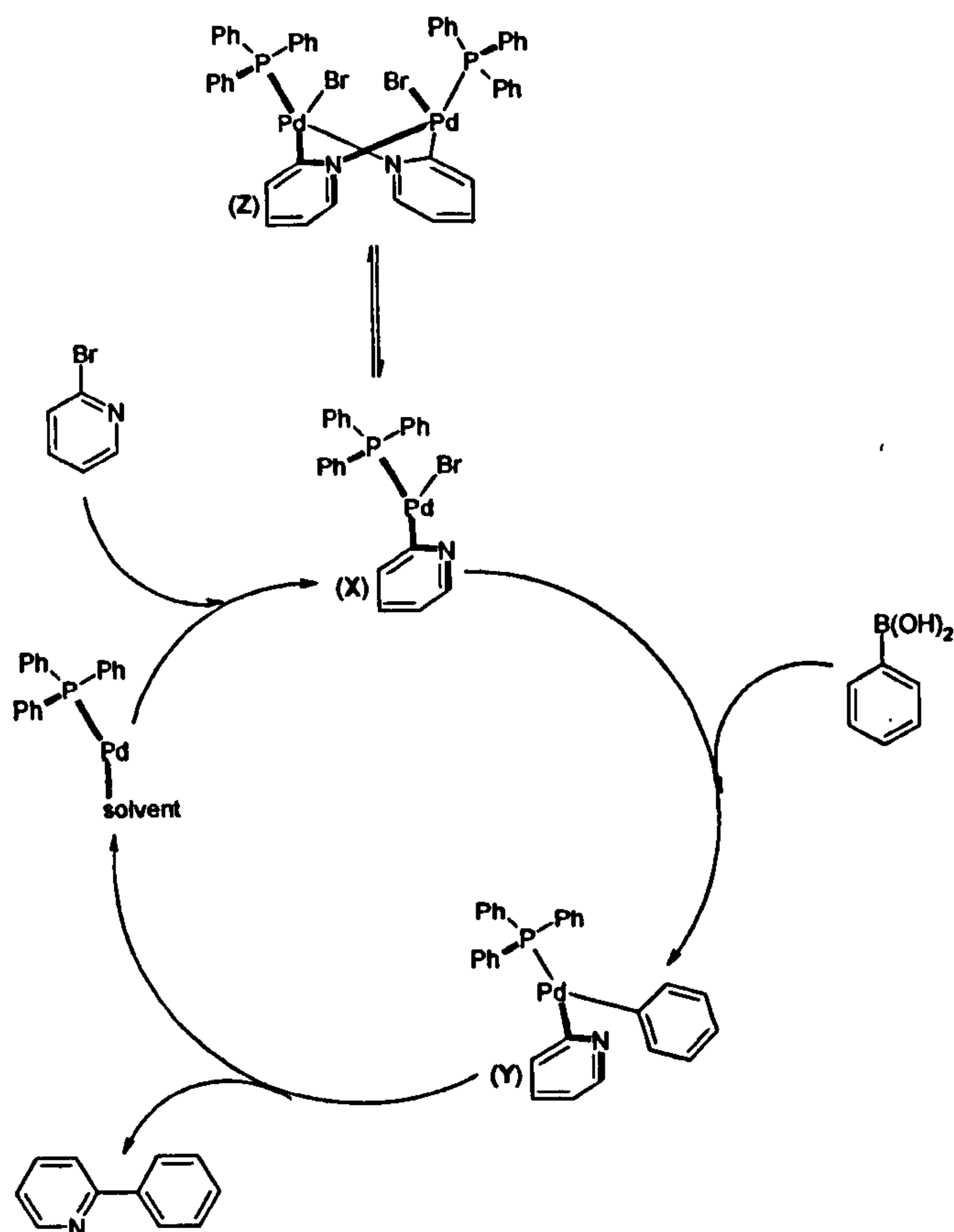


Figure 7.2 Suggested catalytic cycle of the dimeric Pd(II) complex.

A great advantage of these complexes is that they are stable under ambient conditions unlike other commonly used Pd(0) catalysts, e.g. $\text{Pd(PPh}_3)_4$, which are readily oxidised to Pd(II) species in air. These dimeric Pd(II) complexes are also easily synthesised in high yield.⁷

7.4 Alternative preparation of

trans-(P,N)-[PdBr-(μ -C₅H₄N-C²,N)(PPh₃)]₂⁶

Tetrakis(triphenylphosphine) palladium(0) ($\text{Pd(PPh}_3)_4$, 0.60 g, 0.48 mmol) was dissolved in toluene (40 mL) to produce a bright clear yellow solution. After which 2-bromopyridine (0.14 g, 0.87 mmol) was added. The resulting mixture was refluxed at 90 °C for 4 hours, during which the solution became cloudy and pale green-yellow in

colour. The reaction mixture was cooled to room temperature and filtered. The green-yellow precipitate was collected and washed thoroughly with diethyl ether (5 x 10 mL) and subsequently dissolved in chloroform. The filtrate was evaporated to dryness and the solid was recrystallised from chloroform and n-hexane to give the pure product a green-yellow crystalline solid in 81 % yield (0.21 g). ^1H -NMR (300 MHz) δ : 8.58 (1H, m), 7.85 (6H, m), 7.36 (3H, m), 7.28 (6H, m), 6.61 (1H, m), 6.49 (2H, m). ^{31}P -NMR (300 MHz) δ : 30.79. MS (ES+) (CH_3CN): m/z 973 (M-Br) $^+$, 817 ($\text{M-Br}_2\text{C}_6\text{H}_5$) $^+$, 488 ($\text{M-Br}_2+\text{C}_4\text{H}_6\text{N}_2$) $^{2+}$. Electrospray mass spectrometry in acetonitrile are similar to results obtained by Chin *et al.*⁶ It can be concluded from the ^1H -NMR and electrospray mass spectrometry data above that this complex remains stable as a bimetallic Pd species in both chloroform and acetonitrile, unlike the bimetallic μ -chloro-bridged iridium(III) species discussed in chapter 1.

This freshly synthesised palladium complex was also tested for its ability to catalyse Suzuki cross-coupling reactions. This is described in the following reactions, A2 and B2.

7.5 Catalysis - Part 2

7.5.1 Reaction A2

Phenylboronic acid (0.05 g, 0.41 mmol), 2-bromopyridine (0.07 g, 0.45 mmol), Na_2CO_3 (1M (aq), 1 mL), THF (1.5 mL) and Pd-dimer crystals (0.001 g, 0.95 μmol) were degassed by three 'freeze-pump-thaw' cycles. The resulting mixture was heated at 80 $^\circ\text{C}$ overnight during which the clear solution became bright yellow in colour. The reaction mixture was allowed to cool to room temperature after which water (10 mL) was added. The mixture was then extracted with dichloromethane (3 x 10 mL) and the organic extracts were dried over MgSO_4 , filtered and evaporated to dryness. Column chromatography afforded the pure product, 2-phenylpyridine, as a pale yellow liquid, in 32 % yield (0.020 g). ^1H -NMR 300 MHz (CDCl_3) δ : 8.66 (1H, dt, $J = 4.2$ Hz), 7.91 (2H, m), 7.70 (2H, m), 7.42 (3H, m), 7.21 (1H, m). MS (ES+): 156.1 (M+H) $^+$.

7.5.2 Reaction B2

Phenylboronic acid (0.05 mg, 0.41 mmol), bromobenzene (0.07 g, 0.45 mmol), Na₂CO₃ (1M (aq), 1 ml), THF (1.5 mL) and Pd-dimer crystals (0.001 g, 0.95 µmol) were degassed by three 'freeze-pump-thaw' cycles. The resulting mixture was heated at 80 °C overnight during which the clear solution became pale yellow in colour. The reaction mixture was allowed to cool to room temperature after which water (10 mL) was added. The mixture was then extracted with dichloromethane (3 x 10 mL) and the organic extracts were dried over MgSO₄, filtered and evaporated to dryness. Column chromatography afforded the pure product, biphenyl, as a white solid, in 63 % yield (0.040 g). ¹H-NMR 300 MHz (CDCl₃) δ: 7.68 (4H, m), 7.52 (4H, m) 7.42 (2H, m). MS (EI+): 154 (M)⁺.

As expected, reactions A1 and B2 confirmed that the synthesised complex is also catalytically active with respect to Suzuki cross-coupling reactions. The ¹H-NMR and MS (ES+) analysis of the isolated products show them to be the hetero-coupled species in each case.

7.6 Conclusion

The comparison of the Suzuki cross-coupling reactions involving arylboronic acids and arylhalides; in catalysis parts 1 and 2, it has been demonstrated that *trans*-(P,N)-[PdBr(µ-C₅H₄N-C²,N)(PPh₃)]₂ can act as an effective catalyst. In order to ascertain the range of its catalytic activity with respect to substrates, solvents and reaction conditions, additional coupling reactions must be carried out.

7.7 References

- 1 N. Miyuara and A. Suzuki, Palladium Catalysed Cross Coupling Reactions of Organoboron Compounds, *Chem. Rev.*, 1995, 95, 2457-2483.

- 2 A. F. Littke, L. Schwarz and G. C. Fu, Pd/P(t-Bu)₃: A Mild and General Catalyst for Stille Reactions of Aryl Chlorides and Aryl Bromides, *J. Am. Chem. Soc.*, 2002, **124**, 6343-6348.
- 3 (a) D. R. Coulson, Tetrakis(triphenylphosphine)palladium(0), *Inorg. Synth.*, 1990, **28**, 121-124.

(b) C. M. Unrau, M. G. Campbel and V. Snieckus, Directed Ortho Metalation - Suzuki Cross Coupling Connections. Convenient Regiospecific Routes to Functionalised *m*- and *p*-Teraryls and *m*-Quinquearyls, *Tet. Lett.*, 1992, **33**, 2773-2776.
- 4 N. Miyaura, *Advances in Metal-Organic Chemistry*, JAI Press Inc. 1998, **6**, 187-243.
- 5 A. F. Littke, C. Dai and G. C. Fu, Versatile Catalysis for the Suzuki Cross Coupling of Arylboronic Acids with Aryl and Vinyl Halides and Triflates under Mild Conditions, *J. Am. Chem. Soc.*, 2000, **122**, 4020-4028.
- 6 K. Nakatsu, K. Kinoshita, H. Kanda, K. Isobe, Y. Nakamura and S. Kawaguchi, X-ray Molecular Structure of a Pyridyl-bridged Dinuclear Palladium Complex, *trans*-(P,N)-[PdBr(μ-C₅H₄N-C²,N)(PPh₃)]₂, *Chem. Lett.*, 1980, 913-914.
- 6 C. C. H. Chin, J. S. L. Yeo, Z. H. Loh, J. J. Vittal, W. Henderson and T. S. A. Hor, Synthesis and Electrospray Mass Spectrometry of Palladium(II) Diphosphine Complexes from Oxidative Addition of 2-bromopyridine to Pd⁰, *J. Chem. Soc. Dalton. Trans.*, 1998, 3777-3784.
- 8 K. Isobe and S. Kawaguchi, Organopalladium(II) Complexes Containing Carbon-bonded Pyridine and Picoline as a Ligand: Preparation, Structures and Reactions, *Heterocycles*, 1981, **16**, 1603-1612.
- 9 T. A. Anderson, R. J. Barton and B. E. Robertson, Structure of *trans*-(P,N)-bis(μ-pyridyl-C²,N)-bis[chloro(triphenylphosphine)palladium(II)], [Pd₂Cl₂(C₅H₄N)₂{P(C₆H₅)₃}]₂, *Acta. Cryst.*, 1985, **C41**, 1171-1173.

- 10 N. W. Alcock, J. M. Brown and D. I. Hulmes, Synthesis and Resolution of 1-(2diphenylphosphino-1-naphthyl)isoquinoline; a P-N Chelating Ligand for Asymmetric Catalysis, *Tetrahedron*, 1993, 4, 743-756.
- 11 F. H. Allen, *Acta Cryst.*, The Cambridge Structural Database: A quarter of a Million Structures and Rising, 2002, B58, 380-388.
- 12 I. J. Bruno, J. C. Cole, P. R. Edgington, M. Kessler, C. F. Macrae, P. McCabe, J. Pearson and R. Taylor, *Acta Cryst.*, New Software for Searching the Cambridge Structural Database and Visualising Crystal Structures, 2002, B58, 389-397.

Appendix A

Crystallographic Information

The full set of crystallographic data collected for each crystal structure can be found on the enclosed CD (back cover). The file names correspond to the relevant identification codes listed in the tables below.

A1 2-Phenylpyrimidine (3)

Crystal data and structure refinement

Identification code	01srv181	
Empirical formula	C10 H8 N2	
Formula weight	156.18	
Temperature	120(2) K	
Wavelength	0.71073 Å	
Crystal system	Monoclinic	
Space group	P2(1)/c	
Unit cell dimensions	a = 10.9062(11) Å	α = 90°
	b = 5.9256(6) Å	β = 109.040(2)°
	c = 12.9753(13) Å	γ = 90°
Volume	792.66(14) Å³	
Z	4	
Density (calculated)	1.309 Mg/m³	
Absorption coefficient	0.080 mm ⁻¹	
F(000)	328	
Crystal size	0.4 x 0.3 x 0.2 mm³	
Theta range for data collection	1.98 to 27.49°	
Index ranges	-14<=h<=14, -7<=k<=7, -16<=l<=16	
Reflections collected	7918	
Independent reflections	1819 [R(int) = 0.0400]	
Completeness to theta = 27.49°	99.9 %	
Absorption correction	Semi-empirical from equivalents	
Max. and min. transmission	0.9841 and 0.9686	
Refinement method	Full-matrix least-squares on F²	
Data / restraints / parameters	1819 / 0 / 109	
Goodness-of-fit on F²	1.052	
Final R indices [I>2sigma(I)]	R1 = 0.0466, wR2 = 0.1259	
R indices (all data)	R1 = 0.0605, wR2 = 0.1389	
Largest diff. peak and hole	0.286 and -0.180 e.Å ⁻³	

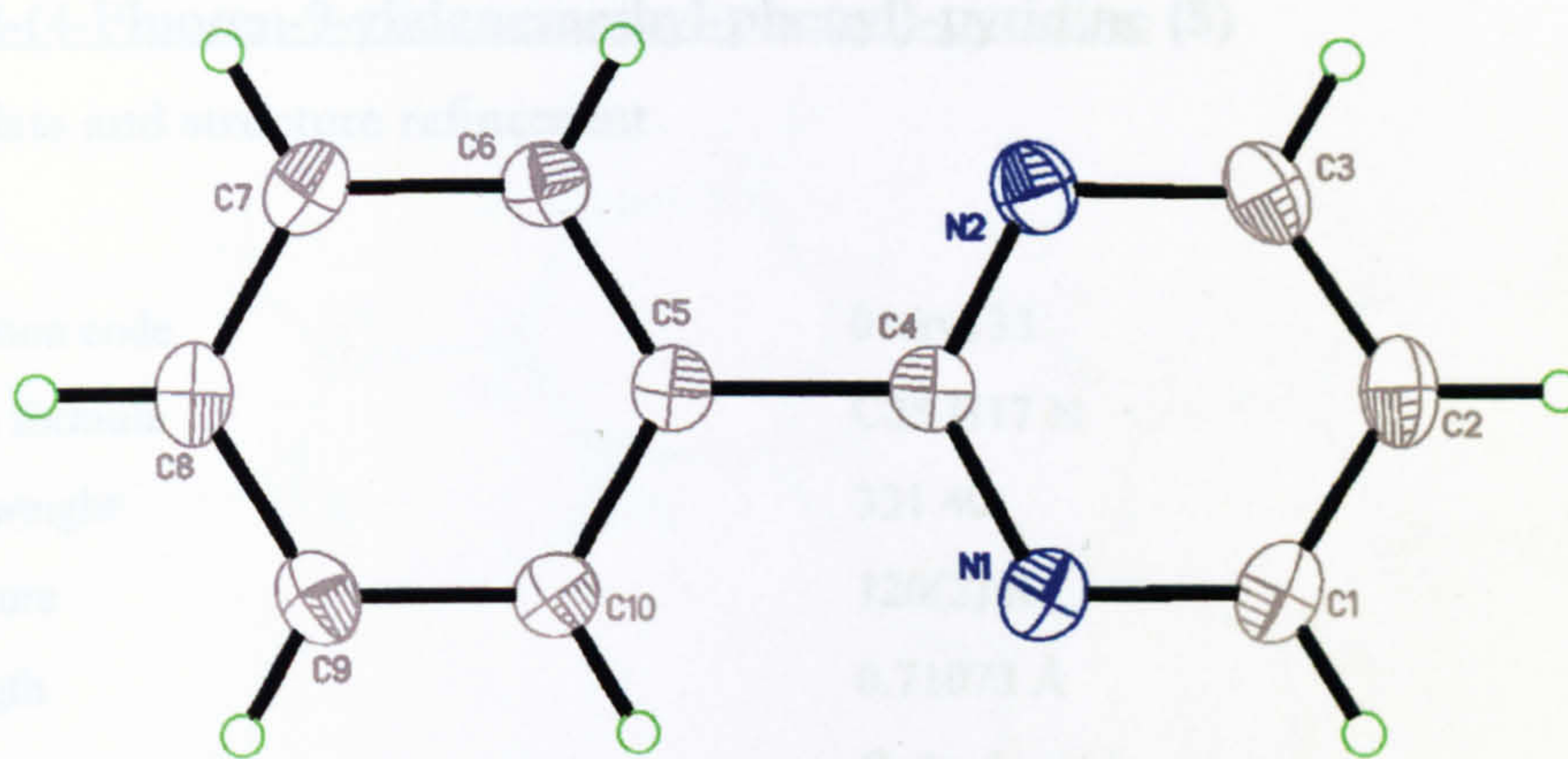


Figure A1 X-ray crystal structure of 2-phenylpyrimidine at 120 K, thermal ellipsoids depict 50 % occupancy.

A2 2-(4-Fluoren-9-ylidenemethyl-phenyl)-pyridine (5)

Crystal data and structure refinement

Identification code	01srv133	
Empirical formula	C25 H17 N	
Formula weight	331.40	
Temperature	120(2) K	
Wavelength	0.71073 Å	
Crystal system	Orthorhombic	
Space group	Pbca	
Unit cell dimensions	a = 7.6835(4) Å	α = 90°
	b = 19.8043(10) Å	β = 90°
	c = 21.8122(11) Å	γ = 90°
Volume	3319.1(3) Å ³	
Z	8	
Density (calculated)	1.326 Mg/m ³	
Absorption coefficient	0.077 mm ⁻¹	
F(000)	1392	
Crystal size	0.4 x 0.28 x 0.16 mm ³	
Theta range for data collection	1.87 to 27.49°	
Index ranges	-9<=h<=9, -25<=k<=25, -28<=l<=28	
Reflections collected	32995	
Independent reflections	3797 [R(int) = 0.0421]	
Completeness to theta = 27.49°	100.0 %	
Absorption correction	Semi-empirical from equivalents	
Max. and min. transmission	0.9879 and 0.9700	
Refinement method	Full-matrix least-squares on F ²	
Data / restraints / parameters	3797 / 0 / 235	
Goodness-of-fit on F ²	1.036	
Final R indices [I>2sigma(I)]	R1 = 0.0406, wR2 = 0.0964	
R indices (all data)	R1 = 0.0569, wR2 = 0.1095	
Largest diff. peak and hole	0.332 and -0.220 e.Å ⁻³	

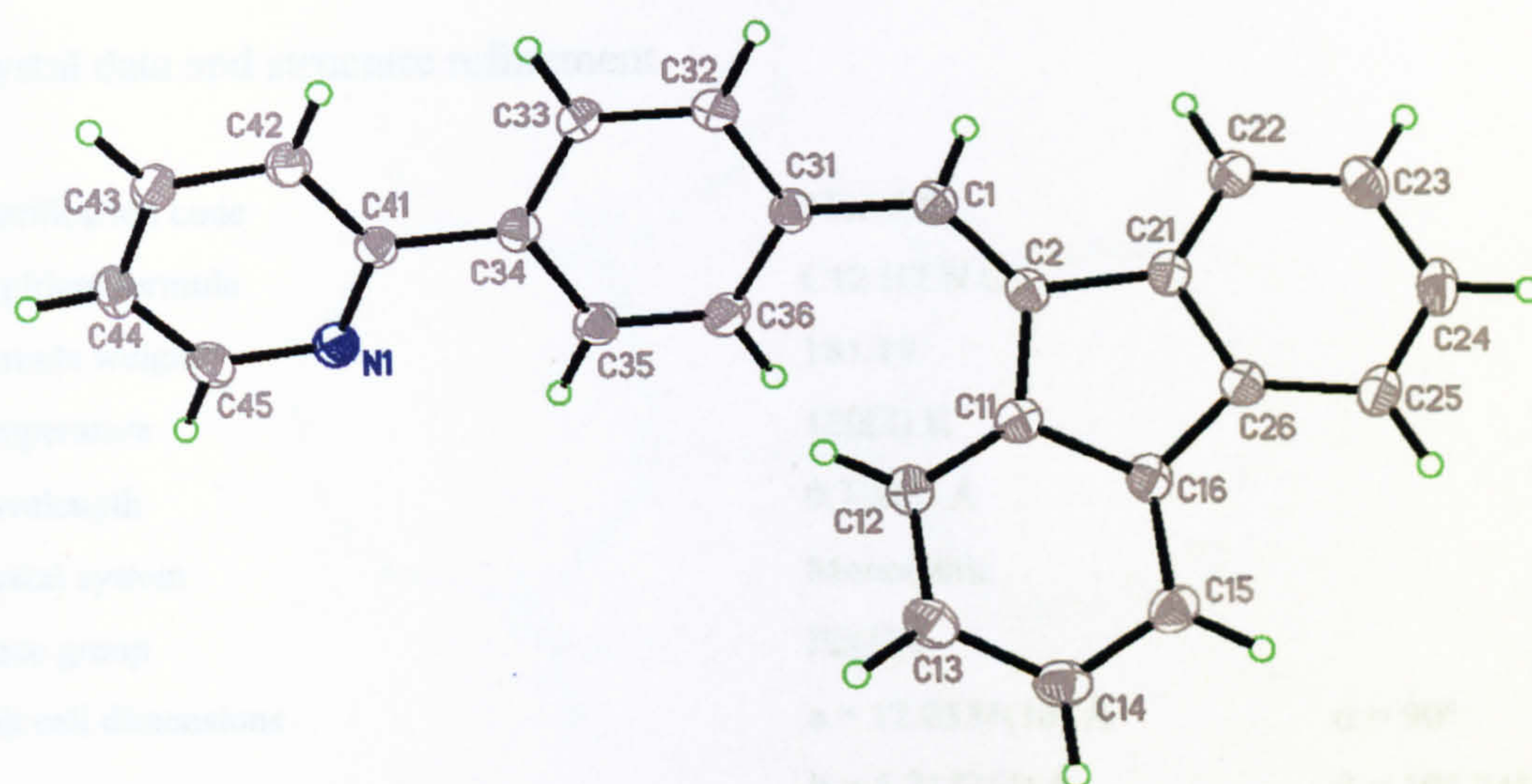


Figure A2 X-ray crystal structure of 2-(4-fluoren-9-ylidenemethyl-phenyl)-pyridine at 120 K, thermal ellipsoids depict 50 % occupancy.

A3 Indeno[1,2-b]pyridin-5-one (7)

Crystal data and structure refinement

Identification code	01srv222	
Empirical formula	C12 H7 N O	
Formula weight	181.19	
Temperature	120(2) K	
Wavelength	0.71073 Å	
Crystal system	Monoclinic	
Space group	P2(1)/c	
Unit cell dimensions	a = 12.0531(10) Å	α = 90°
	b = 5.2183(4) Å	β = 108.745(2)°
	c = 14.4375(11) Å	γ = 90°
Volume	859.91(12) Å ³	
Z	4	
Density (calculated)	1.400 Mg/m ³	
Absorption coefficient	0.090 mm ⁻¹	
F(000)	376	
Crystal size	0.50 x 0.20 x 0.02 mm ³	
Theta range for data collection	2.94 to 27.51°	
Index ranges	-15<=h<=15, -6<=k<=6, -18<=l<=18	
Reflections collected	8845	
Independent reflections	1975 [R(int) = 0.0750]	
Completeness to theta = 27.51°	99.8 %	
Absorption correction	None	
Max. and min. transmission	0.9982 and 0.9562	
Refinement method	Full-matrix least-squares on F ²	
Data / restraints / parameters	1975 / 0 / 127	
Goodness-of-fit on F ²	1.026	
Final R indices [I>2sigma(I)]	R1 = 0.0443, wR2 = 0.1141	
R indices (all data)	R1 = 0.0564, wR2 = 0.1243	
Largest diff. peak and hole	0.274 and -0.198 e.Å ⁻³	

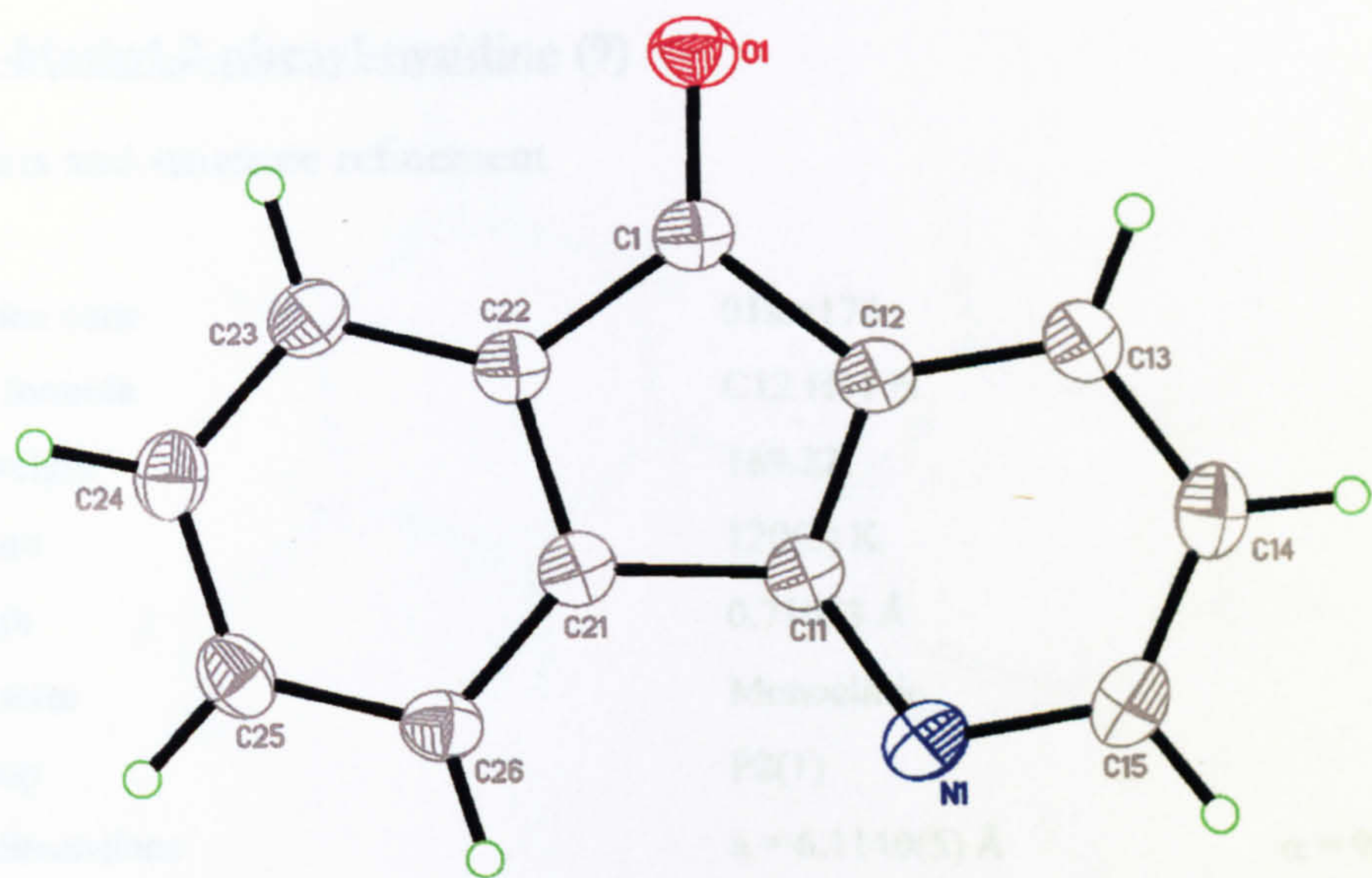


Figure A3 X-ray crystal structure of Indeno[1,2-b]pyridin-5-one at 120 K, thermal ellipsoids depict 50 % occupancy.

A4 4-Methyl-2-phenyl-pyridine (9)

Crystal data and structure refinement

Identification code	01srv170	
Empirical formula	C12 H11 N	
Formula weight	169.22	
Temperature	120(2) K	
Wavelength	0.71073 Å	
Crystal system	Monoclinic	
Space group	P2(1)	
Unit cell dimensions	a = 6.1140(5) Å	α = 90°
	b = 7.3207(6) Å	β = 105.019(1)°
	c = 10.4166(8) Å	γ = 90°
Volume	450.31(6) Å ³	
Z	2	
Density (calculated)	1.248 Mg/m ³	
Absorption coefficient	0.073 mm ⁻¹	
F(000)	180	
Crystal size	0.4 x 0.2 x 0.1 mm ³	
Theta range for data collection	2.02 to 27.47°	
Index ranges	-7<=h<=7, -9<=k<=9, -13<=l<=13	
Reflections collected	4831	
Independent reflections	1117 [R(int) = 0.0277]	
Completeness to theta = 27.47°	99.9 %	
Absorption correction	Semi-empirical from equivalents	
Max. and min. transmission	0.9927 and 0.9714	
Refinement method	Full-matrix least-squares on F ²	
Data / restraints / parameters	1117 / 1 / 119	
Goodness-of-fit on F ²	1.069	
Final R indices [I>2sigma(I)]	R1 = 0.0323, wR2 = 0.0868	
R indices (all data)	R1 = 0.0339, wR2 = 0.0879	
Absolute structure parameter	3(4)	
Largest diff. peak and hole	0.224 and -0.194 e.Å ⁻³	

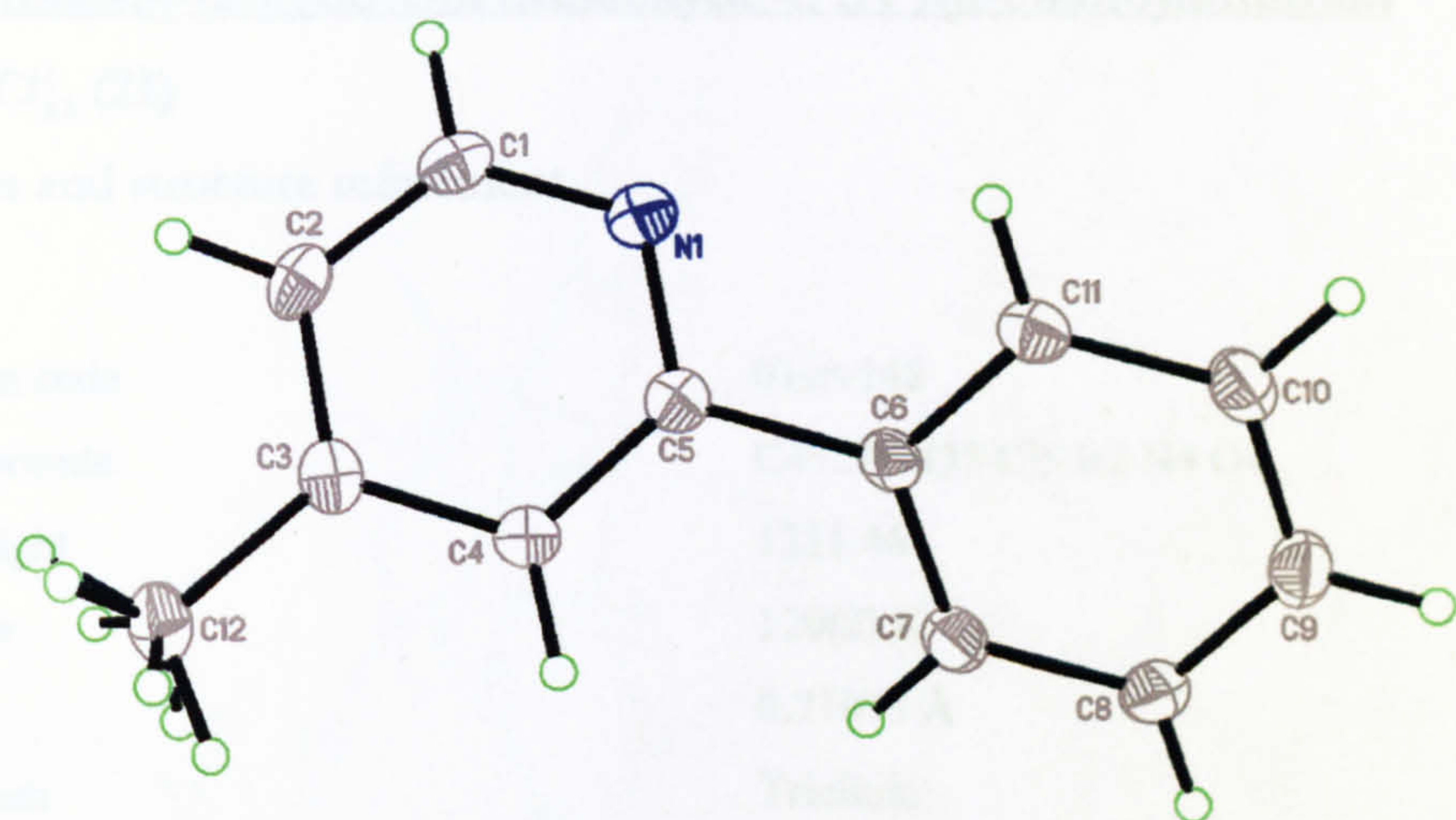


Figure A4 X-ray crystal structure of 4-methyl-2-phenyl-pyridine at 120 K, thermal ellipsoids depict 50 % occupancy.

Volume	223.70(3) Å ³
Z	2
Density (calculated)	1.96 Mg/m ³
Absorption coefficient	6.336 mm ⁻¹
F(000)	1262
Crystal size	0.13 × 0.1 × 0.1 mm ³
Theta range for data collection	1.38 to 27.49°
Index ranges	-13 ≤ h ≤ 13, -16 ≤ k ≤ 16, -23 ≤ l ≤ 23
Reflections collected	23672
Independent reflections	10133 [R(int) = 0.0423]
Data/restraints to data = 27.49°	99.5 %
Absorption correction	Semi-empirical flux equivalents
Max. and min. transmission	0.531 and 0.410
Refinement method	Full-matrix least-squares on F ²
Data / restraints / parameters	10133 / 48 / 430
Goodness-of-fit on F ²	1.037
Final R indices [I ≥ 2-sigma(I)]	R1 = 0.0423, wR2 = 0.0879
R indices (all data)	R1 = 0.0760, wR2 = 0.0935
Largest diff. peak and hole	1.557 and -2.009 e.Å ⁻³

A5 Tetrakis(4-(2-pyridyl)benzaldehyde-C²,N¹)(μ-chloro)diiridium
[Ir(fppy)₂Cl]₂ (21)

Crystal data and structure refinement

Identification code	01srv148	
Empirical formula	C _{49.50} H ₃₅ Cl ₁₅ Ir ₂ N ₄ O ₄	
Formula weight	1311.46	
Temperature	120(2) K	
Wavelength	0.71073 Å	
Crystal system	Triclinic	
Space group	P-1	
Unit cell dimensions	a = 10.577(2) Å	α = 75.562(4)°
	b = 12.779(2) Å	β = 88.993(3)°
	c = 17.924(3) Å	γ = 71.629(3)°
Volume	2221.7(7) Å ³	
Z	2	
Density (calculated)	1.96 Mg/m ³	
Absorption coefficient	6.336 mm ⁻¹	
F(000)	1262	
Crystal size	0.15 x 0.1 x 0.1 mm ³	
Theta range for data collection	1.18 to 27.49°	
Index ranges	-13 ≤ h ≤ 13, -16 ≤ k ≤ 16, -22 ≤ l ≤ 23	
Reflections collected	23672	
Independent reflections	10153 [R(int) = 0.0523]	
Completeness to theta = 27.49°	99.5 %	
Absorption correction	Semi-empirical from equivalents	
Max. and min. transmission	0.531 and 0.419	
Refinement method	Full-matrix least-squares on F ²	
Data / restraints / parameters	10153 / 18 / 620	
Goodness-of-fit on F ²	1.037	
Final R indices [I>2sigma(I)]	R1 = 0.0424, wR2 = 0.0808	
R indices (all data)	R1 = 0.0700, wR2 = 0.0885	
Largest diff. peak and hole	1.857 and -2.609 e.Å ⁻³	

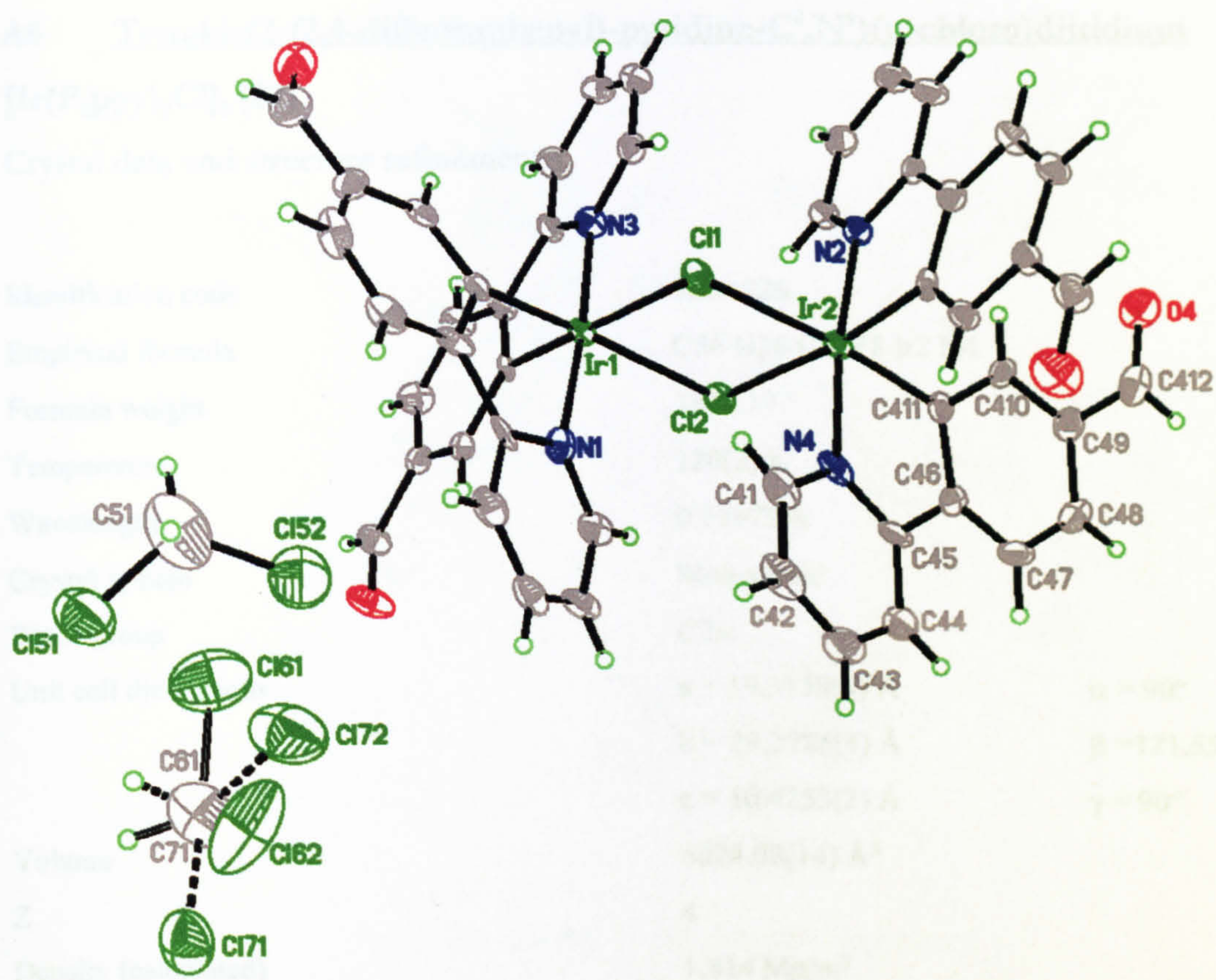


Figure A5 X-ray crystal structure of Tetrakis(4-(2-pyridyl)benzaldehyde-C²,N')(μ -chloro)diiridium at 120 K, thermal ellipsoids depict 50 % occupancy.

A6 Tetrakis(2-(2,4-difluorophenyl)-pyridine-C²,N')(μ -chloro)diiridium
[Ir(F₂ppy)₂Cl]₂ (22)

Crystal data and structure refinement

Identification code	02srv226	
Empirical formula	C ₅₆ H ₃₆ Cl ₂ F ₈ Ir ₂ N ₄	
Formula weight	1372.19	
Temperature	120(2) K	
Wavelength	0.71073 Å	
Crystal system	Monoclinic	
Space group	C2/c	
Unit cell dimensions	a = 19.3158(3) Å	$\alpha = 90^\circ$
	b = 29.2786(4) Å	$\beta = 121.5560(1)^\circ$
	c = 10.4253(2) Å	$\gamma = 90^\circ$
Volume	5024.08(14) Å ³	
Z	4	
Density (calculated)	1.814 Mg/m ³	
Absorption coefficient	5.471 mm ⁻¹	
F(000)	2640	
Crystal size	0.16 x 0.07 x 0.05 mm ³	
Theta range for data collection	2.07 to 29.13°	
Index ranges	-25 ≤ h ≤ 26, -40 ≤ k ≤ 35, -14 ≤ l ≤ 13	
Reflections collected	22403	
Independent reflections	6754 [R(int) = 0.0277]	
Completeness to theta = 29.13°	99.8 %	
Absorption correction	Integration	
Max. and min. transmission	0.7716 and 0.4748	
Refinement method	Full-matrix least-squares on F ²	
Data / restraints / parameters	6754 / 0 / 327	
Goodness-of-fit on F ²	0.967	
Final R indices [I > 2sigma(I)]	R1 = 0.0207, wR2 = 0.0447	
R indices (all data)	R1 = 0.0312, wR2 = 0.0477	
Largest diff. peak and hole	1.480 and -0.594 e.Å ⁻³	

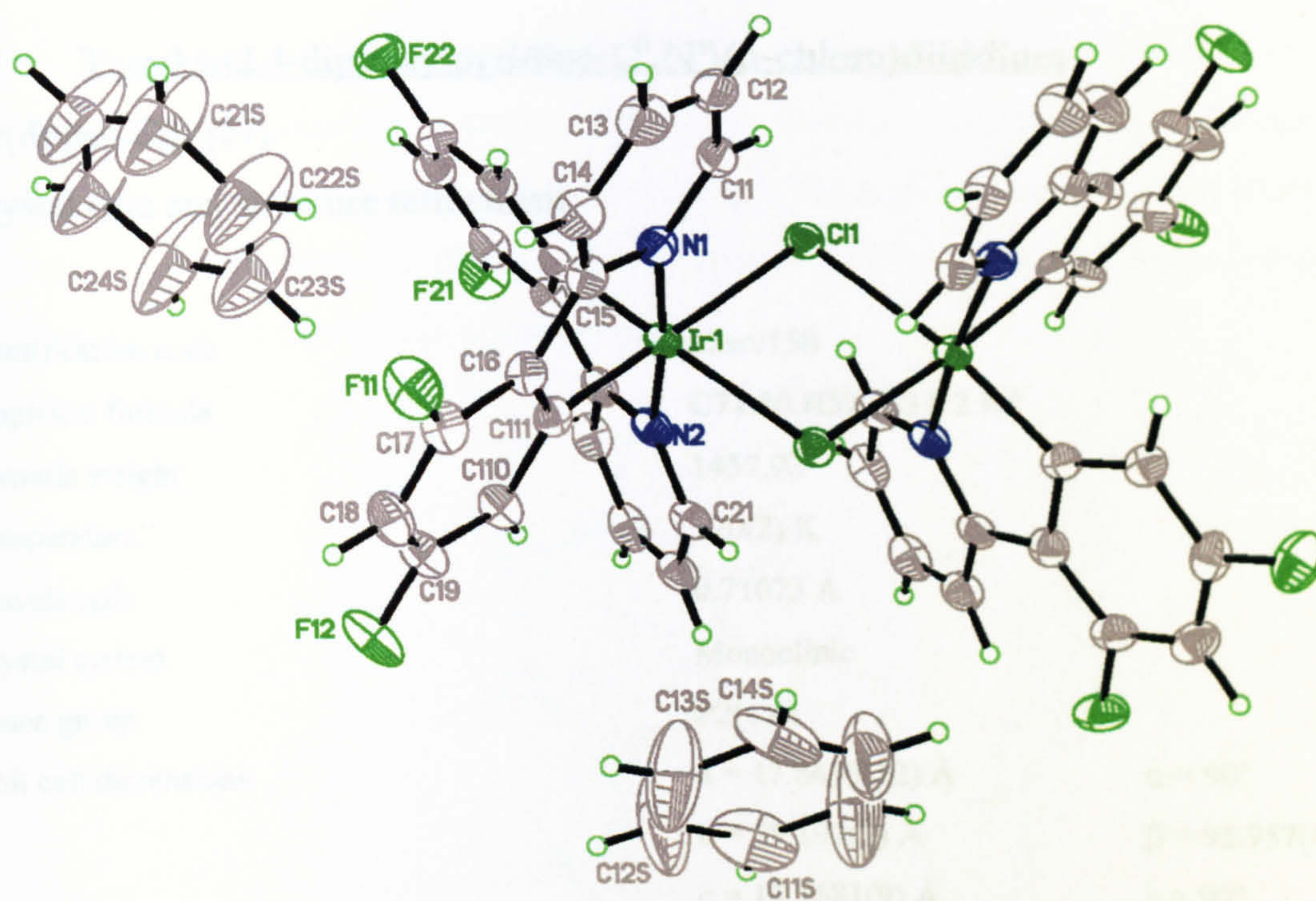


Figure A6 X-ray crystal structure of

Tetrakis(2-(2,4-difluorophenyl)-pyridine- C^2,N')(μ -chloro)diiridium at 120 K,
thermal ellipsoids depict 50 % occupancy.

A7

Tetrakis(2,4-diphenylpyridine-C²,N³)(μ-chloro)diiridium

[Ir(dppy)₂Cl]₂ (27)

Crystal data and structure refinement

Identification code	02srv150	
Empirical formula	C71.50 H52 Cl3 Ir2 N4	
Formula weight	1457.92	
Temperature	120(2) K	
Wavelength	0.71073 Å	
Crystal system	Monoclinic	
Space group	P2(1)/c	
Unit cell dimensions	a = 17.8433(12) Å	α = 90°
	b = 29.193(2) Å	β = 95.957(4)°
	c = 13.7681(9) Å	γ = 90°
Volume	7133.1(8) Å ³	
Z	4	
Density (calculated)	1.358 Mg/m ³	
Absorption coefficient	3.879 mm ⁻¹	
F(000)	2856	
Crystal size	0.20 x 0.15 x 0.10 mm ³	
Theta range for data collection	1.34 to 27.52°	
Index ranges	-19<=h<=23, -37<=k<=37, -17<=l<=17	
Reflections collected	50015	
Independent reflections	16325 [R(int) = 0.1987]	
Completeness to theta = 27.52°	99.5 %	
Refinement method	Full-matrix least-squares on F ²	
Data / restraints / parameters	16325 / 38 / 288	
Goodness-of-fit on F ²	1.852	
Final R indices [I>2sigma(I)]	R1 = 0.1615, wR2 = 0.3565	
R indices (all data)	R1 = 0.2952, wR2 = 0.4112	
Largest diff. peak and hole	13.353 and -4.102 e.Å ⁻³	

The data was so poor that although a solution was possible, a quality structure refinement was unstable with unfeasible atomic displacement parameters. Consequently, despite refining all atoms except the iridium and chlorine atoms as isotropic, possible disorder in the phenyl groups and large errors meant inferring detailed structural information is impossible.

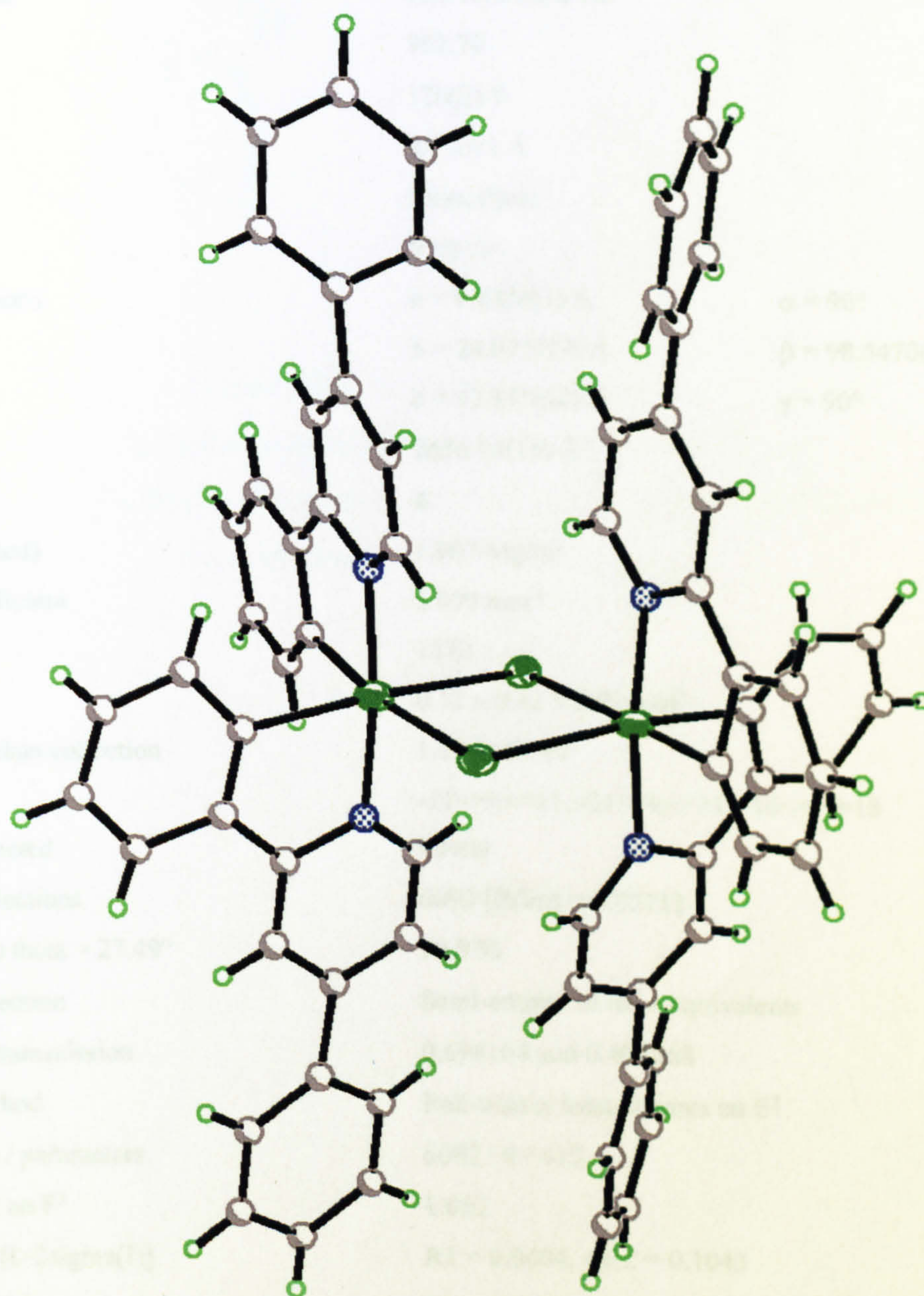


Figure A7 X-ray crystal structure of Tetrakis(2,4-diphenylpyridine- C^2,N')(μ -chloro)diiridium at 120 K, thermal ellipsoids depict 50 % occupancy.

A8 Tris-2-(2,4-difluoro-phenylpyridine-C²,N')iridium**Ir(F₂ppy)₃ (37)****Crystal data and structure refinement**

Identification code	01srv162	
Empirical formula	C ₃₃ H ₁₈ F ₆ Ir N ₃	
Formula weight	762.70	
Temperature	120(2) K	
Wavelength	0.71073 Å	
Crystal system	Monoclinic	
Space group	P2(1)/n	
Unit cell dimensions	a = 9.0356(3) Å	α = 90°
	b = 24.0751(9) Å	β = 98.5470(10)°
	c = 12.3476(4) Å	γ = 90°
Volume	2656.18(16) Å ³	
Z	4	
Density (calculated)	1.907 Mg/m ³	
Absorption coefficient	5.099 mm ⁻¹	
F(000)	1472	
Crystal size	0.12 x 0.12 x 0.02 mm ³	
Theta range for data collection	1.69 to 27.49°	
Index ranges	-11 ≤ h ≤ 11, -31 ≤ k ≤ 31, -16 ≤ l ≤ 16	
Reflections collected	28905	
Independent reflections	6092 [R(int) = 0.0571]	
Completeness to theta = 27.49°	99.9 %	
Absorption correction	Semi-empirical from equivalents	
Max. and min. transmission	0.694164 and 0.493868	
Refinement method	Full-matrix least-squares on F ²	
Data / restraints / parameters	6092 / 0 / 412	
Goodness-of-fit on F ²	1.052	
Final R indices [I > 2σ(I)]	R1 = 0.0404, wR2 = 0.1043	
R indices (all data)	R1 = 0.0612, wR2 = 0.1108	
Largest diff. peak and hole	1.502 and -1.248 e.Å ⁻³	

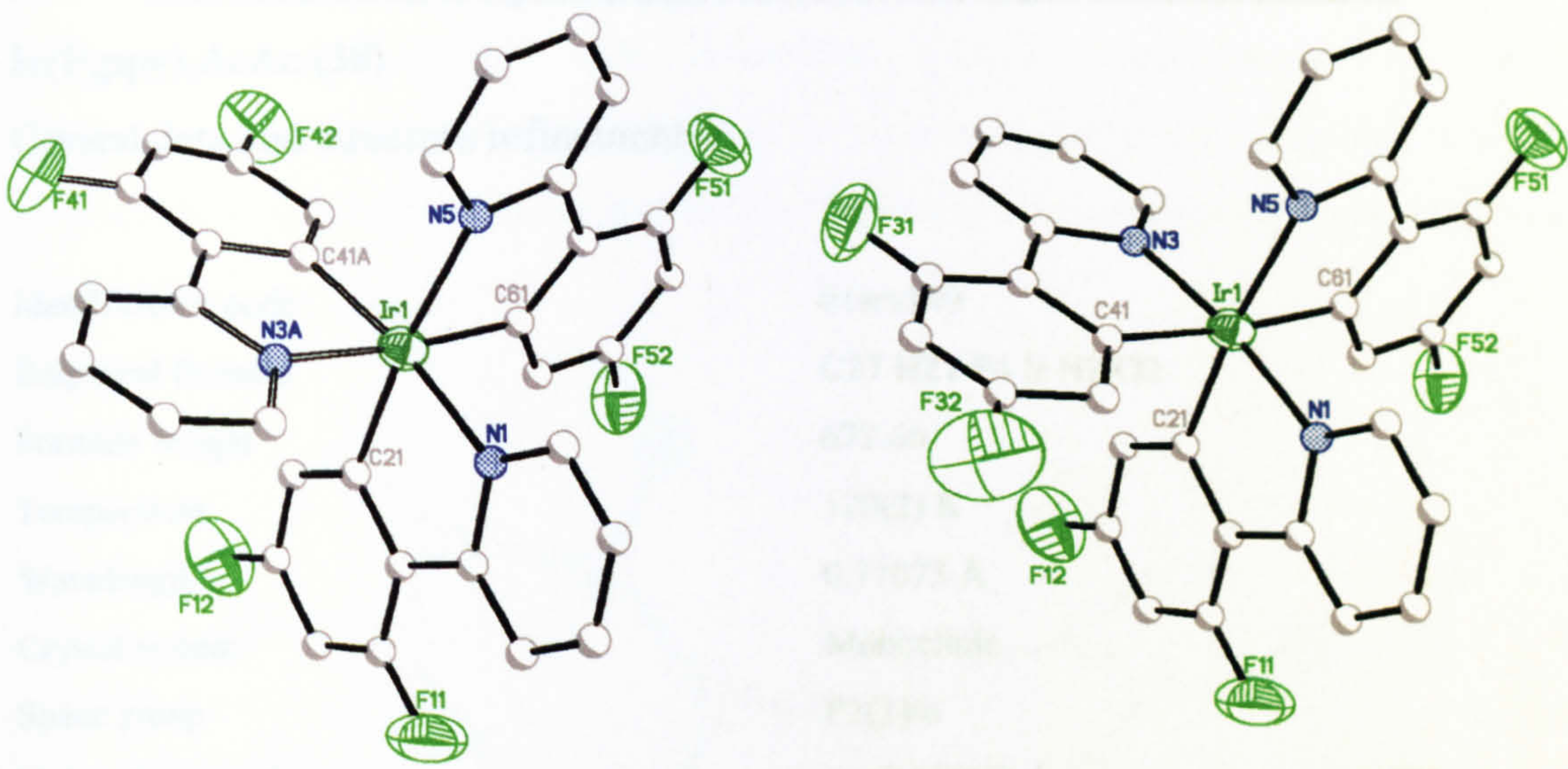


Figure A8 X-ray crystal structures of *Fac*-tris-2-(2,4-difluoro-phenylpyridine- C^2,N')iridium (left) and *Mer*- tris-2-(2,4-difluoro-phenylpyridine- C^2,N')iridium (right) at 120 K, thermal ellipsoids depict 50 % occupancy.

A9 Bis-2-(2,4-difluoro-phenylpyridine-C²,N¹)acetylacetonate iridium**Ir(F₂ppy)₂AcAc (38)****Crystal data and structure refinement**

Identification code	01srv149	
Empirical formula	C ₂₇ H ₂₁ F ₄ Ir N ₂ O ₂	
Formula weight	673.66	
Temperature	120(2) K	
Wavelength	0.71073 Å	
Crystal system	Monoclinic	
Space group	P2(1)/n	
Unit cell dimensions	a = 7.609(5) Å	α = 90°
	b = 19.944(12) Å	β = 98.139(10)°
	c = 15.997(10) Å	γ = 90°
Volume	2403(3) Å ³	
Z	4	
Density (calculated)	1.862 Mg/m ³	
Absorption coefficient	5.615 mm ⁻¹	
F(000)	1304	
Crystal size	0.10 x 0.10 x 0.10 mm ³	
Theta range for data collection	1.64 to 27.49°	
Index ranges	-9 ≤ h ≤ 9, -24 ≤ k ≤ 25, -20 ≤ l ≤ 20	
Reflections collected	22393	
Independent reflections	5503 [R(int) = 0.2199]	
Completeness to theta = 27.49°	99.8 %	
Refinement method	Full-matrix least-squares on F ²	
Data / restraints / parameters	5503 / 0 / 145	
Goodness-of-fit on F ²	1.769	
Final R indices [I > 2σ(I)]	R1 = 0.1551, wR2 = 0.3430	
R indices (all data)	R1 = 0.2601, wR2 = 0.3913	
Largest diff. peak and hole	43.649 and -10.667 e.Å ⁻³	

The data was so poor that although a solution was possible, a quality structure refinement was unstable with unfeasible atomic displacement parameters. Consequently, despite refining all atoms as isotropic, large errors meant inferring detailed structural information is impossible. However, with restraints, the structure can be seen.

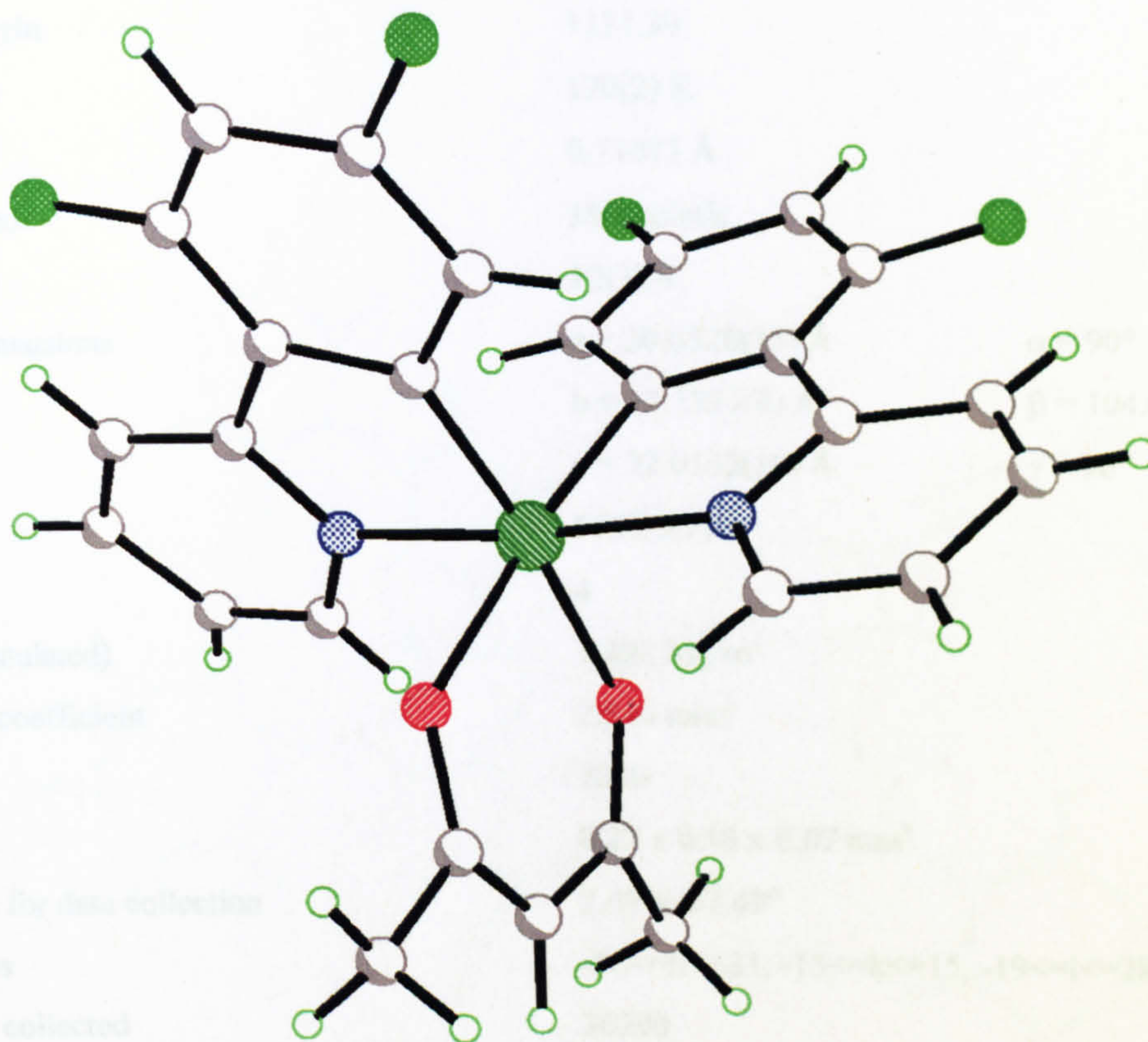


Figure A9 X-ray crystal structure of

Bis-2-(2,4-difluoro-phenylpyridine- C^2,N^n)acetylacetonate iridium at 120 K, thermal ellipsoids depict 50 % occupancy.

A10 Fac-Tris-(2-Biphenyl-3-yl-4-phenyl-pyridine-C²,N')iridium
Fac-Ir(bippy)₃ (48)

Crystal data and structure refinement

Identification code	03srv003	
Empirical formula	C ₆₉ H ₄₈ Ir N ₃	
Formula weight	1111.30	
Temperature	120(2) K	
Wavelength	0.71073 Å	
Crystal system	Monoclinic	
Space group	P2(1)/n	
Unit cell dimensions	a = 20.6528(15) Å	α = 90°
	b = 12.1391(8) Å	β = 104.628(3)°
	c = 22.0132(16) Å	γ = 90°
Volume	5340.0(7) Å ³	
Z	4	
Density (calculated)	1.382 Mg/m ³	
Absorption coefficient	2.546 mm ⁻¹	
F(000)	2240	
Crystal size	0.22 x 0.16 x 0.07 mm ³	
Theta range for data collection	2.07 to 27.49°	
Index ranges	-26 ≤ h ≤ 23, -15 ≤ k ≤ 15, -19 ≤ l ≤ 28	
Reflections collected	36290	
Independent reflections	12213 [R(int) = 0.1162]	
Completeness to theta = 27.49°	99.6 %	
Refinement method	Full-matrix least-squares on F ²	
Data / restraints / parameters	12213 / 0 / 226	
Goodness-of-fit on F ²	1.475	
Final R indices [I > 2σ(I)]	R1 = 0.1093, wR2 = 0.2560	
R indices (all data)	R1 = 0.1639, wR2 = 0.2827	
Largest diff. peak and hole	7.252 and -4.750 e.Å ⁻³	

The data was so poor that although a solution was possible, a quality structure refinement was unstable with unfeasible atomic displacement parameters. Consequently, despite refining all atoms except the central iridium as isotropic, possible disorder in the phenyl groups and large errors meant inferring detailed structural information is impossible.

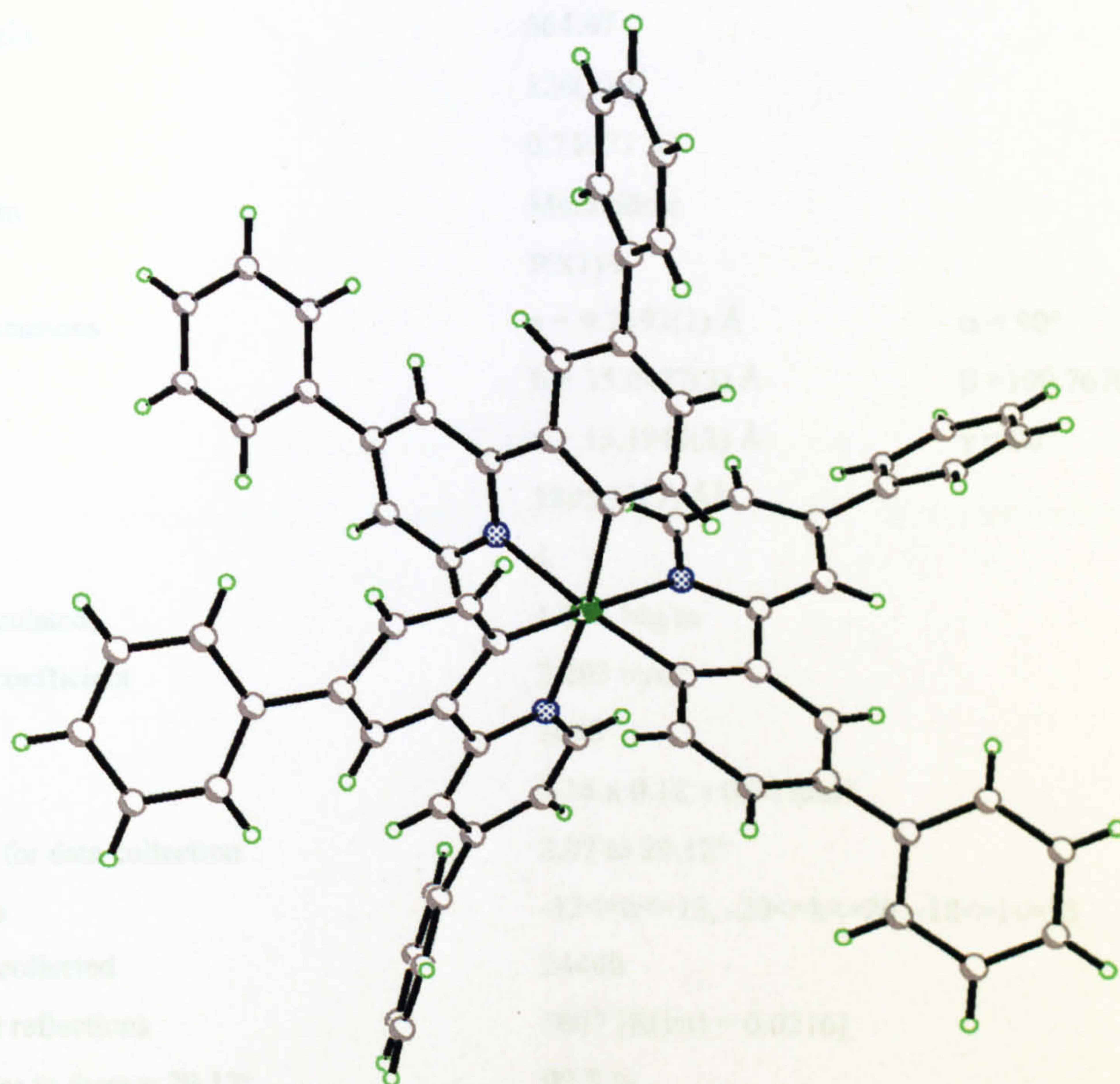


Figure A10 X-ray crystal structure of

Tris-*fac*-(2-Biphenyl-3-yl-4-phenyl-pyridine-C²,N')iridium at 120 K, thermal ellipsoids depict 50 % occupancy.

A11 Bis-(2-phenylpyridine-C²,N')carbonyl iridium chloride

Ir(ppy)₂Cl(CO) (50)

Crystal data and structure refinement

Identification code	02srv209	
Empirical formula	C23 H16 Cl1 Ir1 N2 O1	
Formula weight	564.07	
Temperature	120(2) K	
Wavelength	0.71073 Å	
Crystal system	Monoclinic	
Space group	P2(1)/c	
Unit cell dimensions	a = 9.7192(2) Å	α = 90°
	b = 15.0427(3) Å	β = 100.7670(1)°
	c = 13.1945(3) Å	γ = 90°
Volume	1895.11(7) Å ³	
Z	4	
Density (calculated)	1.977 Mg/m ³	
Absorption coefficient	7.203 mm ⁻¹	
F(000)	1080	
Crystal size	0.16 x 0.12 x 0.06 mm ³	
Theta range for data collection	2.07 to 29.12°	
Index ranges	-13 ≤ h ≤ 13, -20 ≤ k ≤ 20, -18 ≤ l ≤ 18	
Reflections collected	24440	
Independent reflections	5087 [R(int) = 0.0216]	
Completeness to theta = 29.12°	99.8 %	
Absorption correction	Integration	
Max. and min. transmission	0.6718 and 0.3920	
Refinement method	Full-matrix least-squares on F ²	
Data / restraints / parameters	5087 / 0 / 253	
Goodness-of-fit on F ²	1.044	
Final R indices [I>2sigma(I)]	R1 = 0.0190, wR2 = 0.0456	
R indices (all data)	R1 = 0.0211, wR2 = 0.0465	
Largest diff. peak and hole	1.301 and -0.764 e.Å ⁻³	

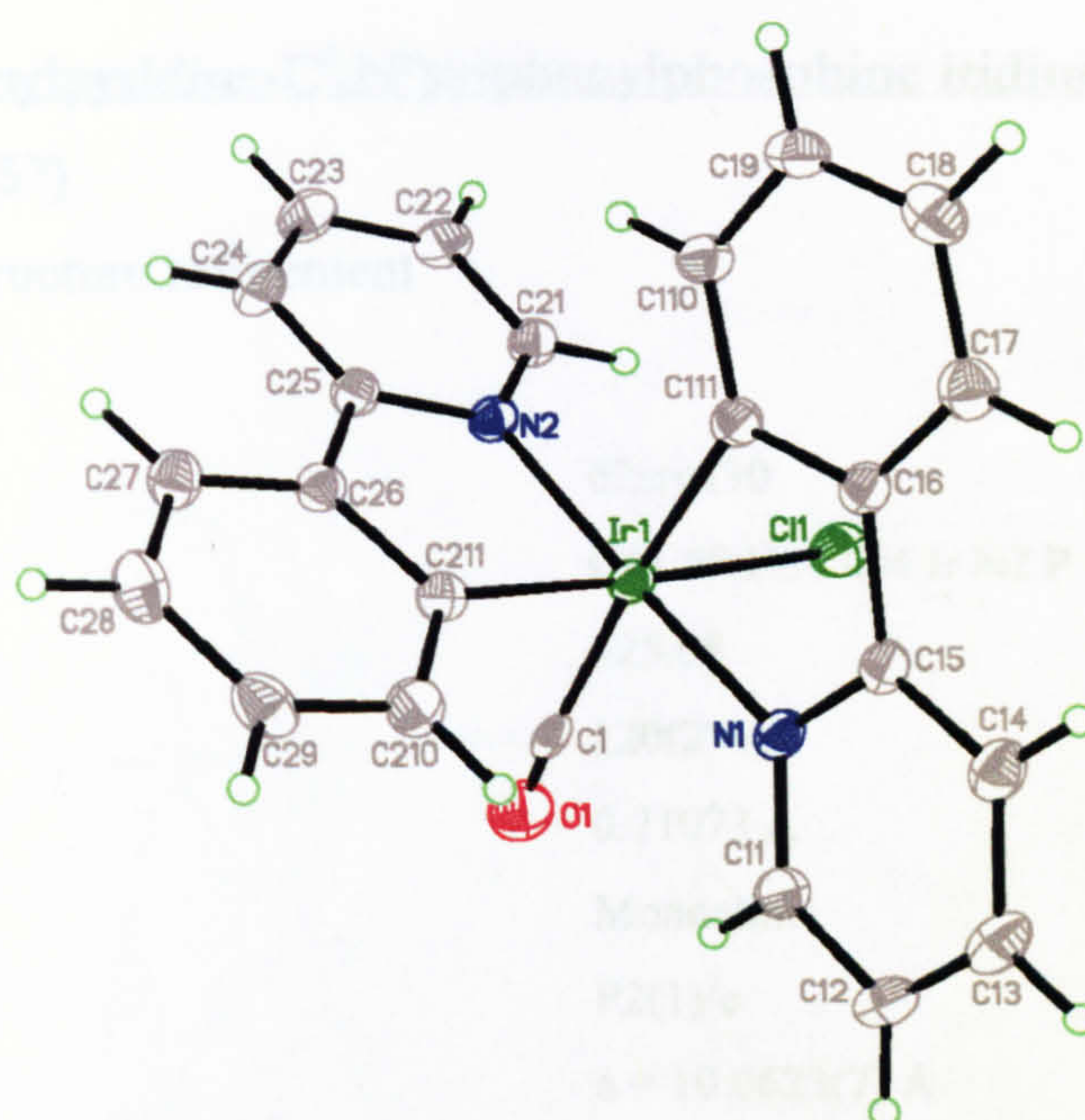


Figure A11 X-ray crystal structure of Bis-(2-phenylpyridine-C²,N')carbonyl iridium chloride at 120 K, thermal ellipsoids depict 50 % occupancy.

A12

Bis-(2-phenylpyridine-C²,N')triphenylphosphine iridium chloride

Ir(ppy)₂Cl(PPh₃) (52)

Crystal data and structure refinement

Identification code	02srv130	
Empirical formula	C41.50 H34 Cl4 Ir N2 P	
Formula weight	925.68	
Temperature	120(2) K	
Wavelength	0.71073 Å	
Crystal system	Monoclinic	
Space group	P2(1)/c	
Unit cell dimensions	a = 10.0623(7) Å	α = 90°.
	b = 14.8387(10) Å	β = 99.864(2)°.
	c = 24.3139(16) Å	γ = 90°.
Volume	3576.7(4) Å ³	
Z	4	
Density (calculated)	1.719 Mg/m ³	
Absorption coefficient	4.111 mm ⁻¹	
F(000)	1828	
Crystal size	0.20 x 0.08 x 0.08 mm ³	
Theta range for data collection	1.61 to 27.51°.	
Index ranges	-13<=h<=13, -19<=k<=19, -31<=l<=31	
Reflections collected	33885	
Independent reflections	8209 [R(int) = 0.1084]	
Completeness to theta = 27.51°	99.9 %	
Absorption correction	Semi-empirical from equivalents	
Max. and min. transmission	0.7345 and 0.4936	
Refinement method	Full-matrix least-squares on F ²	
Data / restraints / parameters	8209 / 3 / 451	
Goodness-of-fit on F ²	0.971	
Final R indices [I>2sigma(I)]	R1 = 0.0502, wR2 = 0.1138	
R indices (all data)	R1 = 0.0684, wR2 = 0.1243	
Largest diff. peak and hole	4.065 and -2.526 e.Å ⁻³	

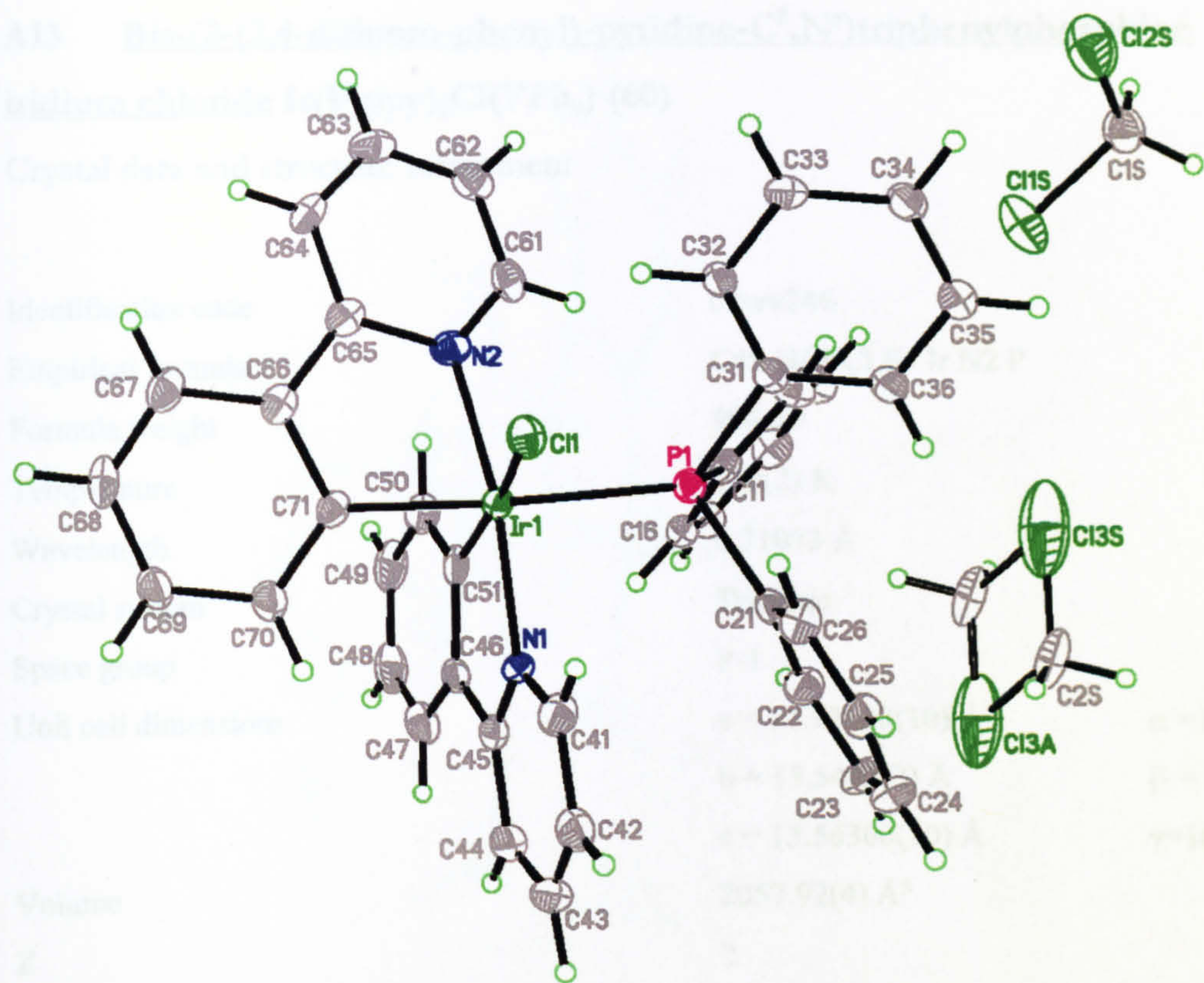


Figure A12 X-ray crystal structure of Bis-(2-phenylpyridine-C²,N³)triphenylphosphine iridium chloride at 120 K, thermal ellipsoids depict 50 % occupancy.

A13

Bis-(2-(2,4-difluoro-phenyl)-pyridine-C²,N')triphenylphosphine
iridium chloride Ir(F₂ppy)₂Cl(PPh₃) (60)

Crystal data and structure refinement

Identification code	02srv246	
Empirical formula	C49 H45 Cl F4 Ir N2 P	
Formula weight	996.49	
Temperature	120(2) K	
Wavelength	0.71073 Å	
Crystal system	Triclinic	
Space group	P-1	
Unit cell dimensions	a = 11.92140(10) Å	α = 101.9410(1)°
	b = 13.5443(2) Å	β = 98.4520(1)°
	c = 13.56360(10) Å	γ = 101.5960(1)°
Volume	2057.92(4) Å ³	
Z	2	
Density (calculated)	1.608 Mg/m ³	
Absorption coefficient	3.404 mm ⁻¹	
F(000)	996	
Crystal size	0.30 x 0.12 x 0.04 mm ³	
Theta range for data collection	1.58 to 28.29°	
Index ranges	-14 ≤ h ≤ 15, -18 ≤ k ≤ 17, -18 ≤ l ≤ 18	
Reflections collected	25950	
Independent reflections	10195 [R(int) = 0.0178]	
Completeness to theta = 28.29°	99.7 %	
Absorption correction	Integration	
Max. and min. transmission	0.8759 and 0.4283	
Refinement method	Full-matrix least-squares on F ²	
Data / restraints / parameters	10195 / 92 / 511	
Goodness-of-fit on F ²	1.033	
Final R indices [I > 2σ(I)]	R1 = 0.0199, wR2 = 0.0481	
R indices (all data)	R1 = 0.0228, wR2 = 0.0495	
Largest diff. peak and hole	1.126 and -0.705 e.Å ⁻³	

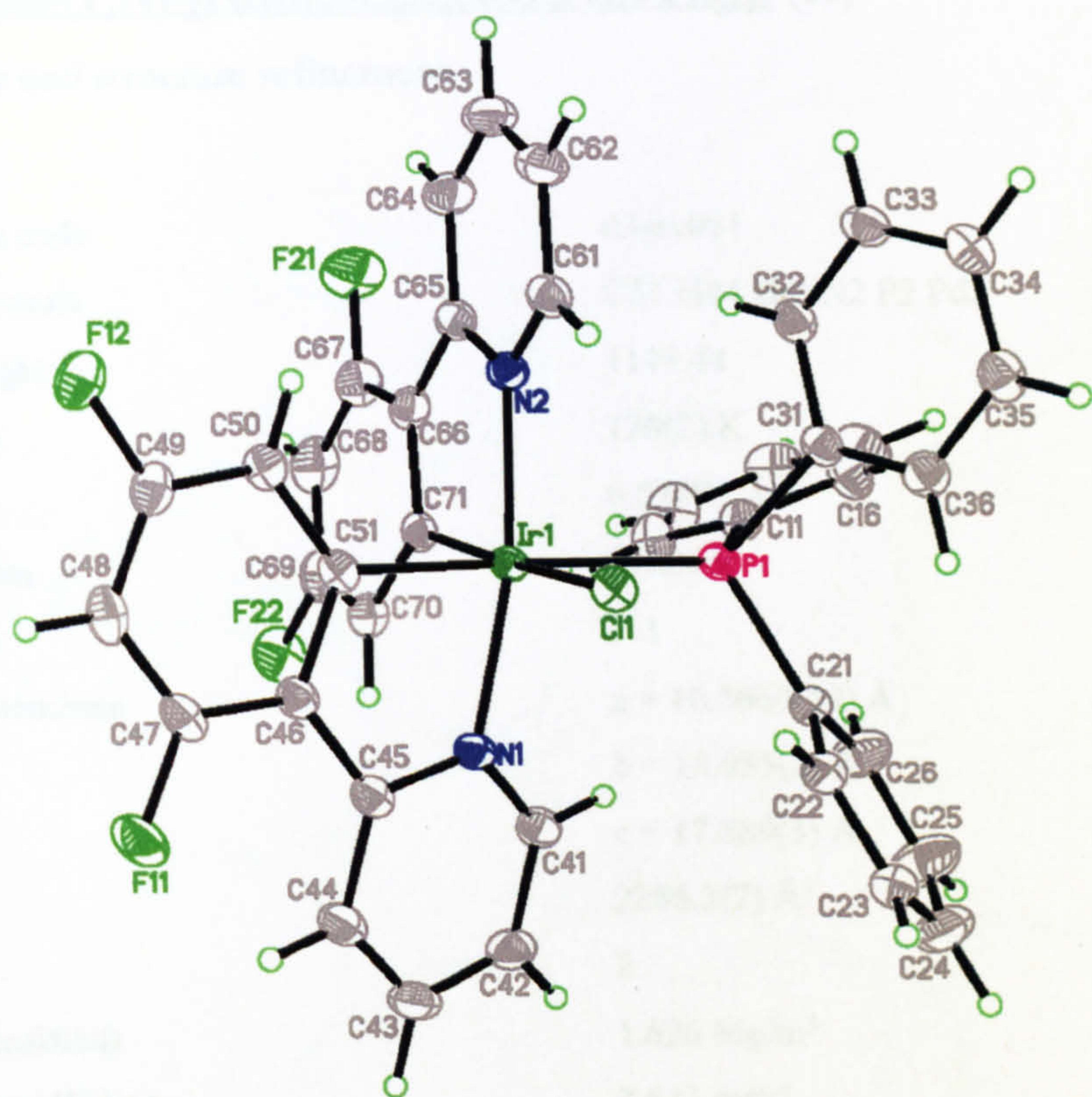


Figure A13 X-ray crystal structure of Bis-(2-(2,4-difluoro-phenyl)-pyridine-C²,N⁷)triphenylphosphine iridium chloride at 120 K, thermal ellipsoids depict 50 % occupancy.

A14 Trans-(P,N)-[PdBr(μ -C₅H₄N-C²,N)(PPh₃)]₂ (61)**Crystal data and structure refinement**

Identification code	03srv081	
Empirical formula	C ₅₁ H ₄₄ Br ₂ N ₂ P ₂ Pd ₂	
Formula weight	1119.44	
Temperature	120(2) K	
Wavelength	0.71073 Å	
Crystal system	Triclinic	
Space group	P-1	
Unit cell dimensions	a = 10.5660(19) Å	$\alpha = 79.502(3)^\circ$
	b = 13.055(2) Å	$\beta = 79.481(4)^\circ$
	c = 17.889(3) Å	$\gamma = 71.984(4)^\circ$
Volume	2286.3(7) Å ³	
Z	2	
Density (calculated)	1.626 Mg/m ³	
Absorption coefficient	2.641 mm ⁻¹	
F(000)	1112	
Crystal size	0.10 x 0.06 x 0.02 mm ³	
Theta range for data collection	1.66 to 27.51°	
Index ranges	-7 ≤ h ≤ 13, -16 ≤ k ≤ 16, -23 ≤ l ≤ 22	
Reflections collected	14605	
Independent reflections	10300 [R(int) = 0.1334]	
Completeness to theta = 27.51°	98.0 %	
Absorption correction	Integration	
Max. and min. transmission	0.9491 and 0.7781	
Refinement method	Full-matrix least-squares on F ²	
Data / restraints / parameters	10300 / 15 / 297	
Goodness-of-fit on F ²	0.914	
Final R indices [I > 2sigma(I)]	R1 = 0.0905, wR2 = 0.1359	
R indices (all data)	R1 = 0.2645, wR2 = 0.1880	
Largest diff. peak and hole	1.175 and -1.206 e.Å ⁻³	

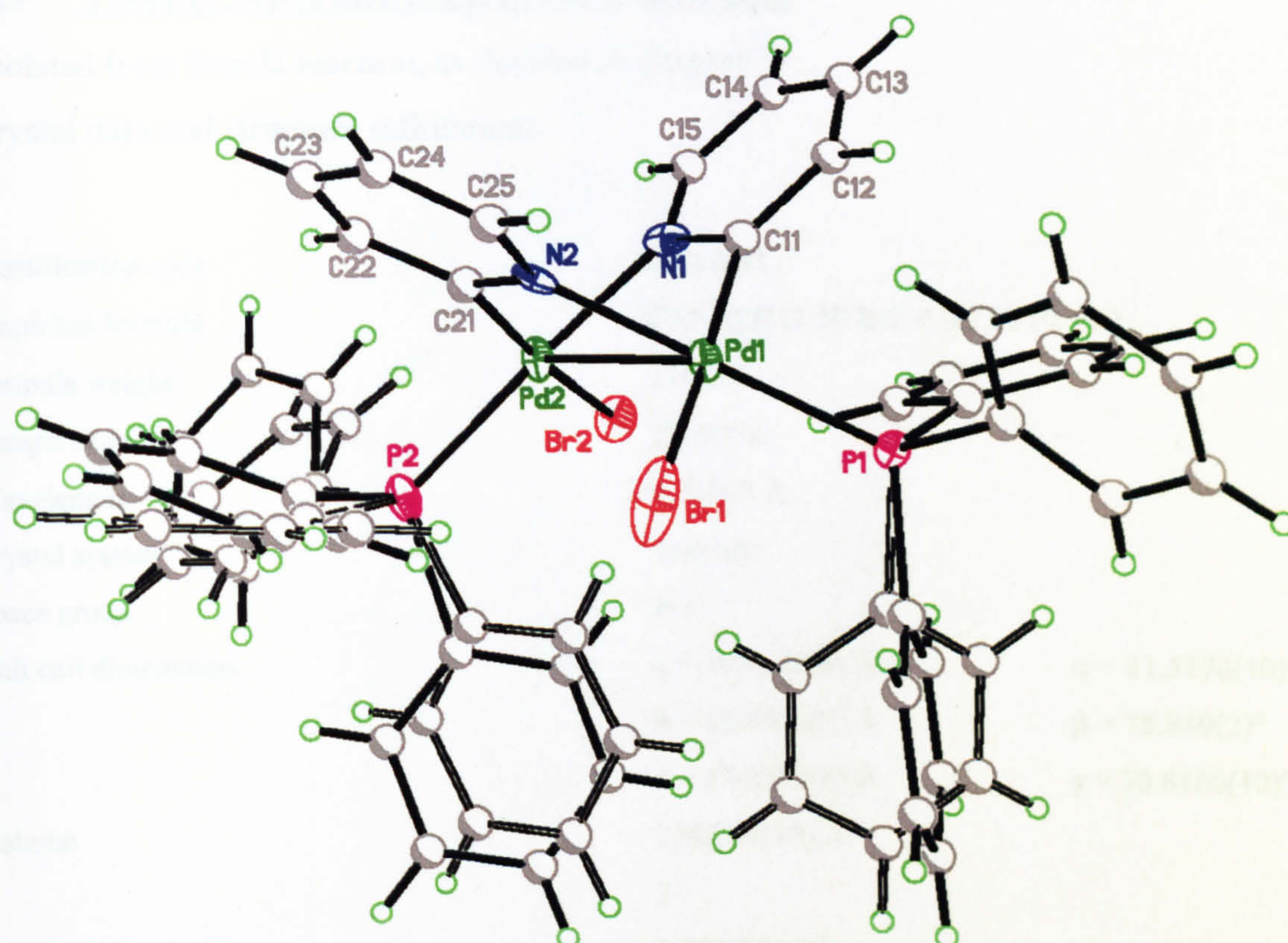


Figure A14 X-ray crystal structure of *Trans*-(P,N)-[PdBr(μ -C₅H₄N-C²,N)(PPh₃)]₂ at 120 K, thermal ellipsoids depict 50 % occupancy.

A15 Trans-(P,N)-[PdBr(μ -C₅H₄N-C²,N)(PPh₃)]₂

(Isolated from Suzuki reaction, as detailed in chapter 7)

Crystal data and structure refinement

Identification code	02srv243	
Empirical formula	C _{51.50} H _{41.50} Br ₂ F N _{2.50} P ₂ Pd ₂	
Formula weight	1148.93	
Temperature	120(2) K	
Wavelength	0.71073 Å	
Crystal system	Triclinic	
Space group	P-1	
Unit cell dimensions	a = 10.4525(4) Å	$\alpha = 81.5170(10)^\circ$
	b = 13.0911(5) Å	$\beta = 78.849(2)^\circ$
	c = 17.7535(6) Å	$\gamma = 70.8180(10)^\circ$
Volume	2241.84(14) Å ³	
Z	2	
Density (calculated)	1.702 Mg/m ³	
Absorption coefficient	2.699 mm ⁻¹	
F(000)	1138	
Crystal size	0.40 x 0.08 x 0.04 mm ³	
Theta range for data collection	1.65 to 29.10°	
Index ranges	-14 ≤ h ≤ 14, -17 ≤ k ≤ 17, -24 ≤ l ≤ 24	
Reflections collected	27278	
Independent reflections	11754 [R(int) = 0.0418]	
Completeness to theta = 29.10°	97.7 %	
Absorption correction	Integration	
Max. and min. transmission	0.8997 and 0.4115	
Refinement method	Full-matrix least-squares on F ²	
Data / restraints / parameters	11754 / 1 / 561	
Goodness-of-fit on F ²	1.035	
Final R indices [I > 2sigma(I)]	R1 = 0.0431, wR2 = 0.0898	
R indices (all data)	R1 = 0.0680, wR2 = 0.1002	
Largest diff. peak and hole	1.057 and -1.705 e.Å ⁻³	

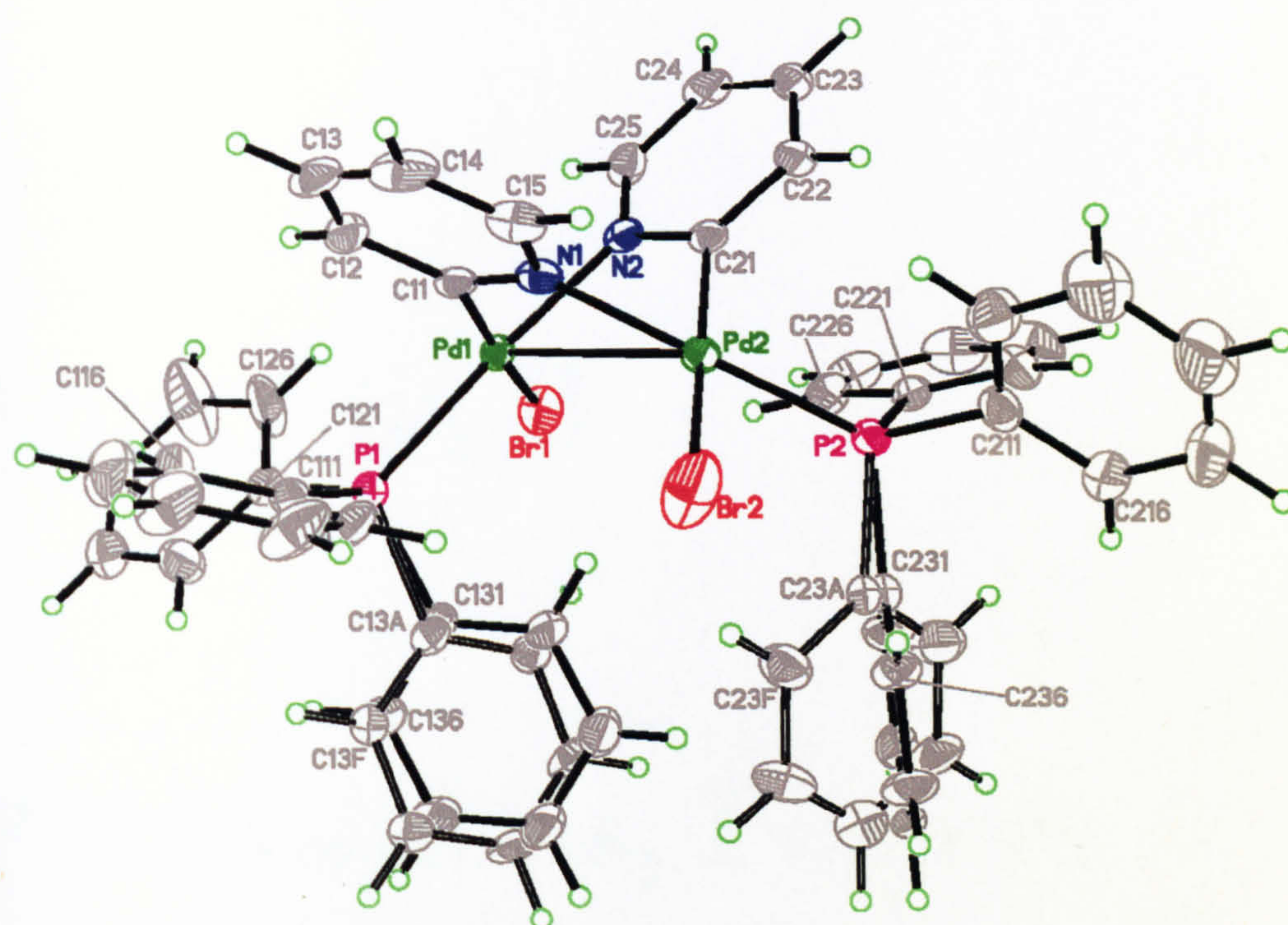


Figure A15 X-ray crystal structure of *Trans*-(P,N)-[PdBr(μ -C₅H₄N-C²,N)(PPh₃)]₂ at 120 K, thermal ellipsoids depict 50 % occupancy.

Appendix B

**Publications, Posters
Presented, Conferences
and Seminars Attended,
Courses and Work
Experience Completed**

B1 Publications**Tuning the Emission of Cyclometalated Iridium Complexes by Simple Ligand Modification**

A. Beeby, S. Bettington, I. D.W. Samuel and Z. Wang, *J. Mater. Chem.*, 2003, **13**, 80-83.

B2 Posters Presented**1 Tuning the Emission of Cyclometalated Iridium(III) Complexes by Simple Ligand Modification**

S. Bettington and A. Beeby

Avecia Postgraduate poster competition - Winner

Department of Chemistry, University of Durham, UK, January 2003

2 The Tuneable Emission of Cyclometalated Iridium(III) Complexes

S. Bettington and A. Beeby

The 8th International Conference of the Platinum Group Metals,

University of Southampton, UK, July 2002

B3 Conferences Attended**CLRC Annual Users Meeting**

Cosener's House

Abingdon, Oxford

9th – 11th May 2001

The 8th International Conference of the Platinum Group Metals

University of Southampton

8th - 12th July 2002

B4 Seminars Attended

- 1 Recent Developments in Organic LED Technology: Organolanthanide Phosphors**
Dr V. Christou, University of Oxford, UK
11th October 2000
- 2 Life, Death and Carotenoids**
Professor T. G. Truscott, University of Keele, UK
29th November 2000
- 3 Dual Activation Approaches to Electroanalysis, Ultrasound and Laser Activation**
Professor R. Compton, University of Oxford, UK
6th December 2000
- 4 Chemical Integrated Circuits: Performing Chemical Analysis on a Single Integrated Device**
Dr A. DeMello, Imperial College, London, UK
24th January 2001
- 5 Analysis of Bond Energy Distribution in Polyatomic Molecules**
Dr S. T. Howard, University of Cardiff, Wales, UK
14th February 2001
- 6 Liquid Crystals of all Shapes and Sizes**
Professor R. Richards, University of Bristol, UK
21st February 2001
- 7 Luminescent Transition Metal Complexes for Chemical Sensing**
Dr G. Williams, University of Durham, UK
5th March 2001

- 8 **Escapades with Arenes and Transition Metals: From Laser Spectroscopy to Synthetic Applications**
Professor R. Perutz, University of York, UK
2nd May 2001
- 9 **Catalysis: Olefin Polymerisation using Ni(II) and Pd(II) Di-imines**
Professor R. Brookhart, University of North Carolina, USA
4th May 2001
- 10 **Towards Benign Supramolecular Chemistry: Synthesis and Self-Organisation**
Professor C. Raston, University of Leeds, UK
31st October 2001
- 11 **Polymers as Building Blocks in Nanotechnology**
Dr W. Huck, University of Cambridge, UK
23rd January 2002
- 12 **Laser Probing the Gas Phase Chemistry Involved in Diamond Chemical Vapour Deposition**
Professor M. Ashfold, University of Bristol, UK
6th March 2002
- 13 **α -, β -Unsaturated Boronates as Versatile Intermediates in Organic Synthesis**
Professor M. Vaultier, University of Rennes, France
20th May 2002
- 14 **Metal Catalysed Routes to Organoboronates Including Direct Functionalisation of C-H Bonds**
Professor T. Marder, University of Durham, UK
20th May 2002

- 15 Design of Molecular and Supramolecular Bipyridyl Metal Complexes for NL Optics**
Professor LeBozec, University of Rennes, France
16th October 2003-07-24
- 16 Fast Time Resolved Spectroscopy from Organometallic Alkane and Noble Gas Complexes to Infrared Probes of DNA**
Professor M. George, University of Nottingham, UK
20th November 2002
- 17 Probing the Spatio-Temporal Organisation of Protein Activities in Early Cell Signalling and Morphogenesis**
Professor P. Bastiaens, EMBL Heidelberg, Germany
16th January 2003
- 18 New Challenges for Chemistry in Signalling Bioactive Species**
Professor David Parker, University of Durham, UK
16th January 2003
- 19 Expanding the View: New Developments in Multi-Dimensional Live Cell Microscopy**
Dr M. Newman, Carl Zeiss
16th January 2003
- B5 Courses Completed**
- 1 Supramolecular Chemistry**
Professor David Parker
University of Durham, UK
Michaelmas Term 2000

2 Experimental Methods

Professor Randal Richards and Dr Andrew Beeby

University of Durham, UK

Epiphany Term 2001

B6 Work Experience

CDT Oxford

Oxford University Begbroke Science Park, Oxford, UK

20th - 24th January 2003

